

Proceedings of the Twentieth NASA Propagation Experimenters Meeting (NAPEX XX)

and the

Advanced Communications Technology Satellite (ACTS) Propagation Studies Miniworkshop

Held in Fairbanks, Alaska
June 4–6, 1996

Nasser Golshan
Editor

September 1, 1996



National Aeronautics and
Space Administration

Jet Propulsion Laboratory
California Institute of Technology
Pasadena, California

JPL Publication 96-20

Proceedings of the Twentieth NASA Propagation Experimenters Meeting (NAPEX XX)

and the

Advanced Communications Technology Satellite (ACTS) Propagation Studies Miniworkshop

Held in Fairbanks, Alaska
June 4–6, 1996

Nasser Golshan
Editor

September 1, 1996



National Aeronautics and
Space Administration

Jet Propulsion Laboratory
California Institute of Technology
Pasadena, California

This publication was prepared by the Jet Propulsion Laboratory, California Institute of Technology, under a contract with the National Aeronautics and Space Administration.

ABSTRACT

The NASA Propagation Experimenters (NAPEX) Meeting is convened each year to discuss studies supported by the NASA Propagation Program. Representatives from the satellite communications (satcom) industry, academia and government who have an interest in space-ground radio wave propagation are invited to NAPEX meetings for discussions and exchange of information. The reports delivered at these meetings by program managers and investigators present recent activities and future plans. This forum provides an opportunity for peer discussion of work in progress, timely dissemination of propagation results, and close interaction with the satcom industry.

NAPEX XX took place in Fairbanks, Alaska, on June 4-5, 1996 and consisted of three sessions. Session 1, entitled "ACTS Propagation Study: Background, Objectives, and Outcomes," covered the results of thirteen station-years of Ka-band experiments. Session 2, "Propagation Studies for Mobile and Personal Satellite Applications," provided the latest developments in measurement, modeling, and dissemination of propagation phenomena of interest to the mobile, personal, and aeronautical satcom industry. Session 3, "Propagation Research Topics," covered a diverse range of topics including space/ground optical propagation experiments, propagation databases, the NASA Propagation Web Site, and plans to revise the NASA propagation effects handbooks.

The ACTS Miniworkshop was held on June 6, 1996 and consisted of a technical session in the morning and a plenary session in the afternoon. The morning session covered updates on the status of the ACTS Project and the ACTS Propagation Program, engineering support for ACTS propagation terminals, and the ACTS Propagation Data Center. The plenary session made specific recommendations for the future direction of the program.

Page intentionally left blank

PREFACE

The NASA Propagation Experimenters (NAPEX) Meeting is convened each year to discuss studies supported by the NASA Propagation Program. The reports delivered at this meeting by program managers and investigators present our recent activities and future plans. Representatives from the satellite communications (satcom) industry, academia and government who have an interest in space-ground radio wave propagation are invited to NAPEX meetings for discussions and exchange of information. This forum provides an opportunity for peer discussion of work in progress, timely dissemination of propagation results, and close interaction with the satcom industry.

NAPEX XX took place at the Wedgewood Resort in Fairbanks Alaska on June 4-5, 1996 and consisted of the welcome, opening remarks, and three sessions. Steve Townes, the manager of the Space Communications Technology Program at JPL, welcomed the participants on behalf of our NASA sponsor, Ramon DePaula, commended the close interaction between the program and industry, and called for even closer partnership and sharing of resources. R. Bauer, ACTS Experiments manager, and N. Golshan, the new JPL technical manager for the Propagation Program, made the opening remarks, recognizing the outstanding services of outgoing Propagation Program manager Faramaz Davarian and commenting on the historic opportunity to leverage the ACTS propagation campaign to serve the propagation needs of proposed Ka-Band systems.

Session 1, entitled "ACTS Propagation Study: Background, Objectives, and Outcomes," was chaired by L. Ippolito of Stanford Telecom. Session 2, "Propagation Studies for Mobile and Personal Satellite Applications," was chaired by R. Bauer of LeRC and provided the latest developments in measurement, modeling, and dissemination of propagation phenomena of interest to the mobile, personal, and aeronautical satcom industry. Session 3, "Propagation Research Topics," was chaired by C. Mayer of the University of Alaska at Fairbanks, and covered a diverse range of topics including space/ground optical propagation experiments, plans to revise the NASA propagation effects handbooks, the expanded NASA Propagation Web Site, and existing propagation databases.

The ACTS Miniworkshop was held on June 6 and consisted of a technical session in the morning and a plenary session in the afternoon. The morning session was chaired by F. Davarian of Hughes Space and Communications and covered updates on the status of the ACTS Project and the Propagation Program, engineering support for ACTS propagation terminals, and the ACTS Data Center. R. Crane of the University of Oklahoma and D. Rogers of Communications Research Center chaired the plenary session.

The success of the meeting owes a lot to the speakers and session chairs and the active participation of all attendees. I have been to many NAPEX meetings and ACTS workshops, but this is the first time I have organized one. I am

touched by the warm and collegial reception from the participants in the NAPEX meeting and ACTS workshop; I look forward to serving the Propagation Community. I would like to express my gratitude to my predecessor, Faramaz Davarian; to Bob Bauer, my counterpart at LeRC; and to Steve Townes, my programmatic manager at JPL, for advice and support during this transition period.

I would like to express my thanks to Professor C. Mayer of the University of Alaska at Fairbanks for hosting this meeting, and for arranging a visit to see the ACTS Propagation Terminal and the SAR facility at the University of Alaska at Fairbanks. Last but not least, I would like to thank Mardy Wilkins of JPL for meticulously taking care of many administrative details of the meetings, and Roger Carlson and Louise Anderson of JPL Technical Information Section for coordinating the publication of this document.

The next ACTS Workshop will be held at the Marriot Suites, near Washington D.C.'s Dulles Airport, on November 19 and 20, 1996. Julie Feil of Stanford Telecom has graciously agreed to be the local host. The next NAPEX meeting will take place in late May/early June of 1997; the exact time and location will be announced by December 1996.

—N. Golshan

**CONTENTS
NAPEX XX MEETING**

SESSION 1. ACTS PROPAGATION STUDY: BACKGROUND, OBJECTIVES, AND OUTCOMES.....	1
<i>L.J. Ippolito (Stanford Telecom)</i>	
ACTS PROPAGATION STUDY: BACKGROUND, OBJECTIVES, AND OUTCOMES...3	
<i>F. Davarian (Hughes Space and Communications Co.)</i>	
ACTS PROPAGATION EXPERIMENT PREPROCESSING SOFTWARE USER'S MANUAL.....	9
<i>R.K. Crane, X. Wang (U. Oklahoma), D. Westenhaver (Westenhaver Wizard Works, Inc.)</i>	
TWO YEARS OF ACTS PROPAGATION STUDIES IN ALASKA.....	41
<i>C.E. Mayer, B.E. Jaeger (U. Alaska, Fairbanks)</i>	
ANALYSIS OF THE ACTS-VANCOUVER PATH PROPAGATION DATA 1ST DECEMBER, 1993--30TH NOVEMBER, 1995.....	67
<i>M. Kharadly, R. Ross, B. Dow (U. British Columbia)</i>	
Ka-BAND PROPAGATION STUDIES USING THE ACTS PROPAGATION TERMINAL AND THE CSU-CHILL MULTIPARAMETER RADAR.....	85
<i>V.N. Bringi, J. Beaver (Colorado State U.)</i>	
PROPAGATION MEASUREMENTS IN FLORIDA.....	113
<i>H. Helmken (Florida Atlantic U.), R. Henning (U. S. Florida)</i>	
ACTS PROPAGATION MEASUREMENTS IN MARYLAND AND VIRGINIA.....	119
<i>A. Dissanayake, K.-T. Lin (COMSAT)</i>	
ACTS PROPAGATION MEASUREMENTS PROGRAM].....	147
<i>J.H. Feil, L.J. Ippolito, S. Horan (Stanford Telecom / New Mexico State U.)</i>	
ACTS PROPAGATION EXPERIMENT, NORMAN, OKLAHOMA.....	167
<i>F. Shimabukuro (Aerospace)</i>	
THIRTEEN STATION YEARS OF ACTS BEACON OBSERVATIONS.....	179
<i>W.J. Vogel, G.W. Torrence (U. Texas, Austin)</i>	
THE NEED FOR MORE MEASUREMENTS IN THE ACTS PROPAGATION EXPERIMENT.....	191
<i>R.K. Crane (U. Oklahoma)</i>	
EASTERN U.S. SPACE-DIVERSITY EXPERIMENT: ONE YEAR OF ACTS 20 GHz MEASUREMENTS.....	199
<i>J. Goldhirsh, B. Musiani (APL), A. Dissanayake, K.T. Lin (COMSAT)</i>	

FADE MITIGATION TECHNIQUES AT Ka-BAND	221
<i>A. Dissanayake (COMSAT)</i>	
SESSION 2. PROPAGATION STUDIES FOR MOBILE AND PERSONAL SATELLITE APPLICATIONS.....	241
<i>R. Bauer (LeRC)</i>	
IMAGE ANALYSIS AS A TOOL FOR SATELLITE-EARTH PROPAGATION STUDIES	243
<i>R. Akturian, H.-P. Lin, W.J. Vogel (U. Texas, Austin)</i>	
GPS MULTIPATH FADE MEASUREMENTS TO DETERMINE L-BAND GROUND REFLECTIVITY PROPERTIES	257
<i>A. Kavak, G. Xu, W.J. Vogel (U. Texas, Austin)</i>	
A PROPOSED CHANGE TO ITU-R RECOMMENDATION 681.....	265
<i>F. Davarian (Hughes Space and Communications Co.)</i>	
DESCRIPTION OF PROPOSED REVISION OF HANDBOOK ON: PROPAGATION EFFECTS FOR LAND MOBILE SATELLITE SYSTEMS	269
<i>J. Goldhirsh (APL), W.J. Vogel (U. Texas, Austin)</i>	
QUICK LOOK ANALYSIS OF BROADBAND AERONAUTICAL DATA OBTAINED FROM THE KUIPER AIRBORNE OBSERVATORY.....	289
<i>E. Satorius, B. Abbe, M. Agan (JPL)</i>	
FADE MEASUREMENTS INTO BUILDINGS FROM 500 TO 3000 MHz	303
<i>W.J. Vogel, G.W. Torrence (U. Texas, Austin)</i>	
SESSION 3. PROPAGATION RESEARCH TOPICS.....	309
<i>C. Mayer (U. Alaska)</i>	
TDRS SPACE-TO-GROUND LINK WEATHER EVENTS	311
<i>S. Horan (New Mexico State U.)</i>	
ATMOSPHERIC VISIBILITY MONITORING (AVM) PROGRAM	327
<i>M. Jeganathan, L. Tong (JPL)</i>	
ATMOSPHERIC TURBULENCE STATISTICS FROM GOLD EXPERIMENTS	343
<i>M. Jeganathan, K. Wilson, J. Lesh (JPL)</i>	
EARTH-SPACE PROPAGATION DATA BASES	363
<i>E.K. Smith (U. Colorado)</i>	
PROPOSED REVISIONS TO THE NASA PROPAGATION HANDBOOKS.....	379
<i>L.J. Ippolito (Stanford Telecom)</i>	

A DATABASE FOR PROPAGATION MODELS AND CONVERSION TO C++ PROGRAMMING LANGUAGE.....	413
<i>A.V. Kantak, K. Angkasa, J. Rucker (JPL)</i>	
NASA PROPAGATION STUDIES WEBSITE.....	423
<i>K.S. Angkasa (JPL)</i>	
ACTS MINIWORKSHOP	429
<i>F. Davarian (Hughes Space and Communications Co.), R.K. Crane, D.V. Rogers (U. Oklahoma)</i>	
ACTS OPENING REMARKS.....	431
<i>F. Davarian (Hughes Space and Communications Co.), N. Golshan (JPL)</i>	
ACTS PROJECT & PROPAGATION PROGRAM UPDATE.....	433
<i>R. Bauer (NASA LeRC)</i>	
ACTS RAIN FADE COMPENSATION.....	443
<i>T.A. Coney (NASA LeRC)</i>	
A SENSITIVITY ANALYSIS OF COMBINED EFFECTS MODELING.....	465
<i>G. Feldhake (Stanford Telecom)</i>	
ACTS PROPAGATION TERMINALS ENGINEERING SUPPORT AND SYSTEM UPGRADES.....	483
<i>D. Westenhaver (Westenhaver Wizard Works, Inc.)</i>	
ACTS DATA CENTER STATUS.....	499
<i>G.W. Torrence (U. Texas, Austin)</i>	
NASA PROPAGATION PROGRAM STATUS AND PROPAGATION NEEDS OF SATCOM INDUSTRY.....	505
<i>N. Golshan (JPL)</i>	
REPORT OF APSW IX PLENARY MEETING.....	515
<i>D.V. Rogers, R.K. Crane (U. Oklahoma)</i>	

Page intentionally left blank

NAPEX XX AND ACTS MINIWORKSHOP ATTENDEES

Ahmed Abdelgany
AT&T Bell Labs
Dept. 7C-152
67 Whippany Road
Whippany, NJ 07981
201-386-7505
201-386-6081 (FAX)
E-mail: Ahmeda@Whstar.wh.att.com

Krisjani Angkasa
Jet Propulsion Laboratory
MS 67-204
4800 Oak Grove Drive
Pasadena, CA 91109
818-354-9250
818-393-0096 (FAX)
E-mail:Krisjani.S.Angkasa@jpl.nasa.gov

Sami Asmar
Jet Propulsion Laboratory
MS 161-260
4800 Oak Grove Drive
Pasadena, CA 91109
818-354-6288
818-393-4643 (FAX)
E-mail: Sami.Asmar@jpl.nasa.gov

Dick Astrom
Motorola
Satellite Communication Div.
2501 S. Price Road
Chandler, AZ 85248
602-732-3178
602-732-3171 (FAX)
E-mail: Dick_Astrom@sat.mot.com

Robert Bauer
NASA Lewis Research Center
21000 Brookpark Rd., MS 54-6
Cleveland, OH 44135
216-433-3431
216-433-6371 (FAX)
E-mail: acbauer@lims01.lerc.nasa.gov

John Beaver
Colorado University
Dept. of EE
Ft. Collins, CO 80523
303-491-6758
303-491-2249 (FAX)
E-mail: jb686028@longs.lance.
colostate.edu

Harvey L. Berger
TRW Space and Electronics Group
One Space Park
Redondo Beach, CA 90278
310-813-7692
310-812-8943 (FAX)
E-mail: berger@gandalf.sp.trw.com

Patricia Camarina
Instituto Politecnico Mexico
La Ideal 31 Col. Industrial
Mexico PI, D.F. C.P. 07800
Mexico D.F.
525-517-88-88
525-586-94-35 (FAX)

David Carpenter
Consultant
1619 Third Street
Manhattan Beach, CA 90266
310-376-4080
310-379-9007 (FAX)

Thom Coney
NASA Lewis Research Center
MS 54-6
21000 Brookpark Rd.
Cleveland, OH 44135
216-433-2652
216-433-6371 (FAX)
E-mail: TCONEY@lerc.nasa.gov

Bob Crane
University of Oklahoma
Room 1248
100 East Boyd St.
Norman, OK 73019-0628
405-325-4419
405-325-7689 (FAX)
E-mail: bcrane@goadm.gcn.uoknor.ed

Faramaz Davarian
Hughes Space and Comm. Company
Bldg. S10, MS S352
1950 Imperial Highway
P.O. 92919
Los Angeles, CA 90009
310-662-5375
E-mail: fdavarian@ccgate.hac.com

Asoka Dissanayake
Comsat Laboratories
22300 Comsat Drive
Clarksburg, MD 20871
301-428-4411
301-428-3686 (FAX)
asoka.dissanayake@comsat.com

David Drucker
KA Star Satellite Comm.
P.O. Box 1471
Evergreen, CO 80437
303-674-7047

Barry Fairbanks
NASA Lewis Research Center
21000 Brookpark Rd., MS 54-6
Cleveland, OH 44135
216-433-3541
216-433-6371 (FAX)
E-mail: acfair@lms01.lerc.nasa.gov

Julie Feil
Stanford Telecom
1761 Business Center Drive
Reston, VA 22090-5333
703-438-7846
703-438-7921 (FAX)
E-mail: jfeil@sed.stel.com

Glen Feldhake
Stanford Telecom
1761 Business Circle Drive
Reston, VA 22090

Paul Flikkema
University of So. Florida
4202 E. Fowler Ave., ENB 118
Tampa, FL 33620
813-974-3940
813-974-5250 (FAX)
flikkema@sunburn.eng.usf.edu

Arthur Garrison
TRW Space and Electronics Group
One Space Park
Redondo Beach, CA 90278
310-813-7928
arthur.garrison@trw.com

Richard Gedney
Advanced Communications Tech. Co.
3721 Cinnamon Way
Westlake, OH 441245
216-777-8549
216-734-2561 (FAX)
rtgedney@aol.co

Julius Goldhirsh
Applied Physics Lab.
Johns Hopkins University
Laurel, MD 20723-6099
301-953-5042
301-953-5458 (FAX)
E-mail: julius-goldhirsh@aplmail.
jhuapl.edu

Nasser Golshan, MS 161-260
Jet Propulsion Laboratory
4800 Oak Grove Drive
Pasadena, CA 91109
818-354-0459
818-393-4643 (FAX)
E-mail: Nasser.Golshan@jpl.nasa.gov

Henry F. Helmken, MS SE/456
Florida Atlantic University
777 W. Glades Road
Boca Raton, FL 33431
407-367-3452
407-367-2336 (FAX)
E-mail: helmkenh@acc.fau.edu

Stephen Horan, Dept, 3-0
New Mexico State University
P.O. Box 30001
Las Cruces, NM 88003-3001
505-646-5870
505-646-1435 (FAX)
E-mail: shoran@nmsu.edu

Sam Houston
Hughes Communications Inc.
Bldg. R35, MS D416
P.O. Box 92919
Los Angeles, CA 90009
310-364-4824
310-364-4712 (FAX)

Louis J. Ippolito
Stanford Telecom.
1761 Business Center Drive
Reston, VA 22090
703-438-8061
703-438-7921 (FAX)
E-mail: lippolito@sed.stel.com

Brad Jaeger, Dept. of EE
University of Alaska
248 Duckering Bldg.
P.O. Box 755900
Fairbanks, AK 99775-5900
907-474-7815
907-474-6087 (FAX)
E-mail: fsbej@aurora.alaska.edu

Muthu Jeganathan
Jet Propulsion Laboratory
MS 161-135
4800 Oak Grove Drive
Pasadena, CA 91109
818-354-9400
818-393-6142 (FAX)
mutha.altair.jpl.nasa.gov

Anil Kantak
Jet Propulsion Laboratory
4800 Oak Grove Drive, MS 161-260
Pasadena, CA 91109
818-354-3836
818-393-4643 (FAX)
E-mail: Anil.V.Kantak@jpl.nasa.gov

M.M.Z. Kharadly
University of British Columbia
2356 Main Mall, Dept. of EE
Vancouver
Canada V666T 1Z4
604-822-2816
604-822-5949 (FAX)
E-mail: acts@ee.ubc.ca

Norbert Kleiner
Motorola
Satellite Communications Div.
2501 S. Price Road
Chandler, AZ 85248
602-732-2963
602-732-3171 (FAX)
E-mail: P21829@e.mail.mot.com

Rick Leacock
Hughes Communications, Inc.
P.O. Box 9712
Long Beach, CA 90810-9928
310-525-5232
310-525-5250 (FAX)
E-mail: rjleacock@ccgate.hac.com

Tong Lee
Hughes Space & Comm.
6th Floor, S10/5319
2260 E. Imperial Highway
Los Angeles, CA 90009
310-662-5382
310-364-7807 (FAX)

Young S.Lee
Orion Satellite Corporation
2440 Research Blvd.
Rockville, MD 20850
301-258-3310
301-258-3319 (FAX)
E-mail: 690-4830@mcimail.com

Charlie Mayer
University of Alaska, EE Dept.
P.O. Box 755900
Fairbanks, AK 99775-5900
907-474-6091
907-474-6087 (FAX)
E-mail: ffcem@aurora.alaska.edu

Carl Mitchell
Space Systems/Loral
MS G-54
3825 Fabian Way
Palo Alto, CA 94303
415-852-7626
415-852-4148 (FAX)
mitchell.carl@ssd.loral.com

Michael Parr
Hughes Network Systems
10450 Pacific Center Court
San Diego, CA 92121
619-452-4737
619-546-8989 (FAX)
E-mail: parr@hns.com

Kenneth Peterson
Motorola
2501 S. Price Road
Chandler, AZ 85248
602-732-2997
602-732-2303 (FAX)

Larry Pond
Hughes Electronics
2260 E. Imperial Highway
El Segundo, CA 90245
310-364-7215
310-364-7004 (FAX)
E-mail: lspond@ccgate.hac.com

David V. Rogers
Communications Research Centre
3701 Carling Avenue
Ottawa, Ontario
Canada K2H 8S2
613-998-5174
613-998-4077 (FAX)
E-mail: dave.rogers@crc.doc.ca

Robert Ross
University of British Columbia
Dept. of EE, 2356 Main Mall
Vancouver, British Columbia
Canada V6T 1Z4
604-822-4241
604-822-9209 (FAX)
E-mail: robr@ee.ubc.ca

Ed Satorius
Jet Propulsion Laboratory
MS 238-420
4800 Oak Grove Drive
Pasadena, CA 91109
818-354-5790
818-354-6825 (FAX)
E-mail: satorius@bolita.jpl.nasa.gov

Ernie K. Smith, ECE Dept.
University of Colorado
Campus Box 425
Boulder, CO 80309-0425
303-492-7004
303-492-2758 (FAX)

Jorge Sosa
ESIME-IPN Mexico
Memerillo 122, Colonia
Noiva Santa Maria
Mexico D.F. 02800
525-556-8497

Murray Steinberg
Space Systems/Loral
MS G54
3825 Fabian Way
Palo Alto, CA 94303-4604
415-852-4499
415-852-4148 (FAX)
E-mail: mos@comsci5.ssd.loral.com

Daniel Stern
NASA Headquarters
Code X
Washington DC, 20546
202-358-4829
202-358-3525 (FAX)
E-mail: dstern@hq.nasa.gov

Steve Townes
Jet Propulsion Laboratory
4800 Oak Grove Drive
MS 238-420
Pasadena, CA 91109
818-354-7525
818-354-6825 (FAX)
E-mail: townes@galway.jpl.nasa.gov

Wolf Vogel
EE Research Laboratory
University of Texas
10100 Burnet Road
Austin, TX 78758
512-471-8608
512-471-8609 (FAX)
E-mail: wolf_vogel@mail.utexas.edu

Charles Wang
National Space Program Office
9 Prosperity Road 1, 8th Fl.
Hsinehu Science Park
Hsinchu, Taiwan, ROC
(011) 886-35-784-208 Ext. 9381
(011) 886-35-770134 (FAX)
ccwang@nspo.gov.tw

Dongming Wang
University of Alaska
EE Dept.
248 Duckering Bldg.
P.O. Box 755900
Fairbanks, AK 99775-5900
907-474-7815
907-474-6087 (FAX)

David B. Westenhaver
WWW, Inc.
746 Lioness Ct. S.W.
Stone Mountain, GA 30087-2855
404-925-1091
404-931-3741 (FAX)
E-mail: 72622.3404@Compuserve.Com

Gung Yur
National Space Program Office
8F, 9 Prosperity 1st Road
Hsinehu Science Park
Hsinchu, Taiwan, ROC
(011) 886-35-784-208 9381
(011) 886-35-770134 (FAX)
pd17@nspo.gov.tw

Administrative Assistant

JPL:

Mardy Wilkins
818-354-7421
818-393-4643 (FAX)
E-mail: Mardith.J.Wilkins.jpl.nasa.gov

ACTS Electronic Address:

acts@java.jpl.nasa.gov

NAPEX XX

SESSION 1

ACTS PROPAGATION STUDY:
BACKGROUND, OBJECTIVES, AND OUTCOMES

L.J. Ippolito (Stanford Telecom / New Mexico State U.)

Page intentionally left blank

**ACTS PROPAGATION STUDY:
BACKGROUND, OBJECTIVES, AND OUTCOMES**

**F. Davarian
Hughes Space and Communications Company**

ACTS Propagation Campaign Milestones

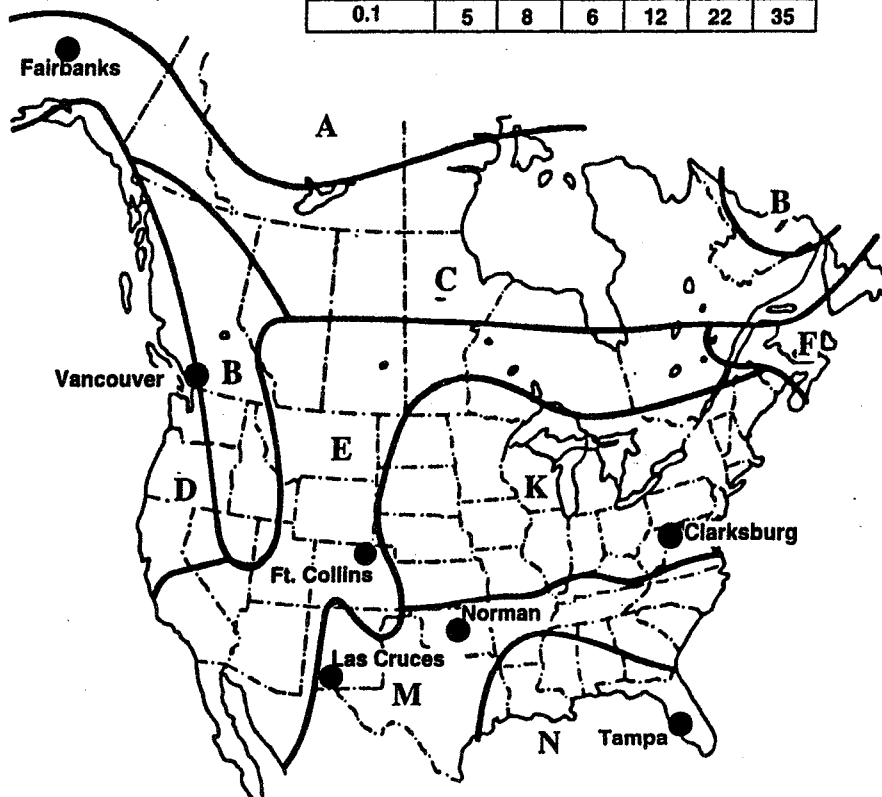
<u>Year</u>	<u>Event</u>
1987	First meeting at COMSAT
1989	First workshop, Santa Monica, CA
1991	Announcement of Opportunity Virginia Polytechnic Institute begins to develop the APT
1993	Terminal delivery and ACTS launch
1996	Data delivery, first two years

Expected Results and Outputs of The Propagation Campaign

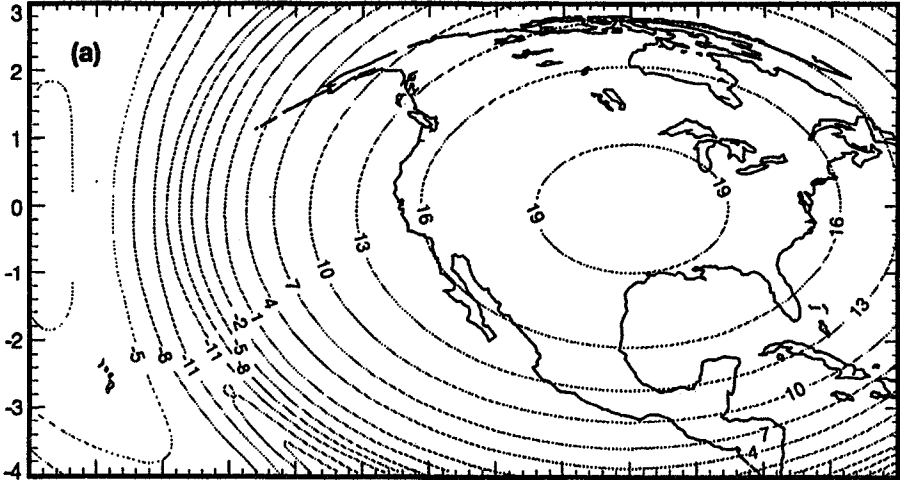
- Ka-band propagation data
- Prediction models of rain and atmospheric attenuation and scintillation
- Fade and nonfade duration distributions
- Frequency scaling models
- Diversity models
- Multiple site analysis
- mitigation schemes for propagation anomalies
- Wet antenna effect model
- Rain climate region map revision
- Contribution to regulatory organizations

ITU-R Rain Zones & Rainfall Rate Exceeded (mm/h)

% of Time	C	D	E	K	M	N
1.0	0.7	2.1	0.6	1.5	4	5
0.1	5	8	6	12	22	35

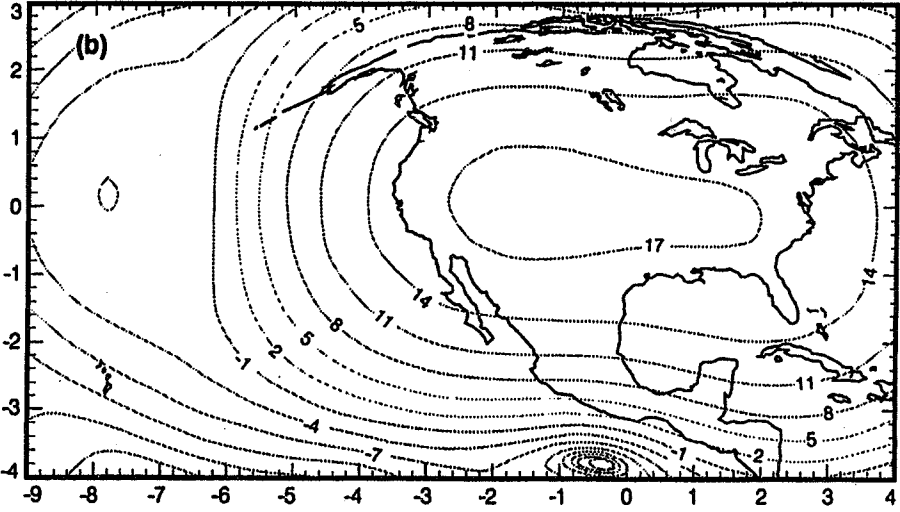


20 GHz
max EIRP 22 dBW



7

27 GHz
max EIRP 19 dBW



Page intentionally left blank

ACTS PROPAGATION EXPERIMENT

Preprocessing Software User's Manual

Robert K. Crane and Xuhe Wang
University of Oklahoma
School of Meteorology
Norman, OK 73019

David Westenhaver
Westenhaver Wizard Works, Inc.
746 Lioness Ct. S.W.
Stone Mountain, GA 30087-2855

January, 1996

Table of Contents	Page
Overview for Experimenters	3
1 Introduction	5
2 Radiometer System Calibration	8
2.1 Background	8
2.2 Calibration procedure	9
3 Attenuation Relative to Clear Sky	17
4 Empirical Distribution Functions	18
5 Preprocessing Program Execution	22
5.1 Overview	22
5.2 Actspp input options	23
5.3 Actspp files and directories	25
5.4 Actspp data calculation and calibration	26
5.5 Sky temperature estimation	27
6 Macro Library for use with Actspp	29
6.1 Introduction	29
6.2 Installation and running the macro	31

Overview for Experimenters

This manual includes by reference the earlier Radiometer Calibration Report of November, 1994, the Preprocessing Software Version 4 report of February 1995 and the README.TXT files provided with the software revisions made available since February 1995. The major changes to the preprocessing software since version 4 were 1) to make the preprocessing software more robust, 2) to make the preprocessing operation user friendly by including all the information required for radiometer system calibration in log files that are read whenever a day is processed or reprocessed, 3) to include a procedure for marking "bad" data, 4) to include modifications to the preprocessing software output (the .pv2 file to replace the .pv1 file - the .xxx notation is to identify the file type extensions used by the DOS operating system on an IBM compatible personal computer) that enables a user to recover the raw data (.rv0 data) from the output file (.pv2 file), and 5) to provide the minimum required output data for the experiment in the output files (.pv2, .edf, .log, .srf, .rtn, and .dfc files). The histogram output (.edf file) contains the monthly histograms of attenuation, rain rate, fade duration and inter-fade interval that comprise the required output for each month for the ACTS Propagation Experiment. In addition, version 66 of the ACTS Preprocessing Program (Actspp) generates histograms of total attenuation averaged over a minute (i.e. attenuation relative to free space), attenuation relative to the clear sky averaged over a minute, sky temperature averaged over one minute and the standard deviations of attenuation calculated for one minute.

The contract between NASA Lewis and the experimenters specifies that the minimum output required from each experimenter includes the monthly and annual distributions of total attenuation at the 20 and 27 GHz frequencies employed in this experiment and the monthly and annual distributions of one minute averaged rain rate. This output is to be provided in two different formats, the digital data files to be archived at the University of Texas (the .pv2, .edf, .log, .srf, .rtn, .dfc, and .edf files), and a report containing plots and tables of the monthly and annual empirical distribution functions for attenuation and rain rate. To assist experimenters, the University of Oklahoma (OU) has provided Microsoft Excel 5 macros that compile the required empirical distribution functions (edf's - cumulative distributions of the observations) plots and tables from the .edf files. The macros are available via ftp from Dave Westenhaver's ftp server: anonymous@ftp.crl.com. Section 6 in this user's manual describes their use.

The ACTS propagation terminal provides simultaneous beacon receiver and radiometer output data at the two beacon frequencies, 20.185 and 27.5 GHz. These data are combined in the preprocessing program to provide estimates of the total path attenuation relative to free space between ACTS and the propagation terminal. The beacon histogram output (.edf file) and the beacon attenuation time series (.pv2 files) are obtained from the combined beacon plus radiometer observations. The radiometer data are used to establish the reference power level for the calculation of beacon attenuation; the beacon data are used to determine the change in power level from the reference value and effectively extend the dynamic range of the radiometer observations. Output for the combined beacon plus radiometer observations (labeled beacon) are provided to satisfy the requirement to produce total path attenuation measurements. The radiometer data are output separately (labeled radiometer) only for use in verifying radiometer system calibration.

The preprocessing program provides daily summaries of the significant observations on a minute-by-minute basis (one-minute averages and standard deviations). This output is the daily .sum file. This output is for use by the experimenter and is not archived at the University of Texas (UT). For the beacon (plus radiometer) attenuation data, the standard

deviation of the beacon signal levels (in dB), the maximum value in a minute, and the minimum value in a minute are also provided. These outputs can be used to separate scintillation effects from the more slowly varying processes that contribute to attenuation. The radiometer derived attenuation values are also reported as minute averages and standard deviations within a minute. The latter can be used to identify periods with rain and/or clouds.

The attenuation relative to clear-sky conditions (total attenuation minus gaseous absorption) cannot be obtained from the beacon and radiometer observations alone. To assist the experimenter, the sum files contain gaseous absorption estimates derived from surface meteorological data. These estimates are accurate to within 0.2 dB if the surface measurements are correct. The surface data input files (.srf) are used to provide surface data to the preprocessing program when the performance of the sensors provided with the propagation terminal is in doubt. Correct surface data are also needed to generate attenuation estimates from the radiometer observations because the preprocessing program uses the surface data to estimate the medium temperature required for the calculation of attenuation. Finally, the gaseous absorption estimates are used in radiometer system calibration because the radiometer derived attenuation values are required to match statistically the gaseous absorption estimates when the sky is clear. To assist the experimenter in verifying the radiometer calibration, the average difference between the gaseous absorption estimate and the radiometer attenuation estimate is output in the .log file for clear-sky conditions.

1 Introduction

The preprocessing software (Actspp) reads the YYMMDDxx.RV0 files (or .rv0 files) where YY is year, MM is month, DD is day and xx is site identifier) generated by the ACTS propagation terminals; performs radiometer calibrations, beacon reference level predictions, and beacon tone modulation corrections as needed to provide valid attenuation estimates at both beacon frequencies; tabulates attenuation histograms for further analysis; prepares one-minute averages or second-by-second output for further spreadsheet analysis; and generates YYMMDDxx.PV2 (or .pv2) files for archival and further analysis. The program was originally developed to observe and diagnose ACTS propagation terminal receiver problems but has been quite useful for automating the preprocessing functions needed to convert the terminal output to useful attenuation estimates. As provided, the preprocessing software will generate .pv2 files automatically. Prior to having data acceptable for archival, the individual receiver systems must be calibrated and the power level shifts caused by ranging tone modulation must be removed.

Actspp provides three output files, the daylog (\DayLog xx\YYMMxx.LOG or .log), the diurnal coefficient file (YYMMxx.DFC or .dfc) and the CALFILE.xxn file that contains calibrate information. All but the CALFILE.xxn file must be archived with the .pv2 files. The auxiliary files, the YYMMxx.SRF (or .srf) file containing corrected surface meteorological data if needed and the YYMMxx.RTN (or .rtn) file containing ranging tone times if different from the standard tone files provided by the University of Oklahoma (OU), must also be archived. They provide sufficient data to verify that the system calibration was performed correctly and to completely recover the input .rv0 data from the archived files. The YYMMxx.EDF files must be archived to comply with the minimum reporting requirements of the experimenter's contracts.

The ranging tones must be removed from the 20 GHz beacon power level data to provide attenuation estimates valid at the low attenuations of interest for VSAT and other low margin communication system designs. The preprocessing software automatically removes most of the ranging tones if the statistical fluctuations in the received signal level are less than about 0.2 dB. During periods with stronger scintillation or rapid fluctuations in rain, the ranging tone detection algorithm may produce false detections and may miss some detections. This problem is critical for sites with observations at low elevation angles such as in Alaska. To circumvent the need for running the ranging tone detection segment of the program, a ranging tone time and level shift file (YYMM.RTN) should be used. OU has prepared these files and they are stored in the RToneTimes subdirectory on Dave Westenhover's ftp server: anonymous@ftp.crl.com. If you have a .rtn file with data for the day you are processing, the system will use the tone start and stop times from the file. It is strongly recommended that you use the prepared ranging tone files.

Actspp automatically marks data as "bad" when the receiver status flags indicate bad data, loss of lock, etc. The experimenter can also mark data as "bad" when some element of a receiver is malfunctioning, or the terminal is not operating correctly, or the antenna is not correctly pointed, or for any other reason. This is done by entering the times (in hours and minutes to begin and end a bad data section in the daylog (.log file). All "bad" data are marked in the .pv2 files. The user defined "bad" periods are also archived in the .log files. Data marked "bad" are considered bad for the entire minute in which a "bad" mark is detected. Data considered bad are not used in the compilation of the histograms or in estimating beacon reference levels.

The preprocessing program prepares an estimate of the undisturbed beacon power level at the receiver for use as a reference for the determination of beacon attenuation. The reference level is obtained from a fourth order harmonic curve fit to the attenuation

corrected beacon power levels from the prior day. The attenuation correction is derived from the radiometer data. An additional diurnal variation correction is required to provide a correction to the fit to the data for the previous day to compensate for day-to-day variations in satellite radiated power. The additional diurnal correction is computed at the end of each hour and applied to predict the correction for the next hour. To provide some smoothing, the coefficients for the additional diurnal corrections are passed through a first order infinite impulse response (IIR) filter with a time constant of about 3 hours. The long time constant is needed to provide valid reference level predictions during periods with rain or times when the rms variation in the radiometer derived attenuation correction exceeds a preset threshold. The preset threshold is site dependent. It varies from 0.1 to 0.5 dB. The constants for the fourth order correction are stored in the daylog (.log file); the constants for the hourly corrections are stored in YYMMxx.DFC (.dfc files). If the program is run a second time, the fourth order curve fit to the current day is used instead of the fit for the prior day unless the program is directed to use only the curve fit for the prior day.

Data with slow variations in signal level with radiometer attenuation corrections of less than 4 dB that also pass a rms variation test and are not marked as "bad" are included in the fourth order fit. If strong unmodeled attenuation events such as due to wet snow on the antenna are present or if bad attenuation adjusted beacon level estimates occur due to radiometer instability or ranging tone detection errors, the reference level for the next day will be in error. In this case run the program for the next day twice. If the data for the current day are in error, force the use of the curve fits for the prior day.

If no reference level predictions are available, the program assumes a constant reference level and computes the hourly diurnal adjustments relative to that constant level. The constant reference level is the received power level in the first second of valid observations. Note that the observations used to compute the fourth order harmonic fit for a day are not contaminated by the fit obtained from the prior day or the diurnal correction to that fit.

The beacon power reference level is obtained from a least squares fit of the diurnal variation model to the recorded beacon power levels after a correction for path attenuation using the attenuation value estimates obtained from the radiometer. This process is equivalent to performing a least squares fit of the beacon attenuation data to the radiometer attenuation data for attenuation values less than about 2 dB. The beacon observations are employed to obtain the signal level change from the reference level established using the radiometer data. The beacon observations extend the dynamic range of the radiometer measurements. The resulting attenuation estimates are for the total attenuation relative to "free space" or propagation in the absence of an atmosphere. The total attenuation is caused by gaseous absorption, extinction by clouds and rain, or by condensed water or wet snow on the antenna surface. In studies of attenuation by rain, only the rain component of the total attenuation is of interest. It is up to each experimenter to ascribe a physical cause to each attenuation event. The histograms produced by the program are for total attenuation not for attenuation due to rain. In Actspp version 66 and later, histograms of one-minute average estimates of attenuation relative to clear-sky conditions are also generated.

The reference level determination procedure produces a maximum reference level estimation error of less than 0.5 dB during an eclipse period at the satellite. The typical reference level estimation error is less than 0.1 dB. Comparisons between radiometer and beacon (plus radiometer) edf's show less than a 0.1 dB difference over a 0 to 2 dB attenuation value range. The main source of error in the estimation of attenuation is the approximately 0.2 dB day-to-day uncertainty in radiometer system calibration stability.

A valid estimate of total attenuation requires a well calibrated radiometer system. Periodic receiver calibrations are performed by the radiometer system to maintain

radiometer calibration but independent system calibrations must be made by each experimenter throughout the entire measurement series. The preprocessing software provides the information necessary to perform a system calibration. An assumption in the design of the preprocessing system is that the surface meteorological measurements, pressure, temperature and relative humidity, are correct. If they are in error, data must be manually entered into the system via the YYMMxx.SRF file (or .srf file). Hourly averages of the three surface variables are needed.

2 Radiometer System Calibration

2.1 Background

The entire radiometer system must be calibrated and the possibility of a change in calibration constants must be monitored over the duration of the experiment. Two types of calibration are performed, a periodic receiver calibration and an aperiodic system calibration. The preprocessing program does the periodic receiver calibration every 15 minutes. Each experimenter must do an independent, aperiodic radiometer system calibration (once per month say) and whenever the receiver rf box is opened or moved. A theoretical description of the radiometer system calibration process was provided in the Radiometer Calibration Report (see also Sections 5.4 and 5.5). Recent changes to Actsp (version 66) make it easy to monitor the adequacy of the calibration constants over periods of a month or more for use in determining when a recalibration is required.

The radiometer system is of total power design and the components in the receiver system may drift in time (i.e. variable amplifier gains, offset voltages, transmission line matches) with a result that the output voltage from the square law power detector is not simply related to the power input to the low noise amplifier (LNA) connected to the antenna. To track and compensate for any possible component variations, standard, known power level signals are introduced into the LNA. They are periodically obtained from the reference load and the noise diode connected to the reference load by switching the LNA from the antenna to the reference diode and turning on then off the noise diode. Under ideal conditions, the noise diode always adds a known amount of power to the power from the thermal noise of the reference load. If, in addition, the match (fraction of power transferred from the reference load to the LNA) between the reference load and the LNA (through a coaxial line switch) is identical to the match between the antenna and the LNA, the response of the square law detector to power received by the LNA can be monitored. Using the automatic periodic calibrations and the two known power levels (the reference load and reference load plus noise diode noise power), the assumed linear relationship between input power and output voltage for each radiometer channel can be measured, monitored and maintained.

For a perfect receiver system with a known input power to output voltage relationship, the response of the system to a known power flux density incident on the antenna is still not known. A second (aperiodic) system calibration must be made to establish this relationship. Unfortunately we do not have a known signal to input to the antenna. The ACTS propagation terminals were supplied with hot and cold loads to supply known signals but these loads do not establish the fraction of the power received from the main lobe of the antenna pattern or the fraction of power received in the "spill-over" side lobes of the antenna pattern. They also do not maintain the same match to the receiver system as the antenna when not covered by the load. Use of the hot and cold load calibration procedure is not recommended. The noise diode calibration system has better stability.

The only signals available for overall system calibration are from the atmosphere and from the satellite. If the signal input from the satellite is constant in time (or changes in time as predicted by the beacon reference level), then attenuation events will change the satellite signal level and simultaneously produce changes in the input power to the radiometer from thermal emission from the atmospheric gases, clouds, or rain producing the attenuation. The attenuation observed using the beacon signals should match statistically the attenuation estimated from the change in sky brightness temperature observed by the radiometer. The beacon signal level change is measured precisely. The match between the beacon signal level change and the observed change in the attenuation estimate obtained from the radiometer may be used to calibrate the radiometer system.

Two calibration constants are required, one that estimates the fraction of the power received from the antenna main lobe and the second that estimates the fraction of the power received from the antenna side lobes. The latter is not easily found from the former because of the possible differences in the matches between the LNA and the antenna and the LNA and the reference load. Two independent calibration signals are necessary to determine the calibration constants. One signal is obtained from the change in power level (or attenuation) recorded for the beacon signal. For a second calibration signal we use the thermal emission from the atmosphere during periods without rain and clouds.

Ideally, we could tilt the antenna in elevation and measure the attenuation produced by a horizontally stratified cloud-free atmosphere to determine the value for thermal emission. For the ACTS propagation terminal this is not possible due to high antenna side lobe levels. The thermal emission can only be calculated theoretically using radiative transfer theory and a measured vertical profile of temperature, pressure, and humidity. In the absence of calculations using sounding data, the clear-sky thermal emission (sky temperature) and attenuation values can be estimated statistically from the surface observations alone. The coefficients for a linear statistical relationship between attenuation and surface temperature and water vapor density were obtained from a regression analysis on the full numerical calculations using a number of measured vertical profiles. The calculations were made at both observing frequencies using 108 soundings from the National Weather Service facility in Norman, Oklahoma. This relationship, adjusted for the elevation angle to the satellite and for the height of the ACTS propagation terminal above mean sea level (i.e. surface pressure), is used to generate the estimated absorption values output in columns BD and BE in the .sum file spreadsheet.

A statistical regression analysis was also made to relate medium temperature to the surface meteorological conditions. This relationship is used in the estimation of attenuation from the sky temperature values observed by the radiometer. The one-minute averaged sky temperature values are also output in the .sum file and histograms of sky temperature values are output to the .edf file (Actspp version 66 and later).

If all the system components were perfectly matched, the two calibration constants needed would be the antenna efficiency (fraction of power in the main lobe) and the spill-over power received via the side lobes. The latter would change from one day to the next as the atmospheric parameters and surface temperature and emissivity change. The spill-over power is characterized by a temperature (K) that must be obtained empirically. The spill-over contribution is also expected to change in proportion to changes in absolute outside air temperature (K).

Note that because the critical matches between system components are unknown, the antenna efficiency and spill-over temperature values that result from the radiometer system calibration are strictly empirical. They are intended for use with the reference level and noise diode power values for radiometer calibration. They are effective values that will not match values calculated for the antenna alone.

2.2 Calibration procedure

The calibration of the radiometer system is iterative. Initially, the software is supplied with the calibration constants used for November 1993 at the Oklahoma site. In Oklahoma the calibration "constants" have changed slowly in time due to noise diode malfunction (drift) and abruptly on occasion when we have disturbed the rf box. Anytime the rf box is moved relative to the antenna surface or removed for servicing or adjustment, the antenna efficiency will be changed unless the box is replaced in exactly the same location relative to

the antenna surface. In practice exact replacement is not possible and a shift in the calibration constants must be assumed.

Calibration must be done over a long enough period of time to sample several cloud-free intervals of long duration and several intervals with rain. Because the underlying calibration procedure is statistical the larger the sample for calibration, the better.

The procedure used to determine the beacon reference power levels for the calculation of attenuation forces a statistical best match between the radiometer and beacon attenuation values at radiometer derived attenuation levels below about 2 dB. Any scattergram of simultaneous observations of attenuation derived from the beacon and radiometer receivers will show agreement within about 0.2 dB between the two estimates of attenuation for attenuation values less than 2 dB (unless an undetected or falsely detected ranging tone is present). Figures 1 and 2 present results for October 18, 1994 obtained in Oklahoma. For both frequencies, the expected agreement is evident. This agreement should be observed even if the radiometer system is not calibrated correctly. It is forced by the preprocessing program.

Figures 1 and 2 show a progressively increasing difference between the attenuation values reported for the beacon and radiometer receivers. The beacon data show the correct change in attenuation from the values around 1 dB (forced by making the radiometer and beacon data agree). The radiometer observations are about 0.5 dB too low at a 5 dB attenuation at 20 GHz and about 0.3 dB too high at 5 dB at 27 GHz. The radiometer observations can be aligned more closely with the beacon receiver attenuation change observations by changing the two calibration constants for each frequency. Exact alignment is not necessary because the radiometer is used to set the reference level (~1dB) for the beacon measurements and the beacon receiver then measures precisely the change from that level. Exact alignment is not possible because the relationship between the radiometer observations of sky temperature and the calculated estimates of attenuation is not exact but depends upon the location of the rain or clouds causing the attenuation relative to the receiving antenna, the physical temperature of the rain or cloud causing the attenuation, the microphysical properties of the rain or clouds (size, shape, orientation, etc.), the distribution of other attenuators along the path, and, for periods with intense rain, the uncertainty in the medium temperature value to be used in the estimation of attenuation because a significant fraction of the power lost by attenuation is redirected due to scattering and the full radiative transfer equation with multiple scattering must be used to determine the correct value for medium temperature. The relationship between attenuation and sky temperature is expected to change within a storm and from storm to storm. A statistical best fit relationship should be used that provides a good match over a number of storms with light to moderate rain intensity. A better fit will not change the beacon (plus radiometer) attenuation distribution that is the required output from this experiment.

The critical test for radiometer calibration is the match between the estimated attenuation due to gaseous absorption and the radiometer attenuation values reported for clear-sky conditions when the only attenuation to be observed is due to gaseous absorption. To perform this part of the calibration, periods without clouds or rain must be identified. This can be done by finding the days within a month having the minimum attenuation observations. The .edf file histograms list the number of seconds (and for Actspp 66, the number of minutes) in the day an attenuation level is observed. Days with a significant number of relatively small attenuation observations should be used for this phase of the calibration process. Locate times without clouds or rain by plotting the radiometer estimated attenuation values vs. the gaseous absorption values (see Figures 3 and 4) and observing the lowest values for the radiometer. If the system is well calibrated, they should be within 0.2 dB of the gaseous

absorption estimates (the 1:1 line on the plots). For Figure 3, good agreement is evident but in Figure 4 a disagreement of about 0.4 dB is evident. This comparison should be made for a number of days within a month. Calibration is achieved when agreement within 0.2 dB is obtained most of the time or when the number of days with a positive difference is equal to the number of days with a negative difference.

The calibration procedure is iterative. A change in effective antenna efficiency to make a better match between the radiometer and beacon observations will affect the radiometer estimate of attenuation during clear-sky conditions. A change in spill-over temperature will in turn affect the comparison of beacon vs. radiometer attenuation values. In practice it is more important to get a good match between the estimated gaseous absorption values and the radiometer values for periods with low attenuation (no clouds). The final adjustments to get a good match can be made using spill-over temperature alone because, in the end, the match between beacon and radiometer attenuation values is not important at attenuations above about 3 dB. Below 3 dB, the radiometer attenuation corrections to beacon received power used in determining the beacon reference power become important and the better the match, the better the reference level determination.

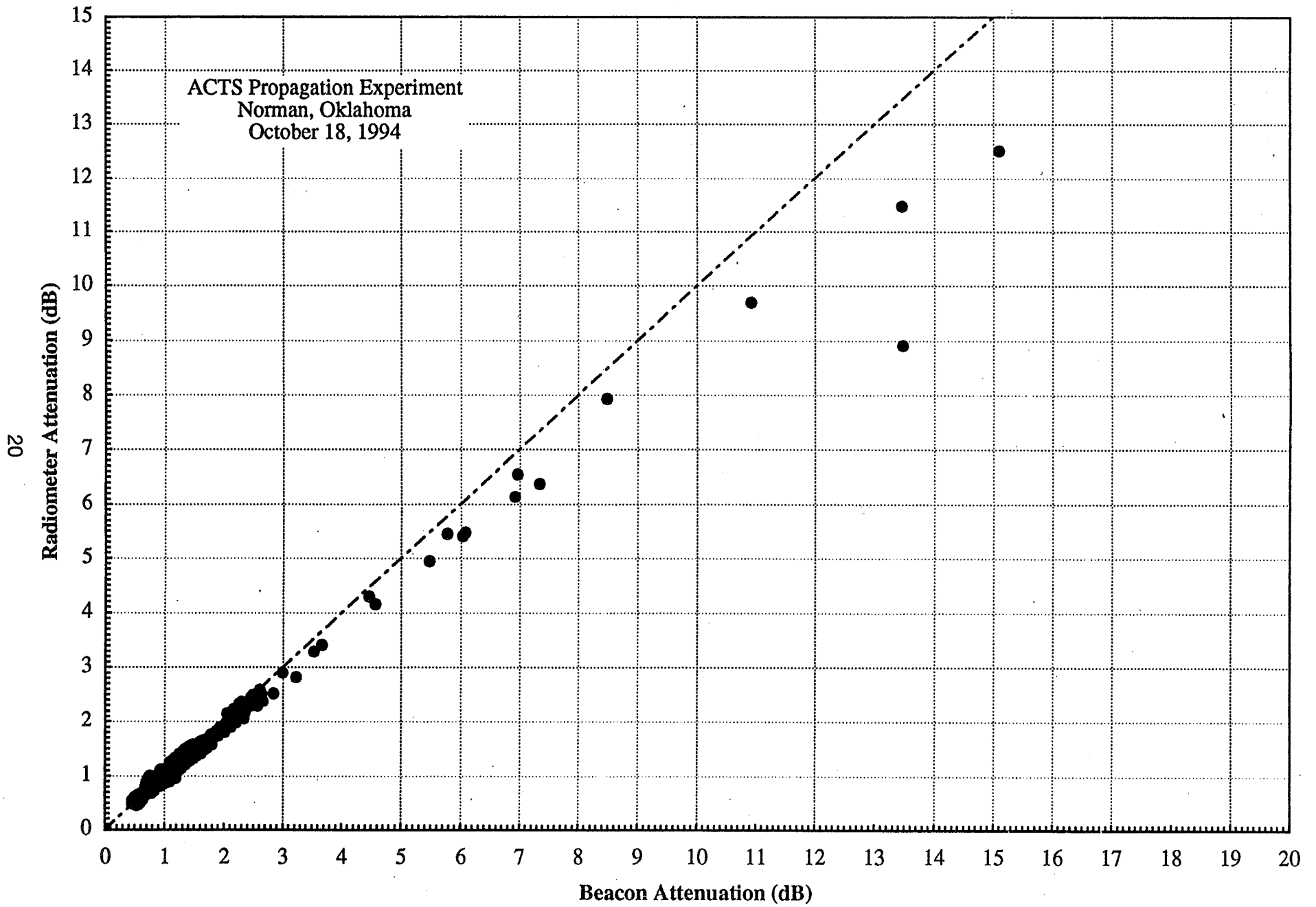
The differences between radiometer and beacon observations evident above 2 dB in Figures 1 and 2 will not affect the performance of the beacon (plus radiometer) estimates of attenuation. A look at the entire month of October shows some days with the radiometer attenuation estimates above the 1:1 line and other days with the radiometer estimates below the line. Such variations are to be expected as the locations of the attenuating regions relative to the antenna, the relative effects of multiple scattering, and the microphysics of the rain process change from day to day.

Any error made in the determination of the clear-sky radiometer attenuation values produces an error of the same magnitude in the attenuation distribution output at all attenuation levels.

Version 66 of Actsp provides daily estimates of the average difference between the gaseous absorption estimates and the radiometer derived attenuation estimates for clear-sky conditions. These data are also listed in the revised .log file output. An easy way to verify system calibration is to plot the daily differences. They should be small except for days with no cloud-free times.

A macro to automatically produce an output from a daily .sum file for calibration checking has been generated by OU and is included in macro set ACTS03.XLS available from Dave Westenhaver's ftp server: anonymous@ftp.crl.com. A sample output is shown in Figure 5 for a well calibrated system.

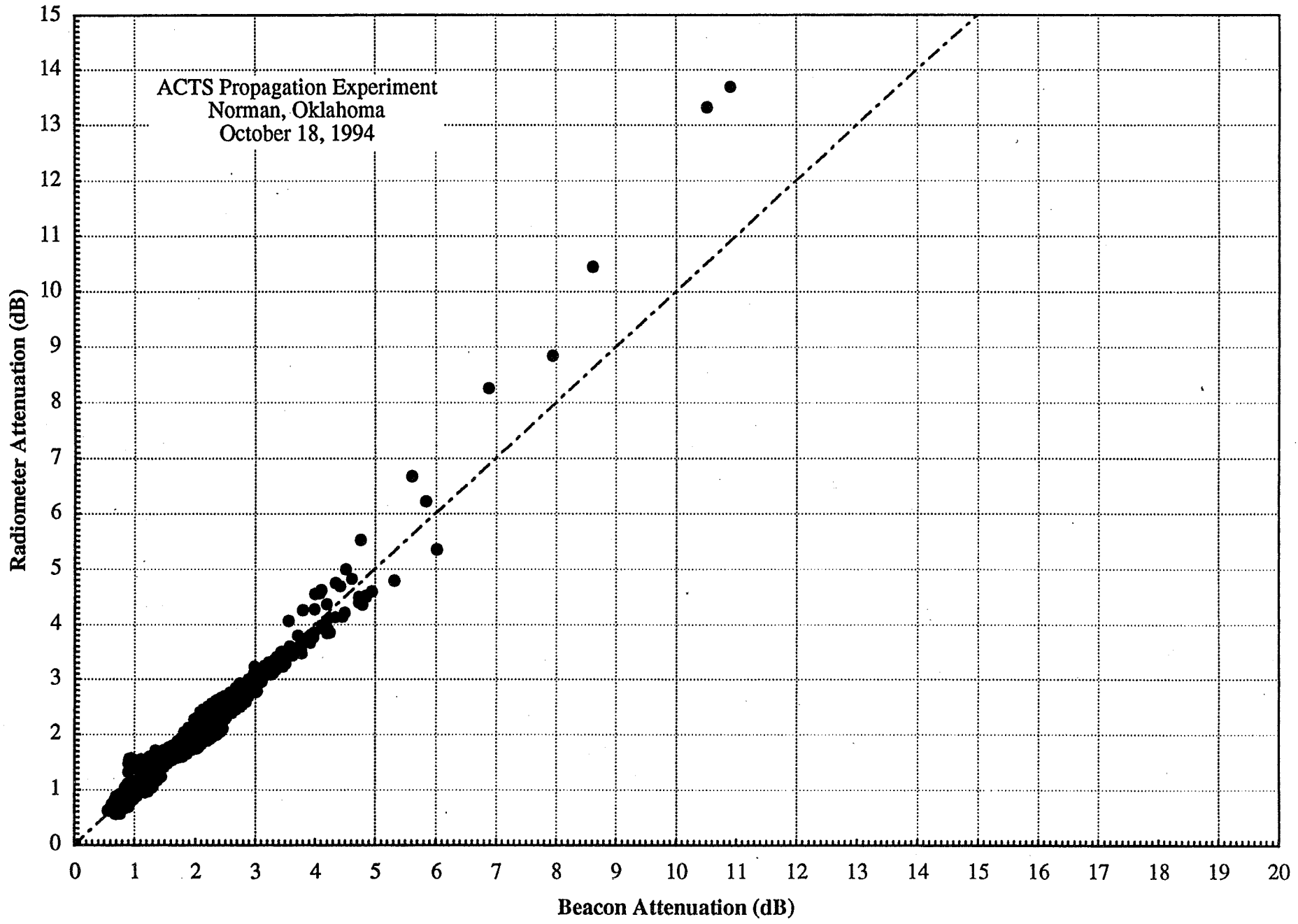
● 20 GHz ----- 1:1



● 27 GHz - - - - - 1:1

ACTS Propagation Experiment
Norman, Oklahoma
October 18, 1994

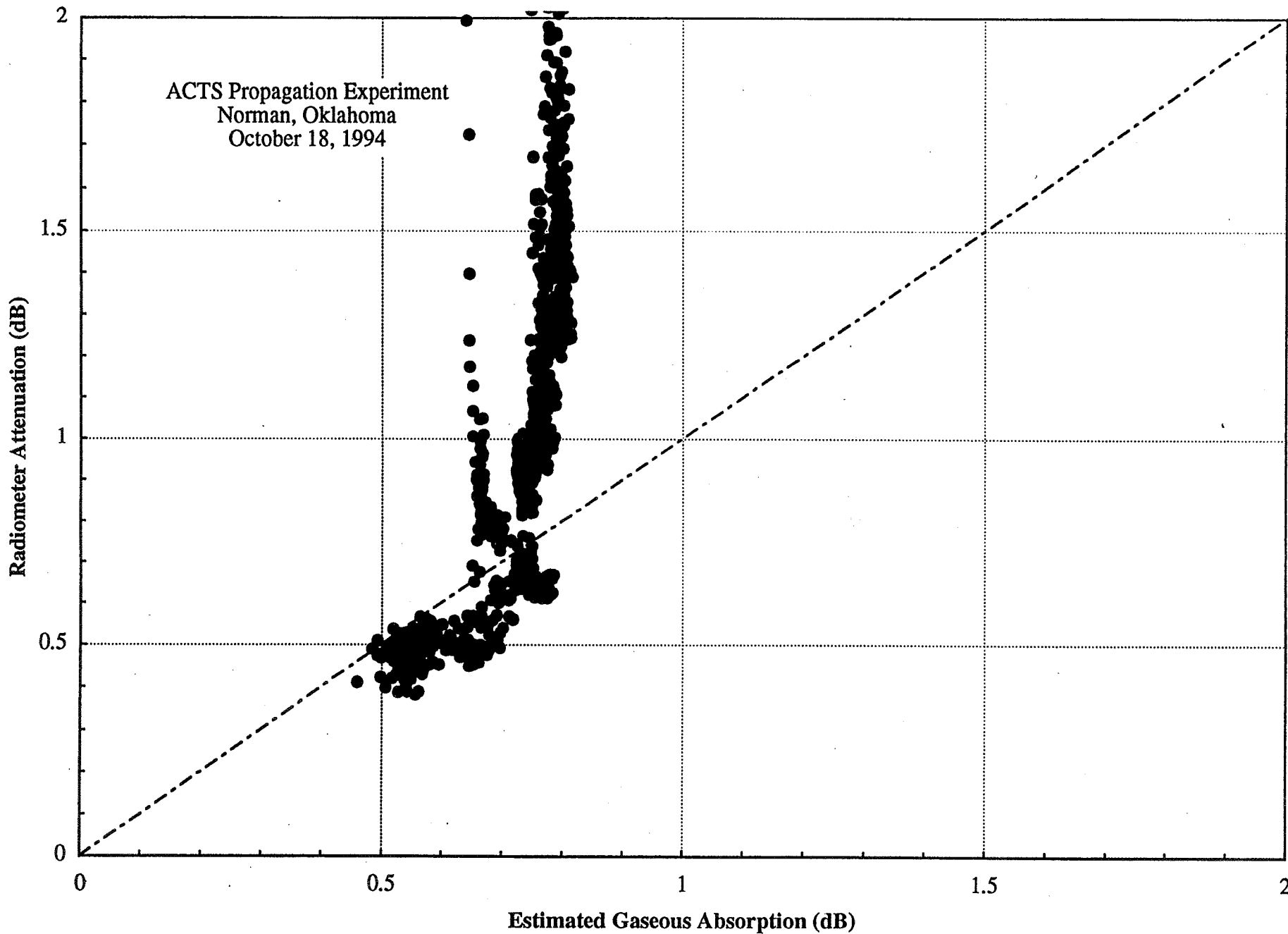
21

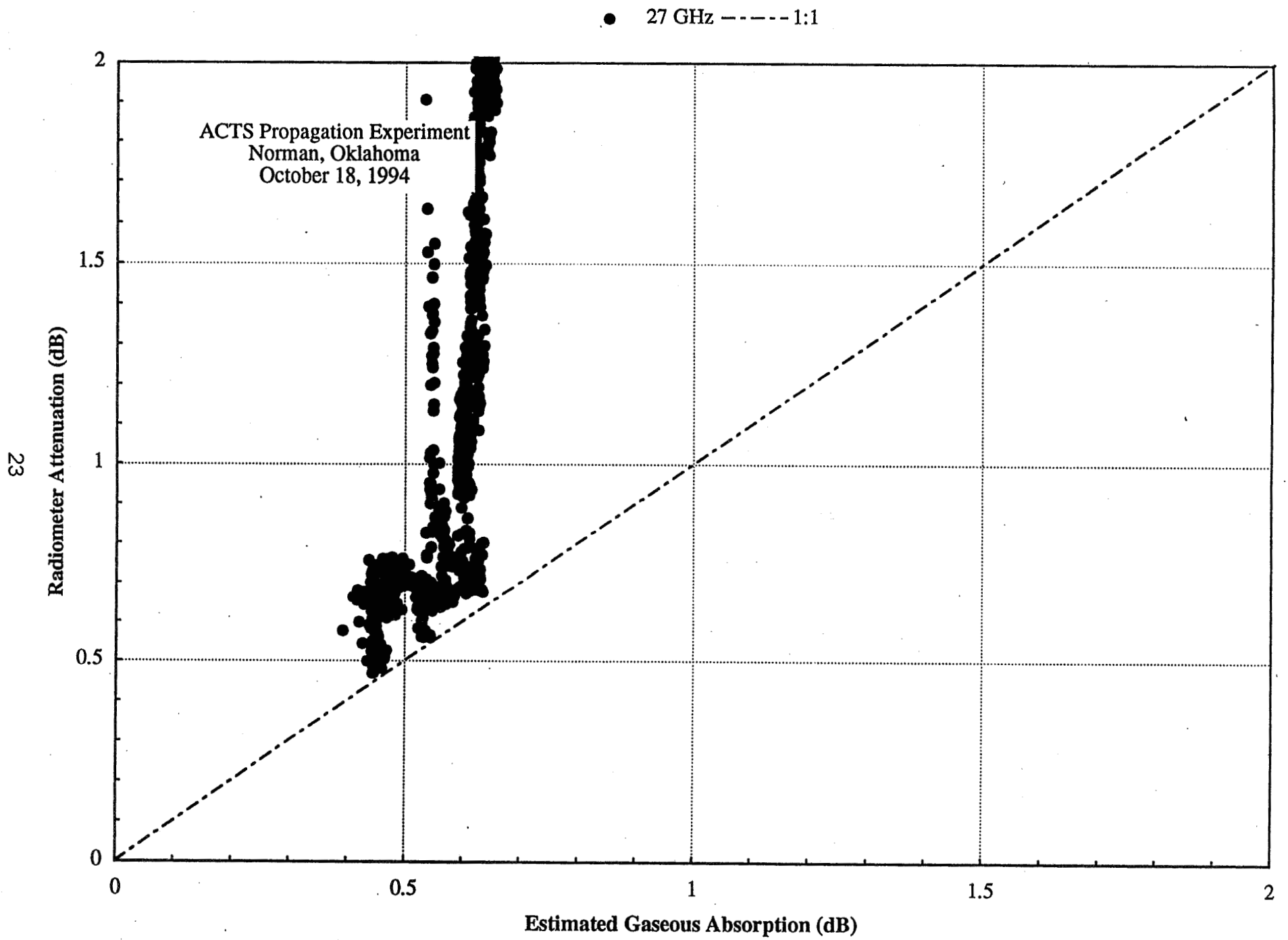


● 20 GHz - - - - - 1:1

ACTS Propagation Experiment
Norman, Oklahoma
October 18, 1994

22

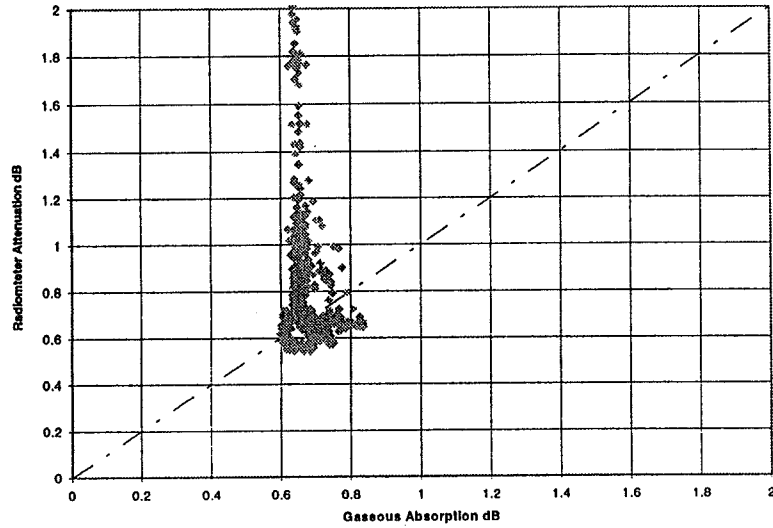




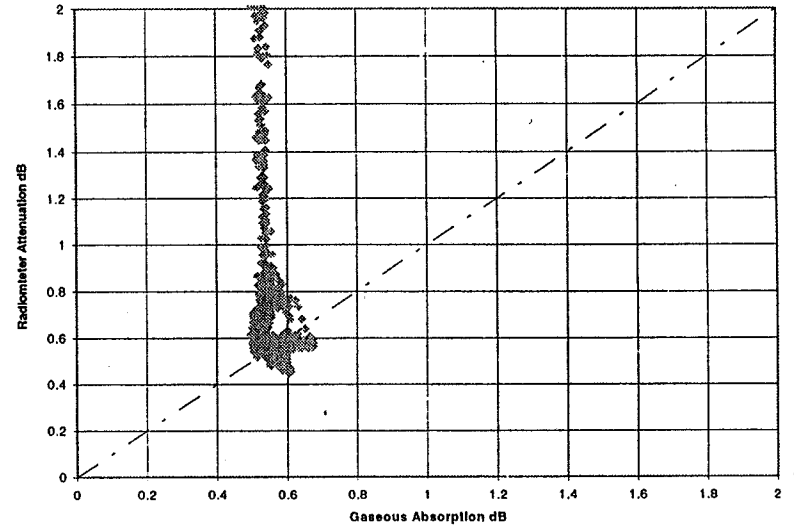
940425OK Calibration Checking

24

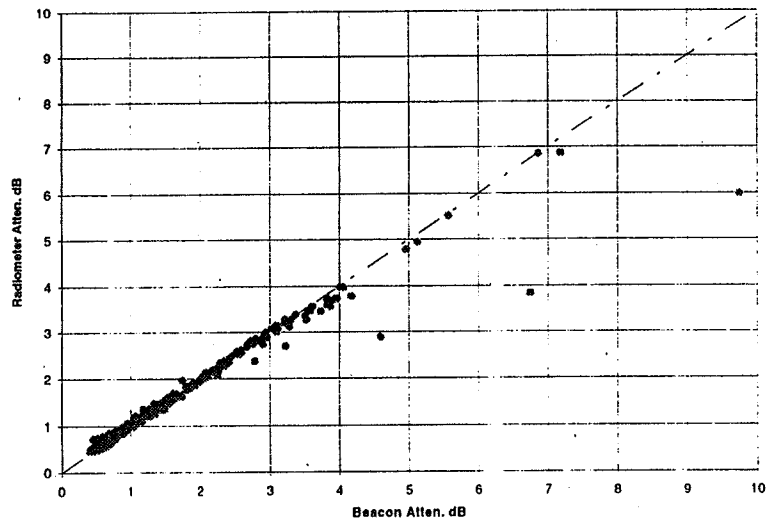
20G Radiometer Atten vs Estimated Gaseous Absorption



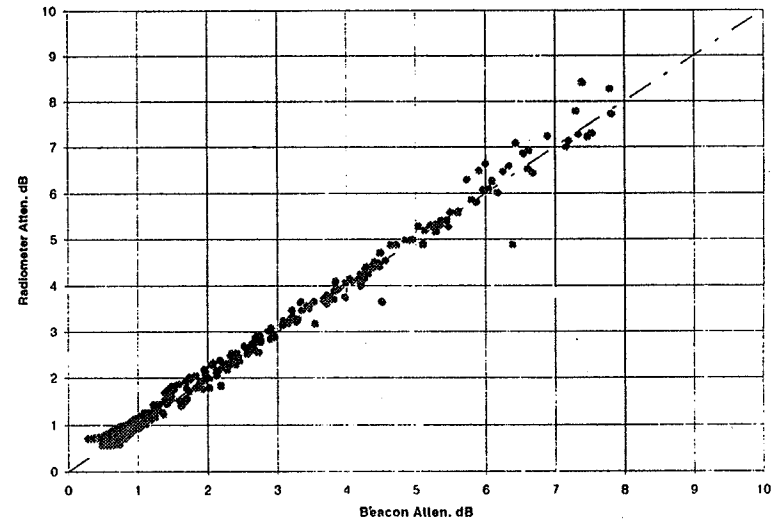
27G Radiometer Atten vs Estimated Gaseous Absorption



20G Radiomtr vs 20G Beacon Atten.



27G Radiomtr vs Beacon Atten.



3 Attenuation Relative to Clear Sky

The preprocessing program provides measurements of attenuation and estimates of gaseous absorption. The difference between these two outputs is the attenuation relative to clear-sky conditions. Distributions of attenuation relative to clear sky are compiled using the one-minute average data and output in the .edf files generated by Actspp version 66 (and higher). These outputs also have had any scintillation effects removed by averaging over a minute.

Time series of the one-minute average total attenuation values and the gaseous absorption estimates are listed in the .sum files. The time series of attenuation relative to clear-sky conditions may be constructed by subtracting the gaseous absorption estimates from the total attenuation values obtained from the beacon receiver.

4 Empirical Distribution Functions

Actspp automatically generates all the statistical data needed to satisfy the minimum reporting requirements of the experimenter's contracts with NASA. Version 66 has added a number of one-minute average and standard deviation histograms of use to the propagation community. They may be regenerated from the archived .pv2 files if an earlier version of Actspp was used in preparing the .pv2 files. The Actspp version number is recorded in the .pv2 file.

The following histograms are recorded in the .edf files:

One-second average beacon (plus radiometer) total attenuation - the basic attenuation data.

One-second average radiometer total attenuation - for calibration only

One-minute rain rate

One-second average fade durations at 3, 5, 7 and 10 dB thresholds

One-second average inter-fade intervals at 3, 5, 7 and 10 dB thresholds

Versions 66 and later

One-minute average beacon (plus radiometer) total attenuation - the basic attenuation data.

One-minute average radiometer total attenuation - for calibration only

One-minute average beacon (plus radiometer) attenuation relative to clear sky

One-minute sky temperature

One-minute standard deviation of beacon received power

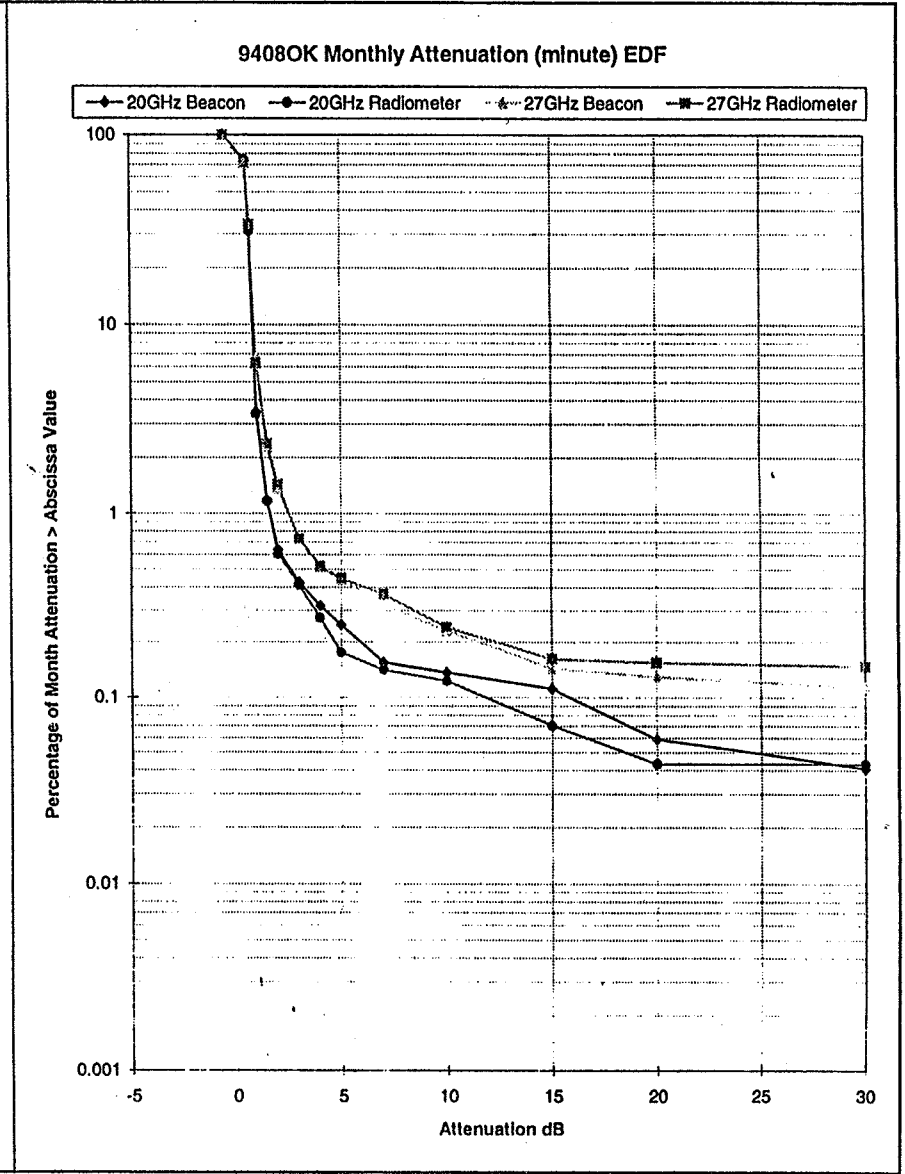
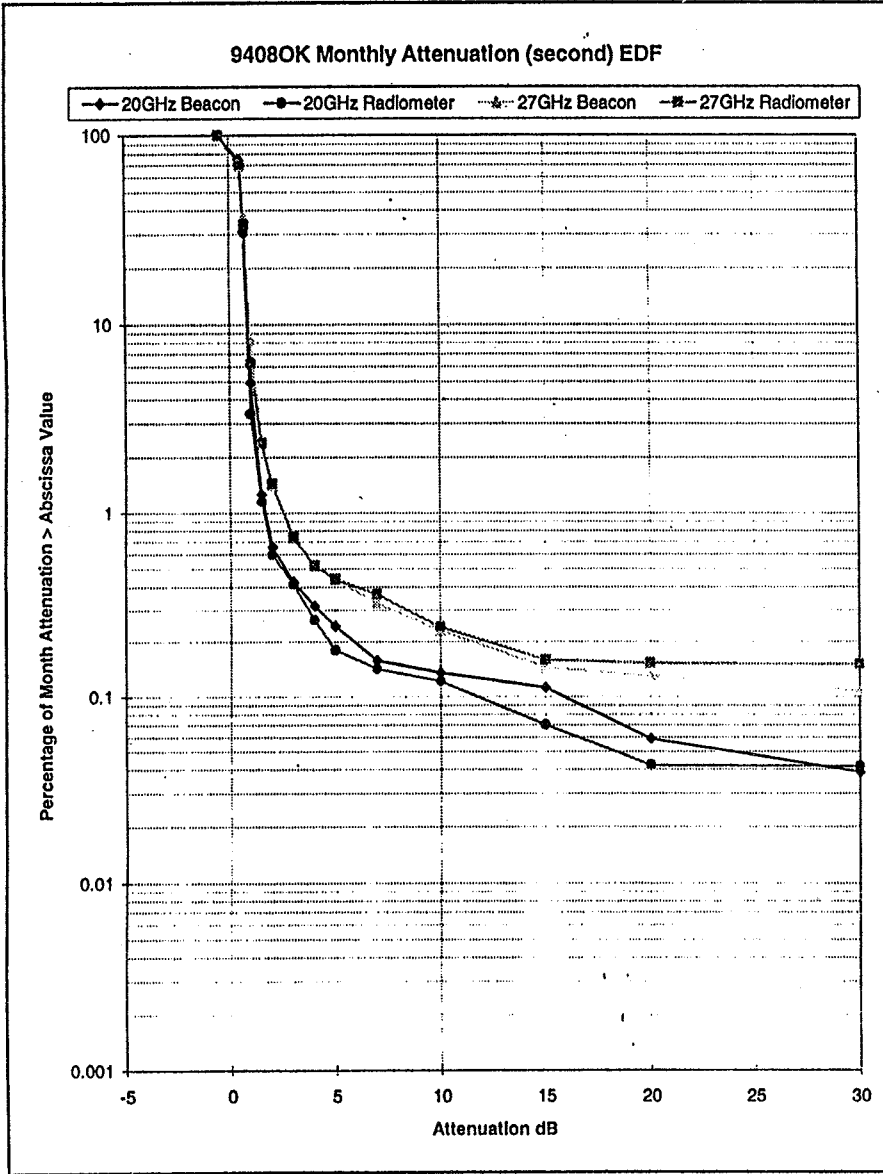
One-minute standard deviation of radiometer attenuation.

The histogram data are in logarithmically spaced attenuation, fade duration, inter-fade interval and standard deviation bin widths. The sky temperature data are reported in linearly spaced bin widths. The data may be readily summed and converted into cumulative distributions of the measurements - empirical distribution functions (edf's). OU has developed a set of macros to do automatically the summations and generate the edf's. They also produce standardized cumulative distribution plots. These plots are sufficient for the final report to NASA.

Sample plots for the required edf's are presented in Figures 6 - 8.

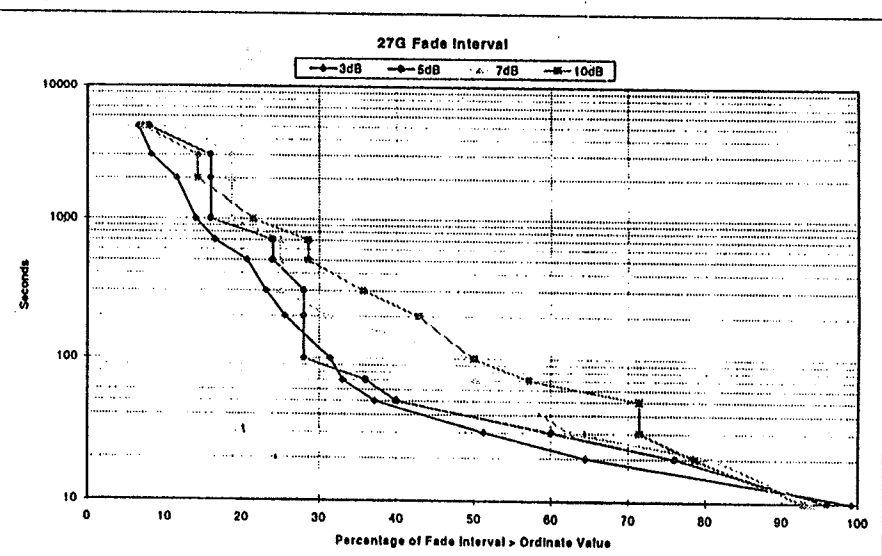
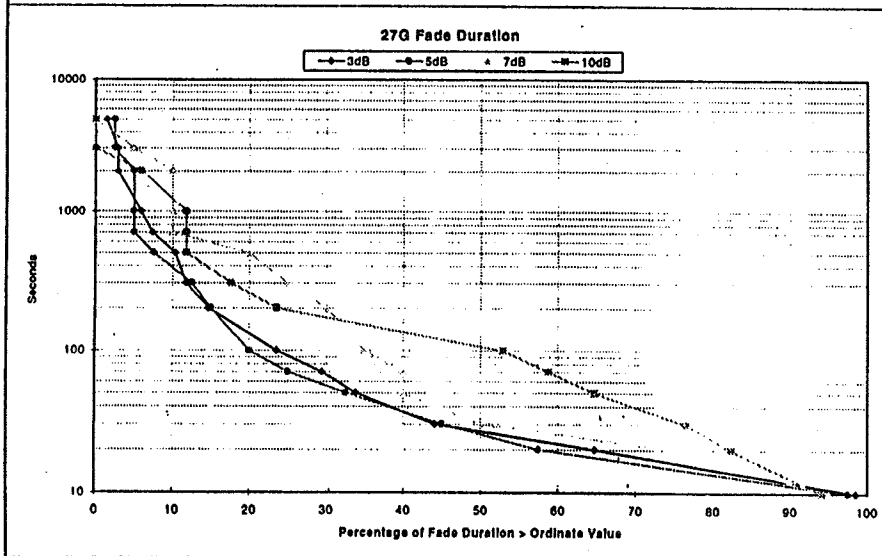
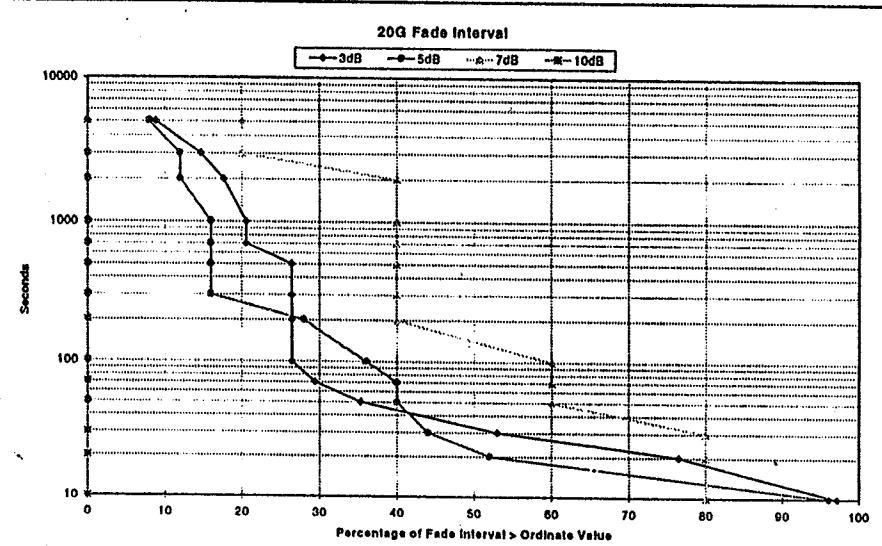
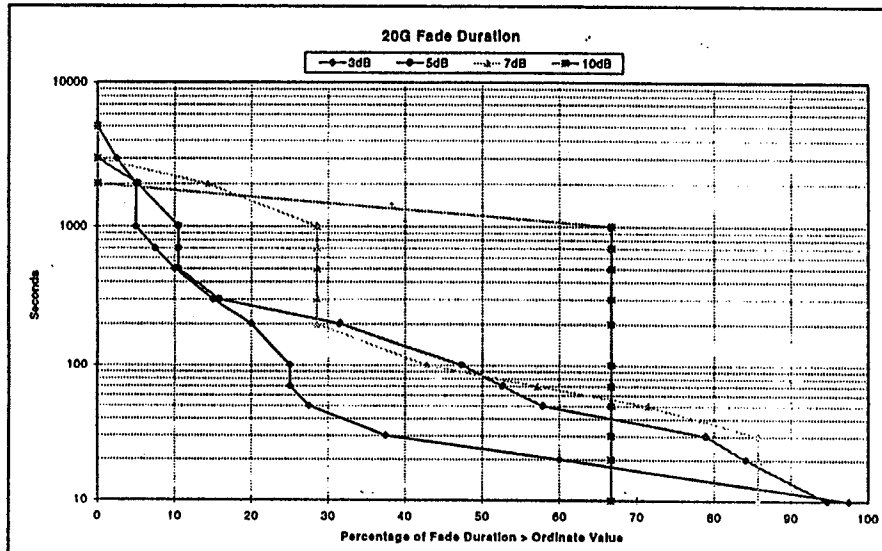
9408OK Monthly Total Attenuation Second and Minute EDFs

27



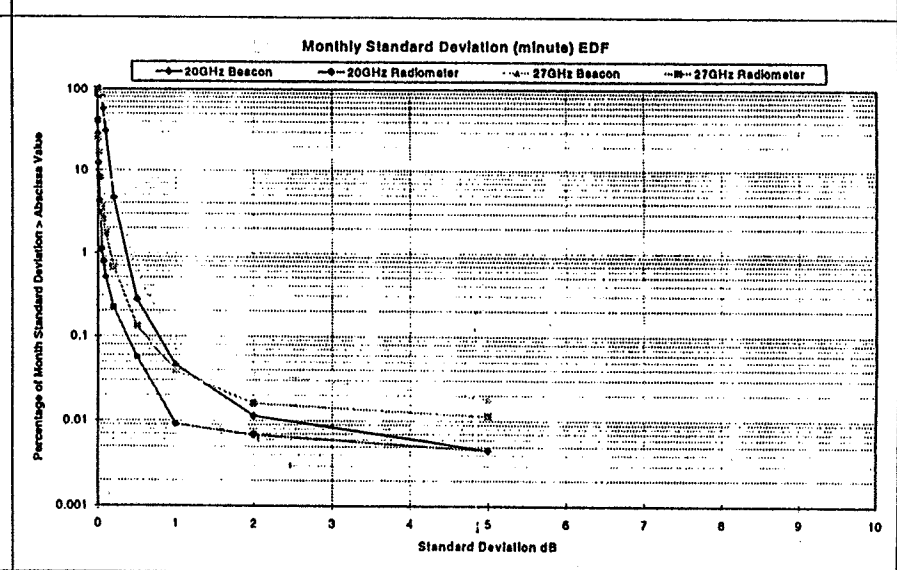
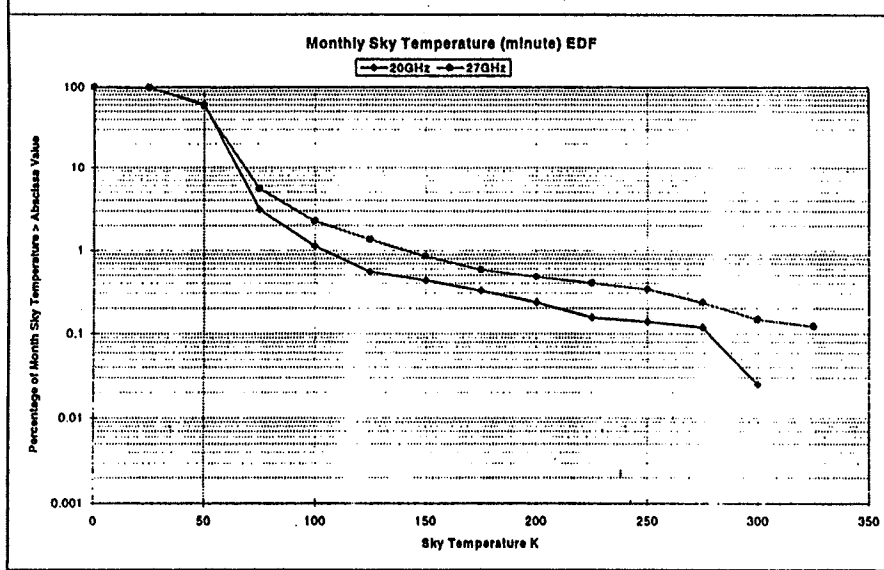
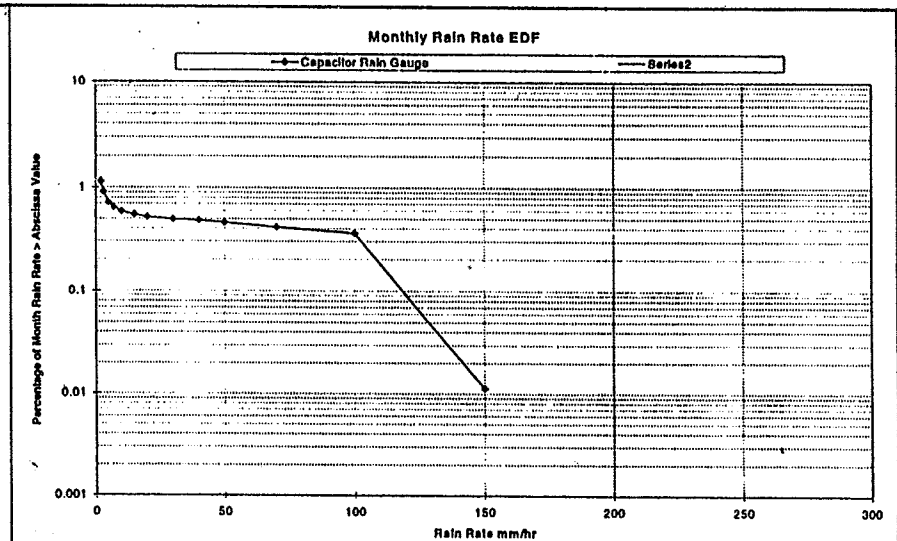
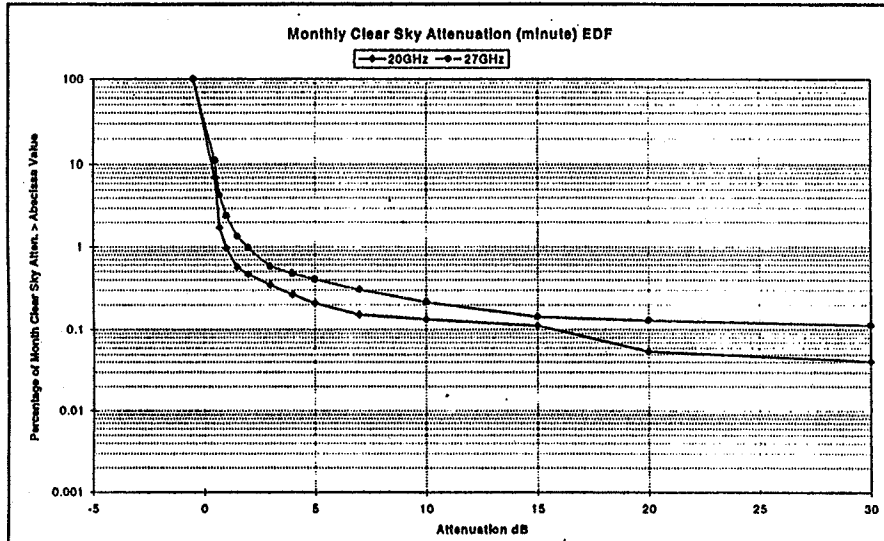
9408OK Fade Duration and Fade Interval EDFs

28



9408OK Monthly Clear Sky Atten., Sky Temp., Rain Rate, Std Deviation EDFs

29



5 Preprocessing Program (Actspp)

5.1 Overview

The information or data processing procedures used within Actspp are described in general terms in this section. At its most basic there is the initial setup, the calculations, and then the summary (conclusions) at the end. The Actspp program is organized with this "top-down" view, but the details are driven from a "bottom-up" view of the information or data. This manual describes some processes of Actspp from the "top-down" view and others from the "bottom-up" point of view. Both are needed to understand how the data is processed and how to use the program and its output files. The goal of Actspp is to remove the site differences and measurements system effects and to distill the one-per-second measurements into more concise measurements of propagation effects.

The lowest unit of information is the one-per-second data record. This 16 byte record contains a time stamp, amplitude and status of the beacon receivers, radiometer voltage readings and two time-multiplexed status words. The time-multiplexed status words have a repeat period of 60 seconds. Thus, it takes a minute of data to obtain a complete, normal set of information. However, the second time-multiplexed status word is used to report two additional asynchronous events when they occur. The highest priority of the two events is the "override" status word that reports specific collection system switch and logical changes. The override status is present several times during each radiometer calibration every 15 minutes. The second priority is the reporting of a tipping bucket rain gauge tip time.

Actspp processes each second of data. The one-minute multiplexed data frames provide the basis for the one-minute data averages. The bias removal (reference level determination) corrections are updated each hour because these corrections change slowly. At the end of the day, summary information is generated. Each day begins with reading the summary information for "yesterday" and "today" and the day ends with writing new summary information for "today". This day "at a time" processing leads to the capability of processing months of data during one session. This process may be extended over many months.

A more detailed description of the processing steps within Actspp begins with an initial setup of the session variables. This is followed by the process of locating the directories and files for the input and output information. Then prior calibration information is retrieved for the day selected from the .log files. Next the auxiliary files are read for surface weather data and ranging tones times. Then the processing begins for the day.

A second of data is read from the input file and decoded into several variables. The radiometer voltages are then converted to sky temperature and the radiometer derived attenuation is calculated. Then the time stamp is checked to determine if there has been a gap in the data. Next the status of this second's information is determined based on the override switch status, beacon receivers status and the beacon levels. This internal status is used to steer the remaining processes. Then Actspp checks for the radiometer calibration events and they are processed. Next the ranging tones are either detected or read from the file and their effect is removed. Then the bias is removed and more consistency checks are made on the beacon and radiometer attenuation to set the internal sample status and "bad data" is identified. This is followed by averaging the one second data for a minute. If the second is 59 then the process of calculating and writing the one-minute averages is called to write the data to the output summary file. Then the summation variables are set to zero and processing is started for the next minute. Next the internal status is converted to the beacon and radiometers attenuation status information for this second of data and written to the

.pv2 output file. Then the attenuation histograms are processed. This basic process is repeated for all the seconds in the input data file.

At the end of the day the summary process updates the calibration information, the empirical distributions, and the other files. If more days are to be processed in this session Actsp initializes internal variables and restarts with the reading of previously processed day's calibration information.

5.2 Actsp input options

Actsp has several input options that are described in order of appearance while running the program.

The first input option appears only if a script file has been found and asks if you want to use this script file or ignore it. If you select to use the script file then the answers to the file selection and input options question are read from the script file. When reading a script file the answers are read one line for each question and then parsed to remove the comments. Only the most used options are allowed. Specifically only .rv0 files are allowed as input and the system calibration parameters cannot be changed with a script file.

The default answers to each question are displayed when not using a script file. If this is the answer you wish to use then pressing the "enter" key will accept the default and move to the next question. An answer of "QUIT" is a valid answer for most questions and stops the program.

Choosing the desired input data file is the next question. The default preprocessing reads .rv0 raw data files but you can also choose to process .pvl or .pv2 data.

If the .pv2 file is input, the program does not rework the radiometer calibrations. It starts with the attenuation data and works backwards through the calibration and reference level adjustment procedures to recover the input data. The required calibration information was stored in the .pv2 file. The additional hourly data needed to reverse the reference level estimation procedure are contained in the .dfc file. If the latter are missing, the program will not provide input beacon level estimates.

Next the full path name of these files must be provided. The default path to the .rv0 or .pvn files is given and you can choose to enter a new path. Actsp then checks the directory for valid input file types and lists the files found before proceeding to the next question. The next question is which input file do you wish to process? The file number or the file name are valid answers. If the file is not found the question is repeated. When a valid input file is found the file name is displayed in the screen.

The default paths to the output subdirectories are displayed and you are allowed to change them. Actsp then checks for the existence of the required subdirectories. The question is repeated if the subdirectories are not found. The drive and path names are saved in the "actsp.ini" file located in the same directory as the Actsp program and this becomes the default path for the next usage.

The program prompts for the desired processing options. Several options are available:

N - the Normal or "Next" in sequence of days which is used for multi-day processing with little output to the screen and selected output to the spreadsheet,

- B - Brief that does an entire day (or multiple days) but writes one-minute average data to the screen and selected output to the spreadsheet,
- F - Full that does an entire day (or multiple days), writes one-minute average data to the screen and writes the full set of output data to the spreadsheet (all receiver voltages, etc. - this mode is recommended only for use in troubleshooting),
- S - a short segment of Second-by-second output, both to the screen and to the spreadsheet file,
- M - a short segment of one-Minute average output, both to the screen and to the spreadsheet file.

The additional options that may appended to the selection are:

- A - for noise diode calibrate factor Adjust,
- C - for change Calibrate constants,
- D - to force ranging tone Detection,
- N - to select multiple days (use if the N processing option was not selected above)
- U - to Use prior day bias reference coefficients if already calculated,
- B - to change radiometer for Bias reference when radiometer fails,
- R - for maintaining the Radiometer and beacon time bases the same for the edf but different as a function of frequency,
- I - for Independent time bases for each edf,
- T - for special Testing outputs.

Please note that when processing a .pv1 or .pv2 input file the only valid additional options are "N", "R" or "T".

The options "A" and "C" will cause the calibration menus to be presented where you can change the calibration constants. The "C" option allows you to change the system calibration constants. The current values are displayed and you can change them. The constants are the antenna efficiencies for 20 and 27 GHz, the spill-over temperatures for 20 and 27 GHz and the humidity sensor calibration adjustment factor. The "A" option allows you to change the noise diode temperature adjustment multiplier factor. This option provides a convenient way to adjust the parameters and keep a reasonable balance between adjusting antenna efficiency and spill-over temperature. It should be used after the system is initially calibrated to provide the incremental changes needed to keep up with system component drift.

The "B" option presents a menu to allow you to select which radiometer channel is in error when one of the radiometers is not working properly or is suffering interference. You are asked to enter 1 for 20 GHz, 2 for 27 GHz to force the use of the other radiometer.

If the "N" option was entered the next question is how many days you wish to process in this session. Because we have already selected the data paths all these files must be in the same sub-directory.

If the processing option was either "N" or "F" or "B" the full day will be processed and you have the option of generating or regenerating the edf's. The default answer is "Yes".

If the option was either "S" or "M" the processing start and stop times are needed from you. The "S" option is for use for processing a limited data set (in time). With this option, bias removal is not attempted.

5.3 Actspp files and directories:

Actspp uses three file types. They are binary files, tab-delimited text files and a text file. The primary input and output files are one-second data records that are binary file types. The tab-delimited text files are used for data input and output. This format is based on one that Microsoft's Excel can read for easy viewing and plotting. In general, the file naming convention is based on the date, site and file type is the extension. In the file name YY is the year, MM is the month, DD is the day and xx is the site identification. The file extension identifies the data type.

The input data file for Actspp is either a YYMMDDxx.RV0 raw binary data file or a YYMMDDxx.PV1 or YYMMDDxx.PV2 preprocessed binary data file. These input files can be located on any logical drive and directory that can be accessed by the PC. This includes a second hard disk, a CD ROM drive or a drive on a network. The drive and path names are saved in the "actspp.ini" file located in the same directory as the Actspp program and this becomes the default path for the next usage.

The output and auxiliary files are located in separate subdirectories. Again there are no restrictions on the drive and path to these subdirectories. The three required subdirectories are "dataout", "datasum" and "daylogxx".

The parent directory for these three sub-directories is where the "screen" file is placed. The file name for this file is "sfMMDDxx.Tss". The last letters in the extension is the PC's clock seconds when the file is opened. This was done so that separate runs of the same day do not automatically overwrite the older data. The screen file is a text file of the messages and data that appear on the screen while the program is running. Many messages flash too fast to be read on the CRT. Also an unattended running of the program leaves a list of the events and the end of day summaries in this text file to be reviewed by the experimenter later.

The subdirectory "dataout" is the directory for the YYMMDDxx.PV2 preprocessed binary data files. The format of this file is similar to the .rv0 file.

The subdirectory "datasum" is the directory for the YYMMDDxx.sum or YYMMDDxx.unk tab-delimited output data files. If the input option is "M", "B", "F" or "S", the .unk file is generated; otherwise, the "N" or normal option generates the .sum file. The input option "S" generates a second-by-second output of a small number of items and is useful in testing by looking at a few minutes of data. The other options place the one-minute averages of various items in the output file.

The "daylogxx" subdirectory contains several monthly summary files. These files are readied and updated for each day processed. If the file does not exist then Actspp will generate it. The first file, calfile.xxn, was originally used for the calibration constants derived from the system calibration and the every-15-minute radiometer calibration. This file is still used but its major function now is to provide default values.

The YYMM.RTN or YYMMxx.RTN is the ranging tone time file with one line for each day in the month. Standard files are provided but are inadequate sometimes because of data collection clock errors. Thus the site specific form YYMMxx.RTN is the first file name in

the search list. If site specific ranging tone times are needed then the standard should be copied or renamed to the site specific name format before using the "D" detect option. If there are no entries in the row for the current day then Actspp automatically switches to the ranging tone detection mode.

The YYMMxx.SRF file is the file to allow experimenters to enter surface weather data for use in place of the collection systems' gauges. To use the external data the experimenter should enter the local barometric pressure, temperature and relative humidity for each hour - 24 triple inputs. If the pressure is zero or there is no entry for the hour then the program uses the site instrument measurements. This file is always present and checked for surface weather data.

The YYMMxx.DFC file is written by Actspp with one line for each day in the month. The diurnal bias removal fit coefficients are listed in this file by hour. This file allows a .pv2 file to be read and regenerates the collected data, creating new one-minute average files and updating the attenuation histograms.

The YYMMxx.EDF file is written by Actspp with one line for each day in the month in each of six data blocks. The first data block is the histogram of the one-second average attenuation and one-minute average rain rates. The second block contains the Fade Duration histograms and the third block has the Inter-Fade Interval histogram information. The fourth and fifth data blocks contain one-minute average total attenuation, attenuation relative to clear sky and sky temperature histogram information. Block 6 contains the standard deviation histogram data. These files are updated by Actspp unless the operator selects the option not to update these files.

The YYMMxx.LOG file is written by Actspp with one line for each day in the month. Additional lines are possible for each day to enter Good and Bad time limits for marking "bad" data or for entering time-tagged comments or weather conditions. The date and times are entered in column 1-4 (A - D in the spreadsheet), the "B" or "G" status indicator is entered in column 5 (E) and the channel (20, 27 or Both) in column 6(F). This file may be edited by the experimenter to change the system calibration, mark the times of known "bad data" or times to "ignore" the data in calculating the histograms (all but rain rate), and add relevant information about the day's collection or weather state. The file contains specific information about the last radiometer calibration in the day and bias removal coefficients derived during the processing. Carrying forward this data allows smooth day to day transitions. Actspp first reads the data from "yesterday" to retrieve the last radiometer calibration in the day, bias removal coefficients and the system calibration values. Actspp then reads data from "today" to update the bias removal coefficients - if the option "U" was not selected - and the system calibration values if they are present.

5.4 Actspp data calculation and calibration

Calibration is necessary because both the beacon and radiometer measurements are needed and they must be forced to agree over the limited dynamic range where they both should agree. The beacon receiver is very linear and has a large dynamic range but there is no way to know the zero dB point and the power from ACTS does slowly change. The radiometer can predict the attenuation during clear sky and for very low attenuation events but it has a very limited dynamic range.

The total power radiometer measures the noise power of the receiver. The major contributors to this power are the LNA (low noise amplifier), the thermal noise from the sky and the thermal noise of the ground received from the side and back lobes of the antenna. The radiometer is a very high gain and wide bandwidth noise power measurement

device. To counteract the system gain changes over time and operating temperatures, the radiometer is "calibrated" every 15 minutes.

This calibration consists of switching the LNA from the antenna to a resistive 20 dB attenuator load - whose temperature is measured - that is in series with a noise source. During the "calibrate" time the noise diode is switched on and off. This gives the power reading for two stable noise temperatures. From this, the "system temperature" can be measured over long periods of time relative to the load and noise diode "temperatures". The "temperature" of the load and noise diode as measured by the radiometer are not known and thus must be inferred through other measurements to get to the sky temperature we want. Also we don't know how to partition this noise between the LNA's large temperature, the side lobe temperature and the sky temperature.

Direct inference of the load and noise diode temperature by using "known temperatures" at the antenna feed has failed, most probably because of the system VSWR matching problems.

Actspp does use an indirect, "total operational system approach" calibration to remove these uncertainties by using the predicted sky temperatures and the variation in these temperatures to derive the system calibration. In fact the approach Actspp uses is much more direct. The downside is that the calibration is driven by weather events and not the operator and has a statistical nature.

While this may be upsetting to some, please remember that the "bottom line" of all of the propagation measurements is statistical.

5.5 Sky temperature estimation

The system noise temperature is calculated from the radiometer voltage by:

$$T_i = a + b * V$$

V is radiometer voltage and is reported to the .sum file in the column "Avg Rad V ...". T_i is the system noise temperature and it is in the column "Avg Trad ...". The calibration constants "a" and "b" are reported to the .sum file when you use the "T" option. The constants are derived during the every 15 minute radiometer calibration. During this calibration the radiometer voltage is collected for both when noise diode is on and off. The temperature for the case when the noise diode is off is the measured temperature of the load. It is about 323 K. The temperature when the noise diode is on is about 613 K when the "Cal Adjust multiplier" is set to 1.

It is not important that we don't know these temperatures because we must perform a system calibration to convert the system temperature to a sky temperature and this system calibration will remove any effect of not knowing the true temperatures. The "Cal Adjust multiplier" is available to remove the effect of the slow drift in the noise diode's noise temperature.

The system calibration is used to convert system temperatures to sky brightness temperatures. The simplified form of this conversion is:

$$T_b = c * T_i - f * ((273+TZ) / (273+TZ_0))$$

where "c" is 1/ "antenna efficiency" and "f" is what we call "spill-over temperature." TZ is the current outside ambient temperature and TZ_0 is a constant = -3 C. With this, the "spill-

over" temperature is scaled to the current ambient temperature. Tb is reported in the column "Avg Sky Temp..." of the .sum file. Ti is the system temperature and we get it from the radiometer's voltage after applying the every-15-minutes radiometer calibration.

Actspp calculates the radiometer attenuation by using the equation:

$$\text{Atten} = -4.343 * \text{LN}((Tm-Tb) / (Tm-2.74))$$

where Tm is the medium temperature and Tb is the sky brightness temperature.

As the sky temperature approaches the medium temperature, the attenuation increases very fast. Thus, a slight error in the sky temperature or in the medium temperature can cause a many dB change in the attenuation for attenuation values above about 10 dB. Actspp estimates the medium temperature from ground based measurements in an effort to extend the range of useful radiometer attenuation estimates.

The goal of the system calibration is to find the two constants "antenna efficiency" and "spill-over temperature". This is done by 1) using a light rain intensity event to match the beacon and radiometer attenuation and 2) using clear sky days to match the radiometer attenuation to the attenuation predicted based on the ground based weather measurements. Matching the predicted sky temperatures to the observed sky temperature values is really the same thing.

A change in the antenna efficiency has little effect at low radiometer voltage reading compared to high readings. Thus you can change antenna efficiency to make a better match at the high attenuation. But remember, we don't know the "sky temperature" during an event. With two constants we could force the beacon to match the radiometer at low attenuation values and we could force the radiometer to match the beacon at high attenuation values (above 10 dB). An exact value for the medium temperature is required to make a match at high attenuation values and have a valid calibration for intermediate attenuation levels. The medium temperature changes during a rain event and between rain events. An exact match that holds for a period of time is not possible. The critical part of the calibration process is the statistical match between the radiometer attenuation values and gaseous absorption values under clear sky conditions.

6 Macro Library for use with Actspp

6.1 Introduction:

The macros in ACTS03.XLS are written in Visual Basic and can only run in Microsoft Excel 5.0 or higher version.

There are 5 macros in ACTS03.XLS. They are written for use with the output files (.sum, .unk, .edf) from Actspp.

Here is a brief description of the function of each macro:

Beacon:

This macro reads .sum files of successive days in a month and automatically prints out the time series of radiometer adjusted beacon power level for the chosen days. User is prompted to give the site ID, the path of the .sum files, the begin and end day he wishes to process, the position of the bad marker on the chart, the number of plots for each day and if he wants to save all the work in Excel files for later checking.

Cal adjust:

This macro is written to assist experimenters checking their APT system calibration. It gives users radiometer attenuation vs. gaseous absorption and radiometer attenuation vs. beacon attenuation charts for both frequencies. A well calibrated system should show that the lowest dots in the radiometer attenuation vs. gaseous absorption chart are less than 0.2 dB apart from the 1:1 line, and the dots in the radiometer attenuation vs. beacon attenuation chart for a "good" rain day are clustered around the 1:1 line.

For details about how to adjust your system calibration please refer to Radiometer System Calibration in ACTS Propagation Experiment Preprocessing Software User's Manual.

DailySummary

This macro is an extension of Beacon. Besides the time series of the beacon power level, it also generates time series of total attenuation, standard deviation and weather information and also can automatically print out sheets which include all these four time series for the user-chosen days. It will ask the user the same questions as Beacon before it runs. A sample output using this macro is shown in Figure 9.

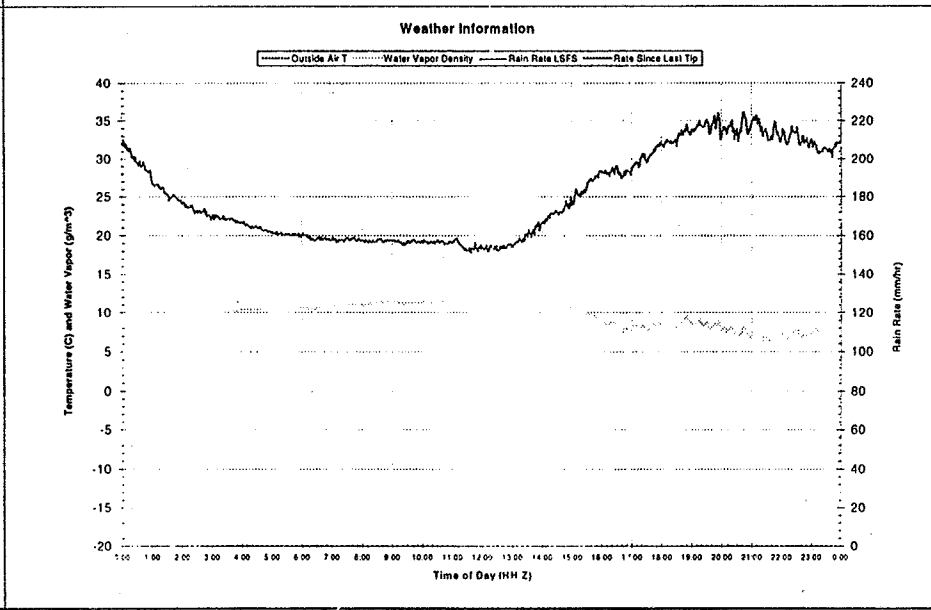
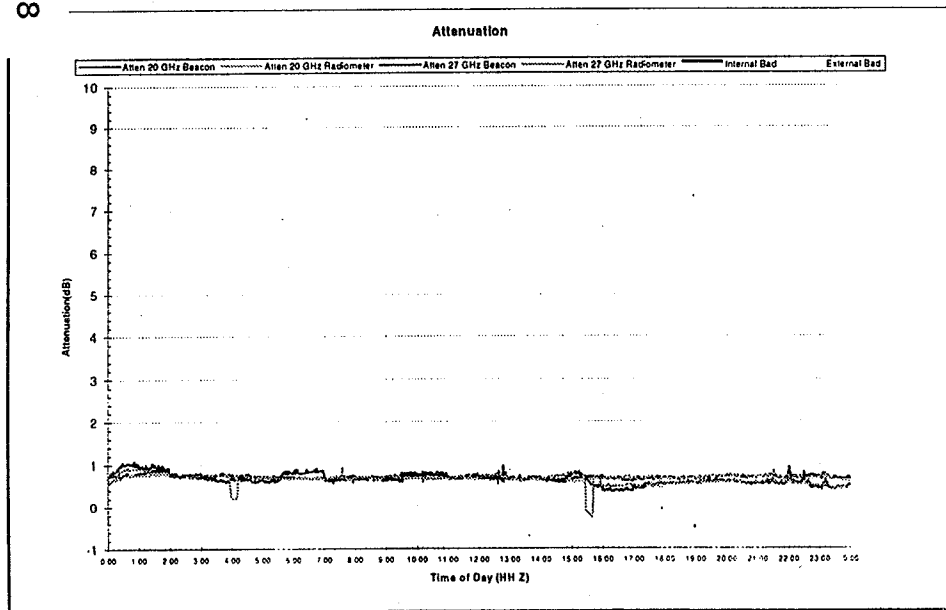
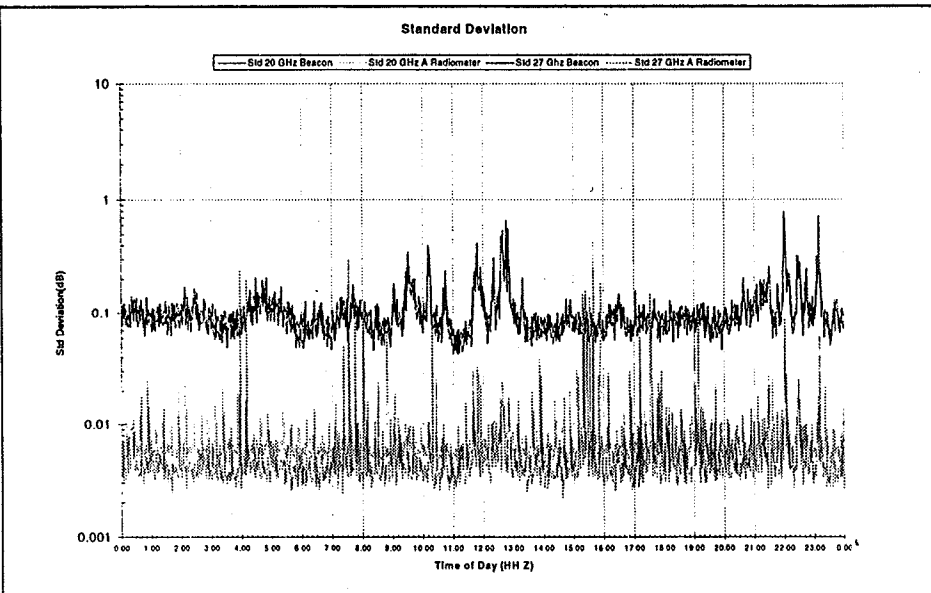
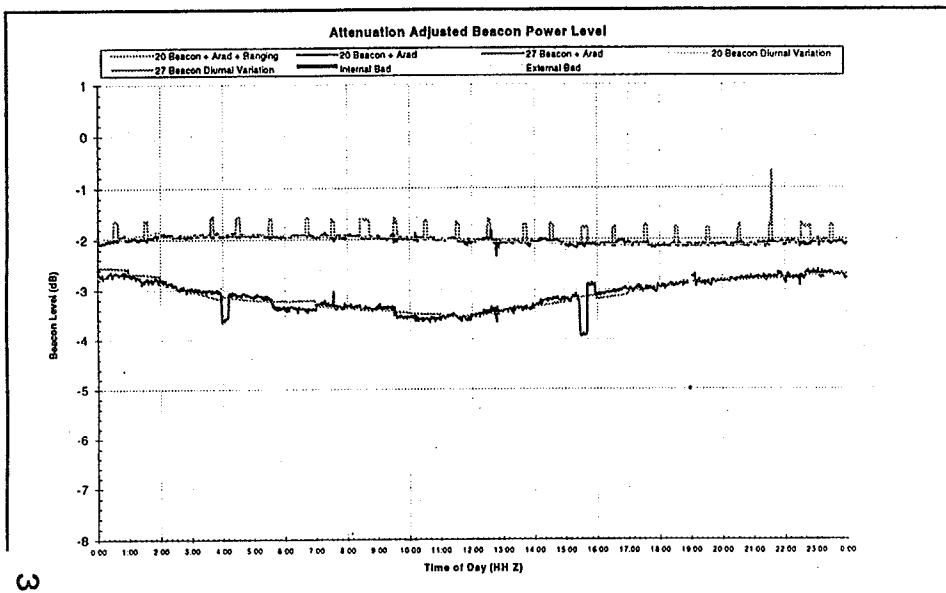
Edf0

This macro reads the .edf file for a month and calculates all the edf's in that file, namely monthly total attenuation by second distribution, monthly total attenuation by minute distribution (these two attenuation edf's are in one sheet), monthly fade duration and fade interval edf's (these two fade statistics are in one sheet), monthly free space attenuation, sky temperature, rain rate and standard deviation edf's (these four edf's are in one sheet). (Note: for .edf file generated by Actspp65 or earlier, only monthly total attenuation edf, fade duration and fade interval edf's are generated.)

ViewUNK

This macro can only work with a short (Sec) segment file (a second by second .unk file generated by choosing option S when you run Actspp). It generates a second by second time series of 20G beacon power level for that short time period and can be used to assist the experimenter in checking ranging tone removal.

940808OK Daily Summary Plots



6.2 Installing and Running the Macros:

> To install the macros:

Two files ACTS03.XLS and XL5GALRY.XLS are needed for installation. You can get them from Dave Westenhaver's ftp server: anonymous@ftp.crl.com (use binary transfer mode).

Before you install the macros, please back up the original xl5galry.xls in your c:\excel\xlstart directory (in case you want to restore your original Excel working environment).

EDF template (for Edf0)

skyattenedf - monthly clear sky attenuation EDF template (for Edf0)

Atten - attenuation time series template (for DailySummary)

Beacon+Arad+(RangTone) - radiometer adjusted beacon power level time series (for DailySummary and Beacon)

RvsEst - radiometer attenuation vs estimated gaseous absorption (for Cal_adjust)

RvsB atten20G - radiometer attenuation vs beacon attenuation (for Cal_adjust)

fadel - fade duration EDF (for Edf0)

fade - fade interval EDF (for Edf0)

Weather - time series of on site weather instrument records (for DailySummary)

UNKchart - second by second time series of 20G beacon level (for ViewUNK)

Note: XL5GALRY.XLS is the Microsoft Excel 5.0 template file, which includes all the chart templates needed for running macros in ACTS03.XLS.

Put the new XL5GALRY.XLS and ACTS03.XLS in your c:\excel\xlstart directory. The installation is finished.

> To run the macros:

1) Start Excel from the Windows Program Manager.

2) Since ACTS03.XLS is put in xlstart directory, it is opened every time Excel starts but it is in hidden mode. You may see an empty window of Excel with only File and Help on the menu bar, or you may see other menus in the menu bar if a file has been already opened in the window. For the first case from File menu, choose Macro... while for the second case from Tools, choose Macro.... A Macro window will pop up, in which available macros are listed. Choose the macro you want to run (e.g., ACTS03.XLS!Edf0) and click Run. Follow the prompts of the macro, then watch the macro finish the operation.

> Adjusting the scales of some charts:

The chart templates for ACTS03.XLS are suitable for the OK site. You may need to adjust the scales of some charts for your site, especially the ordinate scale for Beacon Power Level chart. Here are the steps:

From the File menu choose Open: an Open window will pop up. Change the directory to c:\excel\xlstart (you may also need to change the drive if Excel is in the other hard drive.) Then select xl5galry.xls and click OK. You will see all the chart templates for ACTS03.XLS:

cdf - monthly attenuation EDF template (for chart in Edf0 macro)
rain - monthly rain rate EDF template (for chart in Edf0 macro)
stdedf - monthly standard deviation EDF template (for Edf0)
skytempedf - monthly sky temperature skybrightT - not used by ACTS03.XLS
std - time series of standard deviation (for DailySummary)

If you want to change the ordinate scale for Beacon+Arad+(RangTone), select the tab of Beacon+Arad+(RangTone) from the bottom of the Excel window. The Beacon+Arad+(RangTone) template will show in the window. Now double click on the Y axis; a Format Axis window will pop up. Choose the Scale tab from the top of the Format Axis window. Now you can enter the suitable scale values for your site (e.g., set minimum -14; maximum -2; ...). When you are done, click OK and check the scale of the axis you have just changed; if it is OK, from File choose Save. The next time you run the macro DailySummary or Beacon (these two will use Beacon+Arad+(RangTone) template), changes in the Y axis of the beacon power level time series will show up.

If the beacon level does not drift out of scale over time, you only need to edit this template once.

Changing the other template is much the same as above. For editing other parts of a chart please refer to Excel User's Guide.

> To see the source code of the macros:

Either from File (when only two menus appear in the menu bar) choose Unhide, or from Window choose Unhide. An Unhide window will pop up. Select ACTS03.XLS and click OK. The source codes for all the macros will show up. You can modify the code of a macro to suit your special purpose.

TWO YEARS OF ACTS PROPAGATION STUDIES IN ALASKA

Charles E. Mayer and Bradley E. Jaeger
Electrical Engineering Department
University of Alaska Fairbanks
P.O. Box 755900
Fairbanks, AK 99775-5900

I. INTRODUCTION

The Alaska ACTS Propagation Terminal (APT) is located on top of the engineering building on the University of Alaska Fairbanks campus. The latitude and longitude of the site are $64^{\circ} 51' 28''$ N and $147^{\circ} 48' 59''$ W. The geometrical elevation angle to ACTS is 7.97° . Including a normal atmospheric refractivity, the elevation angle increases to 8.10° . The azimuth angle to ACTS is 129.36° . The terminal is located at 580 feet above mean sea level. The site is located in ITU-R rain zone C and Crane global model zone B1. ACTS transmits vertical polarization beacons at 27.505 and 20.185 GHz. At the APT the polarization tilt angle is 19.4° rotated CCW with respect to vertical when looking toward the satellite. The beacons are transmitted in a CONUS pattern. The ACTS beacon footprint at the Alaska APT site is 9 dB down from the transmission pattern peak at 27.505 GHz and 11 dB down from the pattern peak at 20.185 GHz. We will henceforth refer to the beacon frequencies as 27.5 (or 27) and 20.2 (or 20) GHz for the sake of brevity.

II. FAIRBANKS WEATHER

An understanding of the weather in Fairbanks is pertinent to understanding the displayed results. Fairbanks has very cold and very dry winters. The months November through March can be considered winter, where the only form of precipitation is snow, usually very dry. The transition months of September, October, and April can experience rain, wet snow, or possibly some dry snow. Snow does not greatly attenuate microwave signals. Rain is normally experienced May through September. The annual average precipitation in Fairbanks is 11.0 inches, as shown in Table I below.

Table I. Annual Weather Statistics in Fairbanks by Month

Month	Precipitation (Inches)	No. of Days with ≥ 0.1 in. Precipitation	Mean Minimum Temperature, $^{\circ}$ C	Mean Maximum Temperature, $^{\circ}$ C
January	0.69	2.1	-28.9	-18.9
February	0.58	1.9	-26.1	-12.7
March	0.41	1.1	-20.6	-5.0
April	0.25	0.6	-8.8	4.9
May	0.71	2.0	2.2	14.8
June	1.42	3.2	7.7	21.0
July	1.90	4.0	9.3	22.2
August	2.03	4.2	6.6	18.8
September	1.26	2.6	1.1	12.1
October	0.73	1.9	-7.8	1.1
November	0.48	1.6	-20.6	-11.1
December	0.55	1.8	-27.8	-18.9
Yearly Total	11.00	27.0	-9.4	2.2

III. MONTHLY AND YEARLY ATTENUATION AND RAIN RATE CDFs

The major experimental results of the measurement campaign are the total attenuation and rain rate. The cumulative distribution function (CDF), which is also called an empirical distribution function (EDF), is the primary method of displaying the experiment results. The abscissa on the attenuation CDF plot is total attenuation in dB ranging from -5 to 30 dB, and the ordinate is percentage time the attenuation is greater than the abscissa ranging from 0.001 to 100%. The abscissa on the rain rate CDF plot is rain rate in mm/hr, and the ordinate is percentage time the rain rate is greater than the abscissa. The attenuation and rain rate CDFs are presented for each month and also on a yearly basis. These CDFs are presented time sequentially in the appendix of this document. The attenuation CDFs include both beacon and radiometer distributions for both 20.2 and 27.5 GHz. The monthly attenuation CDFs display results that parallel the discussion of Fairbanks weather above. The CDFs for the cold, dry winters exhibit very low attenuation. The CDFs for the warmer summers exhibit larger percentages of attenuation at a few dB (1 - 4 dB). This attenuation is due to gaseous absorption. At a low elevation angle, the Fairbanks-ACTS link propagates through about 8 airmasses of atmosphere, where one airmass is the amount of atmosphere integrated to zenith. The summer CDFs also exhibit larger attenuation at the lower percentages. This attenuation is due to hydrometeors, mostly rain. The monthly rain rate CDFs clearly correspond to the attenuation measured during that month. The large variability in these CDFs from month to month, the similarity of each month from year to year, and the predictable trends from the above Fairbanks weather discussion indicate the importance of viewing attenuation statistics on a monthly basis. First we will discuss some overall features of these CDFs.

A. Total Attenuation CDFs

Several features must be explained to help interpret the results displayed in these attenuation CDFs. Due to the extra pattern footprint loss in Alaska and the limited dynamic range of the APT, the total attenuation with respect to free space can be accurately measured to a total attenuation level of approximately 18 dB with a sufficiently high signal-to-noise ratio, so that the attenuation value given is accurate. Values of attenuation greater than this threshold are given the value of 35 dB by the preprocessing program and displayed as 30 dB on the CDFs. Thus an attenuation value of 24 dB would be displayed as 30 dB, as would an attenuation value of 40 dB. This method of binning values was chosen so that the total time of attenuation greater than the measurement threshold would be properly accounted for. This tends to flatten out the tails of attenuation CDFs. This is not the shape that the CDFs would show were the measurement dynamic range larger. Values on the CDFs greater than 15 to 20 dB therefore do not accurately represent measured data and should not be taken as valid measurements.

Figure 1 shows the yearly attenuation CDFs for year 1 and year 2. Both the 20 and 27 GHz beacons are displayed. The attenuation displayed is the total attenuation, including gaseous absorption, rain attenuation, snow attenuation, scintillation, antenna wetting, and any other hydrometeor-caused attenuation. The 20.2 GHz beacon experiences more gaseous attenuation and hence has larger attenuation at the lower attenuation levels. The 27.5 GHz beacon experiences more hydrometeor attenuation and hence has larger attenuation at the higher attenuation levels. The crossover point of the two frequency attenuation curves is clearly at the 4 dB and 2% point. The 20.2 GHz beacon is reasonably close to the atmospheric water vapor absorption line at 22.2 GHz. The 27.5 GHz beacon, although higher in frequency, is farther from this absorption line and experiences less specific attenuation due to water vapor. By including year 1 and year 2 together in Figure 1, a measure of the variability between these two years can be readily seen. A word of

caution must be given when interpreting these CDFs. The average of these two years cannot be taken as the "average" year in Fairbanks. Many more years would need to be included to give an accurate assessment of the average year. Thus although these curves show points and narrow lines, it is not accurate to use these curves as an average attenuation.

Often a communications system must be designed to meet worst month statistics. Figure 2 shows the worst month envelope of attenuation. This curve was created comparing equi-attenuation values and selecting the highest percentage time at each of those levels. It should be noted that the 3 summer months of June, July and August were the only months that contributed to this worst month CDF.

B. Rain Rate CDFs

Rain is the only form of precipitation measured in the ACTS experiment; precipitation from snow is not measured. The yearly and monthly rain rate CDFs are shown in the appendix. It is interesting to note that year 1 had a higher percentage of larger rain rate events, but year 2 was a wetter year, demonstrating higher attenuation than year 1. A comparison of the rain rate in year 1, year 2 and the ITU-R rain zone C model is presented in Table II, below. The rain rate measurements were taken with a Young's capacitive rain gauge. The gauge has proven troublesome. Several sites have replaced the capacitive rain gauge with a tipping bucket rain gauge. We have used an optical gauge in conjunction with the capacitive gauge. The two gauges yield similar results for rain rates larger than several mm/hr. The capacitive gauge is noisy, often indicating rain when there is no rain present. We used the optical gauge to remove these anomalous rain indications, and then calculated monthly statistics based upon the amended capacitive gauge numbers.

Table II. Rain Rate in mm/hr

	0.1 %	0.01 %	0.001 %
Year 1 measurements	4.5	9	40
Year 2 measurements	4.5	10	20
ITU-R zone C model	5	15	42

IV. SCINTILLATION ANALYSIS

The impact of rain-induced attenuation on satellite-earth communication links at frequencies above 10 GHz is generally predominant. However, for the design of low margin systems, especially those at high frequencies and low elevation angles, scintillation effects must be properly estimated to accurately complete the link budget.

Scintillations are rapid fluctuations (on the scale of a few seconds to tens of seconds) in the magnitude of the received beacon level. The turbulence in the troposphere is concentrated in the planetary boundary layer, the moist layer of air ranging from the earth's surface up to a height of 1 to 1.5 km. Variations in humidity, pressure, temperature and magnitude and scale size of turbulence in the troposphere change the refractive index along the propagation path. These small scale and time varying perturbations cause amplitude, phase, and angle of arrival fluctuations, known as scintillations. The signal, after propagation through this turbulent layer, can be considered a random variable. This random variable can be described by its probability density function and its power spectrum. Theoretical studies [Tatarskii, Strohbehn, Ishimaru] yield models of these characteristic parameters based upon meteorological parameters that cannot be measured. The lack of knowledge of these meteorological parameters along the propagation path length

has led to the development of semi-empirical-models representing the magnitude and characteristics of scintillations.

The intensity of the scintillations must be accurately portrayed by a measurement unit. The scintillation process is assumed to be a zero-mean process with fluctuations about that mean. The fluctuations can be represented in terms of their root mean square, or rms. Since the mean of the process is zero, the rms can be represented by the standard deviation of the process.

The measure of the intensity of scintillation used will be the standard deviation of the log amplitude of the received signal, that is, the standard deviation of the received signal in decibels. The time duration of the standard deviation calculation will be one minute.

A. Time Series Analysis

Figure 3 shows the received 27.5 GHz beacon level over a period of 10 minutes on August 16, 1994. Large variations of the received beacon level are apparent from this figure. The time behavior of scintillations is demonstrated on this summer day of large scintillations. The day was humid and warm, with a light wind and full sky cover. An expanded view of this period is shown in Figure 4, which covers 1 minute of time on this day. Note that the 20.2 and 27.5 GHz beacons are both displayed, and are closely correlated over most of the time. There is about a 2 dB difference for several seconds. Also of note is the rapid rise of received beacon level in seconds 20 through 25. Both frequencies experience a 5 dB rise in 6 seconds. The mean level of these signals is about -13 dB (the scale is a relative scale), so that the signal enhancement is only about 3 dB above the nominal level. Signal attenuation is thought of as the major impairment to communication systems. However, signal enhancements can also cause problems, especially in multi-carrier transponder operation, where the input power must remain below the nonlinear threshold. If too much input power is supplied, the transponder becomes more nonlinear, producing intermodulation (IM) distortion, which can greatly reduce the overall C/N. Figure 5 is included to present another time series view of scintillation in a representative minute; this example is minute 38 in the hour. Again the behavior of both beacons is highly correlated, with only intervals of several seconds where they differed by several dB. Also note the rapid decrease of 3 to 4 dB during the 3 seconds near the end of the minute. During this hour on August 16, 1994 the beacons experienced large scintillations, as in most of the day. The distribution of scintillations will be studied using PDFs (probability density functions) of one minute standard deviation in several time durations.

B. PDFs

The APT samples each beacon (and each radiometer) once a second. Scintillations were studied by calculating the standard deviation in one minute periods of received beacon data (60 samples at each frequency). The standard deviations, measured in dB, were binned in 0.05 dB width bins. The number of calculated standard deviations (i.e., the number of seconds) in each bin were tabulated, forming a histogram distribution of the number of seconds of scintillation standard deviation at each bin dB value. These histogram distributions were produced over a 1 hour time period, over a 1 day time period, and over a 1 month time period. The nesting hour, day, and month were 18 - 19 GMT, 16th, and August 1994. The number of minutes at each standard deviation value bin were plotted in PDFs, or probability density functions. Figure 6 shows the PDF for one hour of standard deviation values. The time period is 18 - 19 GMT on August 16, 1994. The abscissa of the plot is one minute standard deviations in dB. The ordinate is the probability of occurrence, displayed on a logarithmic axis. For example, there was a 10% probability of the standard deviation being 0.75 dB for the 20.2 GHz beacon and about an 8% probability of the standard deviation being 0.75 dB for the 27.5 GHz beacon. It is clear that the scintillations were large during the hour, as the standard deviation was less than 0.5 dB for only a

few percent of the time for the 20.2 GHz beacon and less than 0.7 dB for a small percentage of time for the 27.5 GHz beacon. The standard deviations for the entire day of August 16, 1994 are shown in Figure 7. It is clear that there were many times of lower magnitude standard deviations over the whole day as compared to the one hour displayed in Figure 6. Also of note is that there were larger standard deviation values for a small percentage of the time. Finally, the PDF of the standard deviations for the entire month of August 1994 is presented in Figure 8. Again the distribution tends to move toward lower values of standard deviations.

C. Scintillation Standard Deviation

Increasingly, models for attenuation due to scintillation, gases, and clouds are becoming important for low margin satellite applications. Total fade distributions have applications in determining link margins and in determining service quality [Salonen, Matsudo]. Models for the fading due to scintillation incorporate the standard deviation of signal amplitude (σ_x) in two ways. First, the formulation of the long term cumulative distribution (CDF) of scintillation log amplitude (χ in dB) is undertaken by assuming two distributions. If a conditional distribution of χ given σ_x and a distribution for σ_x are given, the CDF of log amplitude can be found by integrating over the product of these two distributions [Allnutt]. Second, the models for fading due to scintillation incorporate a prediction of the mean standard deviation of signal amplitude based on the local wet refractivity. The authors present the first year of the standard deviation of signal amplitude. They found that for the first year of observation the standard deviation of signal amplitude was bounded by both the CCIR model and the Karasawa model. They present a typical probability density function for the standard deviation of signal amplitude and measured prediction equations for the mean standard deviation of signal amplitude from wet refractivity for the first year.

D. Two Standard Probability Density Functions of Standard Deviation

Two models are generally accepted for the standard deviation of signal amplitude, the Karasawa gamma distribution and the Mousley-Vilar lognormal distribution. These models describe the standard deviation of attenuation with rain and gas attenuation effects removed. The equation used to perform this operation [Crane] is as follows:

$$\sigma_x = \sqrt{\text{var}(AFS) - \text{var}(ARD)}, \quad (1)$$

where $\text{var}(AFS)$ is the variance in the free space attenuation, or total attenuation, and $\text{var}(ARD)$ is the variance in the radiometer attenuation channel, which accounts for the rain and gaseous attenuation. The Karasawa gamma distribution [Allnutt] describes the distribution of signal standard deviation using parameters β and ζ that could be related to measurements:

$$f = \frac{\beta^\zeta}{\Gamma(\zeta)} \cdot \sigma_x^{\zeta-1} \cdot \exp(-\beta \cdot \sigma_x) \quad (2)$$

$$\beta = \frac{m}{\sigma_{\sigma_x}^2} \quad \text{and} \quad \zeta = \frac{m^2}{\sigma_{\sigma_x}^2}.$$

The mean of the signal standard deviation is equal to m and the variance of the signal standard deviation is $\sigma_{\sigma_x}^2$. This distribution is used to form the CDF of scintillation fading in both the CCIR model and the Karasawa model. Mousley and Vilar obtained cumulative distributions for signal fading by using a lognormal probability density function for the standard deviation of signal fading [Mousley]:

$$f = \frac{1}{\sigma_{\sigma} \cdot \sigma_x} \cdot \sqrt{\frac{2}{\pi}} \cdot \exp\left(\frac{\left[\ln\left(\frac{\sigma_x^2}{\sigma_m^2}\right)\right]^2}{2 \cdot \sigma_{\sigma}^2}\right), \quad (3)$$

where

$$m = \ln(\sigma_m^2) = \text{avg}(\ln(\sigma_x^2)) \text{ and } \sigma_{\sigma} = \text{var}(\ln(\sigma_x^2)).$$

In Fairbanks the authors have obtained measured distributions of signal standard deviation. Statistical K-S tests of these distributions against gamma and lognormal distributions will be presented later in the Proceedings of the IEEE. Typical distributions for each beacon frequency are shown in Figures 9 and 10.

E. Prediction of Average Signal Standard Deviation from Wet Refractivity

There are two accepted models for predicting an average signal standard deviation, the CCIR model and the Karasawa model. Each model makes a prediction of the signal standard deviation from the average wet refractivity and then scales to frequency, elevation angle, and aperture size. Figures 11 and 12 show the annual variation in average hourly standard deviation at Fairbanks. The data for the first year are below both the CCIR model and the Karasawa model predictions.

Using station parameters from Haystack, Massachusetts, the CCIR model scales to frequency, elevation angle, and aperture size as follows:

$$\sigma_{prc} = \frac{\sigma_{ref} \cdot f^{12} \cdot g(x)}{\sin(\theta)^{1.2}} \quad (4)$$

with

$$\sigma_{ref} = 0.0036 + 0.00013 \cdot N_{wet}$$

$$g(x) = \sqrt{3.86 \cdot (x^2 + 1)^{\frac{11}{12}} \cdot \sin\left(\left(\frac{11}{6}\right) \cdot \arctan\left(\frac{1}{x}\right)\right) - 7.08 \cdot x^{\frac{5}{6}}}$$

$$x = 0.00584 \cdot D_{eff}^2 \cdot \frac{k}{L}$$

$$D_{eff} = \sqrt{\eta} \cdot D$$

$$L = \frac{2 \cdot h}{\sqrt{\sin^2(\theta) + \left(\frac{2 \cdot h}{r_e}\right)^2} + \sin(\theta)}$$

$$N_{wet} = \frac{3730 \cdot H \cdot e_s}{(273 + t)^2}$$

$$e_s = \frac{5854 \cdot \left(10^{\left(20 - \frac{2950}{273+t}\right)}\right)}{(273 + t)^5}$$

where

- σ_{pre} is the predicted monthly average standard deviation of signal amplitude (dB)
- L is the effective turbulent path length (m)
- h is the turbulence height (m)
- θ is the elevation angle
- D_{eff} is the effective antenna diameter (m)
- D is the antenna diameter (m)
- k is the wave number (m^{-1})
- η is the antenna efficiency
- r_e is the effective earth radius= $8.5 \cdot 10^6$ (m)
- N_{wet} is the wet refractivity (N units)
- e_s is the monthly average saturated water vapour pressure (mb)
- t is the monthly average surface temperature ($^{\circ}C$).

The Karasawa model is very similar, scaling from its station parameters at Yamaguchi, Japan, to other frequencies, elevation angles, and aperture sizes. The main theoretical difference between the two models is the scaling with frequency, $f^{7/12}$ versus $f^{0.45}$. Karasawa made the argument that Yamaguchi frequencies fell in between the diffraction region and the geometrical optical region. The diffraction region was assumed to be under the Tatarskii model, $f^{7/12}$, and the geometrical optical region was assumed to be under the Yokoi model, f^0 . The Karasawa model is as follows:

$$\sigma_x = \sigma_{x,ref} \cdot \eta_f \cdot \eta_{\theta} \cdot \eta_{D_a} \quad (5)$$

with

$$\sigma_{x,ref} = 0.15 + 0.0052 \cdot N_{wet} \quad \eta_f = \left(\frac{f}{11.5}\right)^{0.45} \quad \eta_{\theta} = \left(\frac{\text{cosec}(\theta)}{\text{cosec}(6.5^{\circ})}\right)^{1.3} \quad \theta > 5^{\circ}$$

$$\eta_{D_a} = \sqrt{\frac{G(D_a)}{G(7.6)}}$$

$$N_{wet} = \frac{3730 \cdot H \cdot e_s}{(273 + t)^2}$$

$$e_s = 6.11 \cdot \exp\left(\frac{19.7 \cdot t}{(t + 273)}\right)$$

$$R = 0.75 \cdot \left(\frac{D_a}{2}\right)$$

$$G(R) = 1.0 - 1.4 \cdot \left(\frac{R}{\sqrt{\lambda \cdot L}}\right) \quad \text{for } 0 \leq \frac{R}{\sqrt{\lambda \cdot L}} \leq 0.5$$

$$L = \frac{2 \cdot h}{\sqrt{\sin^2(\theta) + \left(\frac{2 \cdot h}{r_e}\right)^2} + \sin(\theta)}$$

where

σ_x	is the predicted monthly average standard deviation of signal amplitude (dB)
$\sigma_{x,ref}$	is the unscaled predicted monthly average standard deviation of signal amplitude (dB)
N_{wet}	is the wet refractivity (N units)
η_f	is the frequency scaling, f is the frequency (GHz)
η_θ	is the elevation angle scaling, θ is the elevation angle
η_{Da}	is the antenna diameter scaling, D_a is the antenna diameter (m)
H	is the monthly average relative humidity (%)
e_s	is the monthly average saturated water vapour pressure (mb)
t	is the monthly average surface temperature ($^{\circ}$ C)
G(R)	is the antenna aperture averaging factor
R	is the effective radius of circular aperture (m)
L	is the effective turbulent path length (m)
h	is the turbulence height (2000 m)
r_e	is the effective earth radius= $8.5 \cdot 10^6$ (m).

In Fairbanks the relationship between average hourly standard deviation and wet refractivity, in the first year, was as given in Figure 13 and Figure 14. Additional data will be analyzed before deciding if these relationships are statistically different from the models.

The frequency scaling exponent for the first year was nearly equal to the Karasawa model. The ratio of standard deviations, 1.14, was calculated from an average ratio of standard deviations. The arguments in the average came from interpolating equal percentage points on cumulative distribution functions. Solving the CCIR scaling relation for a:

$$a = \frac{\ln\left(\frac{\sigma(f,\theta)}{\sigma(f_0,\theta_0)}\right) - 1.2 \cdot \ln\left(\frac{\sin(\theta_0)}{\sin(\theta)}\right) - \frac{1}{2} \cdot \ln\left(\frac{G(R)}{G(R_0)}\right)}{\ln\left(\frac{f}{f_0}\right)} \quad (6)$$

Substituting 1.14 for the ratio of standard deviation gives $a=0.44$.

Figure 15 and Figure 16 show the month to month variability in standard deviations. The months of January and August are nominally the months with the smallest and largest scintillations. All other months typically fit between these bounds. Figure 17 shows the one year CDFs of standard deviation and associated power law fits.

V. CONCLUSIONS

The Fairbanks AK APT site is the only APT site with a low elevation angle. This feature allows measurements to be made on a long propagation path length through the atmosphere. Propagation phenomena that are strongly elevation angle dependent include gaseous absorption and scintillations. The AK APT clearly experiences large amounts of gaseous absorption during the humid summer months, as seen in the total attenuation CDFs. Scintillations have been analyzed and presented in PDFs of their standard deviation. For the month of August 1994, one minute standard deviations were greater than 1.5 dB for 0.02% of the month at 20.2 GHz and for 0.03% of the month for 27.5 GHz. It should be noted that the beacon peak-to-peak variation is significantly larger than the standard deviation. For example, the 10 minute time series of beacon data shown in Figure 3 has a standard deviation of 0.88 dB, whereas the peak-to-peak variations are on the order of 5.0 dB. Two models of signal standard deviation (CCIR and Karasawa), which

quantifies the magnitude of scintillations, were compared to the measured data, with the measured values being significantly less than both models.

REFERENCES

- Allnutt, J. E., Y. Karasawa, and M. Yamada, "A New Prediction Method for Tropospheric Scintillation on Earth-Space Paths," *IEEE Transactions on Antennas and Propagation*, pp. 1608-1614, November 1988.
- Crane, R. K., E-mail Communication.
- Ishimaru, A., *Wave Propagation and Scattering in Random Media*. New York: Academic Press, 1978.
- Matsudo, T. and Y. Karasawa, "Characteristics and Prediction methods for the Occurrence Rate of SES in Available Time Affected by Tropospheric Scintillation," *Electronics and Communications in Japan*, pp. 843-851, December 1990.
- Moulsley, T. J., and E. Vilar, "Experimental and Theoretical Statistics of Microwave Amplitude Scintillations on Satellite Down-links," *IEEE Transactions on Antennas and Propagation*, pp. 1099-1106, November 1982.
- Salonen, E. T., J. K. Tervonen, and W. J. Vogel, "Scintillation Effects on Total Fade Distributions for Earth-Satellite Links," *IEEE Transactions on Antennas and Propagation*, pp. 23-27, January 1996.
- Strohbehn, J. W., "Line-of-Sight Wave Propagation Through the Turbulent Atmosphere," *IEEE Proceedings*, vol. 56, no. 8, pp. 1301-1318, August 1968.
- Tatarskii, V. I., *Wave Propagation in a Turbulent Medium* (translated by R. A. Silverman). New York: McGraw-Hill, 1961.

Fig. 1. AK Yearly Beacon Attenuation (second) EDF

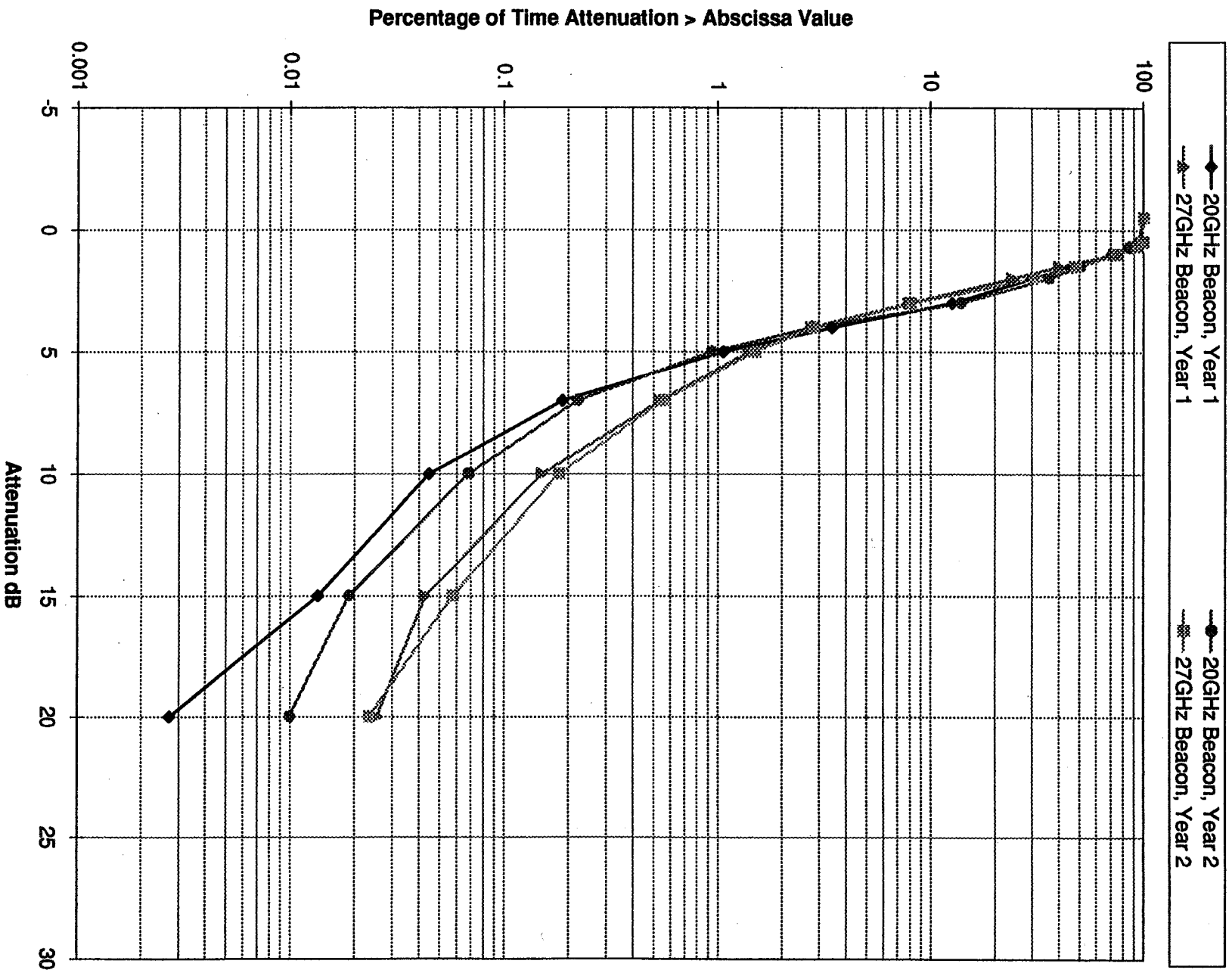


Fig. 2. 2 Year Envelope of Worst Monthly Attenuation (second) EDF

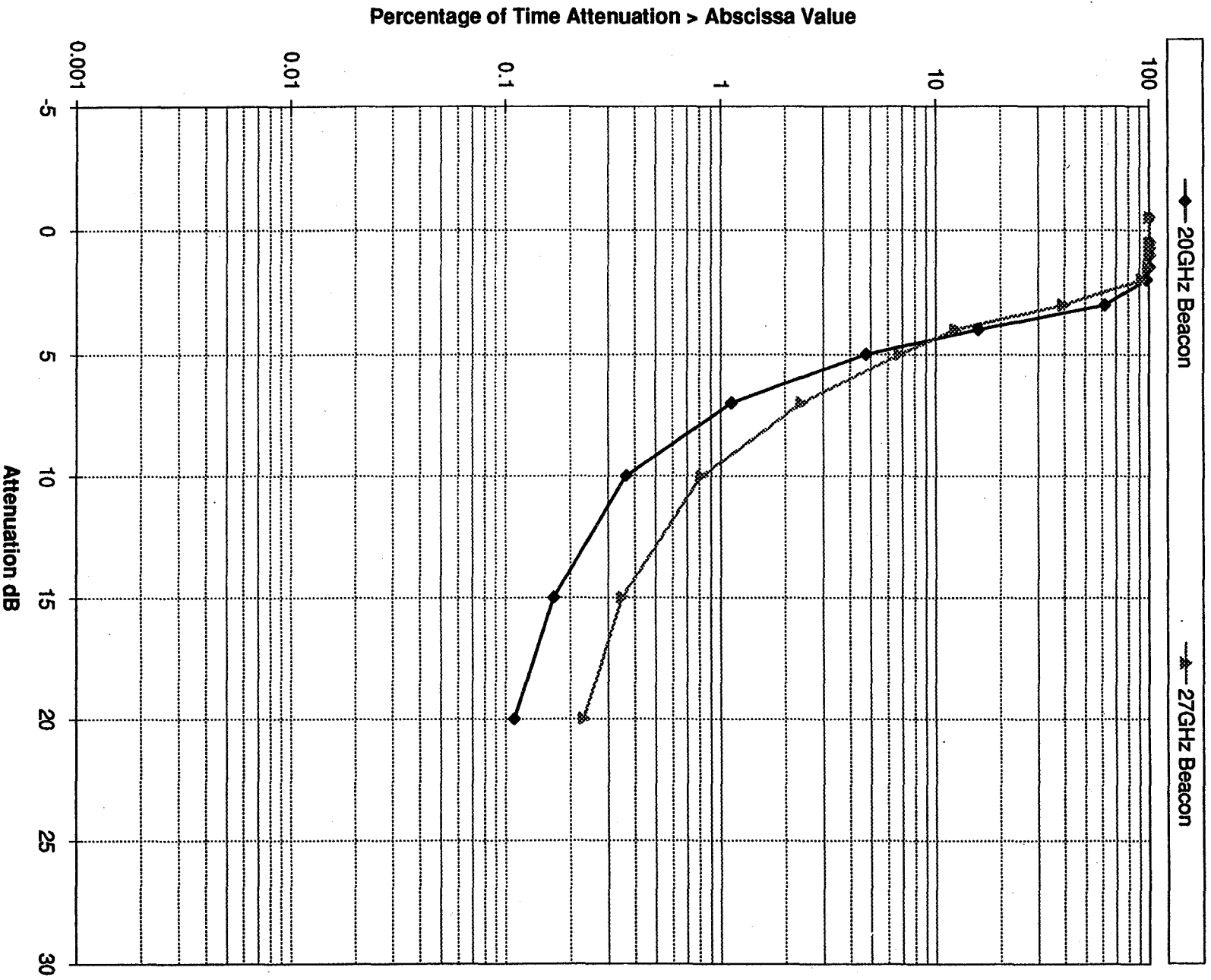


Fig. 3. 27.5 GHz Beacon Levels

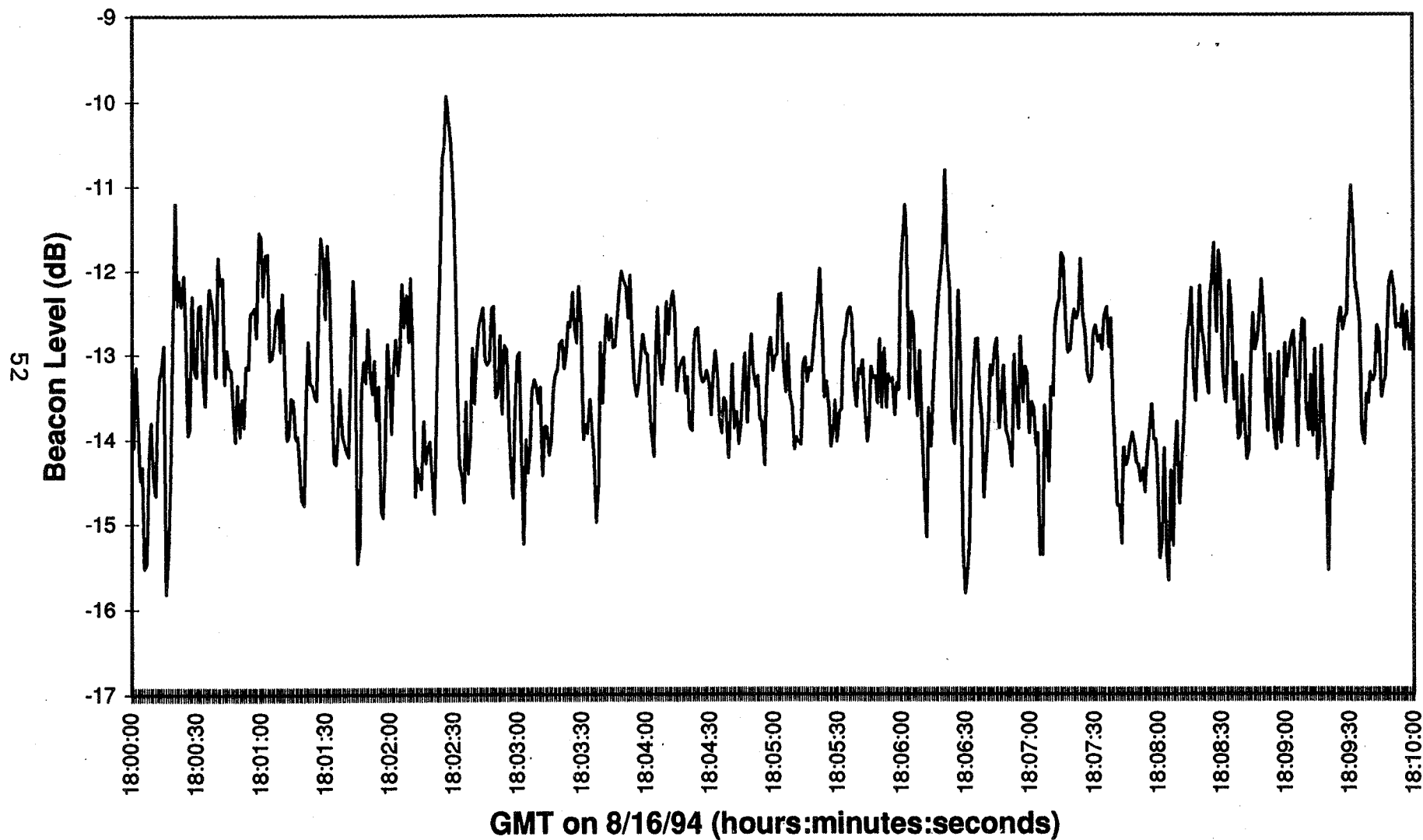


Fig. 4. 20.2 and 27.5 Beacon Levels

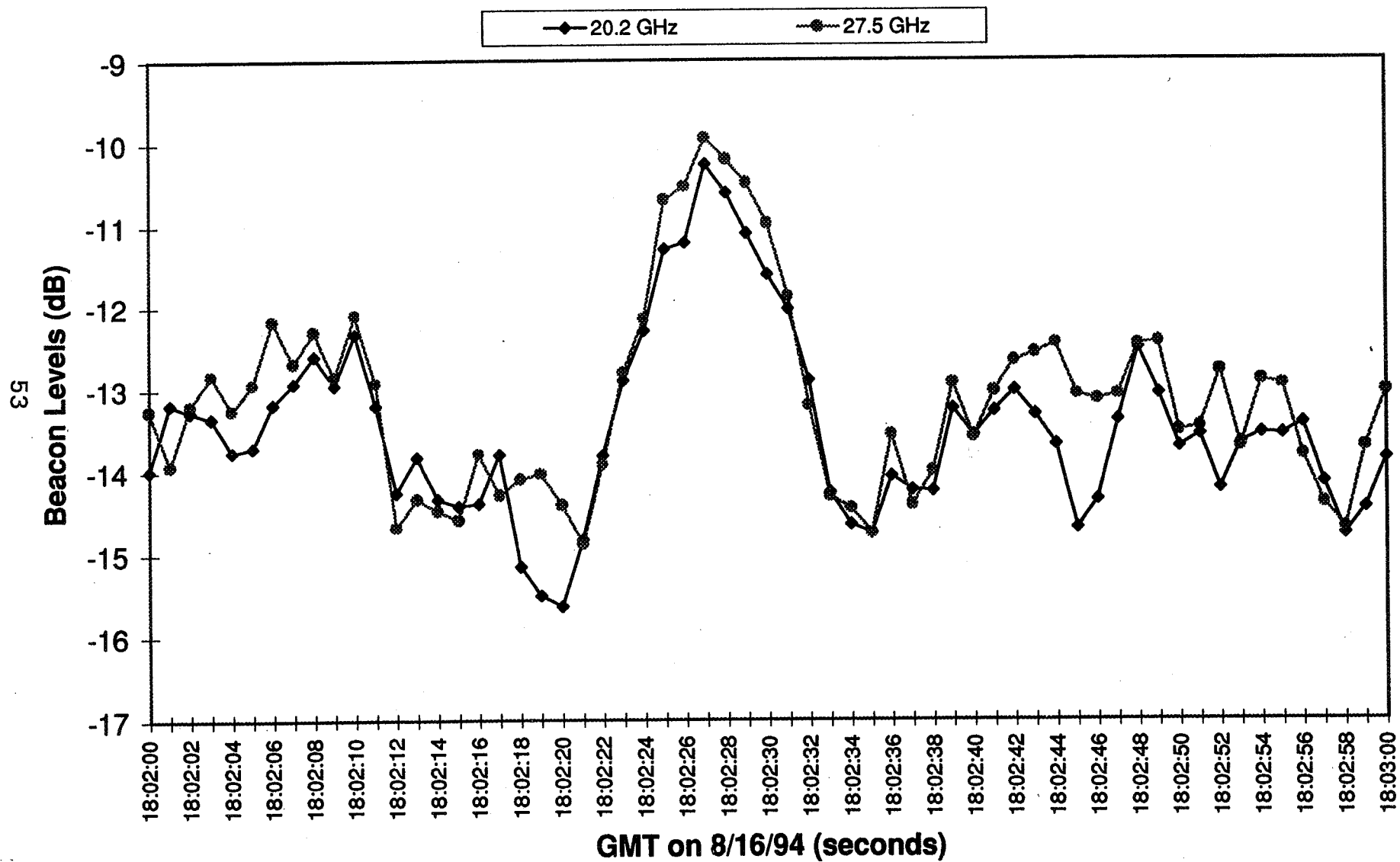
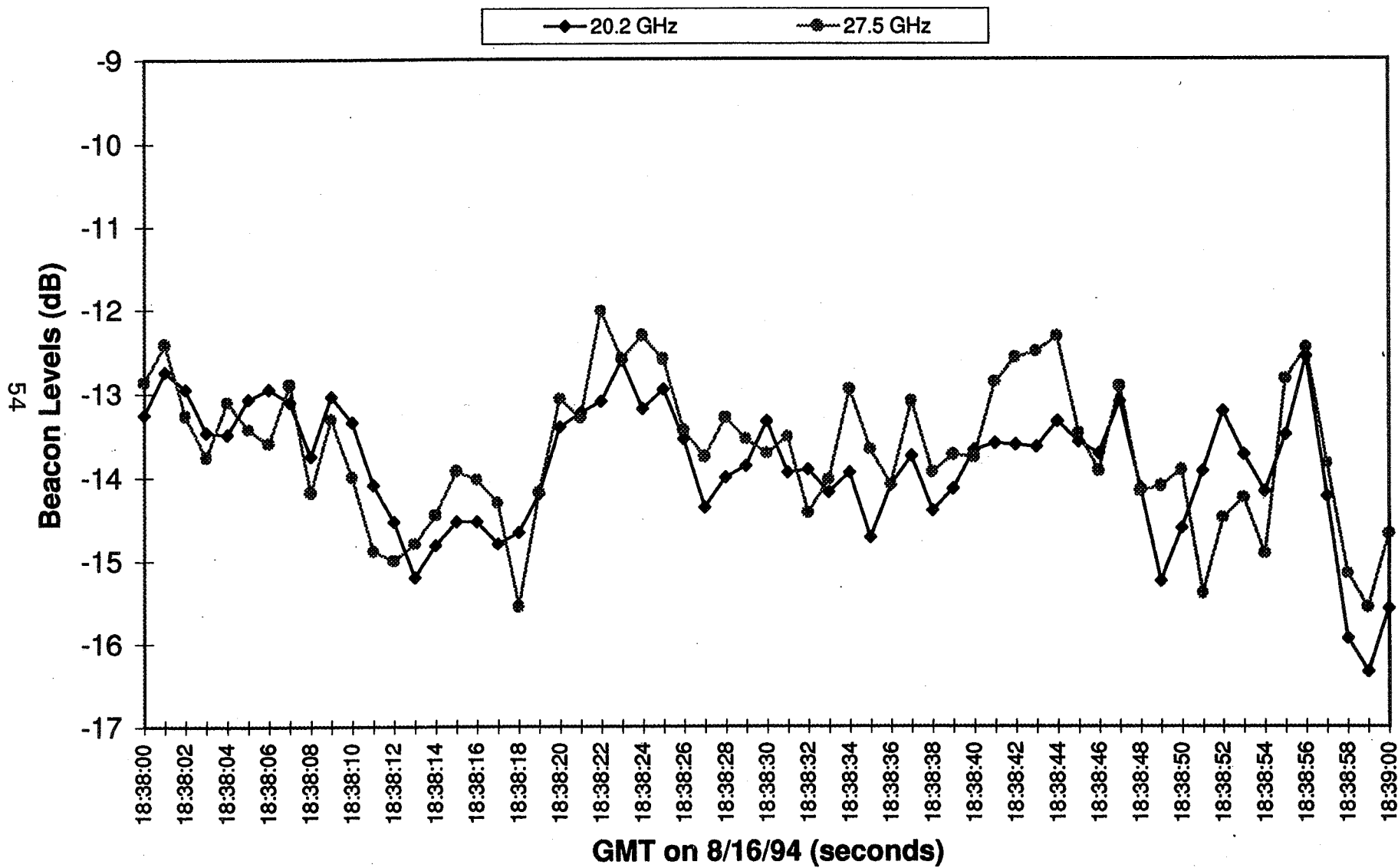
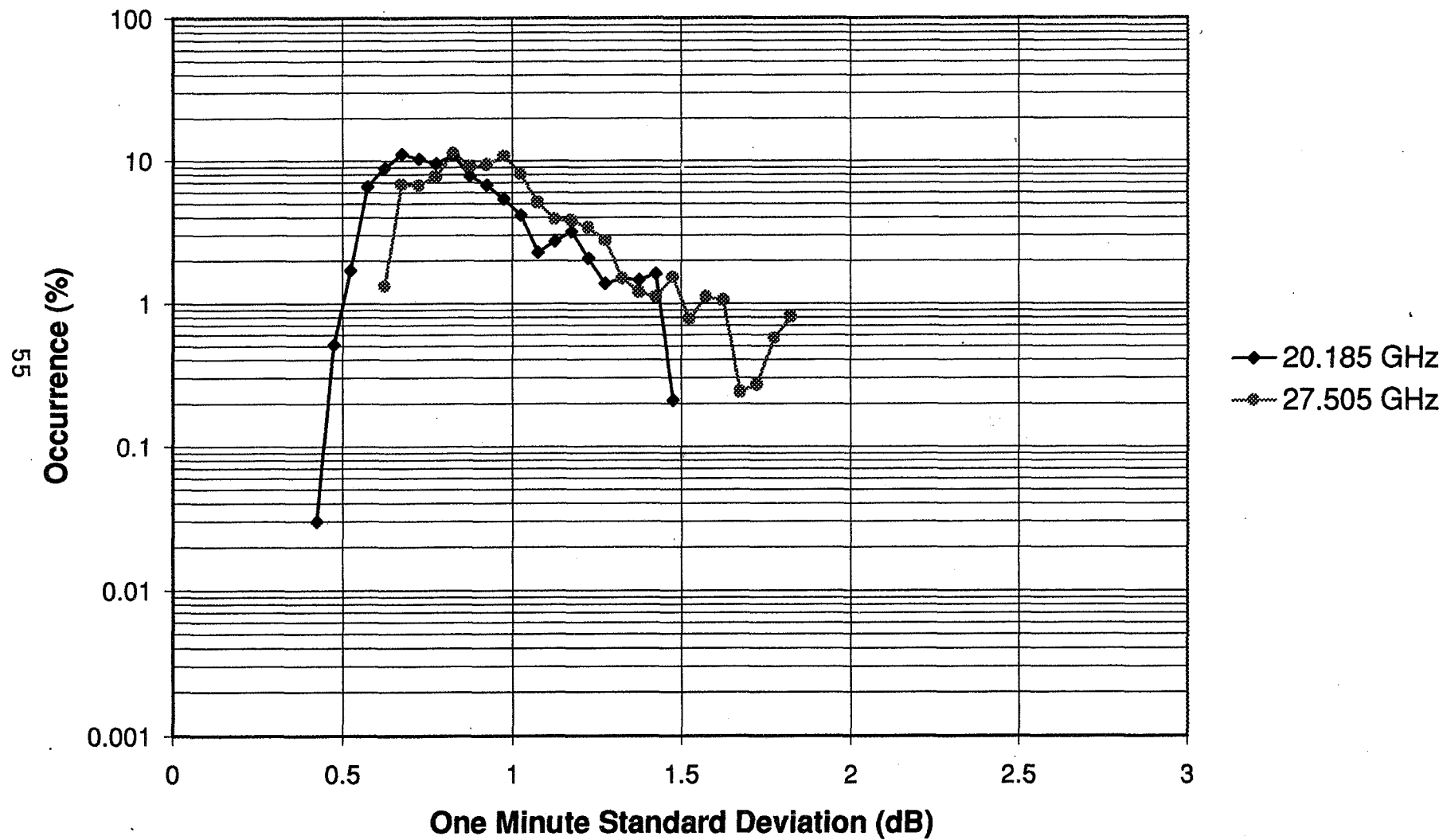


Fig. 5. 20.2 and 27.5 Beacon Levels



**Fig. 6. One Minute Standard Deviation PDF
18-19H GMT 8/16/94**



**Fig. 7. One Minute Standard Deviation PDF
8/16/94**

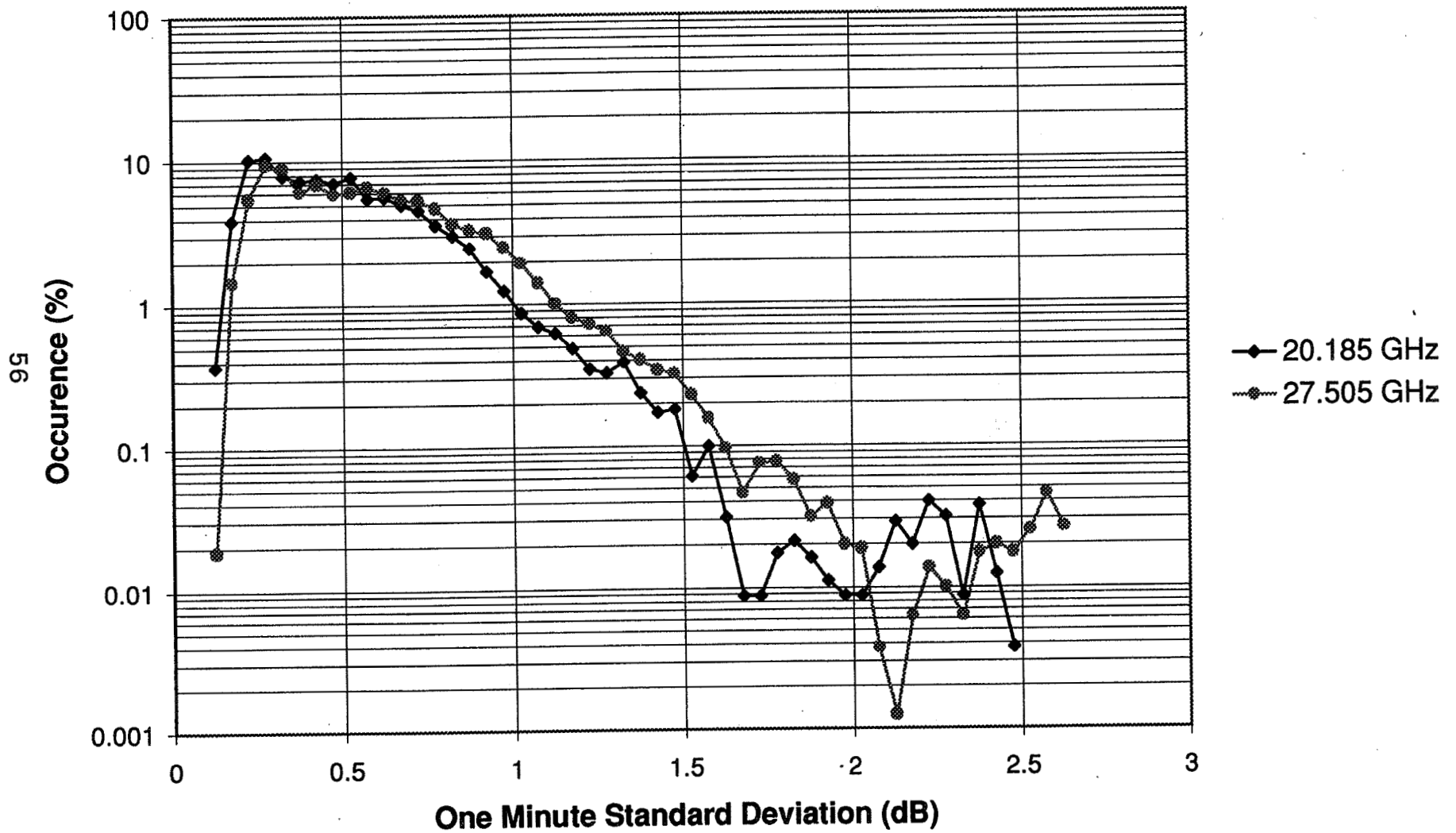


**Fig. 8. One Minute Standard Deviation PDF
August 1994**

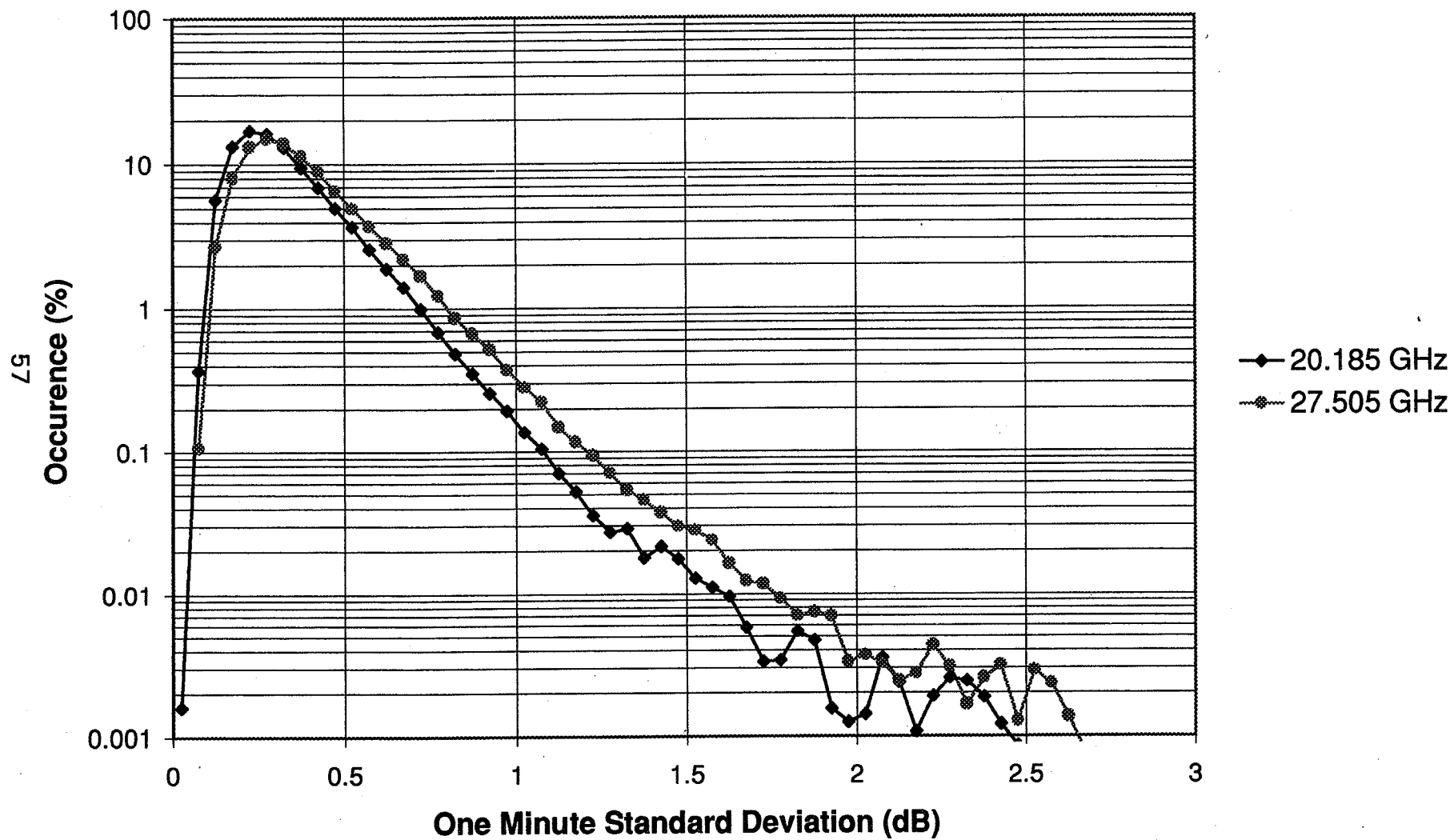


Fig. 9. Probability Density Function of Hourly Standard Deviation

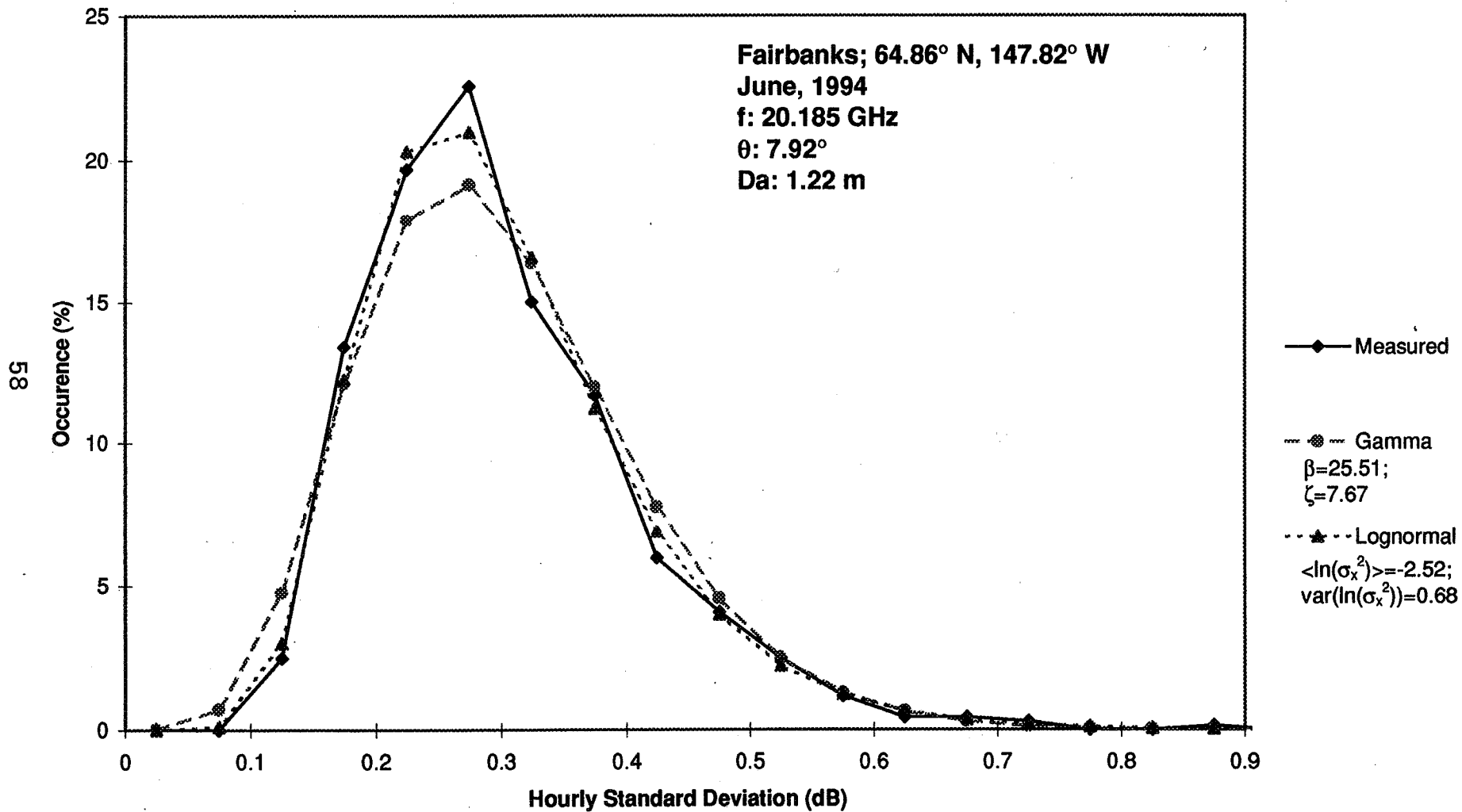


Fig. 10. Probability Density Function of Hourly Standard Deviation

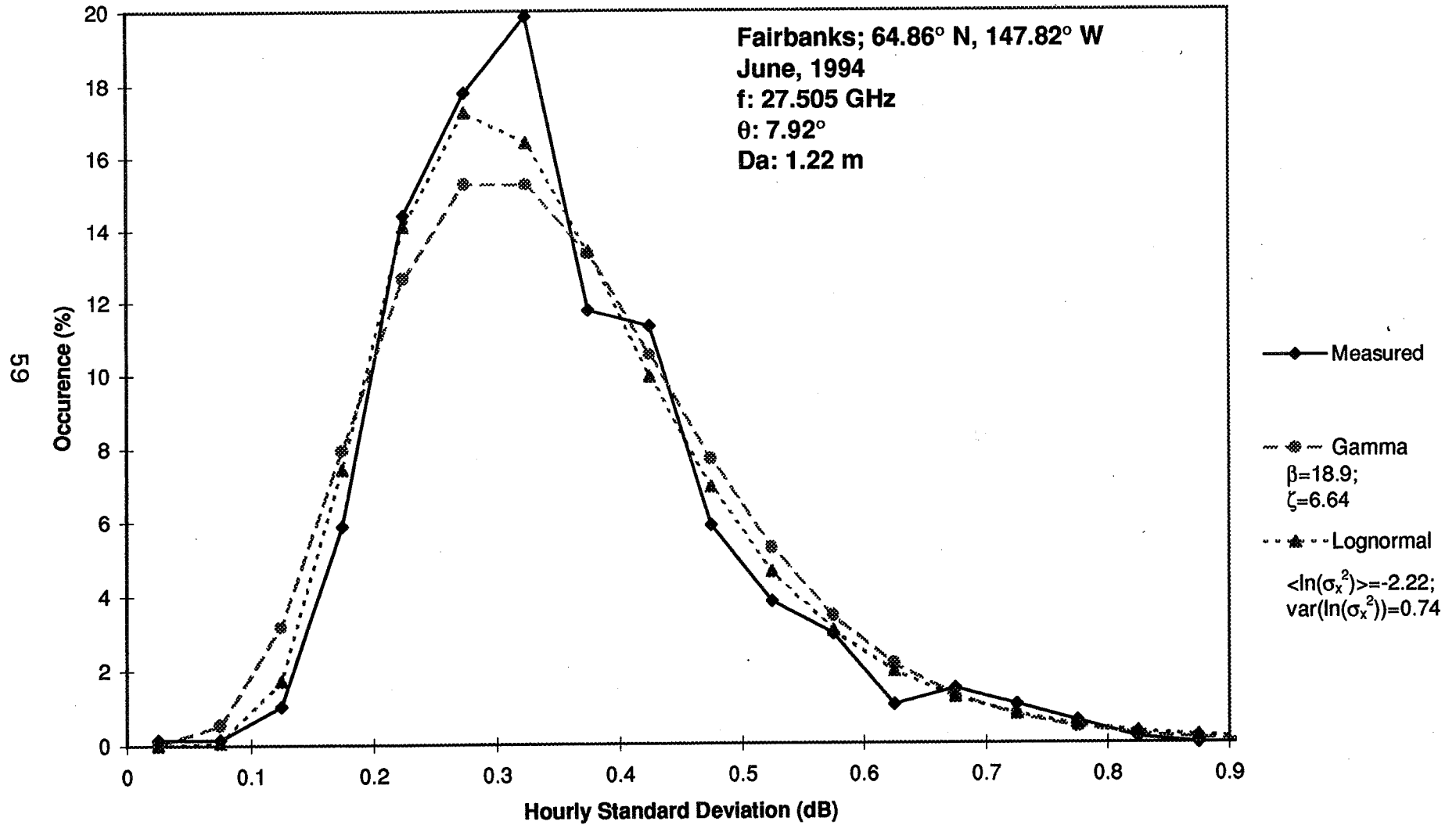


Fig. 11. Annual Variation in Hourly Standard Deviation

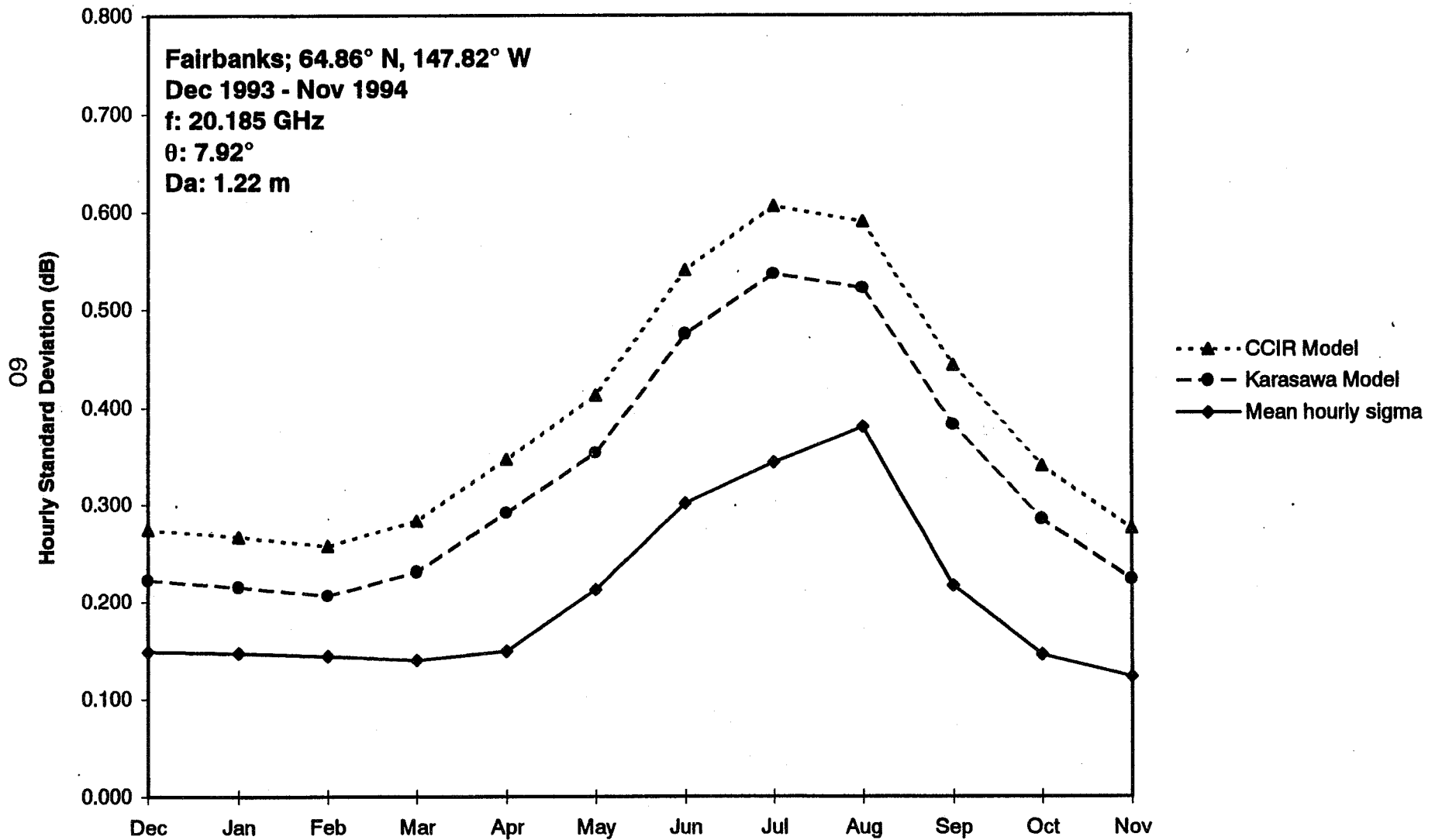


Fig. 12. Annual Variation in Hourly Standard Deviation

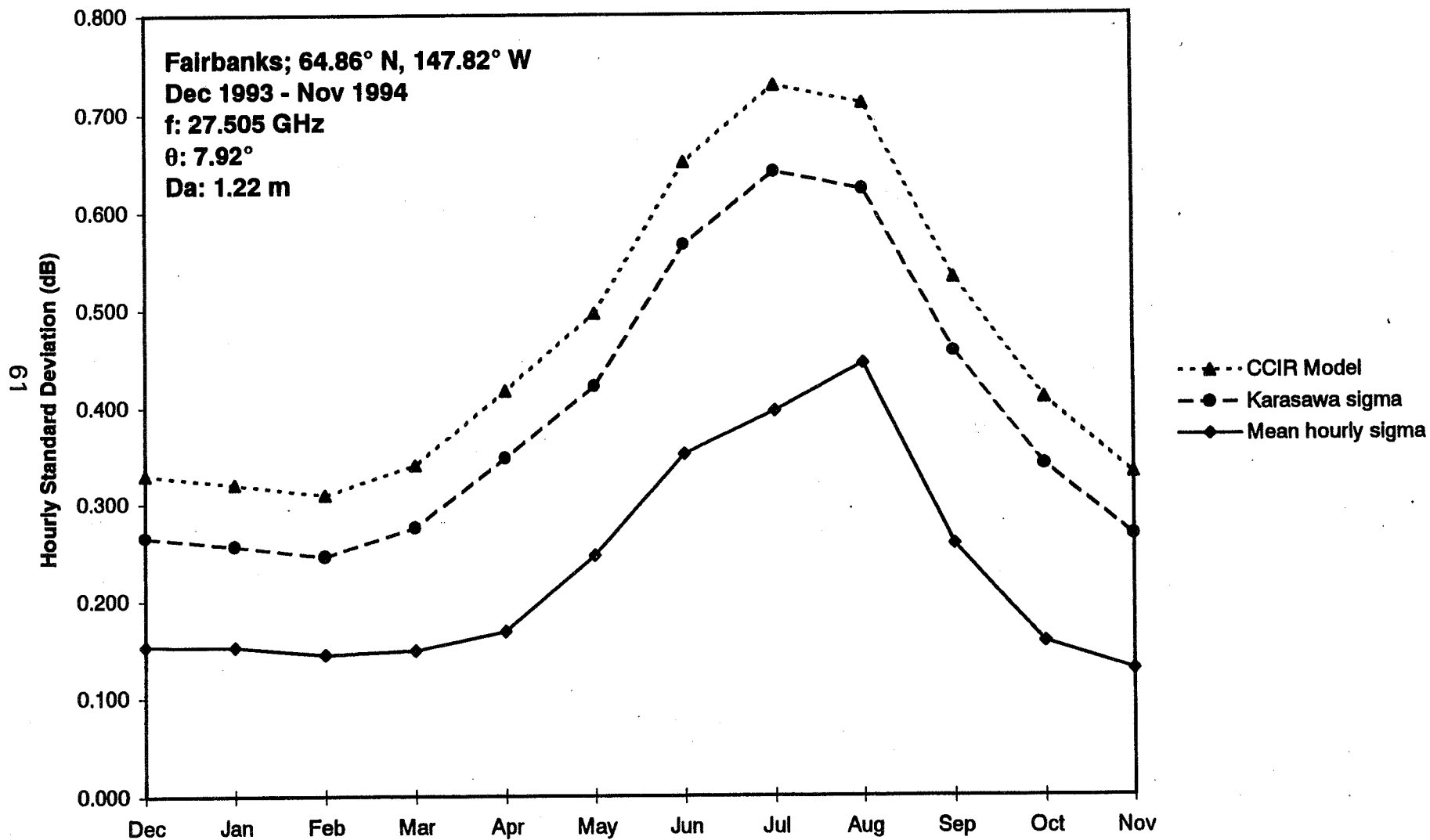


Fig. 13. Linear Regression of Nwet and Hourly Standard Deviation

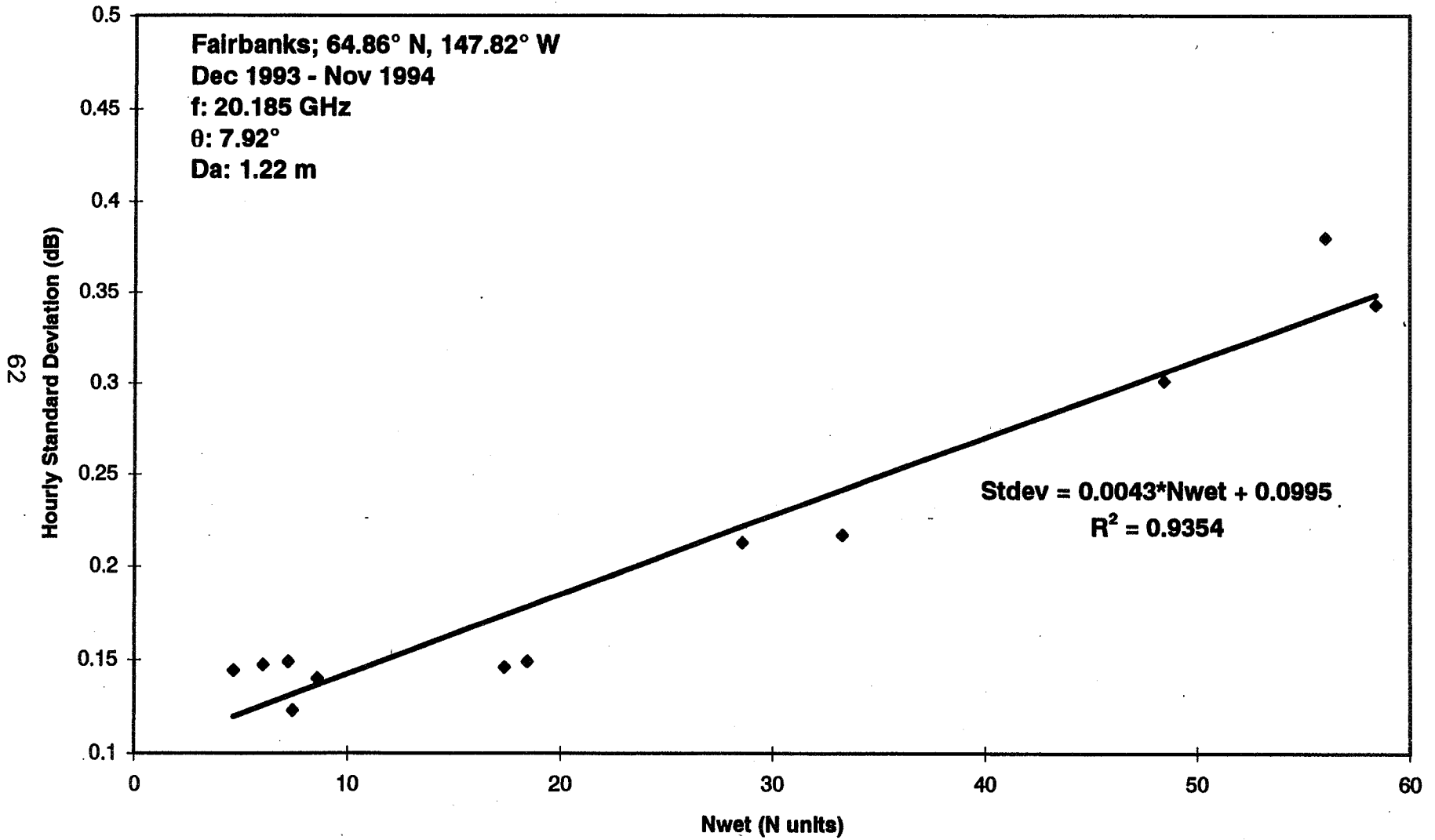


Fig. 14. Linear Regression of Nwet and Hourly Standard Deviation

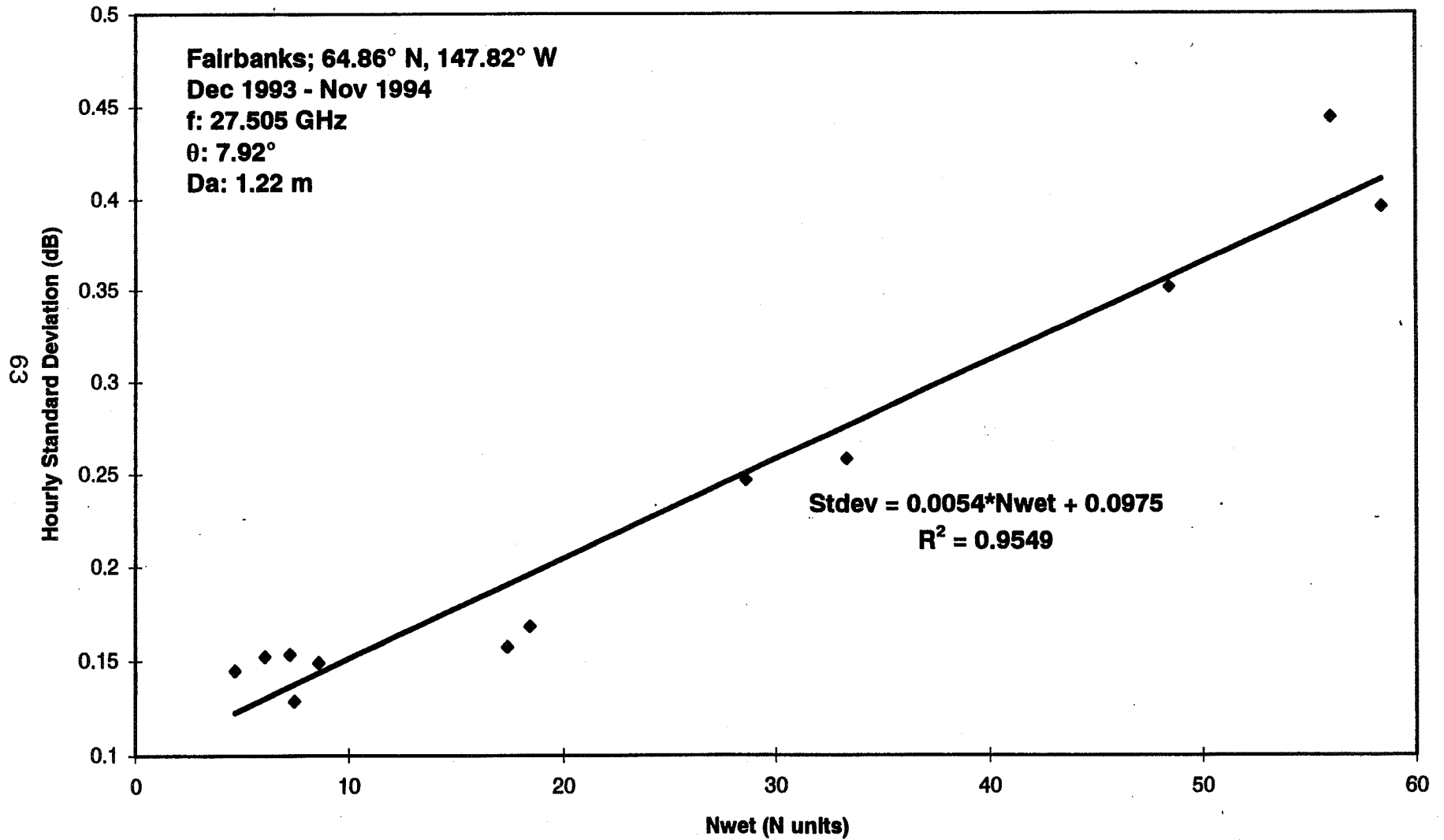


Fig. 15. One Minute Standard Deviation Percentage of Time Functions

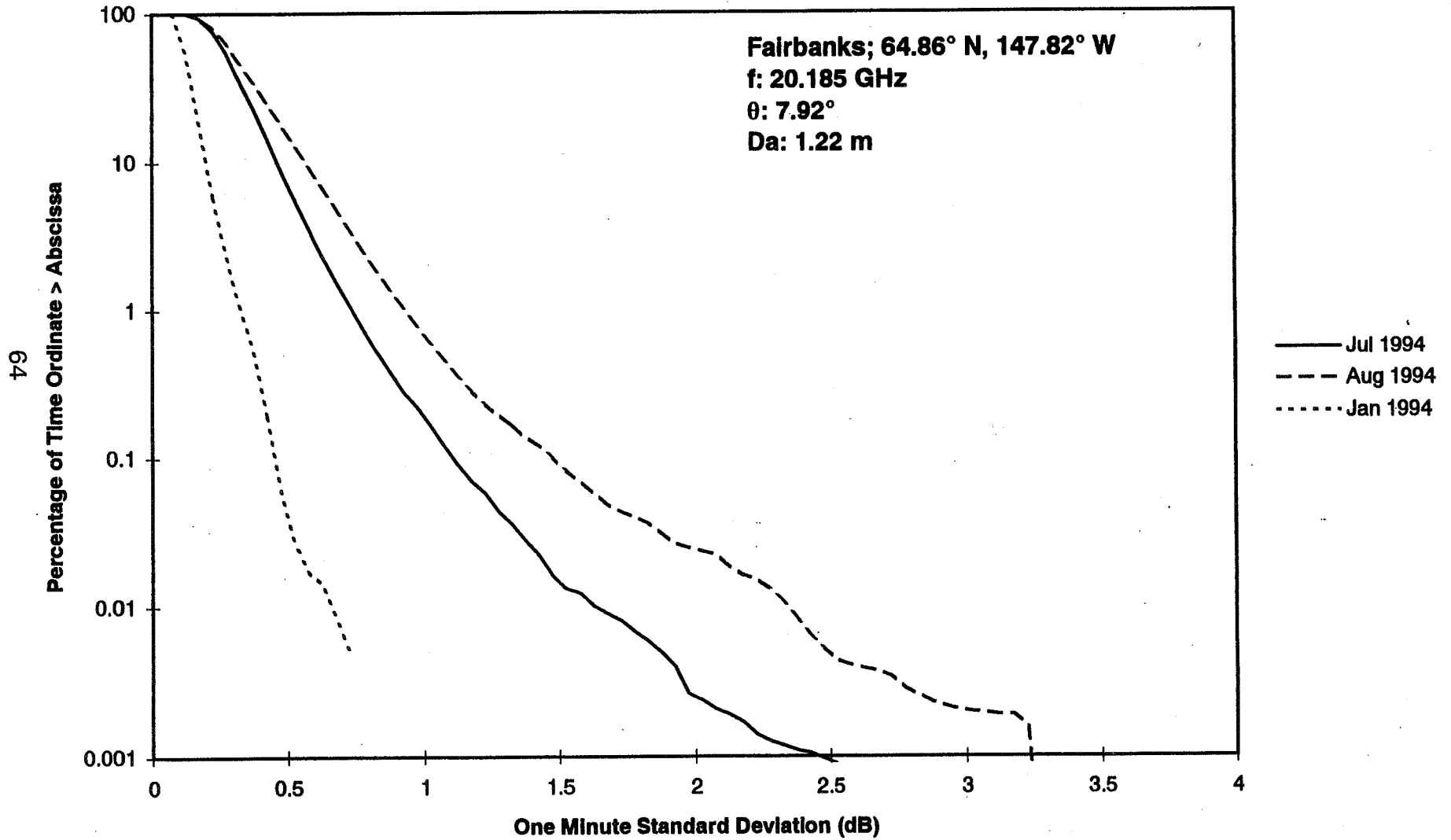


Fig. 16. One Minute Standard Deviation Percent of Time Functions

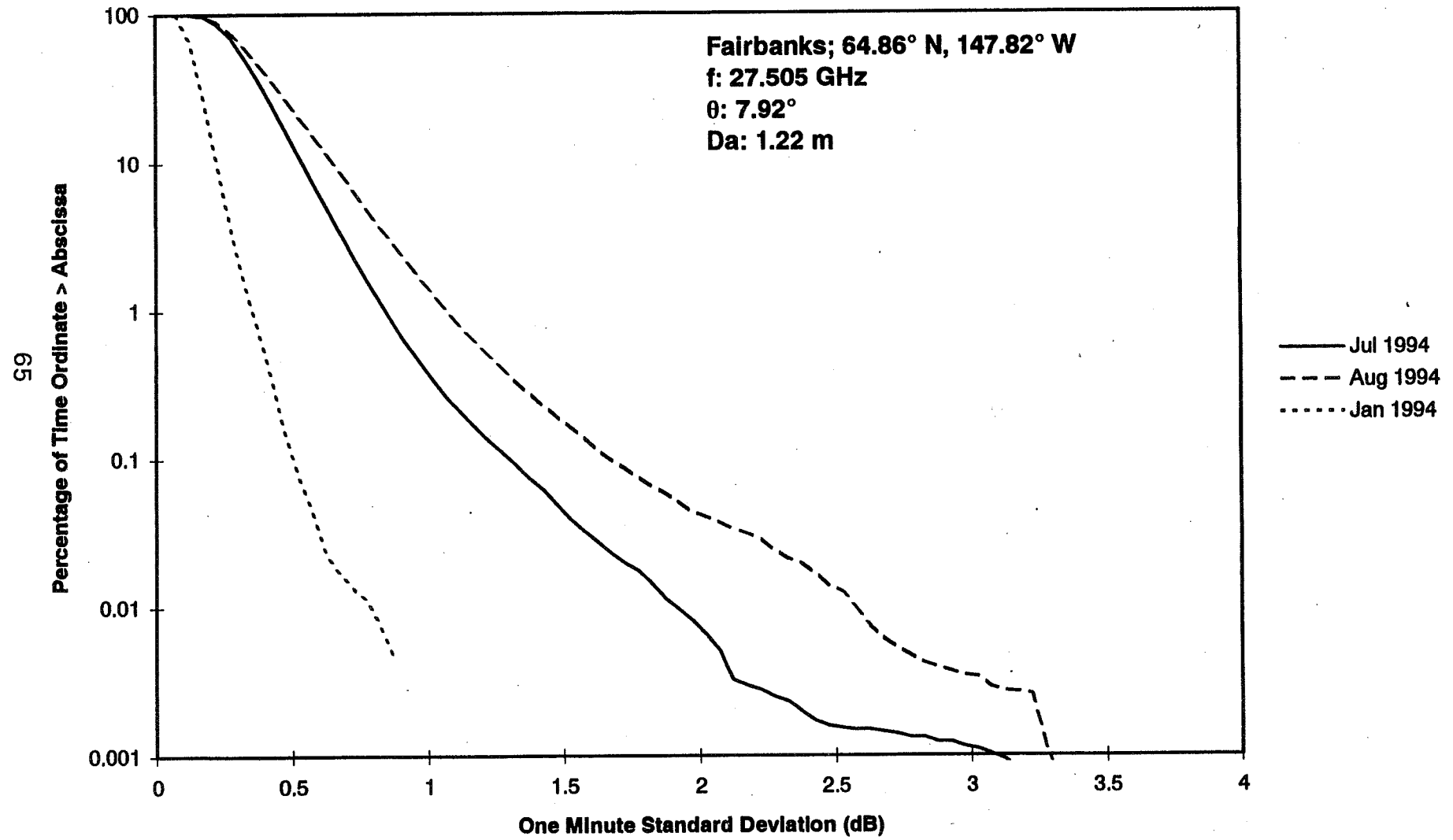
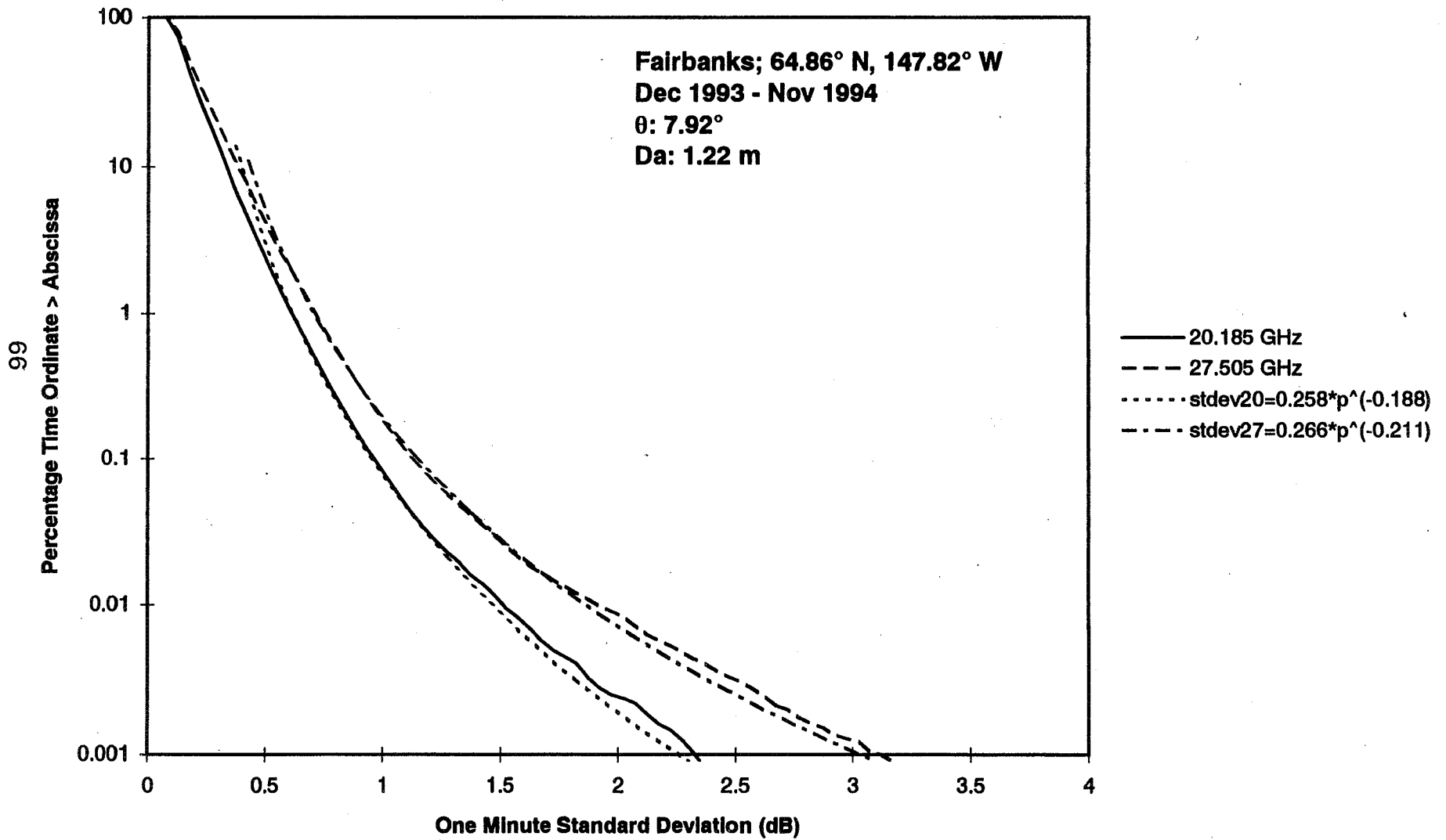


Fig. 17. One Minute Standard Deviation Percent of Time Function



**ANALYSIS OF THE ACTS-VANCOUVER PATH
PROPAGATION DATA**

1st December, 1993 — 30th November, 1995

M. Kharadly

R. Ross

B. Dow

**Department of Electrical Engineering
University of British Columbia**

June, 1996

Outline

1. **Site Description**
2. **Data Description**
3. **Attenuation Due to Wetting of Antenna Surfaces**
4. **Observed (Total) Attenuation Statistics**
5. **Adjusted Attenuation Statistics**
6. **Some Comparisons**
7. **Concluding Remarks**

1. SITE DESCRIPTION

Location

University of British Columbia, Vancouver, Canada

49° 15' N latitude

123° 15' W longitude

Elevation

164.6 metres above mean sea level

Antenna Orientation

Elevation angle: 29.4°

Azimuth: 150° clockwise from true north

Climate

ITU-R rain climatic zone D

Between rain zones B1 and C in Crane's classification

2. DATA DESCRIPTION

The data described here cover a two-year period, 1st December, 1993 to 30th November, 1995. The analysis is done for two sets of valid data:

- (a) observed or total attenuation data, which include all atmospheric effects plus the additional attenuation resulting from wet antenna surfaces during rain events, and
- (b) adjusted attenuation data: the same data as in (a) minus estimated values of attenuation due to wetting of antenna surfaces.

In both cases, average and worst month CDFs, fade-duration statistics and fade-slope statistics for the 20 and 27 GHz beacons are presented.

3. ATTENUATION DUE TO WETTING OF ANTENNA SURFACES

The detailed analysis will be presented in a proposed paper for the Special Issue of the Proceedings of IEEE. The main points are summarized here.

- (i) The surfaces involved are those of the parabolic dish and the membrane covering the feed horn.
- (ii) The theoretical analysis is relatively simple, as it assumes a uniform layer of water on the surfaces. This assumption, however, is far from being representative of a real situation, and the corresponding results can only serve as a guideline, Figs. 1 to 3.
- (iii) Since the effect of wetting depends on many factors (e.g., elevation angle, type and condition of surface, rain rate, drop-size distribution, wind speed and direction, temperature, humidity, etc.), some experimental input was, therefore, considered necessary.
- (iv) Experiments were conducted on clear days using a variety of nozzles pointing upwards and producing showers of different intensity and drop size, which fell on the antenna structure.
- (v) The resulting attenuation time series depicts certain characteristics (e.g., Fig 4). The average attenuation did not, however, exceed about 3 dB for the 20 GHz signal and 4 dB for the 27 GHz signal.

- (vi) Proposed models for incorporating this phenomenon in the analysis were used to separate out the effect of surface wetting, and obtain the adjusted attenuation values due to atmospheric factors only.

4. OBSERVED (TOTAL) ATTENUATION STATISTICS

The data considered in this section are those directly derived from the observations, without adjustment for the effect of antenna wetting. Only examples of the statistics are shown here.

4.1 Cumulative Distribution Functions (CDFs)

Fig. 5 shows the two-year average for the 20 GHz and 27 GHz signals. The results of frequency scaling between the two frequencies, as described in ITU-R rev. rec. 618-1, are also shown in this figure. Fig. 6 depicts the worst-month statistics.

4.2 Fade-duration Statistics

These are shown in Figs. 7 and 8 for the average month in the two-year period for various thresholds and a block-averaging period that includes 11 samples at one second intervals for the 20 GHz and 27 GHz signals, respectively. The corresponding statistics for the worst month are shown in Figs. 9 and 10.

4.3 Fade-slope Statistics

The fade slopes are calculated by the method proposed by the European Space Agency. The statistics are shown in Figs 11 and 12 for the average month in the two-year period, for the same thresholds and block-averaging period as in 4.2. The corresponding worst-month statistics are shown in Figs. 13 and 14.

5. ADJUSTED ATTENUATION STATISTICS

These are the statistics derived by taking into consideration the effect of antenna-surface wetting. They are shown in Figs. 15 to 24, in the same order as in Section 4.

6. SOME COMPARISONS

This section presents the statistics shown in sections 4 and 5 in a manner which will demonstrate the effects of adjustment due to antenna-surface wetting and average versus worst-month statistics.

6.1 Cumulative Distribution Functions (CDFs)

Figs. 25 and 26 compare unadjusted and adjusted CDFs for the two-year average and for the worst month, respectively. The unadjusted two-year average-month and worst-month CDFs are compared in Fig. 27 while the same comparison for adjusted values is presented in Fig. 28.

6.2 Fade-duration Statistics

The unadjusted and adjusted statistics for the 3 dB threshold and 11-sample block-average for the average month are compared in Fig. 29 for the 20 GHz signal. The same comparison for worst-month statistics is shown in Fig. 30. Fig. 31 presents the comparison between unadjusted average-month and worst-month statistics for the same threshold and block averaging period for 27 GHz. The same comparison for adjusted statistics is shown in Fig. 32.

6.3 Fade-slope Statistics

Similar comparisons showing the effects of antenna-surface wetting on fade-slope statistics are presented in Figs. 33 through 36. The same threshold and block-averaging period is used as for the fade-duration statistics.

7. CONCLUDING REMARKS

7.1 Scope of the analysis

The statistics presented are for the period 1st December, 1993 to 30th November, 1995. These include average and worst-month statistics pertaining to the CDFs, fade duration and fade slopes.

7.2 Effect of moisture on the antenna surfaces

Statistics, similar to those in 7.1, are also presented, where the effect of antenna-surface wetting during rain events is taken into consideration in an approximate manner. It is shown that moisture clinging to antenna surfaces can significantly affect propagation-data statistics. It must be emphasized, however, that this effect depends on antenna type and conditions at the receiving site.

- (i) The ITU-R frequency-scaling model appears to apply more closely to the adjusted values rather than the unadjusted.
- (ii) For fade duration, the number of events for any particular duration is almost an order of magnitude lower using the adjusted results than for the unadjusted.
- (iii) The fade-slope statistics show a similar trend as for fade duration.

7.3 New designs for Ka-band antennas

There appears to be a need for developing Ka-band antennas which do not suffer from the effect of moisture on their surfaces. This is particularly important for systems with low fade margin. The development of such antennas is not only possible but also feasible.

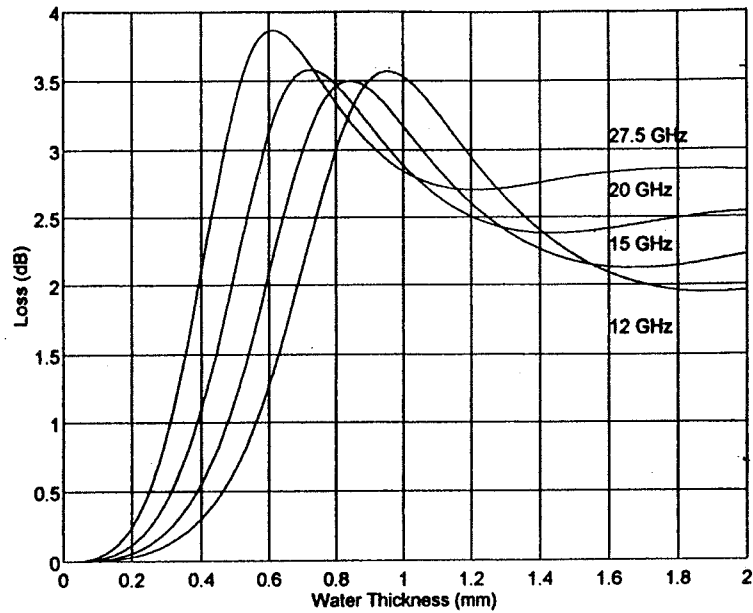


Fig. 1: Reflection Loss from Dish

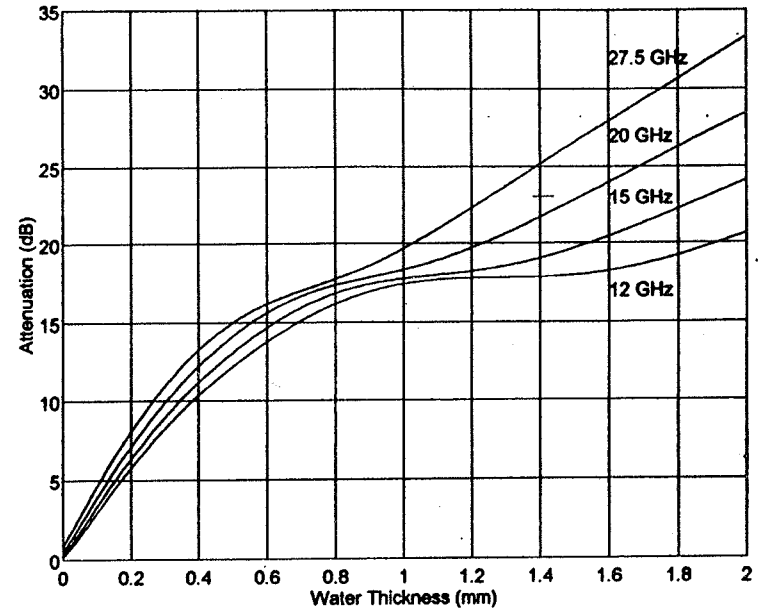


Fig. 2: Total Loss through Membrane

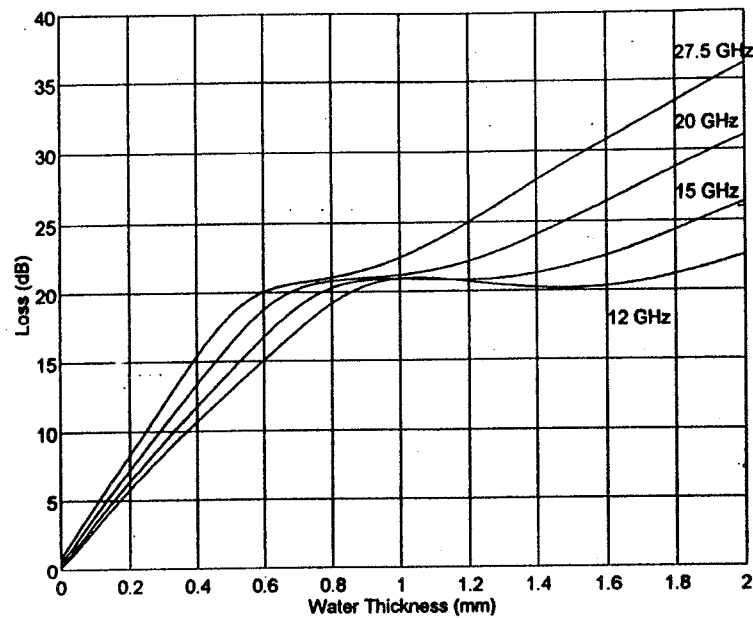


Fig. 3: Total Loss due to Water on Both Dish and Membrane

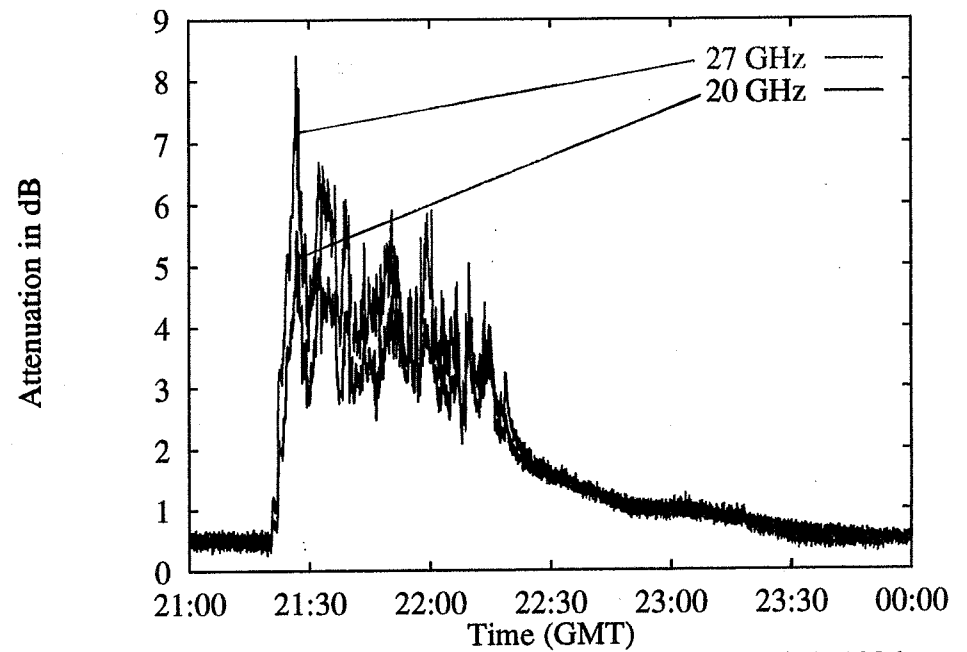


Fig. 4: Antenna Wetting Experiment on March 1, 1996

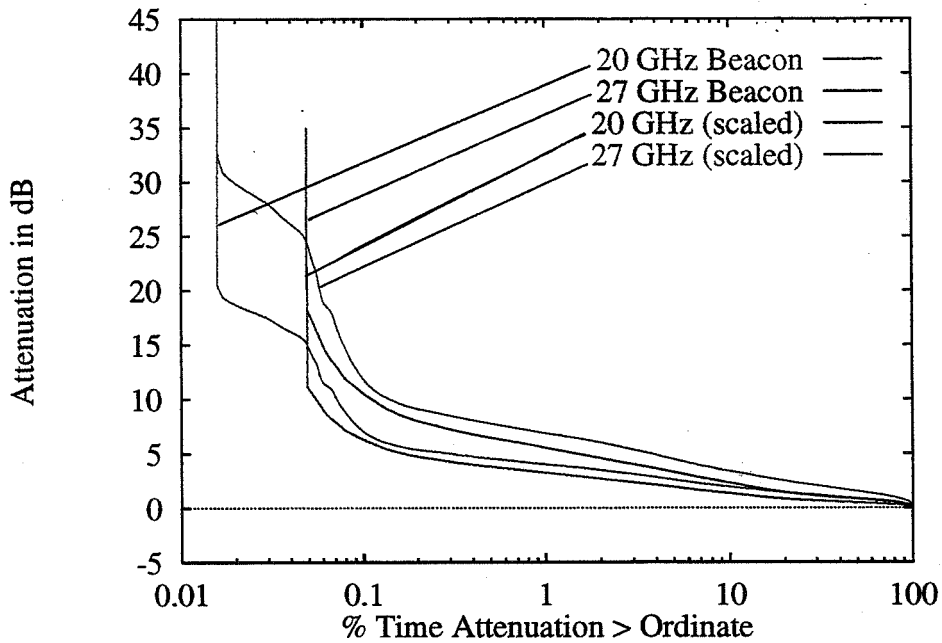


Fig. 5: 9312-9511 Unadjusted CDFs

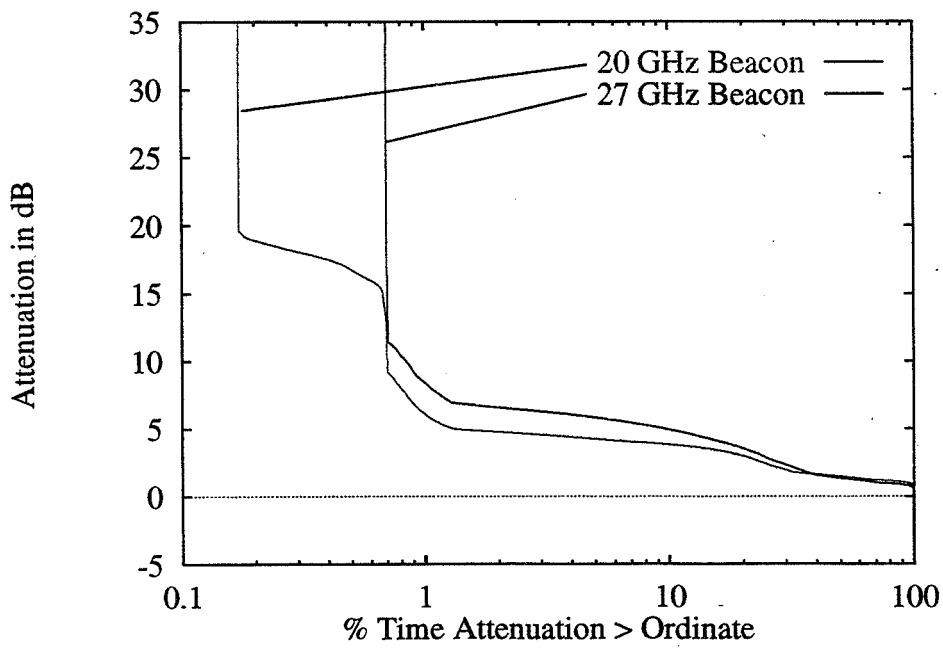


Fig. 6: 9312-9511 Worst-Month Unadjusted CDFs

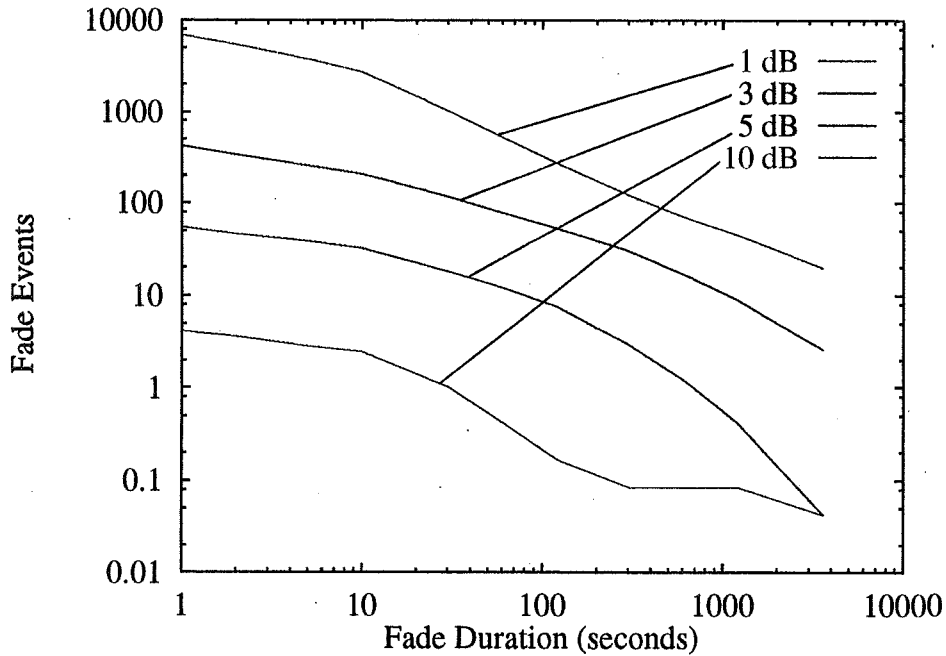


Fig. 7: 9312-9511, Avg-Month, 20 GHz, Block Width 11

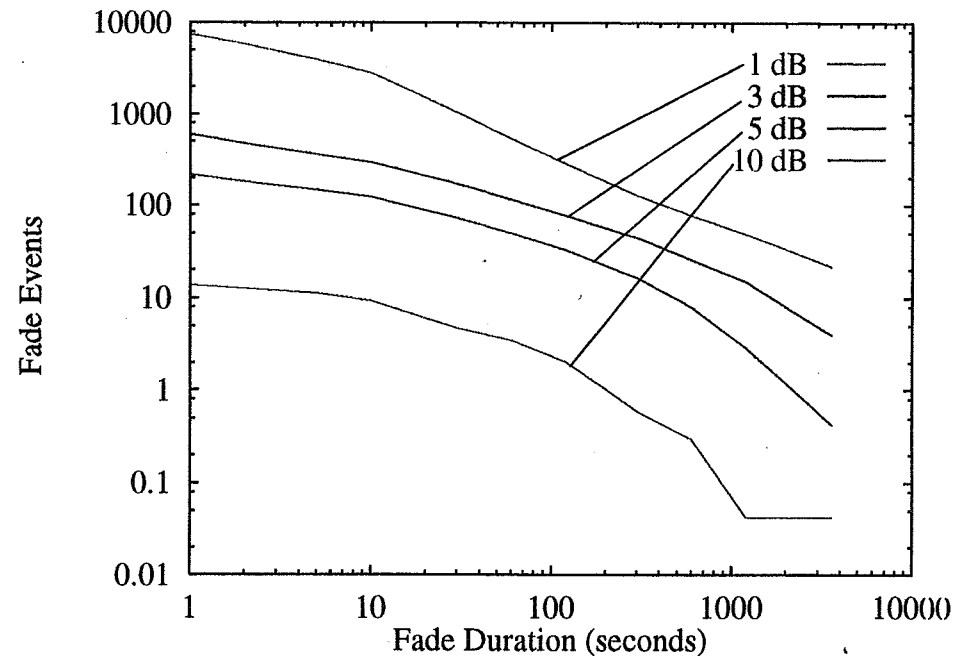


Fig. 8: 9312-9511, Avg-Month, 27 GHz, Block Width 11

97

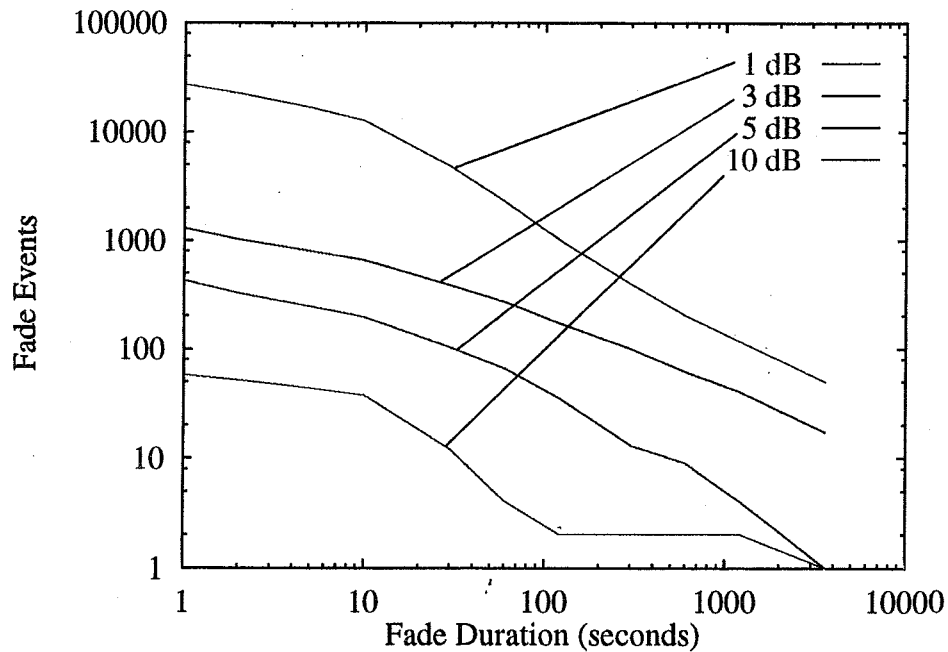


Fig. 9: 9312-9511, Worst-Month, 20 GHz, Block Width 11

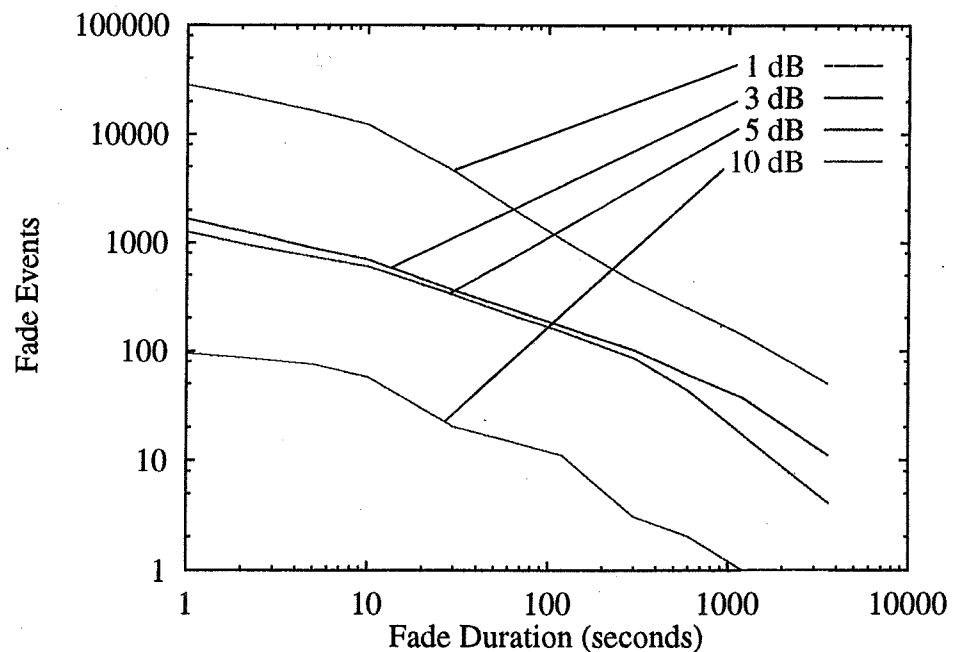


Fig. 10: 9312-9511, Worst-Month, 27 GHz, Block Width 11

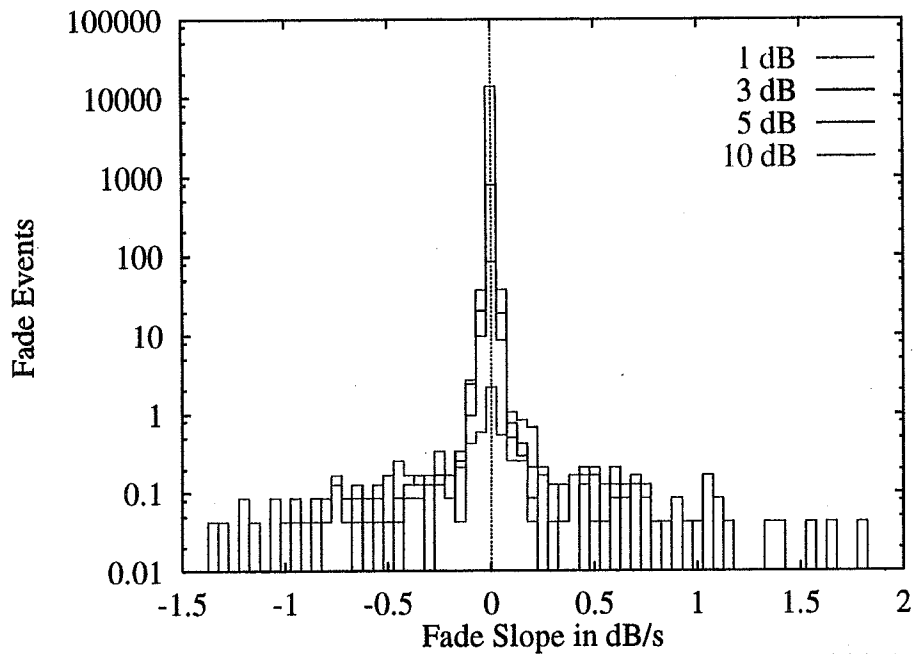


Fig. 11: 9312-9511, Avg-Month, 20 GHz, Block Width 11

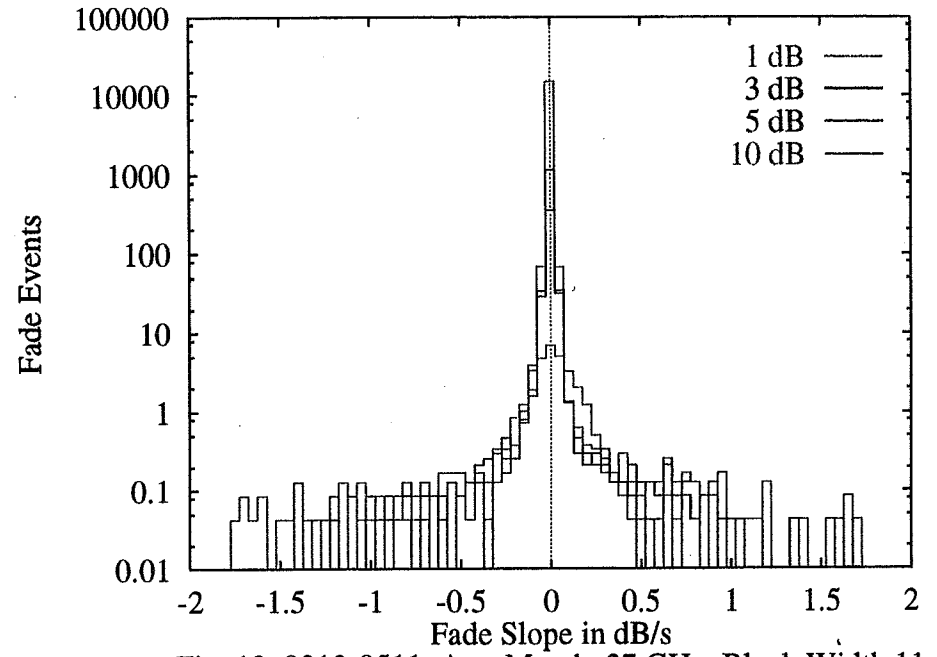


Fig. 12: 9312-9511, Avg-Month, 27 GHz, Block Width 11

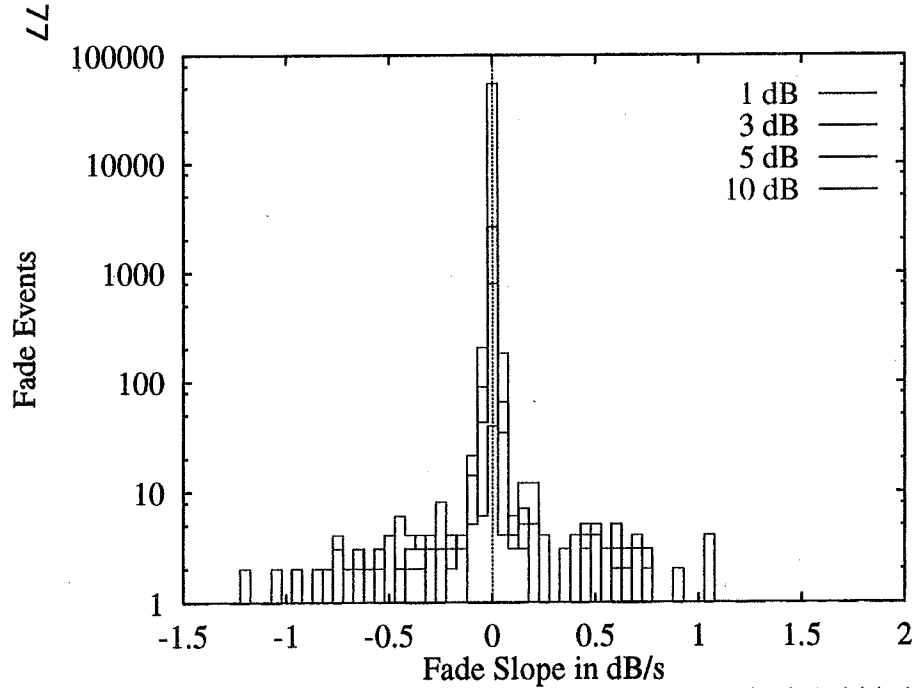


Fig. 13: 9312-9511, Worst-Month, 20 GHz, Block Width 11

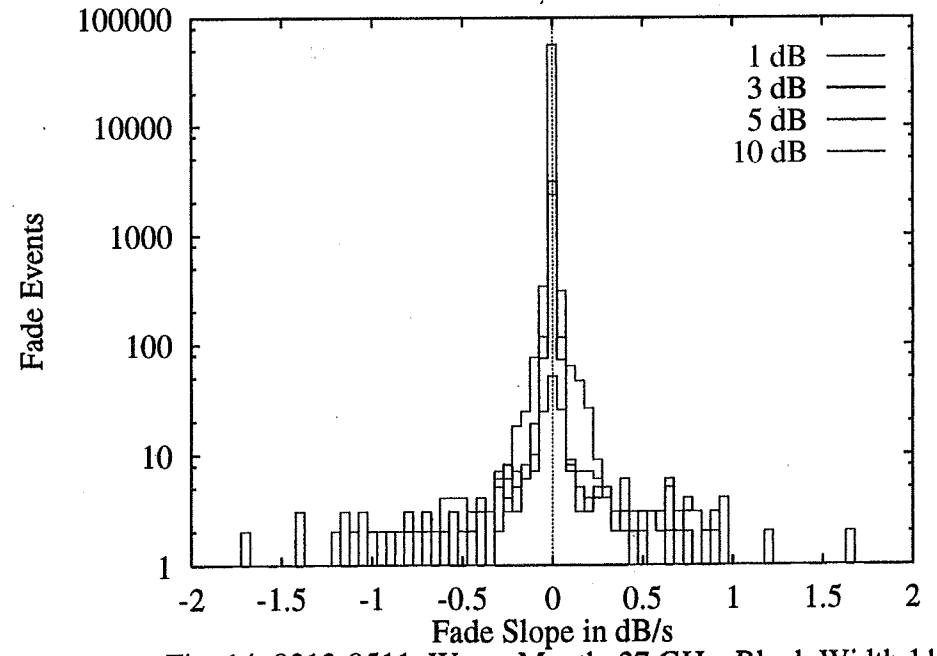


Fig. 14: 9312-9511, Worst-Month, 27 GHz, Block Width 11

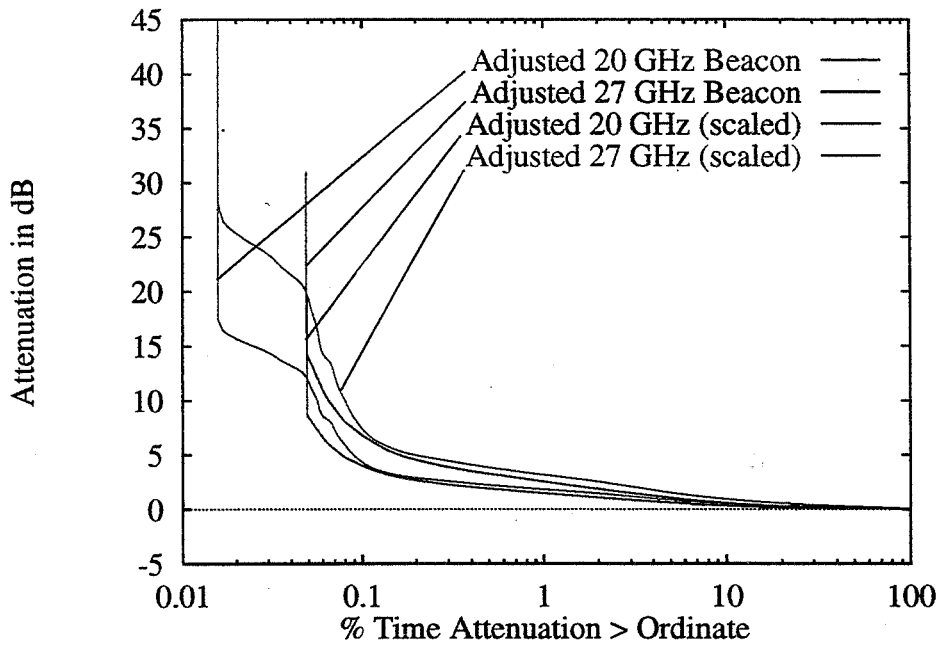


Fig. 15: 9312-9511 Adjusted CDFs

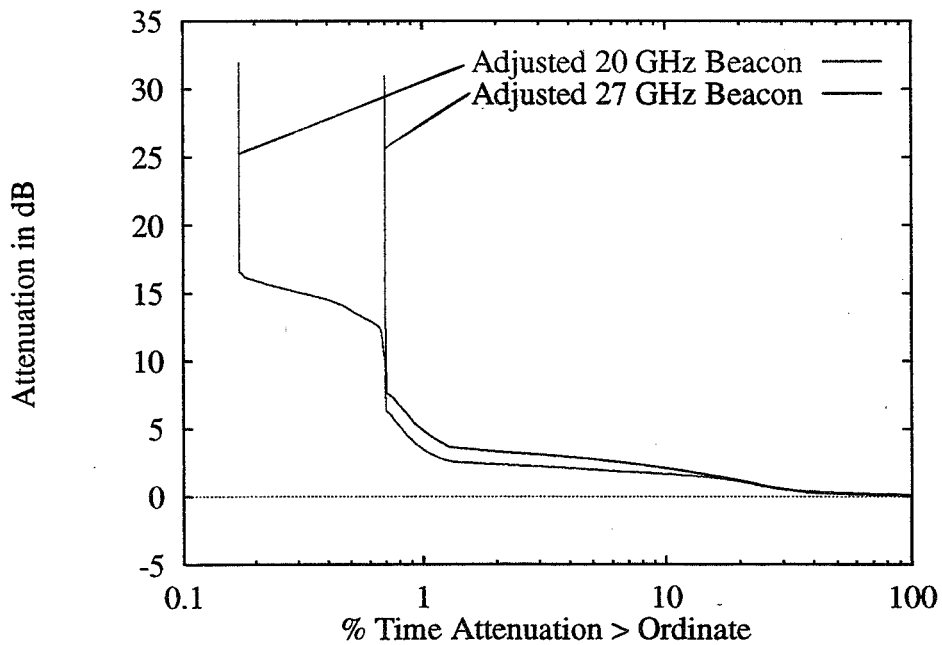


Fig. 16: 9312-9511 Worst-Month Adjusted CDFs

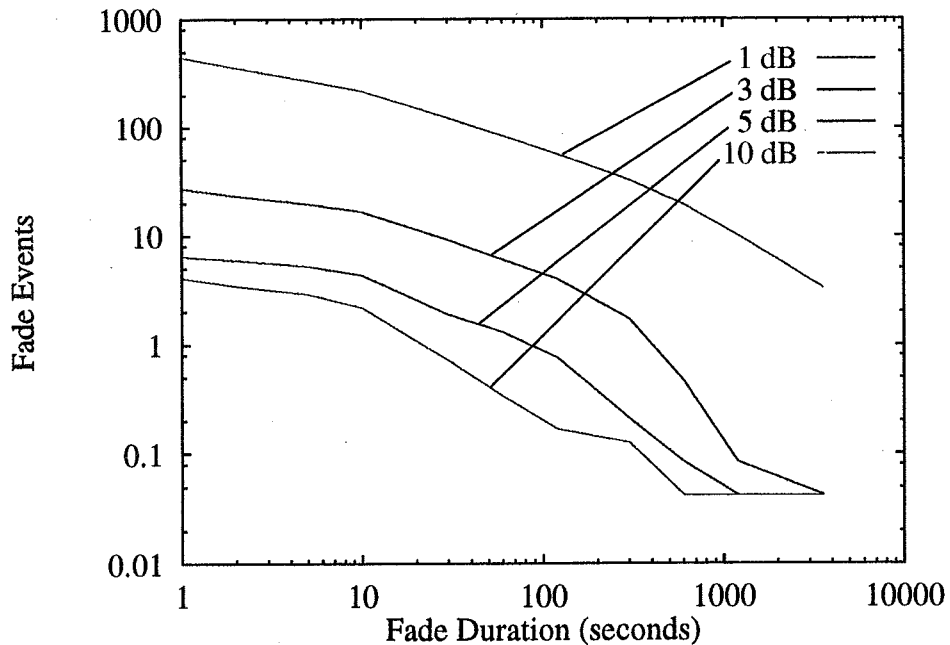


Fig. 17: 9312-9511, Adjusted, Avg-Month, 20 GHz, Block Width 11

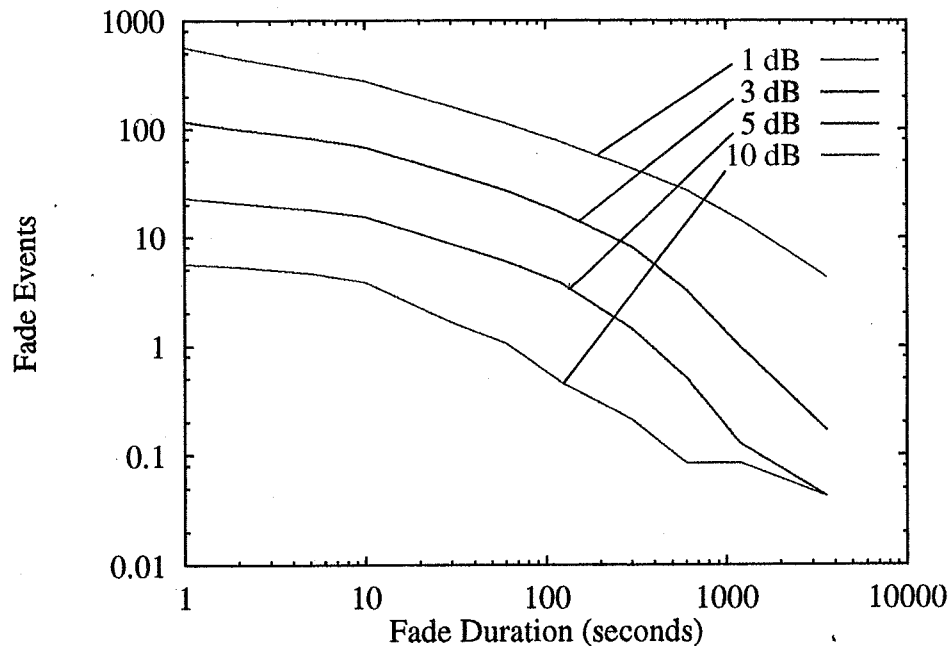


Fig. 18: 9312-9511, Adjusted, Avg-Month, 27 GHz, Block Width 11

67

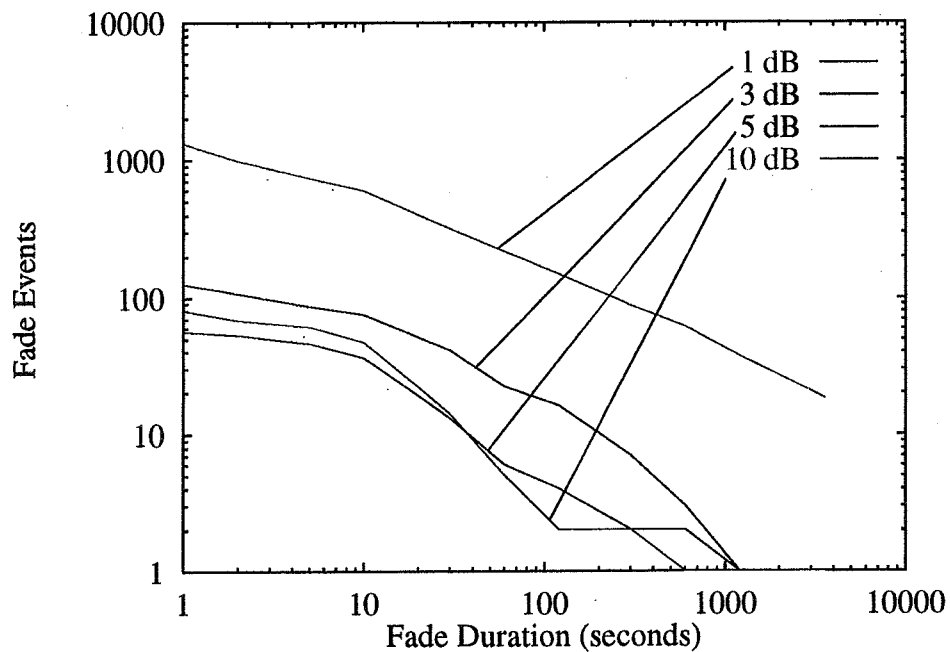


Fig. 19: 9312-9511, Adjusted, Worst-Month, 20 GHz, Block Width 11

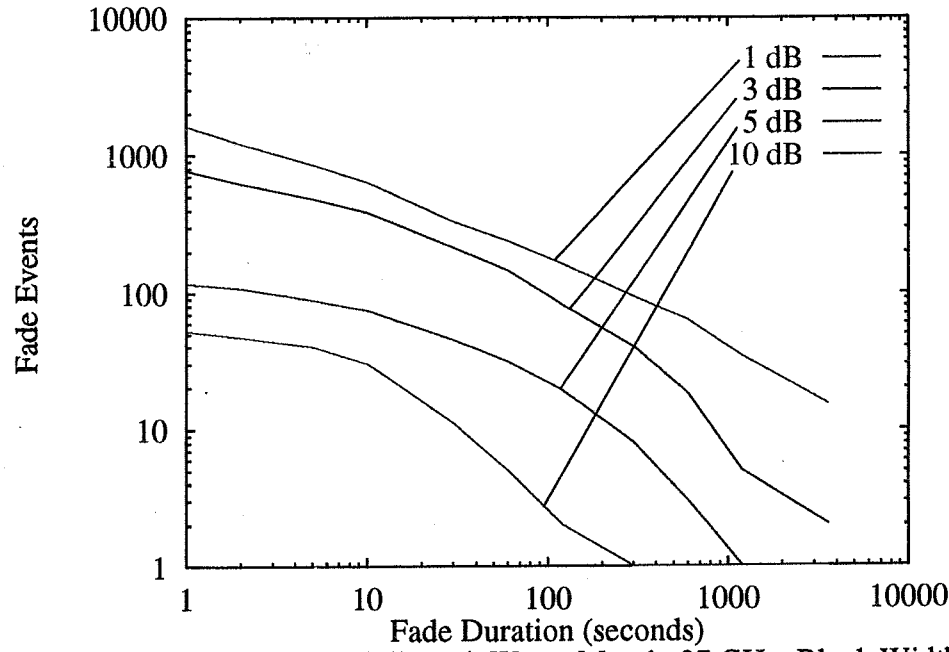


Fig. 20: 9312-9511, Adjusted, Worst-Month, 27 GHz, Block Width 11

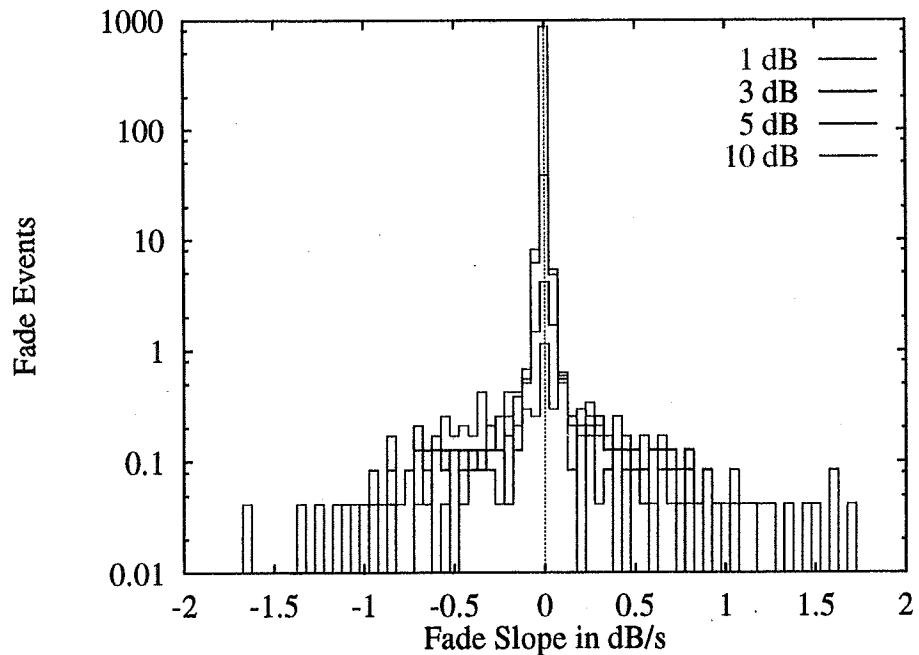


Fig. 21: 9312-9511, Adjusted, Avg-Month, 20 GHz, Block Width 11

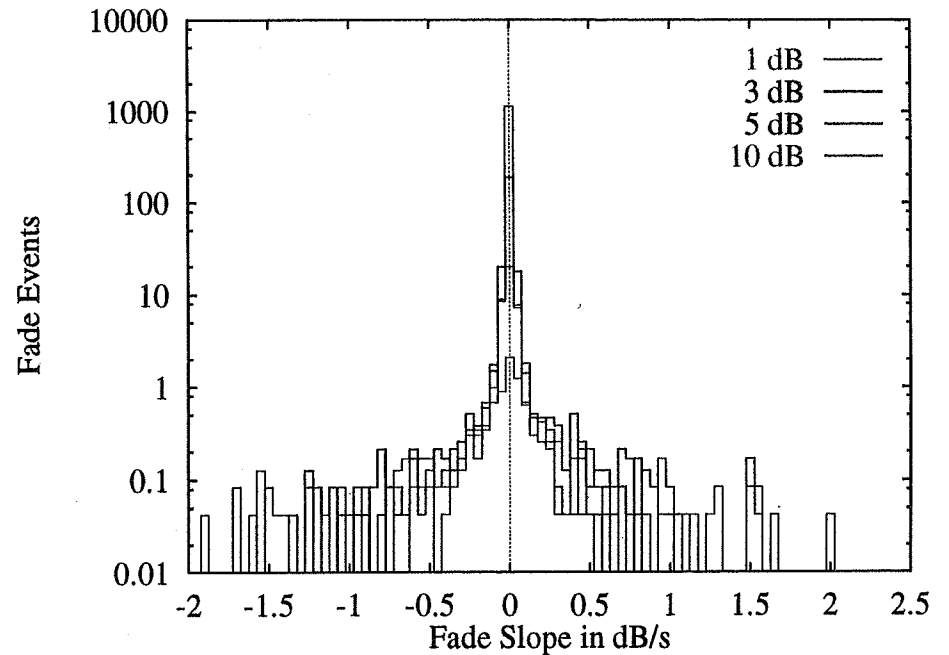


Fig. 22: 9312-9511, Adjusted, Avg-Month, 27 GHz, Block Width 11

08

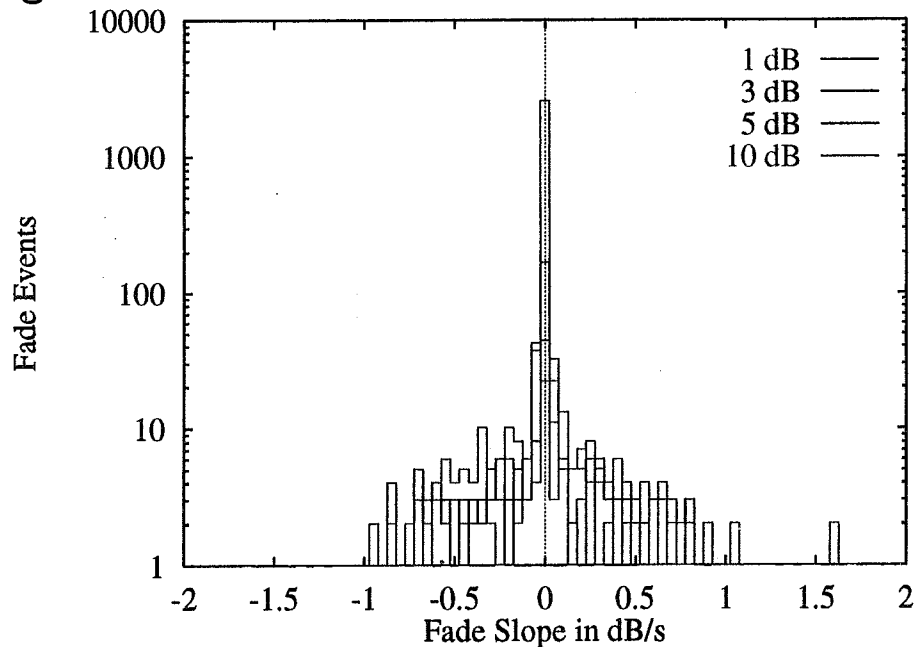


Fig. 23: 9312-9511, Adjusted, Worst-Month, 20 GHz, Block Width 11

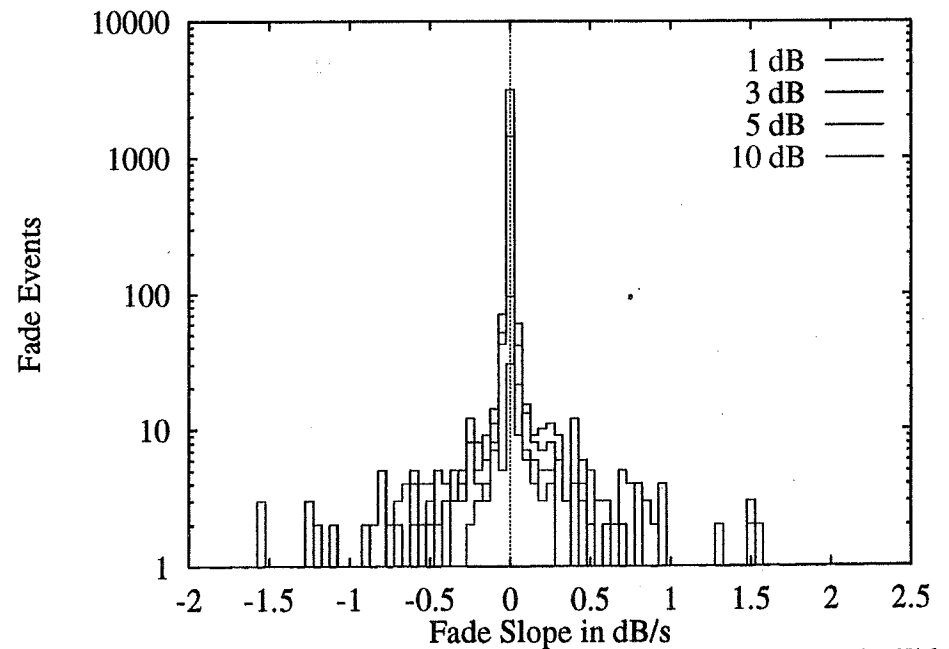
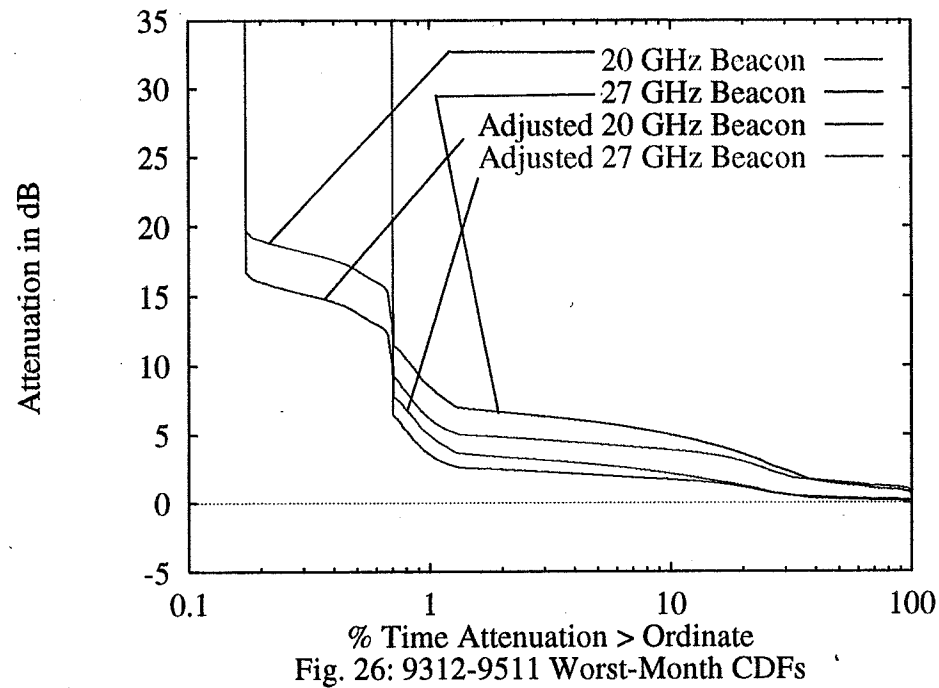
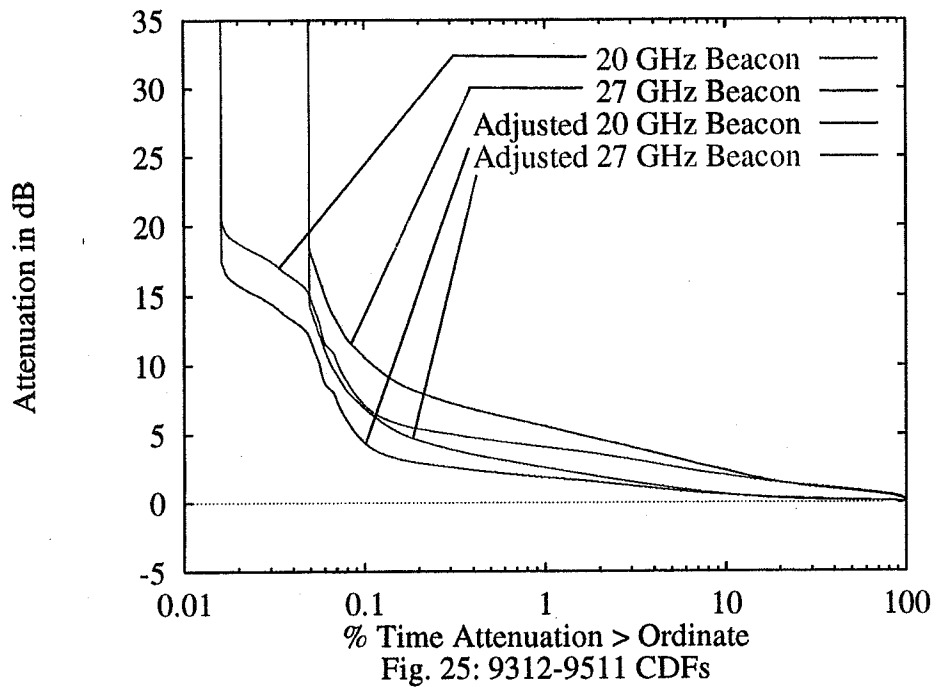
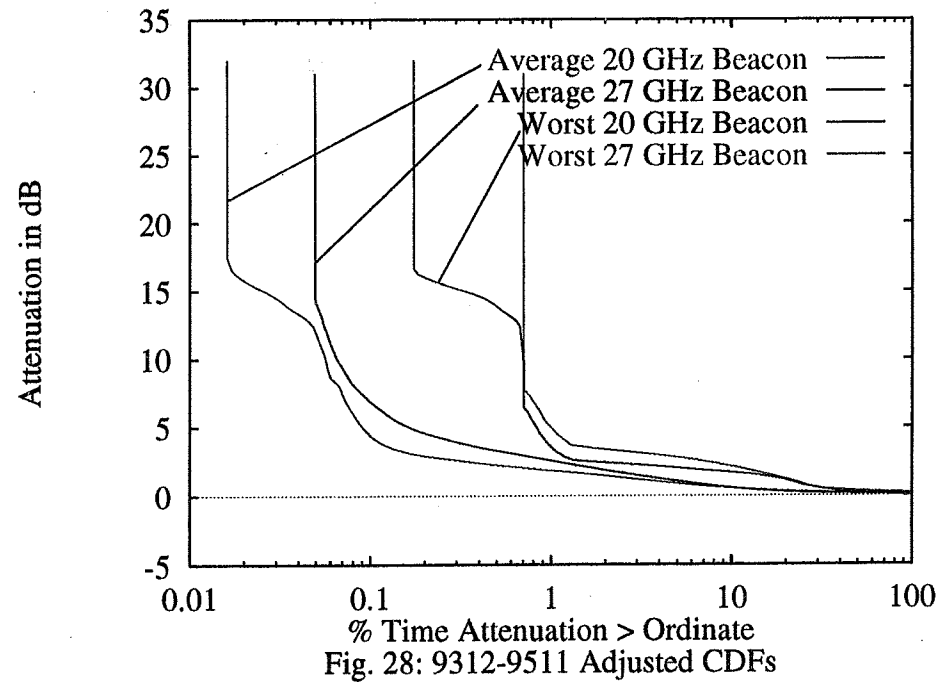
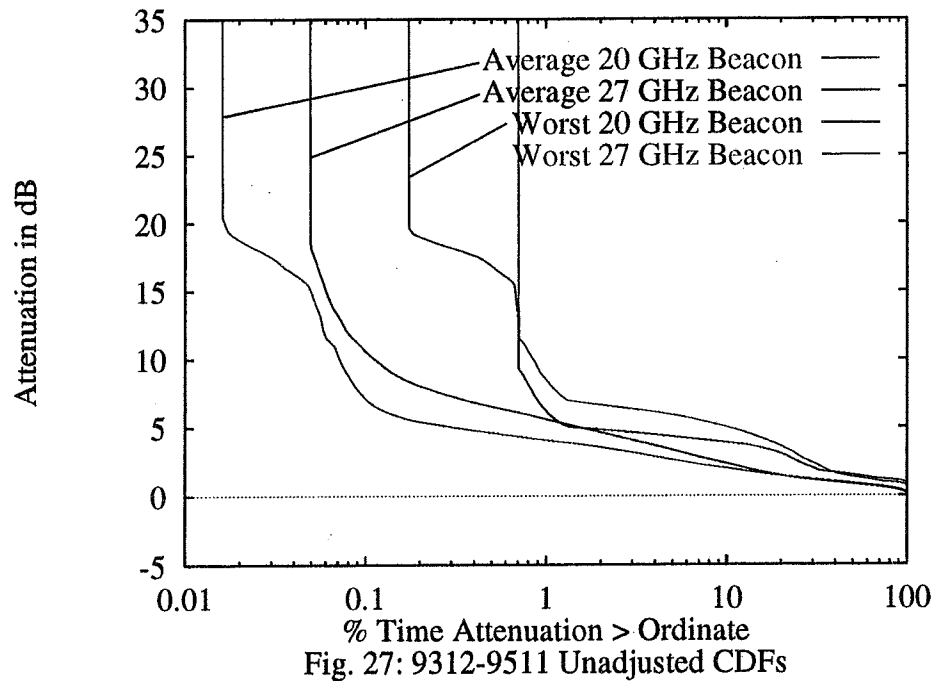


Fig. 24: 9312-9511, Adjusted, Worst-Month, 27 GHz, Block Width 11



18



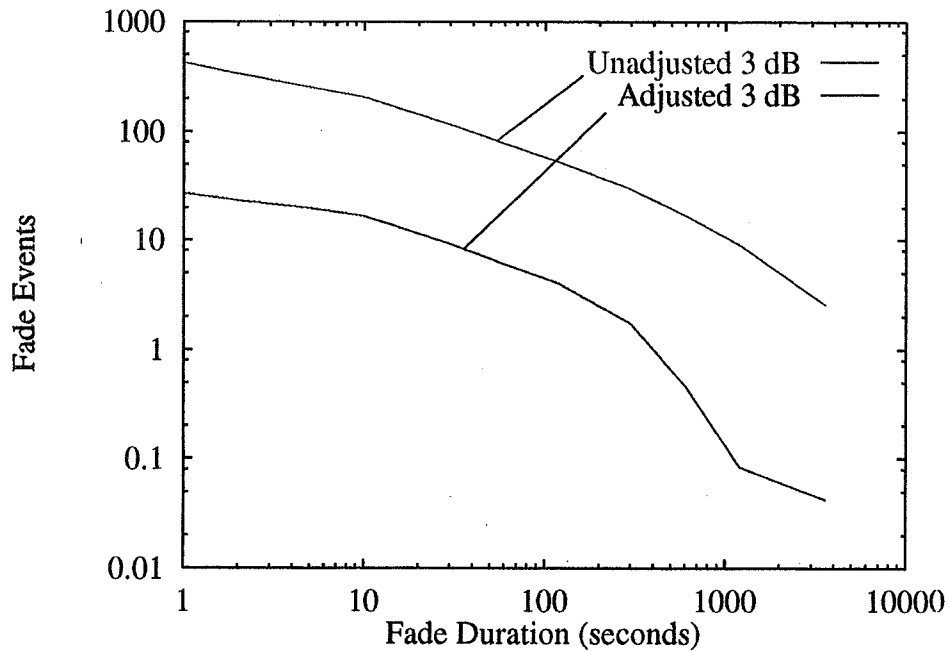


Fig. 29: 9312-9511, Avg-Month, 20 GHz, Block Width 11

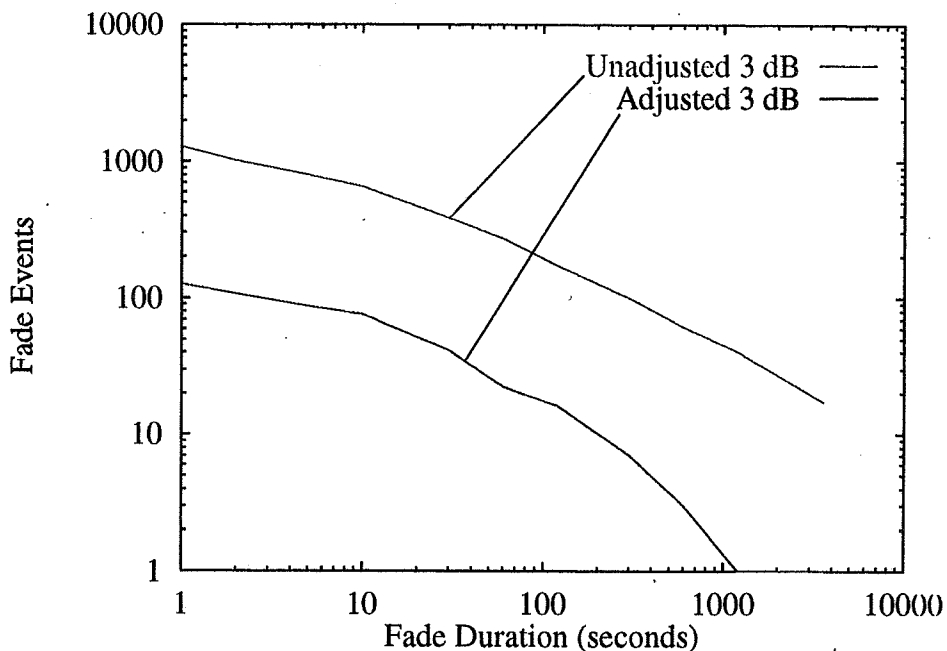


Fig. 30: 9312-9511, Worst-Month, 20 GHz, Block Width 11

82

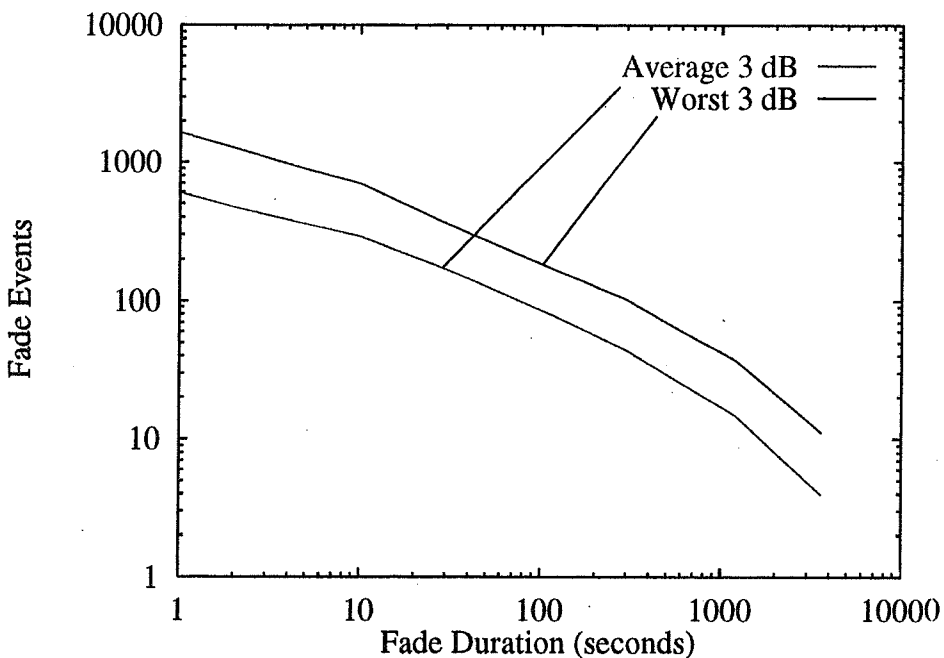


Fig. 31: 9312-9511, Unadjusted, 27 GHz, Block Width 11

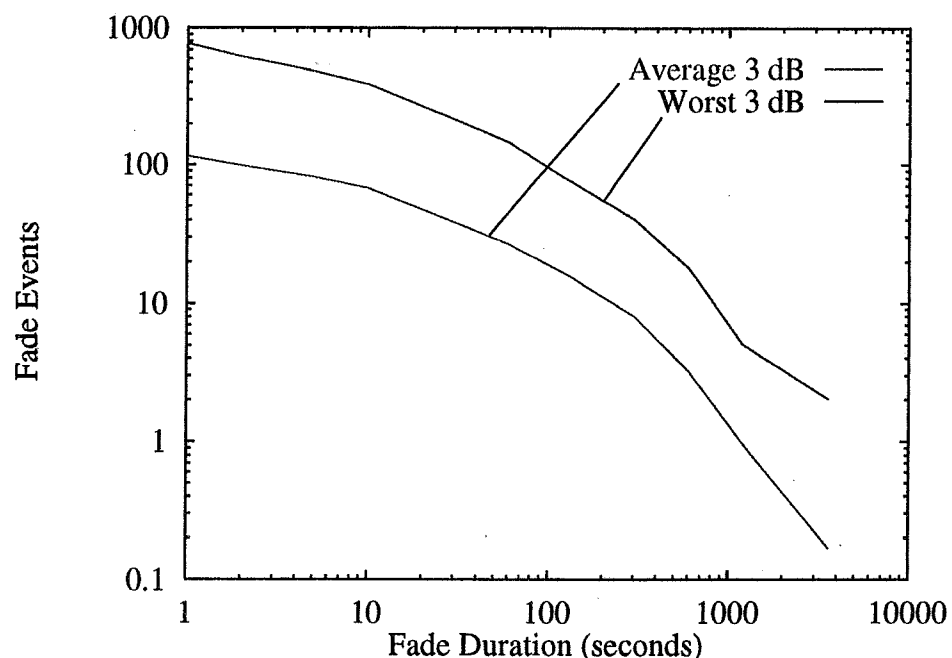


Fig. 32: 9312-9511, Adjusted, 27 GHz, Block Width 11

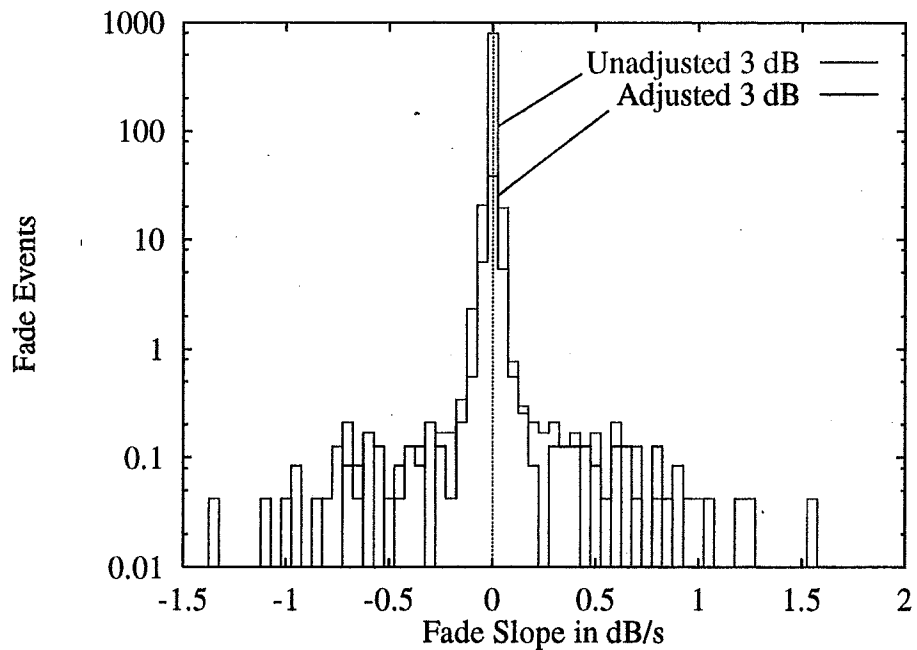


Fig. 33: 9312-9511, Avg-Month, 20 GHz, Block Width 11

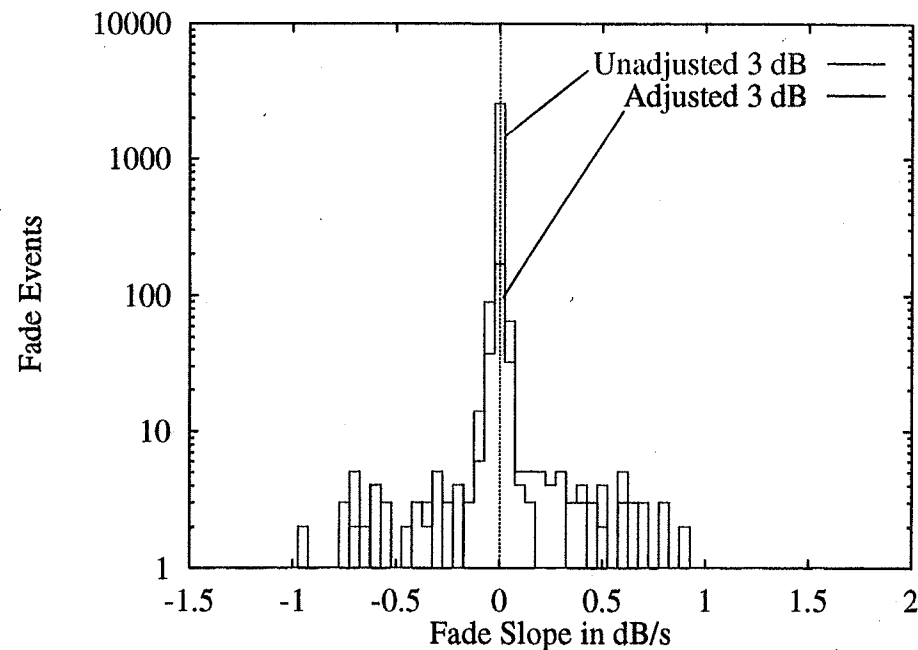


Fig. 34: 9312-9511, Worst-Month, 20 GHz, Block Width 11

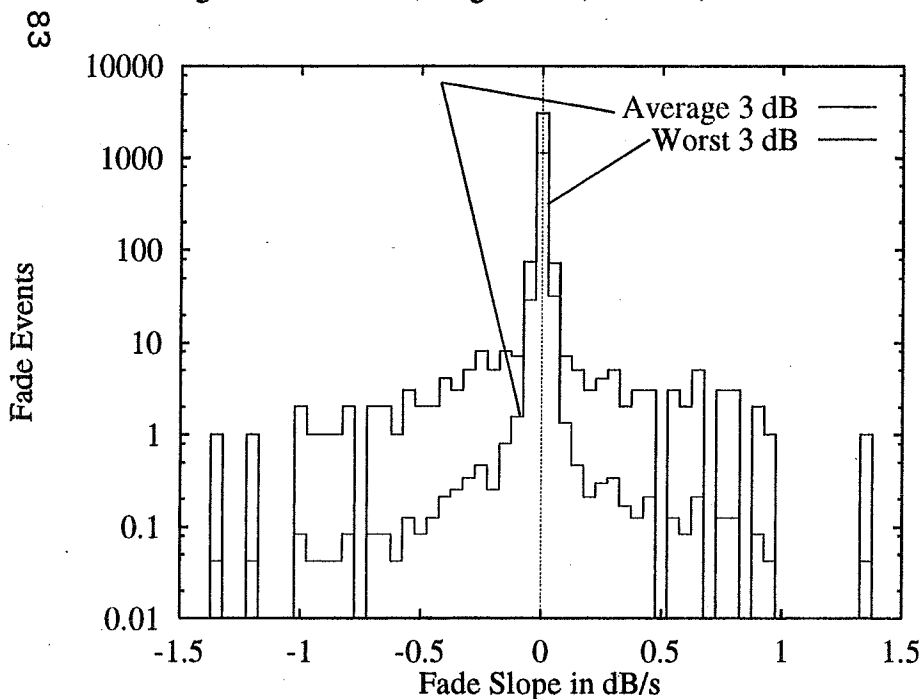


Fig. 35: 9312-9511, Unadjusted 27 GHz, Block Width 11

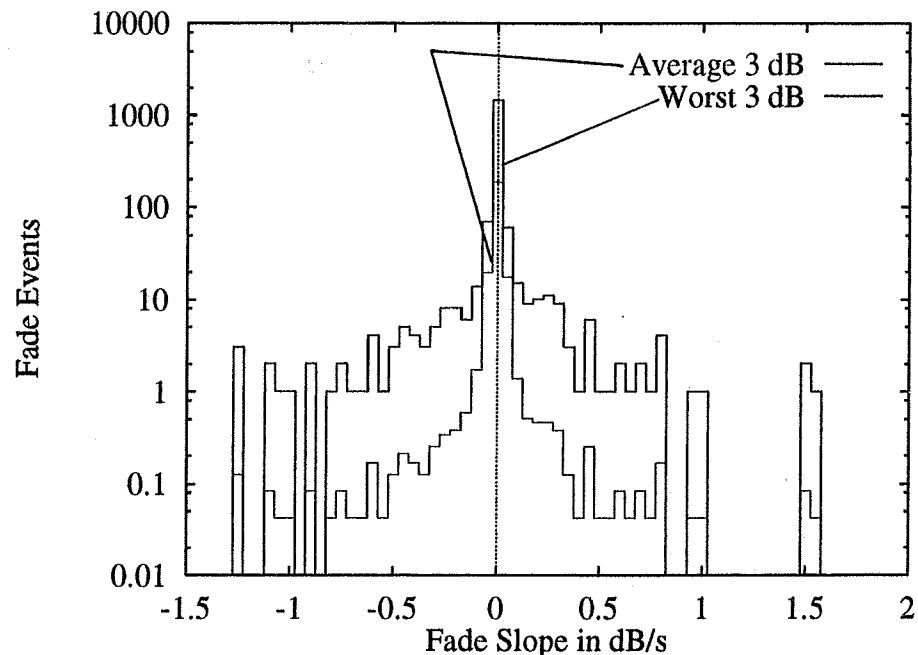


Fig. 36: 9312-9511, Adjusted 27 GHz, Block Width 11

Page intentionally left blank

**Ka-Band Propagation Studies Using the ACTS
Propagation Terminal and the CSU-CHILL
Multiparameter Radar**

(A Two Year Report)

Experimenters

Colorado State University
Department of Electrical Engineering
Ft. Collins, CO 80523

Investigators

V. N. Bringi, Professor
John Beaver

**NASA Propagation Experimenters Meeting
(NAPEX XX)
June 4-6, 1996
Fairbanks, Alaska**

Contents

1	Introduction	2
2	Statistical Attenuation Analysis at Ka-Band	3
2.1	CSU-ACTS Propagation Data	4
2.2	Description of Statistical Quantities	5
3	CSU-CHILL Polarimetric Radar Data	7
3.1	Radar Description	7
3.2	Radar Observables	7
3.3	Attenuation Estimates	10
4	Concurrent CSU-APT and CSU-CHILL Measurements	12
4.1	Attenuation Events	13
4.2	Attenuation Estimates	19
5	Conclusions	27
A	Statistical Results for Analysis Period of December 1, 1993 through November 30, 1995	28
A.1	Monthly Analysis for December 1, 1993 through November 30, 1994	29
A.2	Annual Results for December 1, 1993 through November 30, 1994	84
A.3	Monthly Analysis for December 1, 1994 through November 30, 1995	93
A.4	Annual Results for December 1, 1994 through November 30, 1995	150
A.5	Monthly and Annual CDF Comparisons for 1994 and 1995 . .	159

1 Introduction

There has been an increased interest in utilizing the Ka-band frequency spectrum from industry. Currently several industry leaders are in the process of setting up satellite communication systems that operate at the Ka-band frequencies or already have systems in place. The increased interest in operating such systems at the Ka-band frequencies is mainly due to overcrowding of the current spectrums at C- and Ku-bands. Of course, other benefits exist such as an increase in data transmission rates, an increase in the amount of information that is being transmitted and smaller Earth receiving stations which leads to greater mobility. However, along with the benefits there are some disadvantages of operating at these frequencies, such as increased attenuation effects due to the atmospheric conditions.

One of the attractive features that led to the use of C- and Ku-bands for satellite communications was the low susceptibility to attenuation effects caused by rain or clouds. The larger wavelengths are minimally affected by the atmospheric conditions. The Ka-band frequencies, however are very susceptible to weather-related events. Rain, clouds and even gaseous absorption by oxygen and water vapor can adversely affect the signal and must be considered. Rain can easily produce 20 to 30 dB of attenuation at the Ka-band frequencies. For space-to-Earth links with low elevation angles, tropospheric scintillations can also cause appreciable attenuation. Therefore, before being used commercially, propagation effects at Ka-band must be studied.

One of the first experimental communication satellites using Ka-band technology is the National Aeronautics and Space Administration's (NASA) Advanced Communications Technology Satellite (ACTS). In September 1993, ACTS was deployed into a geostationary orbit near 100° W longitude by the space shuttle Discovery. The ACTS system supports both communication and propagation experiments at the 20/30 GHz frequency bands. The propagation experiment involves multi-year attenuation measurements along the satellite-Earth slant path.

Colorado State University (CSU) and six other sites across the United States and Canada are conducting the propagation studies. Each site is equipped with the ACTS propagation terminal (APT). The APT's were designed and built by Virginia Tech's Satellite Communications Group [8] and

are receive only Earth stations. Each site is located in a different climatic zone, with CSU in the newly designated B2 climate zone. In addition to the Colorado site, other propagation sites include British Columbia, Alaska, New Mexico, Oklahoma, Florida and Maryland.

The overall goal for the propagation experiment is to obtain high quality attenuation measurements in order to construct a data base so that the attenuation effects at Ka-band frequencies can be statistically characterized. This statistical analysis is to be done on a monthly and annual basis. The monthly resolution makes this study a unique one as most attenuation statistics available today are on an annual basis. This is also true for most of the statistical models available to date.

In addition to the overall goal, each site is applying its own expertise to secondary studies. CSU's contribution is the application of polarimetric radar data for attenuation prediction. Radar data taken by the CSU-CHILL fully polarimetric, multiparameter Doppler radar is used to gain a greater understanding of the microphysical processes that are responsible for Ka-band attenuation that occurs along the ACTS slant path. Radar data are used to initialize a radar-based attenuation model that has been developed for this research.

This paper outlines the methods used to obtain the stated goals and presents results from the first two years of data collection. A description of the statistical analysis done at CSU for the first two years of the experiment are presented in Section 2. The statistics presented include cumulative distributions for attenuation measurements, attenuation ratio data, fade and non-fade duration analysis and fade slope computations. Section 3 gives a brief description of the CSU-CHILL radar, along with definitions of several radar observables that will be used in this study. A description of the attenuation model developed for this research is also presented in this chapter. Section 4 presents three case studies for which concurrent measurements from the CSU-APT and CSU-CHILL radar were available. Results using the attenuation model are given and analyzed. Finally, Section 5 presents some conclusions that were obtained from this research.

2 Statistical Attenuation Analysis at Ka-Band

A description of the propagation data and the statistical analysis completed on the measured CSU-APT data is presented in this chapter. The results are presented as primary and secondary statistics, as defined by Virginia

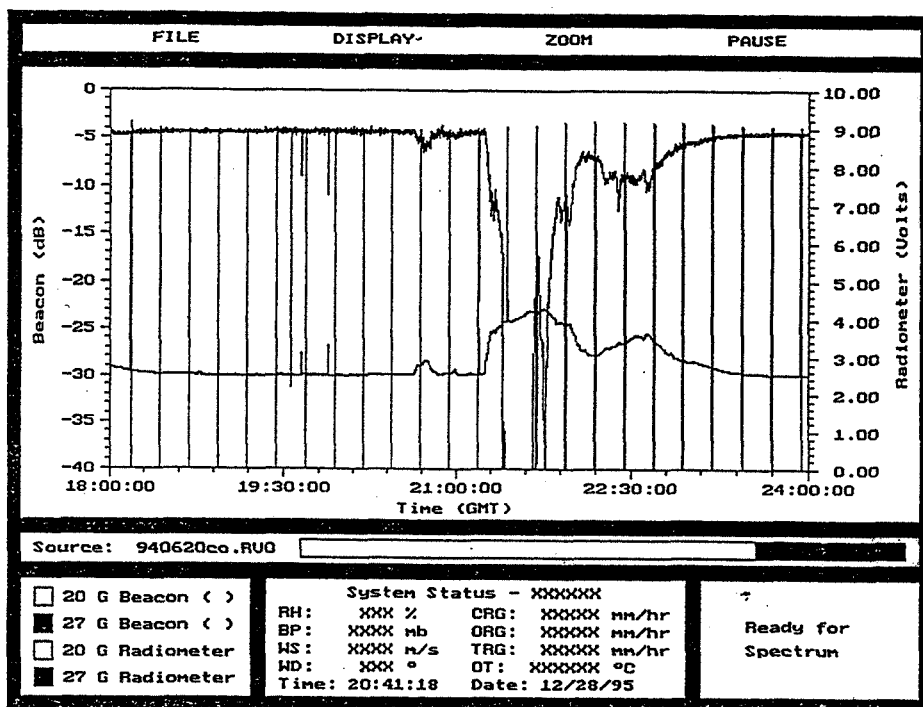


Figure 1: CSU-APT raw propagation data for June 20, 1994 rain event.

Tech during the Olympus propagation experiment [7]. The analysis period is for December 1, 1993 through November 30, 1995. Attenuation statistics are computed for a monthly and annual basis.

2.1 CSU-ACTS Propagation Data

Before a statistical analysis is performed on the data, it must be preprocessed. An example of a raw data set is shown in Figure 1, for the 27 GHz beacon and radiometer channels. The data is taken from June 20, 1994. The raw data is contaminated from various sources; a few will be briefly described here. The periodic dropouts in the beacon data that occur every 15 minutes are points where automatic calibrations occur. The beacon and radiometer data are assigned special values during these calibrations and should not be included in the final attenuation data. Dropouts in the beacon level that are not weather related, such as during maintenance periods, also should not be included in the data. Other factors that may affect the raw data signal include solar and lunar eclipses, satellite maneuvering and diurnal effects.

To obtain “clean” attenuation data, the raw data is processed through software that was developed by Crane and Westenhaver [4]. The prepro-

cessing software automatically marks data bad during calibration periods, eclipse periods and periods of non-thermal events (such as when the Sun is aligned along the propagation path). Diurnal effects are also automatically removed by the preprocessing code. For effects that cannot be automatically determined, such as maintenance periods or the occasional beacon dropout, the data can be manually marked as bad. Finally, system calibration is also incorporated into the preprocessing code [4]. The final output from the software is calibrated attenuation data, with all bad data points removed. Parameters that are used in the statistical analysis are radiometrically derived attenuation (ARD) and attenuation with respect to free space (AFS)[7].

2.2 Description of Statistical Quantities

The statistical analysis presented by Virginia Tech from the Olympus propagation program, was separated into two types – primary and secondary statistics [7]. The primary statistics include cumulative distribution functions of the AFS and ARD data, as well as attenuation ratio data between two frequencies. A common time base is used for all the primary statistics computed so that a valid comparison is made between the quantities of interest. Secondary statistics include fade durations, non-fade durations and fade slope data. For these types of statistics a common time base is not used. The methods used to compute primary statistics is discussed first.

Cumulative distribution functions (CDF) are computed for ARD and AFS data at both 20 and 27 GHz. The data are binned from -3.0 to 30 dB in increments of 0.1 dB. The data are presented as a percentage of time exceeded versus attenuation level. Data used to construct the CDF plots, are taken from the 1-Hz samples of preprocessed data, with no average applied to the data.

Attenuation ratio (RA) data are presented here in the form of a percentage of time exceeded versus dB ratio and dB level exceeded versus dB ratio. First the data are averaged by applying a 30-second moving block average to remove any scintillation effects. The attenuation ratio is then obtained by dividing the 27 GHz AFS with the base frequency of 20 GHz AFS (both values are in dB). The RA values are binned from 0.0 to 10.0 in increments of 0.05 for all base attenuation levels greater than 1 dB. The RA data are also binned for different base dB levels, the base dB level ranges from 0 to 30 dB in increments of 1 dB. RA versus dB level exceeded is used to determine when an RA value, for a specific dB level, exceeds a specific

value for a certain amount of time. The exceedance curves are given for 1%, 10%, 50%, 90% and 99% of the time.

While the primary statistics are used mainly for direct comparison of data between two frequencies or for scaling information, the secondary statistics are used more to look at the individual characteristics at each frequency. They contain information regarding fade duration, inter-fade duration and fade slope characteristics. Fade duration data is discussed first.

Fade duration (FD) is defined as the amount of time that the attenuation level (AFS) exceeds a specified threshold, T [7]

$$FD(\overline{AFS}_T) = t_2 - t_1 \quad (1)$$

where

$$\overline{AFS} \geq \overline{AFS}_T \quad \text{for } t_1 < t < t_2 \quad (2)$$

The bar indicates that a moving average has been applied to the data. In this case a 30-second moving average is used before the fade duration computations were done. Similarly the non-fade or inter-fade duration (IFD) is defined as

$$IFD(\overline{AFS}_T) = t_2 - t_1 \quad (3)$$

where

$$\overline{AFS} \leq \overline{AFS}_T \quad \text{for } t_1 < t < t_2 \quad (4)$$

Data are presented for the number of fade events for a given threshold level versus a specified fade duration. The percentage of time for all fades for a given threshold level versus a specific fade duration is also computed. The threshold level ranges from 0 to 30 db in increments of 1 dB, while the fade duration bins are 0-1, 1-2, 2-3, 3-5, 5-6, 6-10, 10-15, 15-18, 18-20, 20-30, 30-60, 60-120, 120-180, 180-300, 300-600, 600-1200, 1200-1800 and 1800-3600 seconds. Non-fade duration data is computed in the same manner.

Finally, fade slope (FS) information is obtained. The fade slope is computed after applying a 10 second moving average on the AFS data to remove signal fluctuations due to scintillation effects. It is defined only if the attenuation level crosses a specified threshold and remains either larger or smaller than the threshold for more than 10 seconds. The fade slope for a given threshold crossing is defined as [7]

$$FS_i = \frac{\overline{AFS}_{i+5} - \overline{AFS}_{i-5}}{10} \quad (5)$$

where \overline{AFS} is given as

$$\overline{AFS}_k = \frac{1}{10} \sum_{j=k-4}^{j=k+5} \overline{AFS}_j \quad (6)$$

and i is the index value when the attenuation crosses a specified threshold. The threshold values range from 0 to 30 dB in increments of 1 dB, while the fade slope values are binned from -1.25 to 1.25 dB/sec in increments of 0.05 dB/sec.

Primary and secondary statistics are computed on a monthly basis and annually for the period of December 1, 1993 to November 30, 1995. Results obtained at CSU for the two year period are given in Appendix A.

3 CSU-CHILL Polarimetric Radar Data

3.1 Radar Description

The CHILL radar has an historic past as it was one of the first radars to utilize polarization diversity. The radar was originally design and constructed jointly by the University of Chicago and the Illinois Water Survey under the guidance of Mueller and Atlas [2]. In 1990, the CHILL radar was moved to its present location outside of Greeley, Colorado and is now used exclusively as a research radar operated by CSU under the sponsorship of the National Science Foundation. It is a fully polarimetric S-band radar that can alternately send two orthogonally polarized signals and simultaneously receive the co- and cross-polarized signals. With recent upgrades made to the radar it is now ranks as one of the top radars of its kind. A summary of the system characteristics are given in Table 1

3.2 Radar Observables

The CSU-CHILL radar transmits and receives both horizontal and vertical polarizations. Being able to measure both the copolar and cross-polar returns allows measurements of such quantities as the horizontal reflectivity (Z_H), differential reflectivity (Z_{DR}), the specific differential phase between the H and V copolar signals (K_{DP}) and the differential propagation phase shift (ϕ_{DP}). The correlation coefficient between the two copolar signals (ρ_{HV}) and the linear depolarization ratio (LDR) are also measured. The radar observables can be defined in terms of the forward and back scattering amplitudes and the raindrop size distribution. The first subscript of the

Table 1: System Characteristics of the CSU-CHILL Radar

Antenna	
type:	fully steerable, prime focus parabolic reflector
size:	8.5 m
feed:	scalar horn
3 dB beamwidth:	1.0°
directivity :	45 dB
sidelobe level (any ϕ -plane):	≤ -27 dB
cross-pol. level (any ϕ -plane):	≤ -30 dB
polarization radiated:	Horizontal or Vertical
Transmitter	
type:	klystron, modernized FPS-18
wavelength:	10.7 cm
peak Power:	700 – 1000 kW
pulse width:	steps of 0.1 μ s up to a max. of 1 μ s
PRT:	800 – 2500 μ s
max. unambigu. range:	375 km
max. unambigu. velocity:	± 34.3 m/s
Receiver	
noise figure:	0.7 dB
noise power:	- 114 dBm
typical bandwidth:	750 kHz
transfer function:	linear
dynamic range:	90 dB, 0 – 60 dB IAGC in 12 dB steps
Data Acquisition	
signal processor:	SP20 made by Lassen Research
number of range gates:	64 – 2048
range gate spacing:	0.2 μ s or 1 μ s
sampling rate/avg. option:	under micro-code control
video digitizer:	12-bit, in the SP20 input card for I, Q and logP
time series capability:	up to 150 range gates.
Variables Available	
<ul style="list-style-type: none"> • Reflectivity at H polarization (Z_h) • Differential Reflectivity (Z_{dr}) • Mean Doppler Velocity (\bar{v}) and Spectral Width (σ_v) • Differential Phase between H and V states (Ψ_{dp}) • Copolar Correlation Coefficient ($\rho_{hv}(0)$) • Linear Depolarization Ratio (LDR) • Doppler Spectra from FFT processing • I, Q and logP for every pulse in time series mode (up to 150 gates) 	

polarization states given in the following equations refers to the received polarization state, while the second subscript refers to the transmitted polarization state. The horizontal and vertical reflectivity are defined by

$$Z_{HH,VV} = \frac{\lambda^4}{\pi^5 |K|^2} \int \sigma_{HH,VV}(D) N(D) dD, \quad mm^6 m^{-3} \quad (7)$$

where $\sigma_{HH,VV}(D)$ are the copolar radar cross sections at the horizontal and vertical polarizations, $|K| = (\epsilon_r - 1) / (\epsilon_r + 2)$, ϵ_r is the dielectric constant of water and λ is the wavelength [5]. Differential reflectivity is defined as

$$Z_{DR} = 10 \log \frac{Z_{HH}}{Z_{VV}}, \quad dB \quad (8)$$

Defining f_{HH} and f_{VV} as the forward scattering amplitudes of the H and V polarized waves, the specific differential phase is given as

$$K_{DP} = \frac{180\lambda}{\pi} \int \text{Re}[f_{HH}(D) - f_{VV}(D)] N(D) dD \quad (deg/km) \quad (9)$$

Then ϕ_{DP} is defined as

$$\phi_{DP} = \int_{r_1}^{r_2} 2K_{DP}(r) dr \quad (deg) \quad (10)$$

where ϕ_{DP} is the two-way differential phase between range locations, r_1 and r_2 . If the backscatter amplitudes for the horizontal and vertical polarizations are defined as S_{HH} and S_{VV} , then the cross-correlation coefficient is given as

$$\rho_{HV} = \frac{\int S_{HH}(D) S_{VV}^*(D) N(D) dD}{\{[\int |S_{HH}|^2 N(D) dD][\int |S_{VV}|^2 N(D) dD]\}^{1/2}} \quad (11)$$

The linear depolarization ratio can also be defined in terms of the backscatter amplitudes

$$LDR_{VH} = 10 \log \frac{|S_{HV}|^2}{|S_{HH}|^2} \quad (dB) \quad (12)$$

The variable $N(D)$ is the raindrop size distribution in equations 7–12 and is the number of raindrops per unit volume per unit size interval D to $D + \delta D$, where D refers to the equivalent spherical diameter [6].

Each polarimetric parameter provides information about the type of particles present in a given radar range resolution volume. For instance, information regarding a particle's shape can be obtained from the differential reflectivity, while information about a particle's orientation can be

obtained from the linear depolarization ratio. Specific differential phase is sensitive only to non-spherical particles such as oblate rain drops or aligned ice crystals. While each of these parameters provide information on their own, looking at a combination of polarimetric parameters can give an even greater insight to what is occurring in a particular storm cell. For example, reflectivity and differential reflectivity used together can be a good indicator to determine if a range resolution volume contains hail particles. Typically, if hail is present the reflectivity values tend to be high, while the tumbling nature of hail stones results in low values for differential reflectivity. This is just one of many examples of how polarimetric parameters can be used in describing the internal structure of storm events.

3.3 Attenuation Estimates

To obtain K-band attenuation estimates from S-band reflectivity data, simulations were obtained by varying the parameters of a given drop size distribution (DSD). Using a Mie solution for spherical water particles, propagation variables such as K-band attenuation and S-band reflectivity were computed using a wide range of DSD parameters. In this case a gamma DSD was used

$$N(D) = N_0 D^m e^{-\gamma D} \quad (13)$$

where

$$\gamma = \frac{3.67 + m}{D_0} \quad (14)$$

and $N(D)$, given in $mm^{-1}m^{-3}$, is the number of drops per unit volume per unit size interval, D is the equivalent drop size diameter in mm, N_0 is given in $mm^{-1-m}m^{-3}$, D_0 is the median drop size in mm and m is the shape factor. The DSD triplets (N_0, D_0, m) are varied as follows: $100 \leq N_0 \leq 50000$, $1 < D_0 \leq 4$ and $0 \leq m \leq 5$. Results of the simulation are shown in Figure 2. Each point on the scatter plot represents K-band attenuation and S-band reflectivity for a given DSD triplet. The entire range of triplets are representative of actual drop size distributions for a wide variety of rainfall events [1].

The S-band reflectivity/K-band attenuation curves are obtained by applying a power function fit to the simulated data. The equation that relates S-band reflectivity to K-band attenuation is given by

$$A_K = a \left(10^{Z_S/10} \right)^b \quad (15)$$

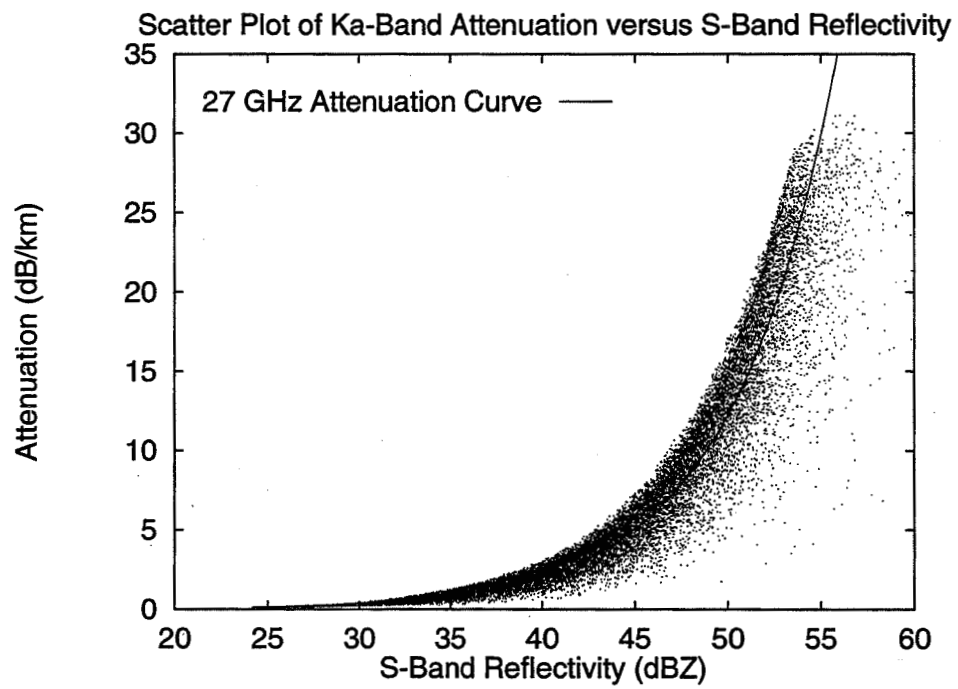
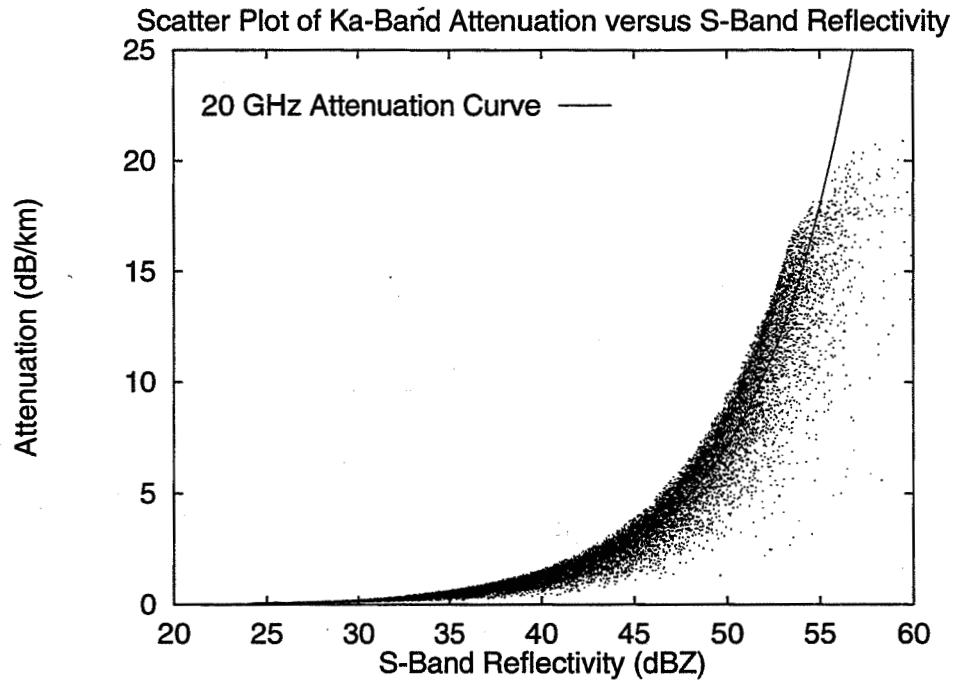


Figure 2: Attenuation for 20 and 27 GHz versus reflectivity at 3 GHz, obtained using a Mie solution for spherical particles.

Table 2: Values for a and b given in equation 15

Frequency	a	b
20 GHz	7.1×10^{-4}	8.0×10^{-1}
27 GHz	1.7×10^{-3}	7.7×10^{-1}

where A_K is K-band attenuation and Z_S (in dB) is S-band reflectivity. Values for a and b are given in Table 2.

Simulations were also conducted using a two-layered Mie solution. Several scatter plots were obtained by simulating water coated ice particles and varying the fraction of ice to water. The gamma DSD triplets were varied as before. Particles that were simulated ranged from spheres with small ice cores and a thick layer of water to spheres with large ice cores and a very thin layer of water. The derived attenuation curves in each case were almost identical to those shown in Figure 3.3. Any variations that were noted fell well within the scatter of the DSD parameters for pure water.

Attenuation curves relating K-band attenuation versus S-band specific differential phase, KDP , were also derived. The T-matrix solution was used to obtain the scattering amplitudes for oblate raindrops ranging in size from 1–8 mm. S-band KDP and specific attenuation at Ka-band were then computed from the Mueller matrix, averaged over an exponential DSD ($m = 0$ in the gamma DSD). The attenuation curves, shown in Figure 3, were obtained by varying the DSD parameter D_0 , while N_0 was fixed at $8000 \text{ mm}^{-1} \text{ m}^{-3}$.

4 Concurrent CSU–APT and CSU–CHILL Measurements

The Colorado Front range experiences a variety of weather events throughout the year, ranging from upslope rain conditions to winter storms producing wet snow and sleet, to widespread convective episodes in the late summer. Three such events are presented in this section. These include one stratiform event with a well defined “bright band”, where there was light-to-moderate precipitation uniformly covering a large area. Also presented are two convective cases, which are highly variable in nature and more localized

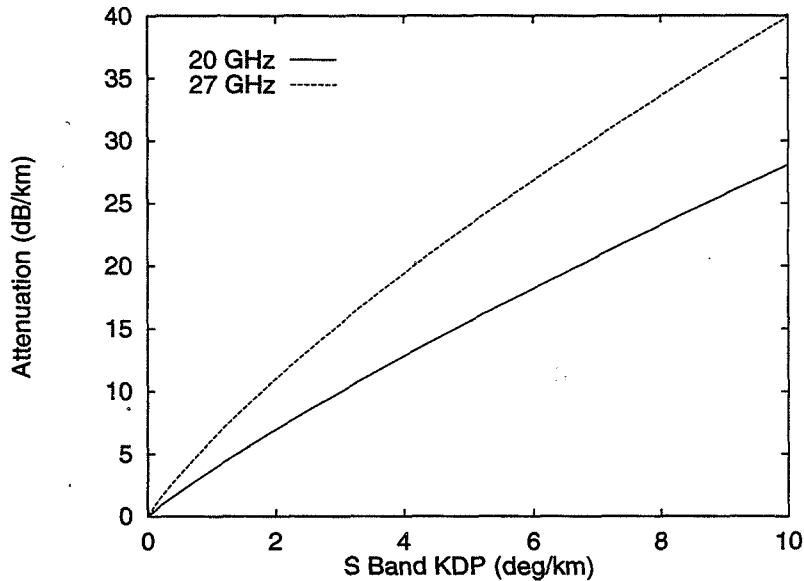


Figure 3: Attenuation for 20 and 27 GHz versus specific differential phase at 3 GHz, obtained via T-matrix and Mueller matrix solutions.

to a particular region.

The events are presented in the order of occurrence and include a June 20, 1994 convective event, a May 18, 1995 convective event and finally, a June 18, 1995 stratiform event. For these three events many radar scans are taken along the ACTS propagation path during the course of the attenuation event. The CSU-APT is co-located at the CSU-CHILL radar site. The APT azimuthal position is 172° from North and its elevation is 43° . This section first gives a description of the concurrent measurements obtained by the CSU-APT and the CSU-CHILL radar and then presents the results obtained using the S-band reflectivity/Ka-band attenuation model presented in Section 3.

4.1 Attenuation Events

A strong convective attenuation event occurred on June 20, 1994 causing a signal loss at 27 GHz for approximately 15 minutes. The 20 GHz signal bounced in and out of lock several times, but for only very short durations. Figure 4 shows the measured APT data for both the 20 and 27 GHz channels. Attenuation levels actually reached the 30 dB level at both frequencies

Attenuation Due to Rain Event

6/20/94 ACTS Propagation Data (CO)

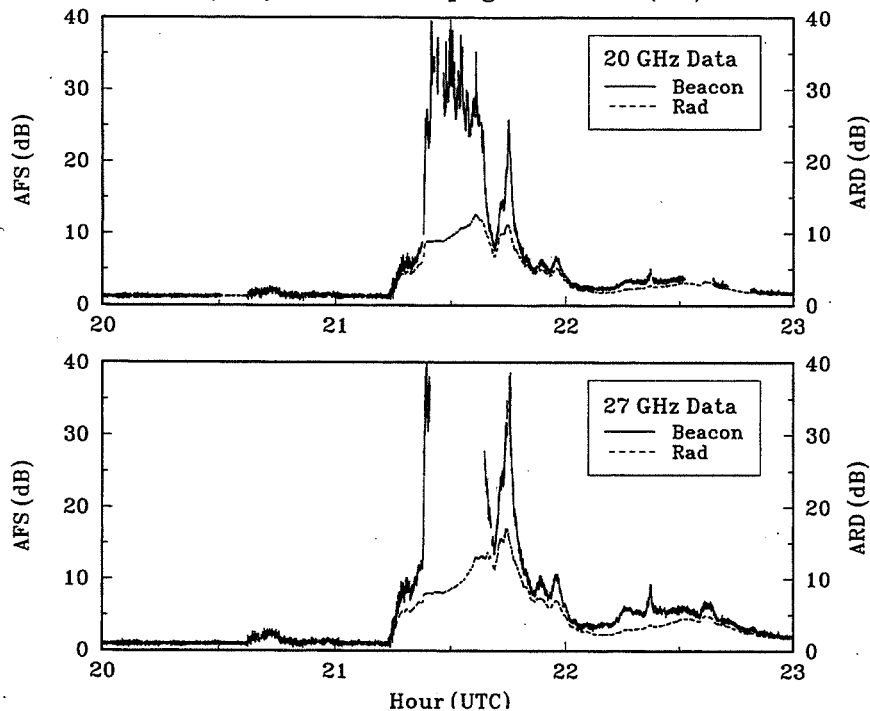


Figure 4: CSU-APT attenuation measurements for the June 20, 1994 convective case.

before the signal began to cut in and out. The event started at approximately 21:14 UTC, with large attenuation present at both frequencies until 22:01 UTC. Concurrent radar data were also taken for the June 20 rain event. Figure 5 shows an RHI plot taken at 21:32 UTC. Reflectivity values along the propagation path are on the order of 45 dBZ, at 6.5 km Z_H reaches a maximum of 54 dBZ. Values of Z_{DR} are on the order of 0.3 to 0.5 dB along the propagation path. In the area of peak reflectivity the Z_{DR} values are approximately 0.5 to 0.8 dB. These low values of Z_{DR} combined with the high reflectivity values gives an indication that there may be tumbling hailstones in that particular region. Panel 3 shows a dip in the cross correlation coefficient in the region of low Z_{DR} and high Z_H , while along the rest of the propagation path it is 0.98 or greater. There are also measurable values of specific differential phase, KDP , at 6.5 km, as shown in Panel 4 of Figure 5. Values of KDP along the slant path were approximately 0.5 to 0.6 deg/km. The presence of KDP and a minimum in the correlation coefficient at 6.5

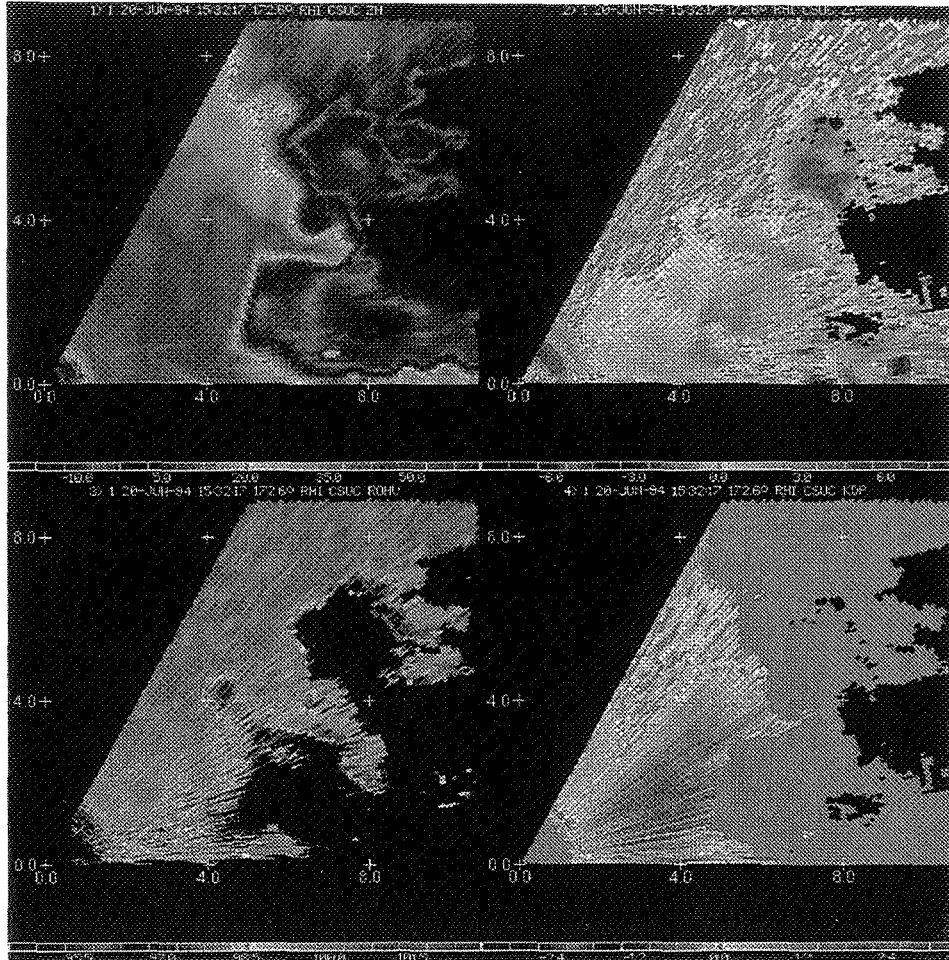


Figure 5: RHI scan for the June 20, 1994 convective case. The scan is taken along the radial of the ACTS propagation path. The CSU-APT elevation angle is 43° . The radar is located at the origin with the height given in km along the y-axis. Distance away from the radar along the 172° azimuthal angle is given in km along the x-axis. Horizontal reflectivity, Z_{HH} (dBZ), is shown in the upper left panel. Differential reflectivity, Z_{DR} (dB), is shown in the upper right panel. The cross correlation coefficient, ρ_{HV} (given as a percentage), is shown in the lower left panel. Specific differential phase, K_{DP} (deg/km), is shown in the lower right panel.

ACTS Data - Convective Case

5/18/95 ACTS Propagation Data (CO)

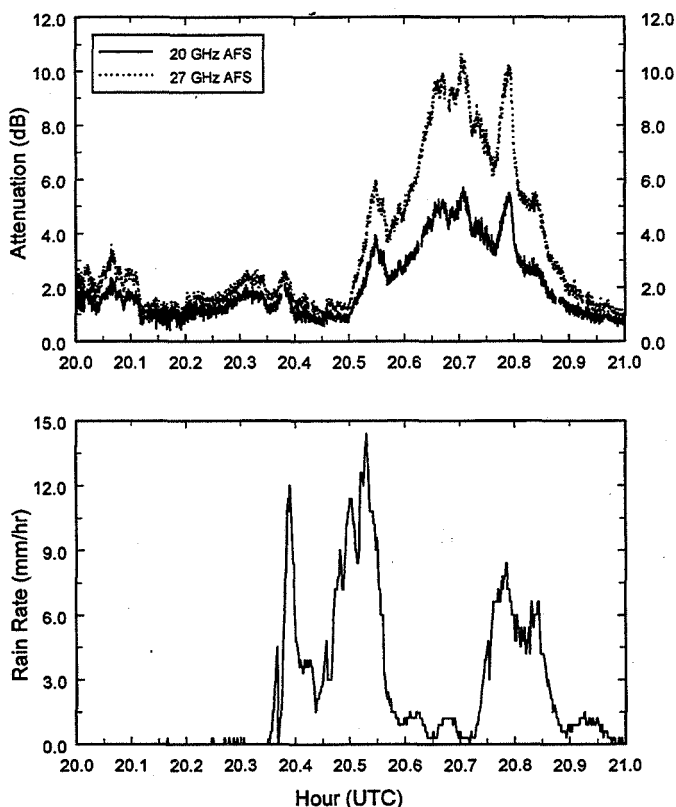


Figure 6: CSU-APT beacon attenuation measurements and the corresponding rain rate for the May 18, 1995 convective case.

km, is an indication that this region is an area of mixed phase. The region consists of tumbling hailstones, along with water coated ice particles, that can produce pure water droplets through a shedding effect. This region of mixed phase occurs right along the along the ACTS propagation path.

A second, weaker, convective event was observed on May 18, 1995. The CSU-APT measured attenuation, along with corresponding rain rates, is shown in Figure 6. The APT measured attenuation reaches a maximum of 10–11 dB for the 27 GHz signal and 5 dB for the 20 GHz signal. The event began at 20:30 UTC and lasted until 20:56 UTC. A total of 72 radar scans taken directly along the slant path between 20:32 to 20:56 UTC were available for this event. A sample of the radar data measured during this event is shown in Figure 7, again as an RHI plot. Panel 1 shows that the reflectivity values range from 15 dBZ to 40 dBZ along the propagation path. Z_{DR} had peak values of 0.7–0.9 dB, while high values of ρ_{HV} is indicative to that of rain. Larger values of KDP , shown in the Panel 4, are mostly present at the lower elevation angles farther out in range from the radar

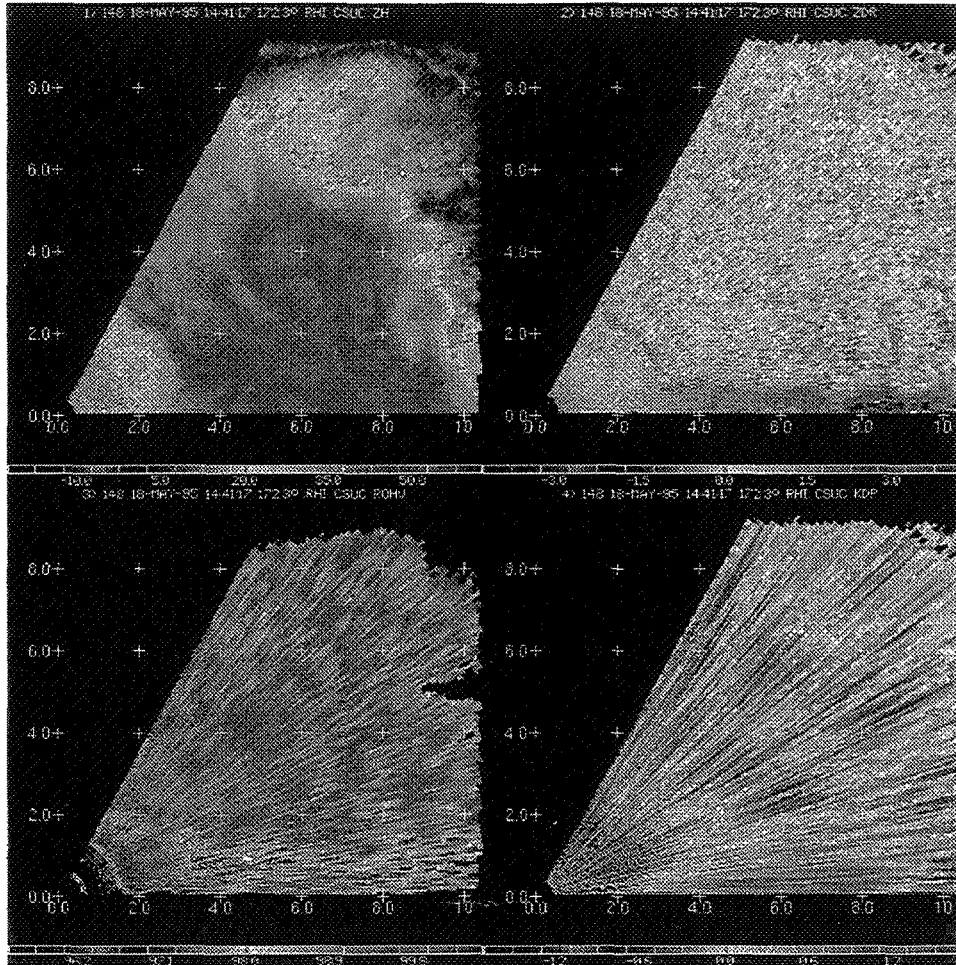


Figure 7: RHI scan for the May 18, 1995 convective case. The scan is taken along the radial of the ACTS propagation path. The CSU-APT elevation angle is 43° . The radar is located at the origin with the height given in km along the y-axis. Distance away from the radar along the 172° azimuthal angle is given in km along the x-axis. Horizontal reflectivity, Z_{HH} (dBZ), is shown in the upper left panel. Differential reflectivity, Z_{DR} (dB), is shown in the upper right panel. The cross correlation coefficient, ρ_{HV} (given as a percentage), is shown in the lower left panel. Specific differential phase, K_{DP} (deg/km), is shown in the lower right panel.

ACTS Data - Stratiform Case

6/18/95 ACTS Propagation Data (CO)

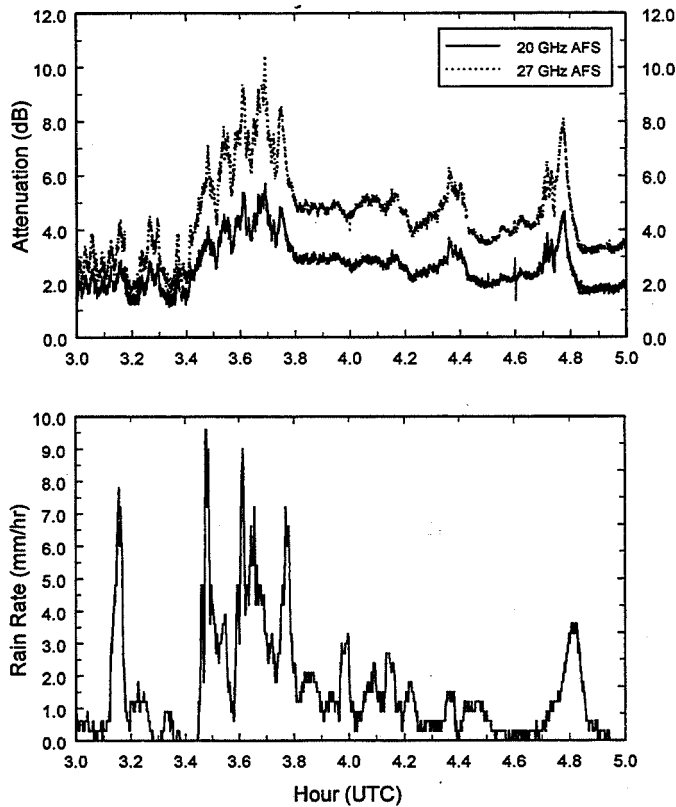


Figure 8: CSU-APT beacon attenuation measurements and the corresponding rain rate for the June 18, 1995 stratiform case.

and not along the slant path. The radar data, along with the rain rate data obtained at the site, indicate that a very light rain has occurred at the site, while most of the attenuation is due to precipitation farther out along the slant path.

The last case to be examined is a stratiform event that occurred on June 18, 1995. As shown in Figure 8, this is actually a stratiform case with some embedded convection in the initial stages of the event. Peak values of attenuation measured by the APT were around 10 dB for the 27 GHz signal and 5 dB for the 20 GHz signal, during the embedded convective part of the event. In the more stable stratiform region the attenuation was approximately 5 and 3 dB, for the 27 and 20 GHz signals respectively. The rain rates for this event are also given, with peak rates of only 6-9 mm/hr during the portion of the event with embedded convection and 1-3 mm/hr during the stratiform only time of the event. For this event, 120 radar scans were taken along the propagation path.

An RHI plot taken at 4:21 UTC is shown in Figure 9. The measured hor-

horizontal reflectivity was about 45 dBZ in the region of the bright band, while values of 30 dBZ are seen along the propagation path below the reflectivity bright band. The height of the reflectivity bright band is approximately 2.45 km. Z_{DR} values in the melting layer were approximately 1.0–1.5 dB, with values of 0.5–0.8 dB below the melting layer. The ρ_{HV} data exhibits the typical decrease in magnitude in the melting region, with values dropping to 0.93. The final radar parameter given in this RHI plot is the linear depolarization ratio (LDR) and it has values up to -18 dB in the melting layer.

The next step in the analysis process is to use the radar information as input to the propagation model on a case-by-case basis. Results using the S-band reflectivity/Ka-band attenuation model are presented in the next section for the three case studies.

4.2 Attenuation Estimates

Attenuation estimates have been computed using the S-band reflectivity/Ka-band attenuation model derived in Section 3.3. Only the reflectivity values have been used to model the cases described in the previous section (KDP estimates were used in the June 20, 1994 convective case), while the polarimetric parameters Z_{DR} , KDP and ρ_{HV} were used to determine the length of the attenuation path. These polarimetric parameters are dependent on the elevation angle of the radar, therefore a correction factor is used to obtain values of Z_{DR} and KDP for an elevation angle of 0° . The corrected values are used as input to the attenuation model.

Radar scans were taken directly along the ACTS propagation path with a range resolution of 150 m. Reflectivity data at 3 GHz were taken at the 150 m increments and used to determine the corresponding 20 and 27 GHz attenuation estimates from the attenuation curves given in Figure 2. The Ka-band attenuation estimates were then multiplied by the appropriate distance along the propagation path.

For the June 20, 1994 convective case, 43 radar scans were taken throughout the duration of the event. Ka-band attenuation estimates were derived from S-band reflectivity data using the procedure described above. For this particular event S-band KDP data are also used to derive Ka-band attenuation estimates. The results are shown in Figure 10

As seen in Figure 10, the CSU-CHILL reflectivity based attenuation estimates follow the attenuation measurements obtained from the APT very closely. The maximum difference is about 5 db, while for the most part the

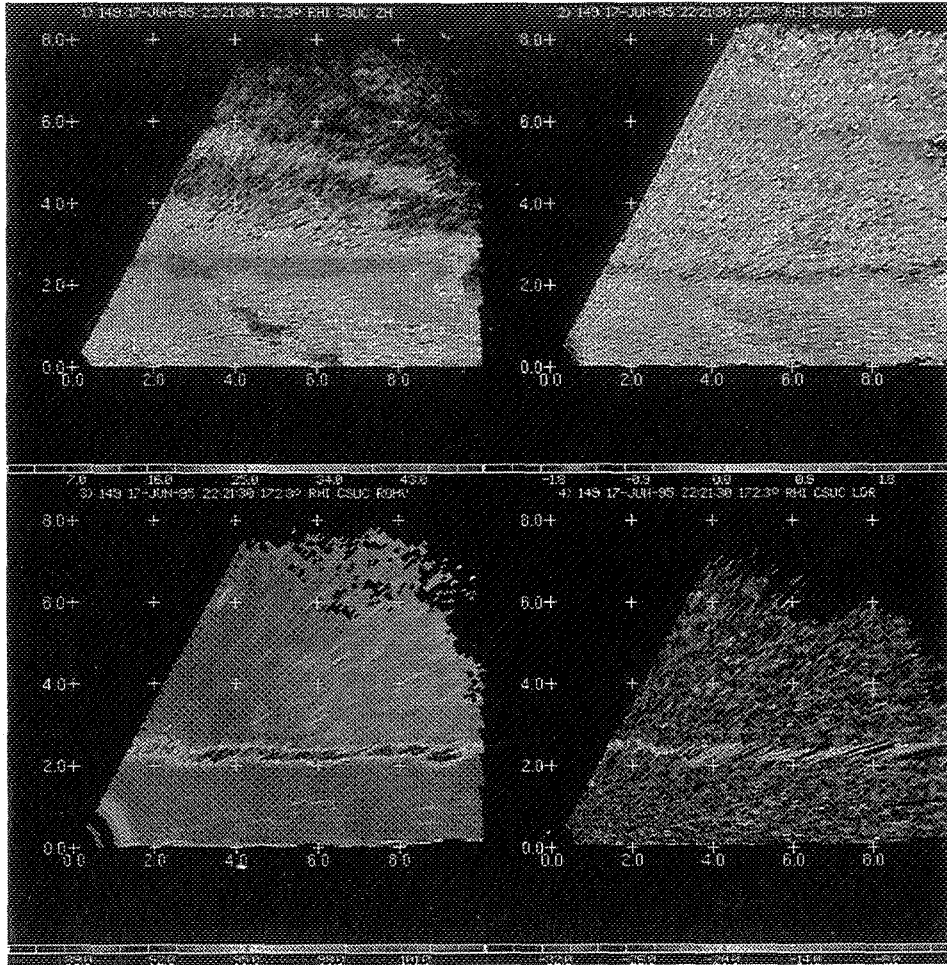


Figure 9: RHI scan for the June 18, 1995 stratiform case. The scan is taken along the radial of the ACTS propagation path. The CSU-APT elevation angle is 43° . The radar is located at the origin with the height given in km along the y-axis. Distance away from the radar along the 172° azimuthal angle is given in km along the x-axis. Horizontal reflectivity, Z_{HH} (dBZ), is shown in the upper left panel. Differential reflectivity, Z_{DR} (dB), is shown in the upper right panel. The cross correlation coefficient, ρ_{HV} (given as a percentage), is shown in the lower left panel. The linear depolarization ratio, LDR (dB), is shown in the lower right panel.

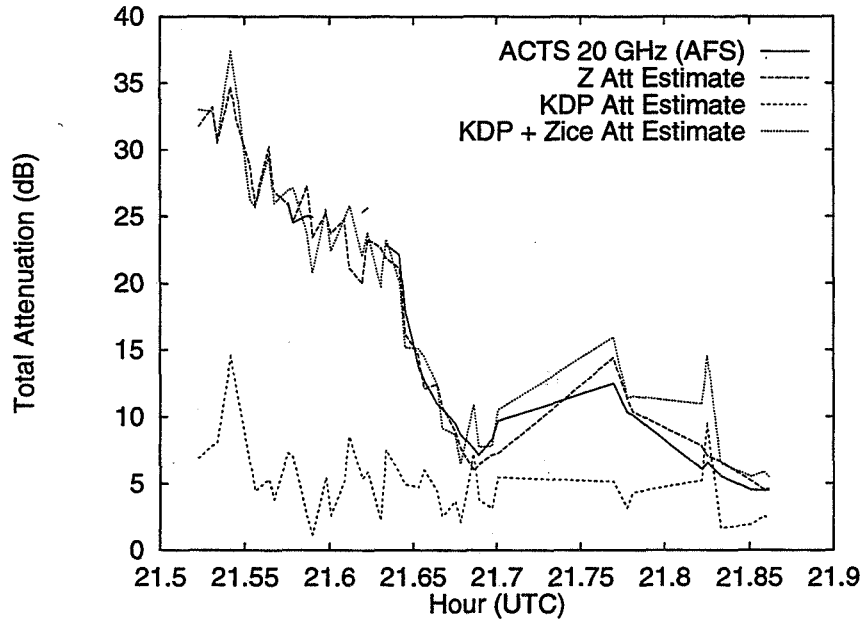


Figure 10: Comparison of measured CSU-APT attenuation and 20 GHz attenuation estimates derived from CSU-CHILL data.

CSU-CHILL derived estimates are within 1-2 dB of those measured by the CSU-APT. The attenuation estimates derived from *KDP* data alone grossly underestimated the attenuation caused by this event. This may be explained by examining Figure 11, a scatter plot of the APT measured 20 GHz attenuation versus the one way differential phase measured by the CSU-CHILL radar.

One way differential phase, Φ_{DP} , and its derivative *KDP* are only sensitive to the oblateness of a particle, therefore the difference seen between the maximum and minimum values of the fitted curve in Figure 11 is caused by the presence of various sizes of oblate rain drops present in the propagation path. If the hydrometeors in the slant path were comprised of only raindrops the y-intercept of the fitted curve would be at zero; however, if the fitted curve is extended back to $\Phi_{DP} = 0$, the y-intercept is at 23.97 dB. This indicates that a large amount of attenuation was due to spherical, water coated ice particles. As indicated previously, there was indeed a region of mixed phase along the propagation path, however from Figure 11 and the fact that *KDP* data alone grossly underestimates the attenuation is an indication

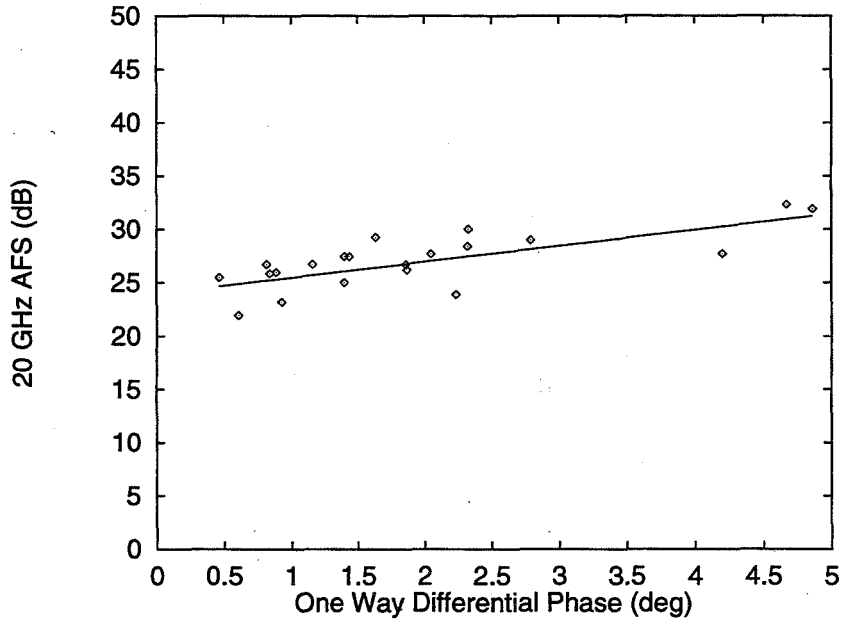


Figure 11: 20 GHz attenuation versus one way differential phase, for the June 20, 1994 convective case.

that water coated ice particles could have been present throughout a large part of the propagation path during this event.

Considering this to be the case, the next step is to determine the reflectivity due only to the water coated ice particles along the propagation path from the total reflectivity measured by the CSU-CHILL radar. This is done using the difference reflectivity, Z_{DP} , to determine the ice fraction content in the radar resolution volume at each 150 m increment along the propagation path. Once the ice fraction content is determined the reflectivity due only to the water coated ice particles, Z_{HH}^{ICE} , can be determined. The S-band reflectivity/Ka-band attenuation model is then used, with Z_{HH}^{ICE} as the input, to determine the attenuation at 20 and 27 GHz for the spherical, water coated hail particles. While the attenuation due to the oblate raindrops, Z_{HH}^{RAIN} , is computed using S-band KDP /Ka-band attenuation model.

The combined results are shown in Figure 10; while the attenuation estimates are still slightly underestimated for the most part, the CSU-CHILL derived attenuation estimates using KDP and Z_{HH}^{ICE} are within 1 to 2 dB of the the attenuation values obtained by the CSU-APT. The 27 GHz results

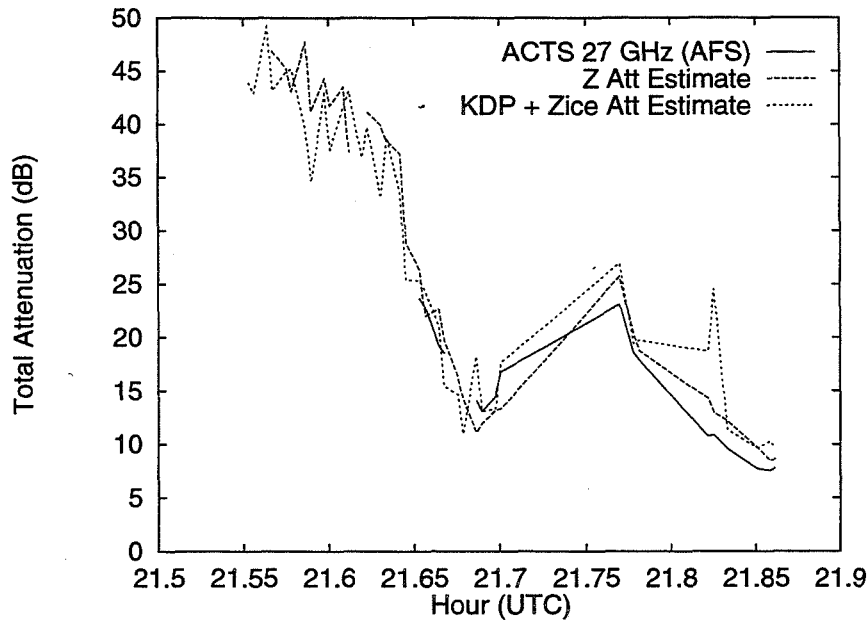


Figure 12: Comparison of measured CSU-APT attenuation and 27 GHz attenuation estimates derived from CSU-CHILL data.

are shown in Figure 12. The 27 GHz signal was interrupted for approximately 16 minutes during this event. At approximately 21:39 UTC, the 27 GHz signal was reacquired and as seen in Figure 12 the CHILL attenuation estimates are very close to the APT measured attenuation.

The results obtained by using the different polarimetric parameters available from the CHILL radar in this case is very encouraging. It is a good example of how the different parameters can be used to determine the nature of precipitation particles along the propagation path and predict Ka-band attenuation using S-band radar data.

Results for the May 18, 1995 convective case are shown in Figure 13. The attenuation estimates obtained from the S-band reflectivity data follow the trend of the beacon attenuation estimates. However, the radar attenuation estimates are off by a constant value at both frequencies, approximately 1.8 dB at 20 GHz and 3.0 dB at 27 GHz. This is also seen in the June 18, 1995 stratiform case, as shown in Figure 14. Here the reflectivity based attenuation estimates underestimate the APT attenuation estimates by 2 dB at 20 GHz and 3.3 dB at 27 GHz. Because of the frequency dependence of the underestimates it is unlikely that it can be attributed to a systematic error in the S-band radar constant, i.e., the absolute calibration of the radar. A simple increase in S-band reflectivity by a few dB would be inconsistent, not only with the frequency dependence, but also the difference in underestimates between the convective and stratiform portions of the same event (see Figure 14).

Underestimation of Ka-band attenuation levels from S-band radar data

May 18, 1995 Convective Case

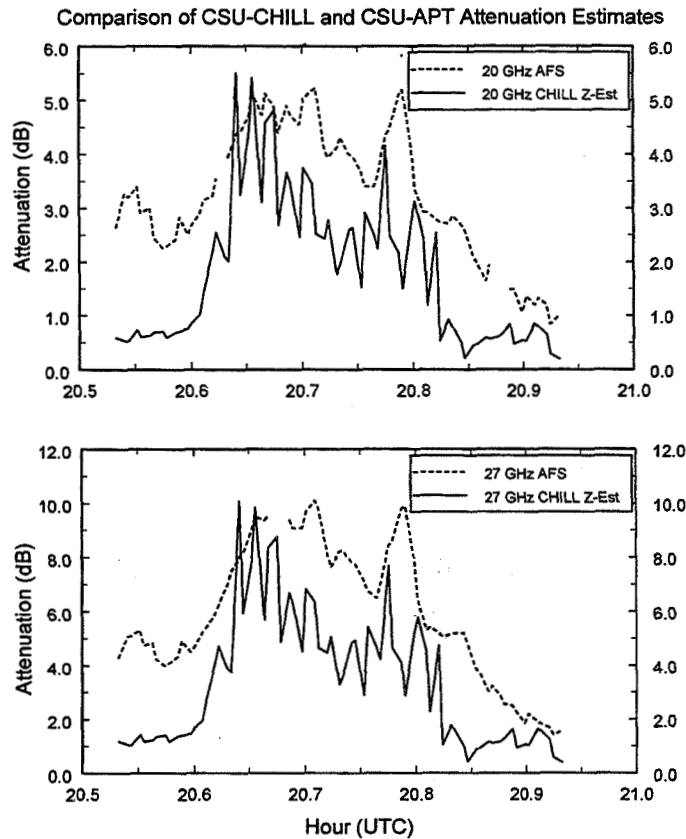


Figure 13: Comparison of measured CSU-APT attenuation at 20 and 27 GHz with attenuation estimates derived from CSU-CHILL S-band reflectivity data. For the May 18, 1995 convective case.

have been noted in previous studies [3], and the differences have been attributed to gaseous attenuation that is not measured at the S-band frequencies. However, in Colorado only 0.4 to 0.5 dB of attenuation can be attributed to the gaseous constituents. These values were determined by using radiometrically derived attenuation, as well as observations from radiosonde data taken from the Denver area. Gaseous attenuation and attenuation from cloud liquid water will contribute partially to the differences seen in the two cases described, but this contribution is small. A possible reason for the remaining difference is that water collecting on the antenna surface in the form of small droplets may cause appreciable amounts of attenuation. This possibility is examined by conducting a water spraying experiment. Under clear sky conditions, a garden hose was used to simulate the effect of rainfall on the antenna surface only, the feed horn surface only and both the antenna surface and feed horn surfaces simultaneously. The results of spraying the antenna surface alone are shown in Figure 15.

June 18, 1995 Stratiform Case

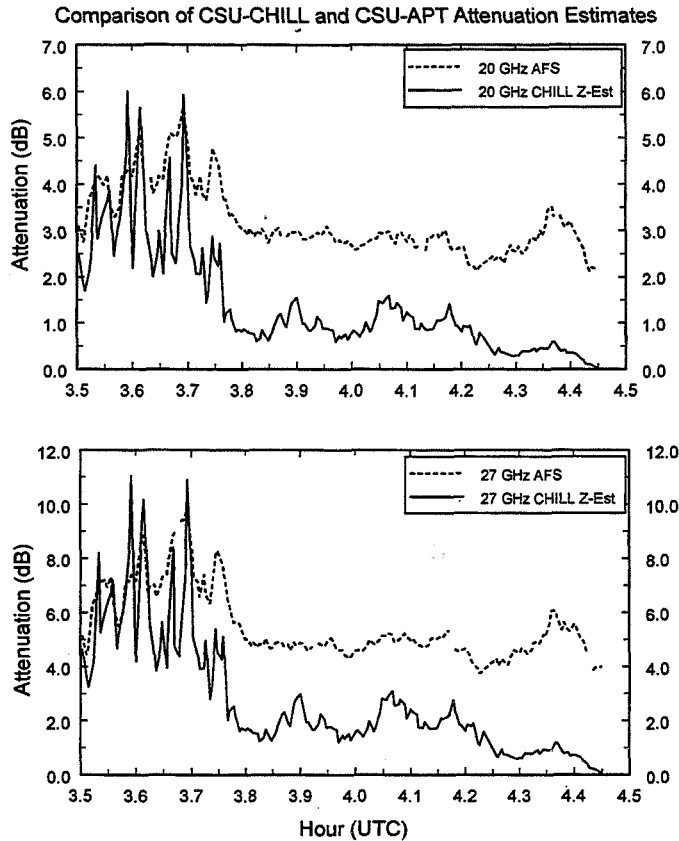


Figure 14: Comparison of measured CSU-APT attenuation at 20 and 27 GHz with attenuation estimates derived from CSU-CHILL S-band reflectivity data. For the June 18, 1995 stratiform case.

The antenna surface was continuously sprayed with water starting at 21:36:00 UTC and ending at 21:37:46 UTC. This is noted by the sustained peak attenuation in Figure 15. After the spraying had stopped there was a quick decrease in attenuation until 21:38:09. At this point, the attenuation continued to decrease but at a much slower rate. This measured attenuation is due to water standing on the antenna surface in the form of small droplets or beads. This beading effect will also occur during rain events and is dependent on the rain rate.

To check if the same type of frequency dependence is exhibited in the water spraying test as that seen in the differences between the attenuation estimates at 20 and 27 GHz shown in Figures 13 and 14, the instantaneous attenuation ratios were compared. The attenuation ratio for the water spraying test and for the June 18, 1995 stratiform case are shown in Figure 15. Once the spraying had stopped, the attenuation ratio between the June 18 event and the attenuation ratio computed from attenuation due to water

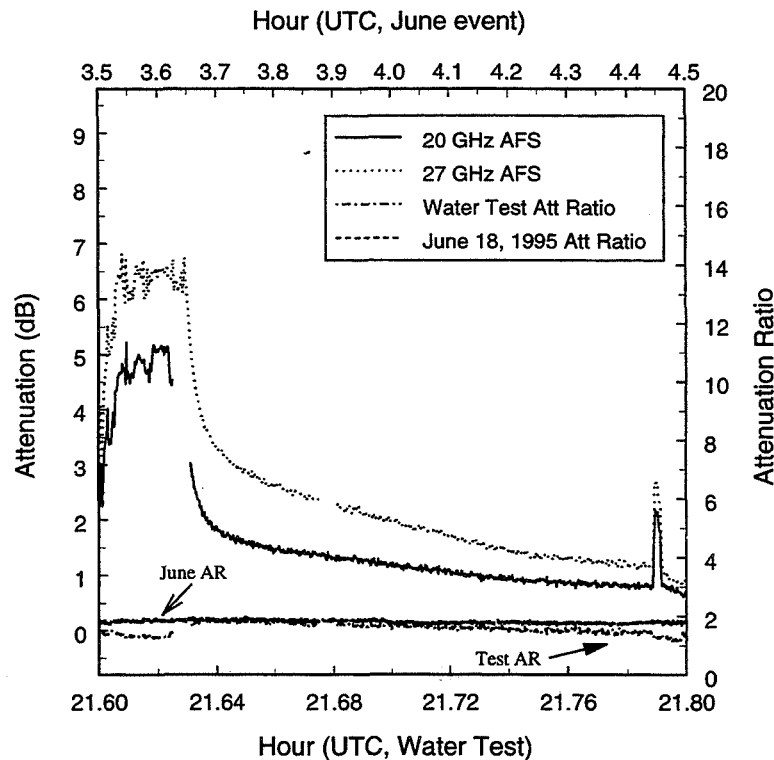


Figure 15: Water spray test results. Water was sprayed only on the antenna surface. Beacon attenuation for 20 and 27 GHz are shown, along with the instantaneous attenuation ratio for the two frequencies (20 GHz is the base frequency).

droplets on the antenna surface are identical for the most part. This gives a good indication that most of the difference seen between the attenuation estimates derived from S-band reflectivity data and CSU-APT attenuation estimates for the May 18 and June 18, 1995 events were due to water droplets that formed on the antenna surface.

The amount of attenuation caused by droplets forming on the antenna surface is dependent on the rain rate, wind direction and speed and the type of event, therefore it is not a systematic error that can be easily removed. While a hydrophobic solution was applied to the antenna surface to minimize this effect, water droplets still collect on the antenna surface. Several experiments were conducted by spraying the antenna surface with water. It was found that 1-5 dB of attenuation could occur at 27 GHz and 1-3 dB of attenuation at 20 GHz, just due to a water build-up on the antenna surface only. Results from spraying the feed horn surface show the beading effect does not occur with the same magnitude as seen on the antenna surface. In addition, the feed horn surface dries much quicker than the antenna surface. While it may be difficult to remove these effects, they do need to be taken into account for model development and in statistical analysis.

5 Conclusions

Due to the high demand for satellite communications, already overused portions of the frequency spectrum (C and Ku-bands) are becoming even more crowded. This necessitates looking at less crowded areas of the spectrum such as the Ka-band frequencies. To study satellite communications at these frequencies, NASA launched the Advanced Communications Technology Satellite (ACTS). The ACTS is an experimental satellite being used to conduct communication and propagation experiments using new Ka-band technology. At Ka-band, weather events can have an adverse affect on the signal being propagated through the atmosphere. Therefore, propagation effects at these frequencies must be studied. This report has outlined the research that has been conducted at CSU during the first two years to meet the ACTS experiment goals and further the understanding of K-band propagation effects.

The main goal of constructing an attenuation data base for the B2 climatic zone at K-band frequencies was met by maintaining a well calibrated ground propagation terminal and ensuring the integrity of the data collected and processed. Data were collected and preprocessed for the two year period of December 1, 1993 through November 30, 1995. A statistical analysis for the CSU-APT data was presented in Section 2 and Appendix A. The analysis was done on a monthly and annual basis.

An attenuation model was developed to relate S-band radar reflectivity to Ka-band attenuation. Several case studies were presented to illustrate the attenuation model. They included a very strong convective case, with known mixed phase, that occurred on June 20, 1994, a second, weaker convective event that occurred on May 18, 1995 and finally a stratiform event that occurred on June 18, 1995. Radar data, collected by the CSU-CHILL radar, for each of these events were used as inputs to the attenuation model. Very good results were obtained for each case.

Finally to conclude, the ACTS propagation experiment is an on-going experiment with two years of data collection completed, the third year in progress and the possibility of a fourth year. With the increased demand from industry to utilize the Ka-Band spectrum, the attenuation data being collected here, as well as at other sites, and its subsequent analysis will be invaluable for the field of satellite communications.

SPACE COMMUNICATIONS TECHNOLOGY CENTER

(SCTC)

PROPAGATION MEASUREMENTS IN FLORIDA

HENRY HELMKEN
FLORIDA ATLANTIC UNIVERSITY (FAU)
&
RUDY HENNING
UNIVERSITY OF SOUTH FLORIDA (USF)

June 4, 1996

FLORIDA PROGRAM GOALS

- * Generate CDF's for Sub-tropical Region
- * Sub-tropical Fading Statistics
- * Radiometer Development
- * Diversity Gain Measurements
- * Sub-tropical Rain Models

ACTS PROPAGATION MEASUREMENTS

- * NASA Propagation Terminal in Tampa, Florida
University of South Florida (USF) Campus
CCIR Rain Zone N, Global Rain Region E
ACTS Elevation Angle: 52 Degrees
ACTS Polarization: 43.6 Degrees
2 Year Collection Efficiency:
99.6% at 20 GHz
98.4% at 27 GHz
- * Diversity Experiments
Extension of GTE Data Base
COMSTAR Beacon Experiments 1978-79

ANALYSIS APPROACH

SUN SPARCstation 20

- * Input Calibrated Data Files (*.pv2) from ACTS edit
- * Interpolate Calibration Intervals
From 20 to 27 GHz or 27 to 20 GHz
Use proximate average attenuation ratio
- * Fill in Small Gaps (< 60 seconds)
Use average AFS value before and after gap
- * Filter Scintillation via Averaging
(30 sec running average)
- * Option to Generate ACA files
Set attenuation threshold from monthly average AFS
- * Generate Data Files for Subsequent Analysis

SOFTWARE OUTPUT

- * Data Matrices for 20 GHz and 27 GHz
At 0, 1, 2,... 35 dB Fade Levels
Number of Fades vs Fade Duration
(>0, >1.... >3600 sec)
Total Time at Fade Duration (>0, >1,... >3600 sec)
Fade Slope Occurrence at Fade Slope
(-1.15....+1.25 dB/sec)
- * Cumulative Distribution Functions
Fad CDF - at 0.1 and 1.0 dB resolution
- * Attenuation Ratio vs Fade Level
- * 20/27 Scatter Plots for Selected Events
- * 20 and 27 GHz Beacon vs Radiometer Scatter Plots
- * 20 and 27 GHz Sky Brightness

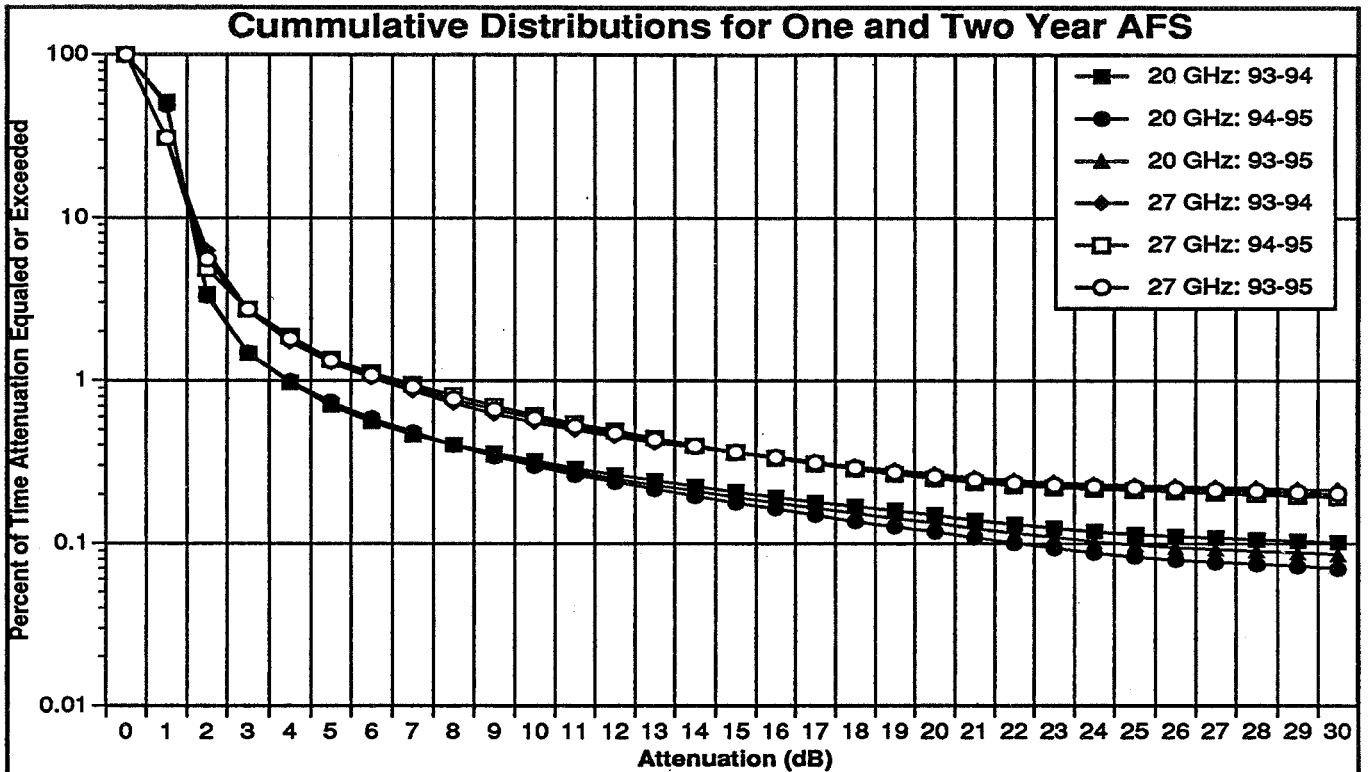


Figure 1. Cumulative distributions of Attenuation with respect to Free Space (AFS) for 1993-1994, 1994-1995 and 1993-1995. Data filtered through 30 second running average. Note excess 20 GHz attenuation at 1 db fade level.

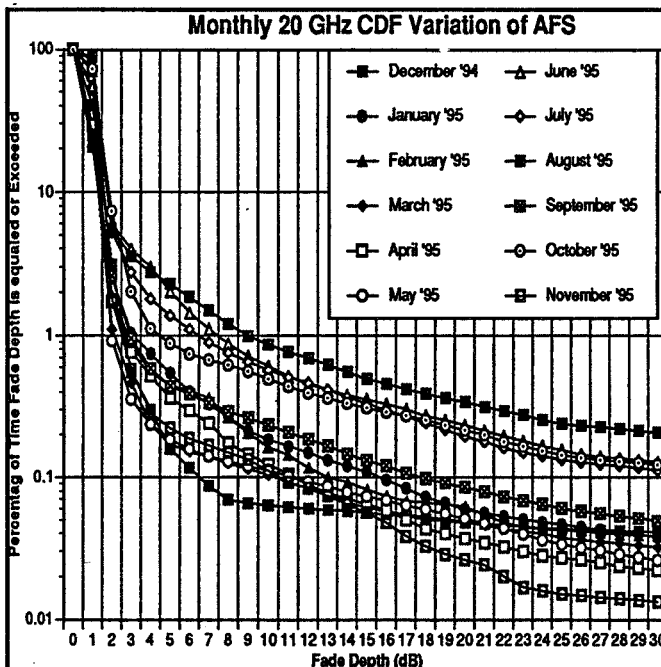


Figure 2. 1993-1994 monthly cumulative distributions (CDF) at 20 GHz. Data filtered through 30 second running average.

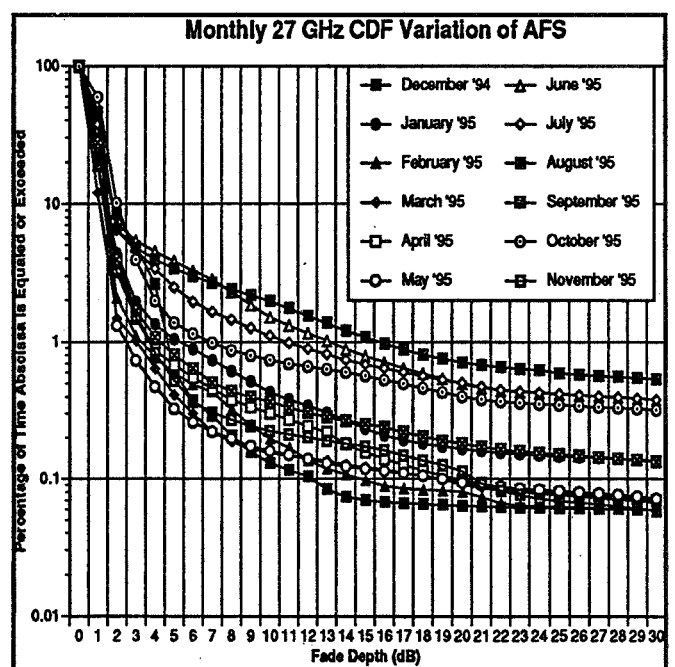


Figure 3. 1993-1994 monthly cumulative distributions (CDF) at 27 GHz. Data filtered through 30 second running average.

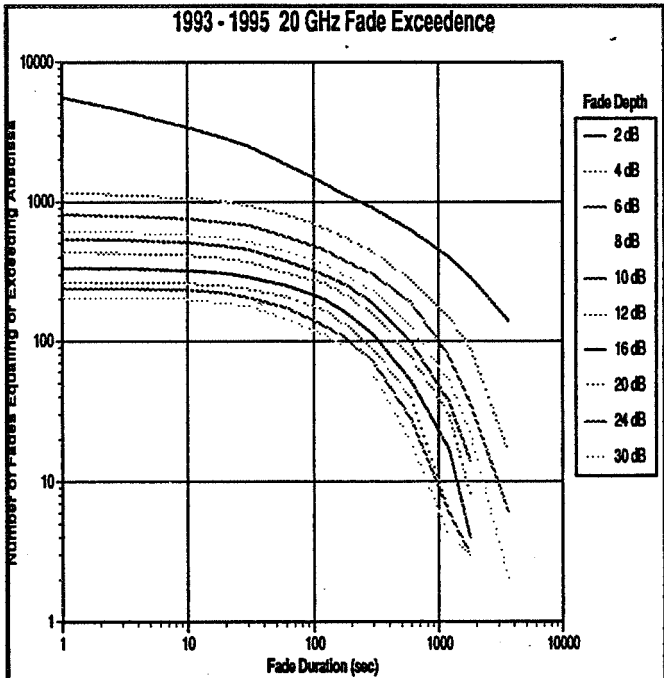


Figure 4. Number of fades at 20 GHz equaling or exceeding abscissa. 30 second running average. Shown for fade depths from 2 db to 30 dB.

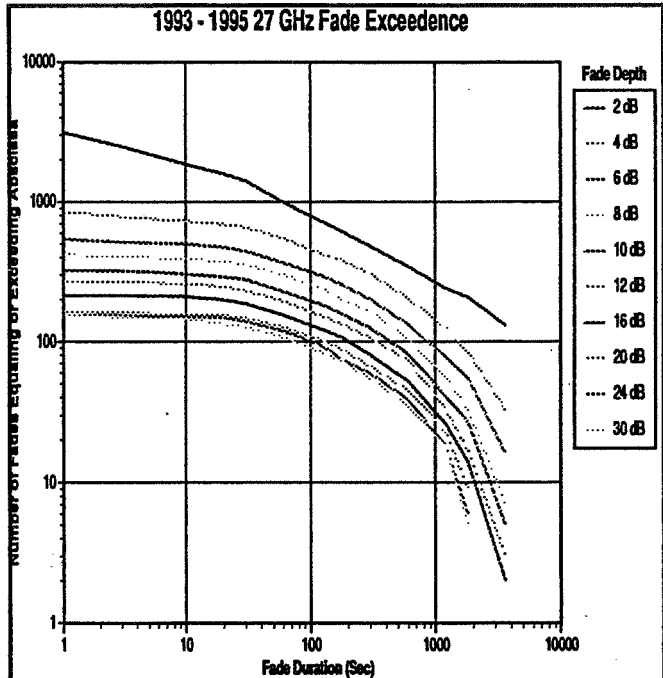


Figure 5. Number of fades at 27 GHz equaling or exceeding abscissa. 30 second running average. Shown for fade depths from 2 db to 30 dB.

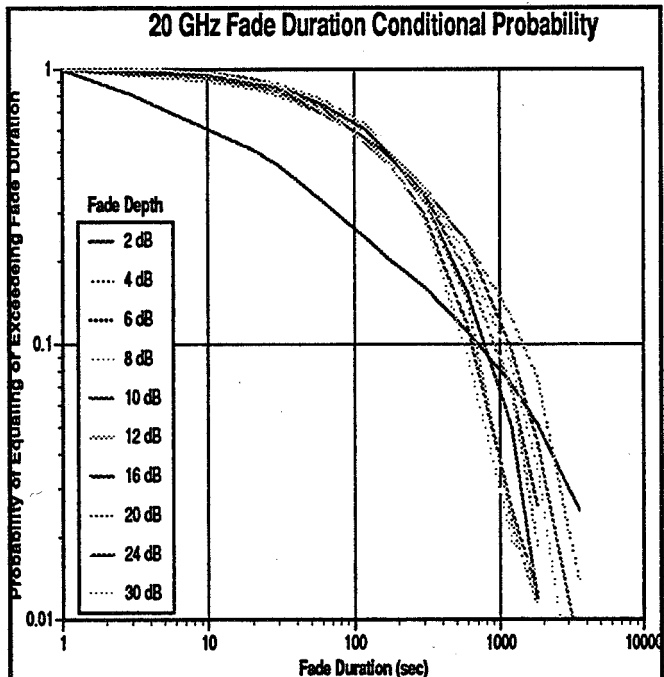


Figure 6. Normalized 20 GHz fade durations shown in figure 4. Plot represents the conditional probability, $p(T|A)$, of observing a fade of T seconds or longer given that a fade of depth A has occurred.

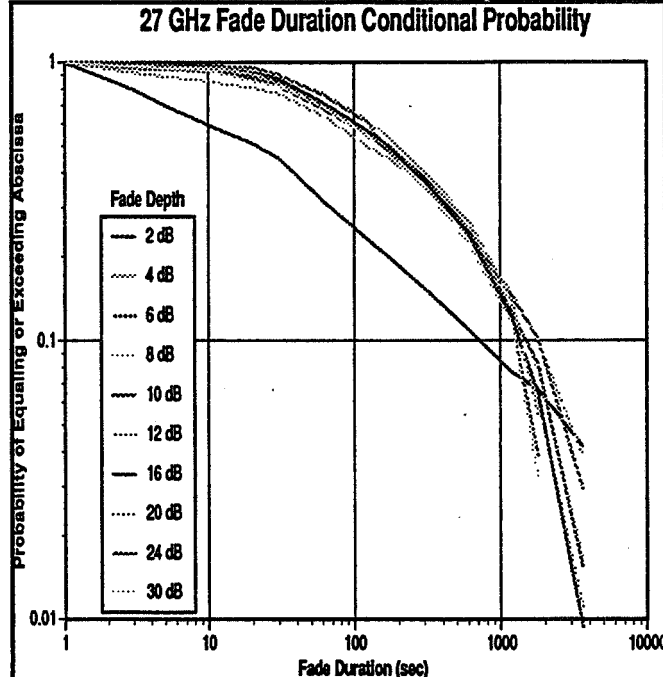


Figure 7. Normalized 27 GHz fade durations shown in figure 5. Plot represents the conditional probability, $p(T|A)$, of observing a fade of T seconds or longer given that a fade of depth A has occurred.

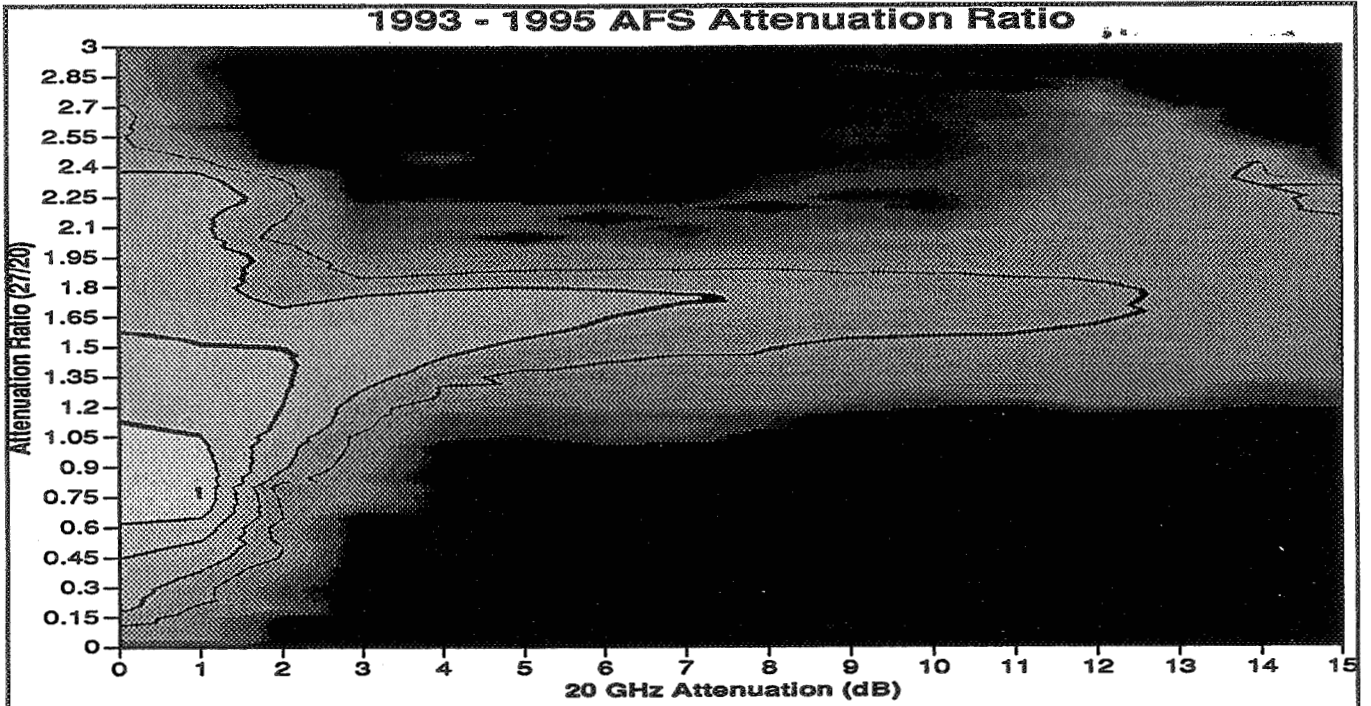


Figure 8. Logarithmic contour plot of instantaneous (no averaging) 27 GHz/20GHz attenuation ratio over the two year observation period. Note transition from ~0.75 at 1 dB attenuation to asymptotic value ~1.75.

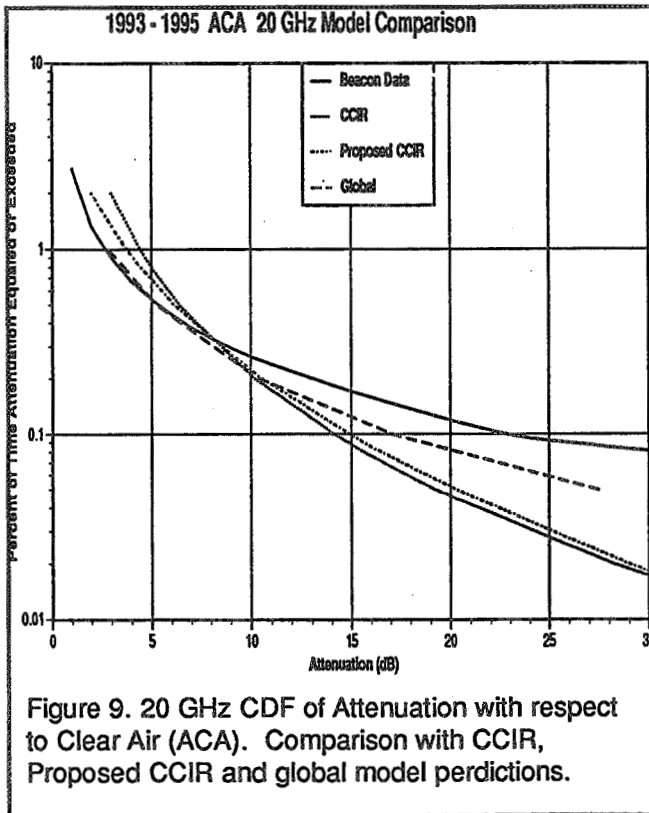


Figure 9. 20 GHz CDF of Attenuation with respect to Clear Air (ACA). Comparison with CCIR, Proposed CCIR and global model predictions.

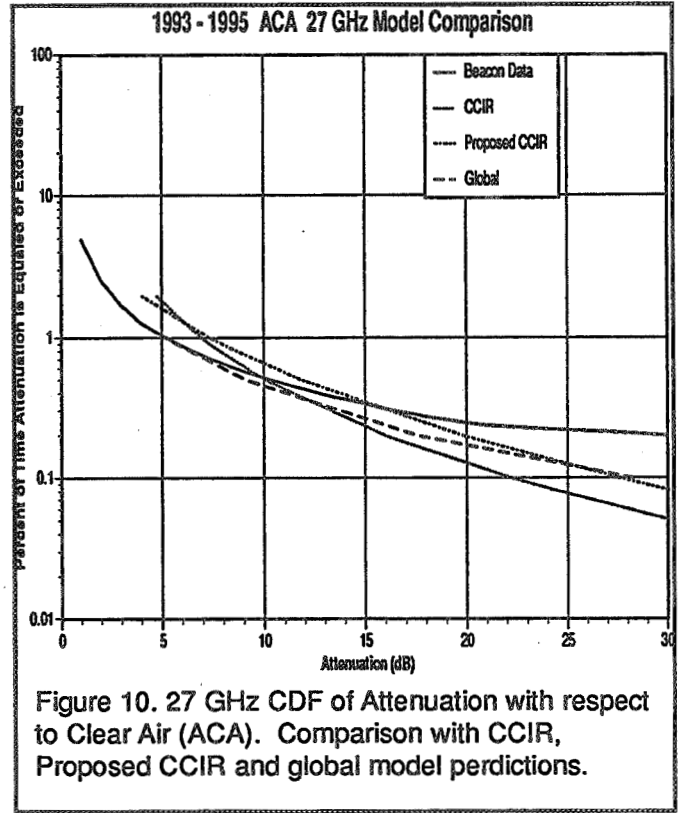


Figure 10. 27 GHz CDF of Attenuation with respect to Clear Air (ACA). Comparison with CCIR, Proposed CCIR and global model predictions.

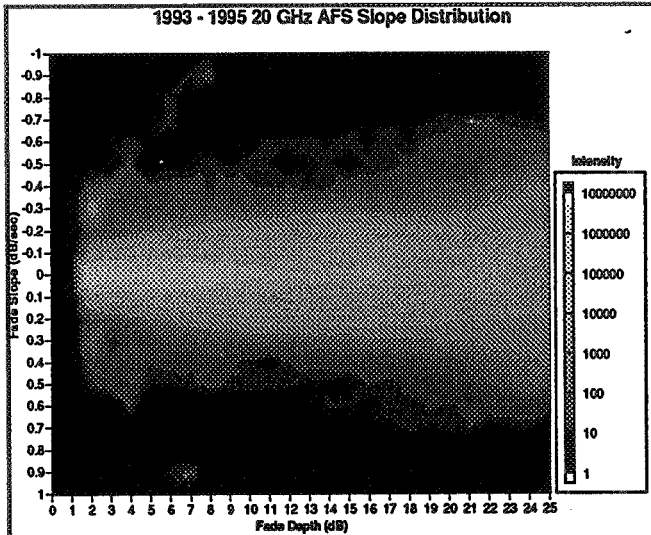


Figure 11. Contour plot of 20 GHz fade slopes. 10 second span of 30 second averaged data.

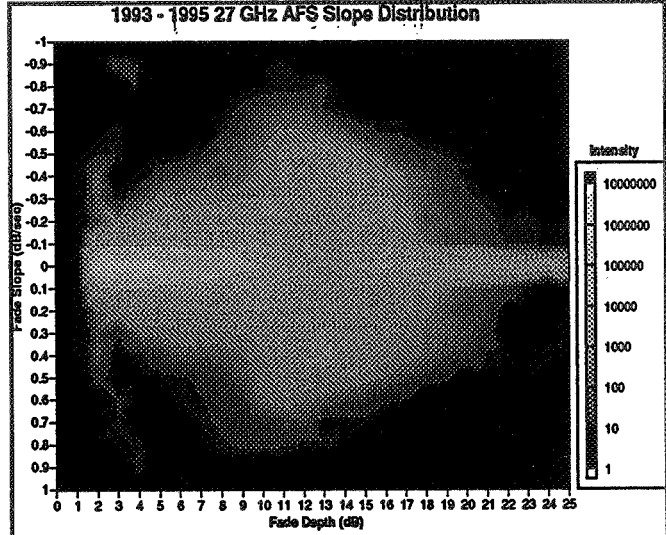


Figure 12. Contour plot of 27 GHz fade slopes. 10 second span of 30 second averaged data.

DIVERSITY MEASUREMENTS

* Diversity Improvement in the Florida sub-tropical Region

Focus on close-in Diversity Improvement < 5km - greatest commercial interest

* 20 GHz Diversity Terminal Operational
 1.2 m APT Dish
 Downconvert to 70 MHz at Feed
 APT Digital Receiver
 486 PC data recording in APT Format
 Easily Replicated (\$20K)

* Operated Successfully 1 Month Adjacent to APT

* In Negotiation on Several off-Campus Sites

* Continue for Duration of the ACTS Propagation Program

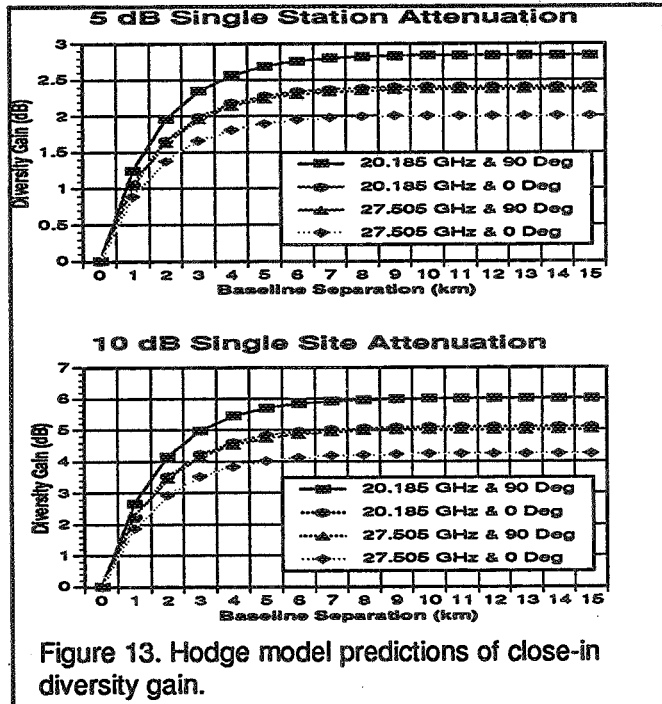


Figure 13. Hodge model predictions of close-in diversity gain.

PROGRAM PLANS

- * Maintain Current APT Terminal Operation
- * Continue Analysis Software Development
- * Detailed Rain Modeling
- * Continue Diversity Experiments
- * Polarization Experiments

CONCLUSION

- * SUCCESSFUL 2 Year Operational Period
- * Robust Software for Automated Analysis
- * Sub-tropical Fading Statistics
- * Diversity Experiments Initiated
- * All Systems "GO" for Continued Operation

Page intentionally left blank

ACTS Propagation Measurements in Maryland and Virginia

Asoka Dissanayake and Kuan-Ting Lin

COMSAT Laboratories

22300 COMSAT Drive, Clarksburg, MD 20871

1. Introduction

Rapid growth in new satellite services incorporating Very Small Aperture Terminals (VSAT) and Ultra Small Aperture Terminals (USAT) is expected in the coming years. Small size terminals allow for widespread use of satellite services in small business and domestic applications. Due to congestion of lower frequency bands such as C and Ku, most of these services will use Ka-band (20/30 GHz) frequencies. Propagation impairments produced by the troposphere is a limiting factor for the effective use of the 20/30 GHz band and the use of smaller earth terminals makes it difficult to provide sufficient link margins for propagation related outages. In this context, reliable prediction of propagation impairments for low-margin systems becomes important. Due to the complexity of propagation phenomena propagation modeling is mainly attempted on empirical basis. As such, availability of reliable measured data that extend to probability levels well in excess of the traditional limit of 1% is of great importance in the development, validation, and refinement of propagation models. The beacon payload on the ACTS satellite together with the propagation measurement terminals developed under the NASA ACTS propagation program provide an excellent opportunity to collect such data on a long-term basis. This paper presents results of ACTS propagation measurements conducted in the Washington DC metropolitan area by COMSAT Laboratories. The measurement program involves three sites, two in Maryland and one in Virginia. Measurements started soon after the launch of the ACTS satellite in September 1993. However, not all three sites were brought on line at the same time. Results from only two sites are presented in this paper; results from the third site are given in Reference 1. Use of multiple sites for the measurement enabled the investigation of site diversity to combat rain fading. Two of the sites use radiometers along with beacon measurement systems, thus allowing a careful estimation of gaseous absorption and other phenomena that produce relatively low attenuation levels. This helps to characterize the attenuation distribution for low availability levels, especially those between 1% and 10%. Several meteorological sensors are also deployed to help evaluate propagation models and to investigate the dependence of propagation impairments on meteorological factors.

A description of the measurement sites and the equipment used is given in Section 2. The three measurement systems are not identical and different data analysis procedures are used for the three systems. However, in each case the underlying analysis principles can be considered the same. Data analysis procedure used to convert raw data collected to a form suitable for the generation of attenuation statistics and other useful results are discussed in Section 3. Section 4 provides the salient results of the experiment. One of the sites reports results over a period of 24 months and the second site reports 21 months of data. Most of the results are presented in the form of monthly statistics. Comparison of standard model predictions with the measurement results is presented under summary and conclusions in Section 5.

2. Experiment Details

Figure 1 shows the measurement configuration. The three sites are located at Clarksburg, MD, Laurel, MD, and Reston, VA. At each site the approximate elevation angle to the ACTS satellite is 39° . The terminal at Clarksburg was developed at COMSAT Laboratories and is capable of receiving both 20 and 27 GHz beacon signals. The Laurel terminal is a Ka-band communication terminal which can receive only the 20 GHz beacon signal. The terminal at Reston is one of the NASA ACTS Propagation Terminals (APT) that can receive both the beacons. Table 1 gives all relevant geographical and receiving terminal parameters for the three sites.

Table 1. Measurement Site Parameters and Receiving System Details

Parameter	Clarksburg, MD	Reston, VA	Laurel, MD
Latitude	39.22° N	38.95° N	39.17° N
Longitude	77.28° W	77.33° W	76.90° W
Elevation Angle	38.8°	39.1°	38.7°
Azimuth Angle	213.5°	213.6°	214.0°
Polarization Angle	64.7°	64.5°	64.3°
Distance from Clarksburg		30.5 km	32.9 km
Antenna Diameter	1.2 m	1.2 m	1.2 m
Antenna Gain 20 GHz	46.0 dB	46.0 dB	46.0 dB
Antenna Gain 27 GHz	48.7	48.7	-
Antenna Beamwidth 20 GHz	0.85°	0.85°	0.85°
Antenna Beamwidth 27 GHz	0.63°	0.62°	-
G/T 20 GHz	14.2 dB/K	14.2 dB/K	15 dB/K
G/T 27 GHz	16.8 dB/K	16.8 dB/K	-
Detection Bandwidth	64 Hz	20 Hz	400 Hz
Dynamic Range 20 GHz	28 dB	30 dB	22 dB
Dynamic Range 27 GHz	26 dB	29 dB	-
Sampling Rate: Beacons	5 Hz	1 Hz	5 Hz
:Radiometers	3 sec.	1 Hz	-
Meteorological Sensors:			
Rain Rate	Yes	Yes	Yes
Temperature	Yes	Yes	No
Humidity	Yes	Yes	No
Pressure	No	Yes	No
Wind Speed	Yes	Yes	No

The APT uses a fully digital receiver with a detection bandwidth of 20 Hz. The receiver at Clarksburg uses the same RF electronics as the APT; the IF receiver is a selective level meter with a detection bandwidth of 64 Hz. The Laurel site also uses a selective level meter as the IF receiver with a somewhat larger detection bandwidth of 400

Hz. Total power radiometers which share the same RF electronics as the beacon receivers are used in the APT. These require periodic calibration using a noise diode and a reference load. The calibration is carried out at 15 minute intervals and lasts approximately 20 seconds. During the calibration the beacon signal is not available. The radiometers are also calibrated using hot and cold loads every six weeks. Radiometers in the Clarksburg terminal also share the RF electronics with the beacon receivers. However, they are of Dicke type where gain variations in the receiving system are removed by switching between the antenna and a highly stable reference load. The switching operation is such that it does not interfere with the beacon reception in any noticeable manner. Calibration of the Dicke radiometers are carried out using hot and cold loads on a bimonthly basis. All three terminals share a common antenna design. The antenna gain was found to degrade appreciably when the antenna surface is subject to wetting. Although the degradation can be somewhat reduced using a hydrophobic coating, the measurements are made without any treatment to the antenna surface.

Data collection at the Clarksburg site started in October 1993, the Reston site in March 1994, and the Laurel site in September 1993. After the first 12 months of measurements the terminal at Reston was moved to a new site approximately 1 km away from the old site. Due to the closeness of the two sites no significant climatological differences are expected and the data from the two sites are treated as belonging to a single site.

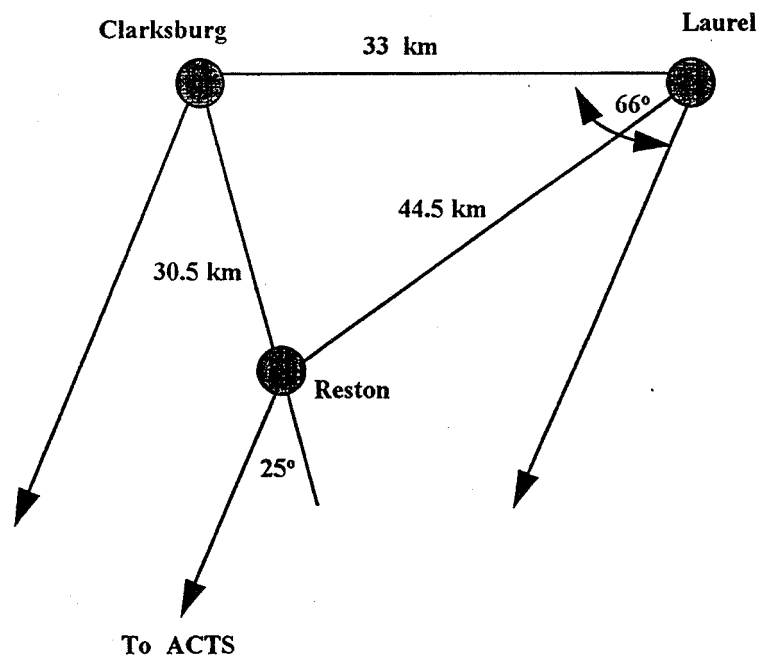


Figure 1 Experiment Site Configuration

3. Data Analysis Procedures

Data analysis is carried out in two stages: a preprocessing stage to remove all undesired features in the raw data and the analysis stage where relevant statistics and other information are generated. The preprocessing stage involves the removal of:

- outliers
- modulation pulses
- calibration intervals
- sun outages
- signal loss due to eclipse operation
- satellite generated interference in the 20 GHz radiometer

Outliers are generated by power line surges and other types of short-lived disturbances. Modulation pulses are present only on the 20 GHz beacon channel and these manifest as signal enhancements ranging from 0.4 dB to 0.8 dB. Both automatic and manual calibration intervals are present in the beacon and radiometer channels and these must be removed and new calibration constants derived to process the subsequent data. Sun interference on radiometer channels occurs twice a year and these must be identified and removed. During the eclipse operation of the satellite, transition from solar to battery power and vice versa generate rapid frequency drifts that cannot be tracked by the receivers; these must be identified and removed. Satellite spot beams generate sufficient noise to interfere with the operation of the 20 GHz radiometers. Frequent use of the east spot beam of the satellite in the Washington DC area by other ACTS experimenters required additional processing to remove these interferences.

In addition, radiometer calibration, bias removal of the beacon signals, and conversion of rain accumulation to rain rate are carried out during the preprocessing stage. The radiometer calibration process involves matching the radiometer estimated attenuation with the attenuation estimations based on meteorological data under clear-sky conditions. The bias removal involves the separation of equipment induced variations in the beacon signal from those due to propagation effects. Bias removal is carried out assuming that the radiometer provides a very good estimate of the signal attenuation under clear-sky and low attenuation conditions. The rain gauge used for the measurement provides sample values of rain accumulation and the preprocessing software converts these into rain rates.

Data analysis for the Reston terminal (APT) was carried out using the standard software supplied by NASA. The analysis software is described in Reference 2. However, the software is not capable of removing all of the undesired contaminants mentioned above. The processed data were visually inspected to identify these contaminants and they were removed manually. As an example, the satellite interferences on the 20 GHz radiometer were removed by declaring such episodes as invalid data. The sun interferences on the radiometer channels were removed by interpolating across the interference event.

Data from the Clarksburg terminal were analyzed using a separate software package. The preprocessing steps are essentially the same as those for the Reston terminal. However, data were subjected to visual inspection before and after the preprocessing stage for the identification and eventual removal of all contaminants. Additionally, the 5 samples per second input data were averaged to obtain one second samples at the output.

The preprocessed data are used to generate different types of statistics. The statistical analysis of the APT data is based on one minute averages; that of the Clarksburg data is based on one second samples.

4. Results

The following list gives the different types of analysis carried out in monthly units and will be presented in an interim report to NASA.

1. Cumulative distribution function of 20.2 GHz beacon attenuation
2. Cumulative distribution function of 27.5 GHz beacon attenuation
3. Cumulative distribution function of 20.2 GHz radiometrically derived attenuation
4. Cumulative distribution function of 27.5 GHz radiometrically derived attenuation
5. Cumulative distribution function of 20.2 GHz clear sky attenuation
6. Cumulative distribution function of 27.5 GHz clear sky attenuation
7. Cumulative distribution function of 20.2 GHz sky noise temperature
8. Cumulative distribution function of 27.5 GHz sky noise temperature
9. Cumulative distribution function of 20.2 GHz beacon standard deviation (1 minute average)
10. Cumulative distribution function of 27.5 GHz beacon standard deviation (1 minute average)
11. Cumulative distribution function of 20.2 GHz radiometrically derived attenuation standard deviation (1 minute average)
12. Cumulative distribution function of 27.5 GHz radiometrically derived attenuation standard deviation (1 minute average)
13. Cumulative distribution function of 20.2 GHz fade duration
14. Cumulative distribution function of 27.5 GHz fade duration
15. Cumulative distribution function of 20.2 GHz inter-fade intervals
16. Cumulative distribution function of 27.5 GHz inter-fade intervals
17. Cumulative distribution function of rain rate
18. Cumulative distribution function of ambient temperature
19. Cumulative distribution function of humidity
20. Cumulative distribution function of pressure

As mentioned in the previous section the results for the Reston site are generated with one minute averages of the various parameters. Results for the Clarksburg site are generated using one second samples; however, these are presented only as annual summaries in the next section. Joint attenuation statistics between Clarksburg and Reston

for the first 12 months of joint operation are also presented in the next section; only the 20 and 27 GHz beacon attenuation are given. Results from the Laurel site can be found in Reference 1.

5. Summary Results

Statistical results presented as monthly units in the previous section were used to generate annual statistics of attenuation and fade durations. In addition, statistics of frequency scaling ratio between the two beacon frequencies were generated. In the ensuing pages, most of the statistical results are compared with appropriate propagation models.

5.1 Rain Rate

Rain measurements at the Reston site was not successful due to difficulties with the rain gauge and only the results from Clarksburg are presented. Figure 2 shows the cumulative distribution of rain rate for the two measurement years (November 1993 to October 1994 and November 1994 to October 1995). It is seen that the second year experienced less rainfall than the first year. Also shown in the figure are the rain rates from three models:

- Rice-Holemborg model [3]
- ITU rain zone classification [4]
- Crane global rain model [5]

The Rice-Holmberg model requires average annual accumulation of rainfall, M (mm), and the fraction of rainfall due to thunderstorm activity, β . Based on long-term meteorological data, these two parameters for the Clarksburg site are: $M = 936$ mm and $\beta = 0.29$. According to ITU rain zone classification the Clarksburg site belongs to rain zone K; global rain zone for the site is D2. It is seen that the Rice-Holmberg and Global models provide closer fits to the measured data averaged over the two year period than the ITU model. However, it should be noted that all three models attempt to provide average rain statistics over a relatively longer measurement period (> 5 years).

5.2 Single Site Attenuation

Attenuation statistics for the two year period from November 1993 to October 1995 for the Clarksburg site are shown in Figure 3 and 4 for the beacon frequencies 20 and 27 GHz, respectively. In Figure 5 same statistics for the Reston site are shown; statistics shown are for the 12 months period from March 1994 to February 1994. Since the two sites belong to the same general rain climate the behavior of attenuation statistics in each case is quite similar. As noted earlier, at Clarksburg attenuation is less severe in the second year.

Model predictions of attenuation statistics for the two sites are also shown in Fig. 3 and 4. Two models are shown: ITU-R rain attenuation model [6], and SPM [7]. The ITU-R models include gaseous absorption based on the ITU-R gaseous absorption model; gaseous absorption corresponding to average temperature and relative humidity conditions is added to the rain attenuation. In the case of SPM, gaseous absorption, cloud attenuation, and melting layer attenuation are included in the prediction. It is seen that SPM provides a better agreement with measured data than the other model.

5.3 Joint Attenuation

Figures 6 through 17 show various joint attenuation statistics for the Clarksburg and Reston sites; measurement period: March, 1994 to February, 1995. These are:

- monthly single site and joint attenuation
- annual single site and joint attenuation with model predictions
- annual statistics of unbalance diversity

From Fig 14 and 15 it is seen that the ITU-R site diversity model generally under predicts the diversity gain for attenuation levels above about 5 dB. Diversity gain is less susceptible to year-to-year variations and therefore, no plausible explanation can be given for the discrepancy.

5.4 Fade Durations

Figures 18 - 21 present statistics of fade durations and inter-fade intervals over a period of 12 months at Clarksburg.

6. References

1. J. Goldhirsh; Diversity Experiments at Ka-Band
NAPEX-96, Fairbanks, AL, 1996
2. R. Crane; Data Processing Procedures
NAPEX-96, Fairbanks, AL, 1996
3. P. L. Rice, N. R. Holmberg; Cumulative Time Statistics of Surface Point Rainfall Rates
IEEE Trans COM-21, 1973
4. CCIR Study Group V; Report 563, 1990
5. R. Crane; A Two-component Rain Model for the Prediction of Attenuation Statistics
Radio Science, Vol. 17, 1982
6. ITU Recommendation 618

7. A. Dissanayake; Propagation Models for Ka-band Applications
ACTS Propagation Workshop, APSW VIII, Norman, OK, 1995

Figure 2 Rain Rate Cumulative Distribution

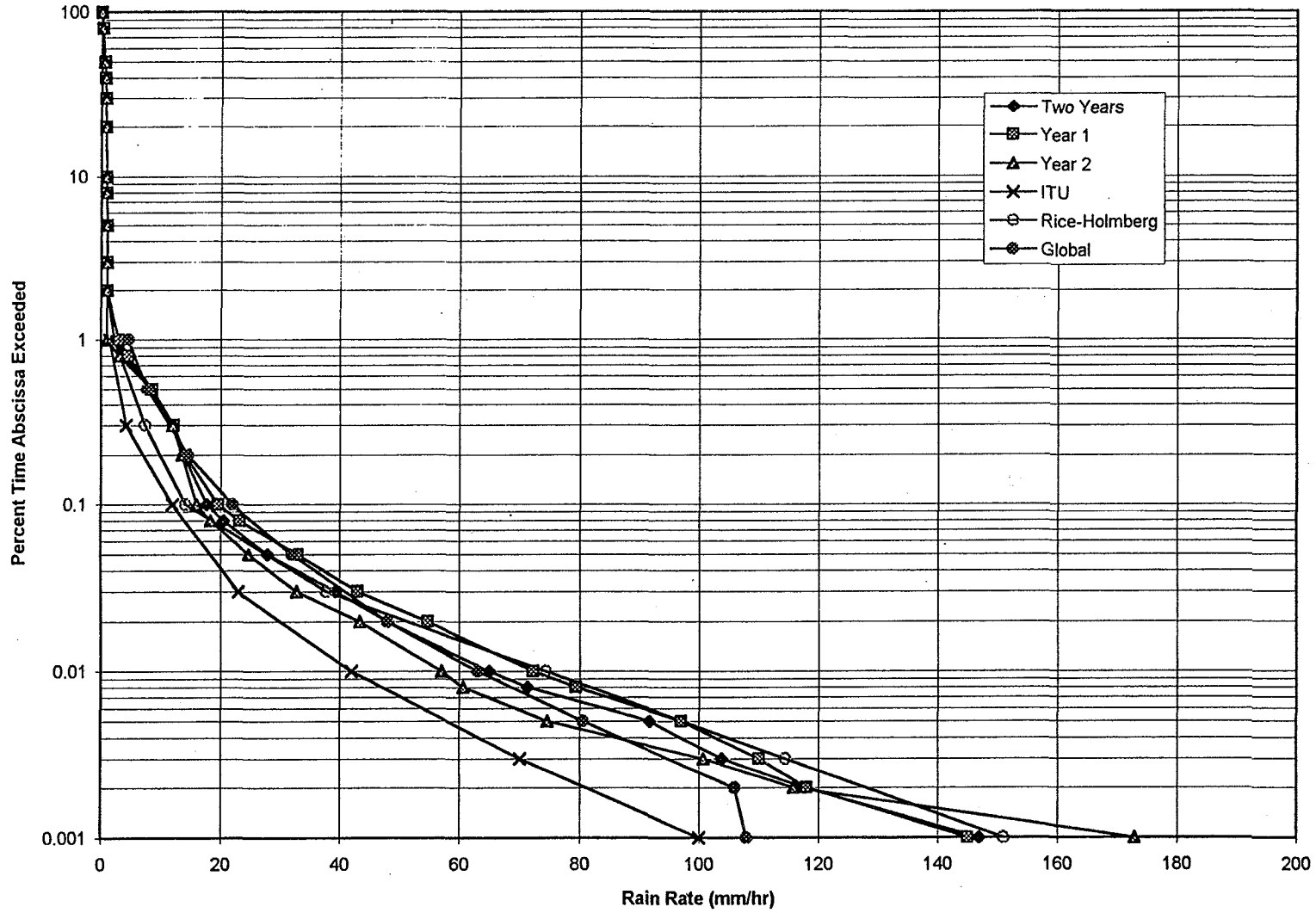


Figure 3 20.2 GHz Attenuation Cumulative Distribution: Clarksburg

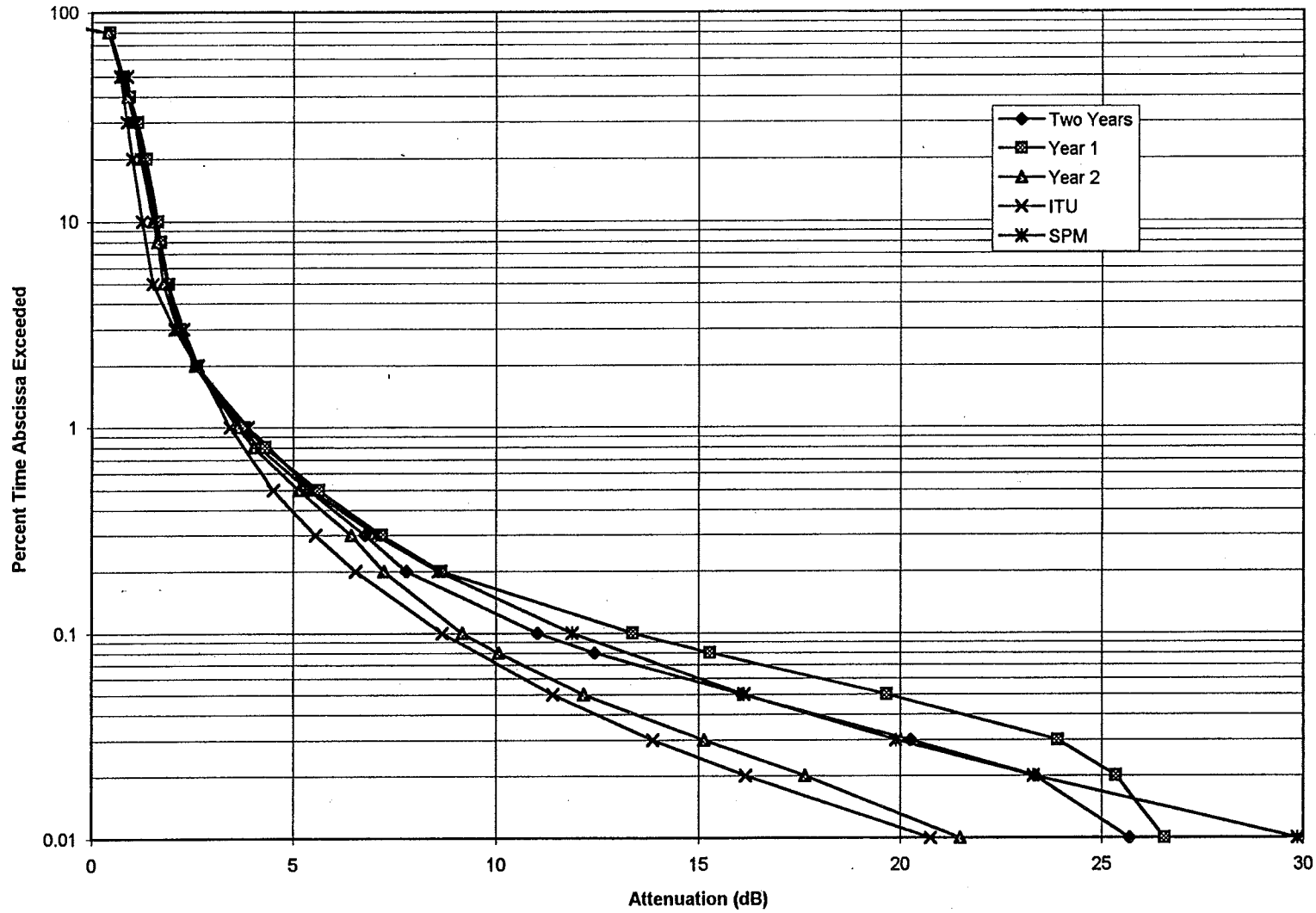


Figure 4 27.5 GHz Attenuation Cumulative Distribution: Clarksburg

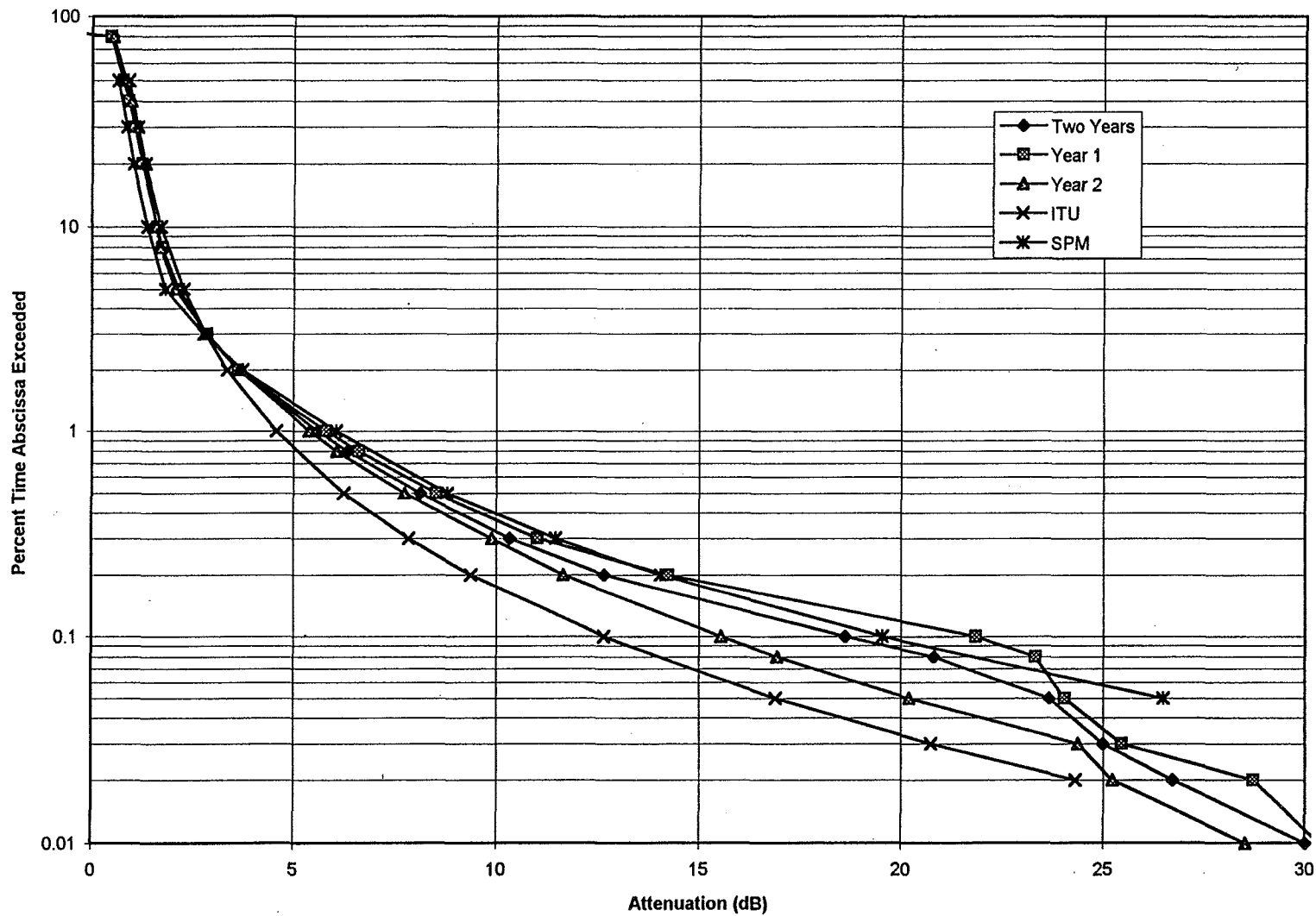
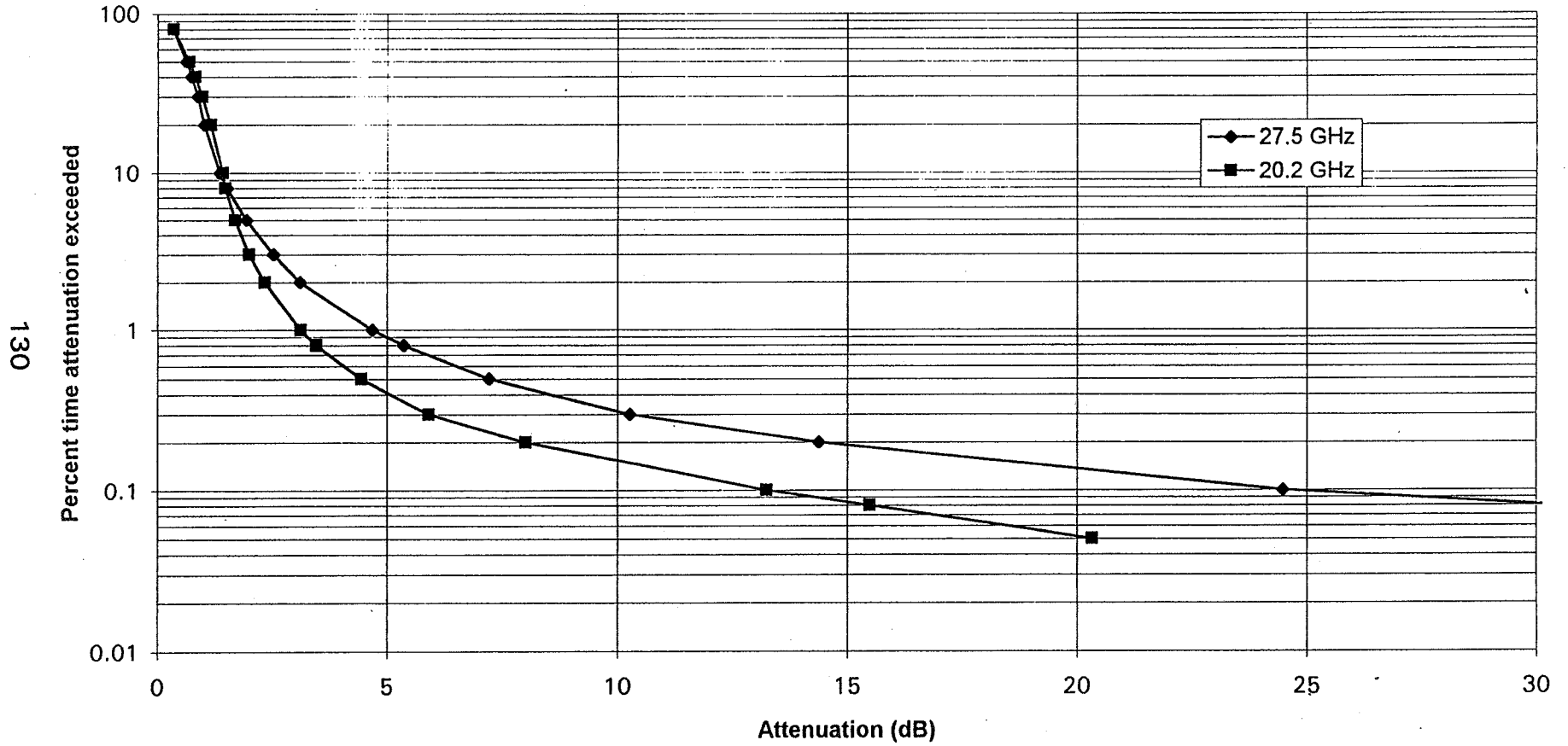


Figure 5. 27.5 and 20.2 GHz Attenuation Distribution: Reston



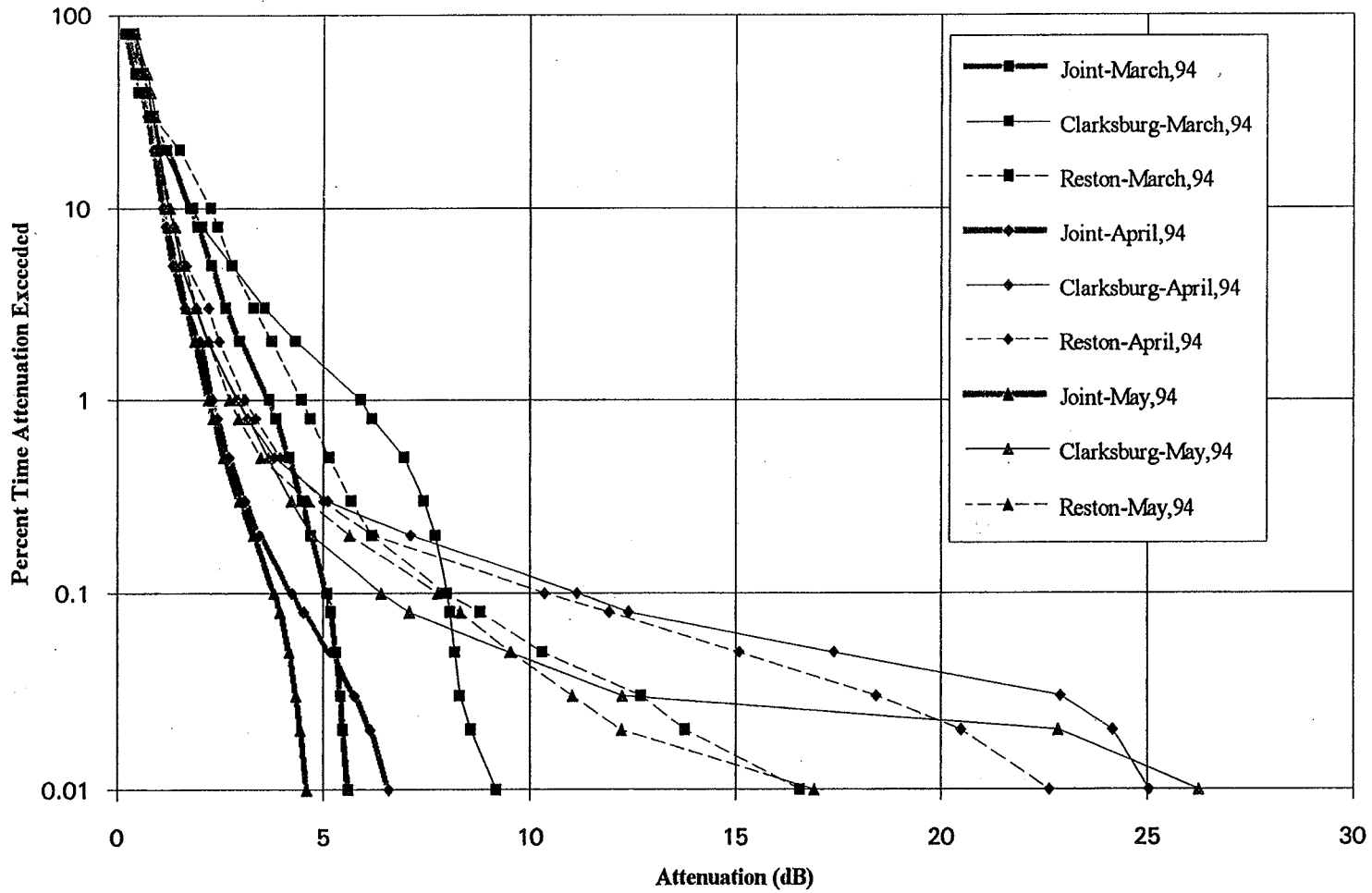


Figure 6 Single Site and Joint Cumulative Distribution of Attenuation at 20 GHz; March, April, and May 1994

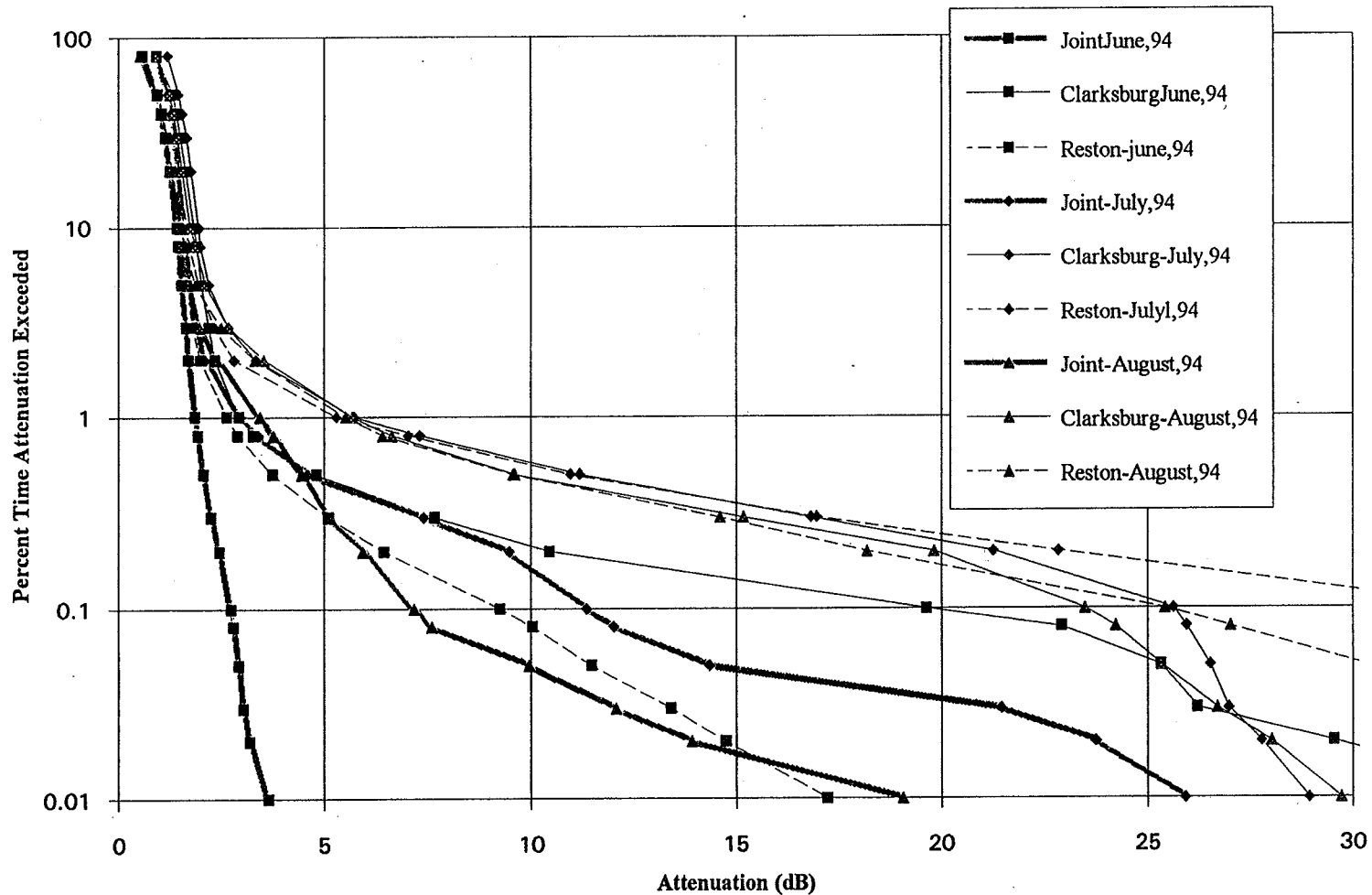


Figure 7 Single Site and Joint Cumulative Distribution of Attenuation at 20 GHz; June, July, and August 1994

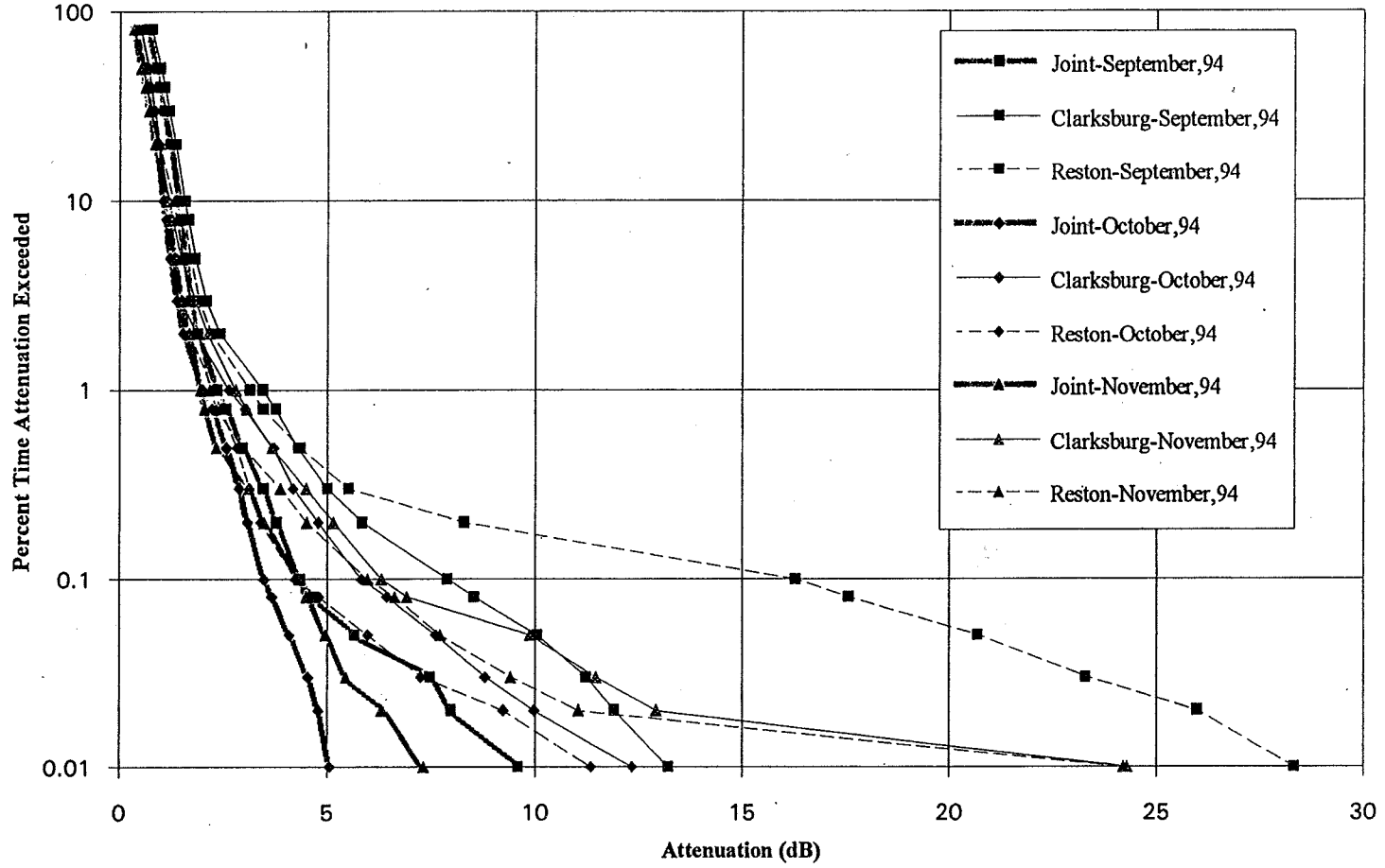
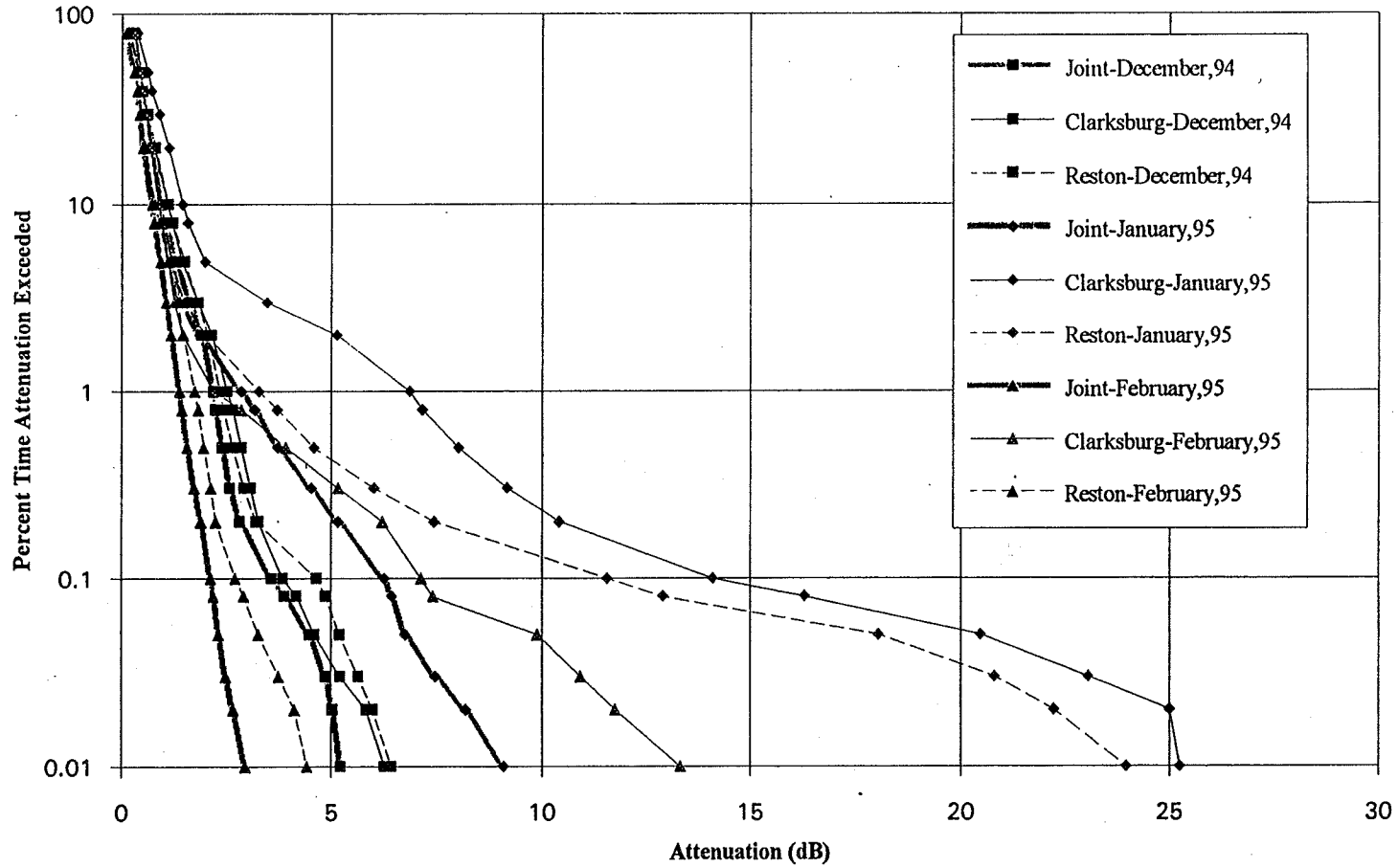


Figure 8 Single Site and Joint Cumulative Distribution of Attenuation at 20 GHz; September, October, and November 1994



**Figure 9 Single Site and Joint Cumulative Distribution of Attenuation at 20 GHz;
December 1994, January and February 1995**

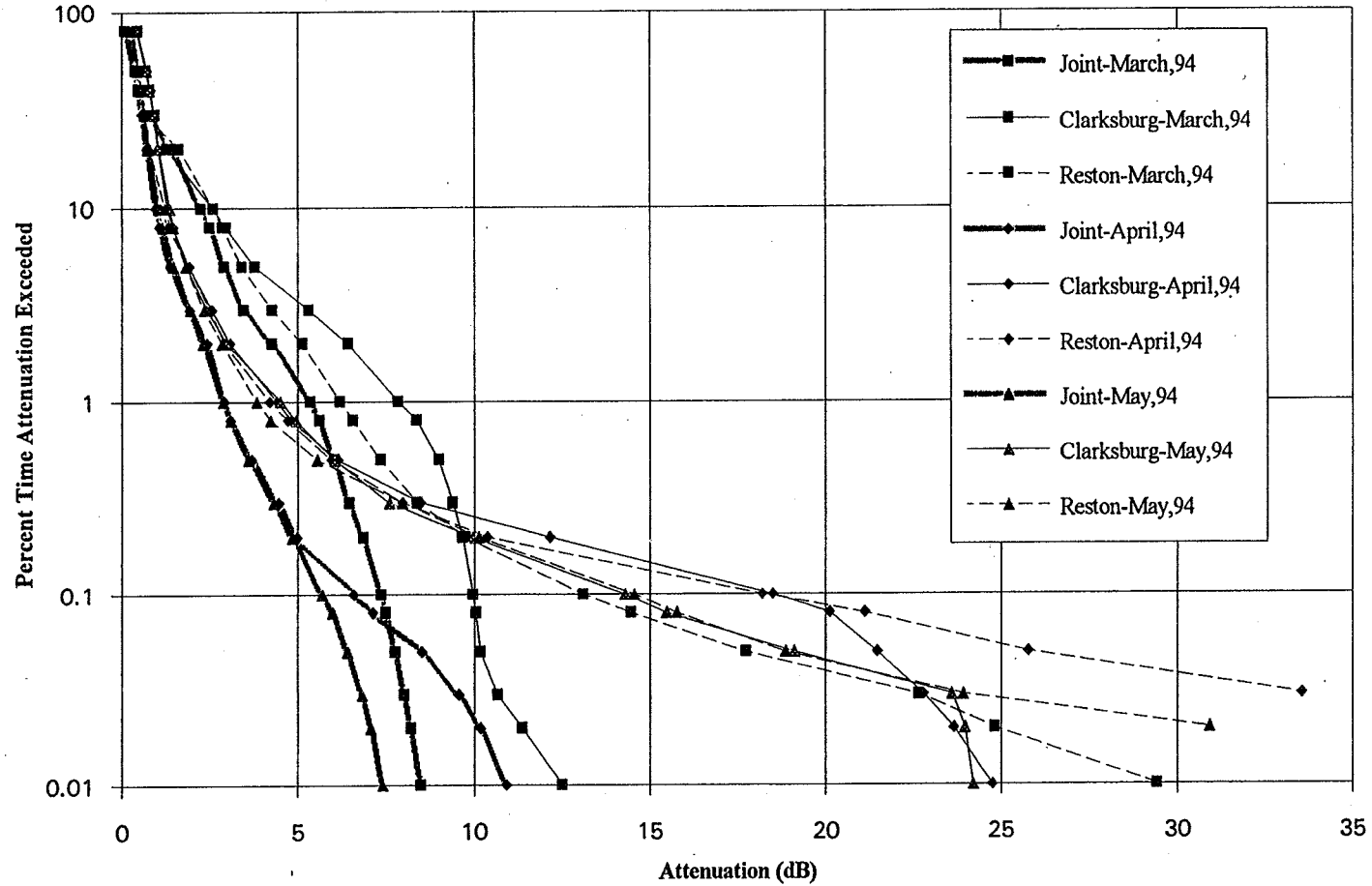


Figure 10 Single Site and Joint Cumulative Distribution of Attenuation at 27.5 GHz; March, April, and May 1994

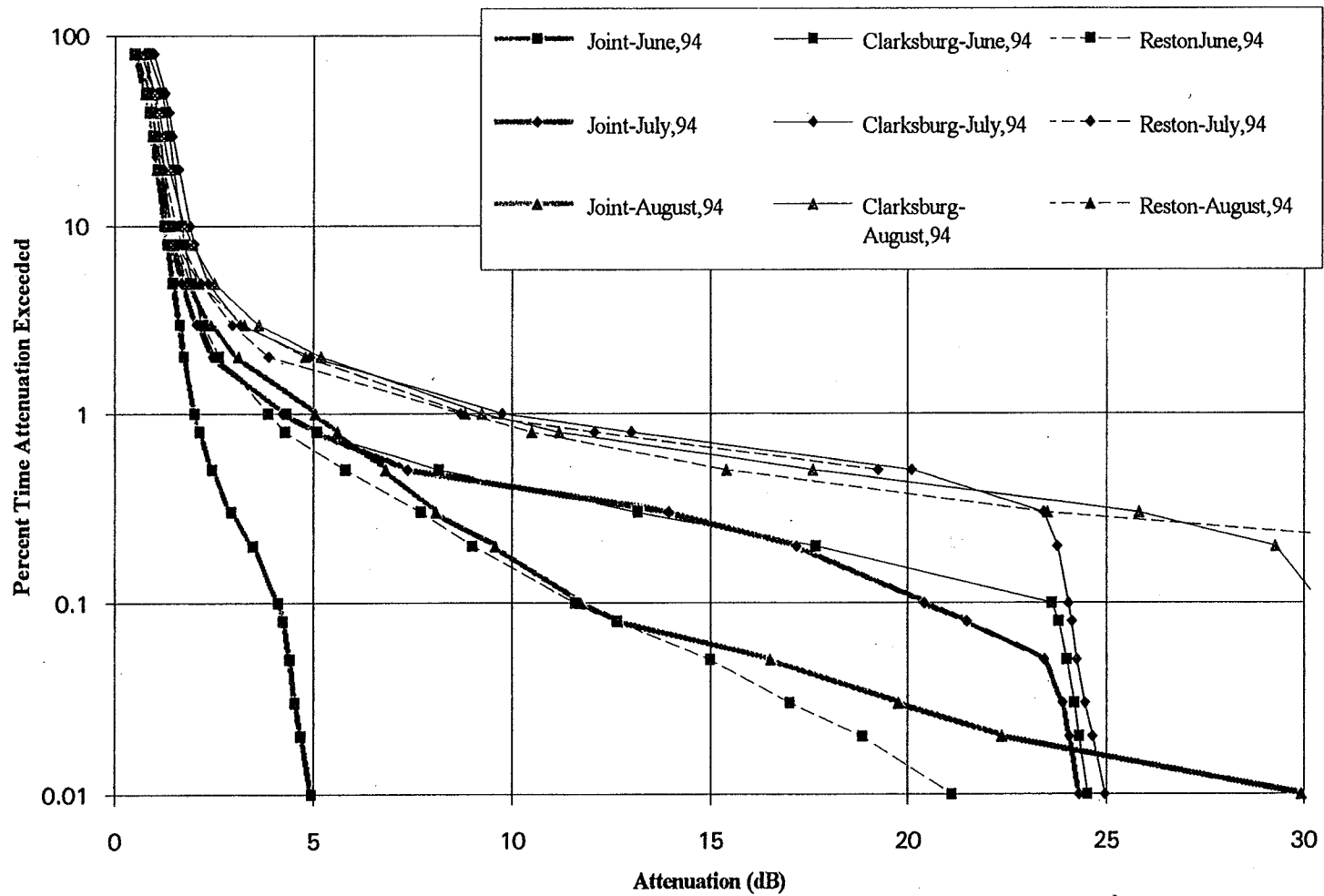
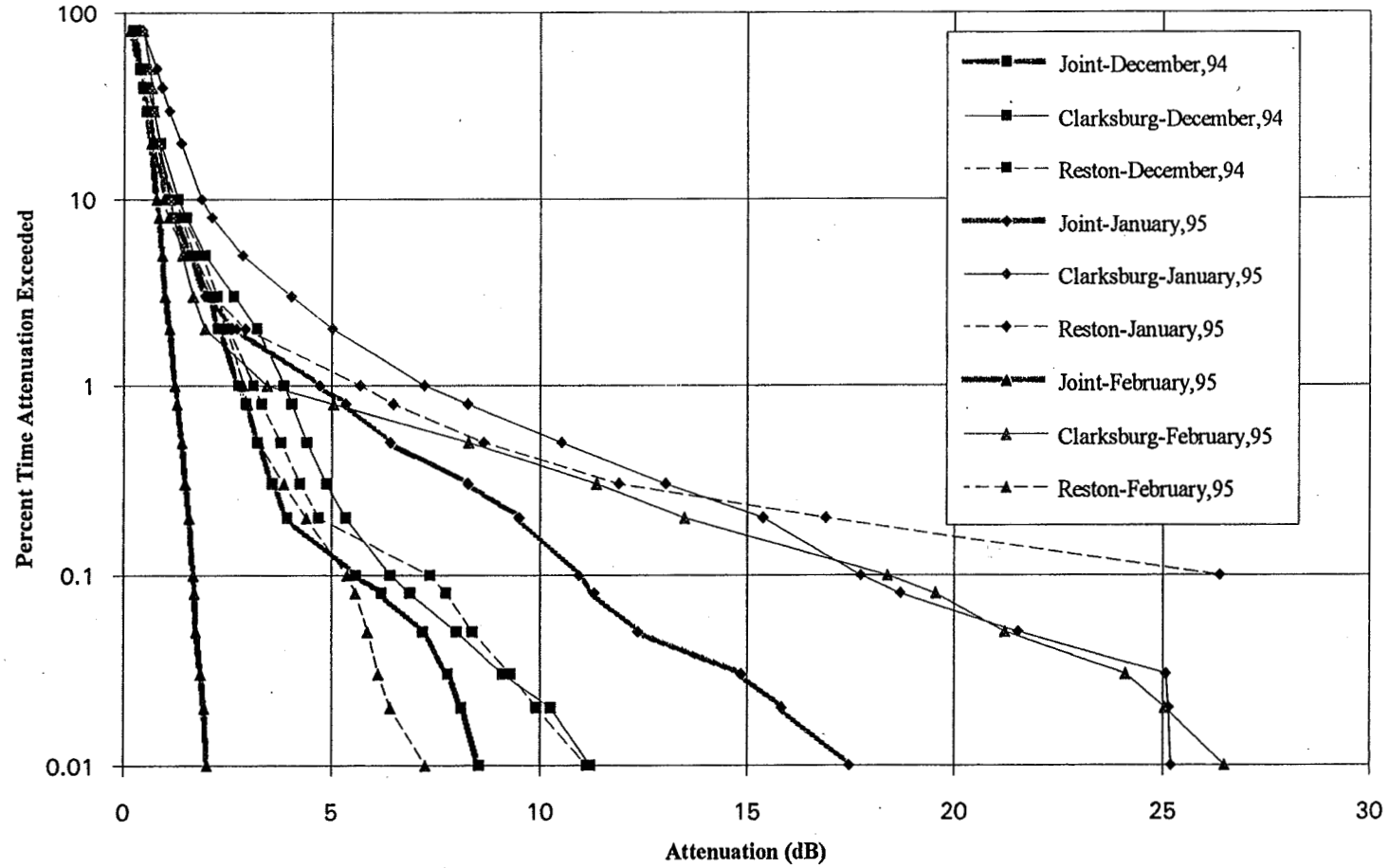
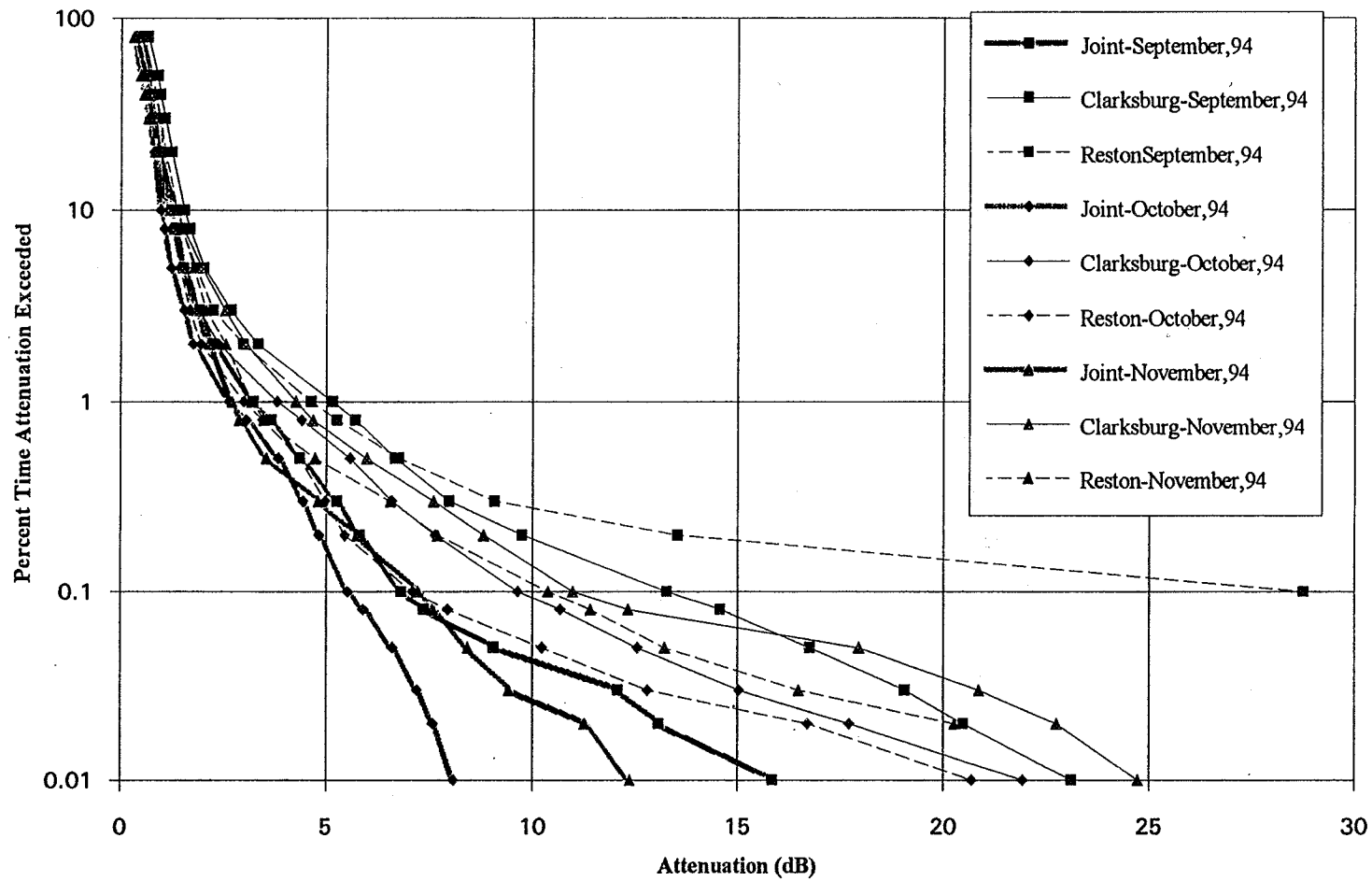


Figure 11 Single Site and Joint Cumulative Distribution of Attenuation at 27.5 GHz; June, July, and August 1994



**Figure 12 Single Site and Joint Cumulative Distribution of Attenuation at 27.5 GHz;
September, October, and November 1994**



*Figure 13 Single Site and Joint Cumulative Distribution of Attenuation at 27.5 GHz;
December 1994, January and February 1995*

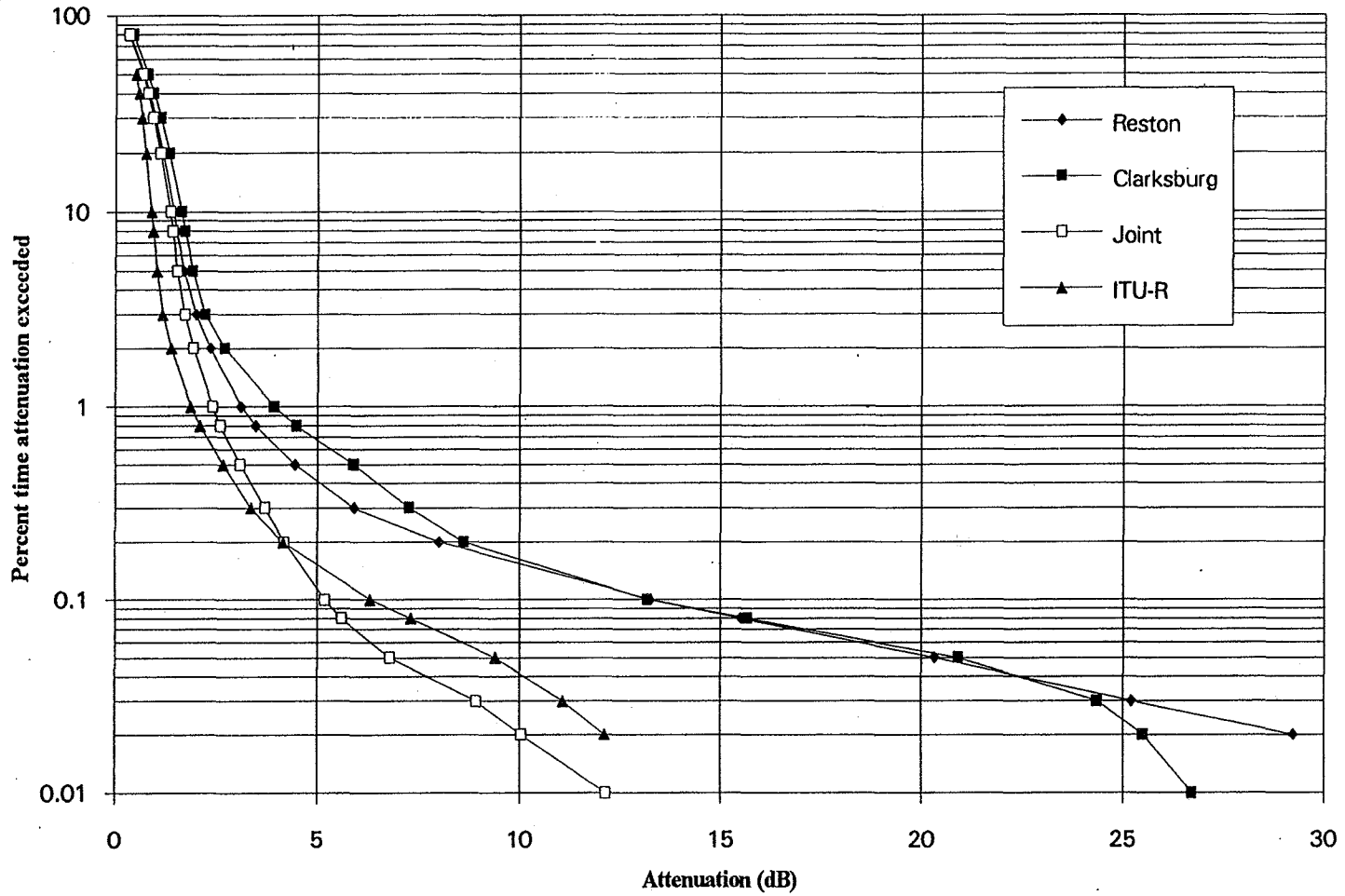


Figure 14 Cumulative Distribution of Single Site and Joint Attenuation at 20 GHz; March 1994 - February 1995

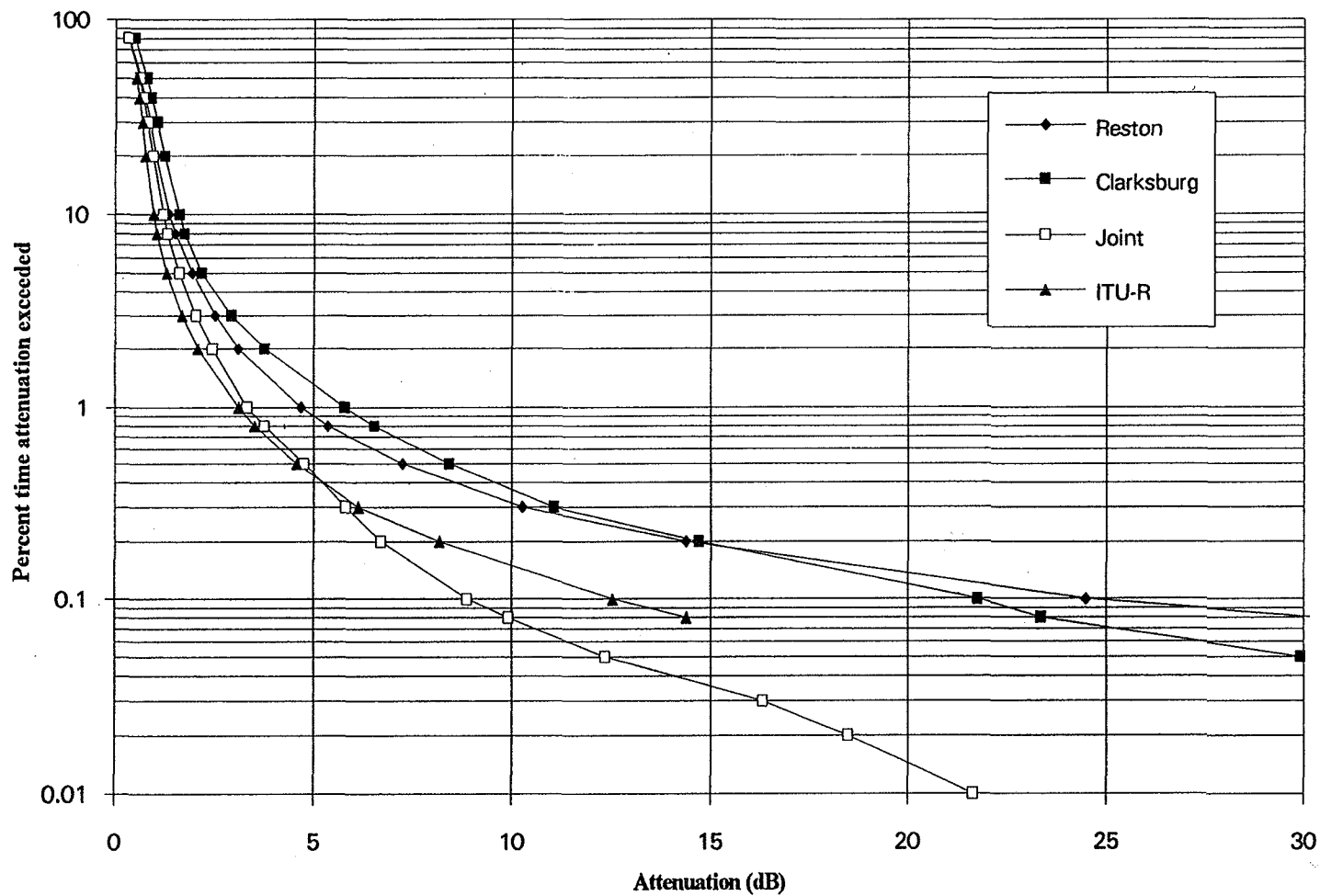


Figure 15 Cumulative Distribution of Single Site and Joint Attenuation at 27.5 GHz; March 1994 - February 1995

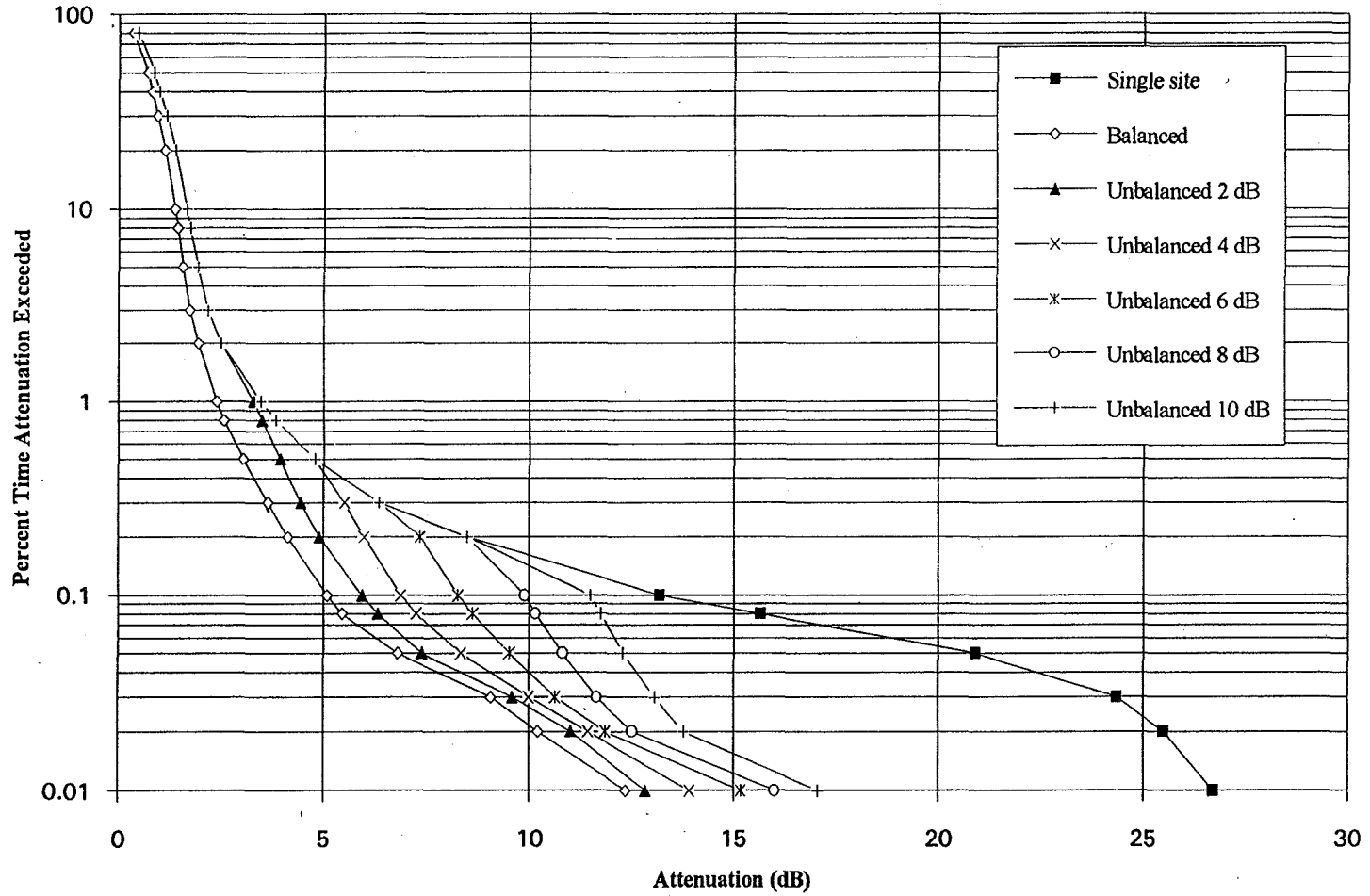


Figure 16 Cumulative Distribution of Joint Attenuation for Unbalanced Diversity at 20 GHz

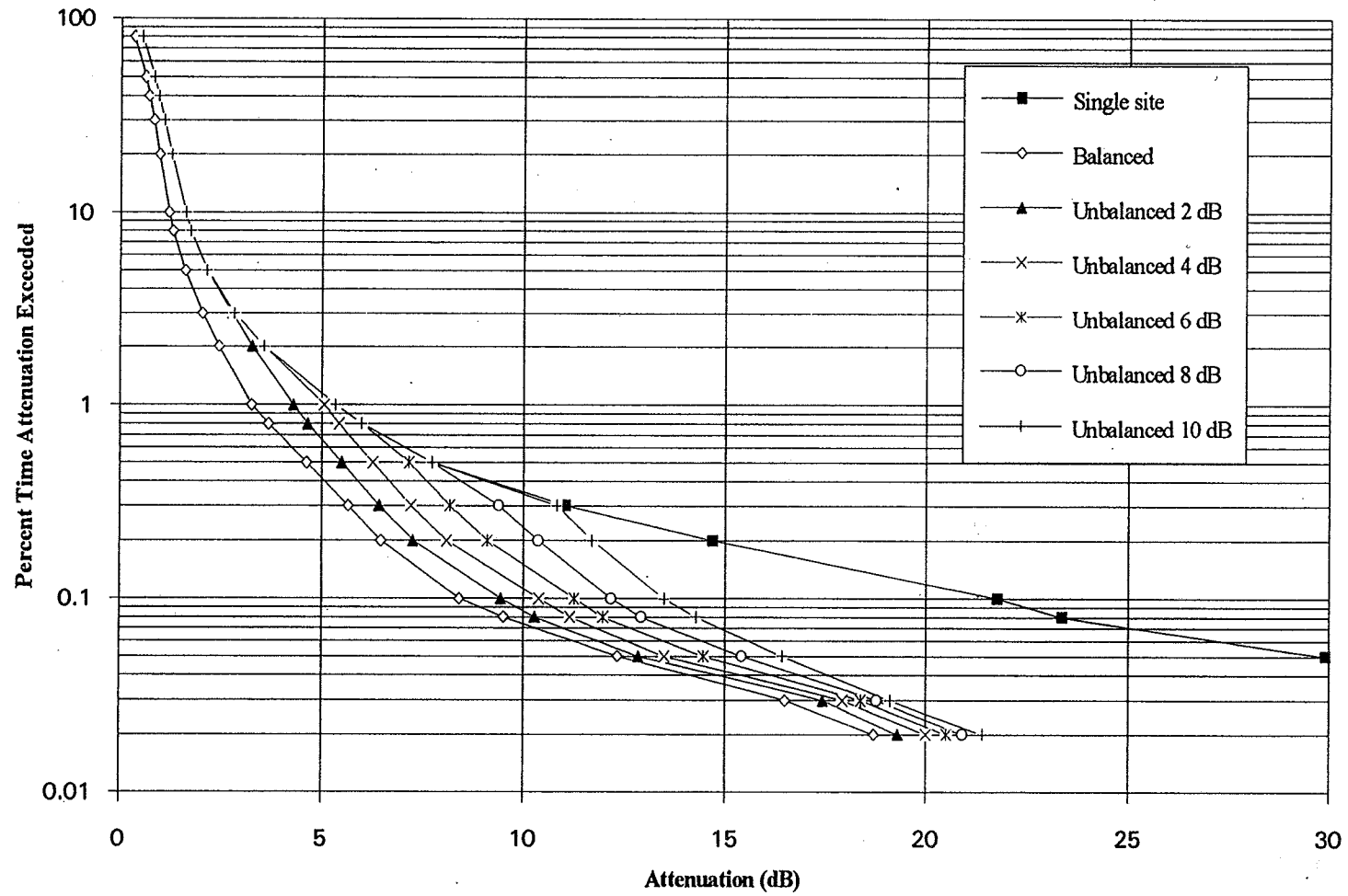


Figure 17 Cumulative Distribution of Joint Attenuation for Unbalanced Diversity at 27.5 GHz

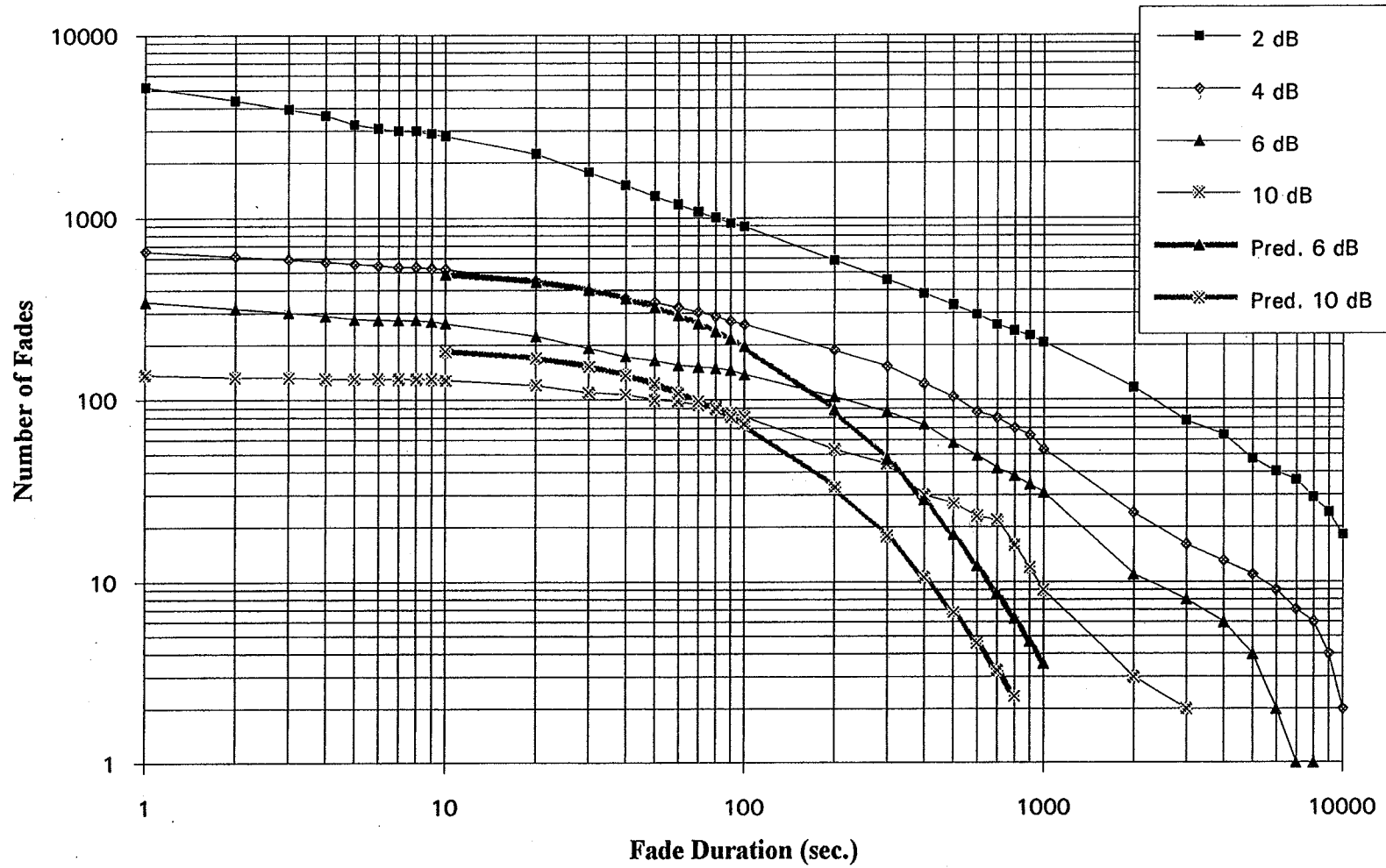


Figure 18 Fade Duration Distribution at 20 GHz; measurement period: March 1994 to February 1995

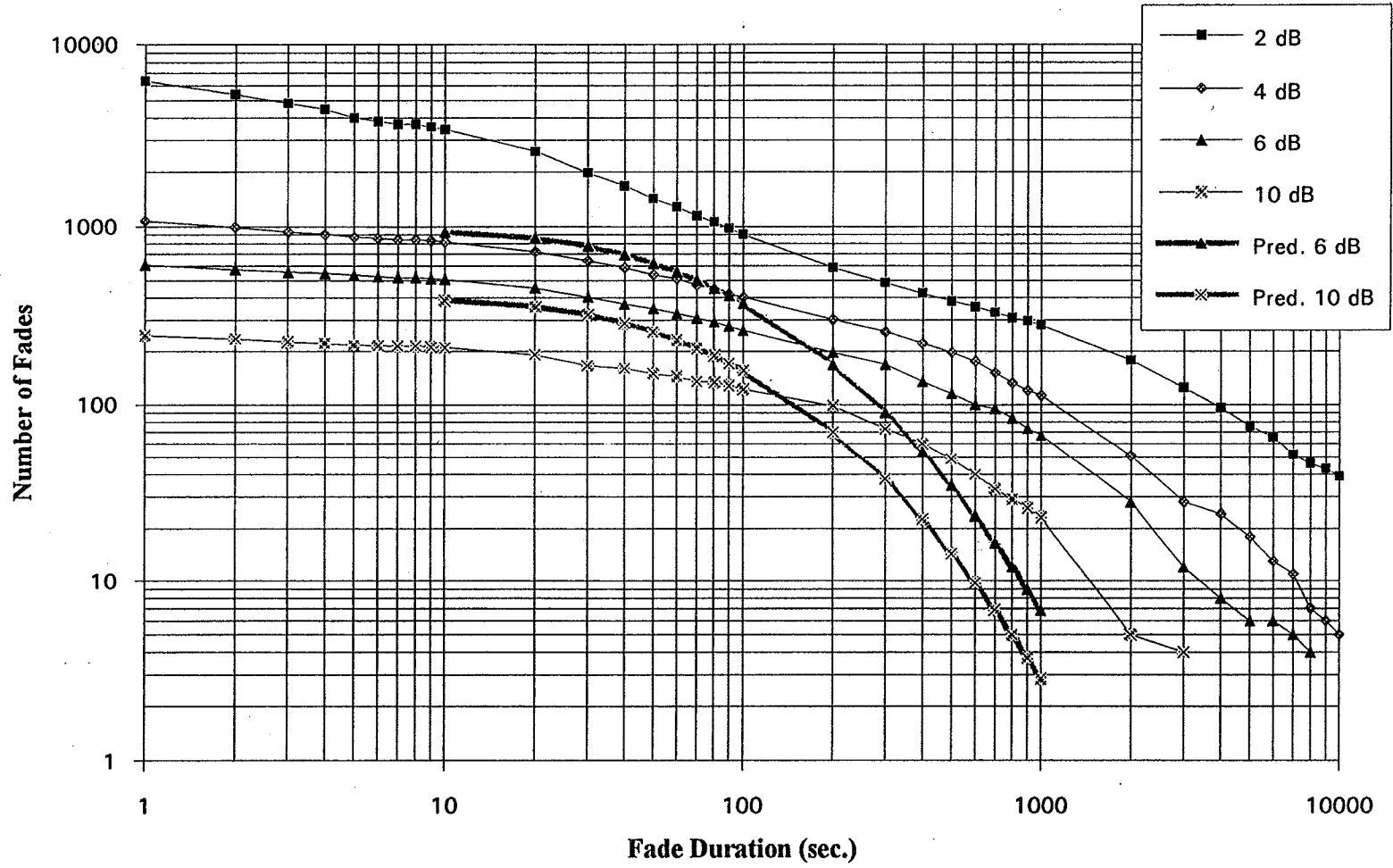


Figure 19 Fade Duration Distribution at 27.5 GHz; measurement period: March 1994 to February 1995

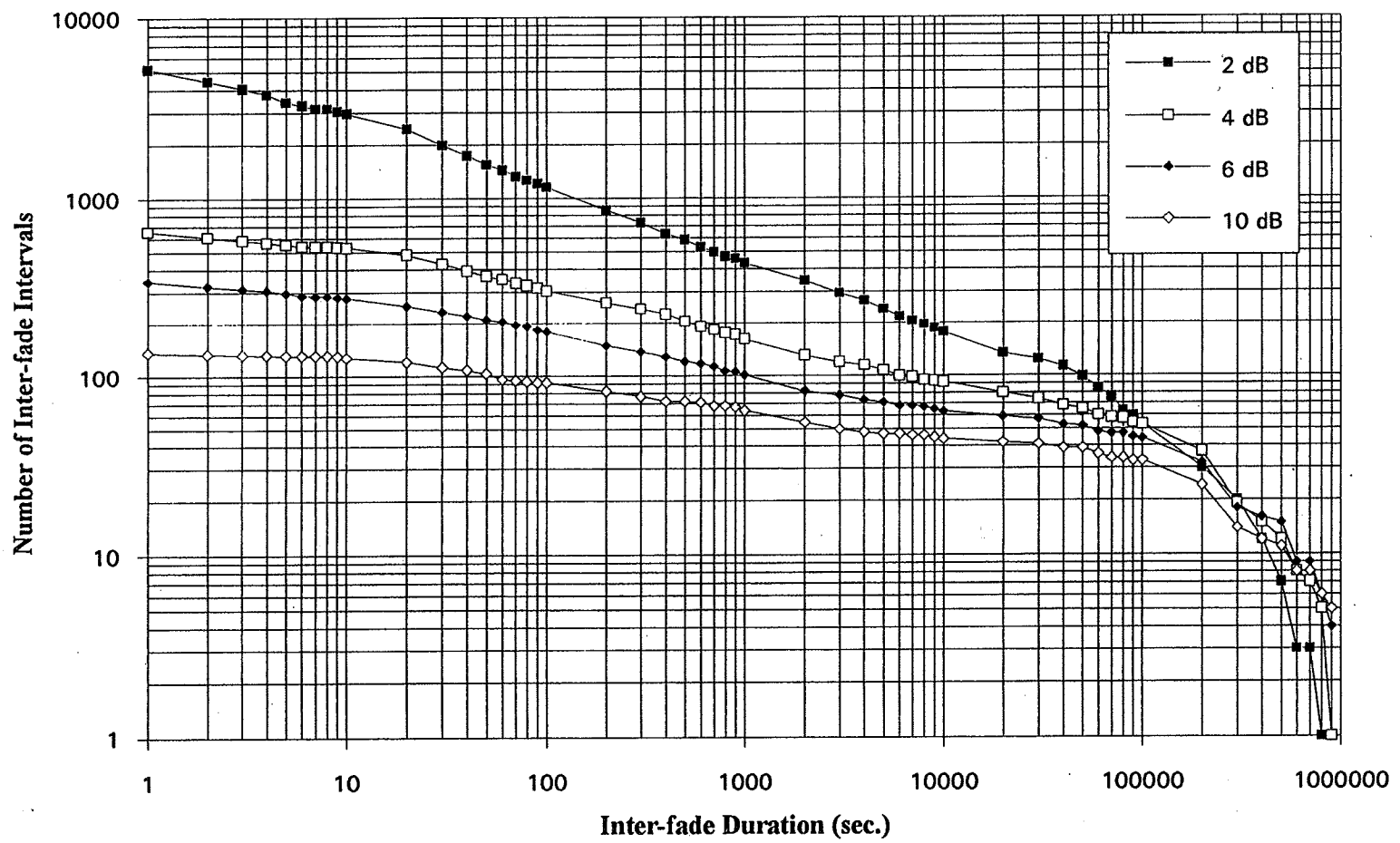


Figure 20 Distribution of Inter-fade Intervals at 20 GHz; measurement period: March 1994 to February 1995

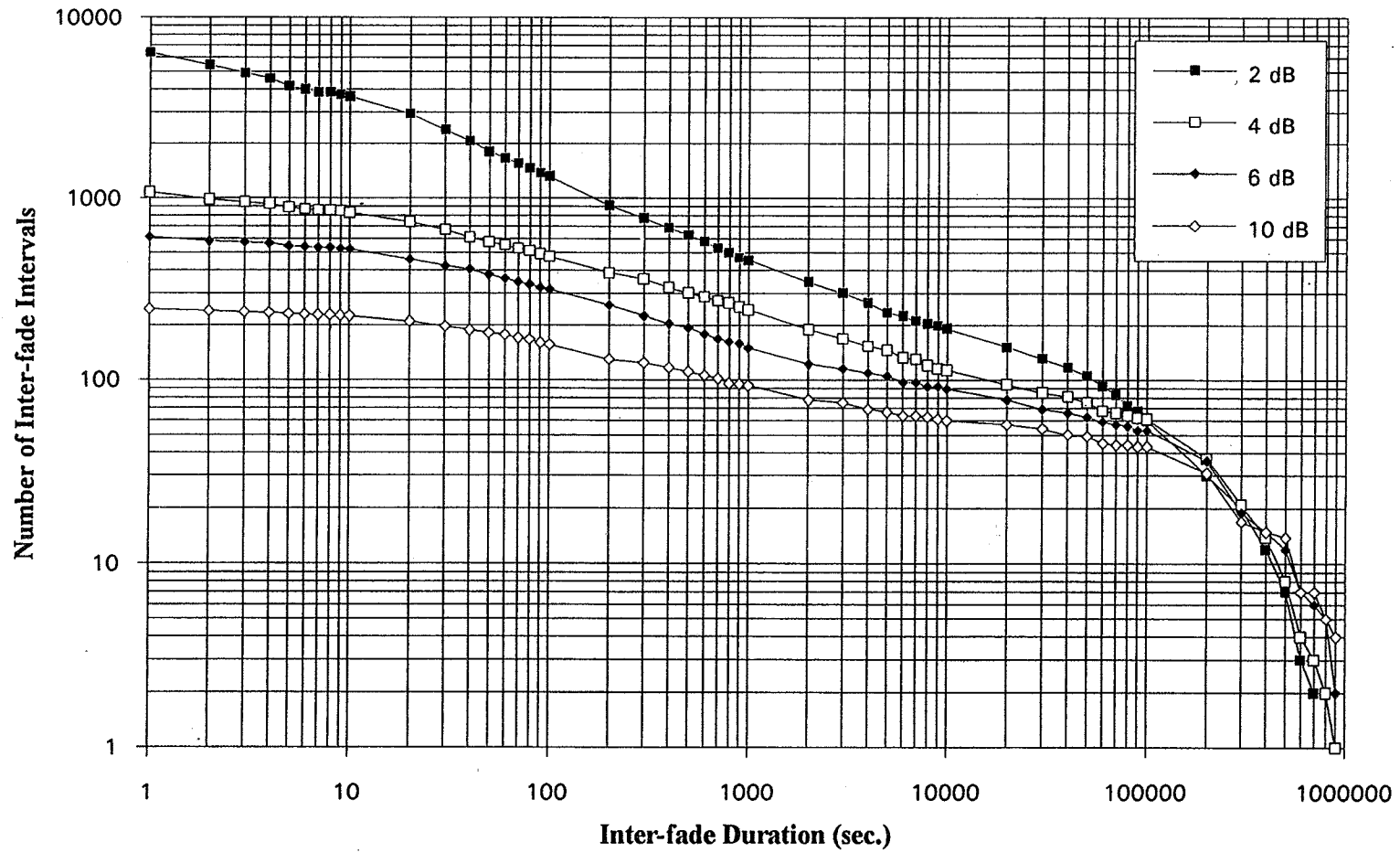


Figure 21 Distribution of Inter-fade Intervals at 20 GHz; measurement period: March 1994 to February 1995



Stanford Telecom / New Mexico State University

ACTS Propagation Measurements Program

Data Analysis Summary

Julie H. Feil
Louis J. Ippolito
Stephen Horan

NAPAX XX & APSW IX
June 4-6, 1996
Fairbanks, Alaska

-1-



Agenda

- Introduction**
 - > Experiment objectives & configuration
- ACTS K_A band measurements and analysis**
 - > Processing technique differences
 - > Worst month attenuation and weather measurements
 - > 24 month (12/93-11/95) propagation statistics
 - > Model comparisons
- Summary and future activities**
- New Mexico State University**
 - > Station Status
 - > Application of ACTS Measurements to TDRS data

-2-



STel ACTS Propagation Experiment Objectives

- Measure and evaluate K_A band propagation effects and link performance for New Mexico
- Develop long-term statistics and prediction modeling techniques for New Mexico climate region for advanced satellite system planning and design
- Apply ACTS measurements (20.185 GHz and 27.505 GHz) to the evaluation of current and planned TDRS Space-to-Ground Link (SGL) performance

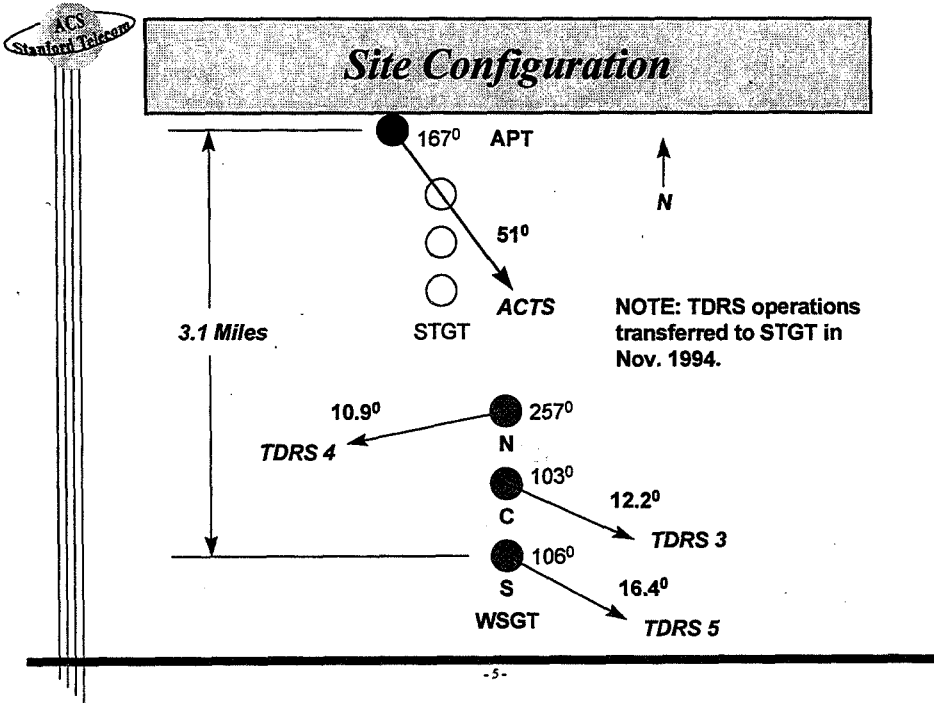
- 3 -



New Mexico APT

- Elevation angle: 51°
- Measured parameters
 - Beacons: 20.185 GHz and 27.505 GHz
 - Radiometers: 20 GHz and 27.505 GHz
 - Rain rate (CRG, TBG)
 - Temperature, Relative Humidity, Wind Vector
- Ancillary Measurements from TDRS
 - 13.5 GHz SGL delogged signal attenuation plots for identified weather events ('Raindance')
 - Coincident Steering Data: date, time, antenna azimuth and elevation

- 4 -



ACTS K_A Band Measurements Summary

- Two years of data processed
- Comparison of old and new processing techniques
- Worst month (in two years): August 1995
- Two year propagation statistics
- Model Comparisons
- Attenuation Ratio
- Fade Duration



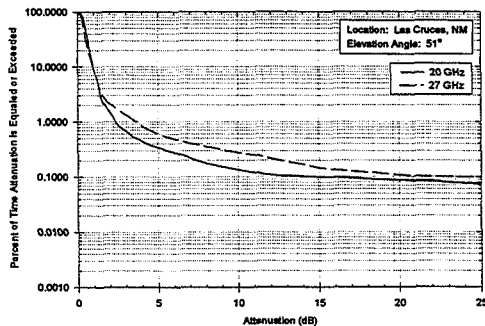
Comparison of Processing Techniques

- ❑ **24 Months Statistics: December 1993 -November 1995**
 - From *.pv0 processing (ACTSEEDIT)
 - From *.pv2 processing (ACTSPP)
- ❑ **Minor differences between two processing techniques**
 - Monthly Statistics are within 1 dB
 - Gaseous absorption is less for *.pv2 than for *.pv0 processing
 - Rain Attenuation is almost identical
 - Snow/ice storms illustrate greatest difference (radiometer delta >1 dB)
- ❑ **Model comparisons performed with *.pv2 processed data**

-7-



August 1995 Free Space Attenuation (AFS)

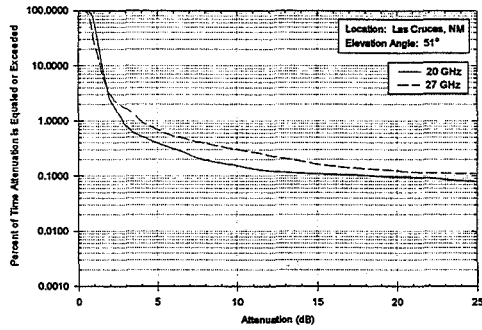


From *.pv2 files

-8-



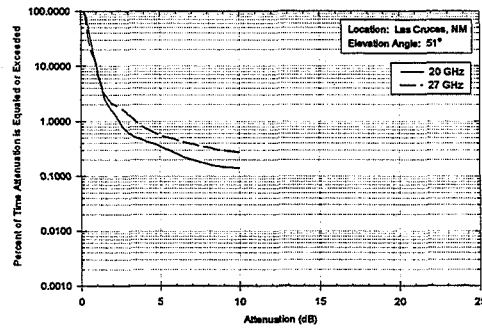
August 1995 Free Space Attenuation (AFS)



From *.pv0 files



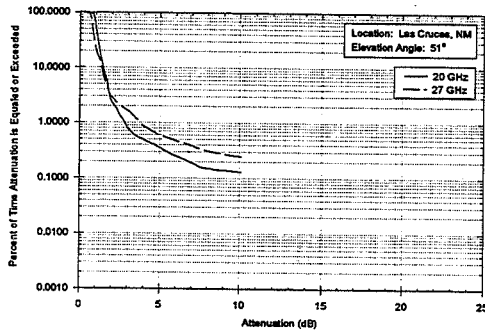
August 1995 Radiometric Derived Attenuation (ARD)



From *.pv2 files



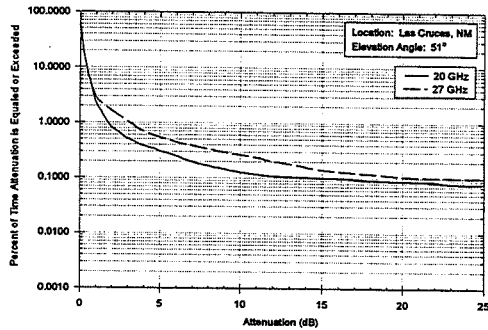
August 1995 Radiometric Derived Attenuation (ARD)



From *.pv0 files



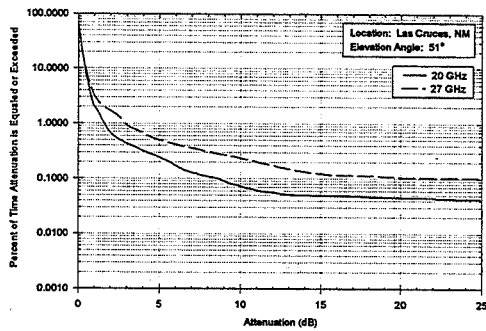
August 1995 Clear Air Attenuation (ACA)



From *.pv2 files



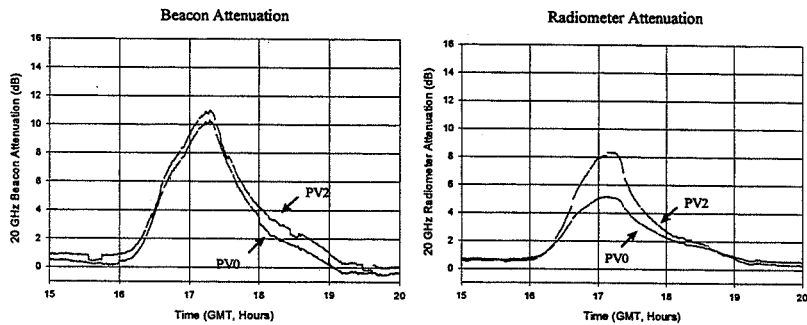
August 1995 Clear Air Attenuation (ACA)



From *.pv0 files

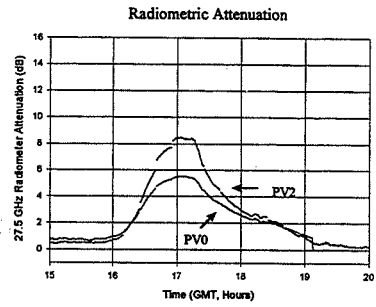
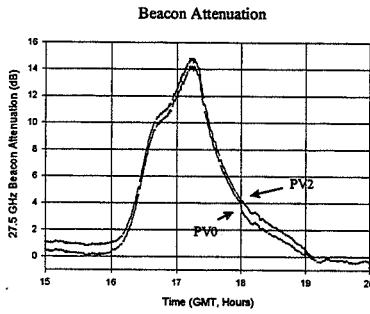


Snow/Ice Event on 20 GHz Channel January 29, 1994

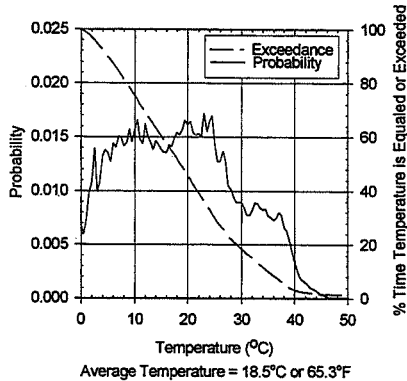




Snow/Ice Event on 27.5 GHz Channel January 29, 1994

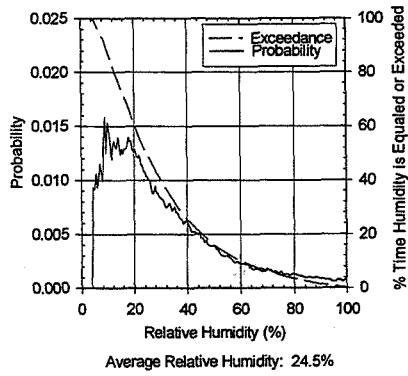


Two Year Surface Temperature





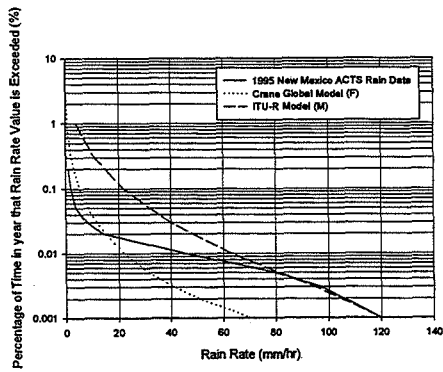
Two Year Relative Humidity



- 17 -



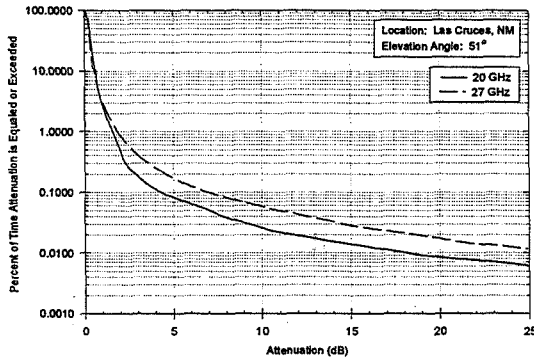
1995 Rain Rate Statistics



- 18 -



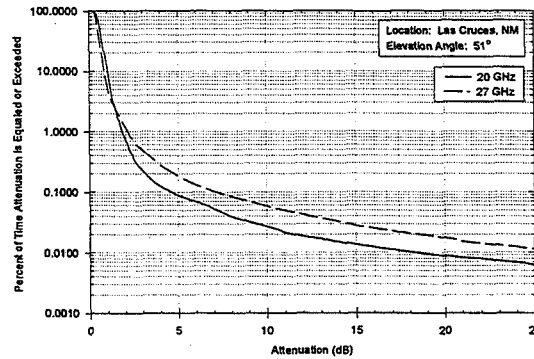
Two Year Attenuation wrt Free Space (AFS)



From *.pv2 file



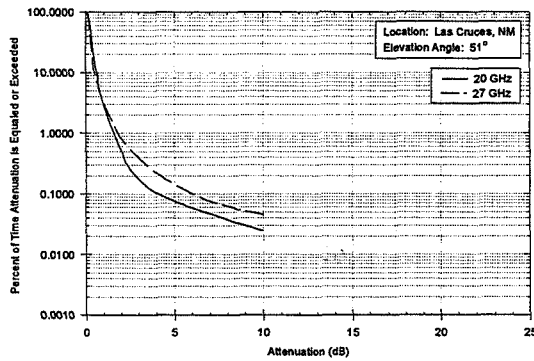
Two Year Attenuation wrt Free Space (AFS)



From *.pv0 file



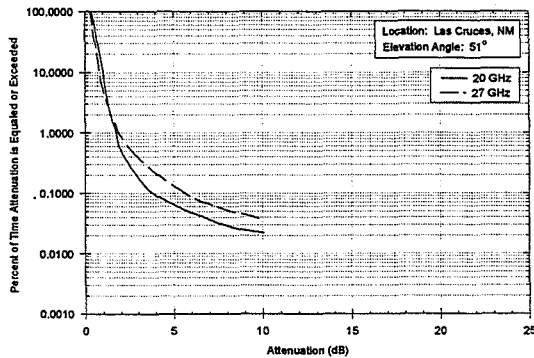
Two Year Radiometric Derived Attenuation (ARD)



From *.pv2 files



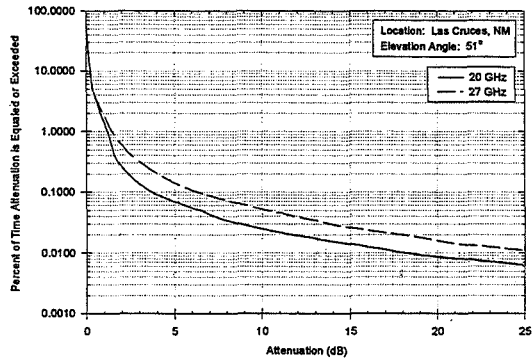
Two Year Radiometric Derived Attenuation (ARD)



From *.pv0 files



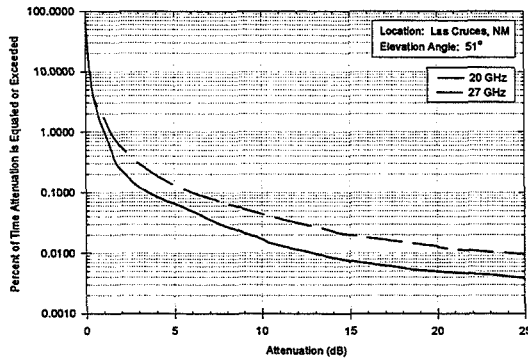
Two Year Attenuation wrt Clear Air (ACA)



From *.pv2 files



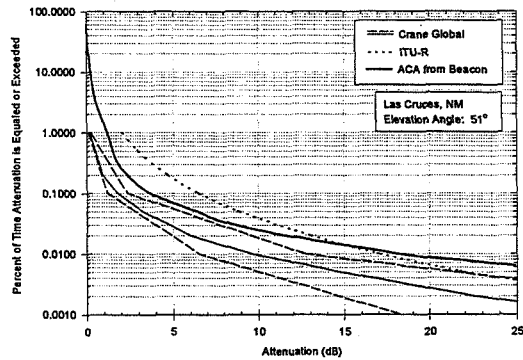
Two Year Attenuation wrt Clear Air (ACA)



From *.pv0 files



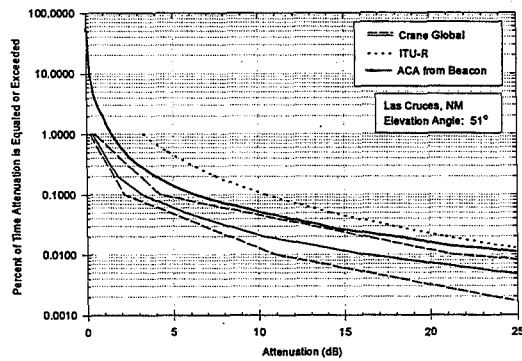
Two Year Comparison 20 GHz Cumulative Distribution



From *.pv2 files



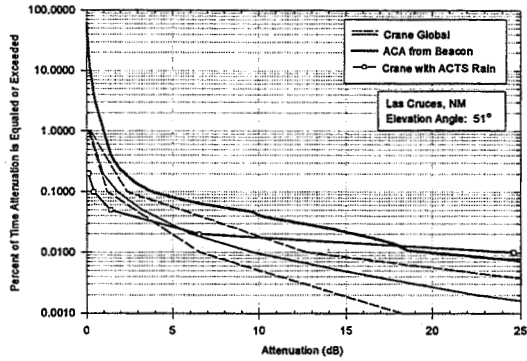
Two Year Comparison of 27 GHz Cumulative Distribution



From *.pv2 files



1995 20 GHz Crane Global Model Rain Statistics

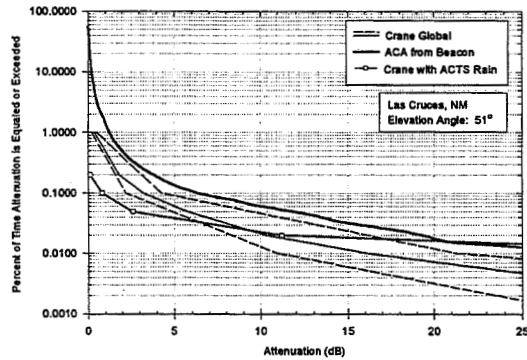


From *.pv2 files

- 27 -



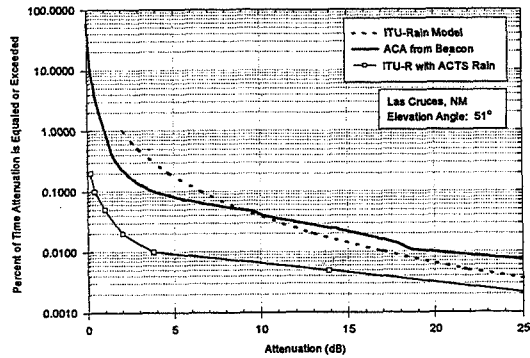
1995 27.5 GHz Crane Global Model Rain Statistics



From *.pv2 files

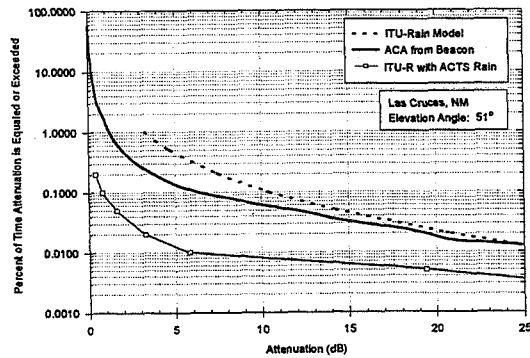
- 28 -

1995 20 GHz ITU Rain Statistics



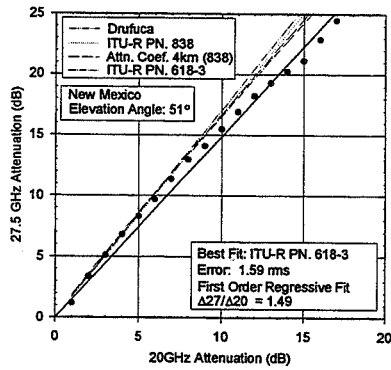
From *.pv2 files

1995 27.5 GHz ITU Rain Statistics



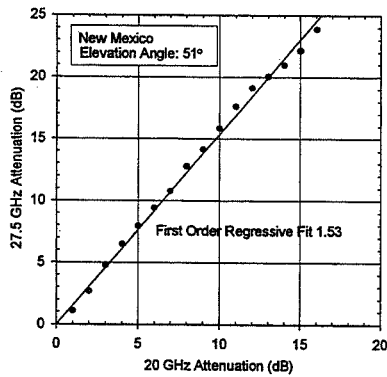
From *.pv2 files

Statistical Attenuation Ratio for ACA



From *.pv2 files

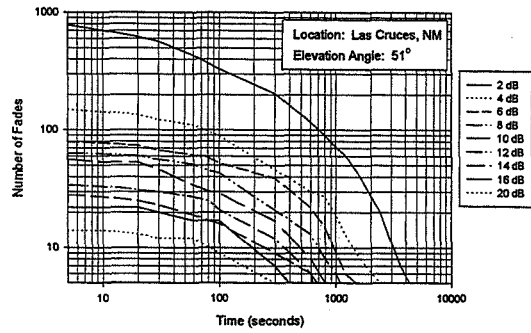
Statistical Attenuation Ratio for AFS



From either *.pv2 or *.pv0 files



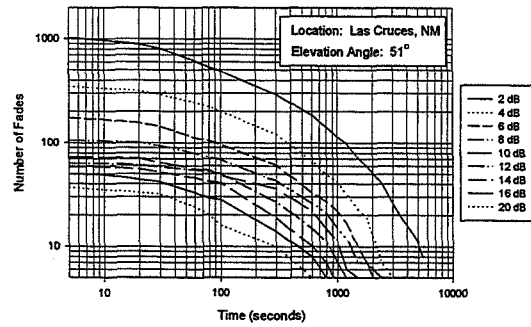
Two Year 20 GHz Fade Duration



From *.pv2 file

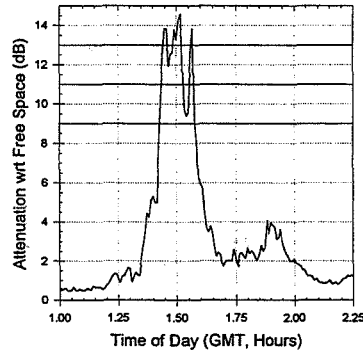


Two Year 27.5 GHz Fade Duration



From *.pv2 file

Fade Event on November 3, 1994



From *.pv0 files

- 35 -

New Mexico ACTS Statistics Summary

- ❑ Comparison of pv0 and pv2 processing for 24 months have minor differences (< 1 dB) in attenuation distributions
- ❑ Measured link performance for two year period

Annual Link Availability	20.185 GHz	27.505 GHz
99.90 %	4.3 dB	6.9 dB
99.95 %	7.0 dB	11.0 dB
99.99 %	18.9 dB	> 25 dB

- 36 -



New Mexico ACTS Statistics Summary (Cont.)

- According to the National Climatic Data Center**
 - > Above average temperature
 - > Average humidity
 - > Slightly below average precipitation
- Rain Attenuation model prediction comparisons**
 - > ITU-R Model over-predicts by 2-4 dB
 - > Crane Global Model under-predicts by 3-15 dB
 - > Use of measured rain statistics does not improve predictions
- Fade duration**
- Attenuation ratio predicted well by models until 12 dB**

- 37 -



Future Activities

- Complete 3 year cumulative distributions from *.pv0 preprocessing**
- Complete 3 year cumulative distributions from *.pv2 preprocessing**
- Compile 3 years of raindanc data for comparison to ACTS data**
- Contract renewal for fourth year statistics**

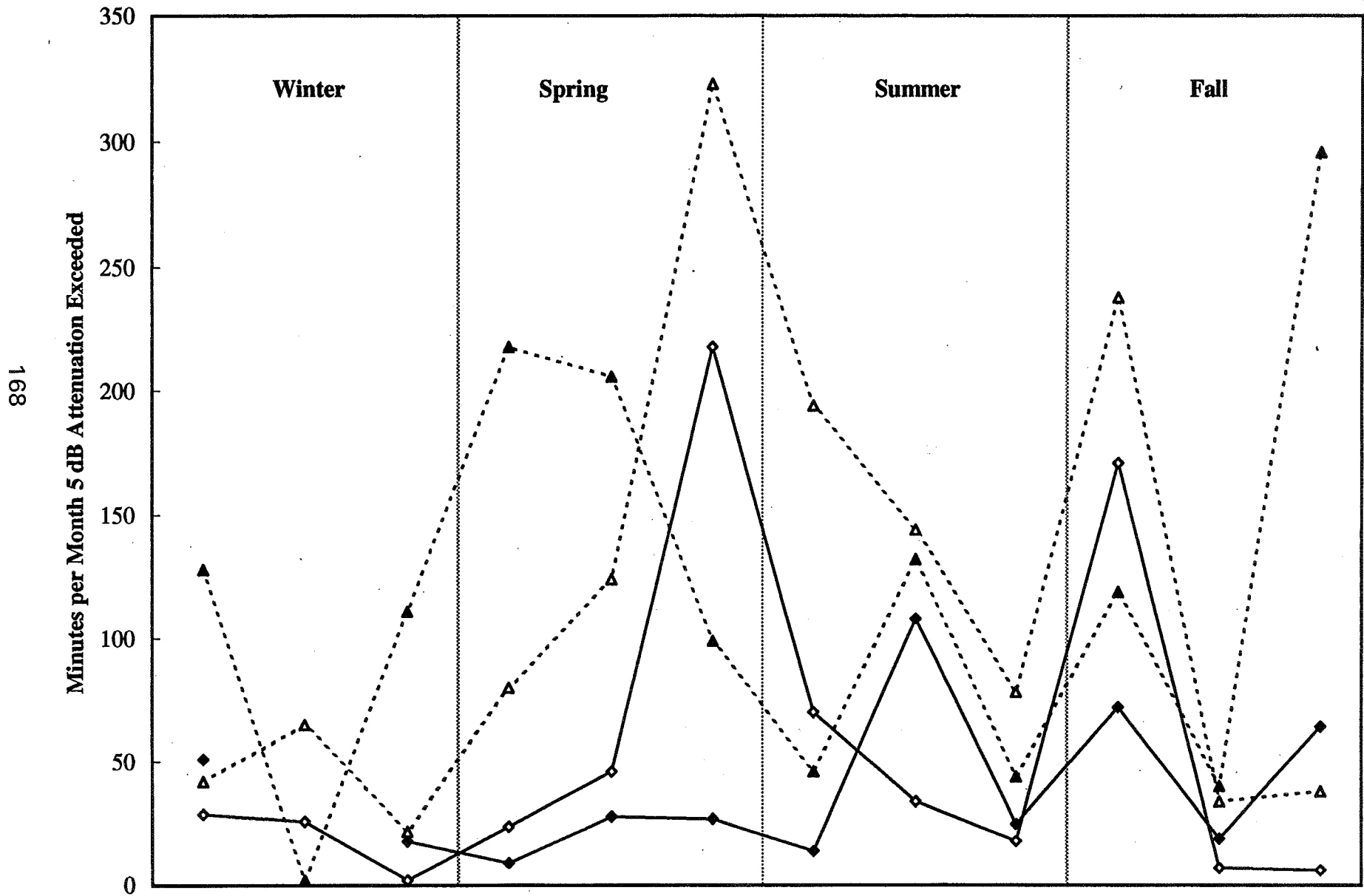
- 38 -

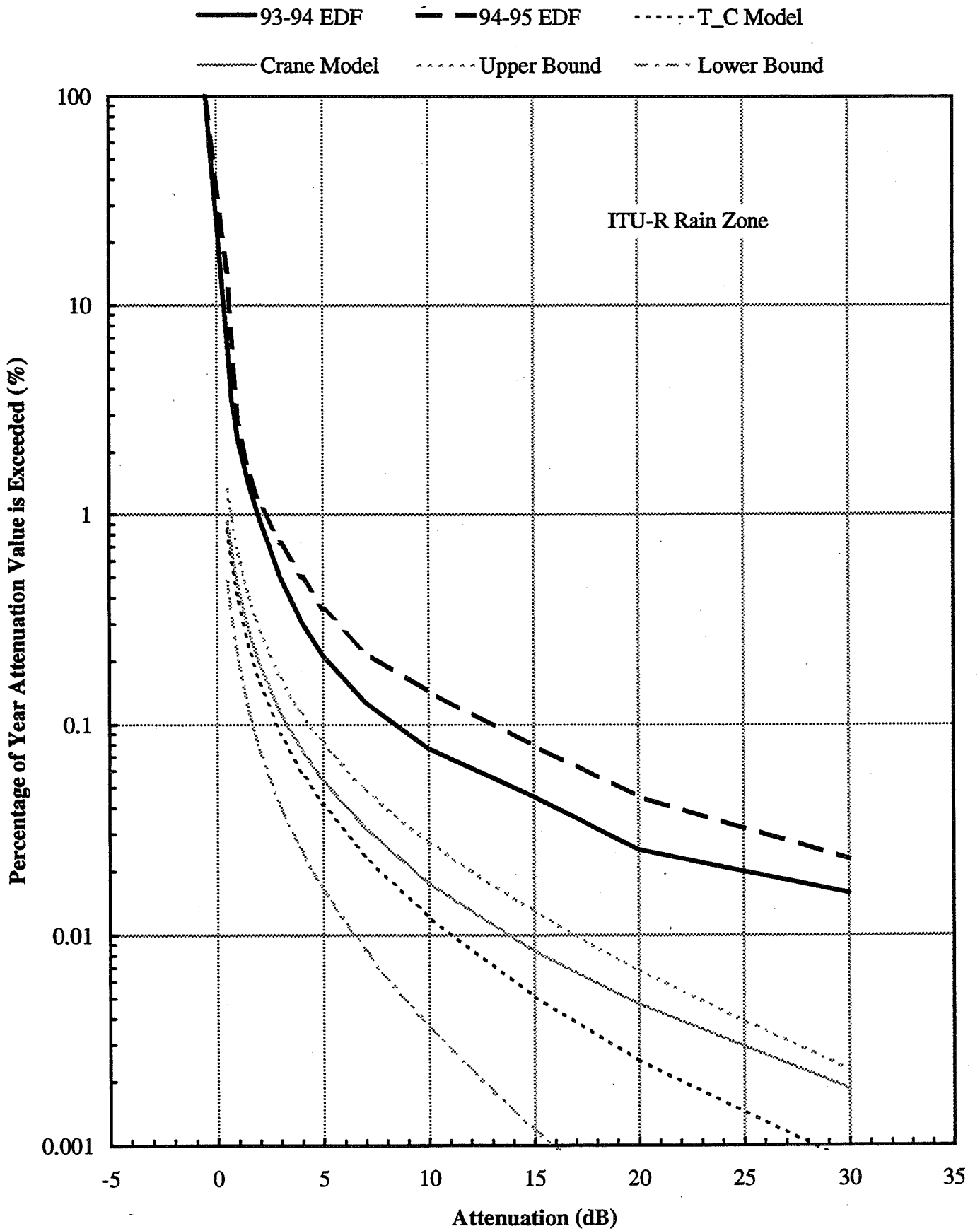
Page intentionally left blank

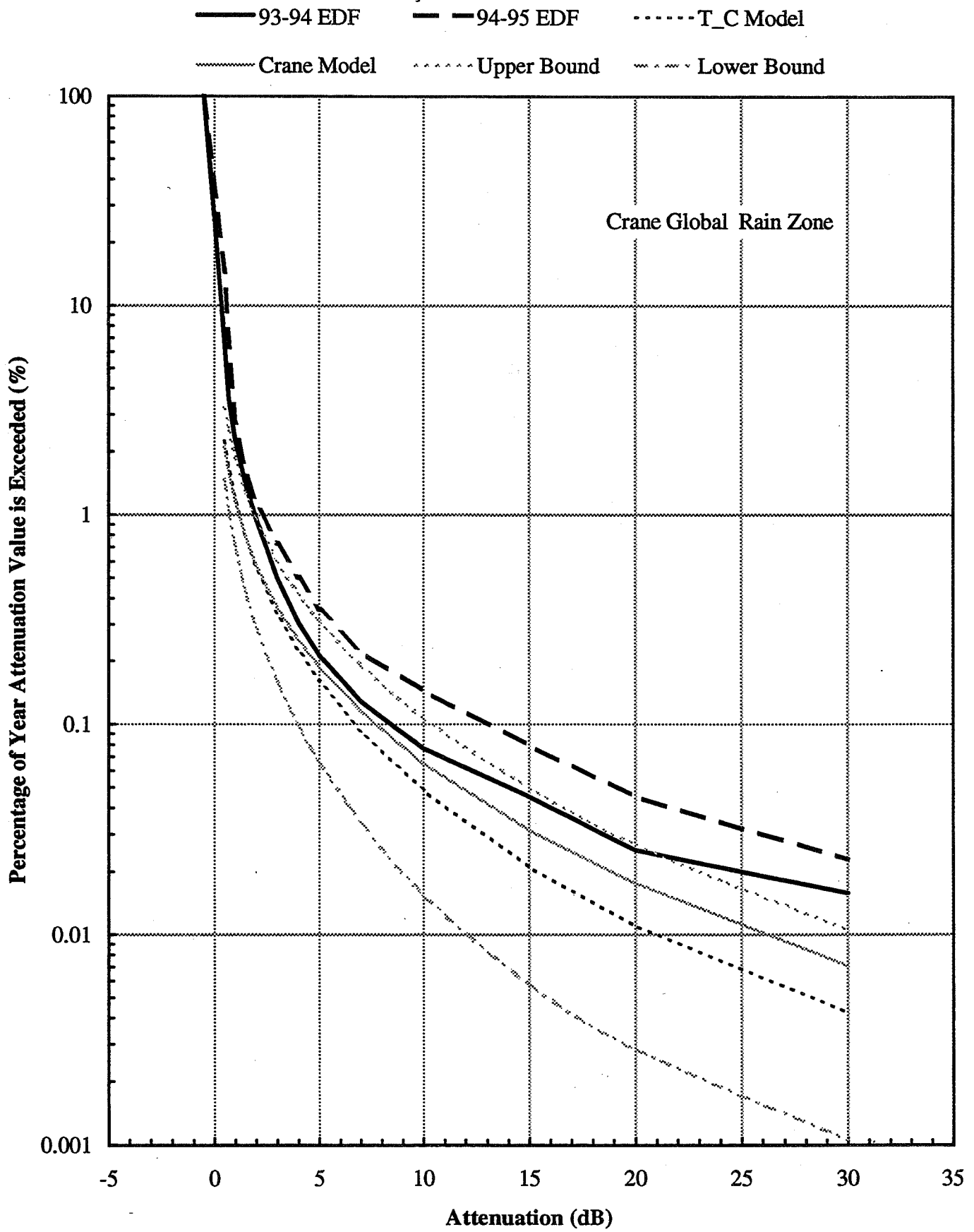
ACTS PROPAGATION EXPERIMENT,
NORMAN, OKLAHOMA

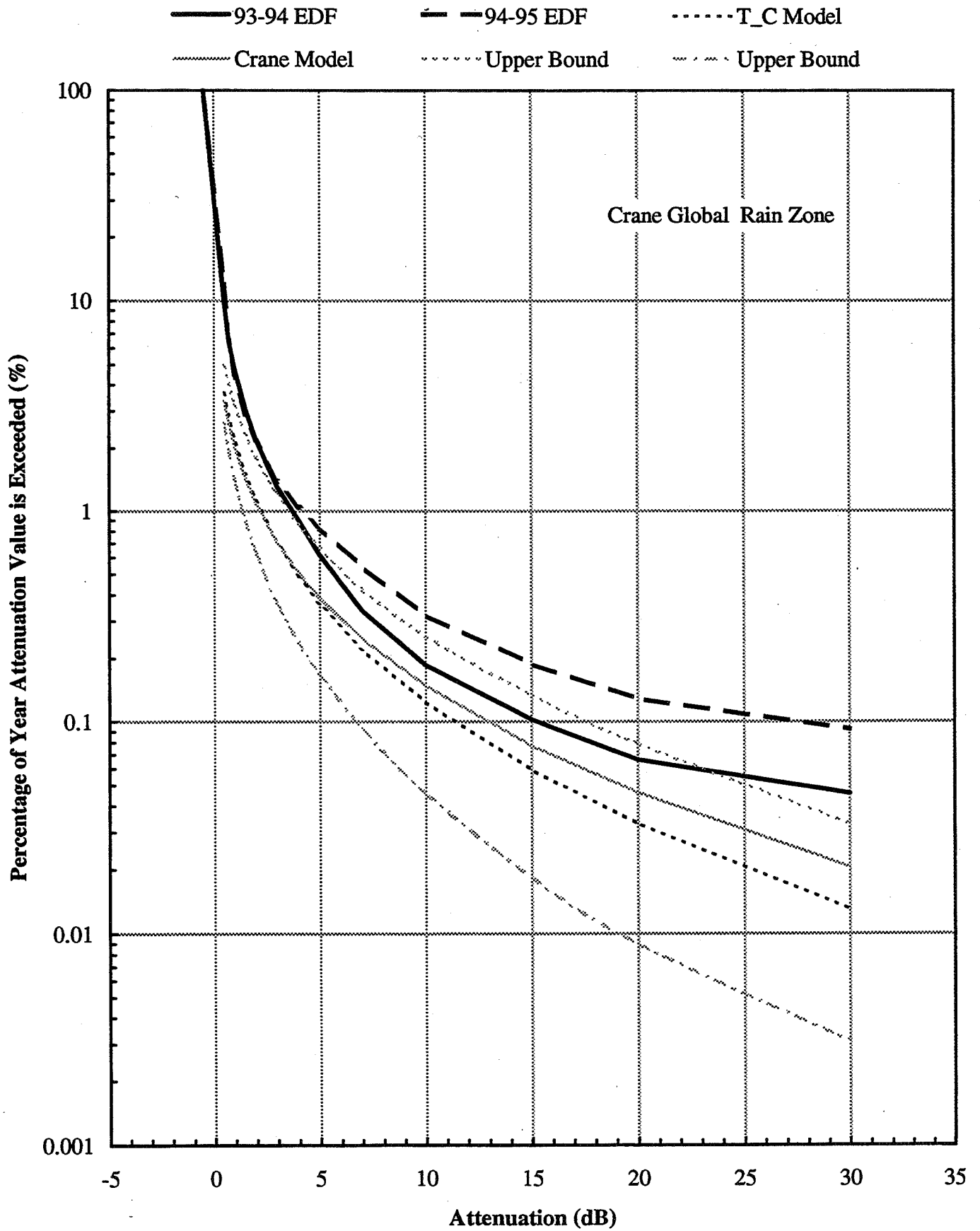
F. Shimabukuro (**Aerospace**)

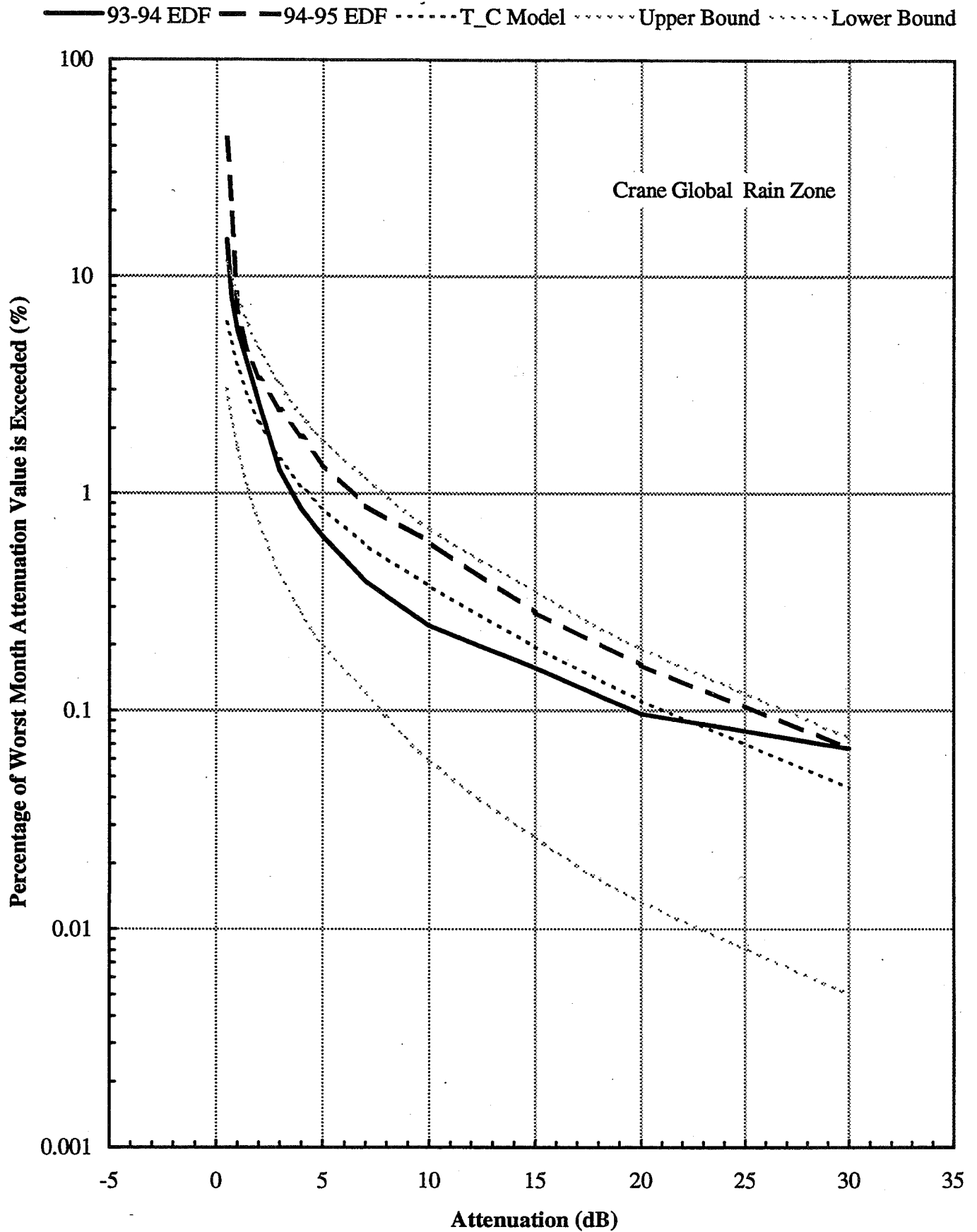
—◆— 5 dB @ 20 GHz 93-94 —◇— 5 dB @ 20 GHz 94-95 --▲-- 5 dB @ 27 GHz 93-94 --△-- 5 dB @ 27 GHz 94-95

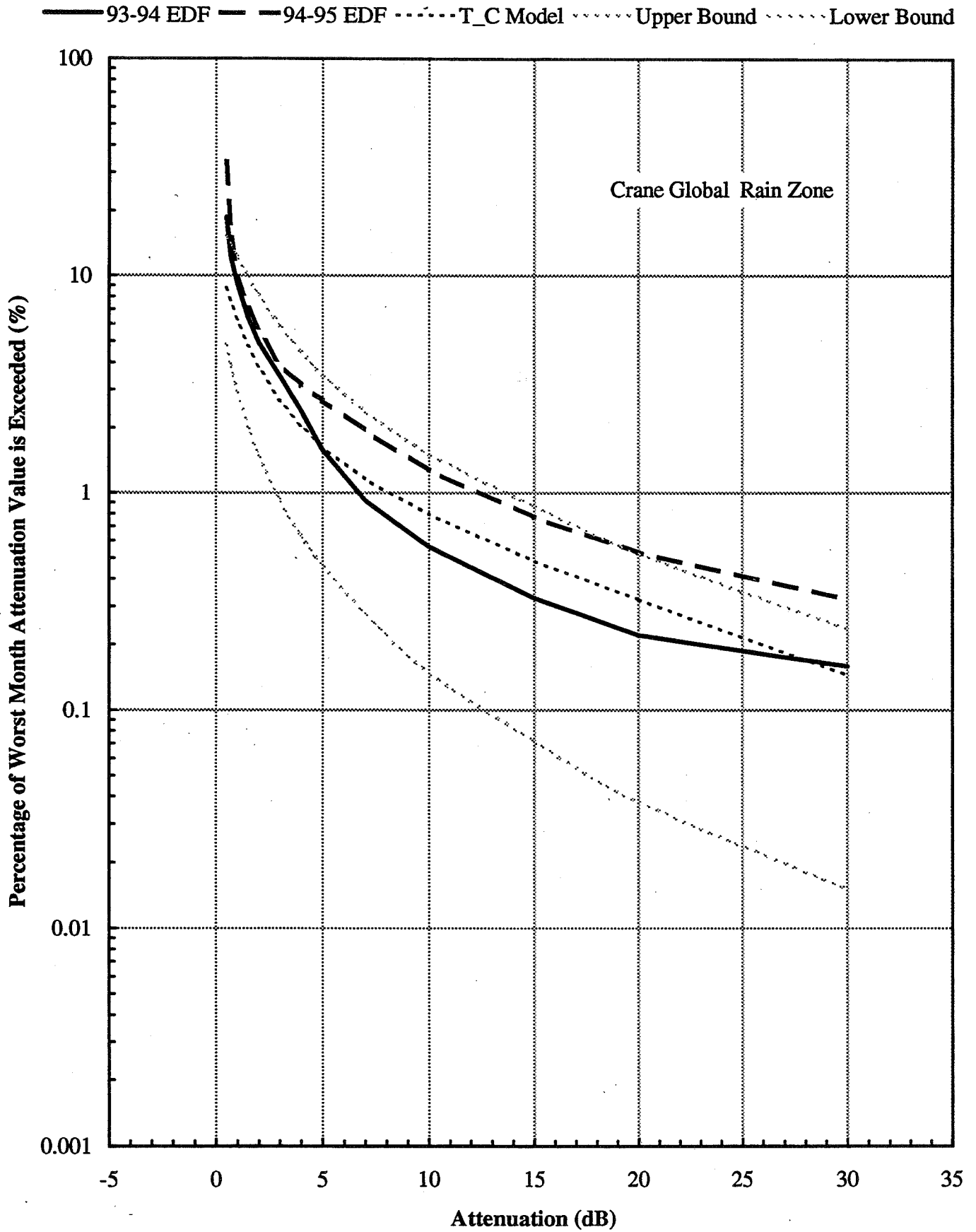


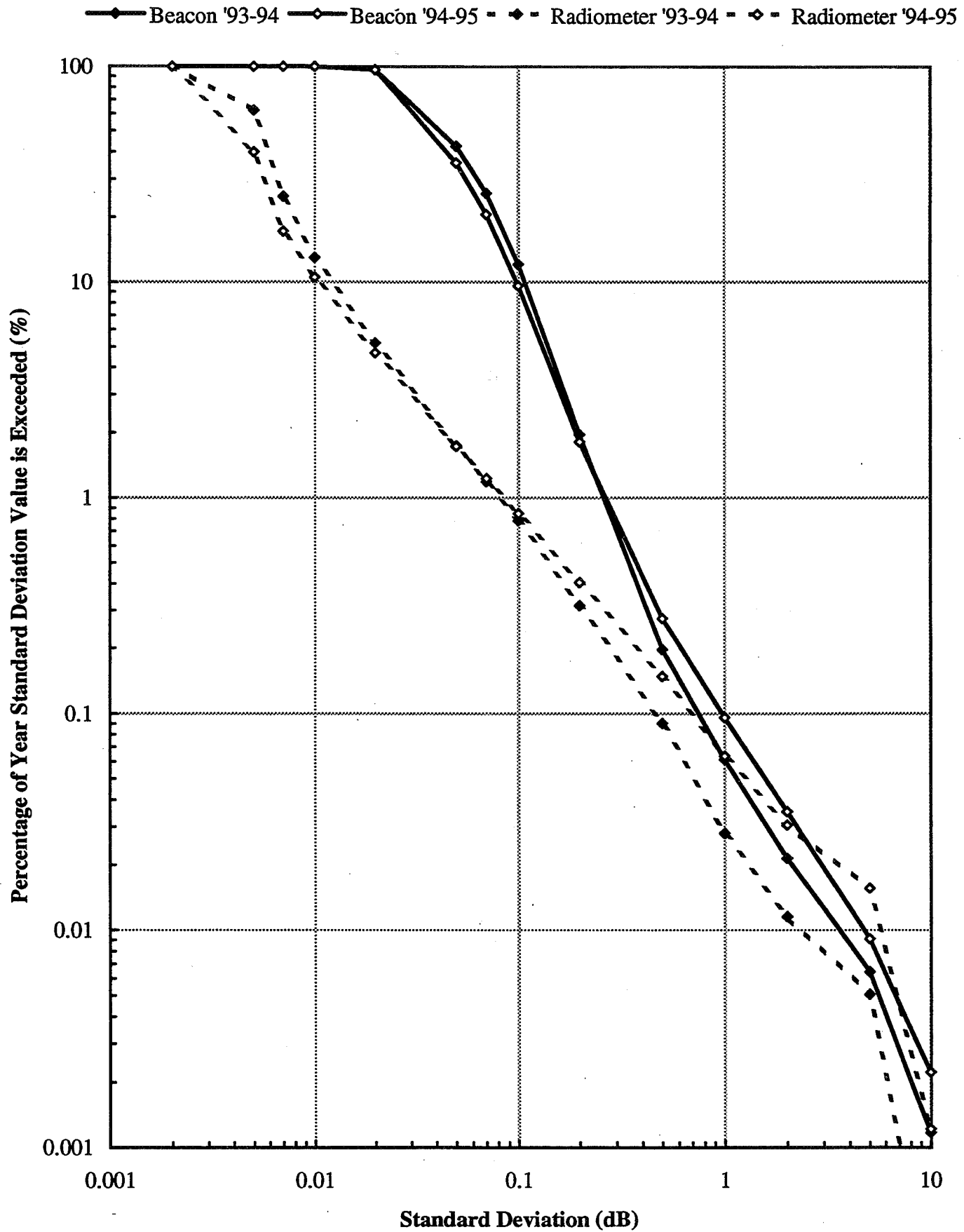


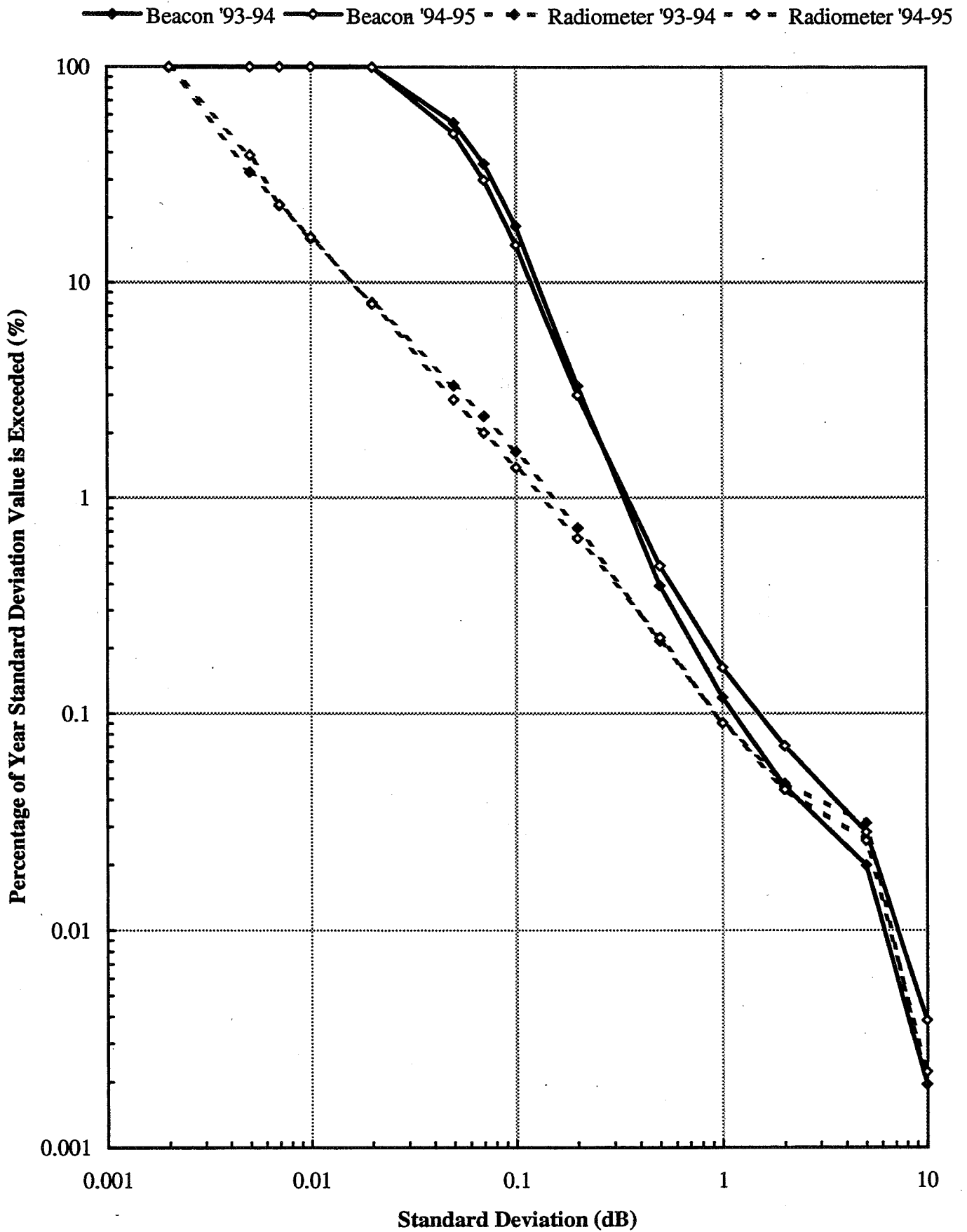


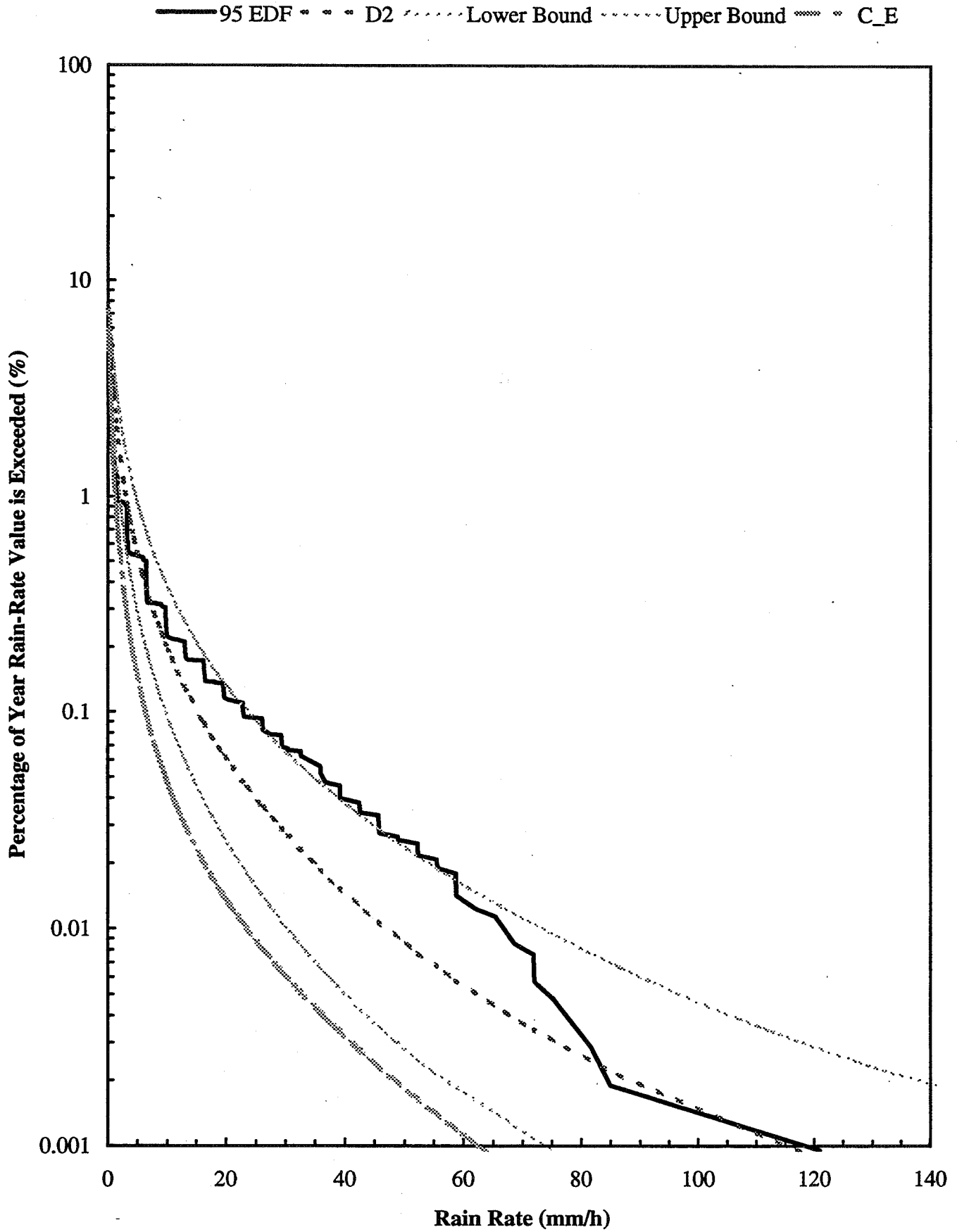












ACTS Propagation Experiment
 Norman, Oklahoma

Block 5 Minute Distributions - Attenuation Relative to Clear Sky

ACTS Ok Total Time Lost Time 20 GHz Beacon Attenuation Relative to Clear Sky Histogram - Minutes above threshold

		Attenuation (dB) =>																
Year	M.	Minutes	Minutes	-0.5	0.5	0.7	1	1.5	2	3	4	5	7	10	15	20	30	Bad
93	12	44624.5	1926.92	39493	406	366	649	226	190	105	47	51	14	6				1036
94	1	44640	5.38333	43091	364	267	139	15	4									739
94	2	40320	18.8333	35947	1091	584	409	192	211	70	18	18	19	7	2	1	4	1353
94	3	44640	6.75	40360	857	1119	776	358	301	189	69	9	3	1	1	1	1	558
94	4	43200	102.217	38201	1013	500	314	227	302	132	44	28	26	9	2	1	1	1965
94	5	44640	15.5167	41502	915	928	422	160	205	60	21	27	15	22	18	11	6	302
94	6	43200	1.35	39487	2955	299	133	71	82	29	13	14	10	6	4	5	20	69
94	7	44640	25.0167	40705	2288	357	242	135	155	115	96	108	52	40	27	13	30	161
94	8	44200		41008	2338	334	178	45	51	37	24	25	8	10	25	6	18	93
94	9	43200	67.5667	39339	1349	465	316	168	165	86	71	72	67	26	11	5		985
94	10	43790.933	245.317	38555	1527	695	475	172	75	18	13	19	13	16	1	4	1	1941
94	11	43200	365.883	38079	1958	703	448	540	606	160	61	64	34	19	10	2		144
94	12	44640	33.6833	39072	1734	817	414	103	75	33	14	29	7	4	1			2301
95	1	44640	100.683	39516	822	324	168	94	81	53	36	26	14	2	1	1	2	3386
95	2	40320	141.133	37564	332	412	138	77	24	10	10	2						1598
95	3	44640		37684	3334	1701	1085	315	210	69	31	24	21	9	3			138
95	4	43200	39.25	39847	840	807	594	243	211	95	54	46	30	30	18	5	11	328
95	5	44640	259.317	34312	4974	914	648	402	432	267	206	218	125	143	55	42	30	1591
95	6	43200	27.35	23459	716	580	432	242	326	126	66	70	57	54	29	18	25	16966
95	7	44640	2.11667	27180	7172	4852	207	39	96	119	113	34	25	17	16	6	15	4745
95	8	44640	22.2667	27251	9628	6669	645	129	108	54	35	18	25	19	8	8	5	12
95	9	43200	6.78333	29868	6976	3671	1009	453	382	219	150	171	61	32	27	21	23	128
95	10	44640	6.75	42299	1647	255	124	74	51	27	2	7	8	7	11	9	1	89
95	11	43150.917	1456.35	39952	158	123	157	82	60	38	22	6	7					589
93-94	An	524295.43	2780.75	475767	17061	6617	4501	2309	2347	1001	477	435	261	162	101	49	81	9346
94-95	An	525550.92	2095.68	418004	38333	21125	5621	2253	2056	1110	739	651	380	317	169	110	112	31871
93-94	Ordered			511169	35402	18341	11724	7223	4914	2567	1566	1089	654	393	231	130	81	
94-95	Ordered			490980	72976	34643	13518	7897	5644	3588	2478	1739	1088	708	391	222	112	
93-94	edf (%)			99.805	6.9122	3.581	2.2891	1.4103	0.9594	0.5012	0.306	0.213	0.128	0.077	0.045	0.025	0.016	
94-95	edf (%)			99.877	14.845	7.0472	2.7499	1.6064	1.1481	0.7299	0.504	0.354	0.221	0.144	0.08	0.045	0.023	

177

ACTS Propagation Experiment
 Norman, Oklahoma

Block 5 Minute Distributions - Attenuation Relative to Clear Sky

ACTS Ok Total Time Lost Time 27 GHz Beacon Attenuation Relative to Clear Sky Histogram - Minutes above threshold

		Attenuation (dB) =>																
Year	M	Minutes	Minutes	-0.5	0.5	0.7	1	1.5	2	3	4	5	7	10	15	20	30	Bad
93	12	44624.5	1926.92	37916	721	526	682	517	648	218	111	128	96	27	8	2		1036
94	1	44640	5.38333	39981	1236	916	1067	465	212	10	2	2						739
94	2	40320	18.8333	35441	893	521	364	345	367	176	133	111	33	15	12	6	7	1353
94	3	44640	6.75	39703	642	754	1017	575	520	221	196	218	35	3	1	1	8	558
94	4	43200	102.217	37077	1261	730	573	365	364	231	162	206	84	28	18	4	3	1965
94	5	44640	15.5167	40337	623	841	908	465	639	127	141	99	47	28	8	20	31	302
94	6	43200	1.35	41289	852	304	302	85	76	60	44	46	15	19	5	3	28	69
94	7	44640	25.0167	40909	1290	628	441	193	223	116	87	132	161	106	44	28	71	161
94	8	44200		39214	2983	853	468	163	172	46	31	44	38	32	6	7	50	93
94	9	43200	67.5667	37315	1821	843	692	409	295	178	107	119	111	95	47	15	19	985
94	10	43790.933	245.317	34988	2563	1192	1233	658	583	200	65	40	22	20	15	6	6	1941
94	11	43200	365.883	36539	1968	1263	726	322	441	480	365	296	136	58	21	13	12	144
94	12	44640	33.6833	37298	1714	1381	969	381	192	69	39	42	24	25	4	2	1	2301
95	1	44640	100.683	38098	880	936	622	138	151	95	34	65	80	20	12	4	5	3386
95	2	40320	141.133	36885	661	255	345	101	90	34	32	22	11	4				1598
95	3	44640		38401	1686	1316	1132	684	778	221	97	80	45	28	13	9		138
95	4	43200	39.25	38340	863	876	955	620	454	197	111	124	74	54	20	22	37	328
95	5	44640	259.317	36993	1531	840	756	375	558	316	217	323	301	226	108	93	144	1591
95	6	43200	27.35	22991	580	494	613	291	338	198	169	194	97	72	44	22	97	16966
95	7	44640	2.11667	33775	4602	769	187	49	50	26	47	144	149	32	13	10	38	4745
95	8	44640	22.2667	34637	8098	844	328	139	185	103	58	78	56	17	22	7	30	12
95	9	43200	6.78333	31268	5601	2473	1161	536	727	331	192	238	250	150	48	10	78	128
95	10	44640	6.75	42750	700	417	328	62	129	41	21	34	7	13	3	3	22	89
95	11	43150.917	1456.35	34682	445	285	212	136	172	75	22	38	41	8	5			589
93-94	An	524295.43	2780.75	460709	16853	9371	8473	4562	4540	2063	1444	1441	778	431	185	105	235	9346
94-95	An	525550.92	2095.68	426118	27361	10886	7608	3512	3824	1706	1039	1382	1135	649	292	182	452	31871
93-94	Ordered			511190	50481	33628	24257	15784	11222	6682	4619	3175	1734	956	525	340	235	
94-95	Ordered			486146	60028	32667	21781	14173	10661	6837	5131	4092	2710	1575	926	634	452	
93-94	edf (%)			99.809	9.8563	6.566	4.7361	3.0818	2.191	1.305	0.902	0.62	0.339	0.187	0.103	0.066	0.046	
94-95	edf (%)			98.894	12.211	6.645	4.4308	2.8831	2.169	1.391	1.044	0.832	0.551	0.32	0.188	0.129	0.092	

Thirteen Station Years of ACTS Beacon Observations

**Wolfhard J. Vogel
Geoffrey W. Torrence**

Electrical Engineering Research Laboratory
The University of Texas at Austin

Presented at NAPEX XX
Fairbanks, AK
June 5, 1996

1

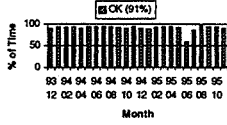
A Preliminary Look at

- **Percent Available Data**
- **2 "Summer" Seasons**
- **2 "Winter" Seasons**
- **2 Years' Statistics**
- **Station by Station Comparison to Crane's Global and 2-Component Models**
- **Summary of Deviations from Models**

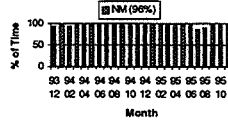
2

EERL / Univ. of Texas

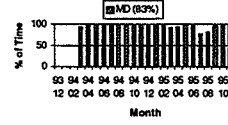
OK 20 GHz Receiver Up-Time



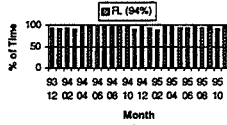
NM 20 GHz Receiver Up-Time



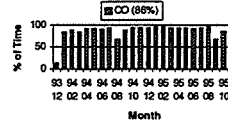
MD 20 GHz Receiver Up-Time



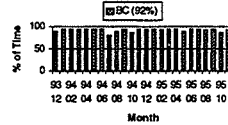
FL 20 GHz Receiver Up-Time



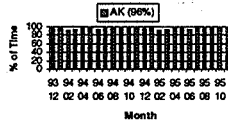
CO 20 GHz Receiver Up-Time



BC 20 GHz Receiver Up-Time



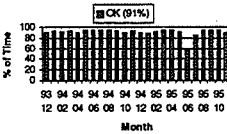
AK 20 GHz Receiver Up-Time



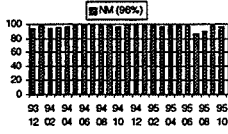
3

EERL / Univ. of Texas

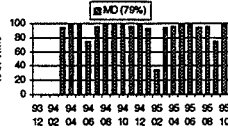
OK 27 GHz Receiver Up-Time



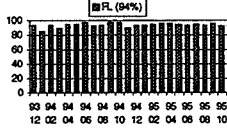
NM 27 GHz Receiver Up-Time



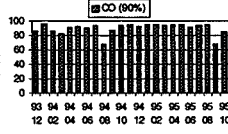
MD 27 GHz Receiver Up-Time



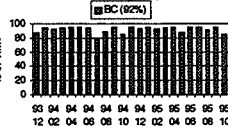
FL 27 GHz Receiver Up-Time



CO 27 GHz Receiver Up-Time



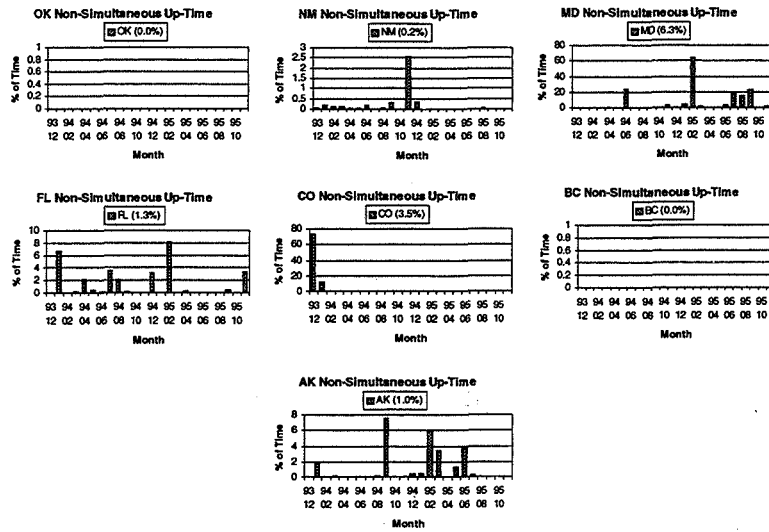
BC 27 GHz Receiver Up-Time



AK 27 GHz Receiver Up-Time

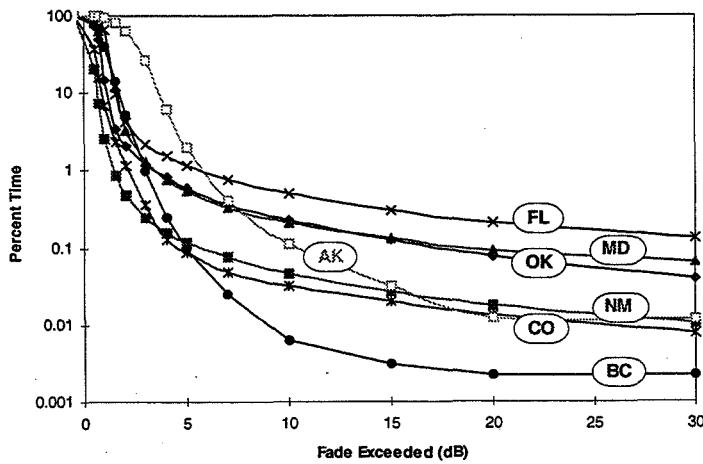


4



5

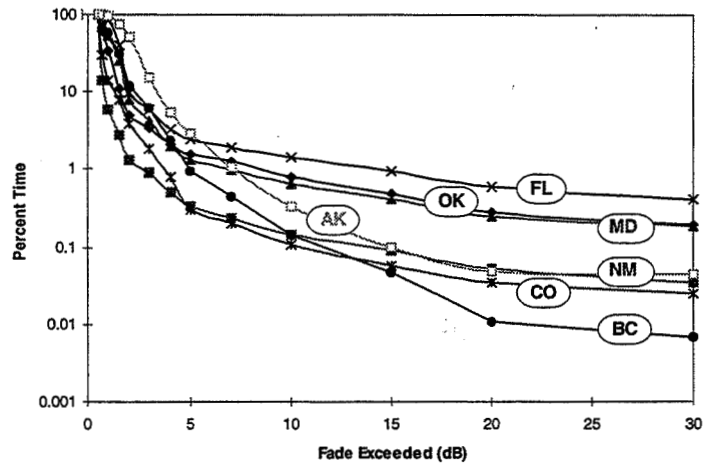
Two-Summer ACTS 20 GHz Beacon Fades



6

EERL / Univ. of Texas

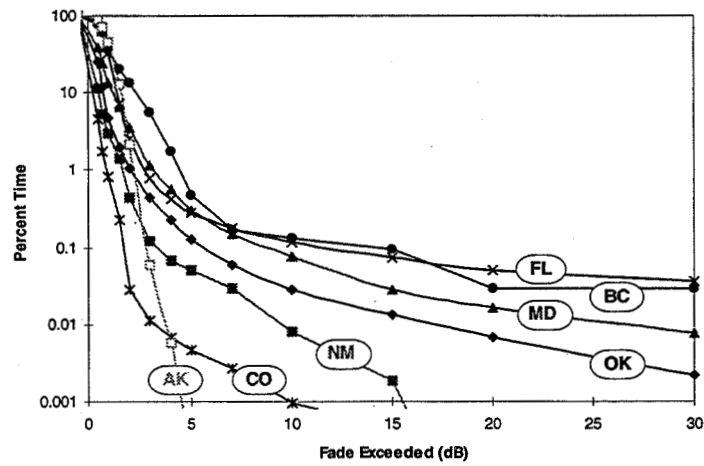
Two-Summer ACTS 27 GHz Beacon Fades



7

EERL / Univ. of Texas

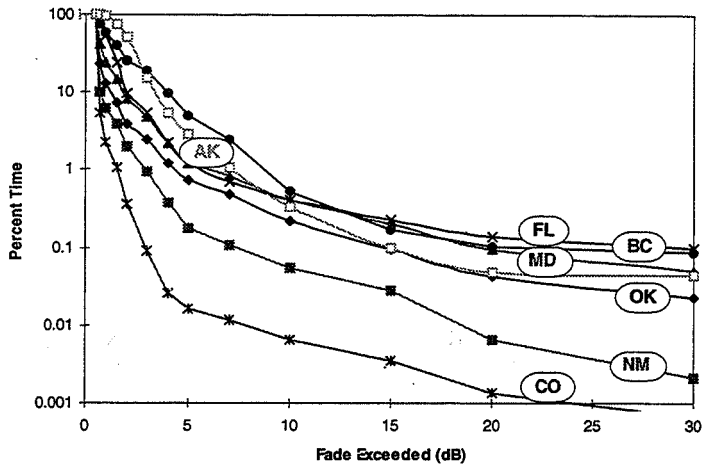
Two-Winter ACTS 20 GHz Beacon Fades



8

EERL / Univ. of Texas

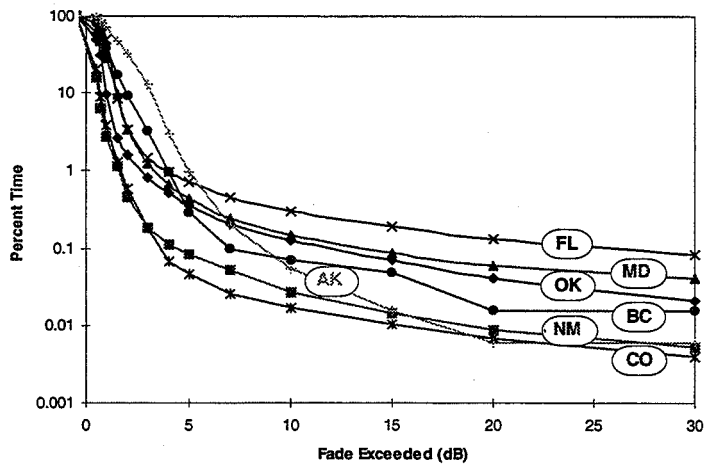
Two-Winter ACTS 27 GHz Beacon Fades



9

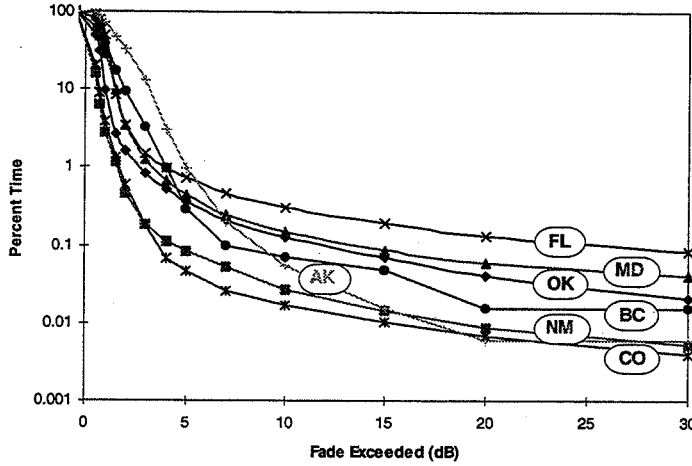
EERL / Univ. of Texas

Two-Year ACTS 20 GHz Beacon Fades

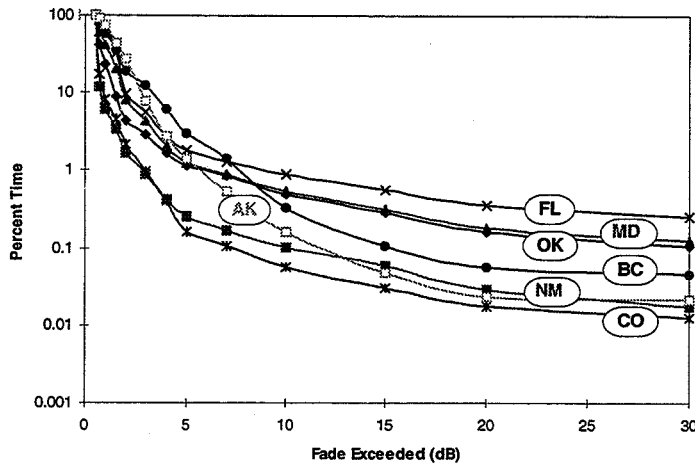


10

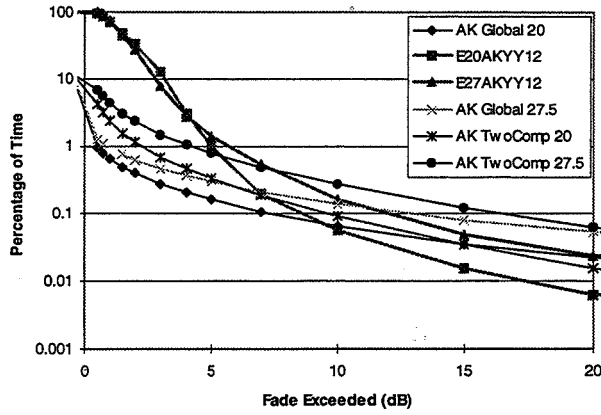
Two-Year ACTS 20 GHz Beacon Fades



Two-Year ACTS 27 GHz Beacon Fades

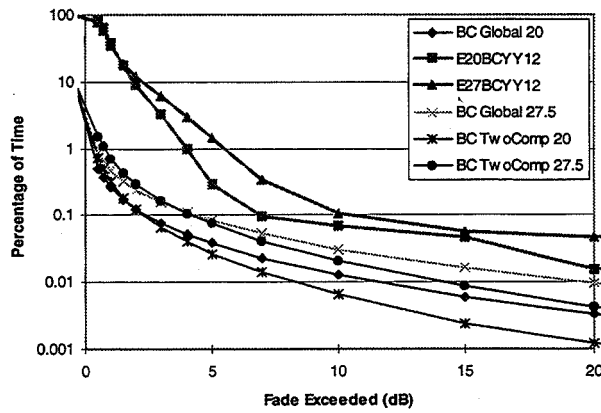


AK vs. Models



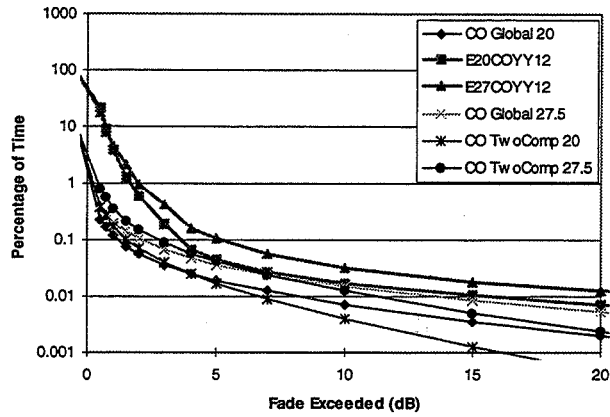
13

BC vs. Models



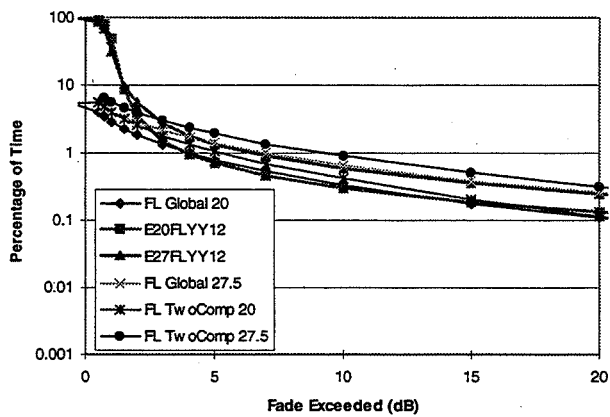
14

CO vs. Models



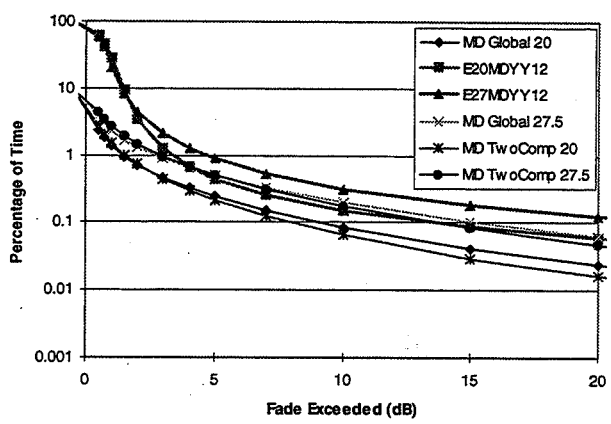
15

FL vs. Models

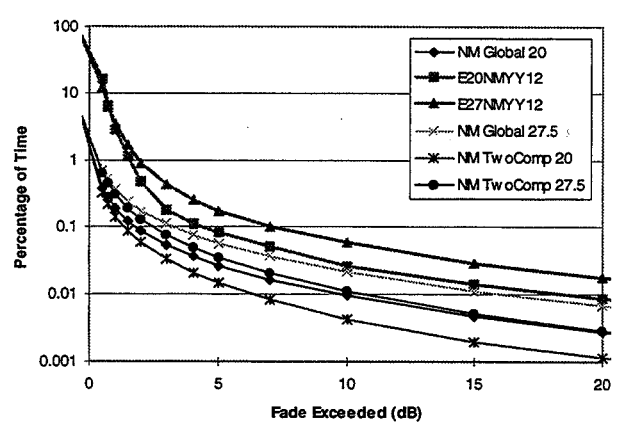


16

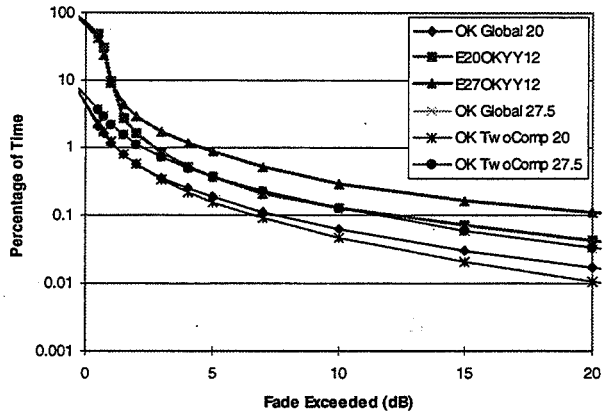
MD vs. Models



NM vs. Models

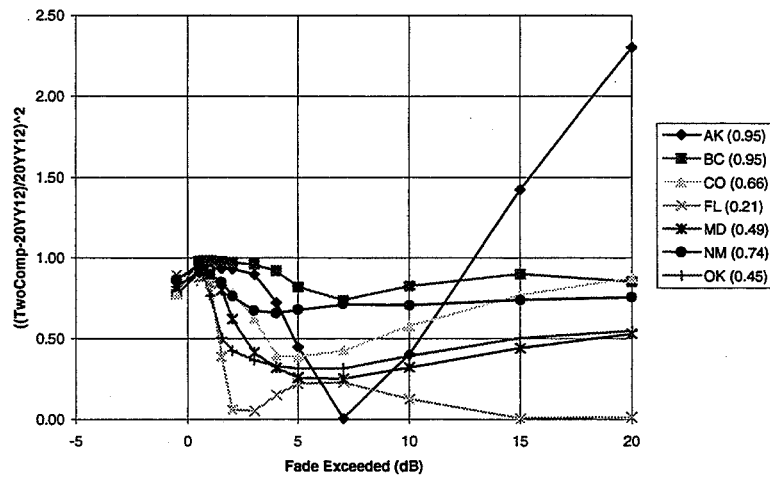


OK vs. Models



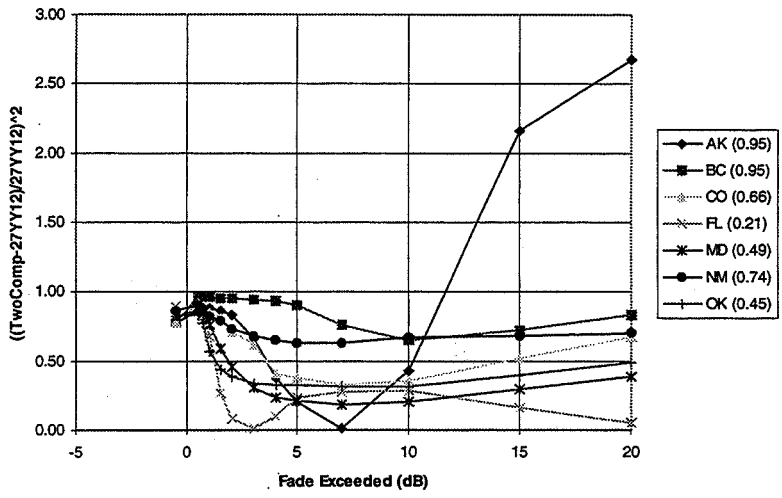
19

20 GHz Annual Fade Probability Prediction Error

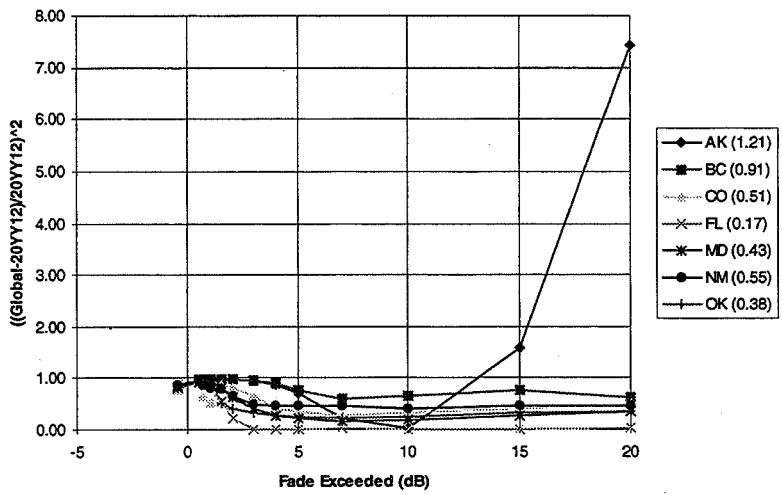


20

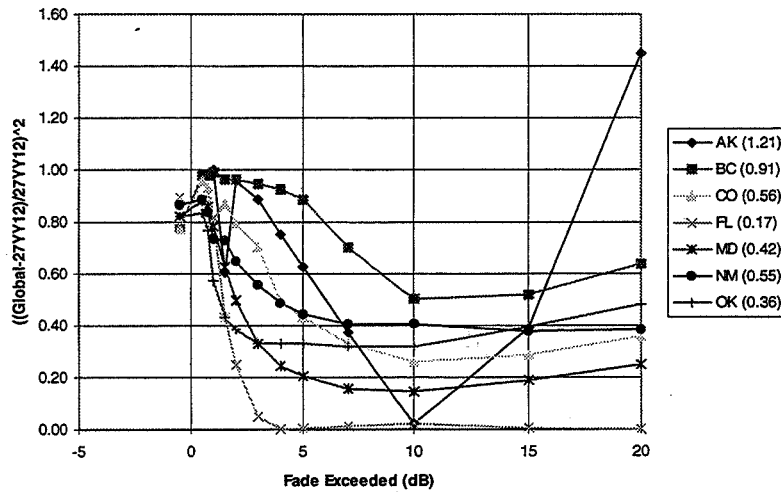
27 GHz Annual Fade Probability Prediction Error



20 GHz Annual Fade Probability Prediction Error



27 GHz Annual Fade Probability Prediction Error



23

Conclusion

- The US propagation data base has been significantly expanded
- West coast distribution function shape is different (more mass in low range)
- Models tend to under-predict fading, but best fit in Florida

24

The Need for More Measurements in the ACTS Propagation Experiment

**R. K. Crane
University of Oklahoma**

June 1996

The study of attenuation by rain at frequencies above 10 GHz started more than four decades ago. At first we collected data to size the problem. Then we expanded data acquisition to provide a sufficient data base to describe the problem statistically. The ITU-R (former CCIR) attenuation prediction model is a statistical summary of the data in the data banks. Recently we have tried to quantify the uncertainty that should be attributed to a prediction of the attenuation distribution for a specified path - the risk to be associated with an attenuation distribution prediction.

Attenuation by rain is a random process. The observed cumulative distribution of the time in a month or year an attenuation value is exceeded is a realization of the results of this random process. The distribution observed in one year may be a poor predictor of the distribution to be observed in the next year. We need to quantify the uncertainty to be associated with a prediction based on one or more years of observations. The Crane models for worst-month distribution prediction [Crane, 1996a] and for the risk to be associated with an annual distribution prediction [Crane, 1996b] are based on a simple empirical model for the expected year-to-year variation in an annual attenuation distribution and for the expected seasonal variations in monthly attenuation distributions. These models are based on the extremely limited set of attenuation data that is available from more than a few years of observation on single, fixed propagation paths. For annual variability, the data were obtained from two 4- and 5-year observation sets taken at two different frequencies on two different paths in Italy. For monthly variability, the data were obtained from a single three-year experiment in coastal Virginia.

The goal for the NASA ACTS Propagation Experiment is to expand the data base on which new attenuation prediction models can be developed or old models can be validated. Seven experiment sites were established, four in climate regions within North America which had not been previously studied, two in regions with insufficient statistical data and one in a region that had been well studied. Figure 1 shows the locations where earlier measurement programs had been conducted and the locations for the ACTS Propagation Experiment. It also indicates the amount of data that had been obtained and the amount of data to be distributed at this meeting. Although the amount of North American data available for application at Ka-band has already been doubled, insufficient data have been collected to provide observations of the annual attenuation distribution within an expected uncertainty of 30% in decibels or of the monthly distribution within an expected uncertainty of 70% in decibels. If the variability values estimated from the simple model for risk are in error, the uncertainties could be higher.

The locations of the ACTS Propagation Experiment sites were chosen to explore climatological regions that had not been adequately investigated. Two rain-rate climate region maps have been published, one the Global climate zones by Crane [1996c] and the other by the ITU-R [CCIR 1992]. They produce widely varying rain-rate distribution estimates for two of the experiment sites. In addition, two experiment sites within the same climate zone (Global D2) have different seasonal variations in rain occurrence yielding different annual to worst-month distribution transformations and possibly different expected year-to-year variability estimates.

Oklahoma is one of the sites with large differences between the predictions of the two rain-zone climate models and with a seasonal variation different from the site used as the model for worst-month predictions. The differences between the model estimates and two years of measurement are shown in Figures 2 (compare with Global model predictions) and 3 (compare with ITU-R model predictions). From the two figures, it is evident that the ITU-R model produces large prediction errors and does not adequately represent the rain climate in central Oklahoma. The Global model gives a better prediction but still underestimates the attenuation for a given probability. For attenuation values less than 15 dB, observations for one year are consistent with the model while observations for the second year are not. For the third year, Oklahoma is in the midst of a major drought and the attenuation for a specified probability may be significantly lower.

The two annual empirical distribution functions differ by about 50% at 0.1% of a year, a result larger than expected on the basis of the variability model. At lower attenuation values corresponding to 1% of a year, the two years of observations are consistent with each other at the level of uncertainty predicted by the variability model. The observations are also consistent with the predictions of the rain climate model if a 1.5 to 2 dB reduction in attenuation is made to compensate for water on the antenna.

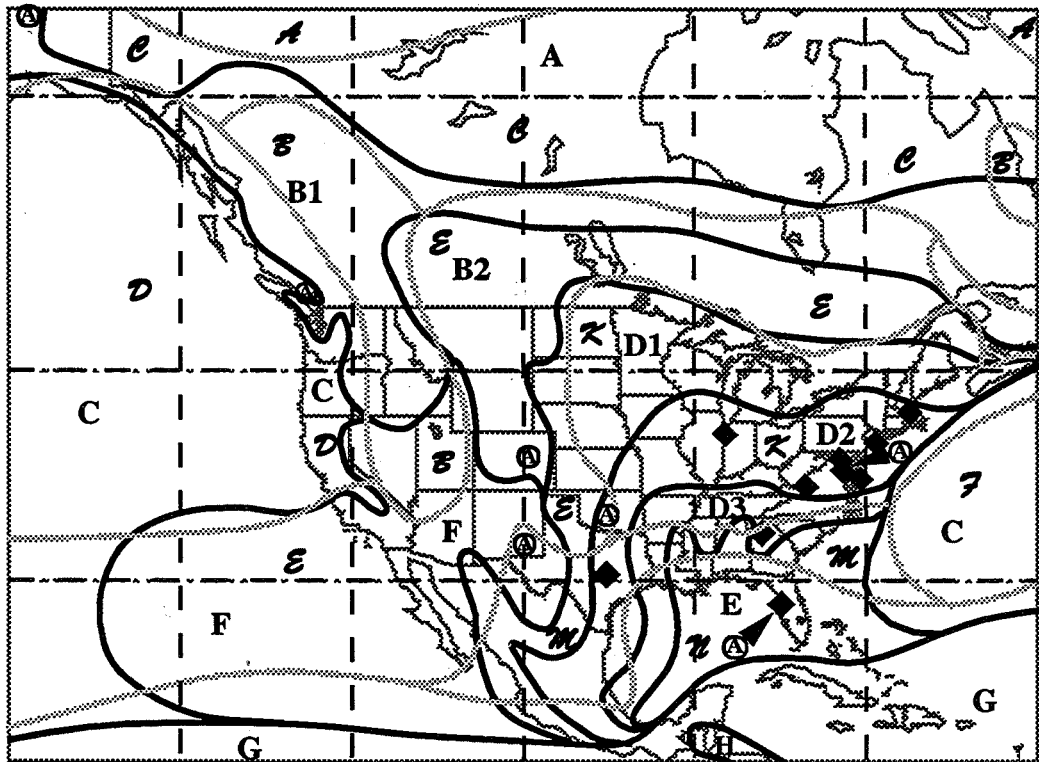
The worst-month attenuation distributions provide a better match to the Global model predictions as illustrated in Figure 4. These results are similar to those presented above with a large difference between the observations for the two years. In this case, both years of observation are within the bounds predicted to be exceeded once in 20 years on average. The data are contradictory with agreement between model and measurement for the worst-month distribution but disagreement for the annual distribution. More observations are needed to resolve this question.

The ACTS Propagation measurement period must be extended to provide observations at each site with small statistical uncertainty sufficient to determine the correct rain climate model and sufficient to establish the variability associated with monthly and annual distribution estimates. Based on the existing model for variability, five years of observation should be sufficient.

References

- CCIR [1992]: Radiometeorological Data, Rept 563, CCIR Study Group 5, International Telecommunications Union, Geneva.
- Crane, R. K. [1996a]: *Electromagnetic Wave Propagation Through Rain*, Wiley-Interscience, New York, NY, Chapt. 6.
- Crane, R. K. [1996b]: *Electromagnetic Wave Propagation Through Rain*, Wiley-Interscience, New York, NY, Chapt. 7.
- Crane, R. K. [1996c]: *Electromagnetic Wave Propagation Through Rain*, Wiley-Interscience, New York, NY, Sect. 3.3.

Crane Global Rain Climate Zones — A
 ITU-R (CCIR) Rain Climate Zones — A



- ◆ Beacon Observation Sites
 - 12 GHz: 5 sites and 12 site years
 - 19 GHz: 7 sites and 15 site years
 - 29 GHz: 9 sites and 14 site years
 - Total of 10 sites
- ⊙ ACTS Propagation Experiment Sites
 - 20 GHz: 7 sites and 14 site years
 - 27 GHz: 7 sites and 14 site years

Figure 1

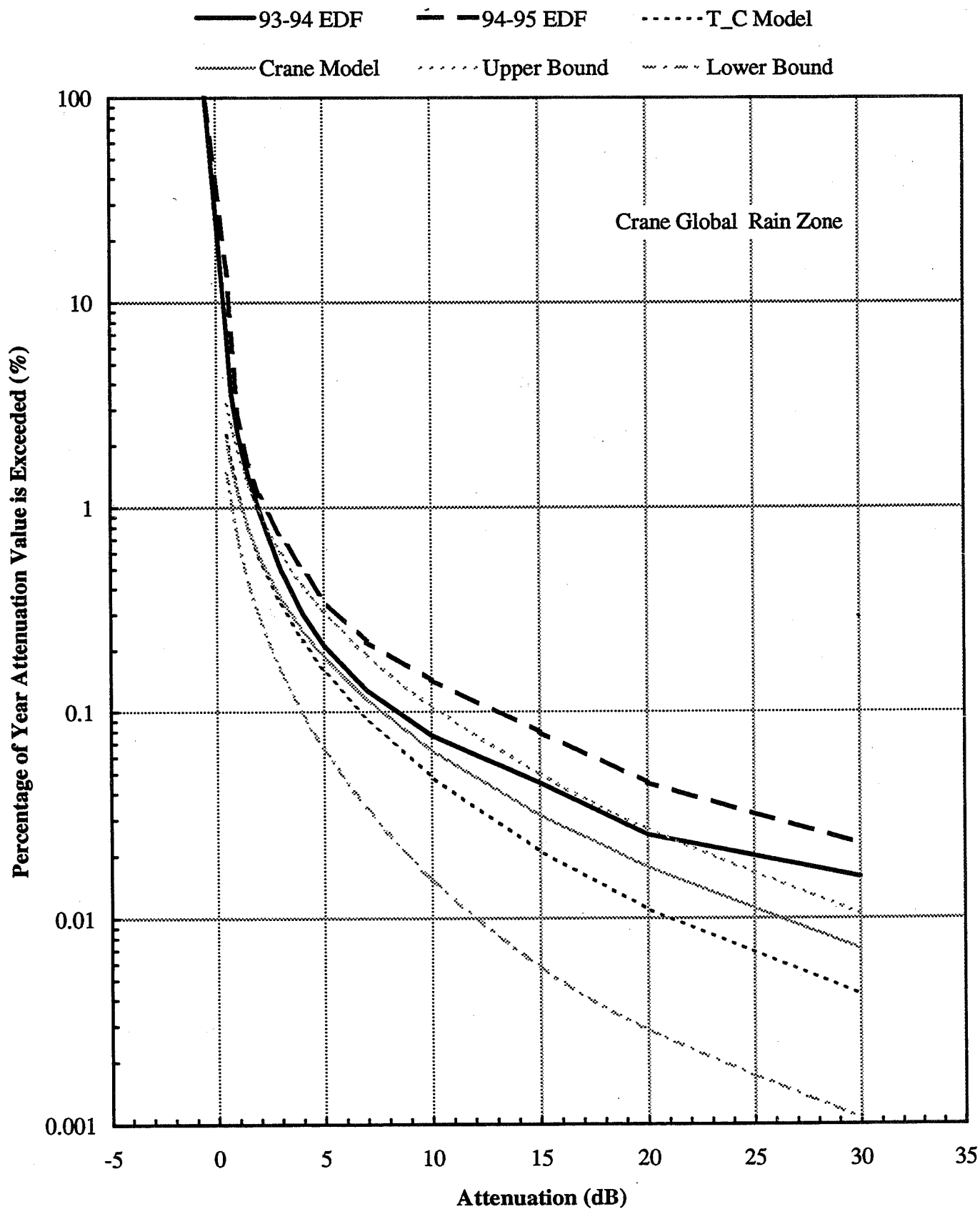


Figure 2 195

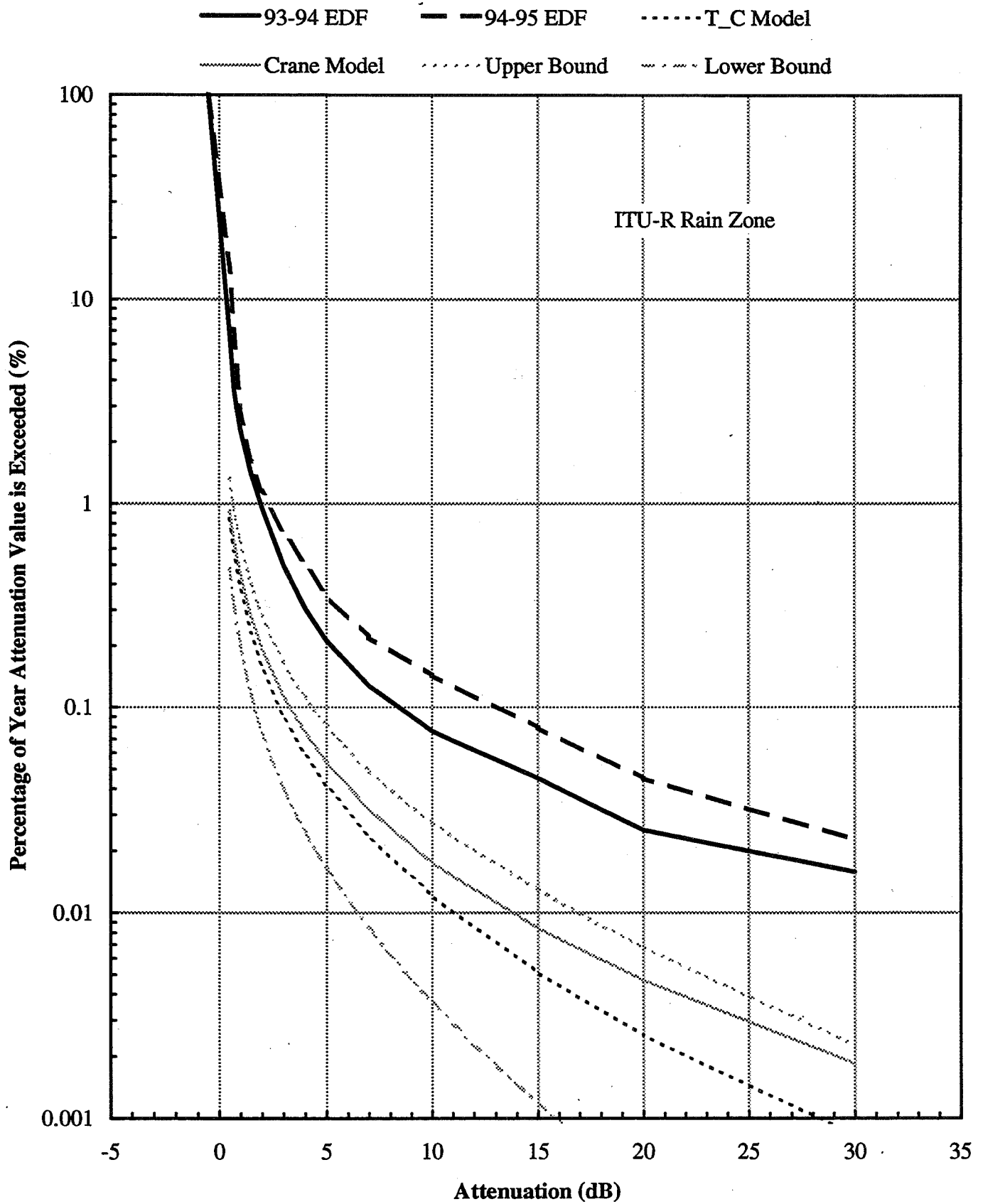


Figure 3 196

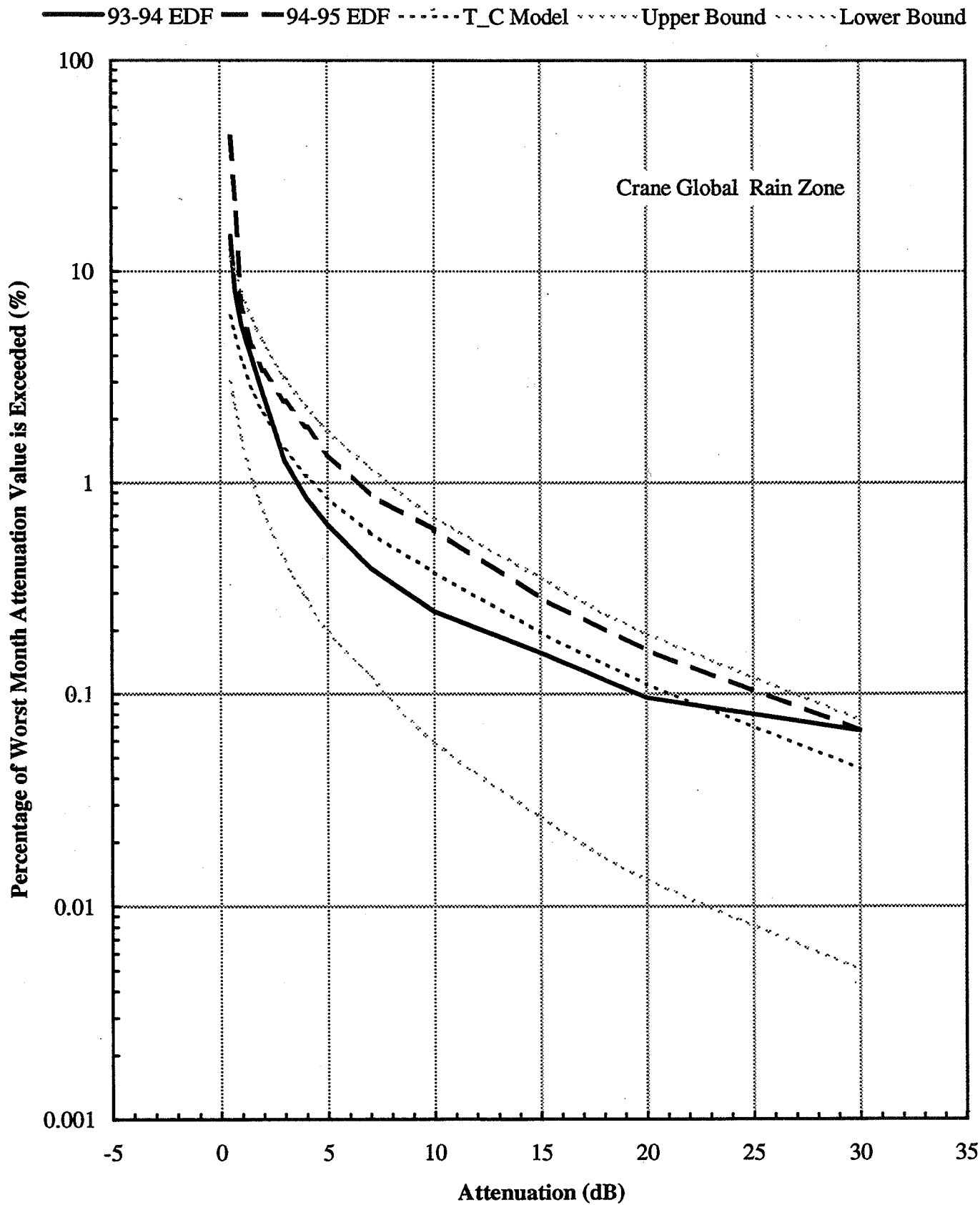


Figure 4 197

Page intentionally left blank

Eastern U.S. Space- Diversity Experiment: One Year of ACTS 20 GHz Measurements

Julius Goldhirsh, Bert Musiani
Applied Physics Laboratory, JHU

Asoka Dissanayake, K. T. Lin
COMSAT Laboratories

Contents of Talk

- Background
 - Geometry
 - Link Budget
- Objectives
- Fade-Time series examples
- Three-site cumulative distributions
 - single terminal, joint
- Three-site diversity gains
 - Versus two-site
- Seasonal Effects
 - Distributions (single and joint)
 - Diversity gains
- Concluding Remarks

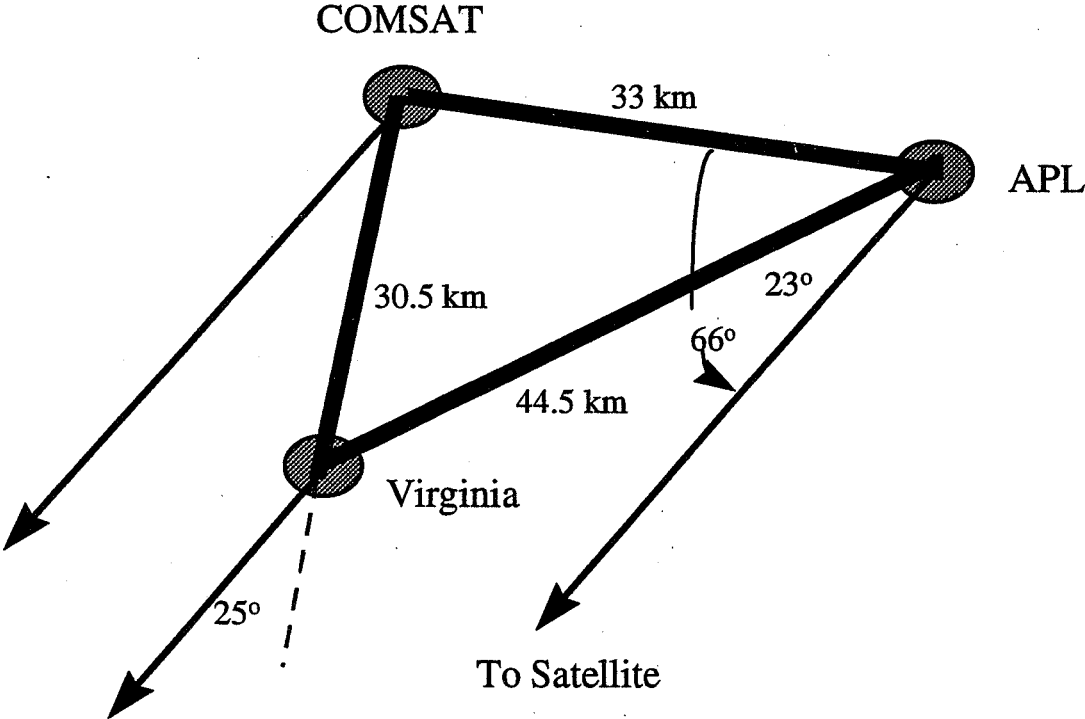
Background

- Three-site diversity experiment initiated September 1, 1994
- 20 GHz receivers located
 - APL (Howard County, MD), COMSAT (Clarksburg, MD)
 - MITRE (Reston, VA) until early April, 1995
 - Stanford Telecom (Reston VA) after April, 1995 (0.5 km distance)
- Time is synchronized with WWV

Background (Continued)

- Details of 1 year results in:
 - “Three-Site Diversity Experiment at 20 GHz Using ACTS,” by Goldhirsh, Musiani, Dissanayake, and Lin, APL/JHU Technical Report F2F-96-U-0-002, March , 1996.

GEOMETRY FOR APL-COMSAT-VIRGINIA DIVERSITY LINK



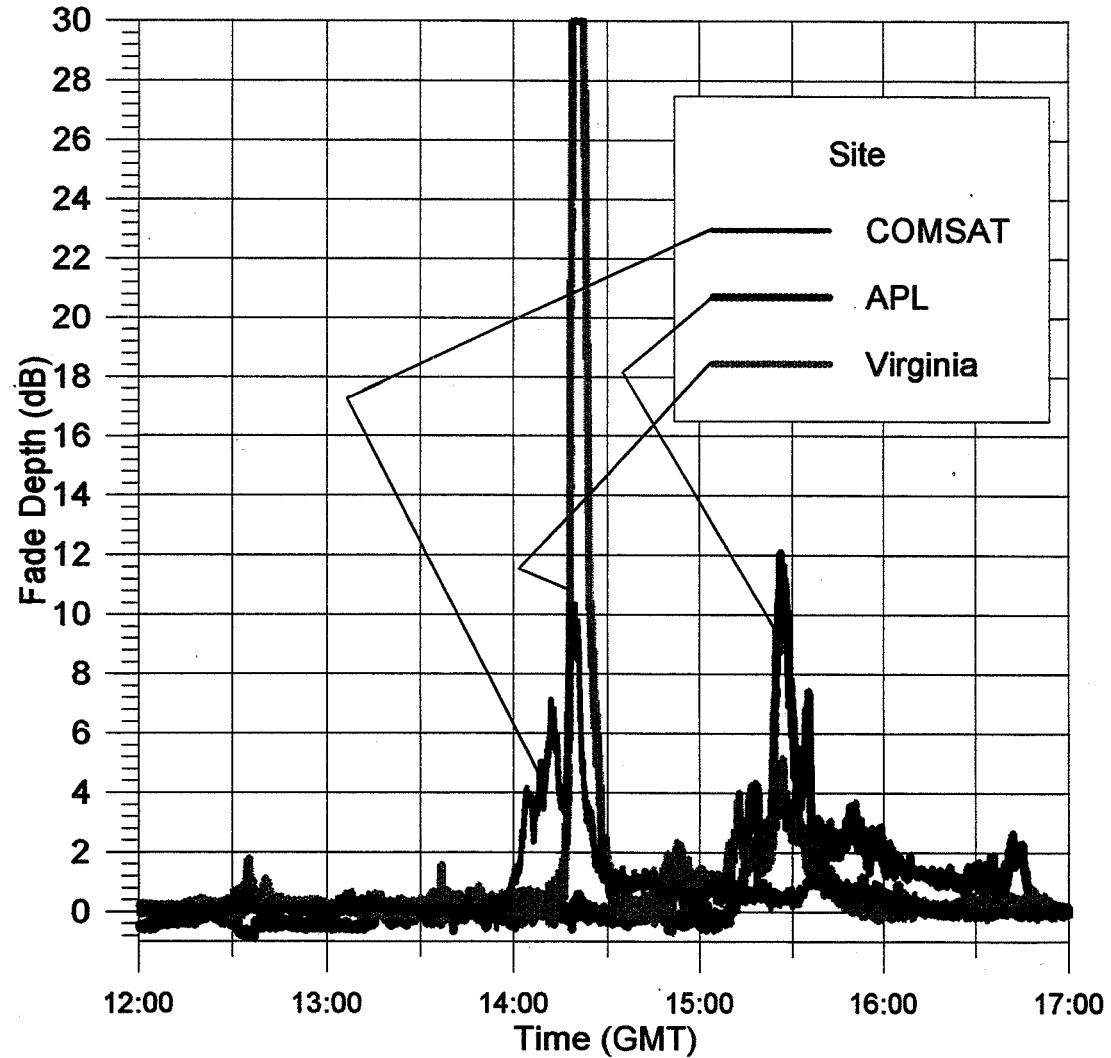
APL-COMSAT-Virginia Link Parameters

PARAMETERS	ALL	APL	COMSAT	Virginia
Frequency	20.185			
Polarization	V			
Beacon EIRP (dBW)	19			
Rec. Antenna Diameter (m)	1.2			
Rec. Antenna Gain (dB)	45.9			
Rec. Beamwidth (deg)	.85			
Rec. Bandwidth (Hz)		400	65	20
Carrier to Noise (dB)		28	34	36
Rec. Dynamic Range (dB)		22	28	30

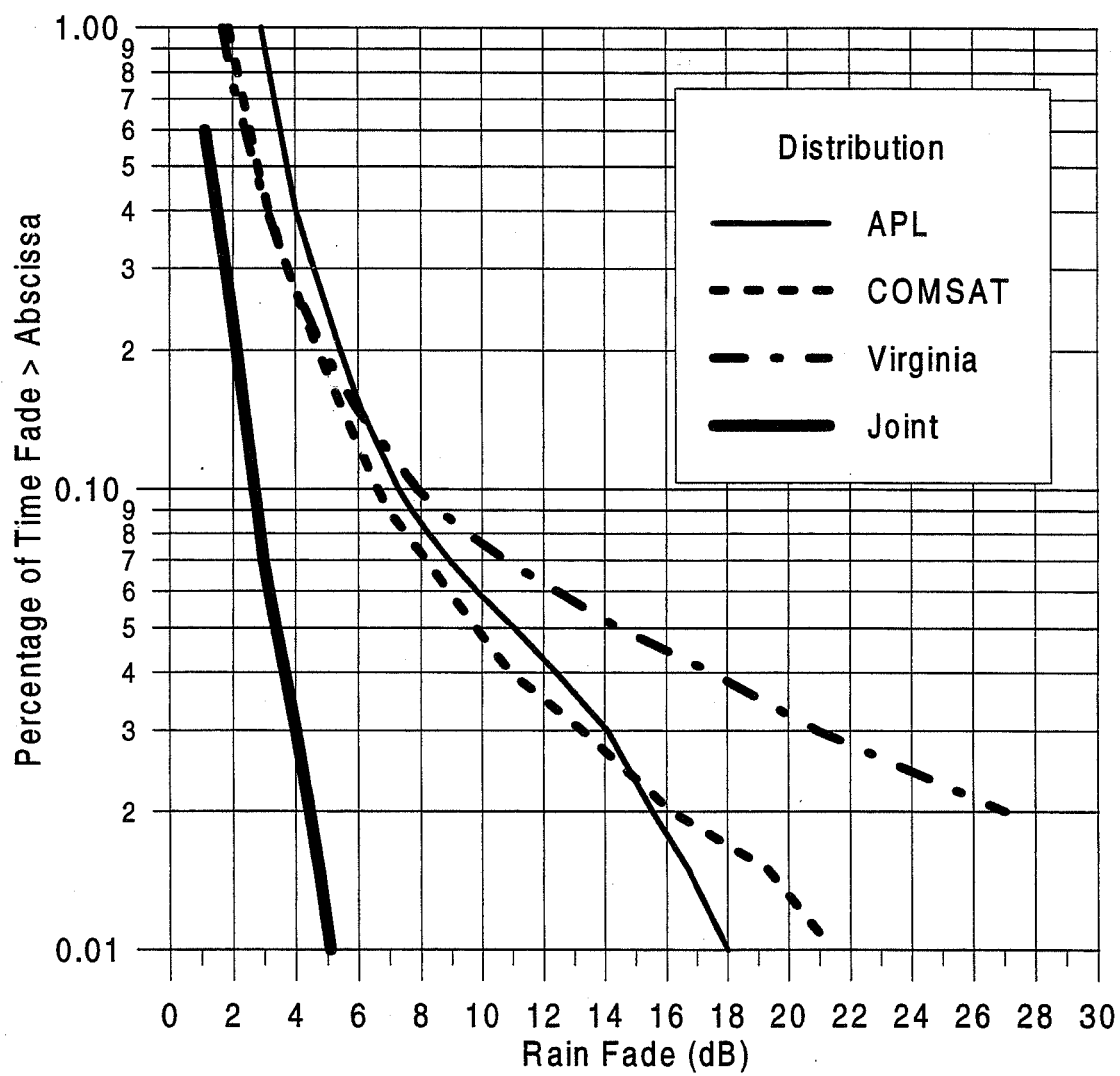
Objectives

- Single terminal, joint probability distributions, diversity gains
 - Three site scenario
 - APL, COMSAT, Virginia
 - Two site scenario combinations
 - APL-COMSAT
 - APL-Virginia
 - COMSAT-Virginia
 - Seasonal Effects
 - Compare results with models
 - Two site scenarios

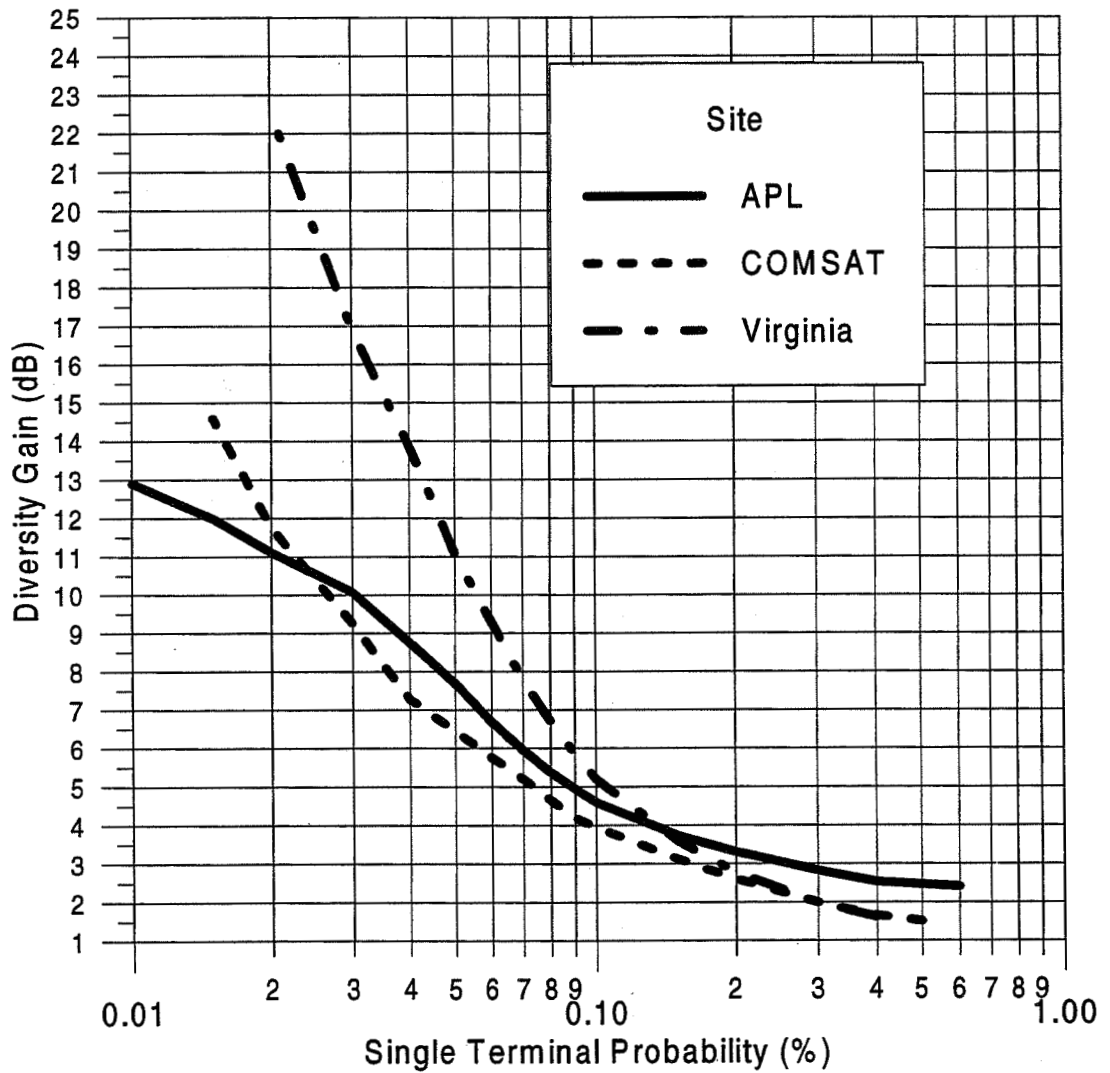
APL, COMSAT and Virginia Rain Fade Time-Series for November 1, 1994



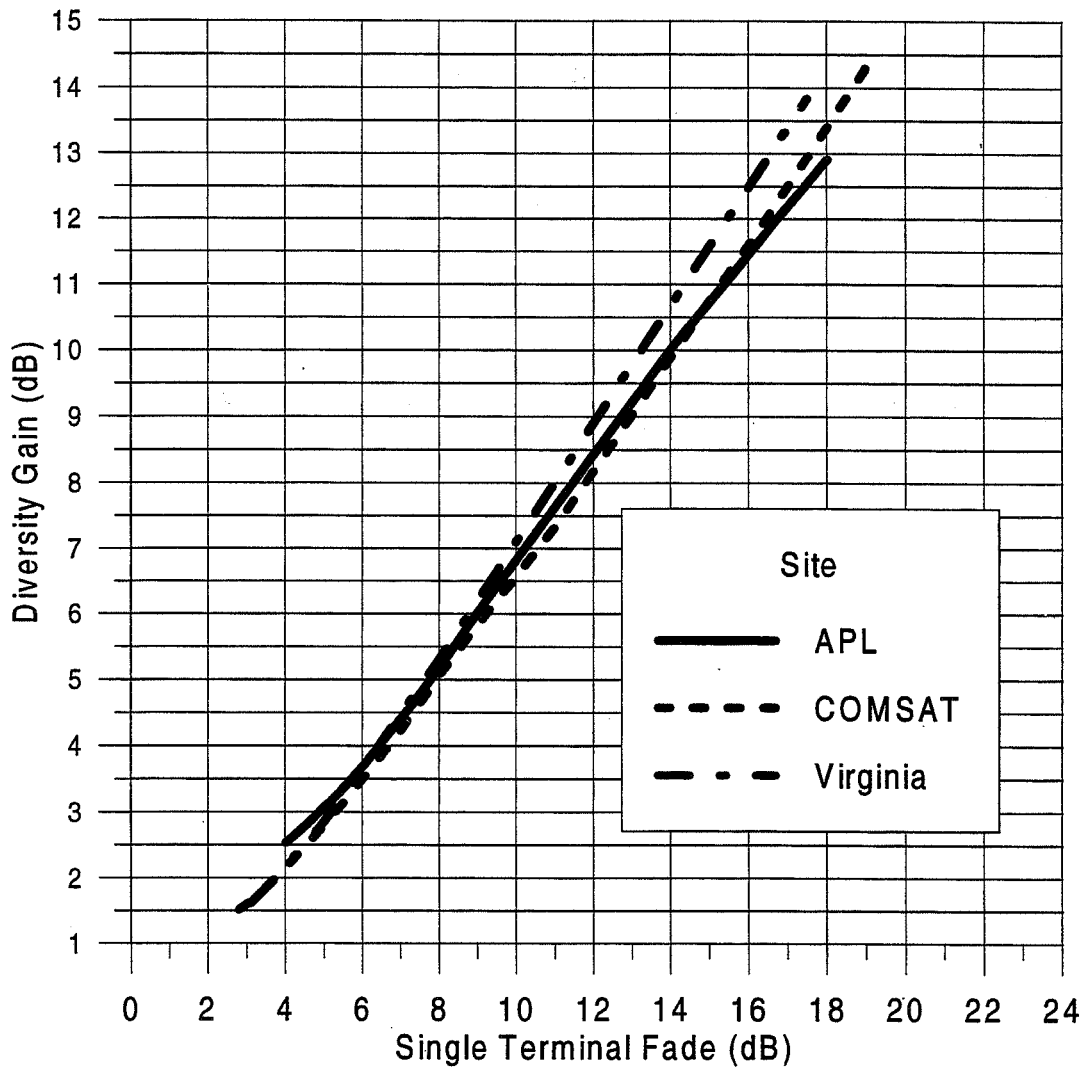
Single Terminal and Three-Site Joint Distributions for 1 Year Period (September 1994 - August 1995)



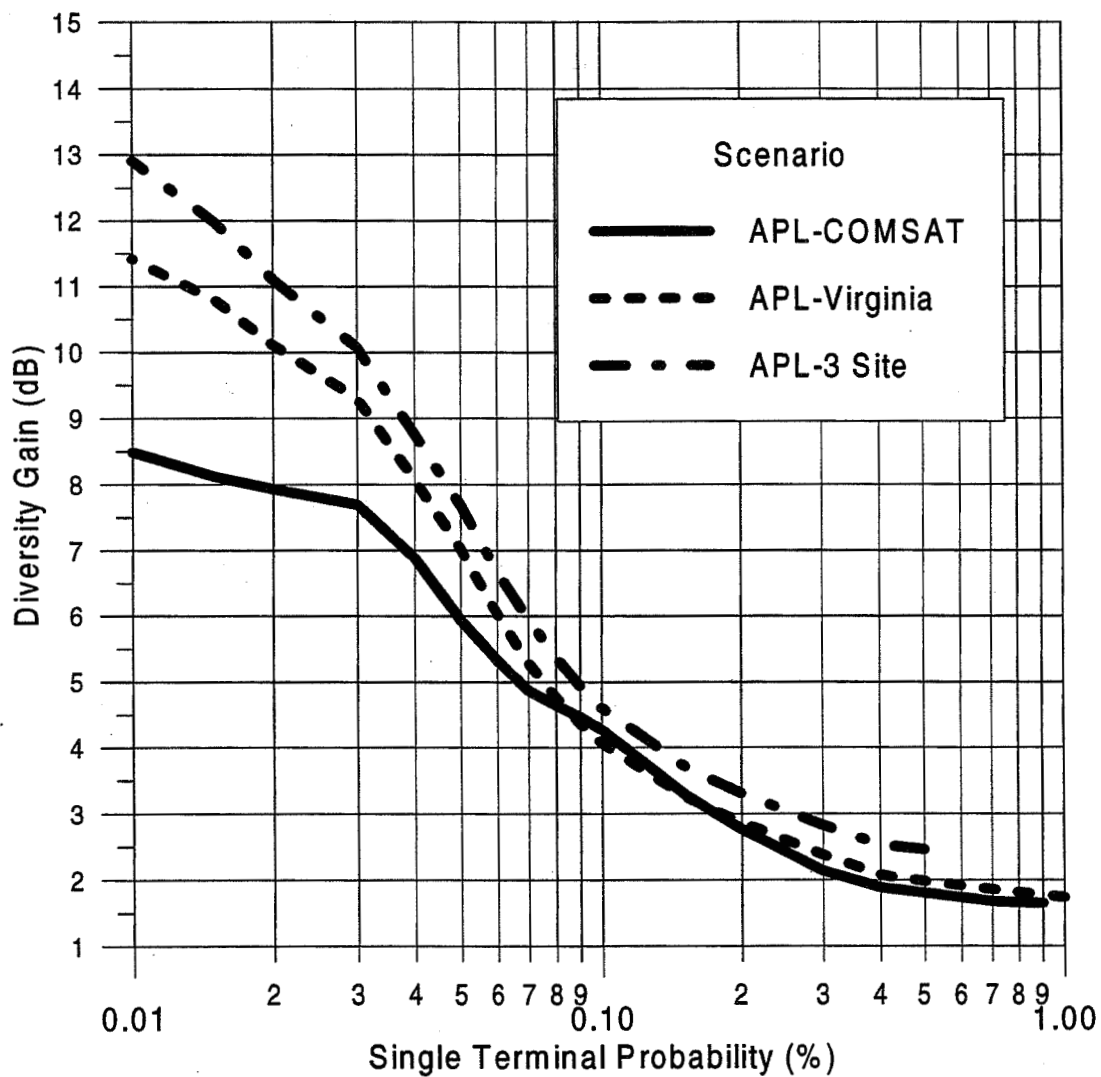
Diversity Gains Versus Single Terminal Probability at APL, COMSAT, and Virginia for Three-Site Diversity Scenario (ACTS 20 GHz)



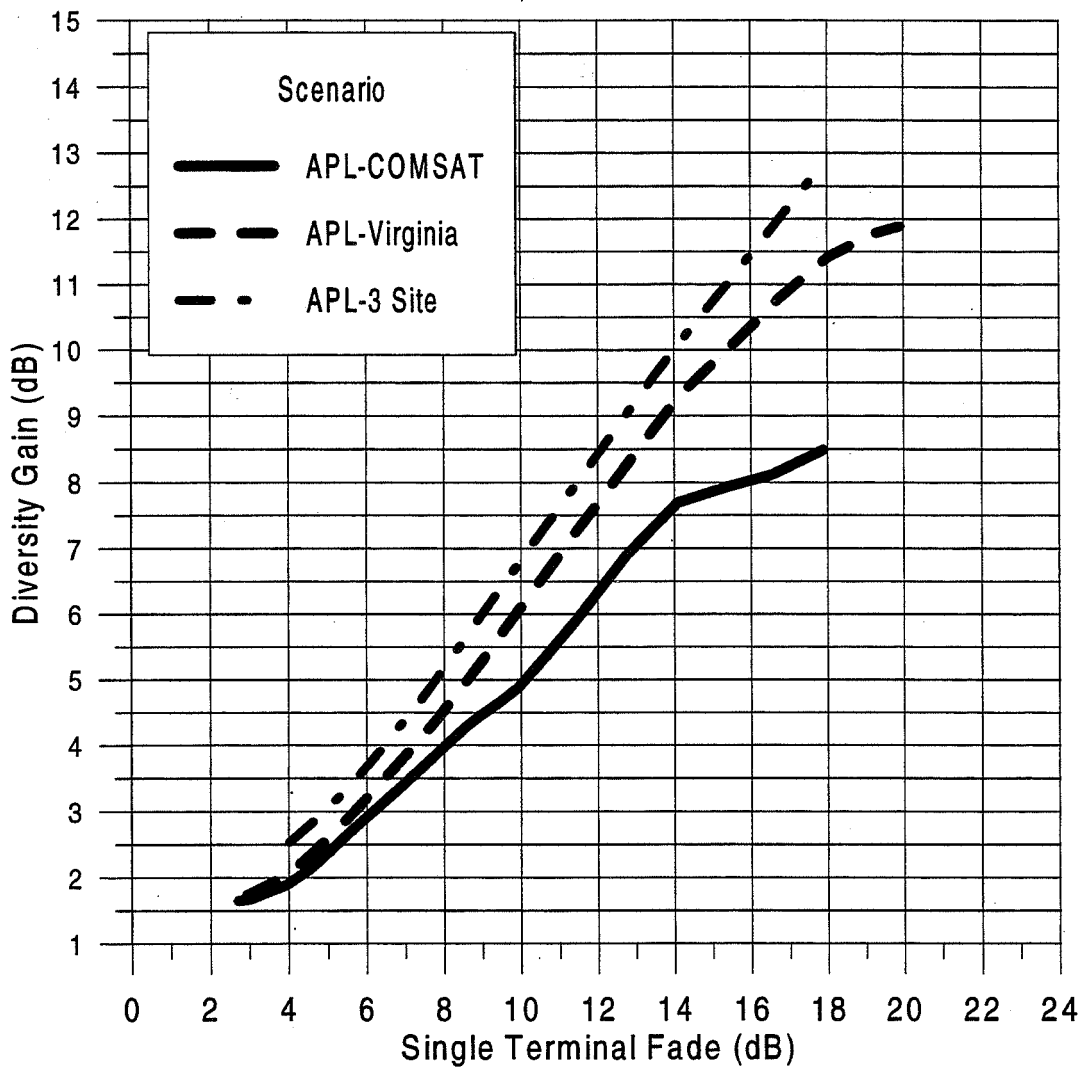
**Diversity Gains Versus Single Terminal Fades at
APL, COMSAT, and Virginia
for Three-Site Diversity Scenario (ACTS 20 GHz)**



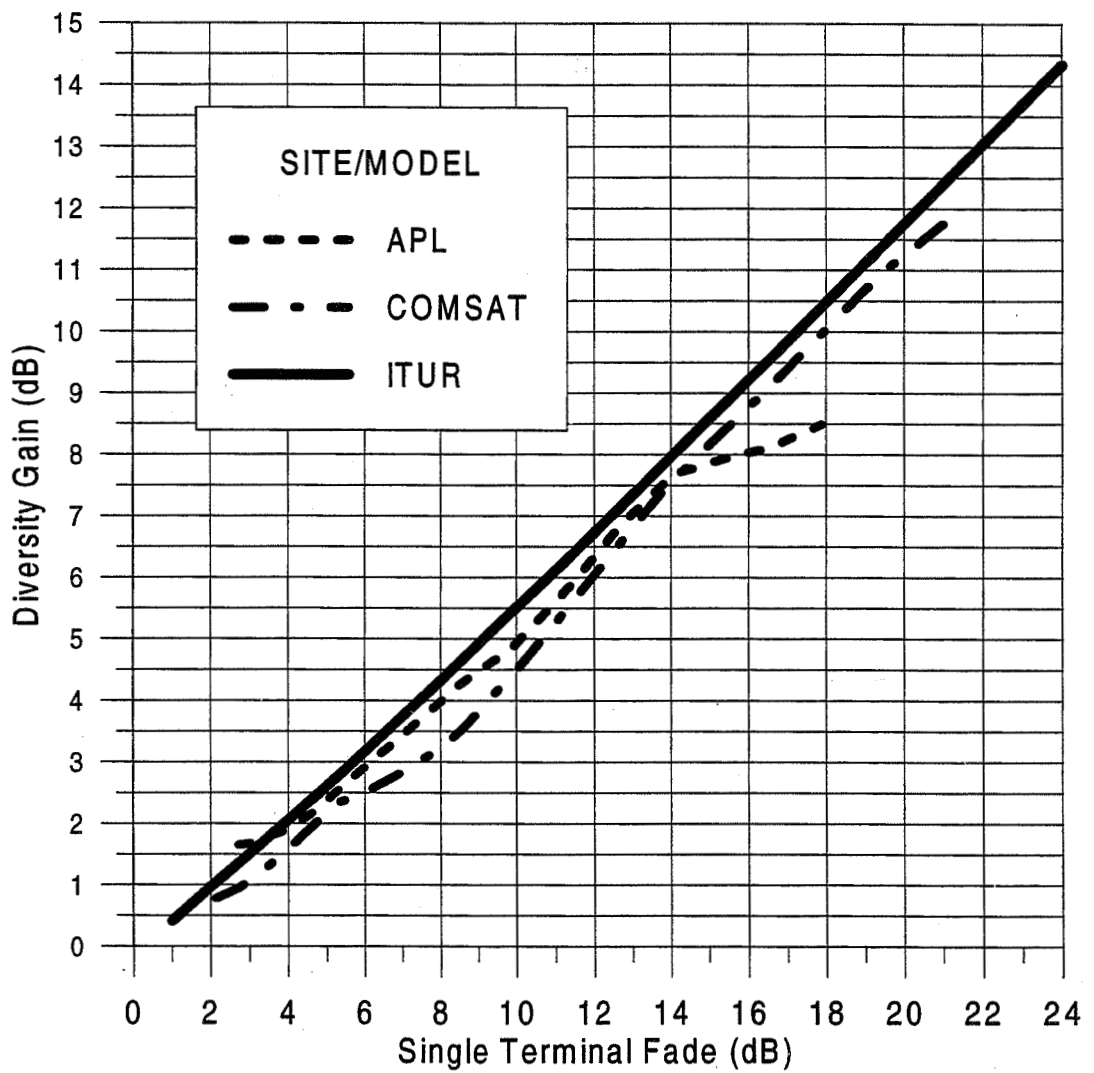
Diversity Gain Versus Single Terminal Probabilities for APL-COMSAT, APL-Virginia, APL-3 Site Diversity



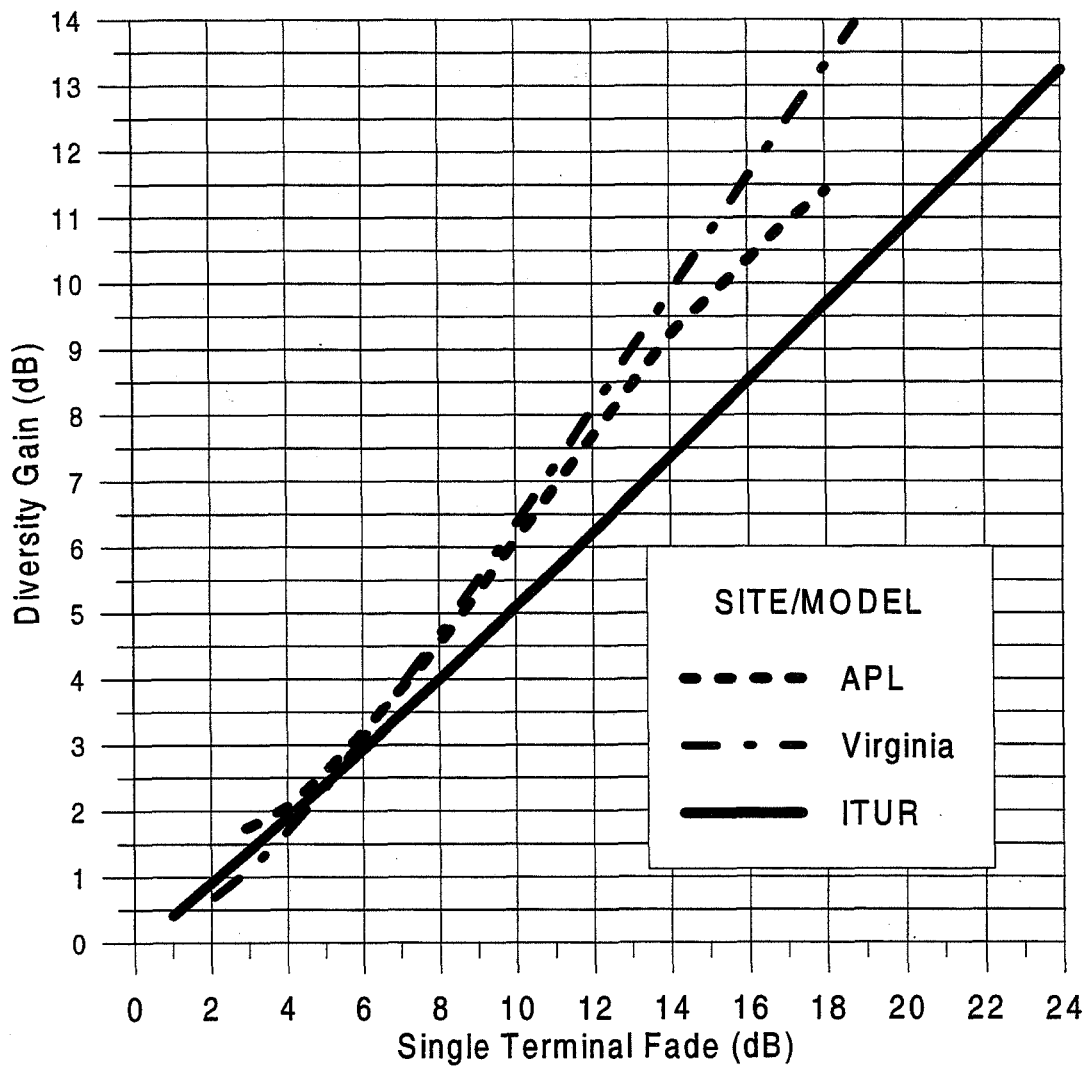
Diversity Gains Versus Single Terminal Fades for APL-COMSAT, APL-Virginia, APL-3 Site Diversity



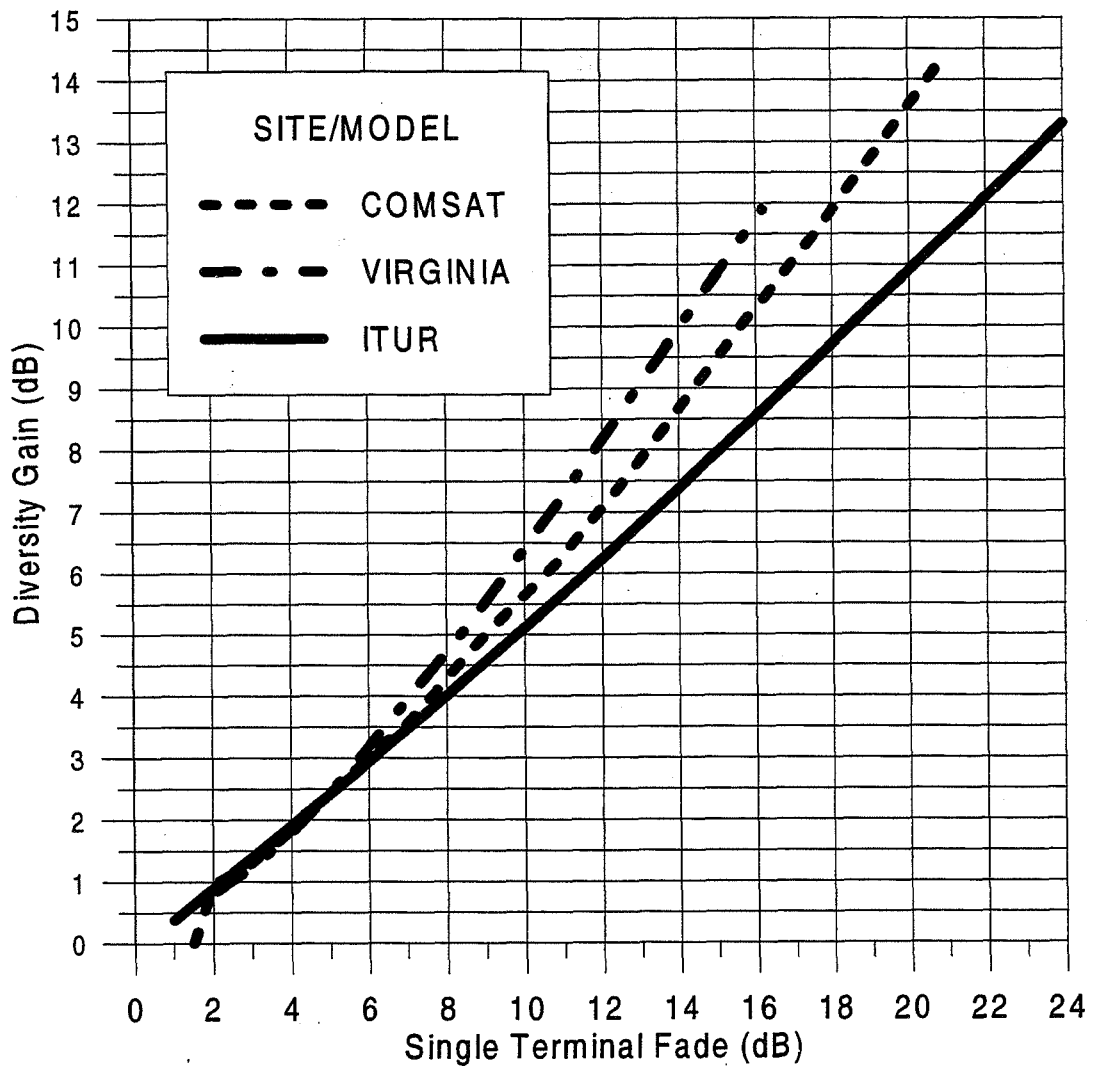
Diversity Gain Versus Single Terminal Fades for APL and COMSAT Two-Site Diversity Scenario



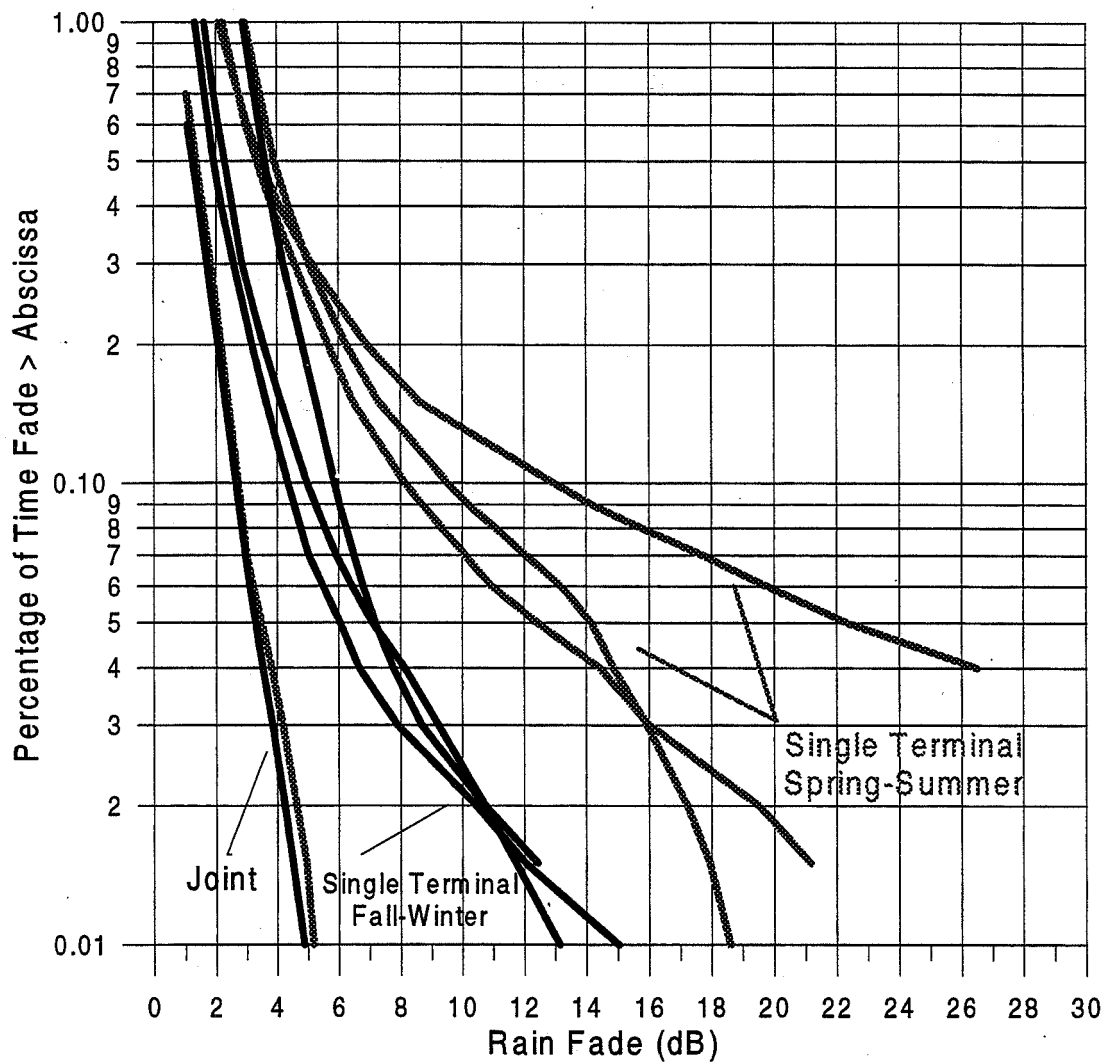
Diversity Gain Versus Single Terminal Fades for APL and Virginia Two-Site Diversity Scenario



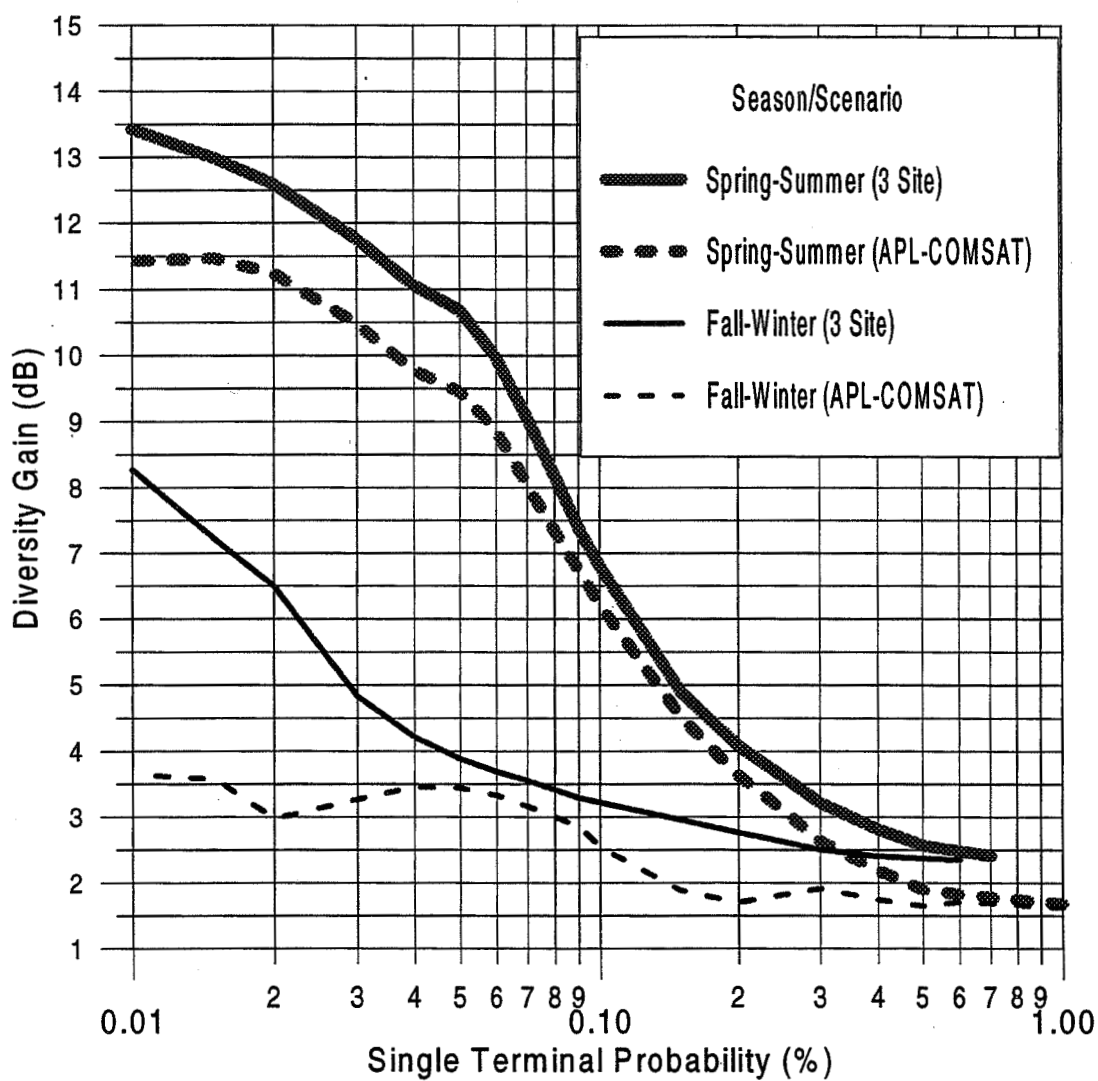
Diversity Gain Versus Single Terminal Fades for COMSAT and Virginia Two-Site Diversity Scenario



Seasonal Dependence on Single and 3-Site Joint Distributions at the Three Site Locations



Diversity Gain Versus Single Terminal Probability Showing Seasonal Effects for APL-3 Site and APL-COMSAT Scenarios



Summary and Conclusions

- Three Site Diversity Required Margins
 - At $P = 0.05\%$ --> 3.5 dB
 - At $P = 0.01\%$ --->5.0 dB
- Two Site Diversity Required Margins
 - 1 to 2 dB more (2 Scenarios)
 - 2 to 4 dB more (APL-COMSAT)

Summary and Conclusions (Continued)

- ITU-R model agrees to within 1 dB as follows:
 - Up to fade margin of 9 dB for two of three scenarios
 - Up to fade margin of 15 dB for APL-COMSAT

Summary and Conclusions (Continued)

- Seasonal Effects
 - Three Site Diversity Fade Margin
 - At $P = 0.01\%$ --> 5 dB (Convective and Stratiform Periods)
 - Significant Increase in Diversity Gain During Convective Season
 - Greater than 6 dB at $P = 0.05\%$
- Second Year of Measurements and Analysis Underway
 - Mitigate statistical noise

Page intentionally left blank

Fade Mitigation Techniques At Ka-Band

Asoka Dissanayake

Introduction

- Rain fading is the dominant propagation impairment affecting Ka-band satellite links and rain fade mitigation is a key element in the design of Ka-band satellite networks. Some of the common fade mitigation techniques include:
 - power control
 - diversity
 - adaptive coding
 - resource sharing
- ACTS provides an excellent opportunity to develop and test Ka-band rain impairment amelioration techniques.
- Up-link power control and diversity are discussed.

UP-link Power Control

- **Up-link power control is one of the fade mitigation techniques that can be implemented relatively easily. Power control at an earth station attempts to maintain a constant power flux density at the satellite irrespective of fading conditions along the propagation path.**
- **Types of up-link power control (ULPC) :**
 - open loop
 - closed loop
 - feedback loop
- **Open loop is the easiest to implement and does not require system-wide considerations.**

Open-loop ULPC

- **Requires estimation of fading/enhancement on the up-link. One of the following methods may be used:**
 - radiometry
 - beacon measurement
 - BER measurement
- **Technique used determines accuracy and cost.**
- **In general, beacon measurement provides a higher accuracy at a modest cost.**



Beacon Measurements

- Attenuation along the satellite path deduced from measured beacon level variations.
- In addition to propagation phenomena, beacon level variations are brought about by:
 - beacon EIRP changes
 - instability of measurement system
 - antenna pointing errors
 - spacecraft maneuvers
 - modulation on beacon signal
- Fade detection based on establishing a clear-sky level that has a dominant diurnal pattern.



Up-link Fade Estimation

- Most satellites carry a beacon sources in the down-link frequency band. When using a down-link beacon for power control, the estimated down-link fade must be frequency scaled to the up-link.
- Propagation factors contributing to fading:
 - gaseous absorption
 - rain attenuation
 - clouds and melting layer
 - tropospheric scintillation
- Each factor has a different average frequency scaling law. In addition, there are random variations around the average scaling ratio.

ULPC Implementation Issues

- Point of application of power control (RF or IF)
- Control accuracy, HPA non-linearities
- Fail safe operation to protect space segment
- Interference:
 - adjacent channel
 - orthogonally polarised channel
 - off axis emission
- Power control dynamic range

Power Control Algorithm

- Detect down-link fade after establishing the reference level; reference level based on long-term observations using an adaptive filter with a time constant of the order of 1 hour
- Down-link fade separated in to rain fade and scintillation components; an averaging time of 20 sec. used in estimating rain fade.
- Current level of rain fade predicted using an adaptive filter
- Frequency scaling of rain and scintillation fades to 29 GHz

Experiment Details

- Power control carried out using a 29 GHz pilot carrier transmitted from the LET at Lewis Center in Cleveland; transponded carrier received at Clarksburg.
- Power control based on down-link attenuation measurements at 20 GHz
- Beacon reception and pilot transmission are done on separate antennas; antenna separation ~ 15 ft; little impact on measurements
- Control applied at IF; power control resolution: 0.2 dB; update rate 5 Hz
- Maximum power control range: 25 dB; however, investigation will be limited to a control range of 15 dB.
- Power controller was able to maintain control accuracy within ± 2.5 dB

Site Diversity

- Site diversity is one of the fade mitigation methods that takes advantage of finite size of rain cells.
- Site diversity applied in the conventional sense involves two earth stations interconnected via a dedicated terrestrial line.
- Relatively high cost of conventional diversity makes it less attractive to network operators.

Factors Affecting Diversity

- Site separation
- Rain climate
- Frequency
- Elevation angle
- Baseline orientation

Wide-area Diversity

- Use of site diversity when interconnecting wide-area networks using satellites. Satellite link serving as a variable bandwidth backbone.
- Presence of more than one earth terminal within a wide-area network; adequate site separation to provide uncorrelated fading.
- Interconnection of earth terminals using an appropriate data service.

Networked Diversity

- **Cost of implementing site diversity can be reduced using:**
 - **public switched network for interconnection**
 - **sharing of earth station resources.**
- **Rain fading is restricted to a small fraction of time in a year and the use of the switched network on as needed basis can bring significant cost advantages.**
- **Sharing of earth station resources implies that not all terminals are fully occupied at all times. This is especially true for VSAT type terminals**

Diversity Implementation

- **Link evaluation (beacon, radiometer, BER, AGC)**
- **Switching with minimum data loss (short-term prediction of fading conditions)**
- **avoidance of frequent switch operations (statistics of fade durations and inter-fade intervals)**
- **Central control or distributed control**

Results

Result	COMSAT	MITRE
Down time due to fading (> 4 dB)	159 min	191 min
Unavailable time with full diversity	33 min	45 min
Networked unavailable time	43 min	54 min
Number of attempted switches	61	55
Number of failed switches	11	9

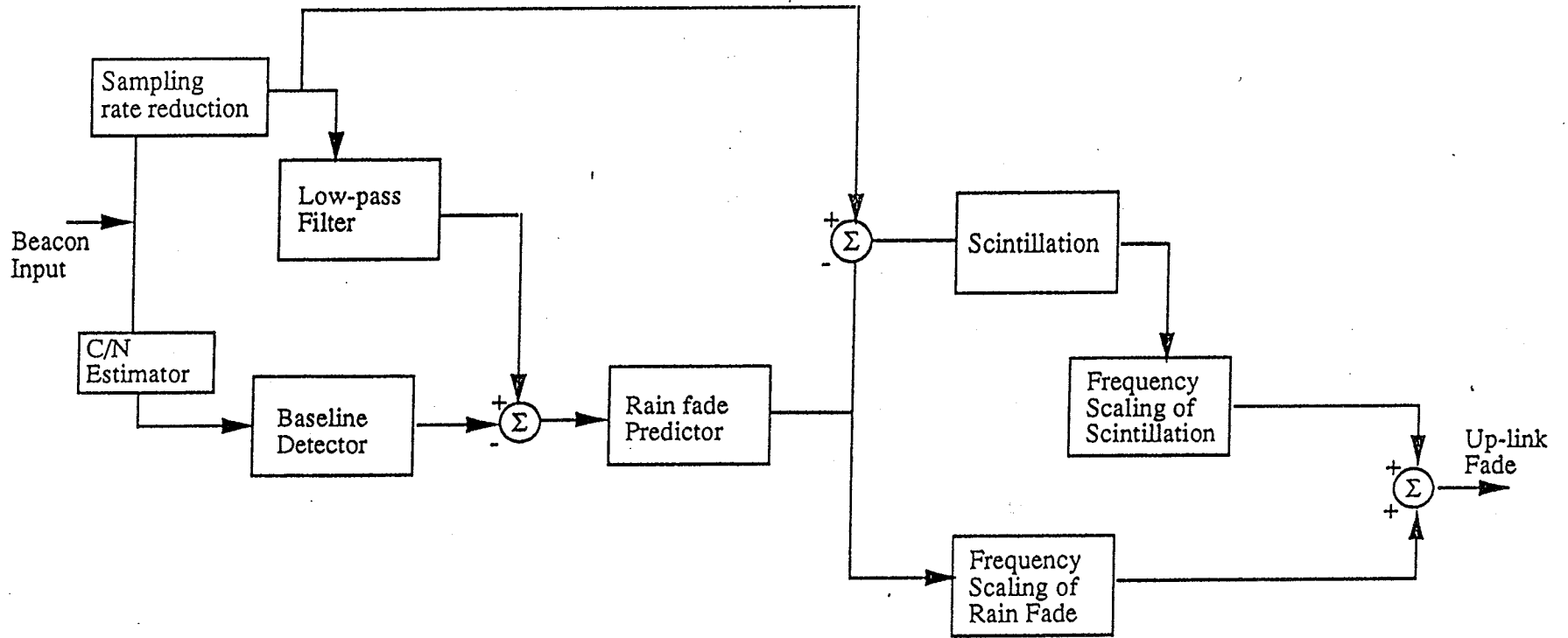
Conclusions

Power Control

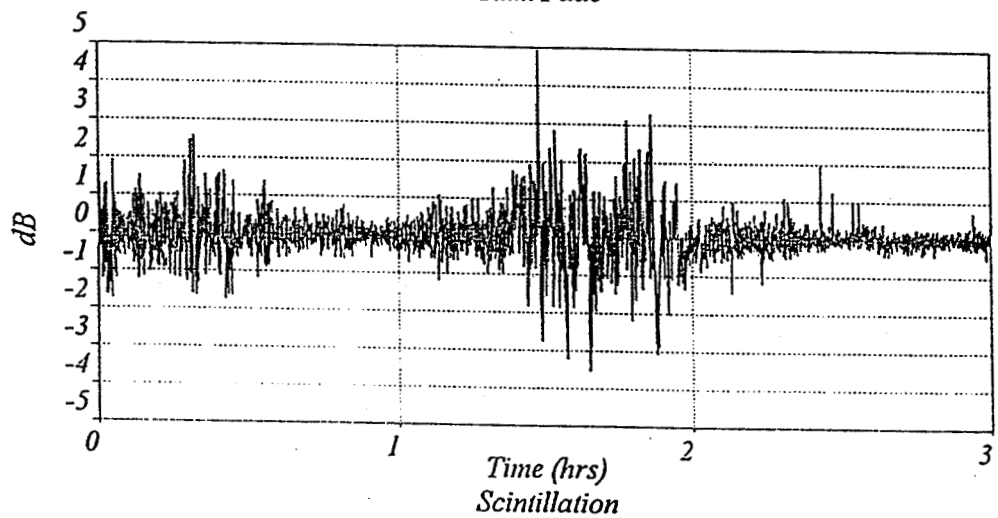
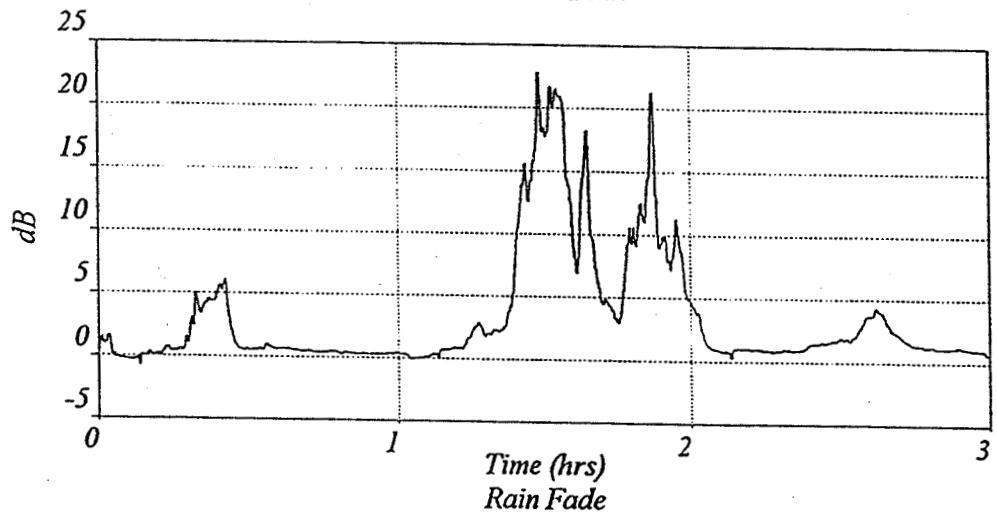
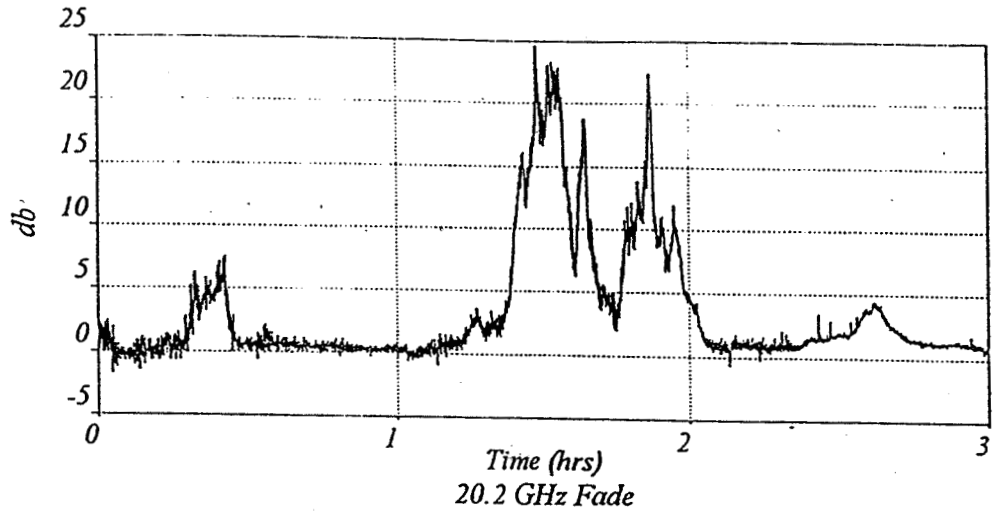
- Experiment demonstrated the usefulness of power control and helped establish design parameters for operational systems.
- When restricted to a power control range of 15 dB, the control accuracy can be maintained within ± 2.5 dB.

Diversity

- Wide-area diversity can be used to increase the availability of Ka-band VSAT terminals.
- It also allows for the increased utilization of both ground and space segment resources.



Up-link Fade Estimation Algorithm



Separation of Rain and Scintillation; Rain Event on 14 August, 1994

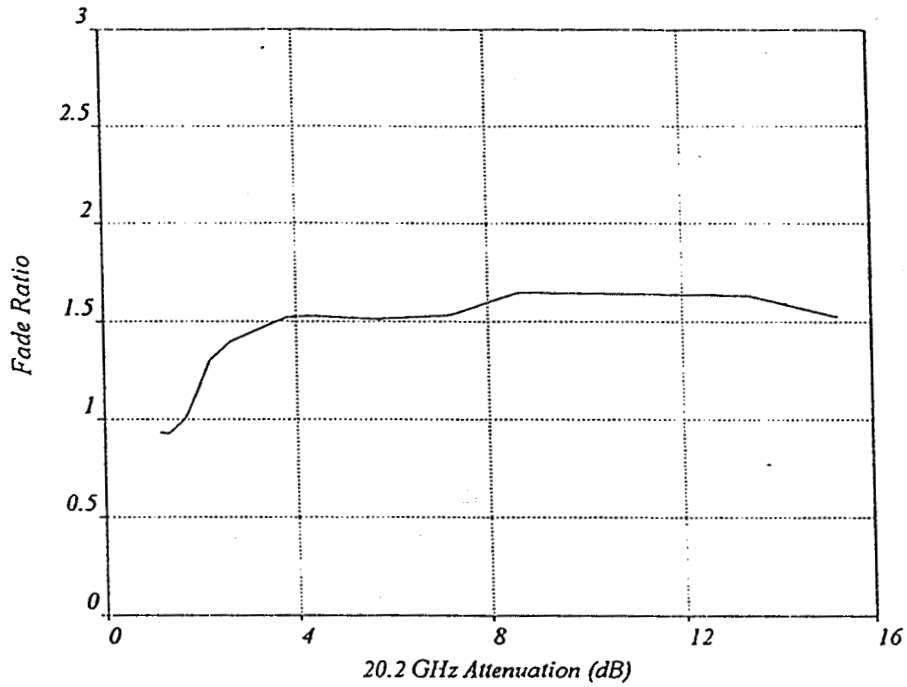
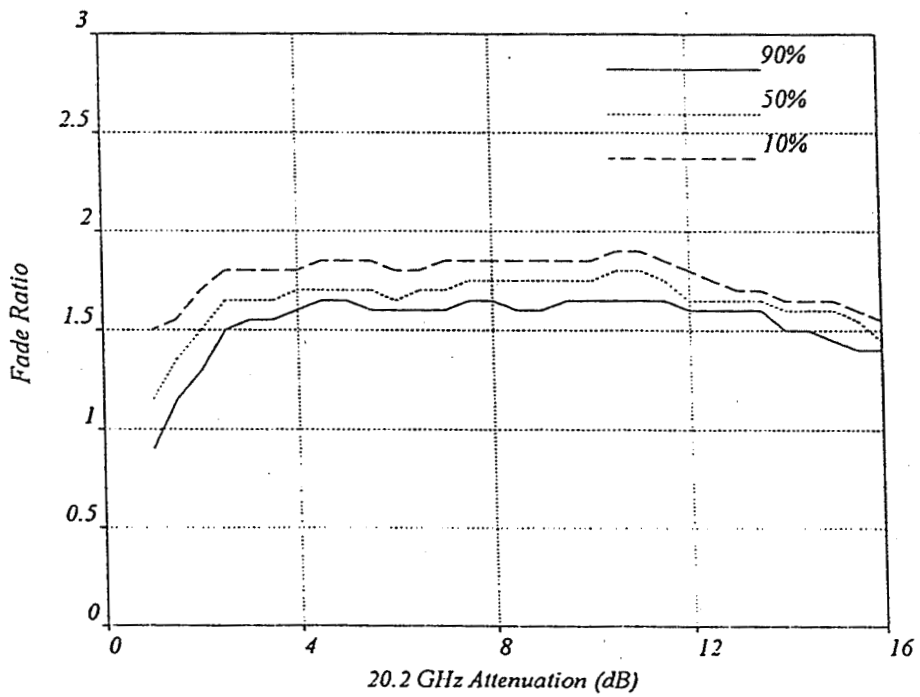
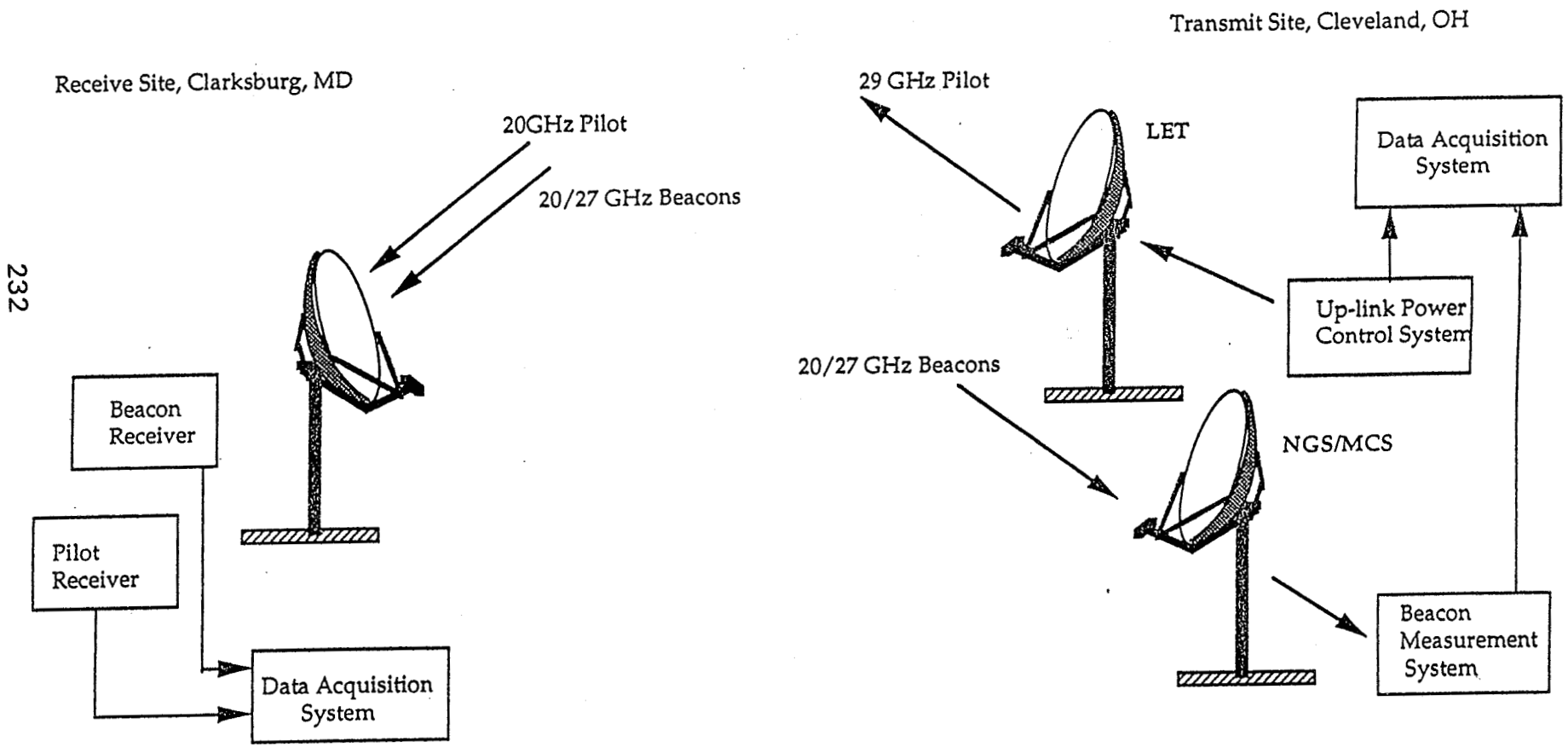
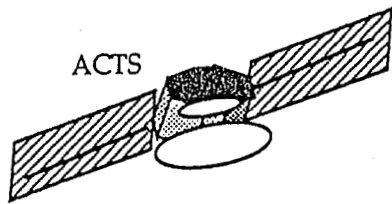


Figure 2.11 Equiprobable Fade Ratio Between 27.5 and 20.2 GHz

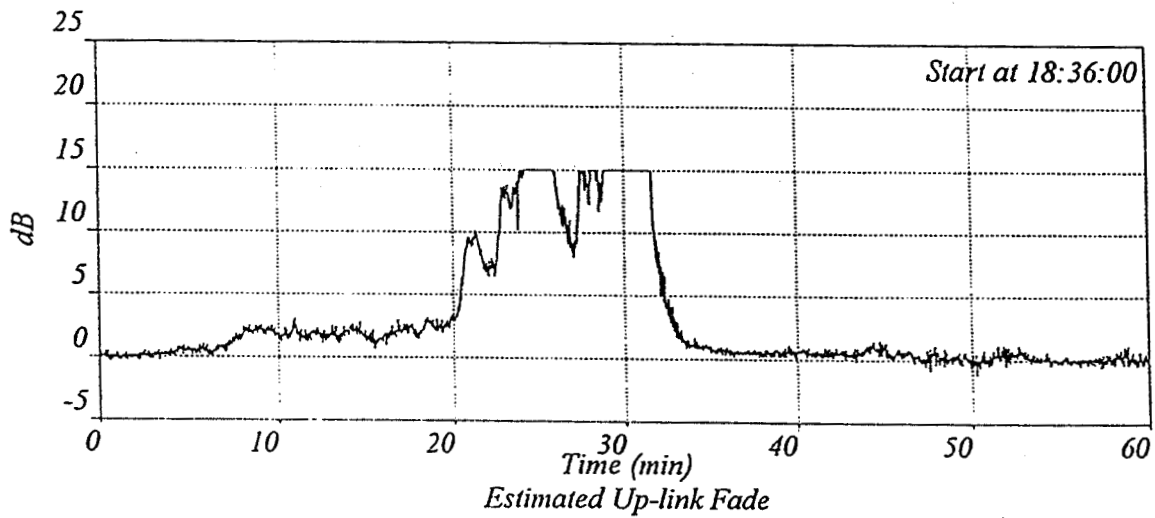
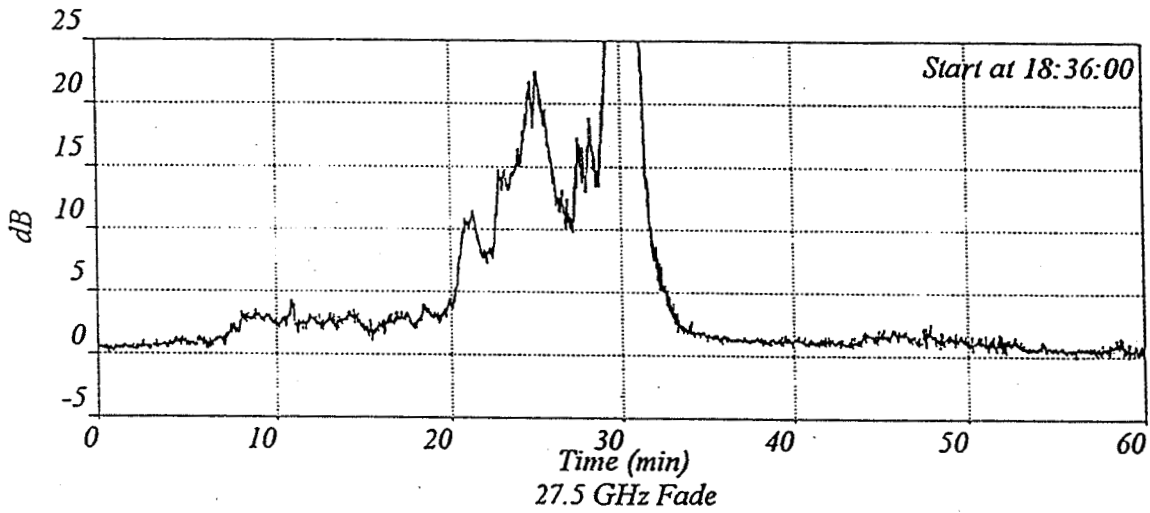
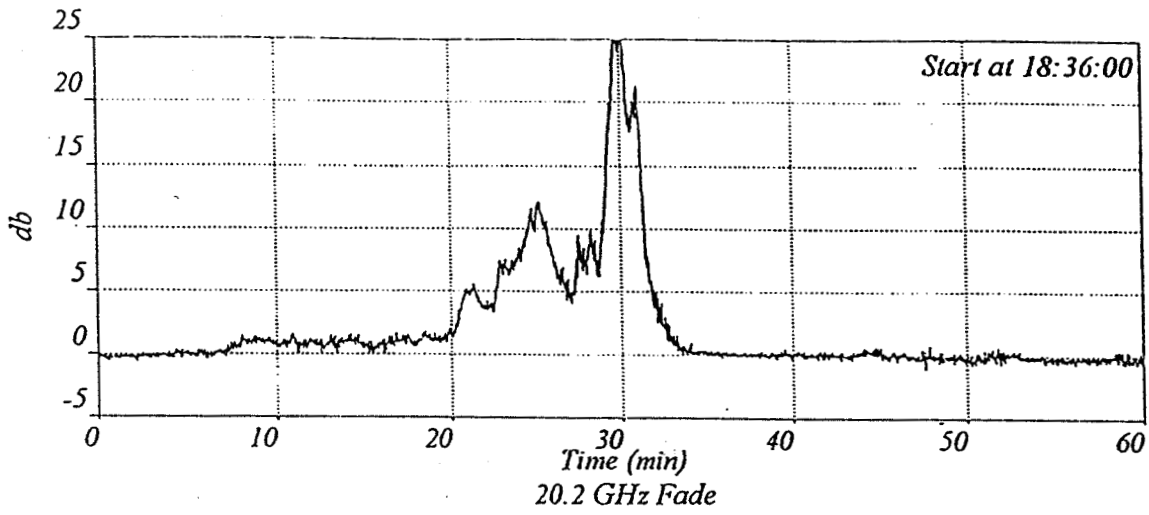


Distribution of Instantaneous Fade Ratio Between 27.5 and 20.2 GHz

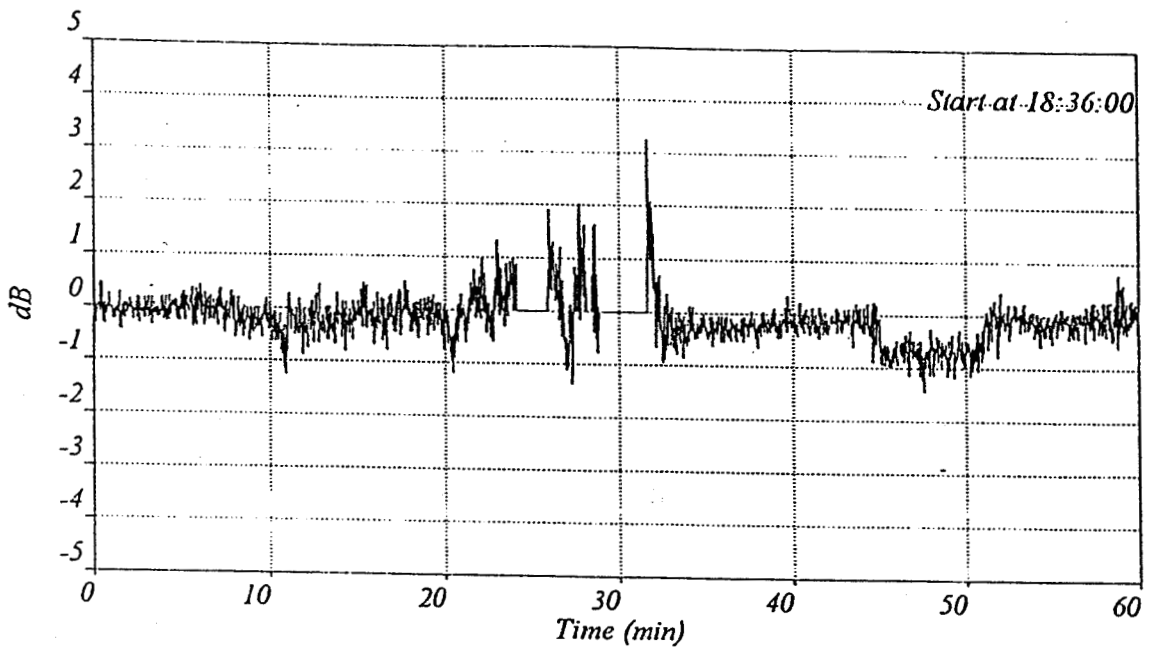


232

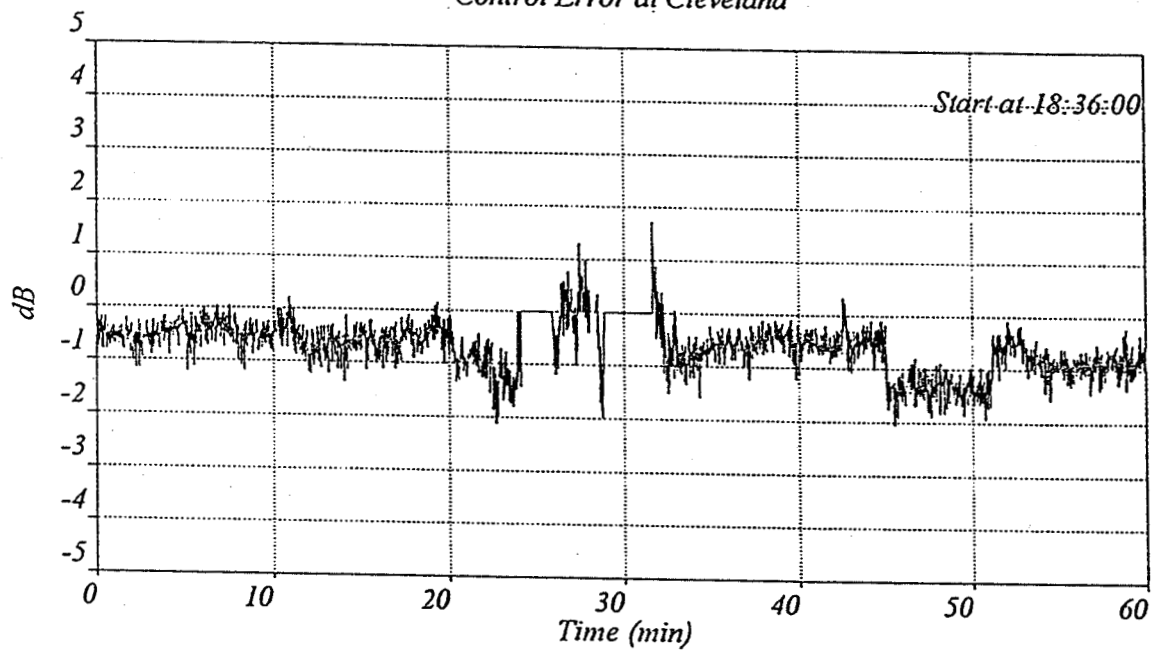
ACTS Up-link Power Control Experiment Configuration



Rain Event 1 on 31 May, 1994

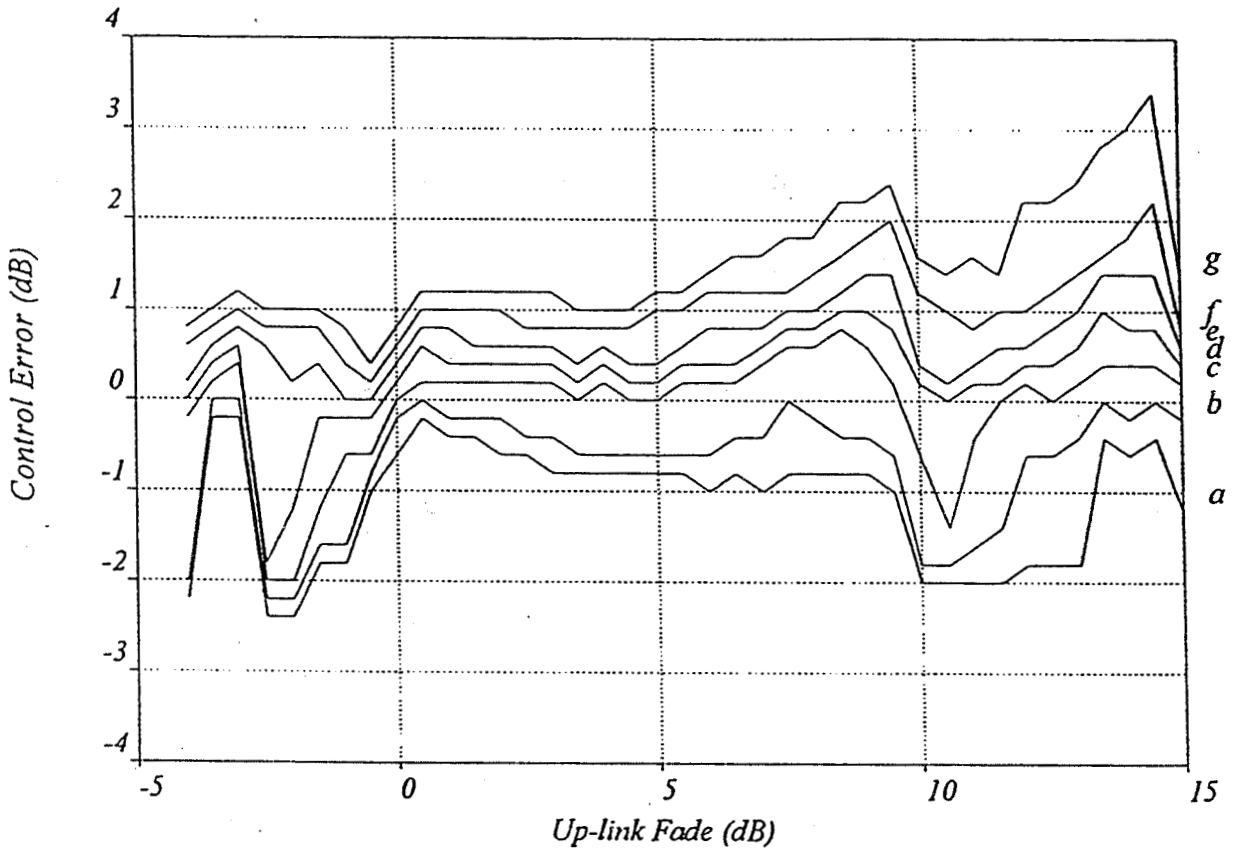


Control Error at Cleveland



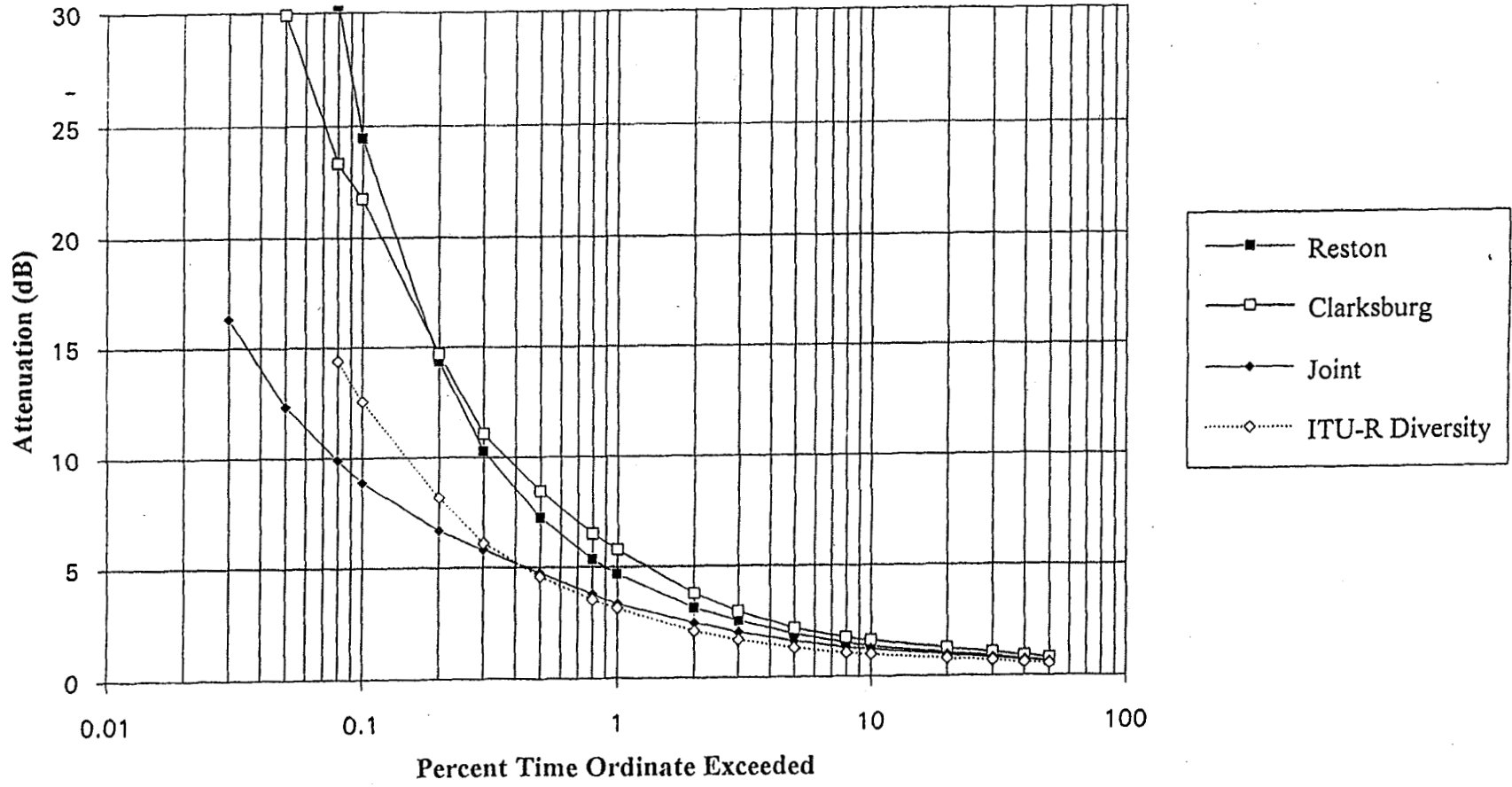
Pilot Level at Clarksburg

Control Error; Rain Event 1; May 31, 1994

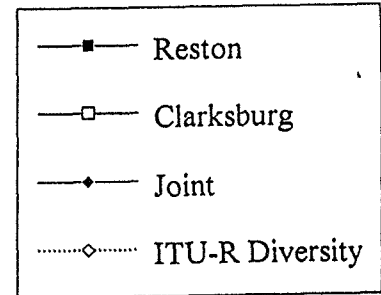
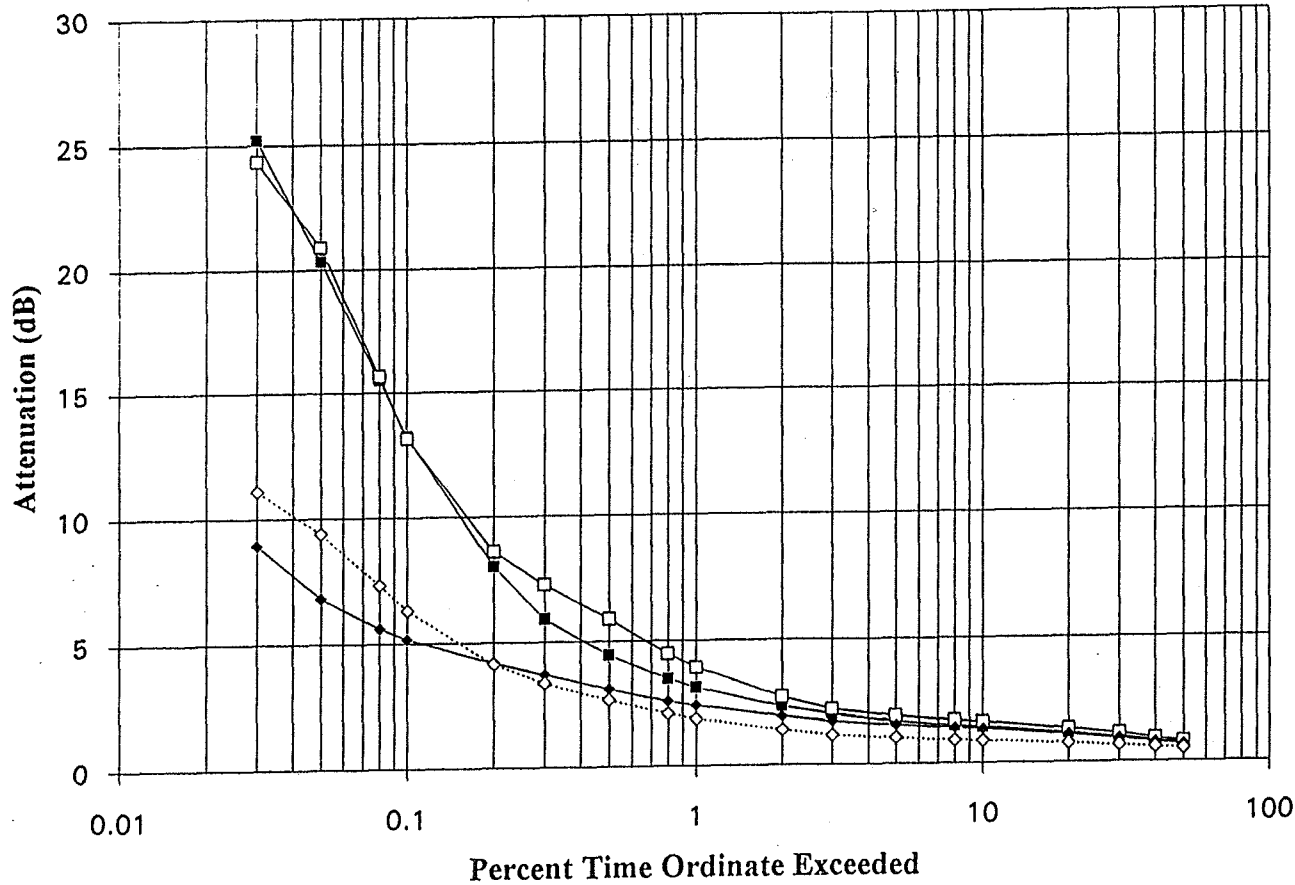


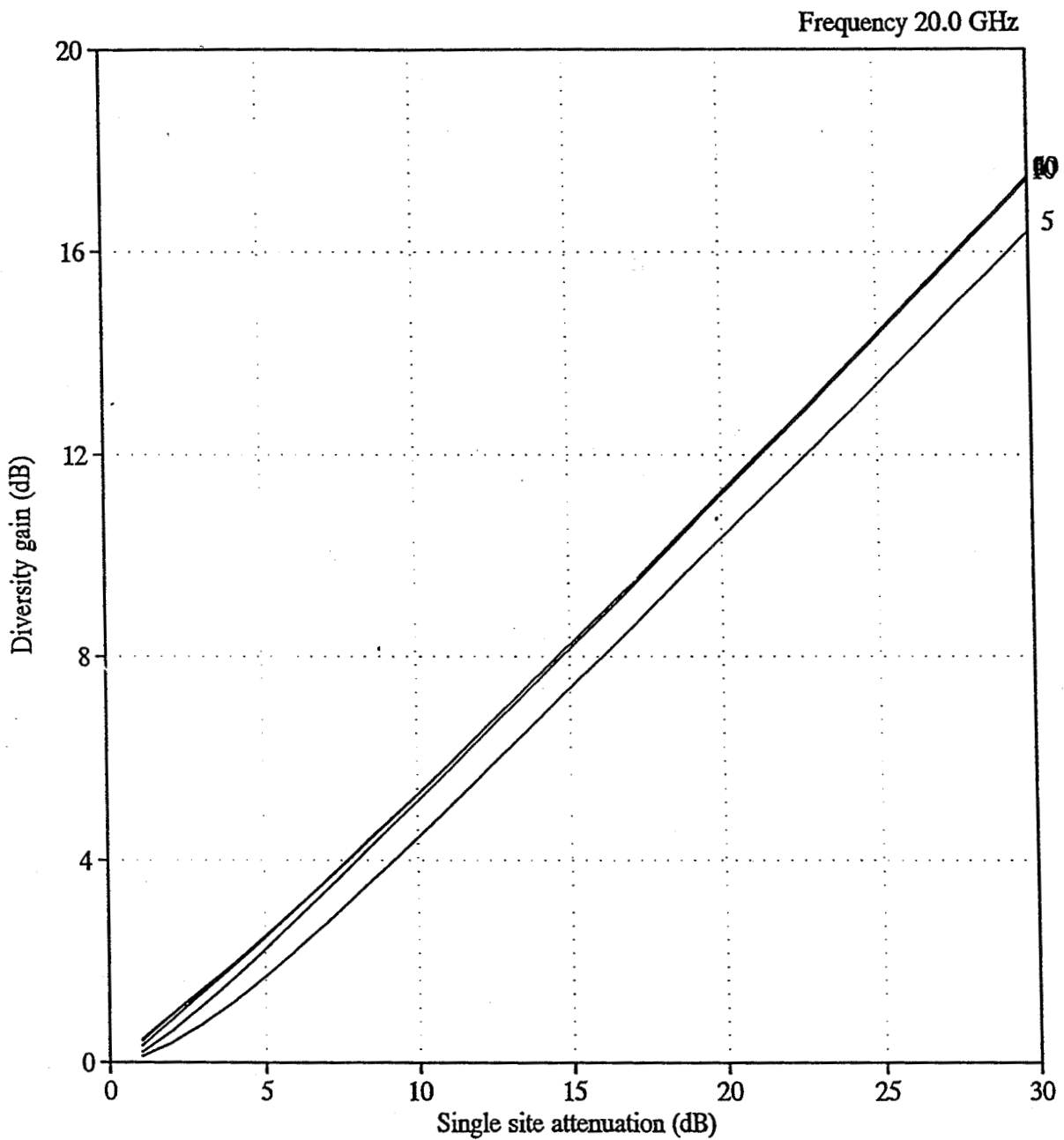
Distribution of Power Control Error;
 a: 99%, b: 95%, c: 75%, d: 50%, e: 25%, f: 5%, g: 1%

27 GHz Attenuation

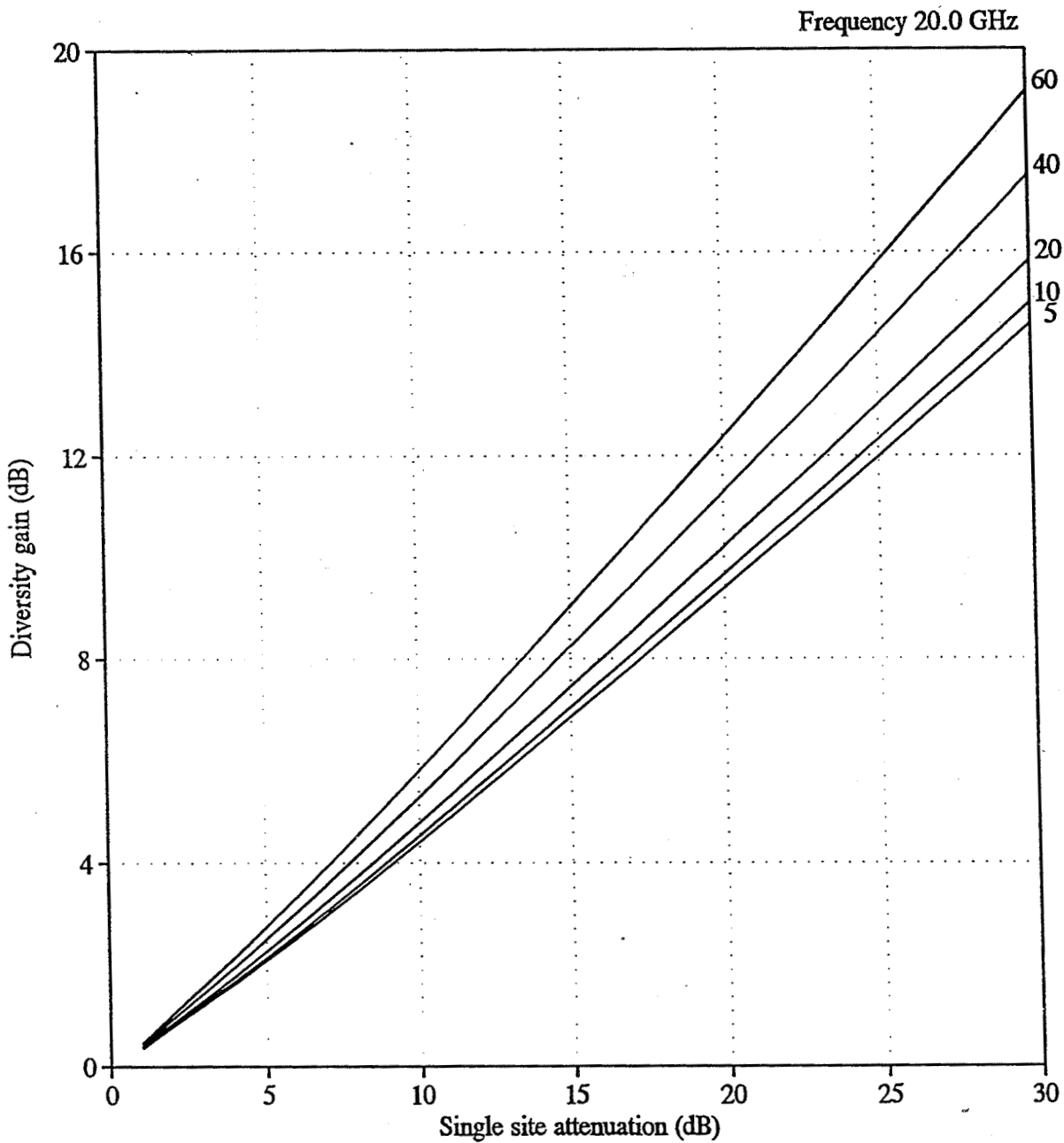


20 GHz Attenuation

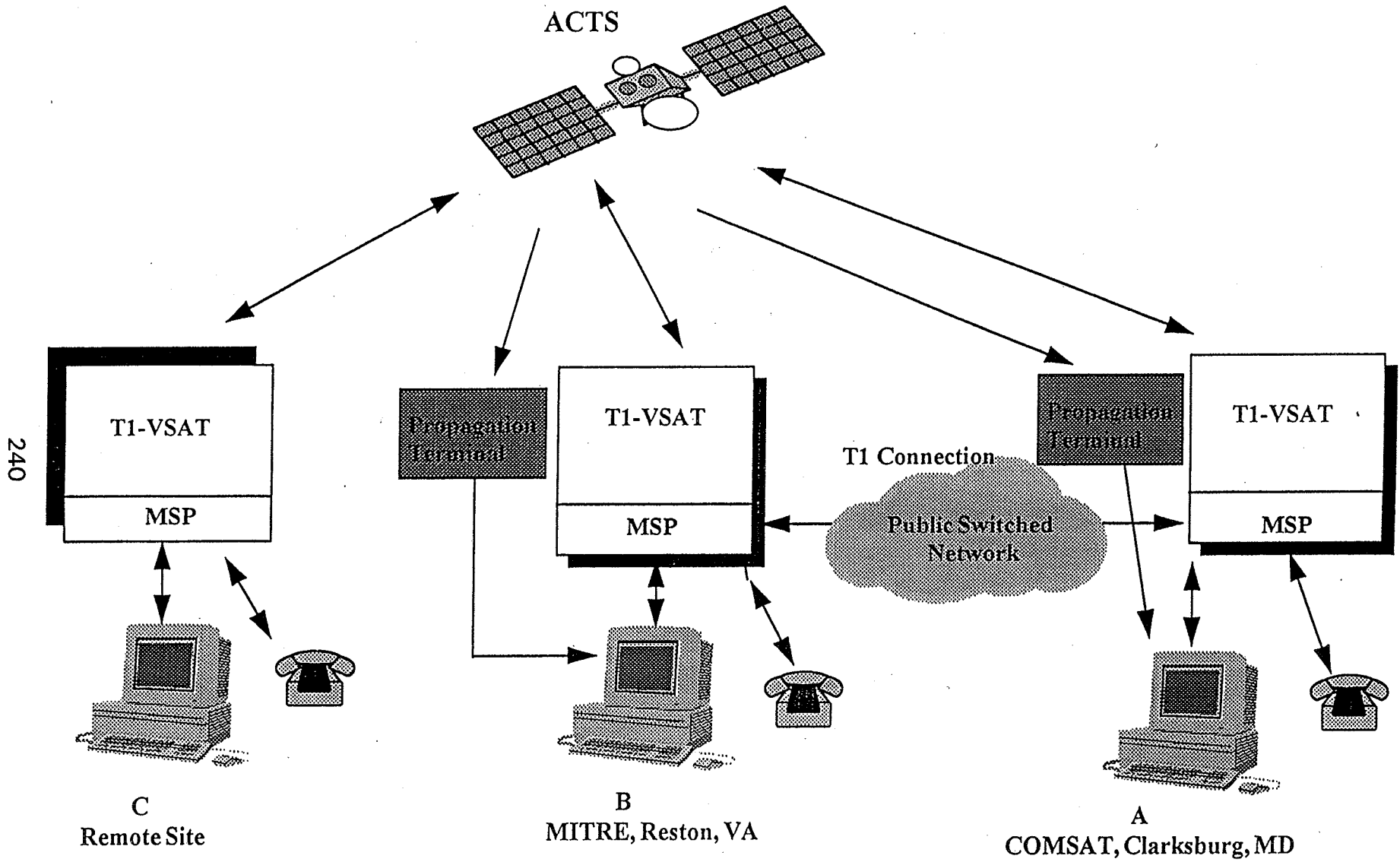




*Diversity gain predictions for Clarksburg, MD.
 Elevation angle: 40° Baseline orientation 45.0°
 Site separations: 5, 10, 20, 40, 60 km*



Diversity gain predictions for Clarksburg, MD.
Site separation 40.0 km; Baseline orientation 45.0°
Elevation angles: 5°, 10°, 20°, 40°, and 60°



Wide-area Diversity Experiment Configuration

NAPEX XX

SESSION 2

PROPAGATION STUDIES FOR MOBILE AND
PERSONAL SATELLITE APPLICATIONS

R. Bauer (LeRC)

Page intentionally left blank

IMAGE ANALYSIS AS A TOOL FOR SATELLITE-EARTH PROPAGATION STUDIES

Riza Akturan, Hsin-Piao Lin and Wolfhard J Vogel
Electrical Engineering Research Laboratory
The University of Texas at Austin
Austin, TX, 78758

Abstract

We present a progress report on a useful new method to assess propagation problems for outdoors mobile Earth-satellite paths. The method, Photogrammetric Satellite Service Prediction (PSSP), is based on the determination of Land Mobile Satellite Systems (LMSS) service attributes at the locations of static or mobile LMSS service users by evaluating fisheye images of their environment. This paper gives an overview of the new method and its products.

Introduction

All personal satellite communications systems (S-PCS), whether targeted for vehicular or personal use and whether operating at UHF, L-, S-Band or higher frequencies [19, 20, 21], are ultimately performance limited by one of three basic propagation states [22]. The line-of-sight signal may be (1) clear, (2) shadowed by trees, or (3) blocked by solid objects, i.e. buildings and mountains. Measurement campaigns to establish a propagation database for system simulation and performance prediction using real or simulated satellite transmissions are very time-consuming and expensive. Thus, a more cost-effective method of determining the probability of the three transmission states is needed.

Previous field measurements [1, 22, 23] have demonstrated a statistical link between fading and the three-state description of signal propagation. This research [2, 4] expands on that viewpoint with measurements with a system that evaluates full images of the upper hemisphere and determines where the sky is clear, where it is shadowed by vegetation, and where it is blocked as illustrated in Figure 1. Assuming that enough images are acquired in a specific environment, one can develop statistics for the three fade states as a function of elevation and azimuth angles [3, 5, 6] and these can be combined with state-dependent propagation data to produce realistic simulated data or fade statistics [9].

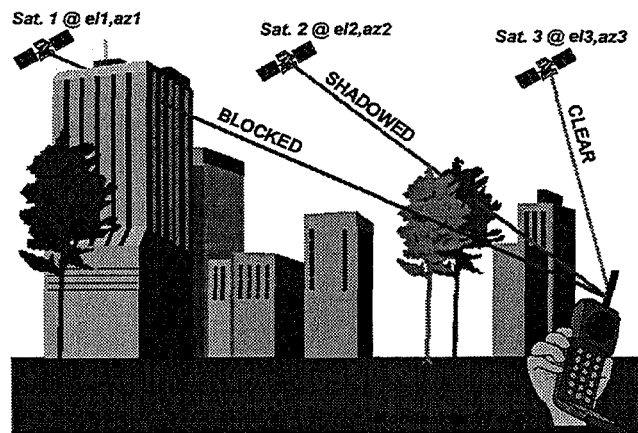


Figure 1. LMSS communication channel illustration.

There are a number of reasons why this method works: (1) Propagation effects for S-PCS are imposed by the physical environment within a short range from a mobile user terminal. (2) The propagation paths are elevated and thus permit visual inspection along their near-terminal extent from the mobile's location. (3) The statistical properties of the received signal levels can be described by a few, physically reasonable distributions which are a function of the fade state. (4) Suitable parameters for the distributions at frequency bands of interest have already been determined by many measurement campaigns.

Hence, provided that the propagation parameters are known for an LMSS service environment, a generalized description of signal propagation is possible when conditioned on path states, and the path states can be readily obtained from optical measurements. This idea permits the cost-effective prediction of service availability in a specific area without the need for new RF measurements [9]. The method is especially effective in (1) predicting fading

probability as a function of elevation angle, (2) path (a.k.a. satellite) diversity gain, or (3) good-call durations for a specific constellation at a given latitude, all in a chosen environment.

In photogrammetric analysis, still and video images of the sky are taken through a fish-eye lens with a 180° field-of-view. Efficient image processing algorithms implement a three-state classification of the fisheye lens images. Using the products of image processing, two- and three-state environment statistics are derived by determining the skyline and three-state fractions in the classified images. This image data is applied to derive the elevation angle dependence of fading in LMSS channels. In addition, by placing satellite constellations on the images, time series of fading and Markov models of the communications channels are generated. From the time series, first order fade statistics are derived, and Markov models of the communication channel are prepared. Again, for the first time, an efficient procedure to derive satellite diversity gain and good-call durations by photogrammetry is introduced. In this text, satellite diversity gain is estimated extensively in urban, suburban and rural environments at different latitudes for different diversity operations. This derivation is performed for a diversity system that is able to operate a k-fold satellite signal combining scheme. Resulting time series of the diversity and non-diversity operations are also used in good-call duration calculations. In the following, this method and its products are presented in a logical order.

Still and Video Image Processing

Our imaging system includes a fisheye lens, a HI-8 camcorder, a 35-mm still camera, a GPS receiver, a scanner, a video frame grabber, and VCR/TV units. Images are either 35-mm stills or 30 frame/second HI-8 videos of the sky taken with a camera through a fisheye lens having a 180° field-of-view, as shown in Figure 2A. Images are digitized and stored on a large capacity medium, typically a CD-ROM. In order to examine propagation characteristics of different environments, pictures are taken in urban, suburban or rural locations. Fisheye pictures are taken at the street-side of the sidewalks in the densely built areas and are taken on the roadsides in rural areas. Sampled locations include the USA, Canada and Japan.

The image processing system includes three steps [7, 8]. They are pre-processing, state separation and state analyzing. Image processing starts with pre-processing of the digitized fisheye images. This involves two steps, north direction adjusting and unwrapping. When taking images, a GPS receiver is used to record the mobile vehicle's heading direction in a log. In processing, the fisheye images are rotated, using the log file, by the azimuth angle from north so that north always stay on the top. Later, image processing continues by unwrapping the images. Unwrapping, as shown in Figure 2B, converts from a circular image in which the zenith is at the center to a rectangular coordinate system in which the zenith is at the top of the frame.

Next, still images are statistically analyzed using their selected spatial features [7]. The image processing system extracts vegetation and blockage features using search windows in the images and evaluates these features to perform the three-state classification in the regions defined by the corresponding search windows. To classify images, initially all image pixels are assumed as clear sky. When the total score of a search window feature density exceeds a threshold value, a state transition occurs; otherwise the pixel stays in the same state. This way, three-state images are obtained based on clear to blocked (Figure 2C) to shadowed (Figure 2D) sky transitions. Lastly, small objects are removed by erosion and dilation. To test the still image analysis algorithm, three-state fractions in urban Japan are measured using automatically and manually classified images. The ratios of clear, shadowed, and blocked sky are found as 58.7%, 4.4%, and 36.9%, respectively. Remarkably, the photogrammetric measurement results of the urban Japan images matched with field signal strength measurements [23]. As an error analysis, automatically classified images are compared with those classified manually using a paint program and mouse. The difference is assumed as the error measure of the image processing algorithm. The largest, 23%, and the lowest, 5%, state recognition errors arose in the urban and rural environments, respectively.

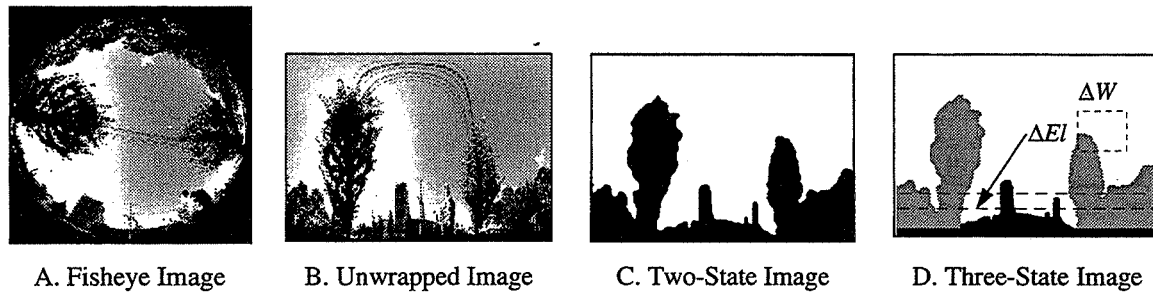


Figure 2. Still image analysis steps

Similarly, our video image processing technique [8] uses the RGB color palette as an object classification set to differentiate the image pixels into one of three state types. Since the algorithm uses spatial image features in classification and only processes images that have changed since the last scene, the processing speed is vastly accelerated [8]. First, fisheye video images are unwrapped, as explained previously. Second, key frames are extracted and third, using these key frames, fisheye videos are processed.

The implementation of the video image analysis procedure shows 80% clear, 14% shadowed and 4% blocked sky in a rural Los Angeles area. Processing errors are 7%, 5%, 4% in urban, suburban and rural Los Angeles environments, respectively. Figures 3A to 3B show the video image analysis steps, sample and processed fisheye images. In this image set, the gray regions correspond to the shadowing objects; the white regions correspond to the open sky. This specific image sequence does not contain blockage objects.

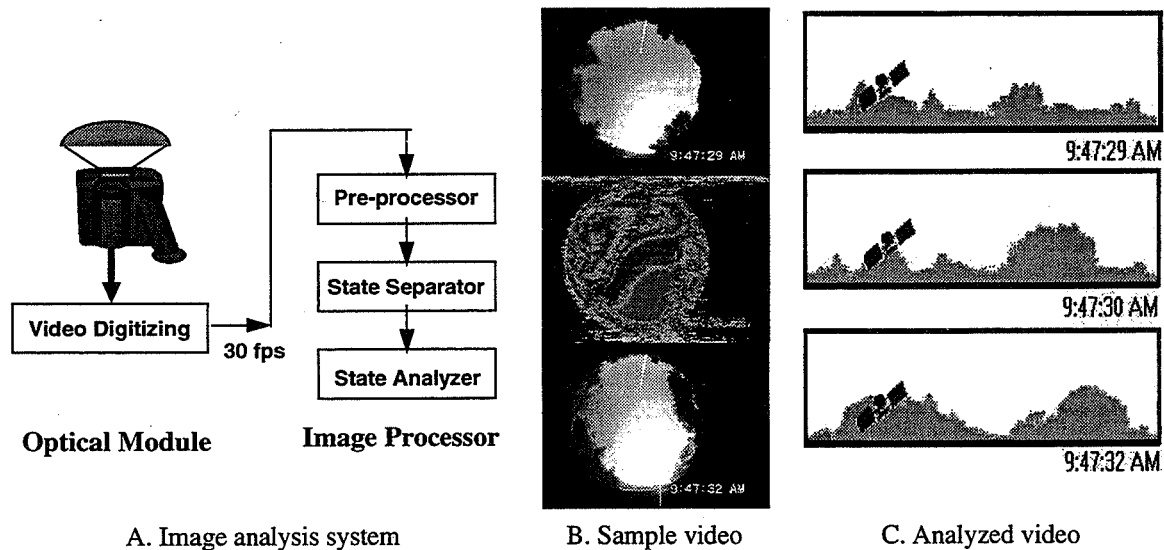


Figure 3. Video image analysis steps

The programming and implementation have been done in C and C++ under a PC-Windows environment on a PC-586-90 platform. The effort has been directed towards developing reliable algorithms as well as minimizing processing speed [4]. An average video image analysis takes less than 5 s/image. Since the required size of the image data to be stored is large compared to the size of available disk space, a lossless 4:1 compression scheme is developed and the compressed images are stored in a binary file [4].

In the fade state analysis, classified three-state images are read from the environment fade state tables as a function of azimuth and elevation. Classified three-state image resolution is 360x90 pixels, which presents a 1°x1° resolution in mapping the environment.

Environment Quantification Using Two-State Model: Skyline Statistics

In this section, results of two-state image processing are presented. The fisheye images of four rural, suburban, and urban Texas locations are analyzed to derive quantitative information about the elevation

angles at which the sky becomes visible, i.e., the skyline [3, 6]. The mean skyline angle for an urban Austin image, Figure 4A, is shown in Figure 4B and the average histogram of skyline elevation angles shown in Figure 4C. Environment average skyline elevation angles in Austin's rural, suburban and urban areas are 5°, 7°, and 26°, respectively. In the three environments, the 90th percentile of the skyline was found to be at 11°, 17°, and near 55°, respectively.

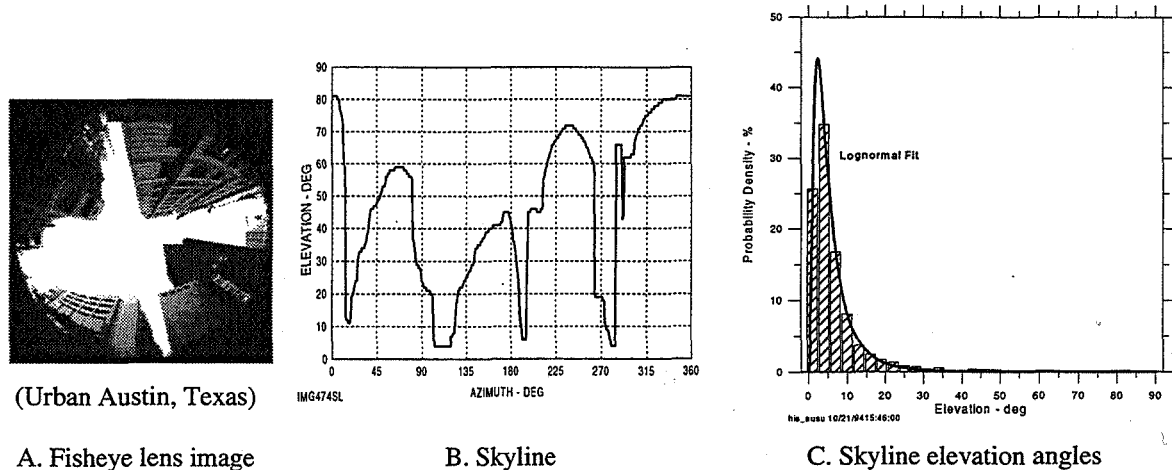


Figure 4. Fisheye image of an urban Austin location, its skyline and skyline histogram

Above 10° elevation, on average 98% of the sky is visible in rural, 95% in suburban, 77% in urban Austin, and 68% in urban San Antonio as shown in Figure 5A. The potential of satellite diversity to mitigate tree-shadowing or blockage depends on the variability and structure of the skyline with azimuth at any particular location and on the satellite constellation. The 10th percentile, mean, and 90th percentile of the skyline autocorrelation in all three environments decreases to 1/e with a lag of about 15°, 30°, and 55°, respectively. The skyline autocorrelations in Figure 5B have a similar shape in all environments. The autocorrelations cross zero near 70° azimuth lag. The median autocorrelation falls to zero near 50°, meaning that for half the locations in urban Austin there is an even chance that at 50° satellite separation the second satellite will be clear if the first one is blocked (or the converse).

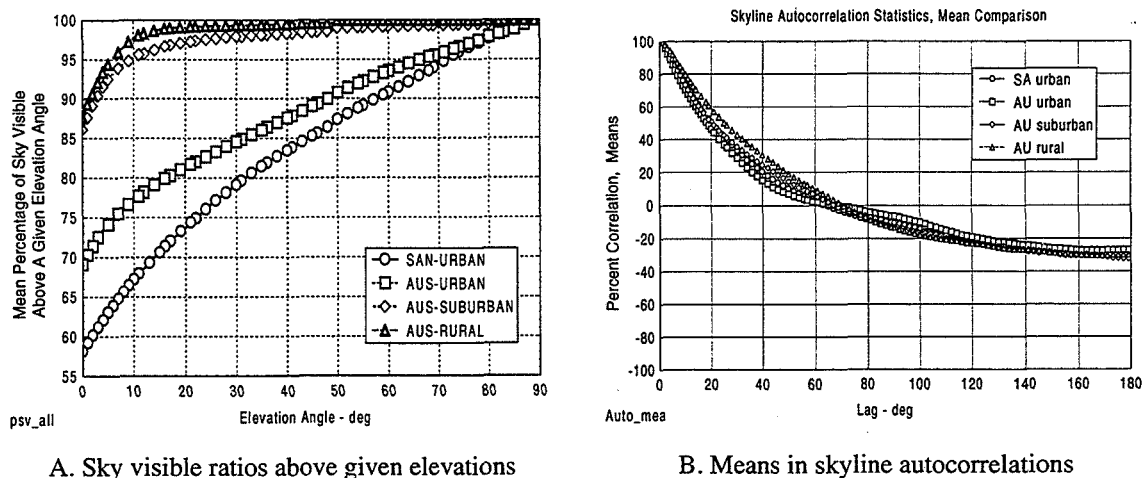


Figure 5. Skyline visibility and autocorrelation statistics

Environment Quantification Using Three-State Model

Until now, environments have been defined verbally such as heavily or lightly shadowed. In this section, an environment quantification method is presented. Using ternary descriptions of environments, three-state

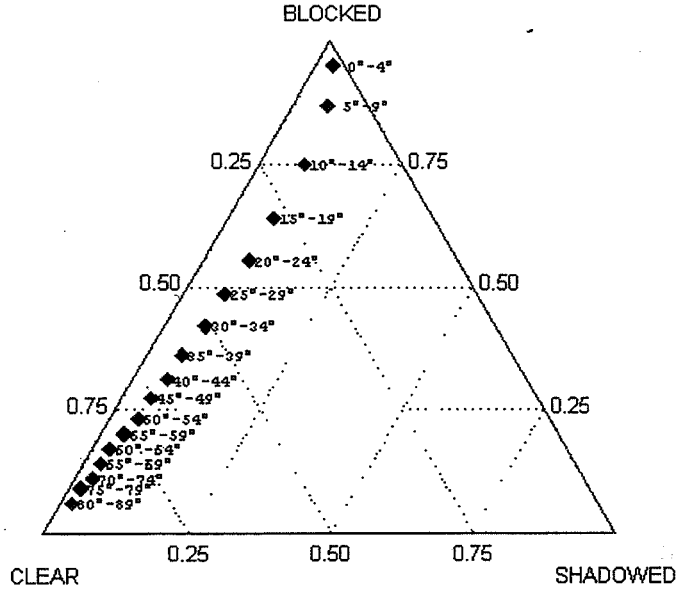


Figure 6. A ternary graph of propagation states in urban Japan as a function of the elevation angle in 5 degree increments.

images, environments were mapped onto environment triangles as illustrated in Figure 6, so that a quantitative ternary description of the environments was obtained [12].

Using the images of urban Japan, the fraction of potential satellite paths with clear, shadowed, or blocked line-of-sight was calculated in 5° elevation angle increments from 0° to 89° [10, 11]. The result has been plotted in Figure 6 in the form of a ternary graph. It is obvious that blockage as opposed to shadowing is of primary importance in the urban environment and that with decreasing elevation less of the sky is clear. For example, in the low-elevation interval from 10° to 14°, 17% of the sky is clear, 8% is shadowed, and 75% is blocked, compared against the higher elevation interval of 60° to 64°, where the state mixture \bar{M} equals (0.8, 0.03, 0.17).

Elevation Angle Dependence of LMSS Fading

Combining each path state derived from images for single or multiple satellites in a specific constellation with frequency-appropriate statistical fade models allows predicting overall performance measures such as fade dependence with elevation angle or path diversity gain [12, 14]. Using the three-state method, for the first time, elevation dependence of fading is derived [10, 11]. In addition, the importance of including specular reflections under urban blockage conditions is established with an urban three-state signal distribution model [12].

Fisheye images of urban Japan were analyzed to derive, as a function of elevation, the fraction of sky that is clear, shadowed by trees, or blocked by buildings. At 32° elevation, the path state vector matches that derived from satellite measurements fit to a 3-state fade model [10]. Using the same model, for the first time the elevation angle dependence of mobile satellite fading is predicted [10, 11]. The dominance of building blockage fading in urban areas is expressed in the terracing of the cumulative distribution. It is found that in the Rayleigh domain, the minimum elevation with 90% coverage decreases by about 5° per dB of additional fade margin [11].

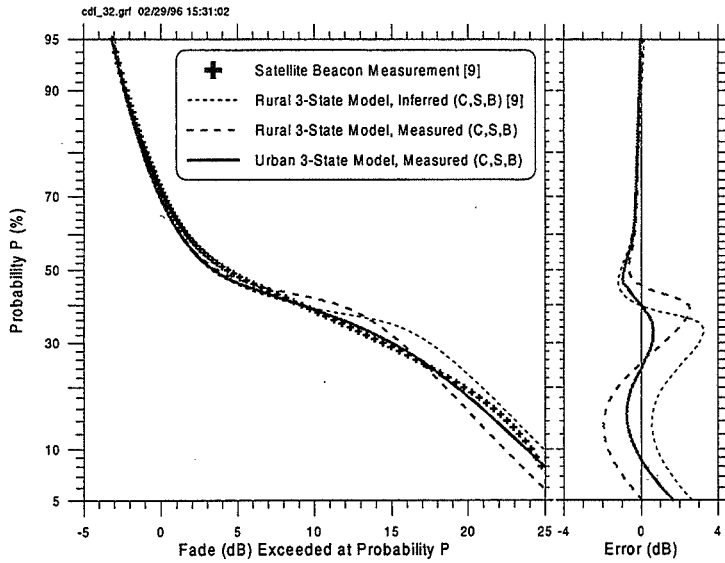
Heuristically, each of the three possible path states of a mobile satellite link can be associated with a distinct fade distribution as expressed in this text. The *clear* state is usually described by a Ricean distribution, which represents the superposition of a line-of-sight (LOS) signal with multipath reflections, but neglects specular effects. The *shadowed* state was modeled by Loo [24] as a combination of a lognormally attenuated line-of-sight signal with Rayleigh distributed diffusely scattered power, and in the *blocked* state only Rayleigh distributed diffusely scattered power is considered.

$$f_v(v) = C \cdot f_{Rice}(v) + S \cdot f_{Loo}(v) + B \cdot f_{Rayleigh}(v) \quad (1)$$

Furthermore, the importance of including specular reflections from nearby illuminated building surfaces under urban blockage conditions is added. This study improved on the model's fit by including potential specular reflections in the blocked state and by refining the distribution parameter estimates. To acknowledge the presence of such specular reflections, the distribution in the urban blocked state was changed from Rayleigh to Loo, resulting in the *urban 3-state model*

$$f_v(v, \alpha) = C(\alpha) \cdot f_{Rice}(v) + S(\alpha) \cdot f_{Loo}(v) + B(\alpha) \cdot f_{Loo}(v) \quad (2)$$

Including specular reflections in the blocked state reduces the rms modeling error (right) from about 1.3 dB to 0.5 dB as shown in Figure 7.



Fade CDFs for urban Japan at elevation angles from 7° to 82°, based on photogrammetrically determined path states and the urban 3-state fade probability model, as shown in Figure 8. Photogrammetry permitted the prediction of fading as a function of the path elevation angle, and simple ternary plots are used to estimate non-diversity fading as a function of the path state vector. In urban Japan, it is found that the required fade margin decreases by about 0.2 dB/degree, from 25.5 dB to 15 dB at the 10% probability level and in the elevation range from 12° to 67° [13, 14].

Figure 7. Comparison of a CDF measured in urban Japan at 32° elevation with three 3-state models.

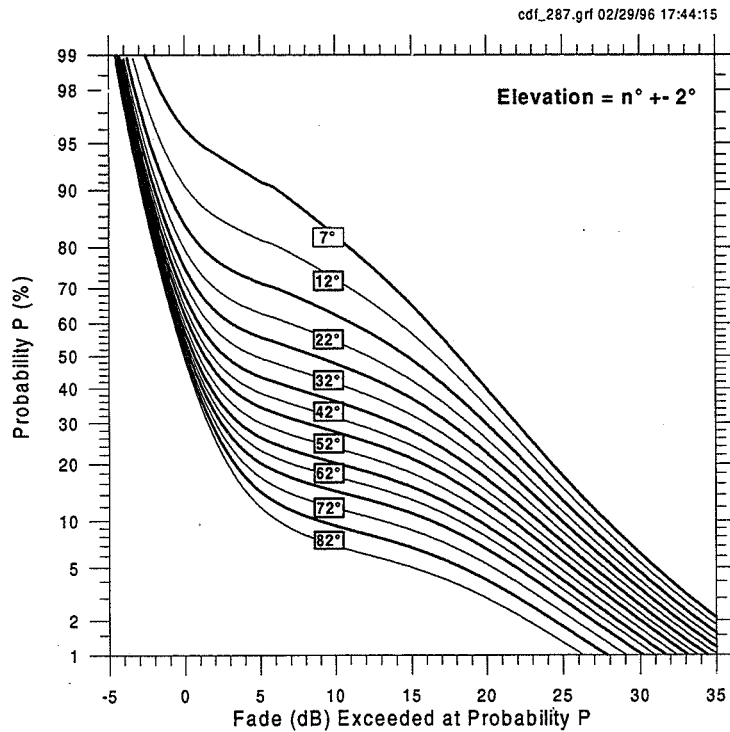
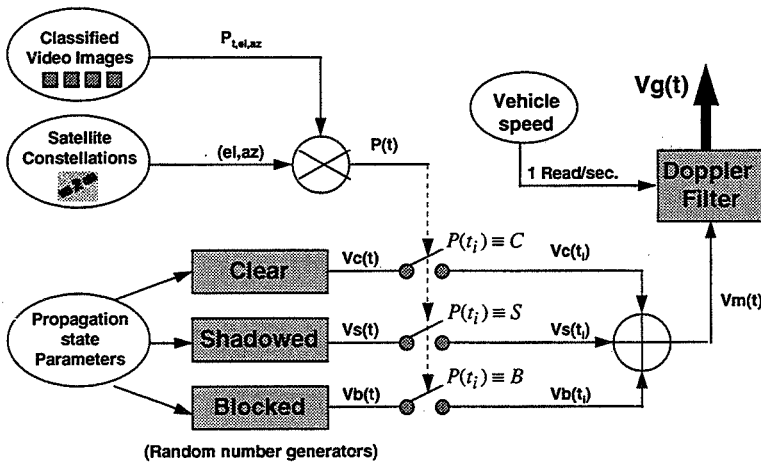


Figure 8. Fade CDFs for urban Japan

Received Signal Generation

The system presented in this section substitutes video image processing for propagation measurements and permits flexible fade simulation of Land Mobile Satellite Communication systems [15]. The video image processing system is used to track the propagation states of the satellites in selected environments. The path state tracking is then applied to generate a satellite to mobile unit path state sequence as a time series. Analyzing sequences of images resulted in a propagation state time series which is input to a channel simulator as shown in Figure 9. By assuming that the channel attributes are quasi-static in each propagation state [22], the statistical models are represented by Rayleigh for urban, Loo's for shadowed and Ricean for open direct LMSC paths. Using these state-specific propagation statistics, a time series of the received signal envelope is generated from the time series of the produced state sequences. The simulated signal time series are subsequently used to derive the first order propagation statistics of the communication channel [15].



In simulation, a one-minute section of a video clip taken in suburban Pasadena is processed. A comparison of the fade series obtained by simulation and by measuring 2055 MHz cw transmissions from a TDRS satellite at 21° elevation and 249° azimuth in Pasadena, CA is shown in Figure 10, right graph. The rms difference between the two PDFs is 0.11. This close match shows the effectiveness of the photogrammetric procedure.

Figure 9. Received signal generation procedure

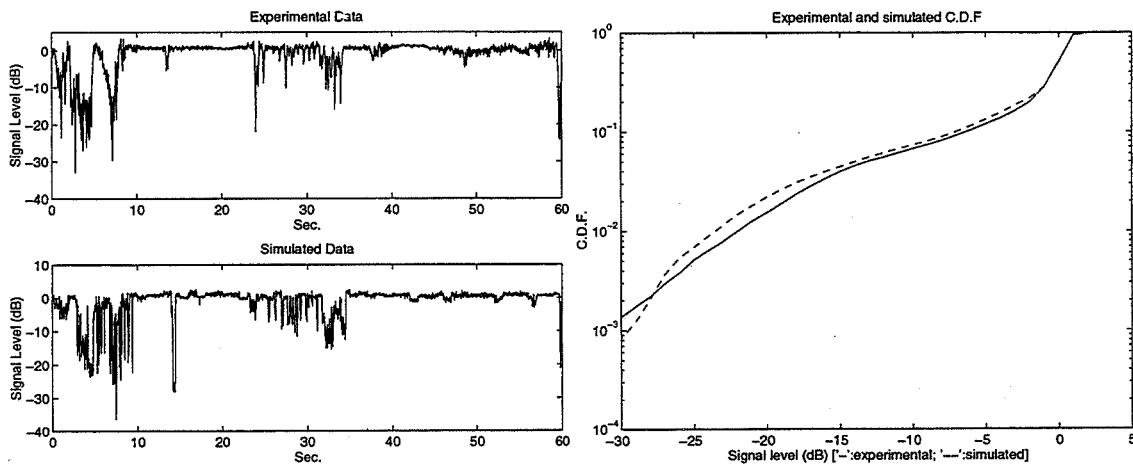


Figure 10. One minute time series of the measured and simulated signals and C.D.F. of one minute data

In a typical LMS scenario, while the mobile unit is in motion, the field strength of the received signal level changes with respect to the time and space according to the changing morphology of the environment. It has been shown [25] that the switching between different attenuation levels can be represented as a Markov stochastic process using the assumption that the channel properties are quasi-stationary in small time periods. Based on this propagation modeling method, our image processing and propagation channel simulation algorithms are employed to obtain a statistical representation of the communication channel [4]. The video image processing system is capable of tracking the propagation state of the path to any satellite in the selected environment, generating a satellite to MES path state sequence time series. Using random

number generators and the state sequences as shown in Figure 11, the received signal levels are predicted based on the state transition probabilities represented by Markov chains [16, 17, 18].

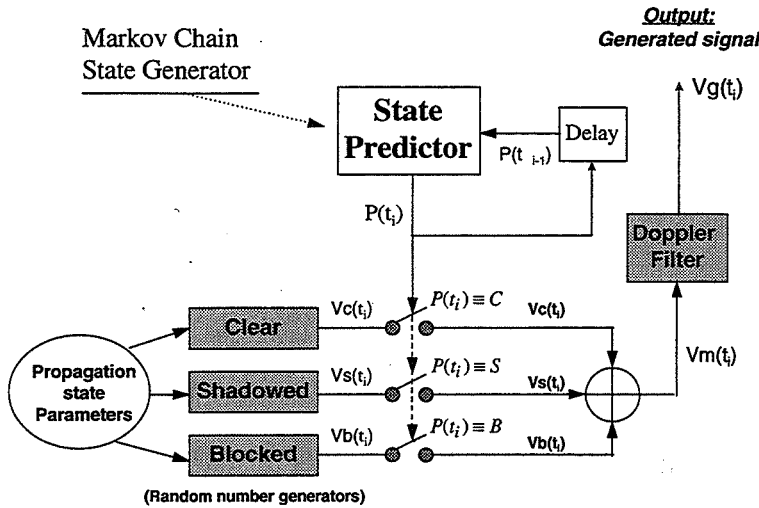


Figure 11. Signal generation using Markov chains

The simulation procedure was applied to the above two-minute section of simultaneous satellite fade data and video clip taken in suburban Pasadena, CA. Using the previously described procedures, the path state sequences, transition matrices and modeling parameters were found in the selected environments for thresholds $T_1 = -2.5\text{dB}$ and $T_2 = -20\text{dB}$.

Comparisons of the simulated fade time series with measured data are shown in Figure 12. Because these time series are generated using the Markov method with state and transition probabilities derived from the entire two minutes of

data, there is no one-to-one correspondence with the measurements.

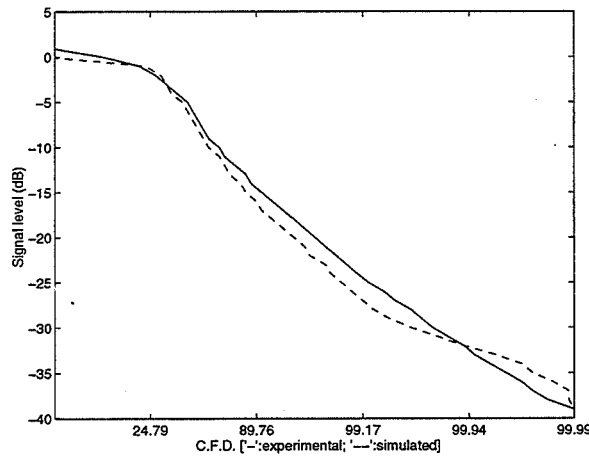


Figure 12. CDF of the suburban Pasadena data

The signal level first and second order statistics, i.e., the cumulative fade distribution (CDF) and level crossing rate (LCR) agree, however. The rms normalized difference between measured and simulated cumulative level probabilities is 2.5% and the rms normalized LCR error in Hz is 3.7 for wooded Pasadena. The best match of the CDFs is obtained in the suburban environment, where the state transitions occurred with regularity throughout the measurement and at a moderate rate that could easily be followed in the video images. Related state duration and transition Markov matrices are given in Figure 13 with a diagram of the Markov process.

As described, fisheye image sequences are used to generate the received signal levels. A sample of the software is shown in Figure 14 to illustrate this process [4]. A Windows-based program processes the fisheye images and extracts states. Then, using the statistical signal distributions in respective states, signal levels are generated as a function of time.

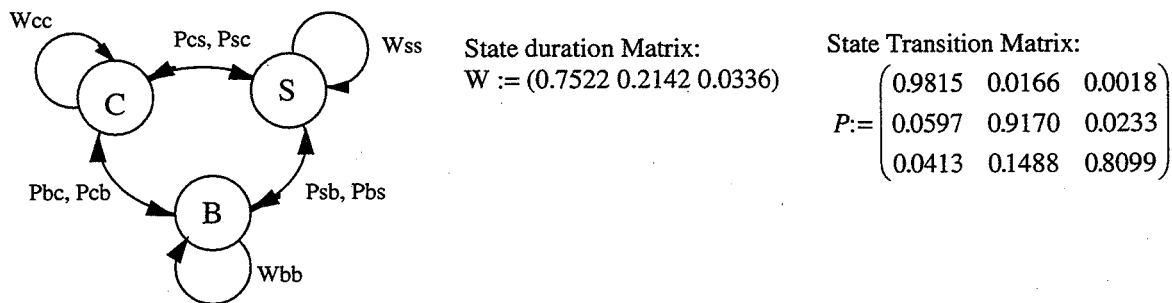


Figure 13. State durations and transitions in suburban Pasadena, CA

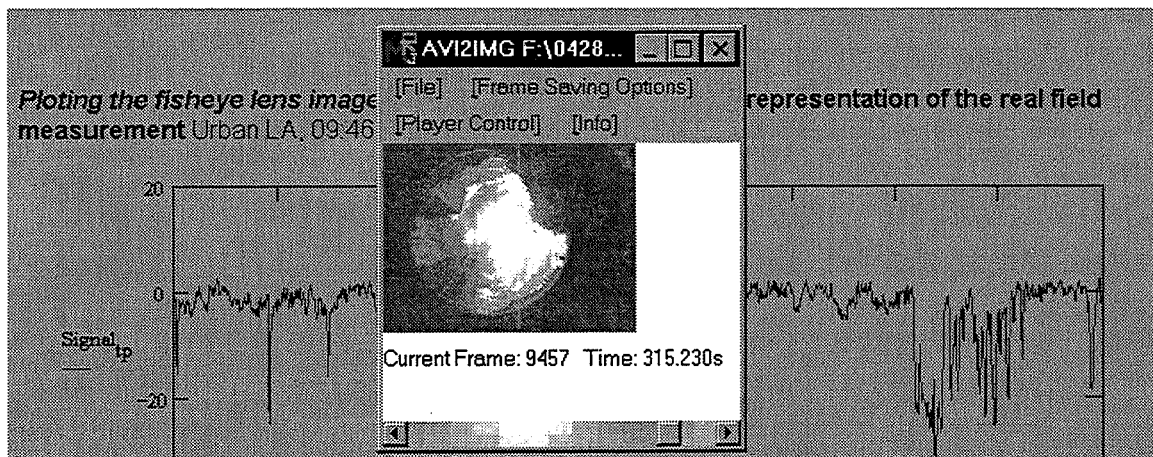


Figure 14. Signal generation software

Satellite Diversity Gain

For the first time [12, 14], diversity gain statistics are estimated for LEO satellite PCS. An image processing procedure to track the visible satellite path states is developed. The diversity gain estimation involves a 4-fold path diversity scheme with k from one to four, where the best k satellites are used in the link [12]. The calculation of k -fold diversity gain involves 4 steps: (a) determining the CDFs according to coherent combining: $v = v_1 + v_2 + \dots + v_k$ and switching combining: $v = \max(v_1, v_2, \dots, v_k)$, (b) placing the satellite constellation into the 3-state images and determining the probability of occurrence for each state combination, (c) summing all CDFs from step (a) weighted by the probabilities of step (b), and (d) subtracting the resulting CDF from the CDF of the highest satellite at the same city at probabilities from 1% to 99%.

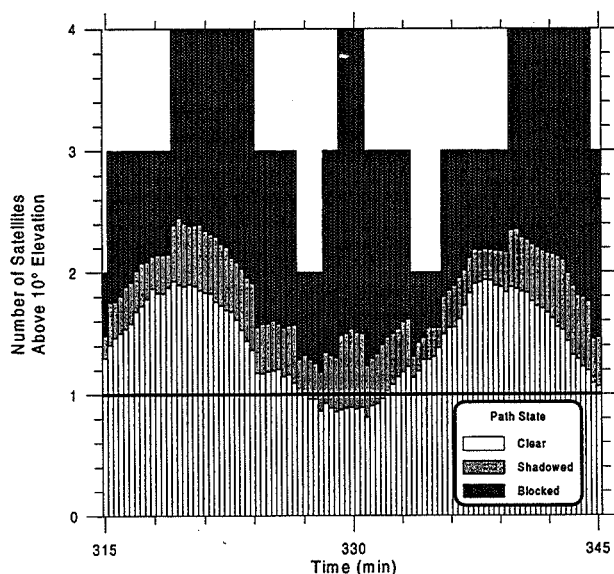


Figure 15. The image-average number of satellites

Stacked bar graphs for 30 minutes of the image-averaged number of satellites visible with (from bottom to top) *clear*, *shadowed*, and *blocked* path states are depicted in Figure 15 for a Globalstar-like constellation, 48 satellites on 8 planes, in Tokyo. The number of *clear* satellites varies periodically between <1 and <2 and most of the time three or four satellites are available. The minimum elevation angle was 10° .

By employing this procedure, satellite diversity gain of any satellite communication system is estimated without actually using any satellites. Measurements have shown that satellite diversity increases availability of the communication channel by introducing more satellites in clear paths. However, satellite diversity gain greatly depends on the constellation's orbiting characteristics. Path diversity gain for combining and hand-off diversity is found for up to 4-fold diversity at a high-, mid- and low-latitude

location for the sample constellation. With 2-fold or higher order diversity, it is near 10 dB and 6 dB at probabilities below 20% when using two or more satellites in the non-equatorial and equatorial locations, respectively.

Figure 16 shows coherent combining path diversity for the Globalstar-like constellation in Tokyo that reduces fading relative to using the highest satellite. Fading at 10% probability, for instance, can be reduced from above 20 dB to below 10 dB by combining signals from as many as four satellites.

Figure 17 shows a comparison of path diversity gain achieved by combining (thick lines) and hand-off (thin lines) diversity with up to four satellites of the Globalstar constellation in Tokyo. Gains for both methods are equal when using the best satellite, but with more satellites combining diversity achieves greater gain.

Figure 18 shows a service comparison between the four environments for the service coverage of 98%, 95%, 90% by receiving signal from only the highest satellite or the two best satellites using hand-off diversity. Using this setup, at 95% coverage, the improvement obtained by using the two best satellites instead of the highest is 9 dB, 9 dB, 6 dB and 3 dB in urban Austin, urban San Antonio, suburban Austin and rural Austin. The two urban environments show similar fade characteristics. As it can be seen clearly, non-diversity fading in a suburban environment is lower than diversity fading in an urban environment. This shows that satellite diversity is mostly valuable in urban environments although it decreases fading in suburban and rural environments. The path diversity gain in mid- and low- probabilities are almost half of the diversity gain in urban Austin.

As a result of the photogrammetric method, it is observed that satellite diversity is useful in providing an adequate link margin [4]. It increases availability of the communication channel and lowers the need for high satellite elevation angles. Diversity gain strongly depends on the constellation's orbit parameters. Large azimuth separations between the visible satellites and a high standard deviation in the average elevations of the visible satellites result in a high diversity gain, recalled from above. Diversity gain is high in heavily shadowed or blocked environments. According to the environment dependence plots [4], a

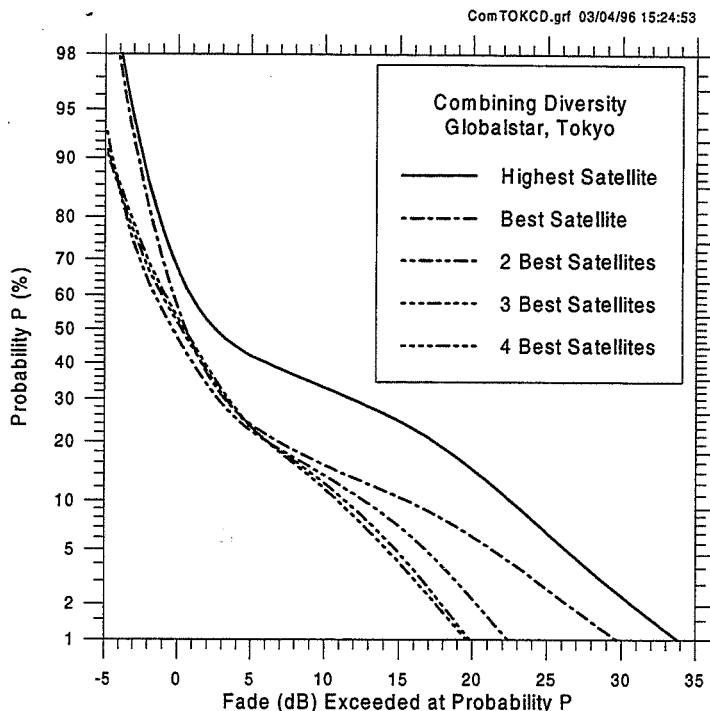


Figure 16. Coherent combining path diversity

the improvement obtained by using the two best satellites instead of the highest is 9 dB, 9 dB, 6 dB and 3 dB in urban Austin, urban San Antonio, suburban Austin and rural Austin. The two urban environments show similar fade characteristics. As it can be seen clearly, non-diversity fading in a suburban environment is lower than diversity fading in an urban environment. This shows that satellite diversity is mostly valuable in urban environments although it decreases fading in suburban and rural environments. The path diversity gain in mid- and low- probabilities are almost half of the diversity gain in urban Austin.

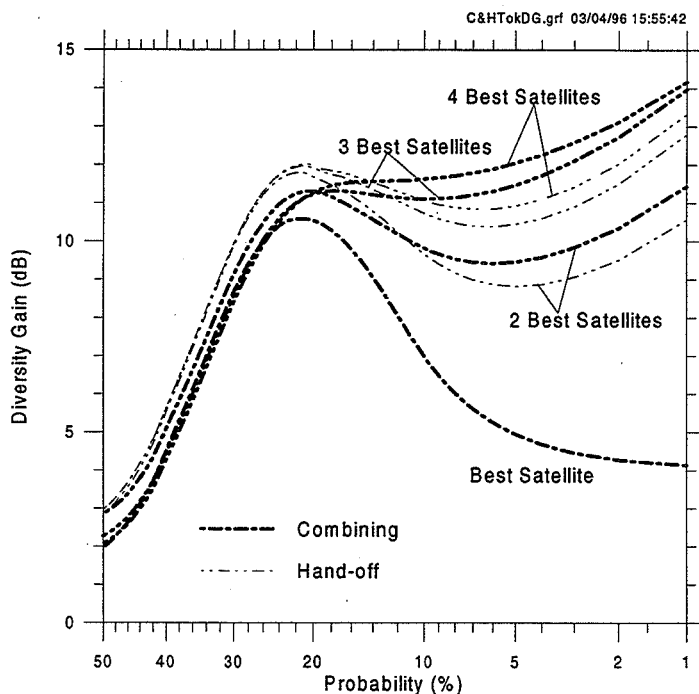


Figure 17 Comparison of combining and hand-off diversity

3 dB/environment gain increase is estimated from the combining diversity gain values that are 10 dB, 7 dB and 4 dB in urban, suburban and rural Austin, respectively.

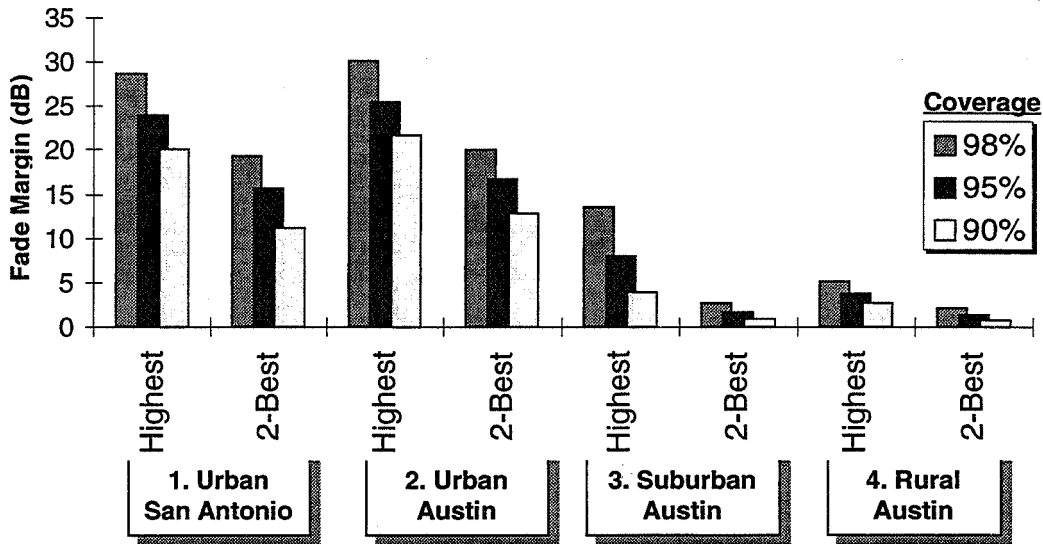


Figure 18 Comparison of path diversity gain using combining diversity with four satellites in Austin, TX.

Communication Channel Stability: Good Call Durations

Similar to [26], a good-call duration analyzer is derived from the diversity analysis procedure [4]. The procedure places the satellite constellations on the classified images [12]. Later, for each time sample, the best satellite and the highest satellites are chosen, and their states are determined as a function of time. The states for these two satellites are written into a state-log file. One log file for the best satellite (non-diversity operation) and one log file for the highest satellite (diversity operation). Then, using a math package, state durations are examined.

A good state or channel occurs when the line of sight (LOS) signal can be transmitted for the duration of the call. Conversely,

a bad state or channel occurs when the LOS signal can not be transmitted for 18 sec. A bad state causes interruption in signal transmission, and the current call is dropped.

To implement this method, it is assumed that the good state occurs when the LOS is clear, when there are no obstructions in the direct path from a mobile or fixed user to the satellite. Therefore, the clear state durations are tracked and call-completion success is

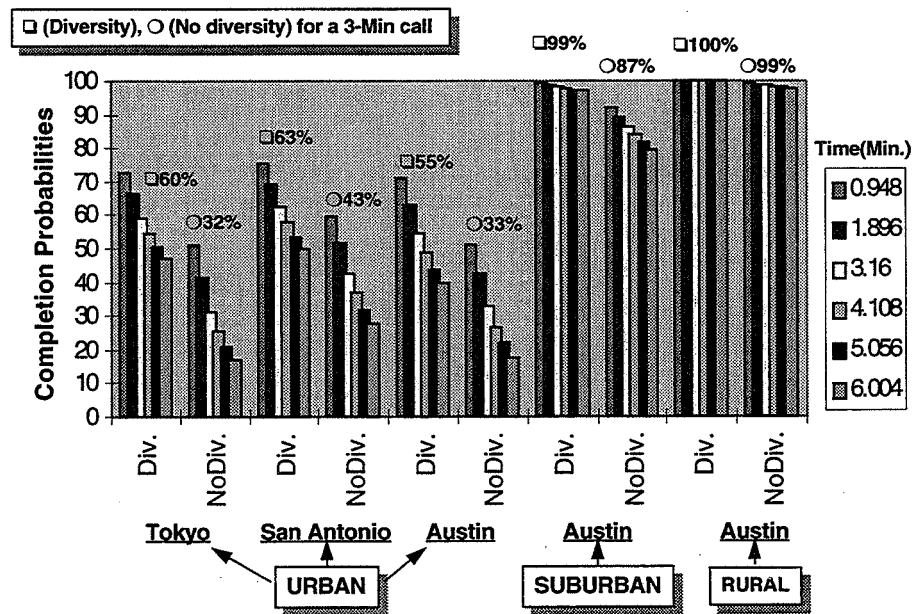


Figure 19. Good-call durations in different environments

calculated using the above procedure. The results are derived using a Globalstar-like constellation without considering specific system parameters and implementations.

As Figure 19 suggests, 60% and 35% of the three-minute calls are successfully completed without an 18 sec channel interruption using diversity and non-diversity operations, respectively, in the three urban environments. These numbers go up to 99% and 100% in suburban and rural environments, respectively, with diversity operation. The rural environment without diversity supports a call completion probability of around 99%, whereas in the suburban environment without diversity operation it drops 12% down to 87%.

Conclusion

As a result of this work, derivation of a ternary description for clear, shadowed and blocked path states allowed one to combine satellite orbit design with propagation statistics to predict performance such as fade probability or diversity gain in a specified environment. Photogrammetry is a new tool with which one can derive service predictions for personal and mobile satellite communications systems in any environment. It is inexpensive and simple compared to other techniques. The data collection process does not require receiving a signal from a satellite or other platform, and results can be applied to any frequency band for which statistical fade parameters are available. The products of photogrammetric satellite service prediction should be of immediate use to satellite system designers. The method opens new capabilities of propagation prediction for Land Mobile Satellite Communication Systems. A milestone table is given in Figure 20.

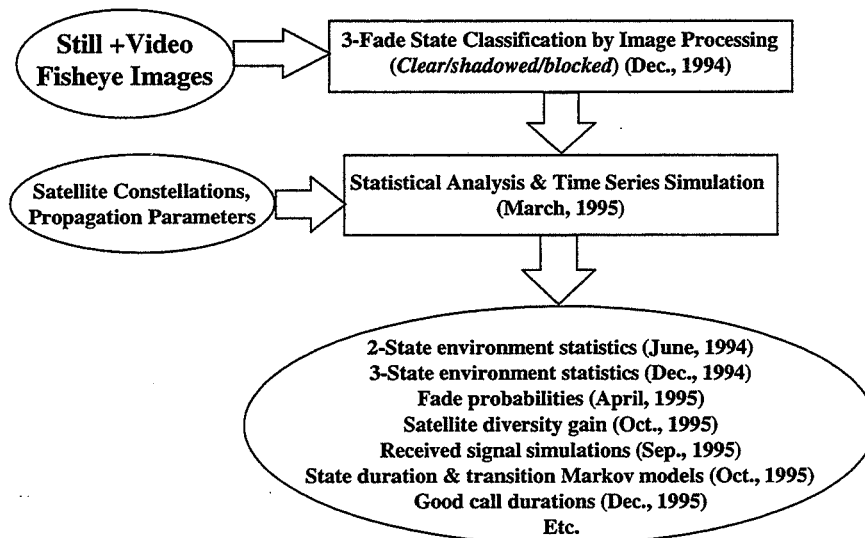


Figure 20. Photogrammetric measurement system architecture with the completion times of its steps.

Bibliography

- [1] Birdwell, B., "Design of an optical sensor system to replicate the effects of signal blockage and shadowing on satellite signal propagation," M.S. Thesis, The University of Texas-Austin, Austin, Texas, May 1993.
- [2] Akturan, R. and Vogel, W.J., "Photogrammetric Mobile Satellite Service Prediction," *Proc. of the Eighteenth NASA Propagation Experiments Meeting, NAPEX XVIII*, Vancouver, BC Canada, June 16-17, 1994.
- [3] Akturan, R. and Vogel, W.J., "Photogrammetric Mobile Satellite Service Prediction," *Project Report, Submitted to Jet Propulsion Laboratory of NASA*, Pasadena, CA, Nov. 1, 1994.
- [4] Akturan, R., "Photogrammetric Mobile Satellite Service Prediction," Ph.D. *Dissertation proposal, Submitted to the Graduate School of the University of Texas-Austin*, Nov. 17, 1994.
- [5] Akturan, R. and Vogel, W.J., "Photogrammetric Mobile Satellite Service Prediction," *National Academy of Sciences and Engineering Meeting, URSI'95*, Boulder, CO, Jan. 3, 1995, p 210.

- [6] Akturan, R. and Vogel, W.J., "Photogrammetric Mobile Satellite Service Prediction," *Electronic Letters*, Feb. 2, 1995, vol. 31, No. 3, p 165.
- [7] Akturan, R. and Vogel, W.J., "Classification of Attenuation Sources In Satellite PCS Using Image Processing," *Proceedings of the Signal and Image Processing Conference*, Las Vegas, NV, Nov 20, 1995.
- [8] Akturan, R., Hudson, F. and Vogel, W.J., "A Fast Video Image Processing Technique For Tracking Attenuating Objects In Satellite Communication Paths," *Proceedings of the Second Joint Conference on Information Sciences*, Wrightsville, NC, Sep.28, 1995.
- [9] Akturan, R., Lin, H.P. and Vogel, W.J., "Elevation Angle Dependence of Fading for Satellite PCS in Urban, Suburban and Rural Environments," *National Academy of Sciences and Engineering Meeting*, Boulder, CO., Jan. 9, 1996.
- [10] Akturan, R. and Vogel, W.J., "Elevation Angle Dependency of Fading for Satellite PCS in an Urban Area," *Electronic Letters*, July 1995, vol. 31, No. 14, pp. 1125-1127.
- [11] Akturan, R. and Vogel, W.J., "Optically Derived Elevation Angle Dependence of Fading For Satellite PCS," *Proc. of the 19th NASA Propagation Experiments Meeting, NAPEX XIX*, Fort Collins, CO, June 14, 1995.
- [12] Akturan, R. and Vogel, W.J., "Path Diversity for LEO Satellite-PCS in the Urban Environment," *Project Report, Submitted to Jet Propulsion Laboratory of NASA*, Pasadena, CA, Dec. 13, 1995.
- [13] Akturan, R. and Vogel, W.J., "A Method to Derive Satellite Diversity," *National Academy of Sciences and Engineering Meeting, URSI'96*, Boulder, CO, Jan. 9, 1996.
- [14] Akturan, R. and Vogel, W.J., "Path Diversity for LEO Satellite-PCS in the Urban Environments" *Submitted to IEEE Trans. on Antennas and Propagation*.
- [15] Akturan, R., Lin, H.P. and Vogel, W.J., "Propagation Modeling In Land Mobile Satellite Sytems Using Photogrammetry," *Proc. of the IEEE Vehicular Technology Conference '96*, Atlanta, GA, April 28, 1996.
- [16] Lin, H.P., Akturan, R. and Vogel, W.J., "Propagation Channel Simulation for LMSS and Satellite PCS," *National Academy of Sciences and Engineering Meeting, URSI'96*, Boulder, CO, Jan. 9, 1996.
- [17] Lin, H.P., Akturan, R. and Vogel, W.J., "Photogrammetric Satellite PCS Channel Modeling Using Markov Chain Approach," *Proc. of the International Conference on Communications'96*, Dallas, TX, June 23, 1996.
- [18] Lin, H.P., Akturan, R. and Vogel, W.J., "Satellite-PCS Channel Simulation in Mobile User Environments Using Photogrammetry and Markov Chains," *Submitted to Special Selected Papers Issue in Communications, ACM/Baltzer Wireless Information Networks (WINET)*.
- [19] Schindall, J., "Concept and Implementation of the Globalstar Mobile Satellite System", *Proceedings of the Fourth International Mobile Satellite Conference*, Ottawa, Canada, June 6-8, 1995.
- [20] Tadano, H., "IRIDIUM- a Lockheed Transition to Commercial Space", *Proceedings of the Fourth International Mobile Satellite Conference*, Ottawa, Canada, June 6-8, 1995.
- [21] Sturza, M., "Architecture of The Teledesic Satellite System," *Proceedings of the Fourth International Mobile Satellite Conference*, Ottawa, Canada, June 6-8, 1995.
- [22] Goldhirsh, J. and Vogel, W.J., "Propagation Effects for Land Mobile Satellite Systems: Overview of Experimental and Modeling Results," *NASA Reference Publication 1274*, February 1992.
- [23] Karasawa, Y., Minamisono, K. and Matsudo, T., "A Propagation Channel Model For Personal Mobile-Satellite Services," *Proc. 1994 Progress in Electromagnets Research Symp., ESA*, (Noordwijk, The Netherlands). 11-15 July, 1994.
- [24] Loo, C., "A Statistical Model for a Land Mobile Satellite Link," *IEEE Trans. on Vehicular Technology*, vol. 34, no. 3, pp. 122-127, Aug. 1985.
- [25] Vucetic, B., and Du, J., "Channel Modeling and Simulation in Satellite Mobile Communication Systems," *IEEE Journal on Selected Areas In Communications*, Vol. 10, No. 8, Oct. 1992.
- [26] Penwarden, K., "Propagation Model for LEO Satellites," *URSI'96, National Academy of Sciences and Eng. Meeting*, Boulder, CO., Jan. 9, 1996.

Page intentionally left blank

GPS Multipath Fade Measurements to Determine L-Band Ground Reflectivity Properties[†]

Adnan Kavak, Guanghan Xu, W. J. Vogel
Electrical Engineering Research Laboratory
The University of Texas at Austin
10100 Burnet Road
Austin, TX 78758-4497

Abstract - In personal satellite communications, especially when the line-of-sight is clear, ground specular reflected signals along with direct signals are received by low gain, almost omni-directional subscriber antennas. A six-channel, C/A code processing, GPS receiver with an almost omni-directional patch antenna was used to take measurements over three types of ground to characterize 1.575 GHz specular ground reflections and ground dielectric properties. Fade measurements were taken over grass, asphalt, and lake water surfaces by placing the antenna in a vertical position at a fixed height from the ground. Electrical characteristics (conductivity and dielectric constant) of these surfaces (grass, asphalt, lake water) were obtained by matching computer simulations to the experimental results.

1. Introduction

In Earth-space communication links, reflections from land, water and obstacles combine with line-of-sight signals to produce fades that can degrade the performance of the communication link. This situation is especially important when a single strong multipath signal interferes destructively with the direct signal. In digital systems, for instance, severe inter-symbol-interference (ISI) may result, increasing the bit error rate (BER). There are, however, also cases in which a multipath signal can improve signal strength, i.e., interfere constructively. The severity of multipath fading depends on the nature and electrical characteristics of the reflecting surface [1, 2, 3], the path length, and the height and directivity of the receiving antenna.

In telecommunications systems employing low-

directivity antennas, such as in land mobile (LMSS), Global Positioning (GPS), or other wireless systems using Low Earth Orbit (LEO) satellites, reflected signals need to be taken into account. Some measurements to characterize multipath fading at L-Band (1.5 GHz) utilized Inmarsat's geostationary satellites in maritime [4, 5] and LMSS [6, 7] scenarios. These studies were performed at low elevation angles and do not fully characterize LEO constellations [8] which cover both low and high elevation angles. For the hand-held phones to be used in LEO telephone, voice and data services, multipath fading may degrade the reception significantly. Under these circumstances, most of the multipath signals are the result of ground reflected signals arriving at the receiver coherently or incoherently depending on the roughness and electrical characteristics of the surface. Coherent components are caused by a smooth surface and are called *specularly reflected* signals as opposed to incoherent components or *diffusely scattered* signals which result from relatively rough surfaces [9, 10].

To model specular reflections for systems design, the permittivity of the ground has to be known. In this paper we demonstrate that it can be measured with a GPS receiver.

2. Background: Specular Reflection and Diffuse Scattering

Signals reflected from a sufficiently smooth surface are called specularly reflected signals. They are directional, phase coherent and contributed by the central Fresnel zones on the surface near the receiver. Figure 1 shows that the total field received by the antenna is the sum of direct signal and specularly reflected signal. Here, an Earth-space link is considered. Compared to the direct component, the reflected component arrives

[†] This work was sponsored in part by National Science Foundation CAREER Program under Grant MIP-9502695, the Joint Services Electronics Program under Contract F49620-95-C-0045, Office of Naval Research under Grant N00014-95-1-0638, the Jet Propulsion Laboratory under Contract JPL 956520, Southwestern Bell Technology Resources, Inc., Motorola, Inc., and Texas Instruments.

with a phase difference that is a result of the physical path length difference and the phase shift caused by the reflection. The phase shift corresponding to the difference in path length can be expressed as

$$\phi = 4\pi h \sin(\theta) / \lambda, \quad (1)$$

where h , θ , and λ are the receiving antenna height, elevation angle to the satellite and wavelength of the transmitted signal, respectively. The reflection coefficient of a plane Earth surface is given by

$$R = \frac{\sin(\theta) - \sqrt{K}}{\sin(\theta) + \sqrt{K}}, \quad (2)$$

where $K = \eta - \cos^2 \theta$ for horizontal polarization, $K = (\eta - \cos^2 \theta) / \eta^2$ for vertical polarization and $\eta = \epsilon_r(f) - j60\lambda\sigma(f)$ is the permittivity of the surface. The dielectric constant, ϵ_r , and conductivity, σ (mho/m) depend not only on the frequency of the electromagnetic wave but also on the nature of the surface, the temperature, and the moisture content. A detailed explanation about these properties of the reflecting surface can be found in [1] and the references therein. Therefore, the reflection coefficient for a smooth surface is a function of the relative dielectric constant, the conductivity, the elevation angle and the frequency of the electromagnetic wave.

The reflection coefficient of the reflecting surface also depends on the polarization of the incident field. If the electric field intensity vector is in the plane of incidence, the polarization is vertical and the reflection coefficient R_v applies, while R_h applies when the wave is polarized perpendicular to the plane of incidence. The Brewster angle θ_p is the angle at which R_v goes to zero:

$$\theta_p = \tan^{-1} \sqrt{(\eta_1 / \eta_2)}. \quad (3)$$

If medium 1 is air so that $\eta_1 = 1$, then

$$\theta_p = \tan^{-1} \sqrt{(1/\eta_2)}. \quad (4)$$

In space-Earth communications, most transmitted signals are circularly polarized to reduce ionospheric effects, namely polarization changes of the wave due to free electrons in the ionosphere (Faraday Rotation) [6]. Reflection coefficients for circularly polarized waves can be derived from

those for horizontal and vertical polarization. In general, if a circularly polarized wave is incident on the surface, the resultant reflected wave will contain a component of the original circular polarization (cp), and a component of orthogonal polarization (xp). If the elevation angle is less than the Brewster angle, the cp component predominates, whereas if the angle is greater than the Brewster angle the xp component predominates. The reflection coefficient for cp and xp components can be expressed as

$$\rho_c = (R_h + R_v) / 2 \text{ and} \quad (5)$$

$$\rho_x = (R_h - R_v) / 2. \quad (6)$$

In many practical cases the ground is not perfectly smooth. If a surface is rough, energy is scattered into various directions, reducing the magnitude of the forward reflection coefficient. The surface roughness (Rayleigh criterion) criterion can be established as

$$\Delta h \leq \frac{\lambda}{4 \sin \theta} \quad (7)$$

The surface roughness factor (reduction factor) ρ_s for slightly rough surfaces with a random height distribution is given by

$$\rho_s = \exp[-(\Delta\phi)^2 / 2]. \quad (8)$$

Miller and Brown [11] have modified (8) to

$$\rho_s = \exp[-(\Delta\phi)^2 / 2] I_0[(\Delta\phi)^2 / 2], \quad (9)$$

where I_0 is the modified Bessel function, with a value of unity or greater.

The specular reflection coefficients R_h and R_v for a rough surface are then modified to

$$R_{hs} = \rho_h \rho_s, \quad R_{vs} = \rho_v \rho_s \quad (10), (11)$$

and the reflection coefficients for circular polarization ρ_c and ρ_x will also be reduced by the same factor ρ_s . Theoretical models were developed especially to characterize sea surface reflections including specular and diffuse components for L-Band multipath [5].

Roughness of the surface tends to decrease specular reflection components and suggests including both specular and diffuse scattering components in the total field expression. Considering all the factors (diffuse scattering, antenna gain, Earth-curvature effect, shadowing factor), the total field at the receiving antenna is:

$$\begin{aligned}
E = E_0 & \left[1 + g_{cr}(2\theta)\rho_s FD\rho_{cd} e^{j\phi} \right. \\
& + g_{xr}(2\theta)\rho_s FD\rho_x e^{j\phi} \\
& + g_{cr}(\theta_d)\rho_{cd} \\
& \left. + g_{xr}(\theta_d)\rho_{xd} \right] \quad (12)
\end{aligned}$$

where

- ϕ path length difference between direct and reflected signals,
- F blockage or shadowing factor, $F=2$ maximum, usually $0.1 < F < 1.2$,
- D divergence factor due to Earth's curvature $0 < D \leq 1$,
- ρ_s roughness parameter ≤ 1 ,
- ρ_c, ρ_x complex reflection coefficients for cp and xp components,
- $g_{cr}(2\theta)$ antenna gain relative to direct path for cp component,
- $g_{xr}(2\theta)$ antenna gain relative to direct path for xp component,
- ρ_{cd} reflection coefficient for diffuse scatter, $=R_c\rho_d$
- $g_{cr}(\theta_d)$ antenna gain relative to that for the direct path at an angle, is average effective angle for diffuse scatter.

If we neglect the diffuse scattering component, and assume that there is no shadowing and a relatively smooth surface $D=F=1$, the normalized field intensity will fall within the values of

$$1 \pm \left[\left| g_{cr}(2\theta) \right| \left| \rho_{cs} \right| + \left| g_{xr}(2\theta) \right| \left| \rho_{xs} \right| \right] \quad (13)$$

3. Experimental Setup

A picture of the experimental setup for taking L-Band ground specular reflection measurement is shown in Figure 2. The system consists of four main units; an antenna-preamplifier unit, a GPS receiver board-set, a portable computer and a 12 volt DC power supply.

Antenna-Preamplifier Unit

The antenna-preamplifier unit consists of a 60 mm diameter low profile circularly polarized patch antenna element and preamplifier circuit which amplifies the noise-like GPS spread spectrum signal within a single unit. It is attached to a large aluminum disk acting as a ground plane and mounted on a tripod in vertical position so as to receive the direct and ground reflected signals.

Normally, when used as a location determination device, the antenna is mounted horizontally.

Receiver Board-Set

Trimble's OEM commercial SVeeSix receiver [12] is used. The signal is received through the antenna feed-line connector. The receiver has six processing channels, operating at the L1 frequency using the C/A code. It processes 6 satellite signals at a time, controls the selection of tracked satellites, and extracts position and velocity information from the 50 bps data. The complete process is performed in a 16-bit microprocessor.

Portable Computer

A portable lap-top data acquisition computer is programmed for interacting with the GPS receiver and connected to the receiver via RS-232 interface. The program monitors the health of the receiver and stores the information decoded by it. This information, i.e., time, location, satellite position (azimuth and elevation angles) and signal strength, are transmitted to the PC up to twice per second. The signal level for each monitored satellite is based on an estimate of the carrier-to-noise ratio (C/N_0) and is reported in amplitude measurement units (AMU), which can be converted to a dB scale by the approximate relation

$$P_{dB} = 20 \log \left(\frac{64 P_{AMU}}{90 \sqrt{1000}} - 100.7 \right) \quad (14)$$

Three different environments were selected for L-Band ground reflection measurements: a) a grass field at the research campus of The University of Texas at Austin, b) an asphalt parking lot at the Texas Department of Human Services, and c) Lake Travis.

Table 1: Summary of GPS Ground Specular Reflection Measurements Details

Environment	antenna azimuth	satellite PRN	surface characteristics
grass	90°	23	dry, flat, clear LOS
asphalt	105°	23	dry, flat, clear LOS
water	315°	14	waves, clear LOS

4. Experimental and Simulation Results

In this section, we present experimental and computer simulation results obtained for the three locations. The most pertinent details of the experiments have been summarized in Table 1. For each case, the results are presented with three figures:

- 1.Measurement Results: GPS Satellite Position Change (PRN which is ID of the selected GPS satellite in the constellation, azimuth and elevation angles) and the received power variation.
- 2.Simulation and measurement results for the received power variation at 1.575 GHz due to direct and ground reflected signals.
- 3.Magnitude and phase of the estimated ground reflection coefficients for vertical and horizontal polarization.

In the simulation, (13) was used to characterize the total power fluctuation of the signal. As relatively flat measurement environments without blockage and shadowing effects were selected, the diffuse scattering component was assumed to be zero, and F and D set to 1. Signal power levels in both measurement and simulation results have been normalized to maximum signal levels. The data was collected for approximately 50-60 minutes in order to characterize the effect of the ground reflection for long-term variation relative to the 2-samples per second data rate recorded by the portable computer. Power levels recorded in AMU have been converted into dB scale as described in [12].

Figure 3 illustrates the measurement results on the grassy field. Satellite PRN 23 was chosen among the available GPS satellites of the constellation, as it had the best position that avoided shadowing and blockage. The elevation angle decreased from 25° to 6°. On the other hand, the azimuth angle increased from 110° to 130°. Both angles varied nearly linearly with respect to the 50 minute observation time interval. The observed fluctuations of the power level were almost periodic and the peak-to-peak variation was around 20 dB. This behavior was caused by the path length difference and change in the complex reflection coefficient, both of which depend on the elevation angle.

Deep fades occurred at around 1500th and 2500th seconds epoch time. Small irregularities on the grass resulted in short-term, random fluctuations imposed on the long-term variation of the signal level. However, the short-term changes do not mask the specular characteristics of the environment. Both experimental and simulation results of the received GPS signal power for the grass field are shown in Figure 4. The power levels were matched closest for conductivity $\sigma=0.08$ mho/m and dielectric constants $\epsilon_r=3.8$. Magnitude and phase characteristics of the complex reflection coefficients of dry grass at L-Band are given in Figure 6 for vertically and horizontally polarized fields. The estimated parameters, σ and ϵ_r , are used in determining these coefficients. As expected, the phase of the reflection coefficient for horizontal polarization is 180°. The phase for the vertical polarization, however, shifts from -140° to -180°. The magnitude of both coefficients increases as the elevation angle decreases.

The measurement results for the asphalt covered ground are presented in Figure 5. The same GPS satellite (PRN 23) was tracked as in the grass field measurement. Again, data was recorded for approximately 50 minutes. Similar changes in azimuth and elevation angle of the satellite were observed. The minimum fade level in the received power level, in this case, was around -15 dB and occurred at the 2500th second epoch time. As compared to the grass field (Figure 3), scattering caused higher short-term fluctuations.

Figure 7 compares simulated and measured GPS signals. A good fit is achieved with $\sigma=0.03$ and $\epsilon_r=1.5$. Specularly reflected signals from the asphalt pavement caused shallower fading than those from the grassy field. The reflection coefficient of the asphalt ground for vertical and horizontal polarization cases is plotted in Figure 8. In this case, the phase of both coefficients was almost 180° and their magnitude increased with decreasing elevation angle.

The relevant measurement results for the lake are given in Figure 10. Compared to the results for the grass and asphalt, we observed more diffuse scattering components, most likely because of the waves. The deepest null was limited to the level of -8 dB, implying lower specular signals. The selected satellite was PRN 14. Its position change

in azimuth followed non-linear variation with respect to the observation time unlike those in the grass and the asphalt measurements. The azimuth angle decreased from 318° to 296° and the elevation angle increased from 36° to 58°. The comparison of simulation and measurement results for the power variation due to the reflection from the lake are presented in Fig 10. The simulation results are matched to the experimental results by setting the parameters $\sigma=0.018$ and $\epsilon_r=2.1$, respectively. The reflection coefficients of the lake water are shown in Fig 11. The magnitude of the horizontal polarization decreased while that of the vertical polarization increased. The phase of the horizontal polarization was 180° for all values of the observed elevation angle.

Conclusions

In this paper, the effect of ground reflected L-Band signals on the received power level in satellite communication systems has been studied. The GPS system was used for making constitutive parameter measurements of a grass field, an asphalt parking lot, and lake water. Received power variations caused by the interference of direct and ground reflected signals were analyzed. In the experiments, the most favorable GPS satellite's signal among six satellites during the measurement time interval (50-60 minutes) was picked and recorded while the elevation and azimuth angle of the satellite changed. Computer simulations modeled the power variations. By matching simulated results to experimental results, conductivity and dielectric constants of the ground (grass, asphalt, and lake water) have been derived, presenting a novel way of estimating ground electrical characteristics at 1.5 GHz. If the peak-to-peak fluctuations of the normalized power (P) level are considered, the following conclusion can be made:

$$P_{\text{lake}} < P_{\text{asphalt}} < P_{\text{grass}} \quad (15)$$

We expected that the peak-to-peak fluctuation caused by the lake would be the greater because water has a large relative dielectric constant near 70. Besides making the lake measurement at a higher elevation angle, the surface was also quite wavy. The waves probably diffused the energy of the incident wave and yielded less specular reflection.

Bibliography

- [1] ITU, "Electrical Characteristics of the Surface of the Earth," *Propagation in Non-Ionized Media*, Report 229-6, 1990 Annex to Vol. V
- [2] ITU, "Methods for Estimating Effective Electrical Characteristics of the Surface of the Earth," *Propagation in Non-Ionized Media*, Report 879-1, 1990 Annex to Vol. V
- [3] ITU, "Reflection from the Surface of the Earth," *Propagation in Non-Ionized Media*, Report 1008-1, 1990 Annex to Vol. V
- [4] D. J. Fang, F.-T. Tseng and T. O. Calvit, "A Low Elevation Angle Propagation Measurement of 1.5 GHz Satellite Signals in the Gulf of Mexico," *IEEE Trans. on Ant. and Prop.*, Vol. 30, No. 1, Jan. 1982
- [5] Y. Karasawa and T. Shiokawa, "Characteristics of L-Band Multipath Fading due to Sea Surface Reflection," *IEEE Trans. on Ant. and Prop.*, Vol. 32, No. 6, pp. 618-623, Jun. 1984
- [6] J. Goldhirsh and W. J. Vogel, *Propagation Effects for Land Mobile Satellite Systems: Overview of Experimental and Modeling Results*, NASA Reference Publication 1274, Feb. 1992
- [7] W. J. Vogel and J. Goldhirsh, "Multipath Fading at L Band for Low Elevation Angle, Land Mobile Satellite Scenarios," *IEEE J. Select. Areas in Comm.*, Vol. 13, No. 2, pp. 197-204, Feb. 1995
- [8] R. J. Leopold and A. Miller, "The Iridium Communications System," *IEEE MTT-S Digest*, pp. 575-578, 1993
- [9] P. Beckmann and A. Spicichino, *Scattering of Electromagnetic Waves from Rough Surfaces*, Pergamon Press, Oxford, UK, 1963
- [10] J. R. Wait, *Electromagnetic Waves in Stratified Media*, Pergamon Press Inc., New York, 1962
- [11] A. R. Miller, R. W. Brown and E. Vegh, "New Derivation for the Rough-Surface Reflection Coefficient and for the Distribution of Sea-Wave Elevations," *IEEE Proc.*, Vol. 131, pp. 114-116, April 1984
- [12] *Trimble Standard Interface Protocol Toolkit User's Manual*, Trimble Navigation Inc., Jun. 1993

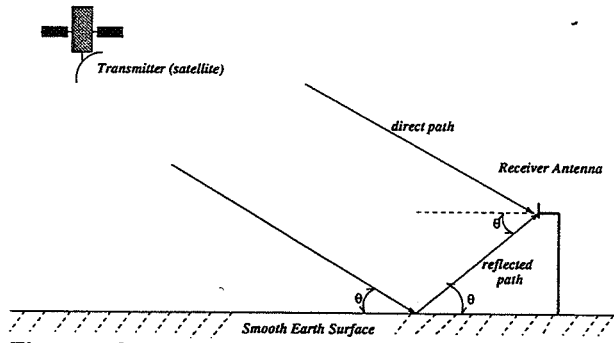


Figure 1: Specular Reflection Model



Figure 2: Experimental Setup for L-Band Specular Reflection Measurement

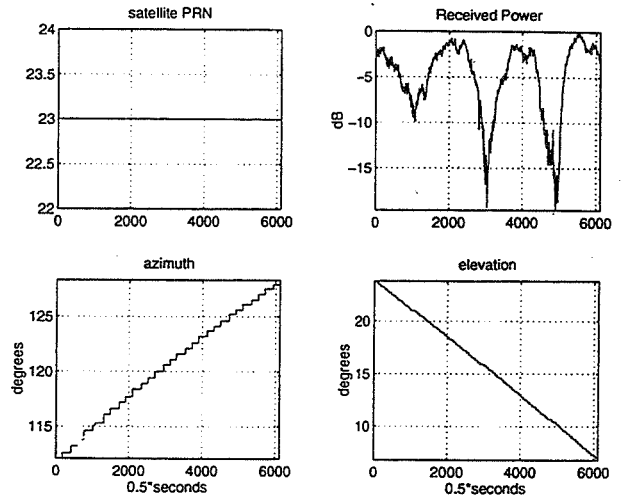


Figure 3: Grassy Field GPS Measurement Details

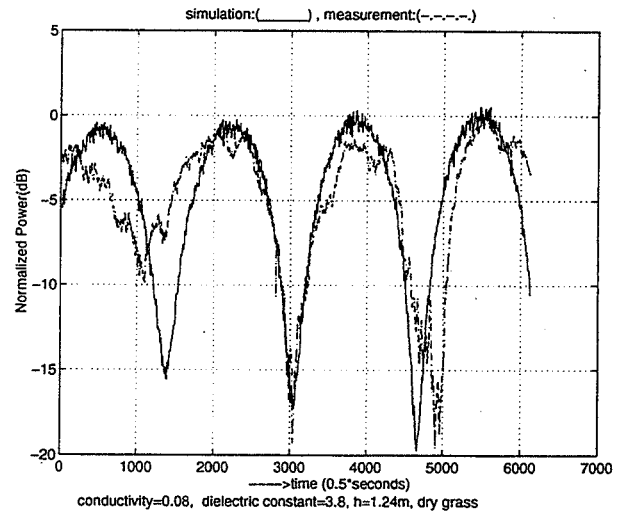


Figure 4: Modeled and Measured Signal Variations Received on a Dry Grass Field

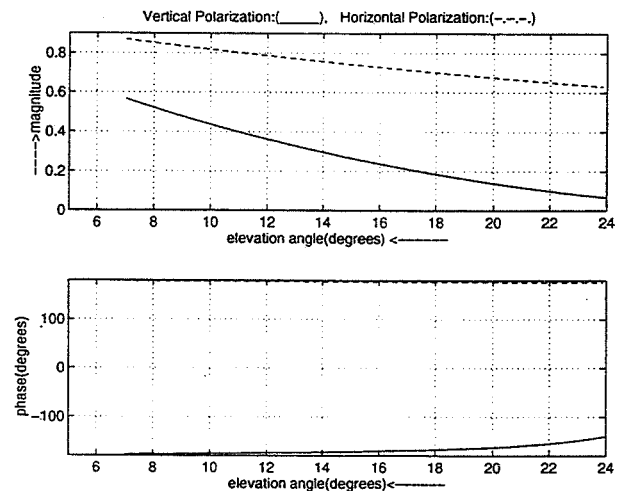


Figure 5: Reflection Coefficients for Dry Grass at 1.575 GHz

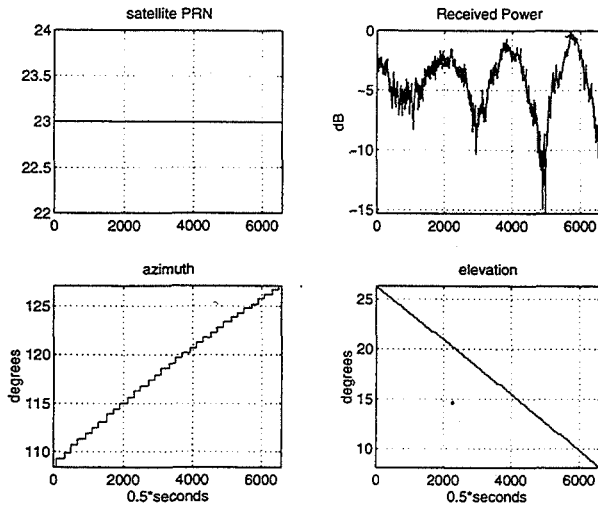


Figure 6: Asphalt Pavement GPS Measurement Details

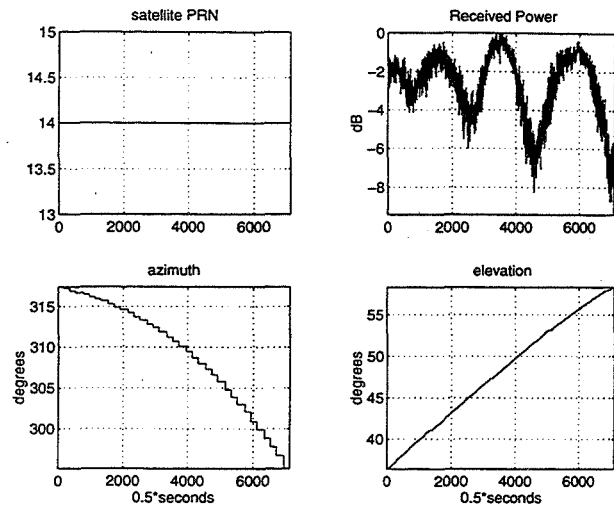


Figure 9: Lake Water GPS Measurement Details

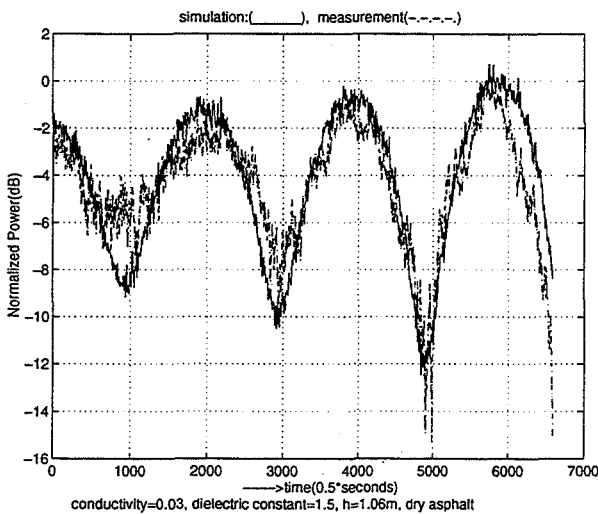


Figure 7: Modeled and Measured Signal Variations Received on an Asphalt Parking Lot

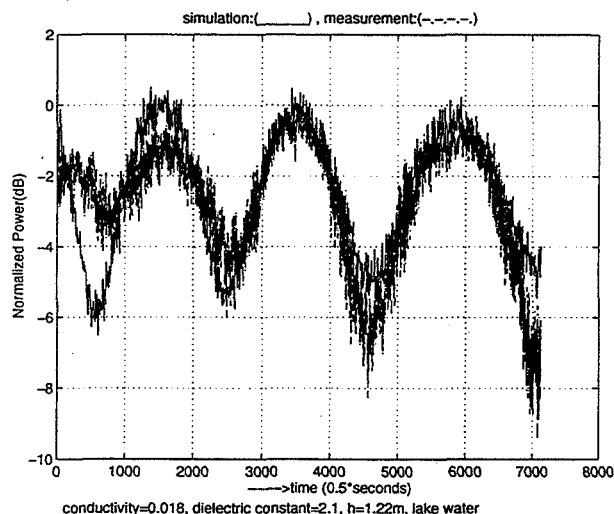


Figure 10: Modeled and Measured Signal Variations Received Over Water at the Lake

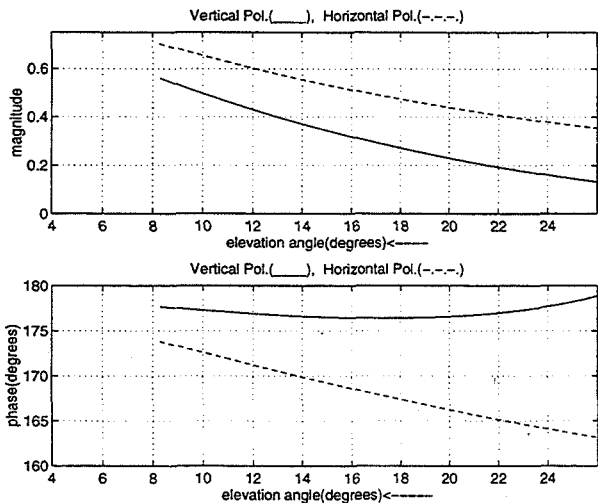


Figure 8: Reflection Coefficients for Dry Asphalt Pavement at 1.575 GHz

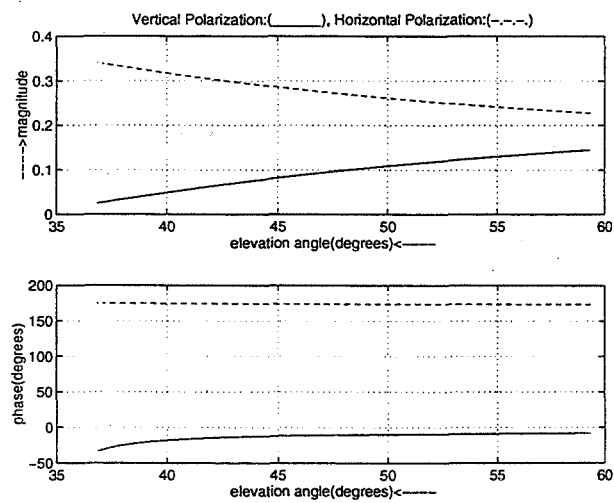


Figure 11: Reflection Coefficients for Lake Water at 1.575 GHz

Page intentionally left blank

A Proposed Change to ITU-R Recommendation 681

F. Davarian
Hughes Space and Communications Company

Introduction

Rec. 681 of the ITU-R [1] provides five models for the prediction of propagation effects on land mobile satellite links which are listed below:

1. Empirical Roadside Shadowing (ERS)
2. Attenuation Frequency Scaling
3. Fade Duration Distribution
4. Non-Fade Duration Distribution
5. Fading due to Multipath

Because the above prediction models have been empirically derived using a limited amount of data, these schemes work only for restricted ranges of link parameters. With the first two models, for example, the frequency and the elevation angle parameters are restricted to 0.8 to 2.7 GHz and 20 to 60 degrees, respectively. Recently measured data have enabled us to enhance the range of the first two schemes. Moreover, for convenience, they have been combined into a single scheme named the Extended Empirical Roadside Shadowing (EERS) model.

The Extended Roadside Shadowing Model

The EERS model estimates the effect of roadside tree shadowing on land mobile satellite links [2]. The inputs to this model are link frequency, elevation angle, and the percentage of link outage. The output is the fade depth experienced at the given percentage, or stated differently, the required margin for the given percentage of link outage. The ranges of frequency f (GHz), elevation angle θ (degrees), and percentage p , are

$$\begin{aligned}0.8 &\leq f \leq 20 \\7 &\leq \theta \leq 60 \\1 &\leq p \leq 80\end{aligned}$$

The EERS is an empirical model based on cumulative fade distribution measurements at UHF (870 MHz), L-band (1.6 GHz) and Ka-band (20 GHz). The population density of trees along the roadside is represented by the percentage of optical shadowing caused by roadside trees at a path elevation angle of 45 degrees in the direction of the signal source, that is the satellite. The EERS model is valid for the percentage of optical shadowing ranging from 55 to 75%.

For $1\% \leq p \leq 20\%$, the EERS model can be presented by

$$A(p, \theta, f) = A(p, \theta, f_L) \exp\left\{1.5\left(\frac{1}{\sqrt{f_L}} - \frac{1}{\sqrt{f}}\right)\right\} \quad (1)$$

and for $20\% < p \leq 80\%$ the model is given by

$$A(p, \theta, f) = A(20\%, \theta, f) \frac{\ln\left(\frac{80}{p}\right)}{\ln 4} \quad (2)$$

where $A(p, \theta, f)$ is the attenuation at the frequency f (GHz) exceeded at the percentage of the driving distance p for a path angle θ , and $A(p, \theta, f_L)$ is the corresponding attenuation at $f_L = 1.6$ GHz. The attenuation is defined relative to non-shadowed and negligible multipath condition.

For $20 \leq \theta \leq 60$ deg, the attenuation $A(p, \theta, f_L)$ is given by

$$A(p, \theta, f_L) = \alpha(p) + \beta(p)\theta + \gamma(p)\theta^2$$

and for $7 \leq \theta < 20$ deg,

$$A(p, \theta, f_L) = A(p, 20^\circ, f_L)$$

where

- A : fade exceeded in dB with respect to unshadowed propagation,
- p : percentage of the distance traveled over which the fade is exceeded, and
- θ : path elevation angle to the satellite in degrees.

The parameters $\alpha(p)$, $\beta(p)$, and $\gamma(p)$ are tabulated in Table 1.

Table 1. Values of $\alpha(p)$, $\beta(p)$, and $\gamma(p)$ of the EERS Model

Percentage	$\alpha(p)$	$\beta(p)$	$\gamma(p)$
20	24.45	-0.7351	5.991×10^{-3}
10	26.84	-0.6775	4.605×10^{-3}
5	29.22	-0.6000	3.219×10^{-3}
2	32.38	-0.5106	1.386×10^{-3}
1	34.76	-0.4430	0.0

The EERS model corresponds to an average propagation condition with the vehicle driving in lanes on both sides of the highway -- lanes close to and far from roadside trees. The model applies to highway and rural roads where the overall aspect of the propagation path is, for the most part, orthogonal to the line of roadside trees and utility poles, a slightly conservative scenario. It is assumed that the dominant cause of signal attenuation is canopy shadowing (see Recommendation ITU-R PN. 833). Figure 1 shows plots of fade exceeded versus the path elevation angle for several constant percentages, p .

Although the EERS model has been tested only for the frequency rang of 0.8-3 GHz and a single frequency of 20 GHz, it is suggested for use as a straw model for in between frequencies, i.e., 3 to 20 GHz.

Extension of Elevation Angle Upper Bound.

Data from the UK indicate that the elevation angle range of the EERS model for L- and S-band frequencies (1 to 3 GHz) and $p \leq 30\%$ can be extended to 90 degrees. This can be achieved by linear interpolation between the EERS model at 60 deg and the data provided in Table 2 at 80 degrees. The value of attenuation at 90 degrees is suggested to approach zero.

Table 2. Fade Exceeded (dB) at 80 deg (measurements in the UK)

Tree-Shadowing: mature deciduous trees of varying density and distance from the road.		
p (%)	1.6 GHz	2.6 GHz
1	4.1	9.0
5	2.0	5.2
10	1.5	3.8
15	1.4	3.2
20	1.3	2.8
30	1.2	2.5

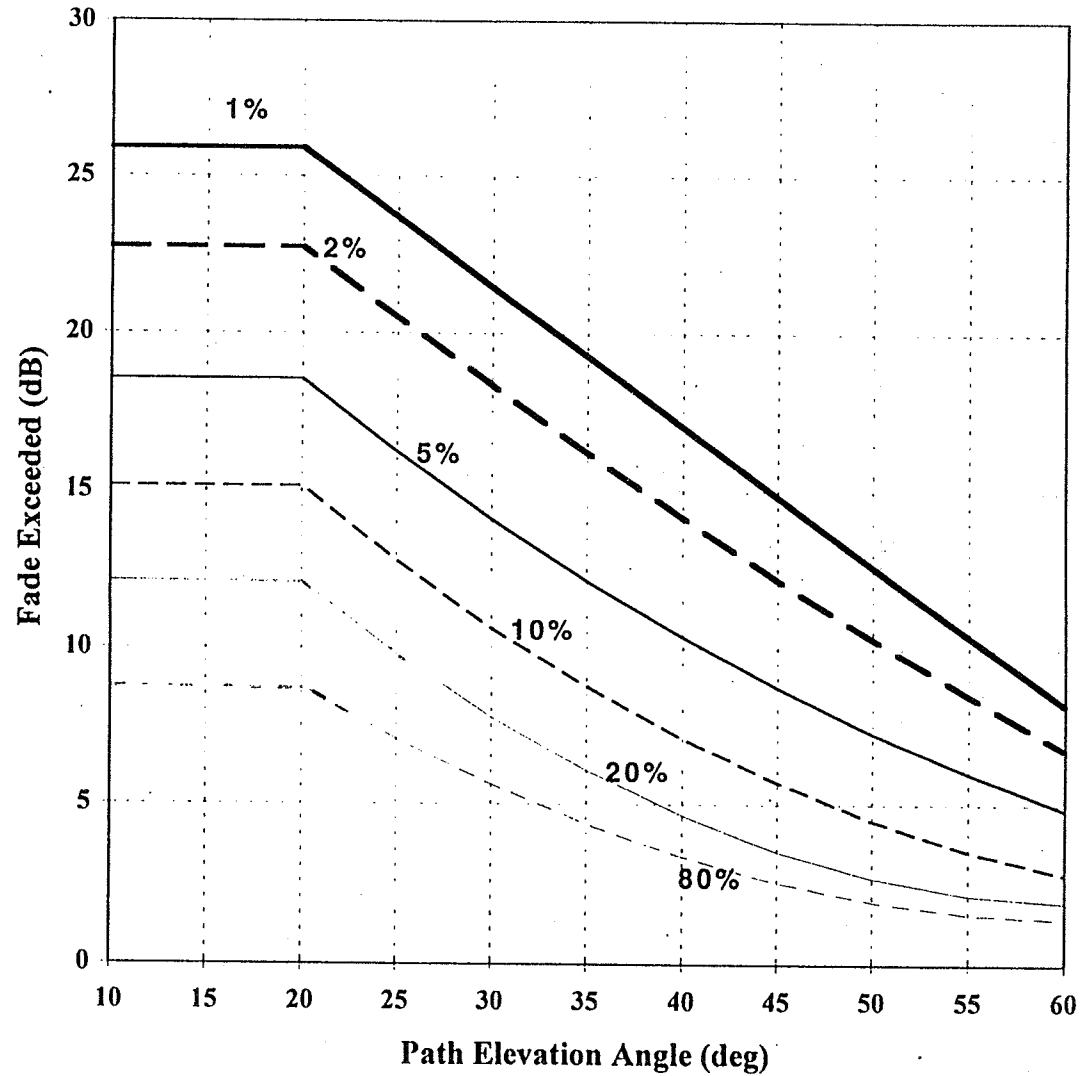
Summary

The extended road side shadowing model is a tool for the prediction of fades on mobile satellite links. EERS is an empirical model based on data obtained on U.S. roads and highways with tree shadowing as the primary source of fading and a small contribution from utility poles, man-made objects, and natural obstacles. This model corresponds to an average propagation condition.

Reference

1. ITU-R Recommendations, 1994 PN Series, Geneva, Switzerland, 1995, pp. 358-365.
2. J. Goldhirsh and W. Vogel, "Extended Empirical Roadside Shadowing Model from ACTS Mobile Measurements," Proceedings of NAPEX XIX, JPL Pub. 95-15, Aug. 1, 1995, pp. 91-102.

FIGURE 1
Fading at 1.5 GHz due to Roadside Shadowing versus
Path Elevation Angle



Description of Proposed Revision of Handbook on: Propagation Effects for Land Mobile Satellite Systems

Julius Goldhirsh

Applied Physics Laboratory, The Johns Hopkins University
Johns Hopkins Road, Laurel, MD 20723-6099
email: Julius_goldhirsh@jhuapl.edu

Wolfhard J. Vogel

Electrical Engineering Research Laboratory, The University of Texas at Austin
10100 Burnet Road, Austin, Texas 78758-4497
email: wolf_vogel@mail.utexas.edu

1. Introduction

The Applied Physics Laboratory, The University of Texas at Austin, JPL, and NASA are exploring the need for revising the Handbook on Propagation Effects for Land Mobile Satellite Systems published as NASA Reference Publication 1274 in February 1992 (Figure 1). The original publication was an outgrowth of a series of joint mobile propagation experiments performed by the Electrical Engineering Research Laboratory of The University of Texas at Austin and the Applied Physics Laboratory of The Johns Hopkins University between 1983 and 1988. When published, the text served the purpose of providing a state of the art manual describing experiments, results, concepts, and models associated with propagation effects for land mobile satellite scenarios. Investigations were cited from within and outside the United States. Although published in 1992, the text contains only referenced material through 1991. Since this time, a number of other mobile satellite experiments and modeling efforts have been performed throughout the world. In addition, new areas of investigation such as personal access and mobile-aeronautical communications have approached a level of maturity and importance requiring descriptions of propagation effects. The intent of the proposed effort is therefore to revise the manual such that it contains pertinent new information, to broaden its scope by adding new subject material, and to delete outdated material (Figure 2).

2. Contents of Talk

The elements of the talk are summarized in Figure 3. To establish a common reference point, the major topics contained in the present text will first be reviewed. As a demonstration of the need for revising the previous text, examples of some pertinent mobile satellite experiments performed and modeling results obtained since 1991 will be cited. A suggested title will be proposed and a summary of the type of new material to be included in the revised text will be given.

3. Review of Salient Subjects in Existing Handbook

In Figures 4–6 are given the salient topics contained in the present mobile satellite handbook where each bullet constitutes an individual chapter. The first theme (Figure 4) covered in the text deals with attenuation due to individual trees. The path attenuation and attenuation coefficient due to tree canopies are derived for static scenarios and are given at UHF (870 MHz) and L-Band (1.5 GHz). A scaling factor valid from UHF to L-Band is also presented along with a formulation characterizing the attenuation effects due to trees with and without foliage. The second theme given in Figure 4 deals with attenuation due to roadside trees. In this chapter the empirical roadside shadowing model is presented. This model describes the percentage of the distance traveled with fades greater than designated levels. The roads are assumed to be lined with trees, the frequency ranges from UHF to S-Band, the elevation angles are from 20° to 60°, and percentages range from 1% to 20%. Also given is a formulation describing the attenuation effects of foliage versus bare tree conditions at UHF (870 MHz). A scaling factor is presented here for mobile satellite scenarios valid over the frequency range UHF (870 MHz) to S-Band (3 GHz).

The next theme presented (Figure 5) deals with fading due to multi-path for both mountain and tree environments. Cumulative fade distributions are presented where line-of-sight between the source and the receiver was generally maintained. The next bullet in Figure 5 corresponds to a chapter where cumulative distributions at L-Band are presented for fade and non-fade durations and for phase spreads. The distributions were obtained from tree shadowing mobile-satellite scenarios. Results are presented in a following chapter which give the cross polarization isolation at 1.5 GHz as a function of co-polarization fade at equal probability levels. Also given are results pertaining to repeat measurements where high and low gain receiving antennas were used. Also presented are the results of a simulation based on real data of a space diversity scenario where two antennas on the vehicle are presumed to be located at different spacings. Diversity improvement factor and gains are described.

A Chapter (Figure 6) is presented reviewing investigations from other countries such as Australia, Canada, Belgium, England, and Japan. In a subsequent chapter, modeling aspects are covered associated with both empirical and theoretical results. This is followed by general conclusions and recommendations for follow-on efforts.

4. Examples of Land-Mobile Satellite Experiments Since 1991

Figures 7 through 12 give examples of pertinent investigations which provide new information. Although, these examples represent only a small sampling of investigations performed since 1991, they reinforce the rationale for updating the present mobile satellite handbook. In 1995 Vogel and Goldhirsh published results pertaining to low elevation angle mobile measurements (7°–14°) at L-Band made in the western part of the United States using the MARECS B-2 satellite (Figure 7). Both multipath effects and tree shadowing of low-elevation angle measurements are covered in this paper. In 1995, Goldhirsh and Vogel published a paper describing the Extended Empirical Roadside Shadowing (EERS) model which was an outgrowth of measurements in Central Maryland, Texas, the western United States, and Alaska (Figure 8). This model extends the results of the previous Empirical Roadside Shadowing (ERS) model such that the following are applicable: (a) the frequency range is between

870 MHz and 20 GHz, (b) the elevation angle range is 7° and 60° , and (c) the probability of fading is 1% to 80%. The attenuation effects of foliage versus no foliage conditions are modeled in this paper and are demonstrated to be dramatically different from the effects at 870 MHz.

Gargione et al. in 1995 reported on the JPL ACTS mobile terminal (Figure 9). In this publication, fade distributions at 20 GHz are presented for a rural free-way run and a suburban road characterized by rolling hills and roadside foliage. Butt et al. in 1995 reported on an extension of the ERS model in elevation angle from 60° to 80° (Figure 10). In 1995, Murr et al. reported on a European Space Agency investigation involving a tracking antenna receiving an 18.7 GHz signal from ITALSAT (Figure 11). Measurements were performed in the Netherlands, France, Germany, and Austria for different driving scenarios at elevation angles between 30° – 35° and satellite azimuths of 0° , 45° , and 90° . Driving scenarios included open rural, tree shadowed, suburban, and urban mixed.

In 1993, Obara et al. reported on land-mobile satellite propagation measurements at 1.5 GHz using the ETS-V satellite. Measurements were predominantly carried out along major expressways connecting cities as well as along several rural roads (Figure 12). The authors give cumulative fade, fade duration, and non-fade duration distributions for the individual roads traveled.

5. Summary of Revisions

In Figures 13-15 is given a summary of suggested revisions for the mobile-satellite handbook. This listing is at present preliminary and is expected to be modified based on feedback from the mobile-satellite community. The present title of the text is "Propagation Effects for Land Mobile Satellite Systems: Overview of Experimental and Modeling Results." A suggested revised title is "Propagation Effects for Vehicular and Personal Mobile Satellite Systems: Overview of Experimental and Modeling Results." As the title suggests, the revised text will cover additional mobile platforms corresponding to air, marine, and personal (Figure 13).

The revised handbook will contain pertinent land-mobile satellite results obtained since 1991 (Figure 14). These include a description of experiments and new theoretical and empirical models. Revisions of models previously described will also be included. These revisions will include extensions of the frequency range, elevation angle, and probability range. A review of existing information in the handbook will also be made, and non-relevant material will be removed.

New subject material will also be added (Figure 15). This includes an overview of material accepted as recommendations by the International Telecommunication Union—Radiocommunication (ITU-R). Propagation experiments involving delay spread spectrum measurements will be covered. New methodologies for arriving at mobile results will also be added. These will include optical procedures pursued by the University of Texas at Austin. The scope of the text will also be broadened such that it includes propagation effects associated with personal, marine, and aeronautical scenarios.

**Description of Proposed Revision
of Handbook
Propagation Effects for Land
Mobile Satellite Systems**

Julius Goldhirsh

Applied Physics Laboratory
The Johns Hopkins University

Wolfhard J. Vogel

Electrical Engineering Research
Laboratory
The University of Texas at Austin

**NASA
Reference
Publication
1274**

February 1992

Figure 1

Propagation Effects
for Land Mobile
Satellite Systems:
Overview of Experimental
and Modeling Results

Julius Goldhirsh
and Wolfhard J. Vogel

NASA

Figure 2

Background and Rationale for Revising Text

- Outgrowth of mobile propagation experiments between 1983 and 1988
 - UOT and JHU
- Text provided state-of-art experimental results, concepts, and models
- Text contains material only through 1991
- Many additional experiments and results published since 1991
 - New and revised results should be added
- Scope of text broadened
- Outdated results should be deleted

Figure 3

Contents of Talk

- Review major topics of present mobile-satellite handbook
- Examples of pertinent land-mobile satellite experiments and results since 1991
- Summary of modifications
 - Suggested title
 - Revisions of existing subject material
 - New subject material in revised text
 - Scope broadened

Figure 4

Topics in Present Handbook (NASA Ref. Pub. 1274 - Feb. 1992)

- Attenuation due to individual trees-static case
 - UHF (870 MHz) and L-Band (1.5 GHz)
 - Attenuation and attenuation coefficient
 - L-Band versus UHF scaling factor
 - Effects of foliage
- Attenuation due to roadside trees: mobile scenarios
 - Empirical Roadside Shadowing (ERS) model
 - Effects of foliage
 - Frequency scaling

Figure 5

Topics in Present Handbook (NASA Ref. Pub. 1274 - Feb. 1992) (Continued)

- Signal degradation for line-of-sight communications
 - Multipath for mountain and tree environments
- Fade and non-Fade durations and phase spreads
 - cumulative Distributions
- Propagation effects due to cross polarization, antenna gain, and space diversity
 - Frequency re-use
 - Low and high gain antenna effects
 - Diversity improvement factor
 - Diversity gain

Figure 6

Topics in Present Handbook (NASA Ref. Pub. 1274 - Feb. 1992) (Continued)

- Investigations from different countries
 - Australia, Canada, Belgium, England, United States, Japan
- Modeling for LMSS scenarios
 - Background concepts used in modeling
 - Empirical regression models
 - Probability distribution models
 - Geometrical-analytical models
- General conclusions
- Recommendations for follow-on efforts

Figure 7

Examples of Land-Mobile Satellite Experiments Since 1991

- Low Elevation Angle Measurements at L-Band
 - 1995, Vogel and Goldhirsh
 - IEEE Journal on Selected Areas in Communications, Vol. 13, No. 2, Feb. 1995
 - Multipath and tree shadowing effects in western U.S.A. using MARECS B-2 satellite
 - Elevation angles 7° to 14°

Figure 8

Examples of Land-Mobile Satellite Experiments Since 1991 (Continued)

- Extended Empirical Roadside Shadowing Model (EERS)
 - Goldhirsh and Vogel, 1995
 - Space Communications, Vol. 13, No. 3, 1995
 - Reviewed ACTS mobile results in central MD, Texas, and Alaska
 - Extended ERS model to 20 GHz
 - Extended ERS model to probability of 80%
 - 0 dB fade
 - Extended ERS model to elevation angle = 7 degrees
 - Effects of foliage at 20 GHz

Figure 9

Examples of Land-Mobile Satellite Experiments Since 1991 (Continued)

- Mobile Experiments Using ACTS
 - 1995, Gargione et al.
 - Space Communications, Vol. 13, No. 3, 1995
 - JPL-ACTS mobile terminal results
 - Cumulative distribution for rural freeway and suburban road at 20 GHz

Figure 10

Examples of Land-Mobile Satellite Experiments Since 1991 (Continued)

- Modelling the Mobile Satellite Channel for Communication System Design
 - Butt et al., 1995
 - 9th International Conference on Antennas and Propagation, Eindhoven, The Netherlands
 - Extended ERS model from 60° to 80°

Figure 11

Examples of Land-Mobile Satellite Experiments Since 1991 (Continued)

- Land Mobile Satellite Narrowband Propagation Campaign at Ka Band
 - Murr et al., 1995
 - IMSC 95, Ottawa, Canada, June 6-8 1995
 - ESA funded investigation
 - Mobile measurements at 18.7 GHz using ITALSAT
 - Open rural, tree-shadowed, suburban, urban, mixed
 - Netherlands, France, Germany, Austria
 - Fade distributions for different azimuth pointing (0° , 45° , 90°)

Figure 12

Examples of Land-Mobile Satellite Experiments Since 1991 (Continued)

- Land Mobile Satellite Propagation Measurements in Japan Using ETS-V Satellite
 - Obara et al., 1993
 - IMSC, 1993, Pasadena, CA, June 16-18, 1993
 - ETS-V at 1.5 GHz at 40° - 50°
 - Measurements in Japan
 - Major expressway measurements (4000 km)
 - Fade and fade duration distributions

Figure 13

Summary of Revisions (Preliminary)

- Old Title
 - Propagation Effects for Land Mobile Satellite Systems: Overview of Experimental and Modeling Results
- New (Suggested) Title
 - Propagation Effects for Vehicular and Personal Mobile Satellite Systems: Overview of Experimental and Modeling Results
 - Land-mobile
 - Personal mobile
 - Air-mobile
 - Marine-mobile

Figure 14

Summary of Revisions (Preliminary) (Continued)

- Revision of existing subject material
 - Add pertinent land-mobile satellite results since 1991
 - Experiments
 - New Models
 - Theoretical
 - Empirical
 - Update existing models
 - Frequency
 - Elevation angle
 - Probability range
 - Shadowing types
 - Deletions of non-pertinent material

Figure 15

Summary of Material to Be Added to Revised Text (Preliminary)

- Review ITU-R models
- Wideband propagation effects
 - Delay spread experiments
- New methodologies for arriving at mobile propagation results
 - Optical methods (University of Texas)
- Experiments and propagation effects pertaining to:
 - Aeronautical-mobile satellite
 - Personal-mobile satellite
 - Marine-mobile satellite

Page intentionally left blank



**Quick Look Analysis of Broadband Aeronautical Data
obtained from the Kuiper Airborne Observatory**

by

**Edgar Satorius, Brian Abbe, Martin Agan
Jet Propulsion Laboratory, California Institute of Technology,
Pasadena, Ca**

K/Ka-Band ACTS Aeronautical Experiments

- **AERO-X Experiments:**

- Purpose: Test viability of speech/data transmissions at: 2.4, 4.8, 9.6, 64 kbps
- Link: NASA Learjet - ACTS - HBR-LET at LeRC
- Aircraft antennas: electronically steerable phased arrays
- Where: Between Cleveland and Washington, DC
- When: Spring/summer 1994

- **Broadband Aeronautical Terminal (BAT) Experiments:**

- Δ **Rockwell International Aeronautical tracking and high data rate experiments**

- Purpose: Test viability of high data rate transmissions at: 512, 768 kbps
- Link: Rockwell Saberliner- ACTS - JPL
- Aircraft antennas: mechanically steerable (az-el tracking)
- Where: Midwest
- When: August 1995

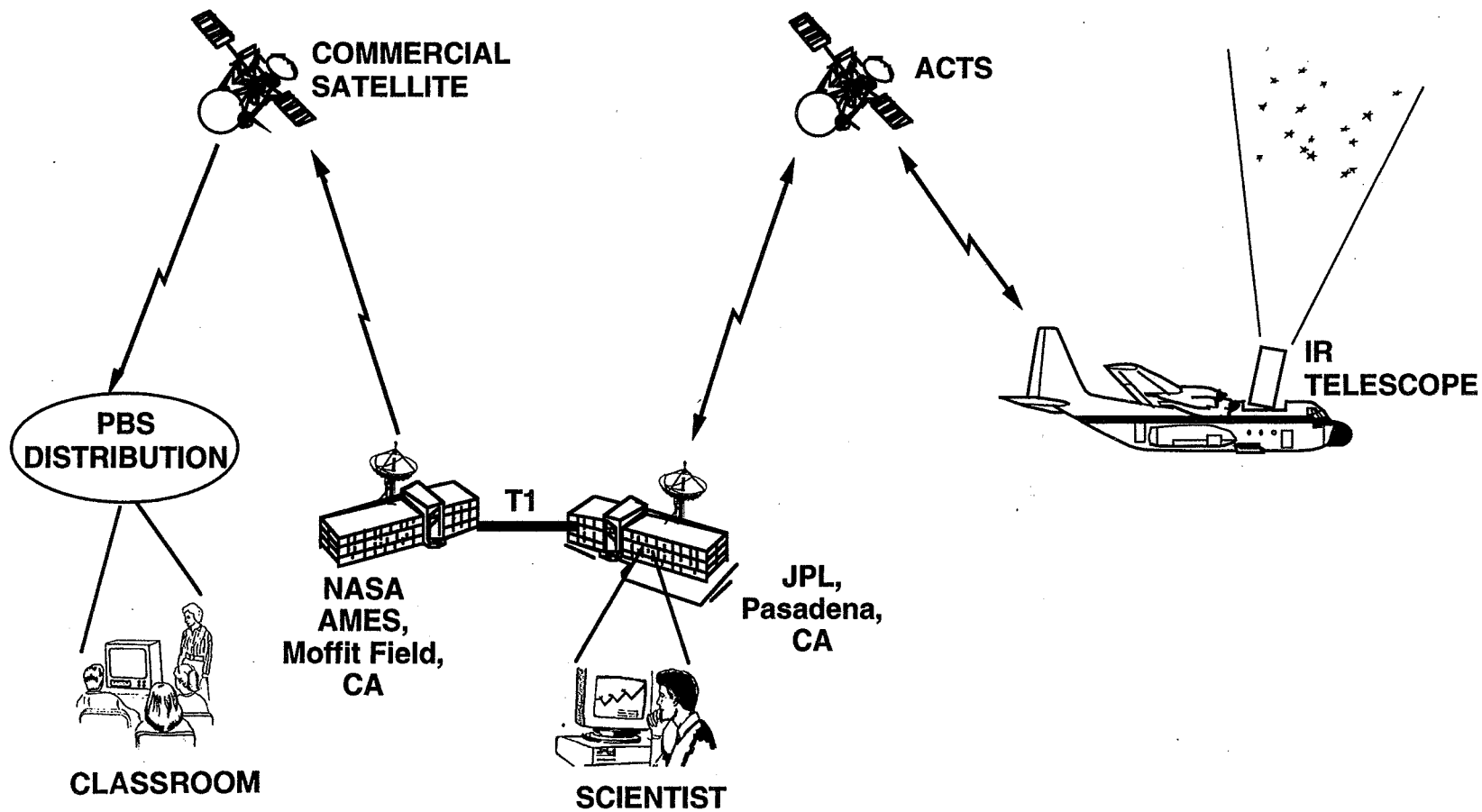
- Δ **Kuiper Airborne Observatory (KAO) live TV broadcast**

- Purpose: Test viability of high data rate transmissions to/from turbojet up to 384 kbps
- Link: KAO (C-141) - ACTS - JPL -(T1)- NASA AMES - ComSat - Classrooms
- Aircraft antennas: mechanically steerable (az-el tracking)
- Where: Northwest US + Houston, TX
- When: Summer/Fall 1995

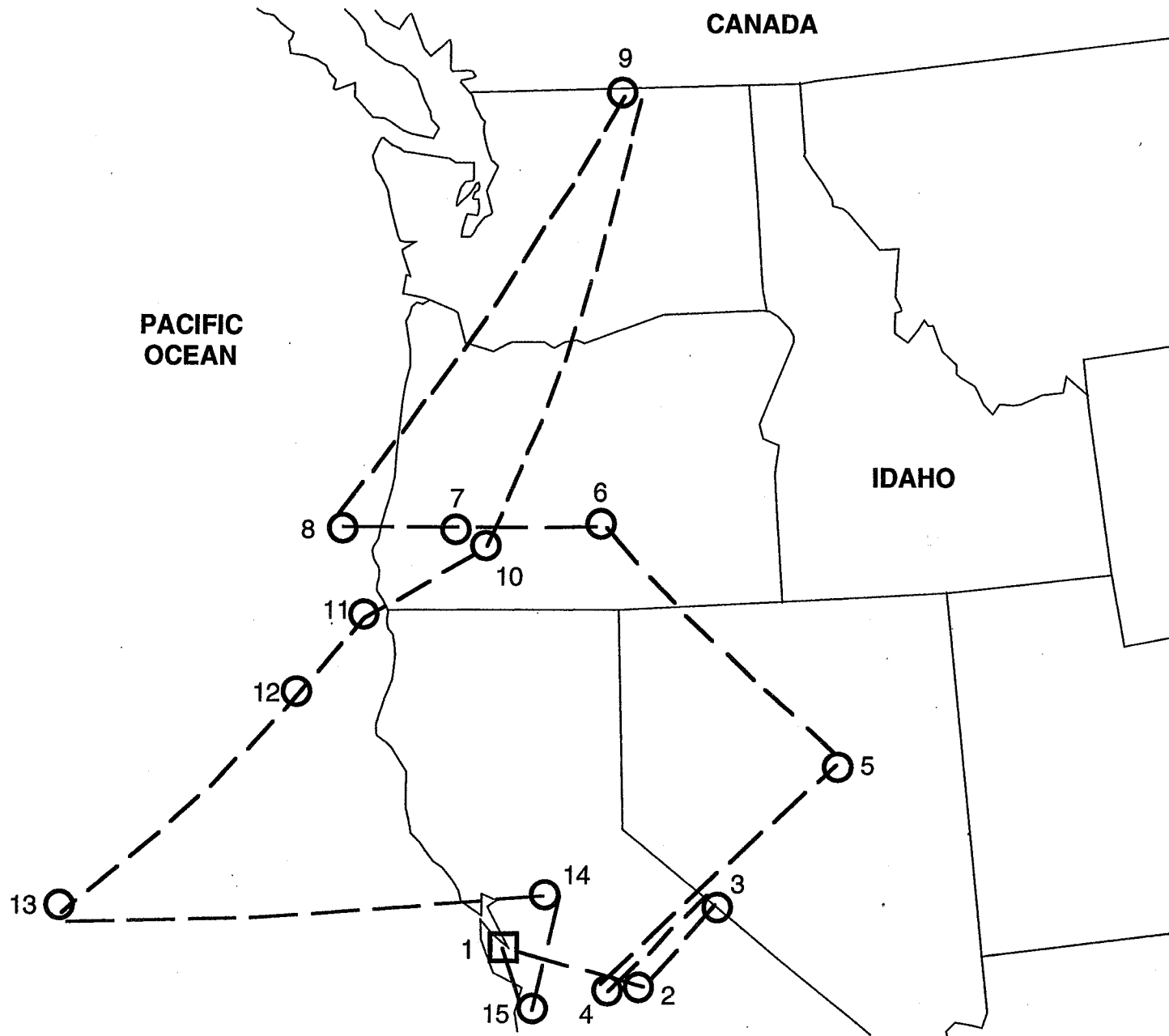
- Δ

KAO Experiment Configuration

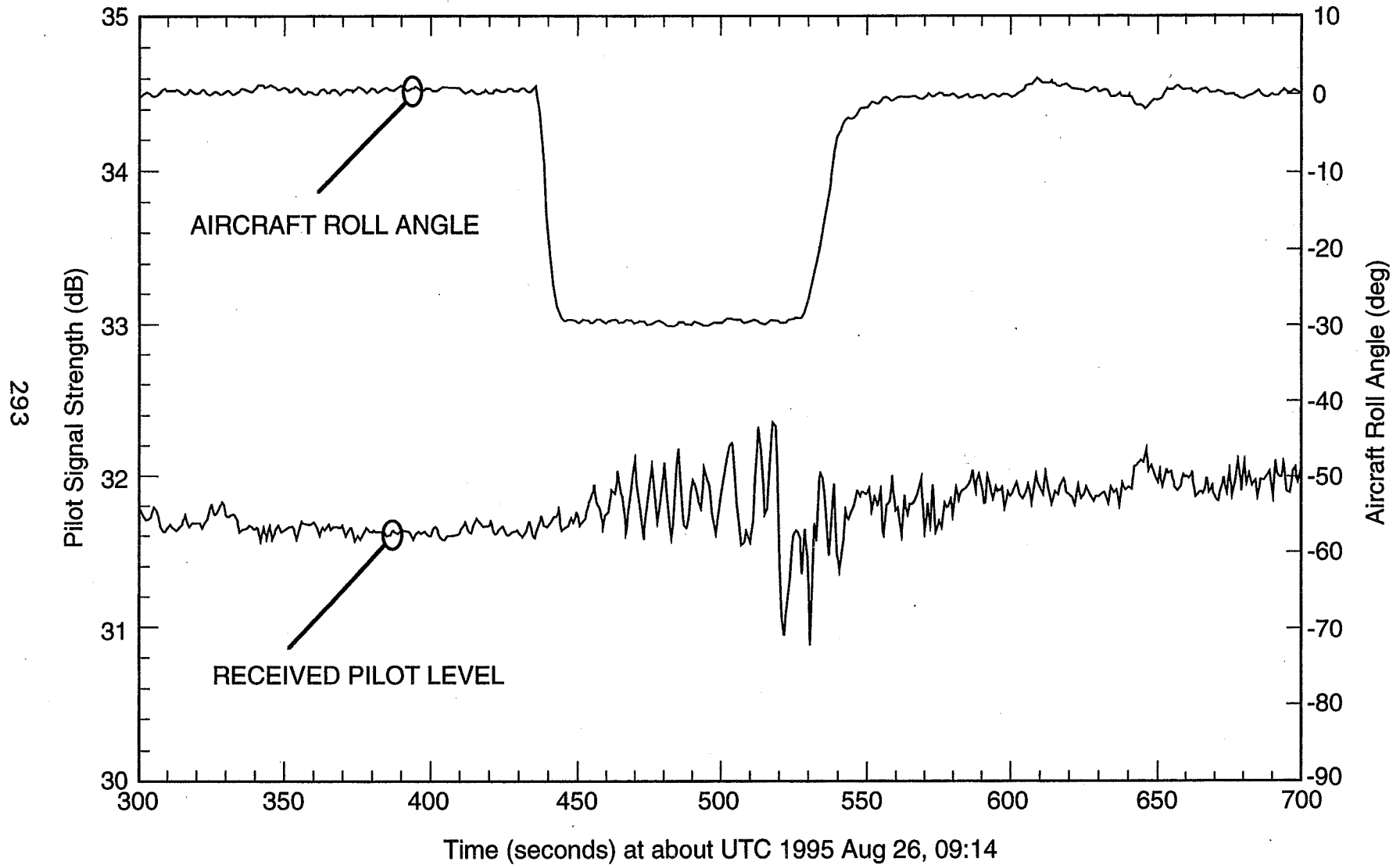
291



292

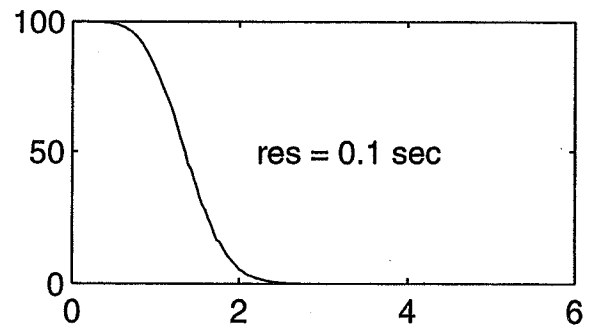
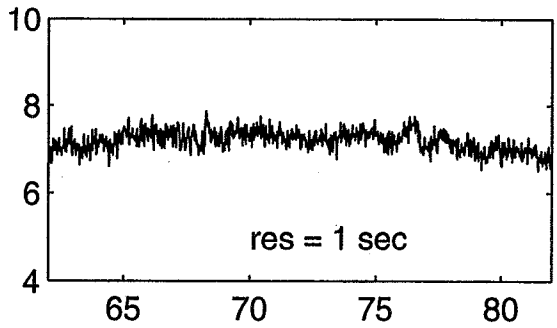
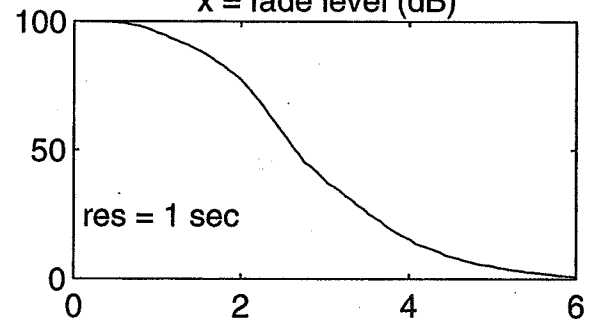
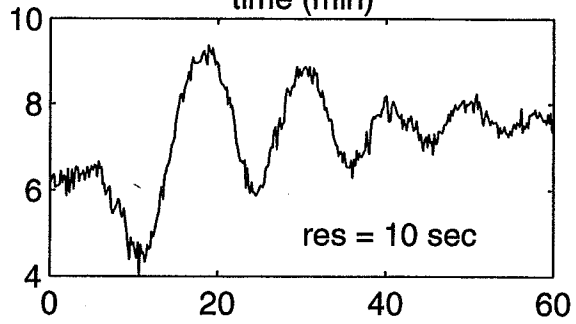
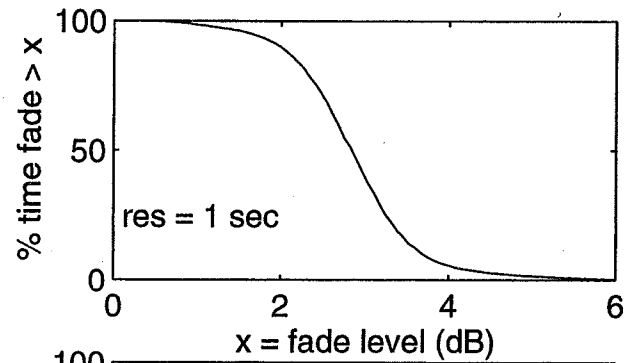
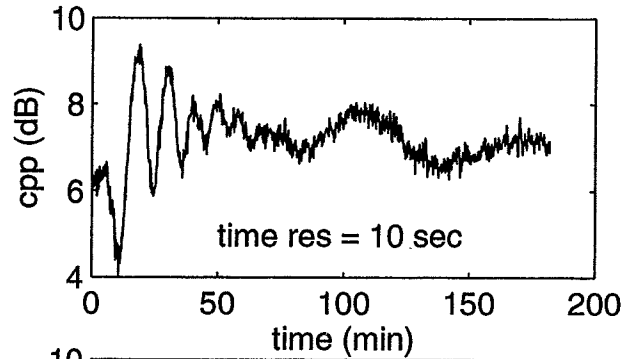


Antenna Tracking Performance (KAO Flight 8-25-95)



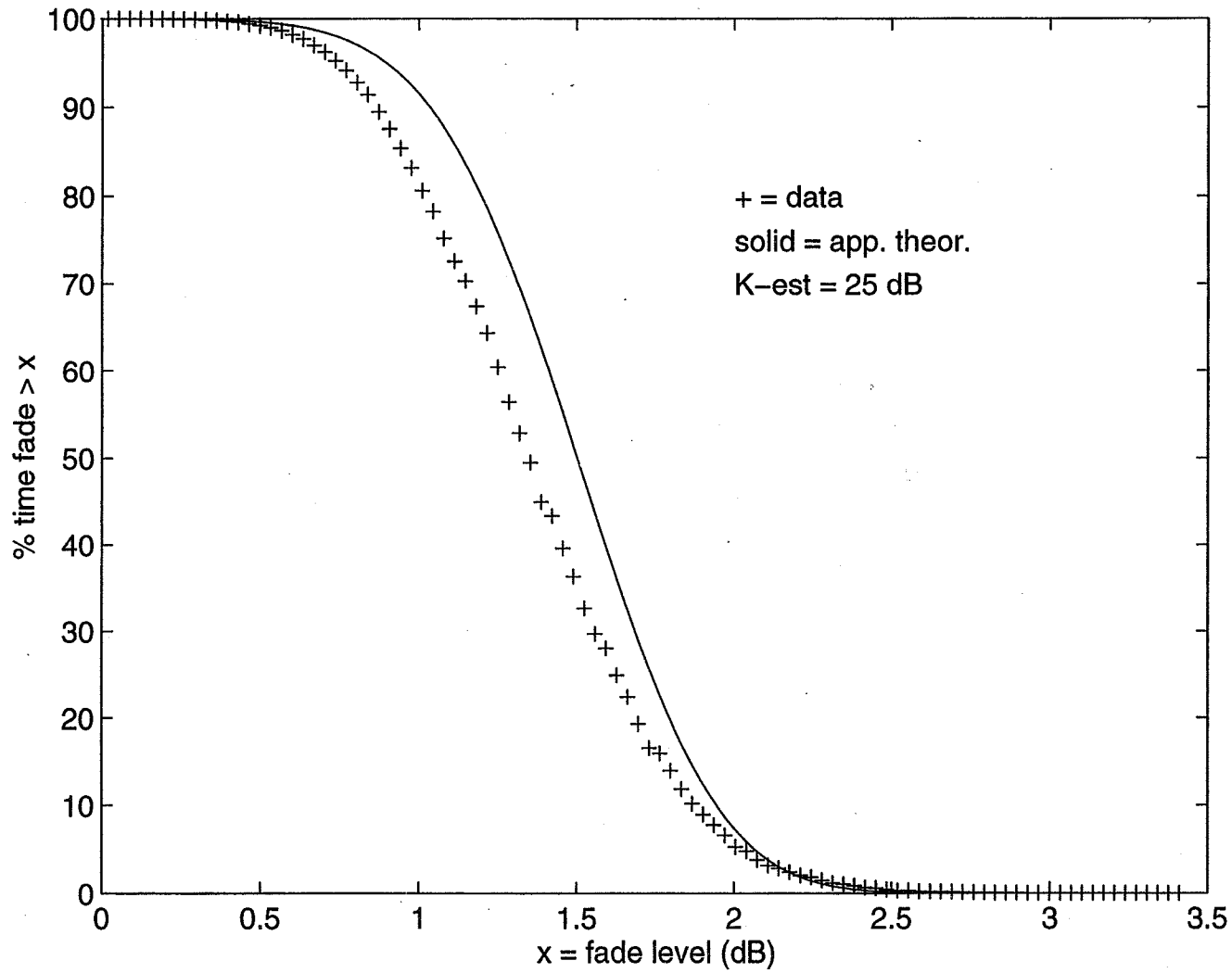


Coherent Pilot Power and Cumulative Fade Distributions
for 12 October 1995 starting at 15:08:00





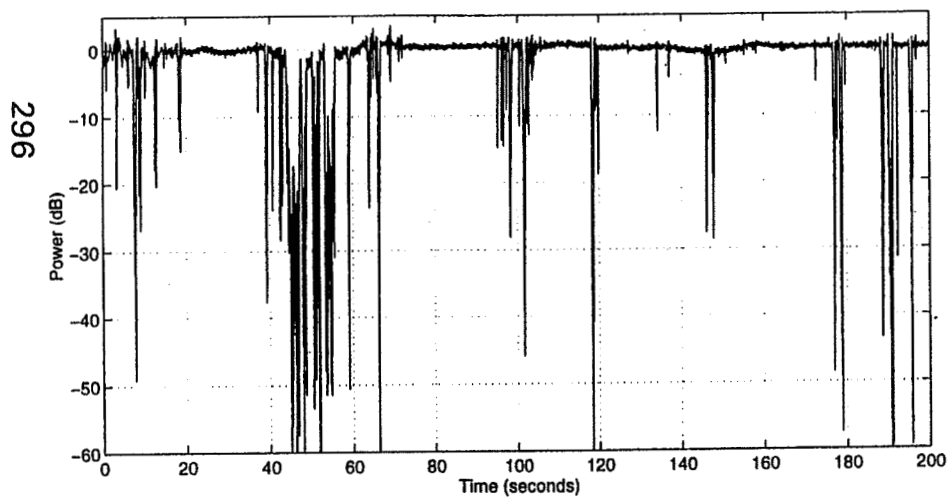
**Approximate Fit Between Coherent Pilot Power Cumulative Fade Distribution and LOS Model
for 12 October 1995 between 16:10:00 and 16:30:00 (0.1 sec sampling)**



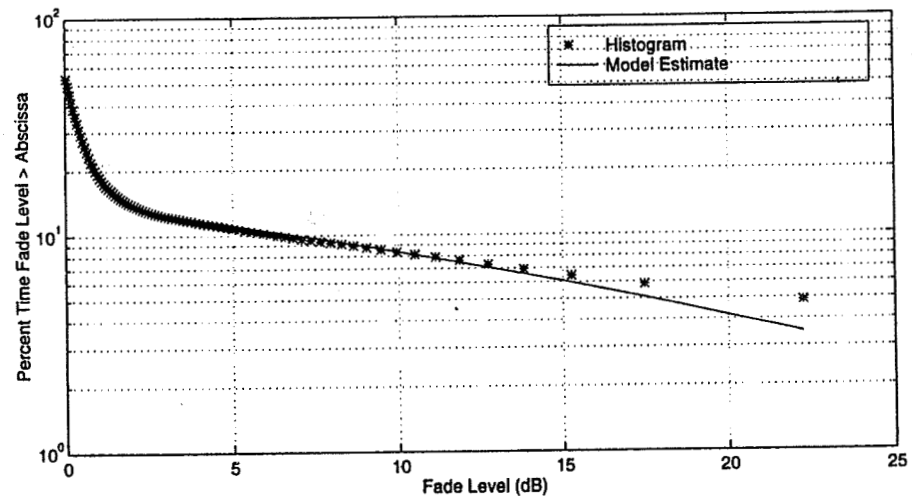


Coherent Pilot Power and Cumulative Fade Distribution for a typical K-Band Land Mobile Satellite Channel

Time Series



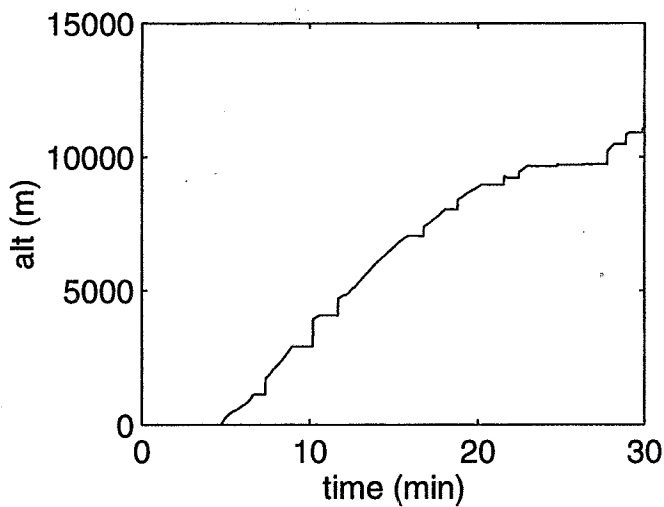
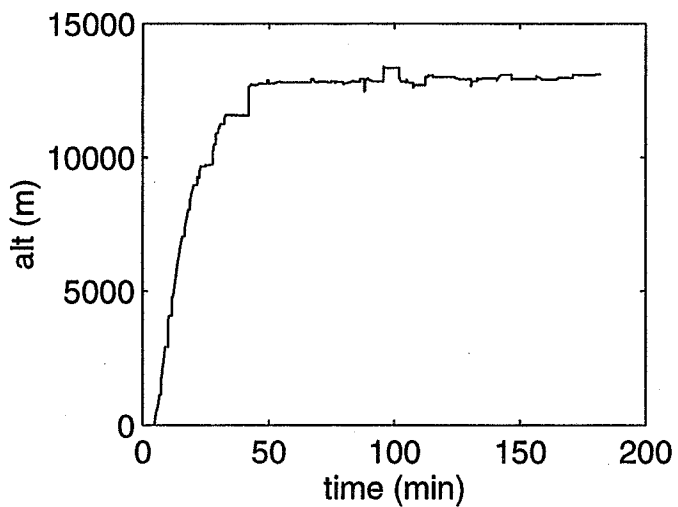
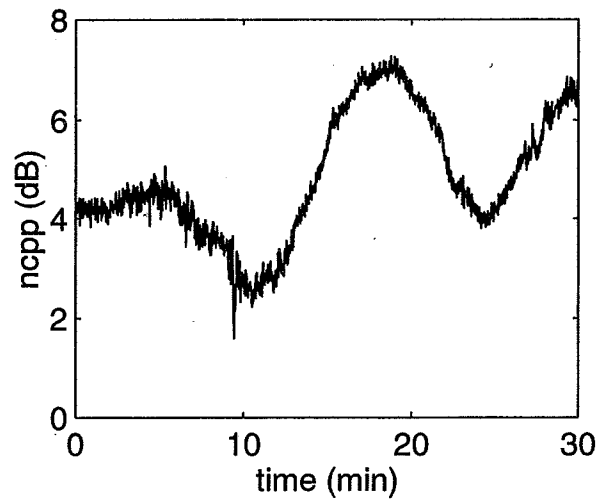
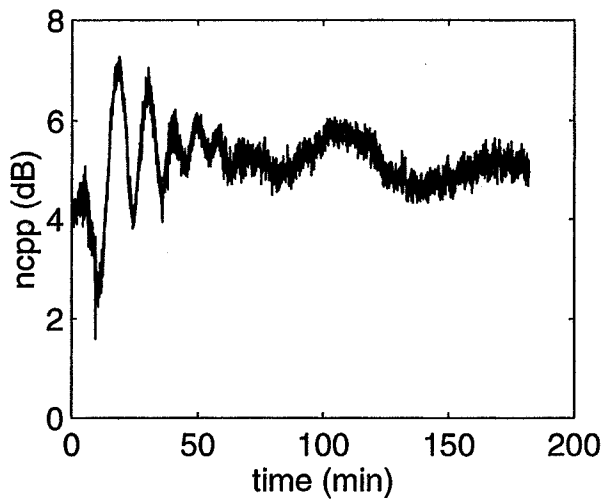
Cumulative Fade Distribution





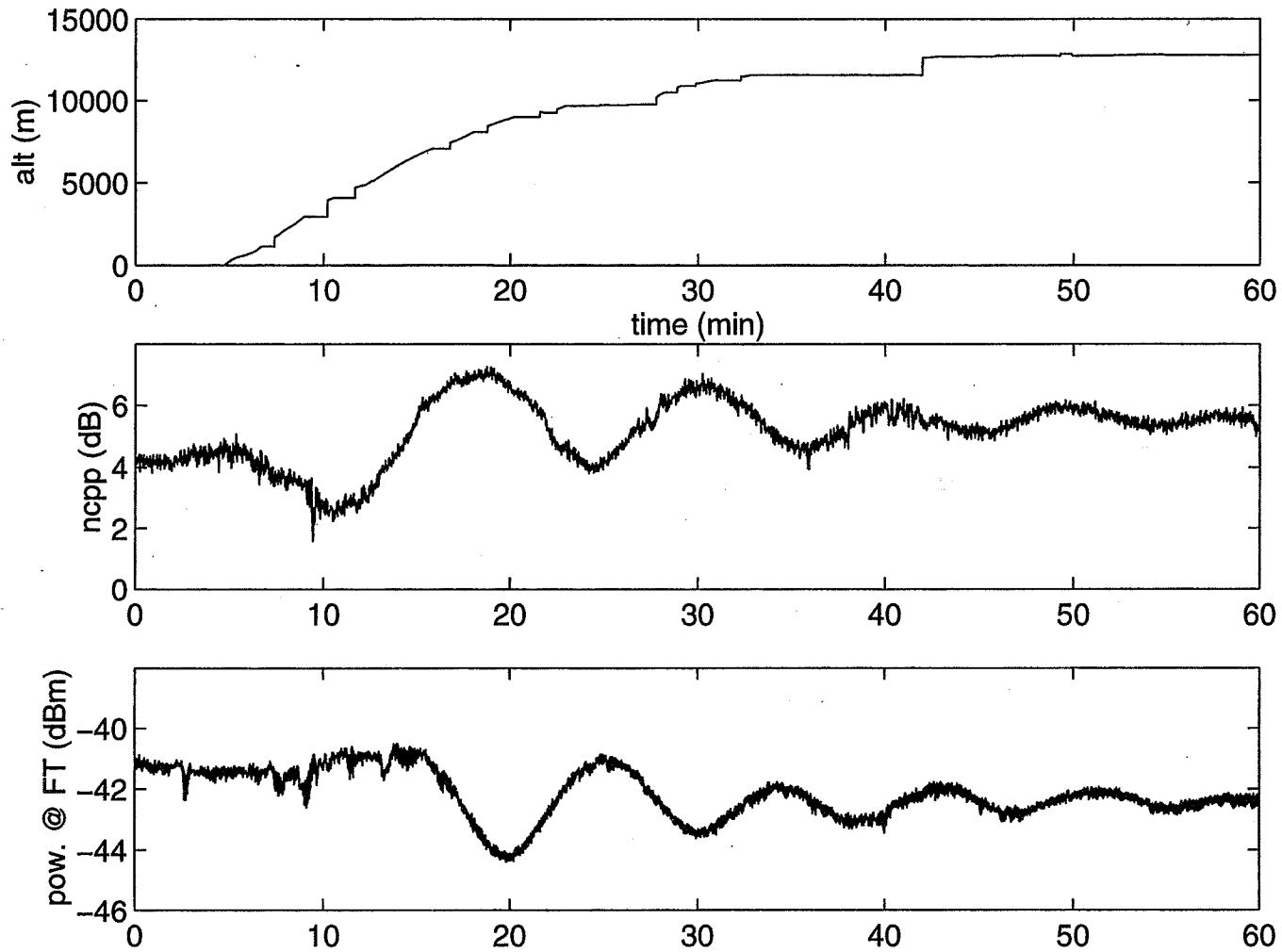
Noncoherent Pilot Power and Altitude for 12 October 1995 starting at 15:08:00

297



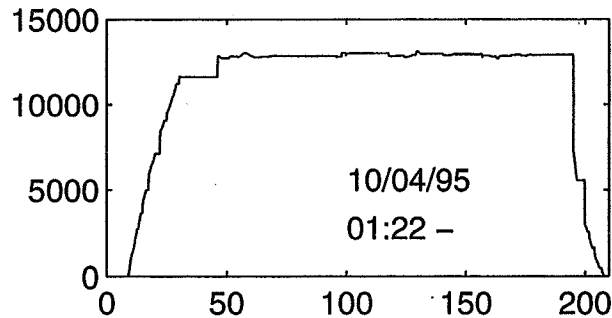
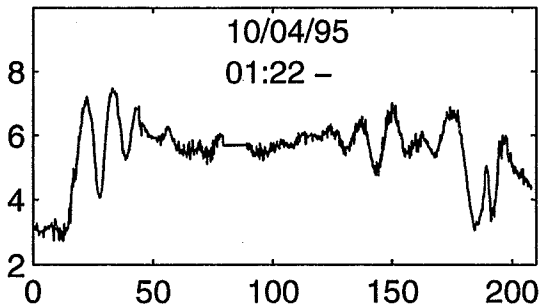
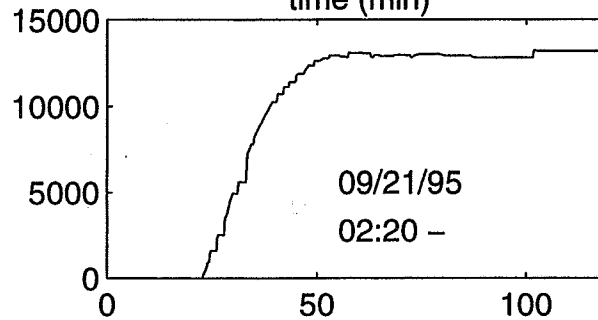
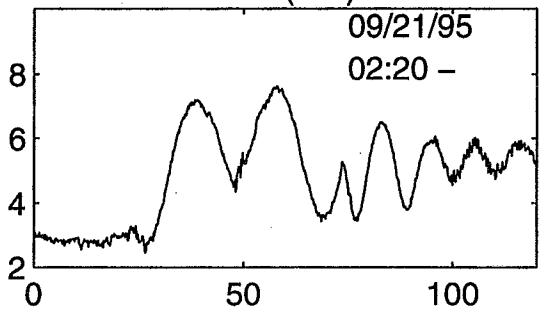
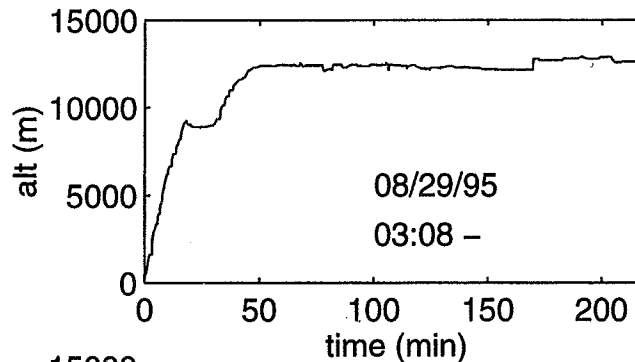
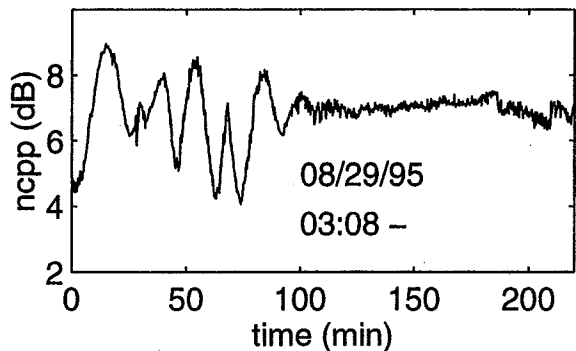


Altitude, Noncoherent Pilot Power and Received Power in the Data Channel at the FT
for 12 October 1995 starting at 15:08:00





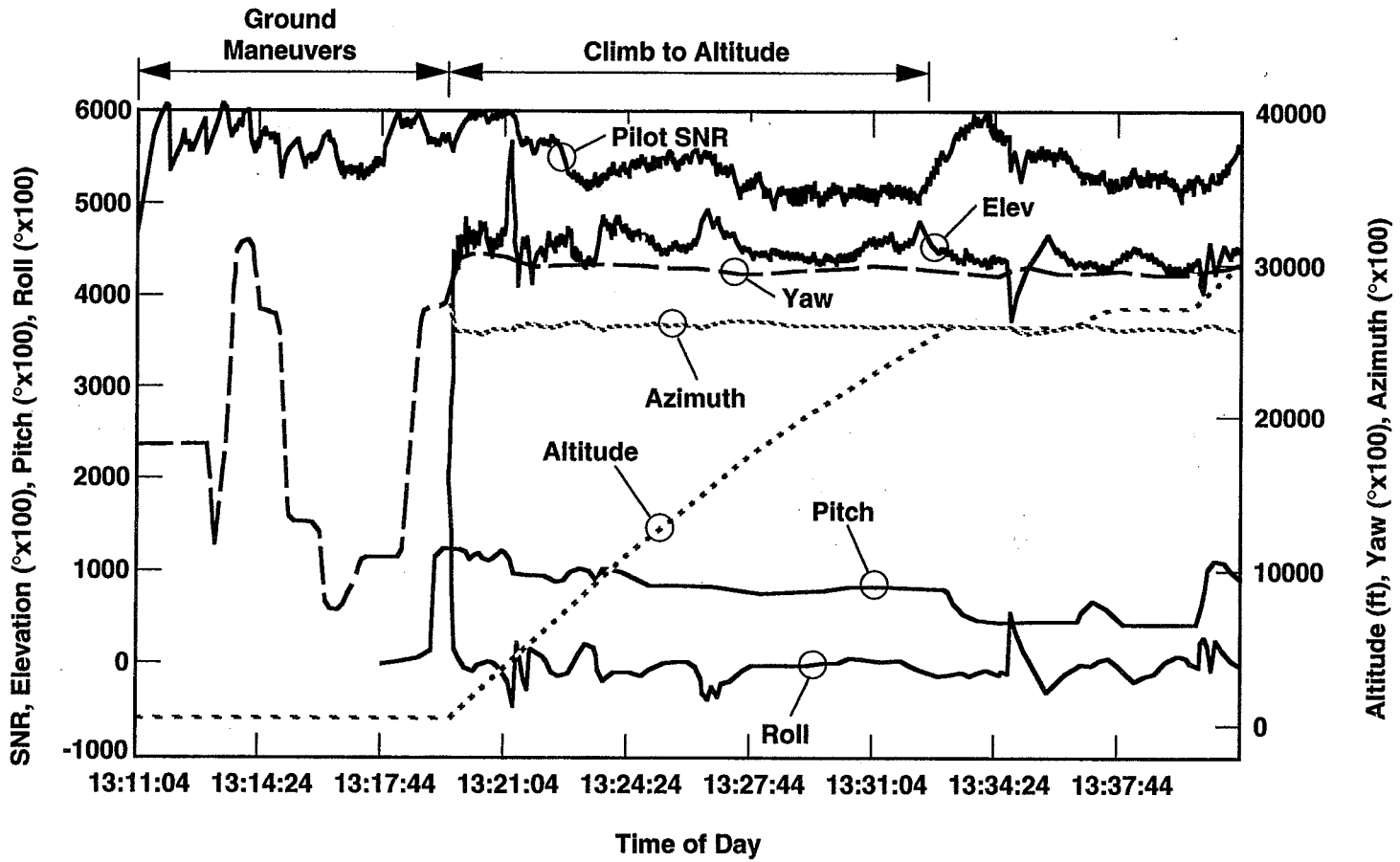
Noncoherent Pilot Power and Altitude for Various Days





Rockwell Sabreliner Flight Test Data for Take-off and Climb to Altitude

300





Preliminary Conclusions

- Received pilot power data characterized by slowly varying amplitude ($< \pm 2.5$ dB) during aircraft ascent/descent:
 - Antenna tracking does not "appear" to be the cause, but final determination can only be made after antenna pointing error data are extracted
 - Temperature-induced changes in Rx/Tx gain is a possibility
 - Atmospheric attenuation is not likely since a lot of the flights were conducted under clear sky conditions
 - Shadowing/scattering from the tail structure may contribute
 - ACTS steerable beam (SB) pointing does not appear to be the cause, e.g., on 10/12/95 the SB was initially pointed to Moffett Field and was incrementally moved about 6 steps every five minutes in an easterly direction in response to the GPS inputs -- similarly for the other days
 - Comparable variability in received pilot power is not observed on ascent in the Rockwell Saberliner data set - but aircraft is much smaller

- Received power in the data channel at the fixed ground terminal reveals similar variability
 - Changes in received power at the ground terminal during ascent are not synchronous with the changes in received pilot power at the aircraft but are of the same magnitude (lack of synchronicity possibly caused in part by the difference in propagation frequencies)
 - This variability in received power at the ground station is consistent with either temperature variations in Rx/Tx gain at the aircraft or propagation-related phenomena

- Over time scales < 10 min and at level altitude, pilot propagation can be characterized by LOS propagation with large Rician parameter (> 25 dB)

- Work is on-going to better understand this airborne propagation channel

Page intentionally left blank

Fade Measurements Into Buildings From 500 To 3000 MHz

Wolfhard J. Vogel and Geoffrey W. Torrence
Electrical Engineering Research Laboratory
The University of Texas at Austin
Austin, Texas 78758, USA

Abstract - Slant-path fade measurements from 500 to 3000 MHz were made into six different buildings employing a vector network analyzer, a tower-mounted transmitting antenna and an automatically positioned receiving antenna. The objective of the measurements was to provide information for satellite audio broadcasting and personal communications satellite design on the correlation of fading inside buildings. Fades were measured with 5 cm spatial separation and every 0.2% of the frequency. Median fades ranged from 10 to 20 dB in woodframe houses with metal roofs and walls without and with an aluminum heat-shield, respectively. The median decorrelation distance was from 0.5 to 1.1 m and was independent of frequency. The attenuation into the buildings increased only moderately with frequency in most of the buildings with a median slope of about 1 to 3 dB/GHz, but increased fastest in the least attenuating building with a slope of 5 dB/GHz. The median decorrelation bandwidth ranged from 1.2 to 3.8% of frequency in five of the buildings, and was largest in the least attenuating building, with 20.2% of frequency.

frequency structure of the satellite signal

Propagation measurements for slant-path into-building fading have previously been reported for the frequency range from 700 to 1800 MHz (swept) [1] and at 1.6 and 2.5 GHz (simultaneously) [2]. The latter measurements were made to provide guidance for the design of satellite telephony and paging systems using CDMA modulation and requiring power control, while the former were targeted towards the application of broadcasting from geostationary satellites. Each set of experiments used receiving antennas with reasonably realistic patterns, i.e., the dual frequency measurements employed azimuthally omnidirectional antennas interacting more fully with the multipath environment inside buildings than the relatively directive receiving antenna of the broadcast reception measurements. This experiment used one each wide-band transmit and receive antenna. Data were generated in the swept-cw mode, thus permitting a deterministic comparative assessment of the spatial and frequency structure of the received power levels over the frequency range from 500 to 3000 MHz.

I. INTRODUCTION

Slant path indoor fade data are needed to support the design of satellite services such as audio broadcasting, messaging, paging, and telephony with information about the temporal, spatial and

After describing the experimental setup and data acquisition procedures and locations, we present the results from our wideband swept into-building measurements in terms of the observed spatial and frequency characteristics and draw some conclusions.

Table 1: Building Names, Construction Details, and Elevation Angles.

Building Name	Approx. Year of Constr.	Wall Type	No. of Stories	Roof Type	Avg. Elev. (°)	Avg. Dist. (m)
Commons Entry	1987	concrete tilt wall	1	tar	18	16
EERL Office	1944	block brick	1	tar	38	8.8
Farmhouse	1880	wood frame	2	metal	33	19.2
House Hallway + LR	1976	wood frame	2	metal	41	12
MER Lobby	1992	glass, concrete	2	tar	26	8
Motel Room	1980	brick	2	compos.	37	16

II. EXPERIMENTAL SETUP

The major components for this experiment were a 20 m crank-up transmitter tower mounted to the top of a van, a vector network analyzer (VNA), a personal computer (PC) and a linear positioner. The "Device Under Test" in this case consisted of a pair of wide-band antennas and the intervening path. The measurement determined the path loss as a function of frequency and location. The PC controlled the VNA and linear positioner, and stored the data from the VNA.

The measurement strategy was to mount the transmitting antenna on the fully extended tower outside of the building to be tested. To establish a calibration, the receiving antenna first was positioned directly outside of the building, at a location without obstructions of the line-of-sight path, and both antennas were pointed at each other. Then one or more series of 16 sweeps were recorded, as the positioner was moving the receiving antenna in the direction of the transmitter in 5 cm steps between each sweep. This motion changed the multipath for each sweep. The smoothed average of the 16 unobstructed sweeps gives a very good estimate of the free space received power. For the measurements, the receiving antenna was moved inside, both antennas were re-pointed, and another series of 16 sweeps was taken. The fully extended positioner was then retracted and moved to place the antenna 5 cm past the last sweep's position, and another series of 16 sweeps was taken. This was repeated as often as the size of the building under test allowed. Each set of 16 sweeps took about half an hour, with measurements in a large building taking many hours to complete. To make the measurements repeatable over a long duration, the tower was held rigid with guy wires.

Calibrations were repeatable to < 1 dB inside the 700-2500 MHz range and < 2 dB outside of it. In the absence of interference there was about 1 dB uncertainty due to thermal noise at 40 dB loss up to 2 GHz, falling to 30 dB at 2.5 GHz, and only about 20 dB at 3 GHz. In the city, when near cellular phone towers, interference added about 1 dB uncertainty at 30 dB loss and rapidly worsens below 900 MHz and above 2.5 GHz. However, this is for outdoors reception; for measurements inside buildings the interfering signals were attenuated as were the measurement signal, and therefore had only a small effect.

III. MEASUREMENT DETAILS

Measurements were made into six different buildings. Pertinent details are summarized in Table 1. All buildings were in the far-field of the transmitting antenna. A picture of the farmhouse, a sketch detailing the locations of walls, windows, and doors and the transmitter tower is shown in Figure 1. The measurement tracks are designated by dashed lines and the positioner locations for each series of 16 sweeps are numbered. Although the transmitting antenna has large beamwidth, it was re-pointed repeatedly (by remote control) to track the moving receiver direction to within $\pm 10^\circ$. The measurements were performed in dry weather.

IV. RESULTS

A. Time Variability

Previous experiments [1,2] have demonstrated conclusively that as long as the transmitting antenna and the receiving antenna are held stable, the time variability of transmissions into a building is very small, i.e., time variations are due to spatial variations converted to time variations by motion. In this new measurement campaign, therefore, no new time variability data were obtained.

B. Space Variability

Average signal levels over the entire 500 to 3000 MHz band were calculated for each receiver position. The results are summarized in Figure 2 by a box and whisker plot, which shows the mean, ± 1 , and ± 1.96 standard deviation with respect to position in each of the six buildings. The building with the best radio frequency penetration was the Farmhouse (median = -5 dB), the worst was the House (median = -19.5 dB). Both have metal roofs, but the House also has an aluminum heat shield in all exterior walls. The other buildings fell into the range of -9 dB to -13 dB. Note that these data include some positions for which the receiving antenna was located in an open door or window in sight of the transmitter.

Examples of the signal level as a function of position at four frequencies (1023, 1463, 2093, 2992 MHz) for the Motel have been plotted in Figure 3. At measurement sites where the receiving antenna was moved towards an open door or window, a dramatic increase of received power can be observed as the antenna comes within the view of the transmitter. In the Motel, for instance, the signal is 15 to 30 dB below the line-of-sight level while the direct path penetrates the wall. It increases

to near 0 dB as the antenna moves through the open door. The levels inside the House, with 25 to 45 dB below the line-of-sight, were the lowest of all the buildings measured, probably because its construction includes a metal roof and a tight energy-conserving aluminum heat shield under the cedar exterior.

To quantify the spatial variability of the signal level, autocorrelations were calculated at all 897 sample frequencies for lags from 0 to 3.2 m. Figure 4 is an example of the spatial autocorrelation vs. frequency for EERL at a lag of 50 cm, where the median value of the correlation has decreased to 1/e (37%). Contrary to intuition, the overall data do not exhibit a clear frequency dependence. One would expect that the spatial autocorrelation in a strong

Table 2: Spatial Decorrelation Distance

Building Name	Median Decorrelation Distance (m)
Commons Entry	1.1
EERL Office	0.5
Farmhouse	0.85
House Hall + LR	0.55
MER Lobby	0.7
Motel Room	0.55

multipath environment decreases twice as fast at 3000 MHz than at 1500 MHz, because the wavelength at 1500 MHz is 20 cm compared to 10 cm at 3000 MHz. One reason for this may be the 15 cm diameter aperture size of the antenna.

The decrease of the autocorrelation with distance at 1625 MHz has been plotted in Figure 5 for the House, MER, and the Motel. The slowest decrease was observed in the Commons, with a decorrelation distance of 1.1 m. The other buildings had more rapidly decreasing autocorrelation, with decorrelation distances from 0.85 to 0.5 m. Table 2 summarizes these results.

A normal probability plot of the autocorrelation at lag L , the median decorrelation distance for each building, has been plotted in Figure 6. A straight line in this graph would indicate a normal distribution. None of the curves represent a normal distribution, but the graph illustrates the variability of the decorrelation distance with frequency.

C. Frequency Variability

Figure 7 is an example of the signal level changes with frequency. The 8th sweep of the first series of 16 sweeps was plotted. Generally, variations with frequency are quite rapid, as would

be expected in a multipath environment. The slowest changes were observed in the Farmhouse, and it also exhibited the most decrease in level from the low to the high end of the band. A typical example of the frequency dependence of building penetration is depicted in Figure 8 for the Farmhouse, where the level decreased by 6 dB/GHz. The signal level slope, in dB/MHz, has been calculated for each sweep and the results are summarized in Figure 9 by a box and whisker plot, which shows the mean, ± 1 , and ± 1.96 standard deviation with respect to slope in each of the six buildings. The largest slopes were found in the Farmhouse. The least slope was measured at MER. This building has a glass curtain wall. The glass used for this building is energy-conserving, i.e., it reflects at RF. It is well known that the transmission through glass depends on the surface resistivity of its metallic coating and is not a function of frequency.

The autocorrelation of frequency variability reveals information about the utility of rake receivers to mitigate fading and the possibility of power control on the up-link (mobile to satellite) at one frequency using knowledge of the fade on the down-link (satellite to mobile) at another frequency. An example of the autocorrelation at a given receiver location is plotted for each building in Figure 10. In five of six buildings the decorrelation bandwidth ranges from about 1% to 4% of the frequency. Noticeably slower decorrelation occurs in the Farmhouse with a decorrelation bandwidth of about 12%. Table 3 summarizes the frequency decorrelation results.

A normal probability plot of the autocorrelation at lag L , the median decorrelation bandwidth for each building, has been plotted in Figure 11. A straight line in this graph would indicate a normal distribution. None of the curves represent a normal distribution, but the graph illustrates the variability of the decorrelation bandwidth with position.

V. CONCLUSIONS

We have observed the space and frequency

Table 3: Decorrelation Bandwidth

Building Name	Median Decorrelation Bandwidth (% frequency)
Commons Entry	2.0
EERL Office	3.6
Farmhouse	20.2
House Hallway + LR	1.6
MER Lobby	1.2
Motel Room	3.8

domain structures of simulated satellite signals from 500 to 3000 MHz propagated into six buildings on a slant path. Our findings are:

1. The attenuation of slant-path microwaves transmitted into buildings depends on the type of construction; the best (10 dB median) and worst (20 dB median) cases were woodframe houses with metal roofs and walls without and with an aluminum heat-shield, respectively (Fig. 2).
2. Attenuation was greater when the line-of-sight was obstructed by a concrete wall than by window glass, for instance.
3. The median decorrelation distance ranged from 0.5 to 1.1 m (Fig. 6) and was not dependent on frequency (Fig. 4).
4. The attenuation into the buildings increased only moderately with frequency in four of the buildings with a mean slope of about 1 to 3 dB/GHz, but increased fastest in the least attenuating building with a mean slope of 6

dB/GHz. The mean slope was near zero for the glass-walled MER building.

5. The median decorrelation bandwidth ranged from 1.2 to 3.8% of frequency in five of the buildings, and was largest in the Farmhouse, with 20.2% of frequency.

ACKNOWLEDGMENT

This effort was supported by JPL under Contract JPL 956520.

REFERENCES

- [1] Vogel, W. J. and G. W. Torrence, "Propagation Measurements for Satellite Radio Reception Inside Buildings," *IEEE Transactions on Antennas and Propagation*, Vol. 41, No. 7, pp. 954-961, July 1993
- [2] Vogel, W. J., G. W. Torrence, and H.-P. Lin, "Slant-Path Building Penetration Measurements at L- and S-Band," *Electrical Engineering Research Laboratory Report*, EERL-95-301, 23 March 1995



Fig. 1a: The Farmhouse, now with a sheet-metal roof.

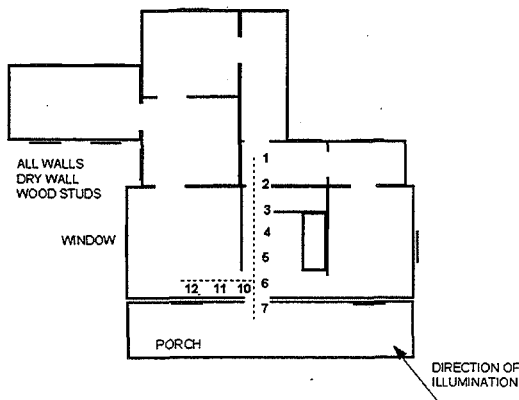


Fig. 1b: Floorplan of the measurement locations in the Farmhouse.

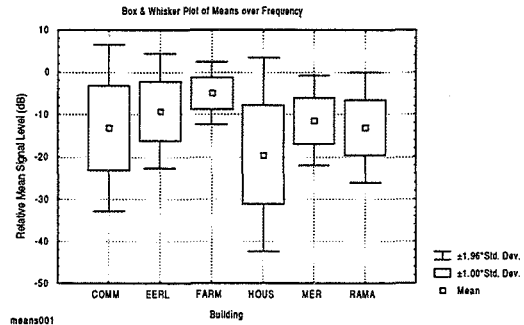


Fig. 2: Box and whisker plot for the distribution of the mean signal levels with respect to frequency.

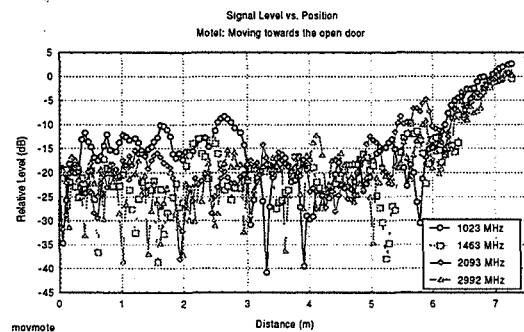


Fig. 3: The relative signal level vs. position at four frequencies in the Motel.

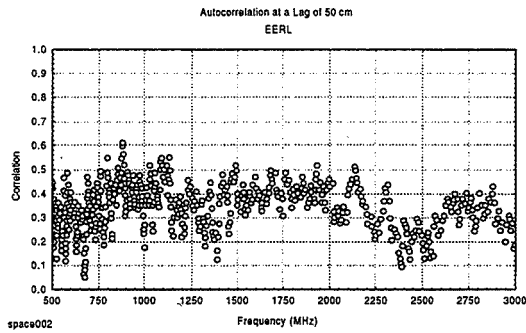


Fig. 4: Spatial autocorrelation at a lag of 50 cm in EERL.

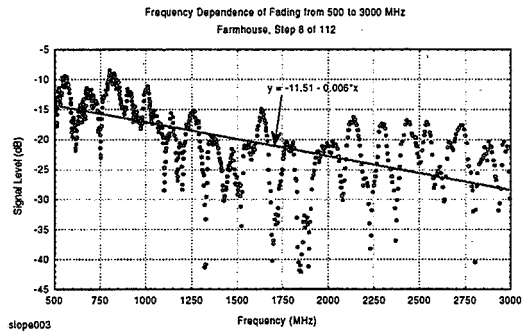


Fig. 8: Frequency dependence of fading from 500 to 3000 MHz in the Farmhouse.

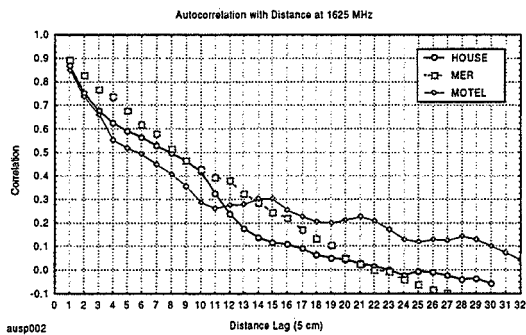


Fig. 5: The spatial autocorrelation vs. distance lag in the House, MER, and the Motel.

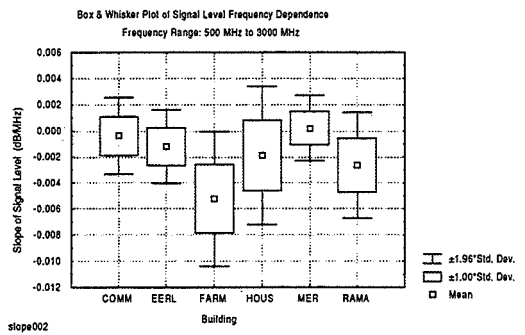


Fig. 9: Box and whisker plot of the signal level slope with frequency in the six buildings.

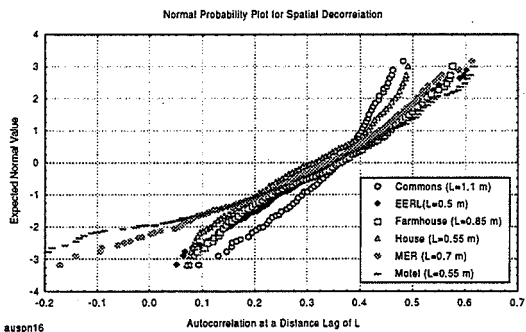


Fig. 6: A normal probability plot for the spatial autocorrelation at the decorrelation distance in the six buildings.

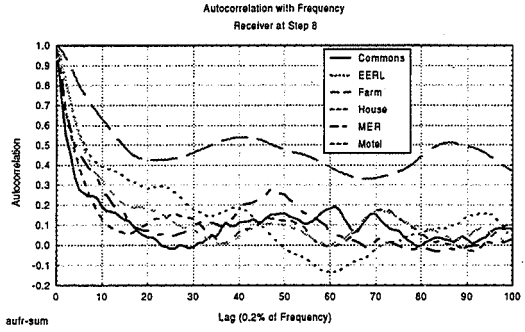


Fig. 10: The frequency autocorrelation in each building at Step 8 for lags from 0 to 20% of the frequency.

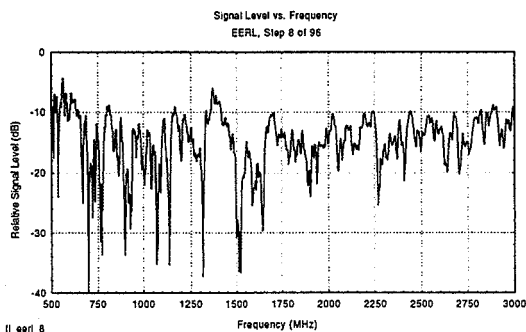


Fig. 7: Signal level vs. frequency in EERL.

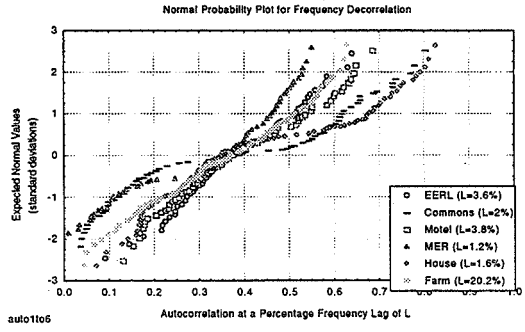


Fig. 11: Frequency autocorrelation at the decorrelation bandwidth in the six buildings.

Page intentionally left blank

NAPEX XX

SESSION 3
PROPAGATION RESEARCH TOPICS

C. Mayer (U. Alaska)

Page intentionally left blank

TDRS Space-to-Ground Link Weather Events

Stephen Horan

Klipsch School of Electrical and Computer Engineering

New Mexico State University

Las Cruces, NM 88003

shoran@nmsu.edu

June 1, 1996

1995 Comparison With White Sands Complex Data

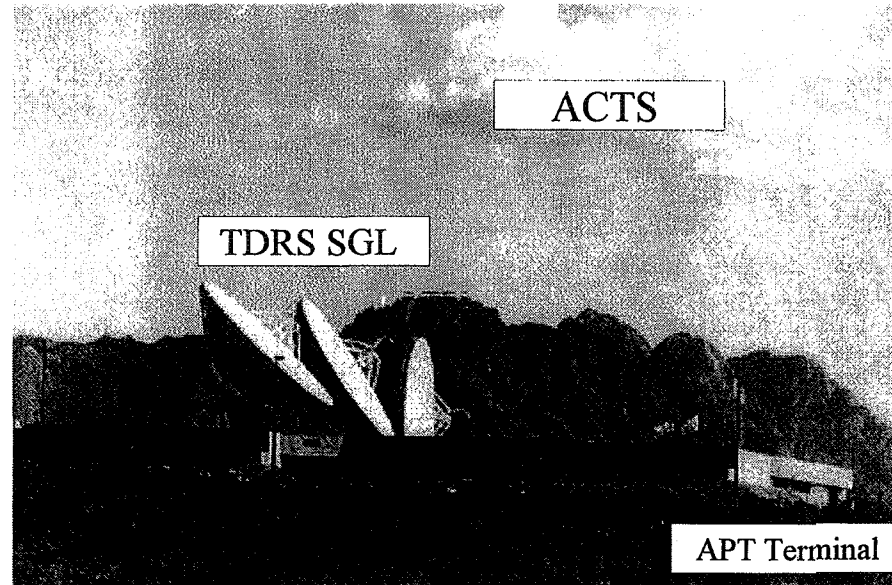


Figure 1 - APT Location at the WSC.

Differences from 1994 WSC Data Collection to the 1995 Data Collection

1. 1995 collection only at the STGT (Danzante)
2. APT and TDRS SGL antennas are within about ½ mile - APT to 1994 collection antenna approximately 3 miles
3. WSC measurements based on the AGC voltage (millivolts) readings from the TDRS SGL antenna system and not a separate system as in the Raindence data reported for 1994
4. Data from TDRS East (TDE) and TDRS West (TDW) provided; no data from spare satellites

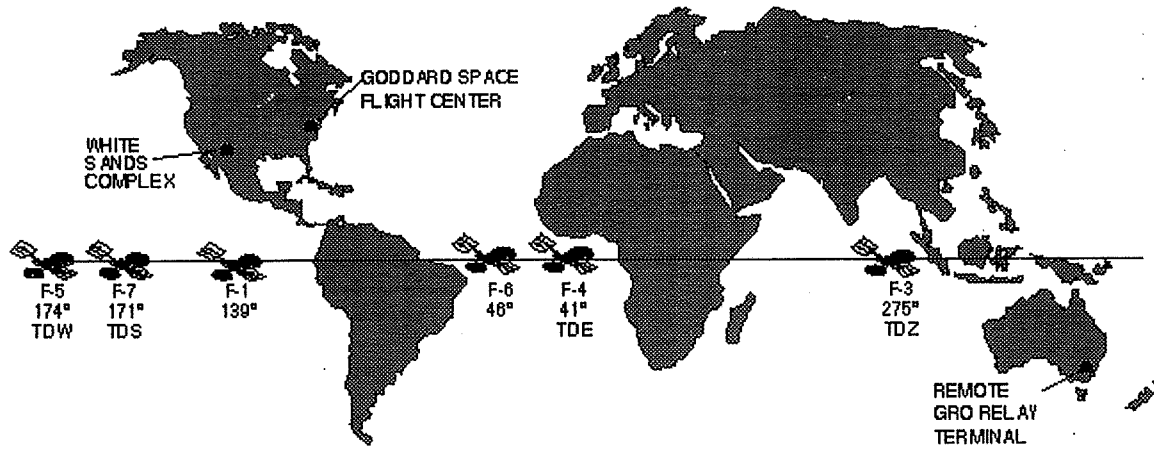


Figure 2 - TDRS Constellation

Satellites			
Spacecraft	Apparent Azimuth Angle	Apparent Elevation Angle	Operating Frequency
TDRS East	103	12	13.7 GHz
TDRS West	257	11	13.7 GHz
ACTS	168	51	20/27 GHz

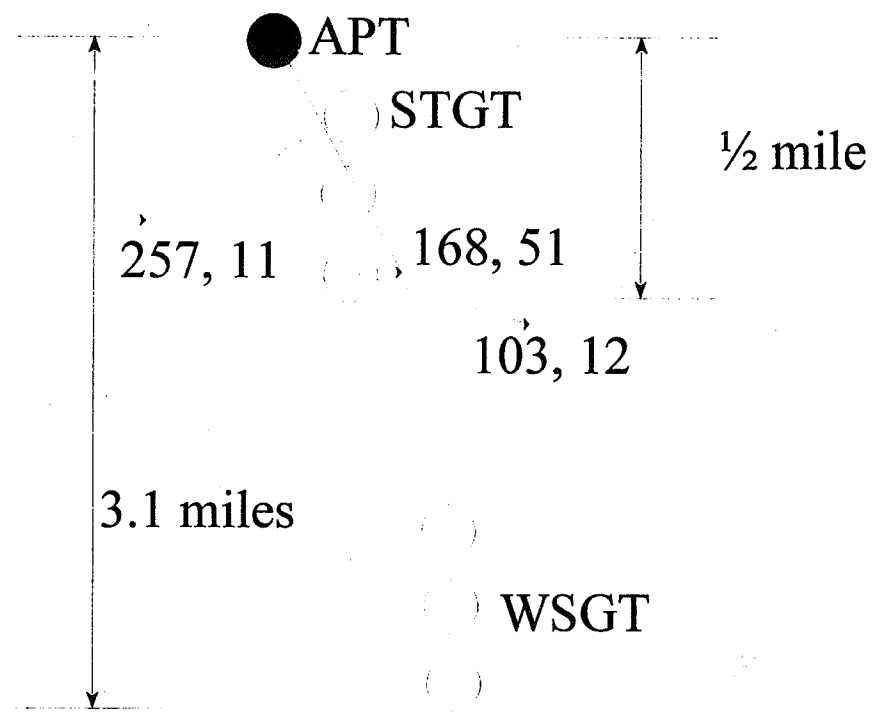
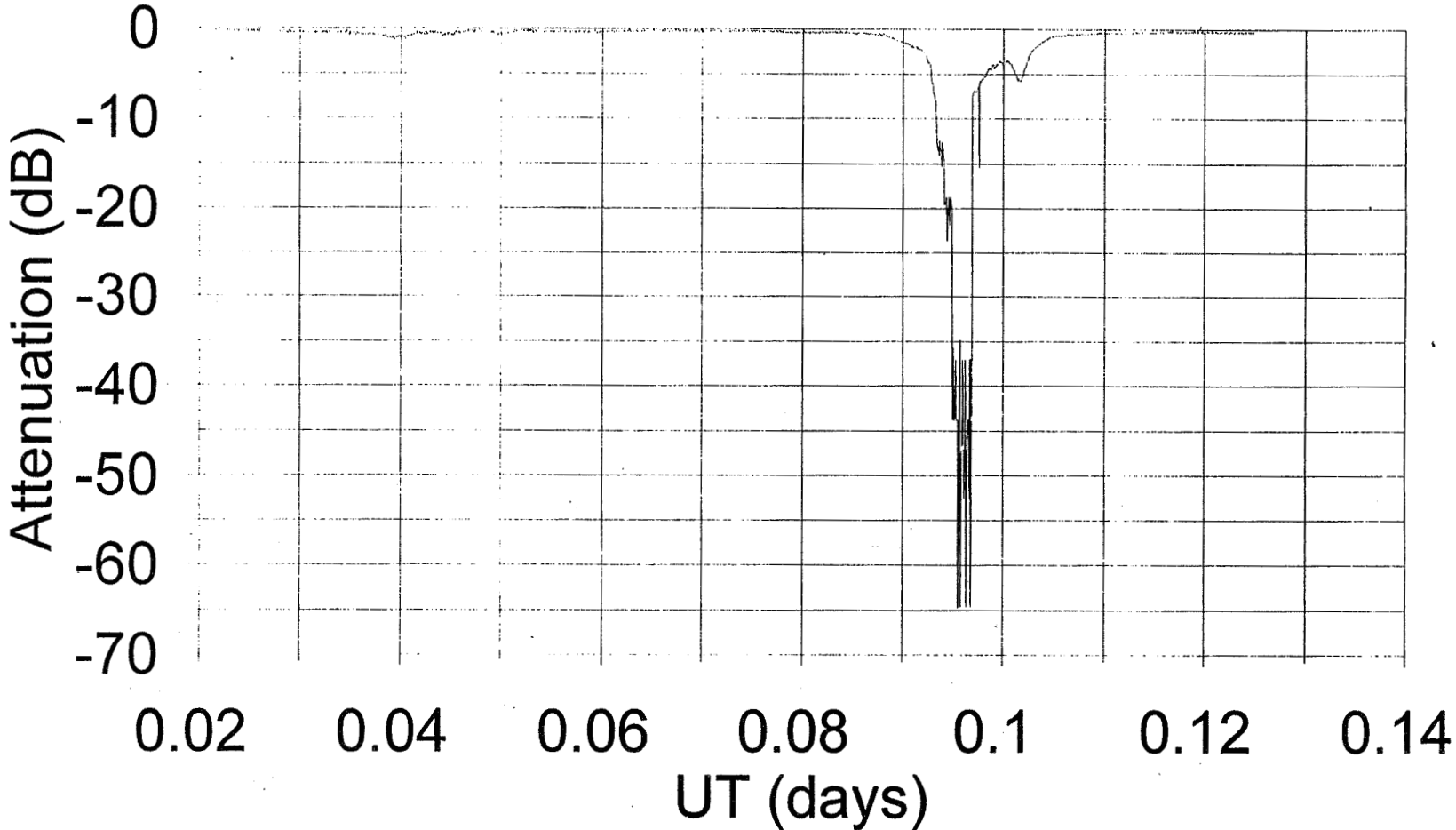
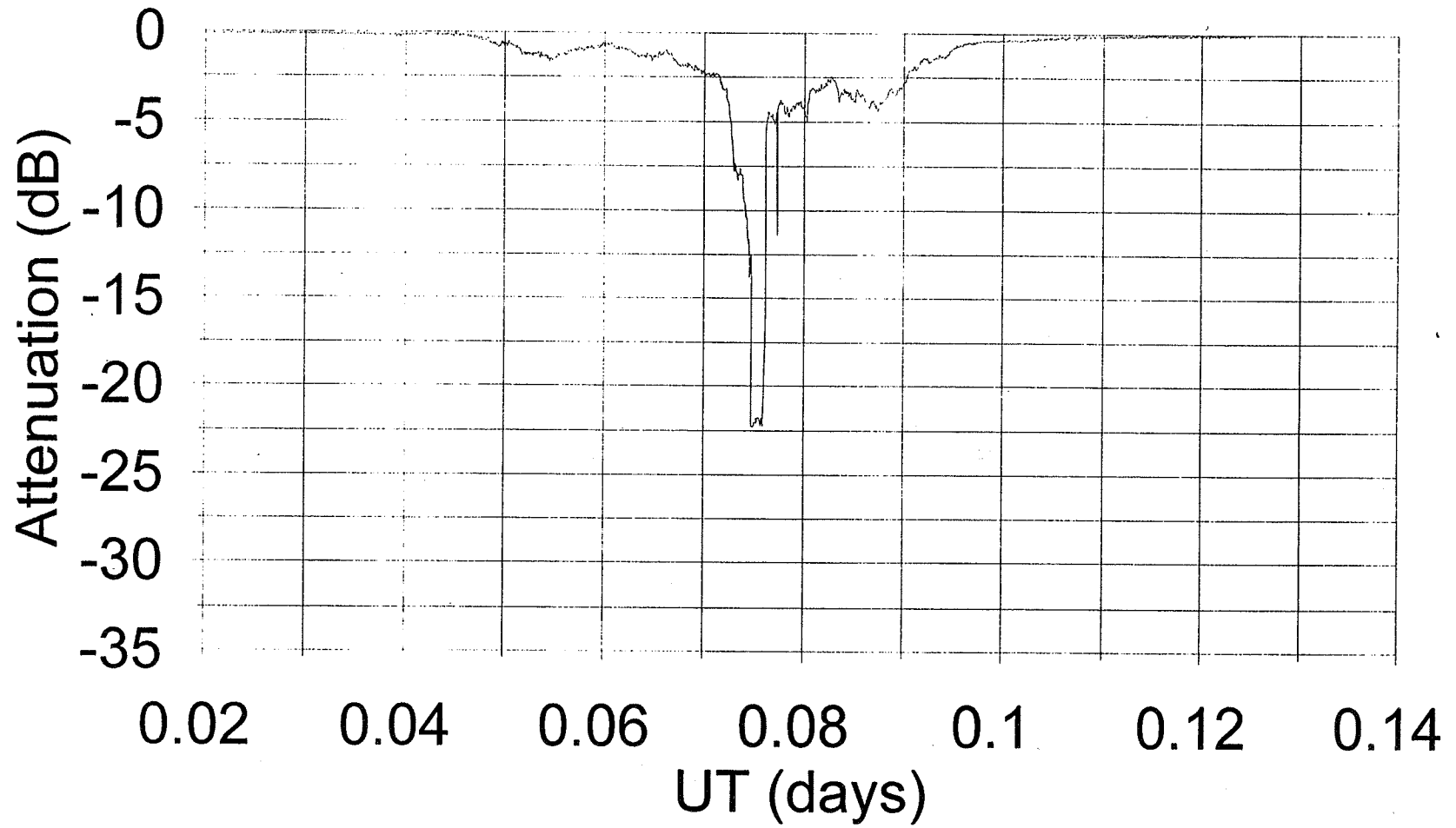


Figure 3 - Pointing Angles (Az, El) from data collection sites to the satellites.

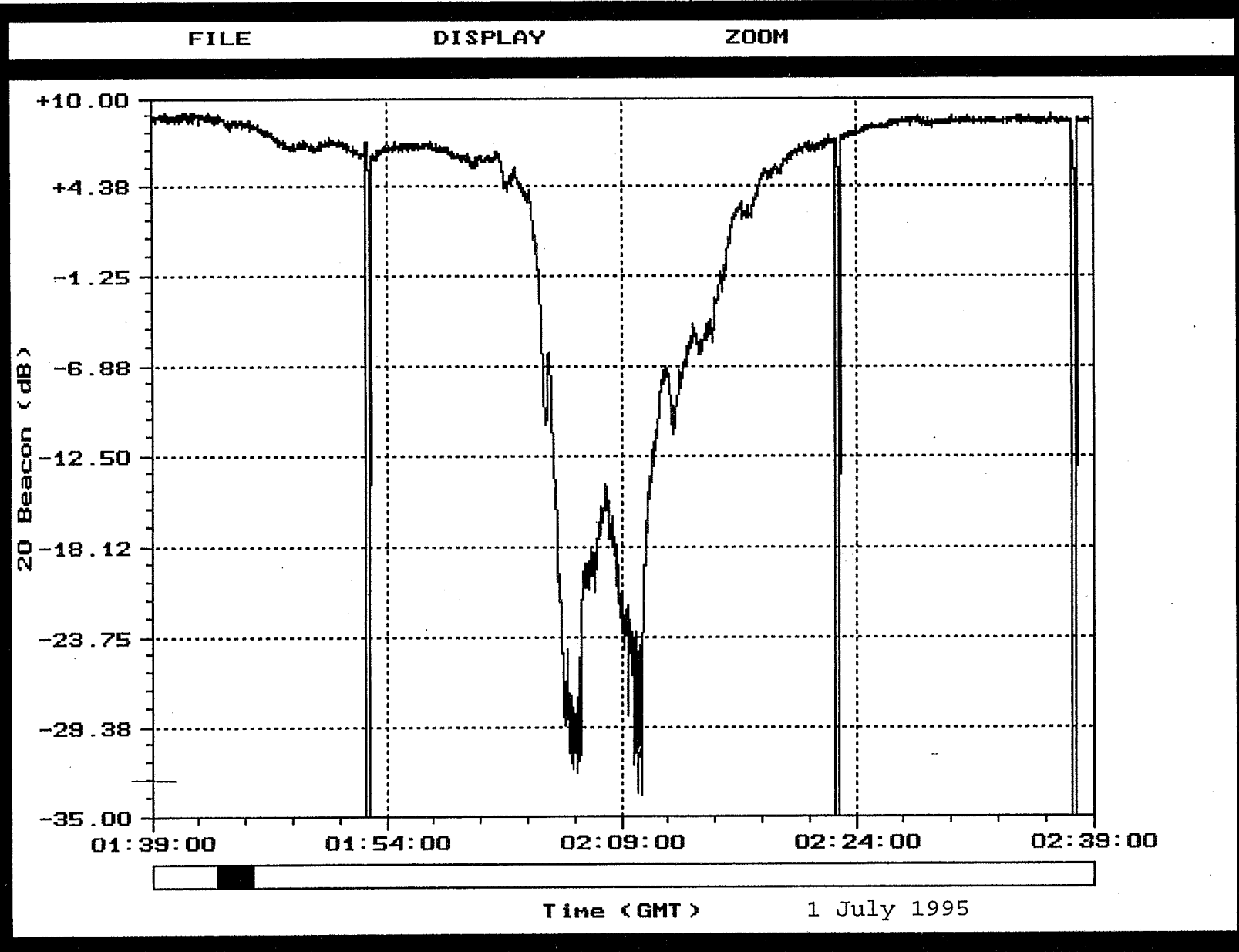
01-Jul-95
TDRS East

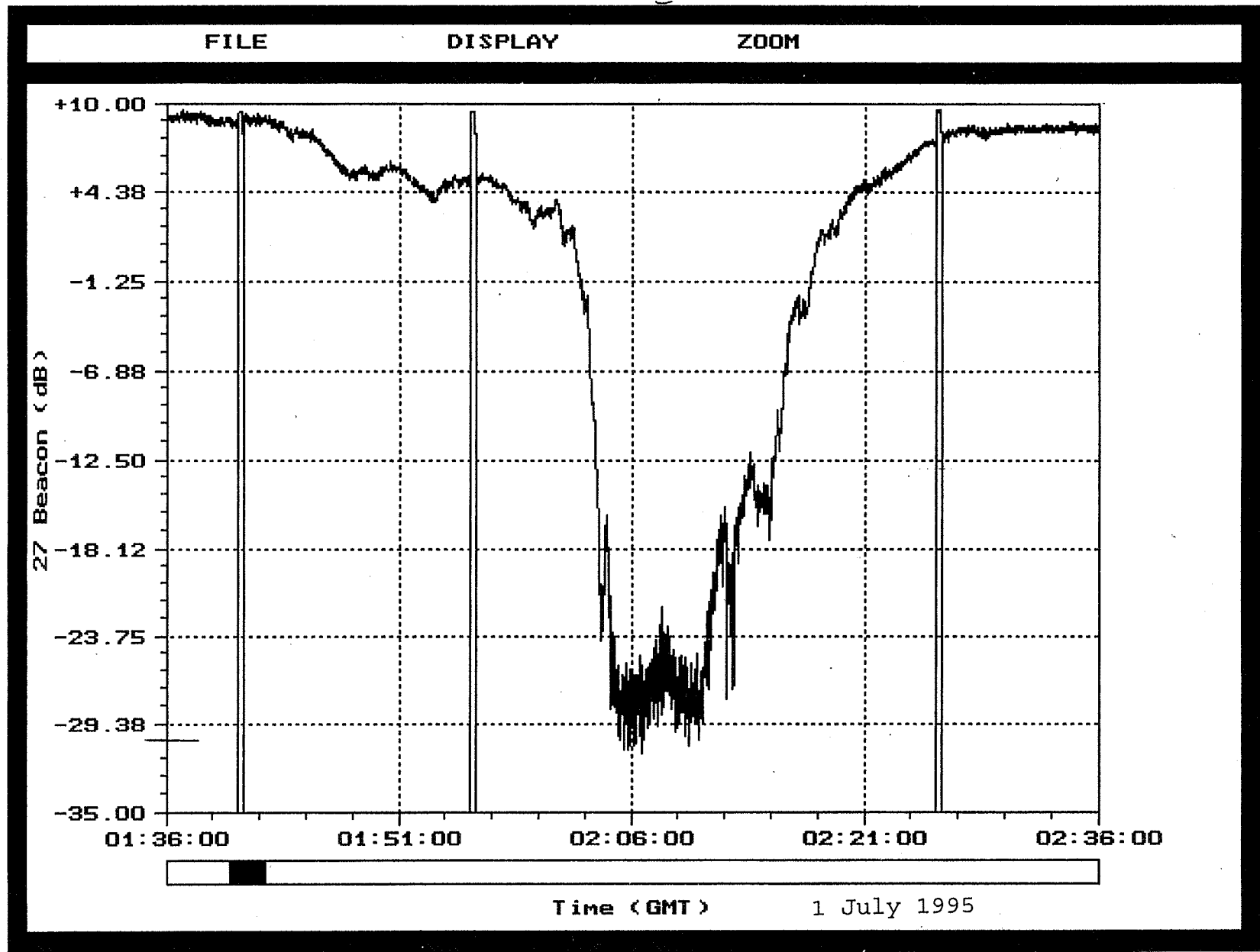


01-Jul-95
TDRS West



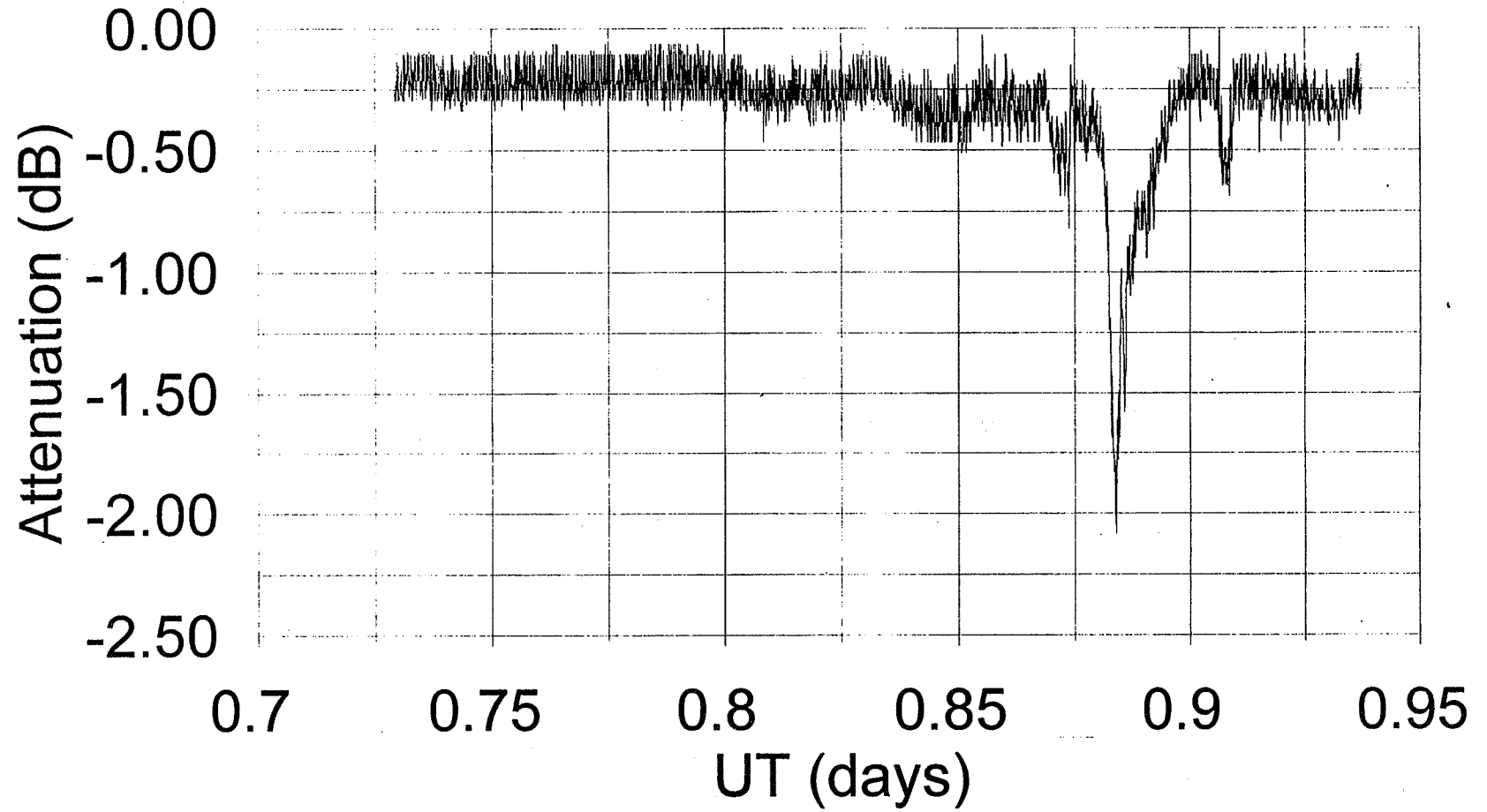
317



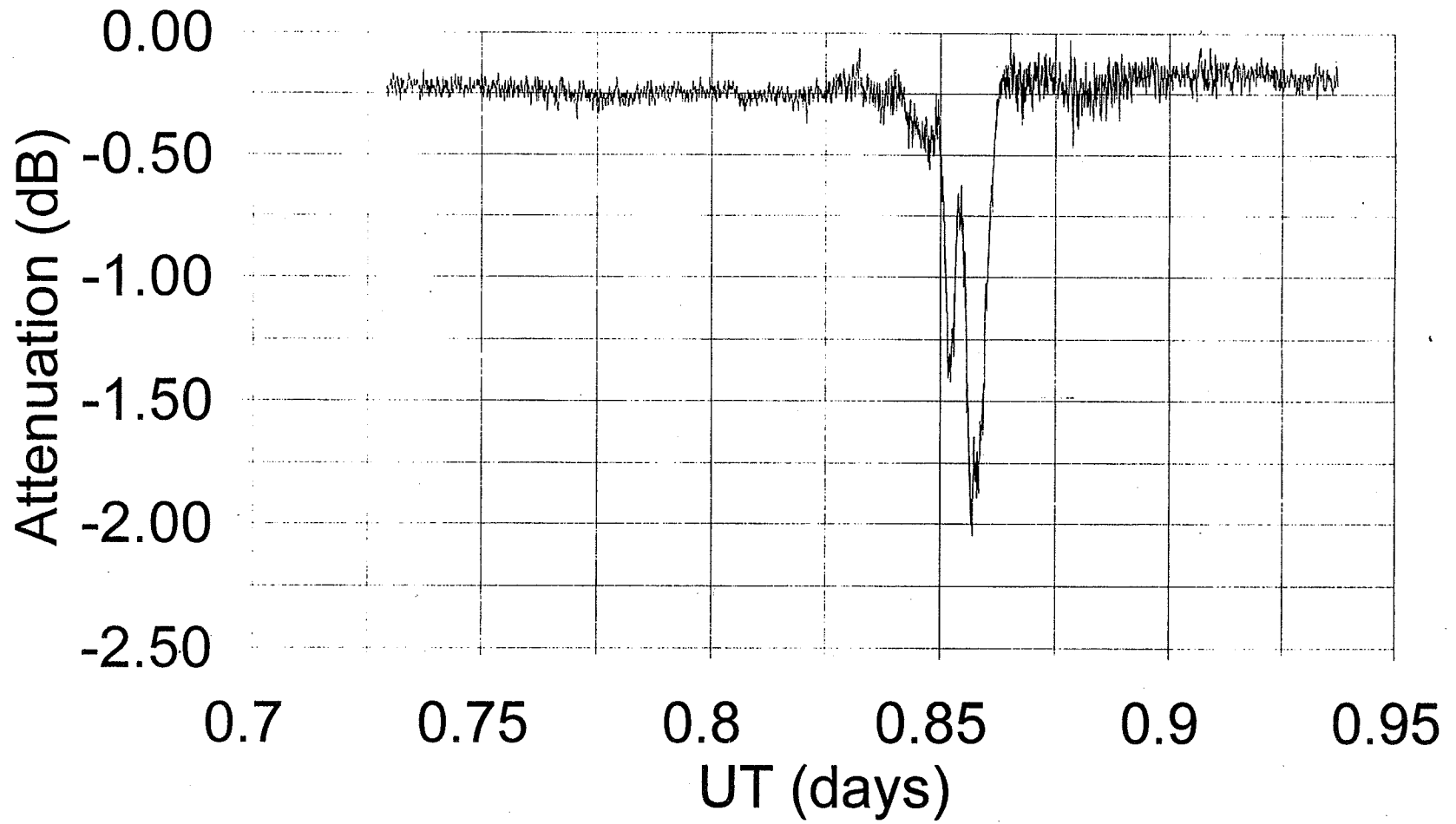


17-Jul-95

TDRS East



17-Jul-95
TDRS West

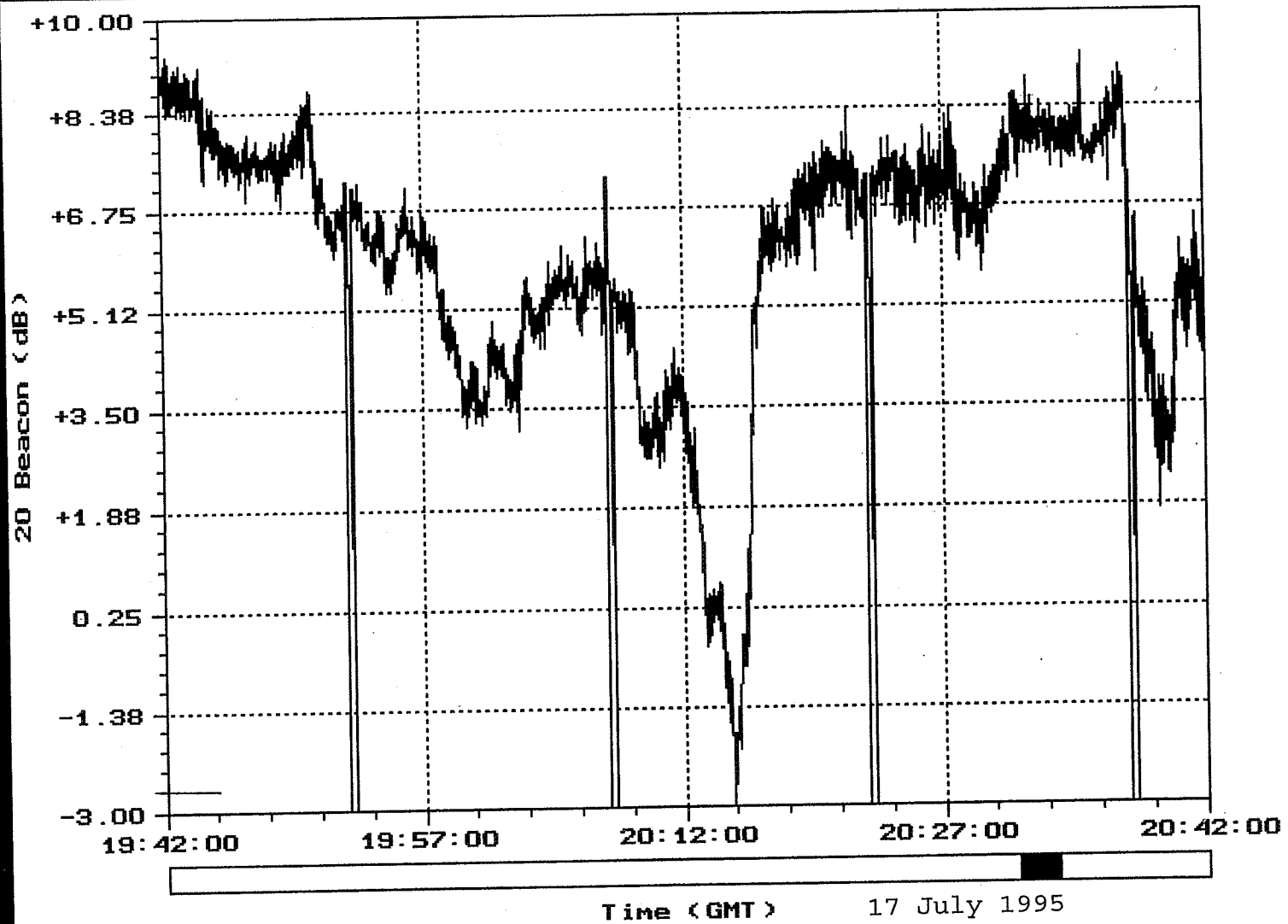


320

FILE

DISPLAY

ZOOM

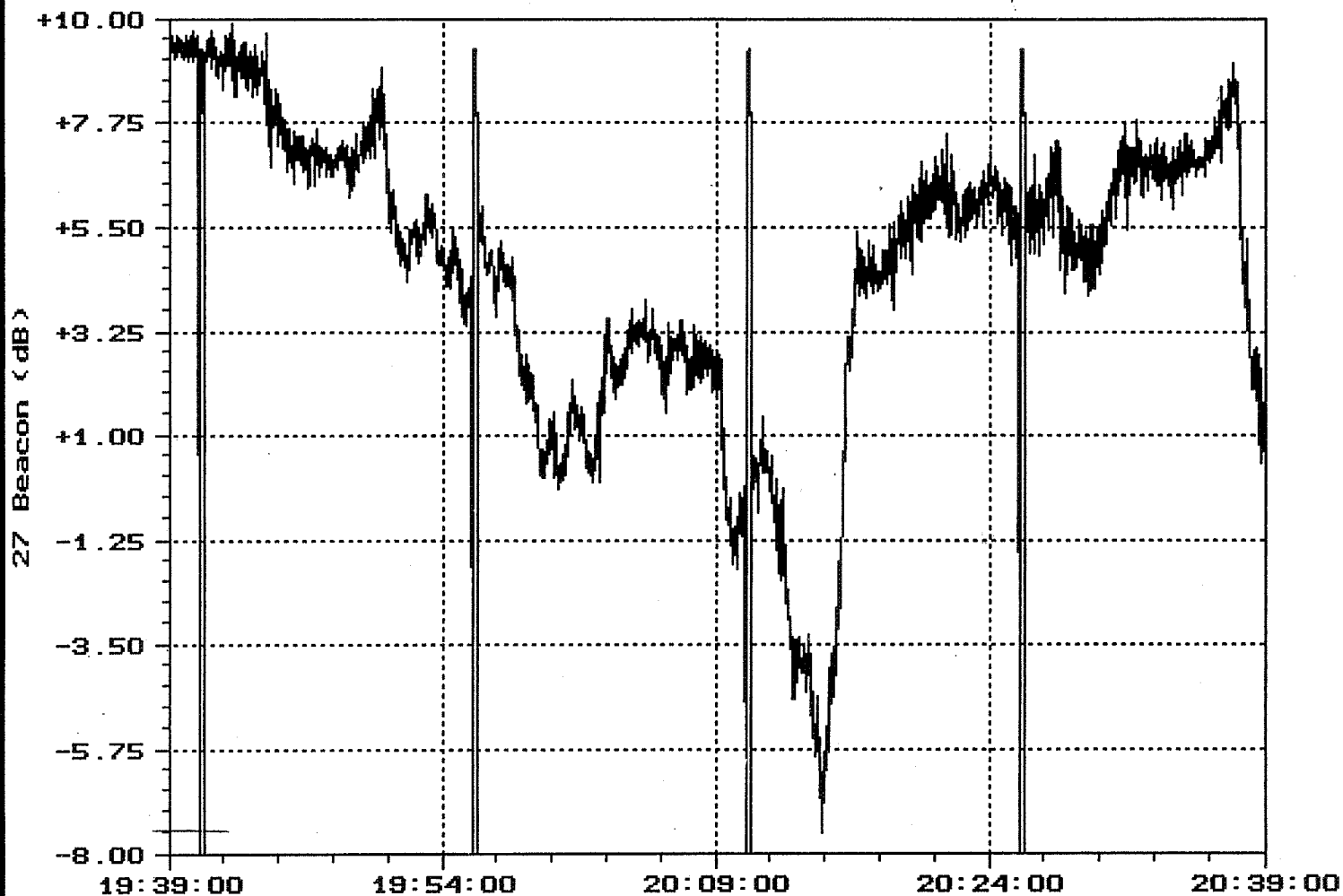


321

FILE

DISPLAY

ZOOM



Time (GMT)

17 July 1995

TDRS SGL Attenuation Measurements (January - August 1995)		
	Satellite	
Parameter	TDRS East	TDRS West
Measured Peak Attenuation	44 dB	22 dB
Date	1-Jul-95	1-Jul-95
Minutes > 1 dB	212	181
Minutes > 3 dB	73	55
Minutes > 10 dB	5	4

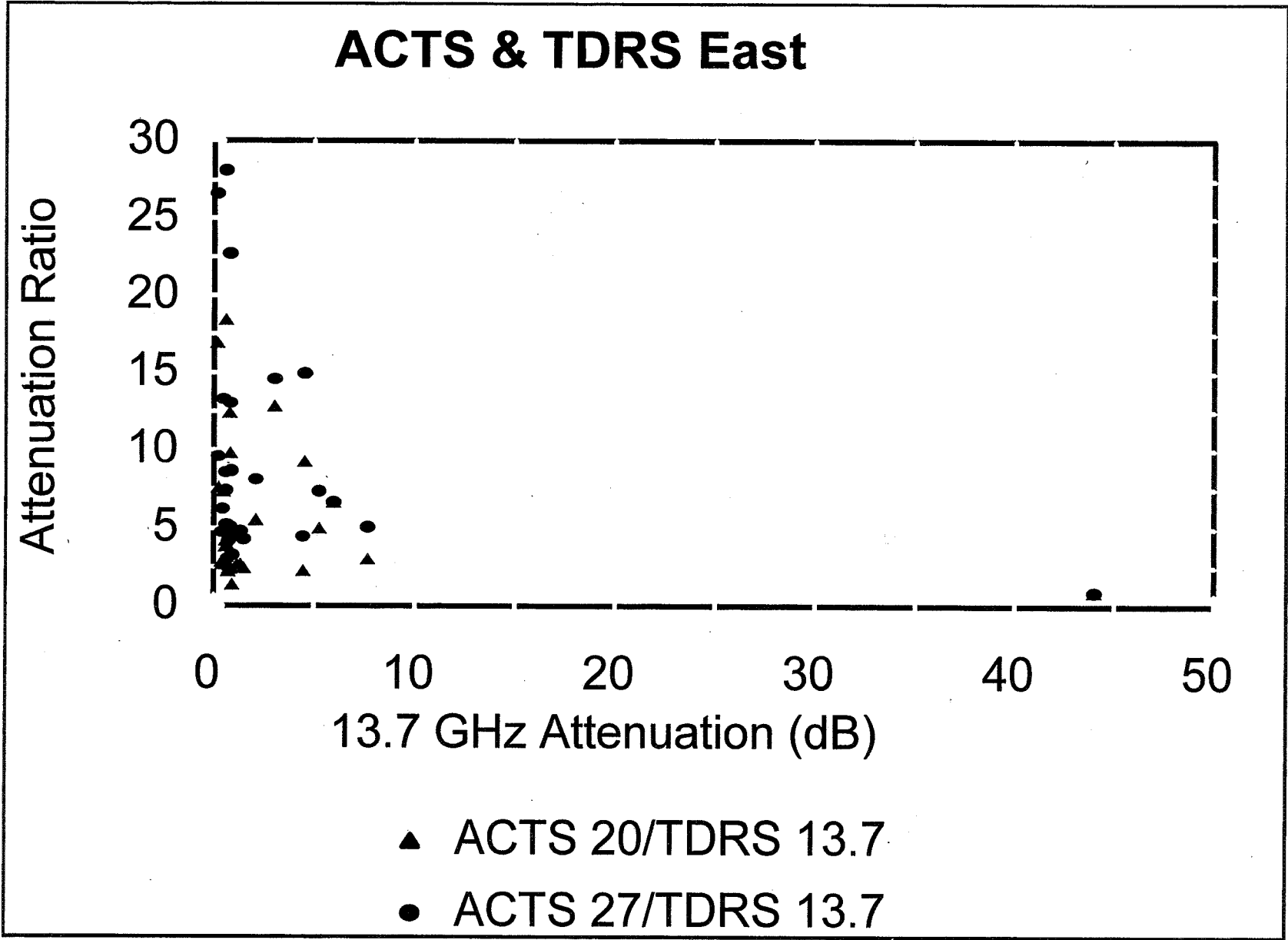


Figure 4 - Attenuation Ratios between ACTS and TDRS SGL

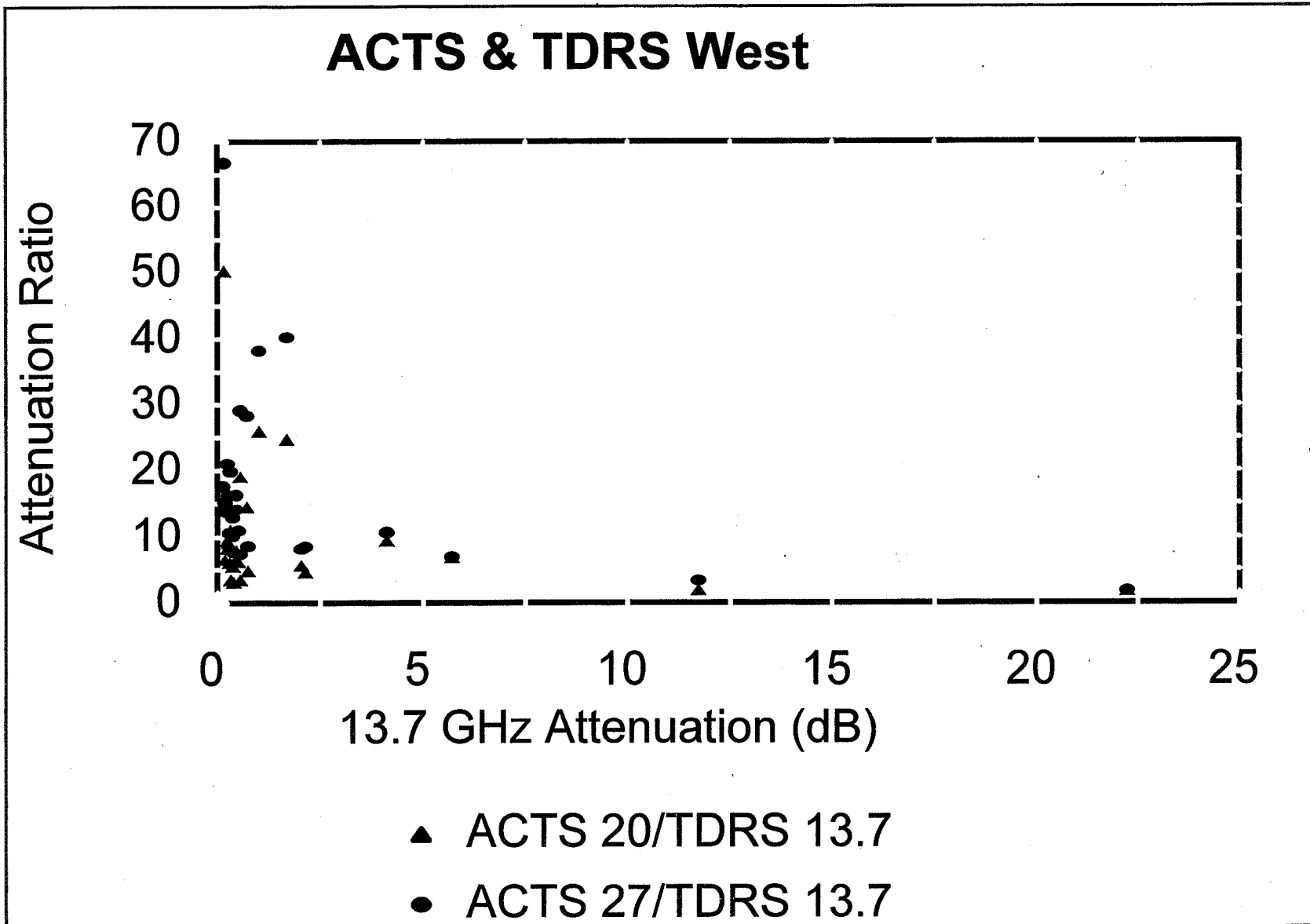
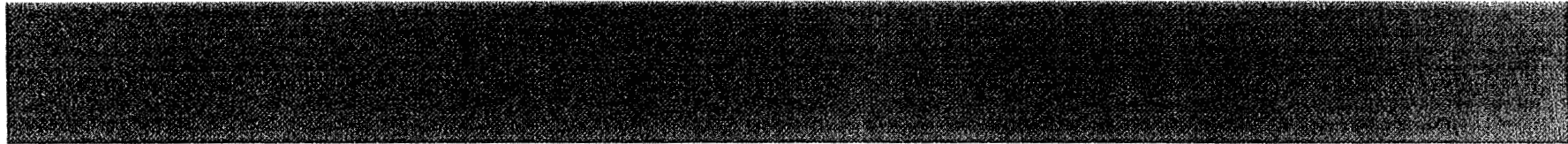


Figure 5 - Attenuation Ratios between ACTS and TDRS SGL

Page intentionally left blank

Atmospheric Visibility Monitoring
(AVM) Program



327



**Muthu Jeganathan and
Loretta Tong**



Jet Propulsion Laboratory



Outline



- **Program objective**
- **Project overview and description**
- **Atmospheric transmission data**
- **Future upgrades & enhancements**
- **Summary**



➤ Obtain Atmospheric Transmission Statistics Data to Support Optical Communications

- ◆ Atmospheric loss in optical comm. channel
- ◆ Joint PDFs for multiple site reception
- ◆ Statistical modeling
- ◆ Extrapolate PDFs for other sites



AVM: Description



➔ **An autonomous system that measures ground intensity of stars through different filters**

- ◆ 10-inch (4-cm) diameter f/10 telescope
- ◆ Six spectral filters (5 operational)
- ◆ Cooled slow-scan CCD camera
- ◆ Weather station to guard system
- ◆ 386 powered PC controls all subsystems and collects data



A VM: Description



- **One star observed every 15 minutes**
 - ◆ Standard stars between 0 & 4 magnitude
 - ◆ About 50 stars in list covering entire sky
- **Each star observed through 6 filters**
 - ◆ Narrow band: 532 nm, 830 nm & ~~1.06 μm~~
 - ◆ Broad band: Astronomical V, R & I
- **24 observations (images) per hour**

A VM: Description



- **Collected data is automatically sent via modem to a dedicated computer at JPL on a daily basis**
- **Image/data processing reveals star intensity values on ground**
- **Attenuation determined by normalizing ground intensity values to above-the-atmosphere intensity values**
- **Subsequent data analysis provides statistical information of interest**



➤ Table Mountain Facility (TMF)

◆ Altitude: 2.3 km (7500 ft)

➤ Mt. Lemmon near Tucson Arizona

◆ Altitude: 2.8 km (9150 ft)

➤ ~~Mesa near JPL~~

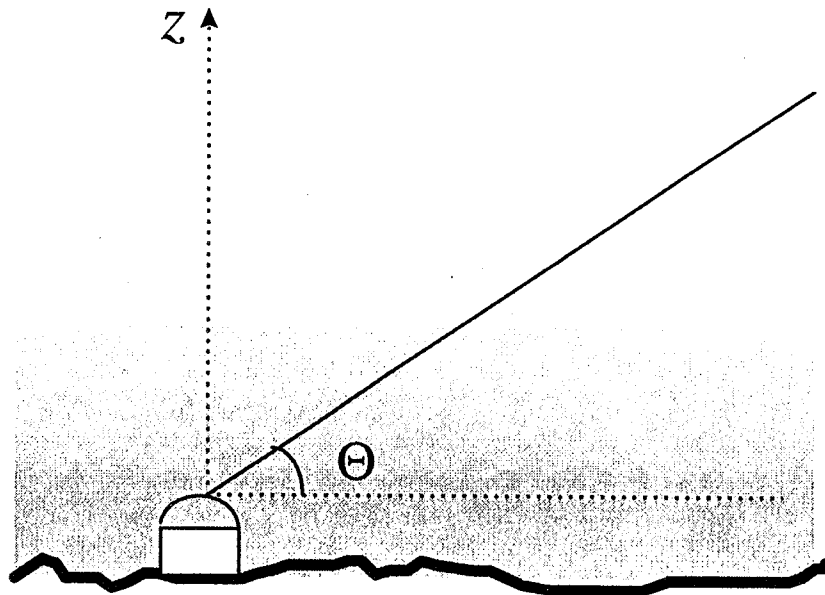
➤ Goldstone (as of August 1996)

◆ Altitude: 1 km (3400 ft)

System Calibration



- ➔ Calibration achieved from observation of stars through different air-mass



$$I = I_0 \exp(-\sec \theta \int \alpha(z) dz)$$

$$I = I_0 \eta^{-\sec \theta}$$

$$y = \ln I$$

$$y_0 = \ln I_0$$

$$x = \sec \theta \text{ (air mass)}$$

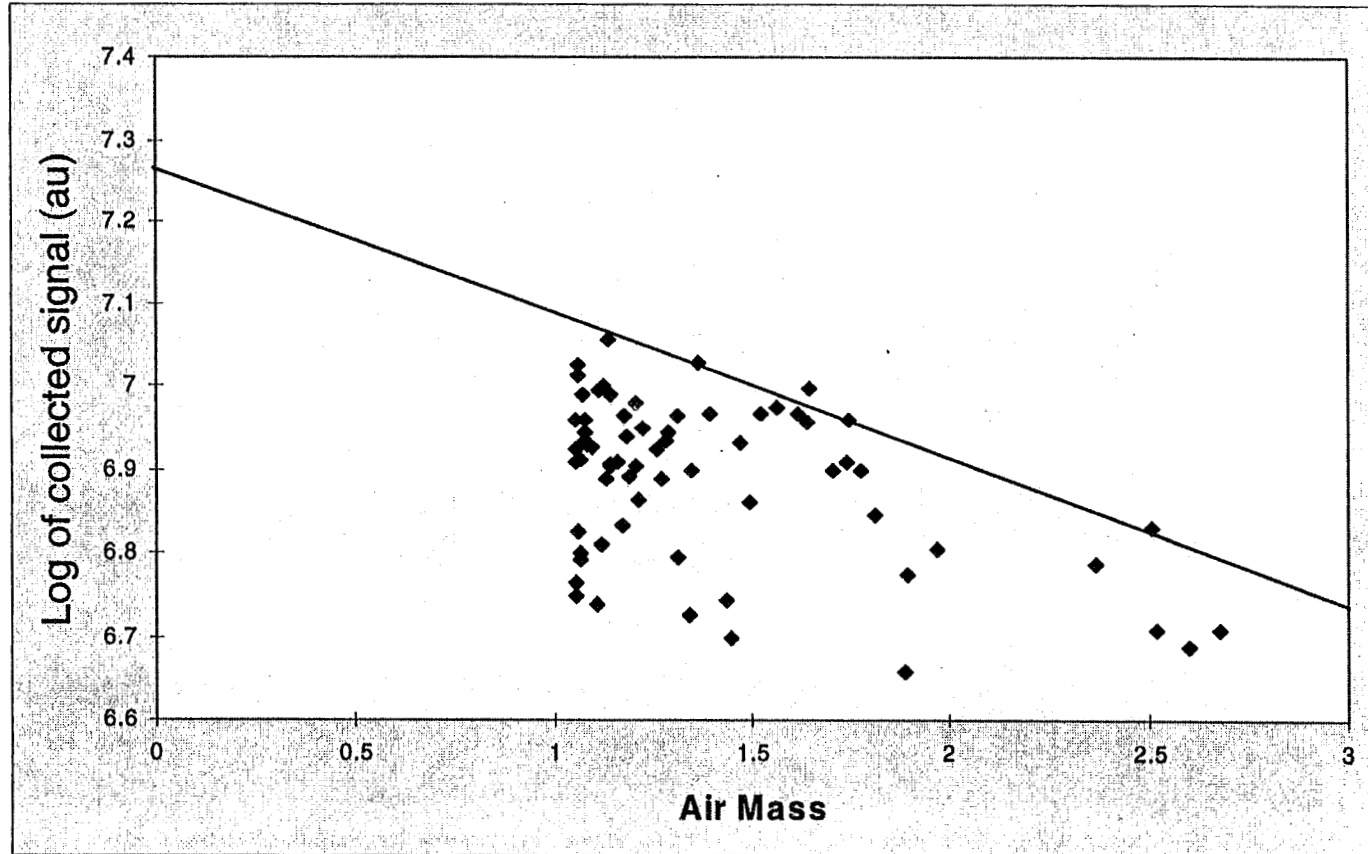
$$y = y_0 - \eta x$$



Calibration



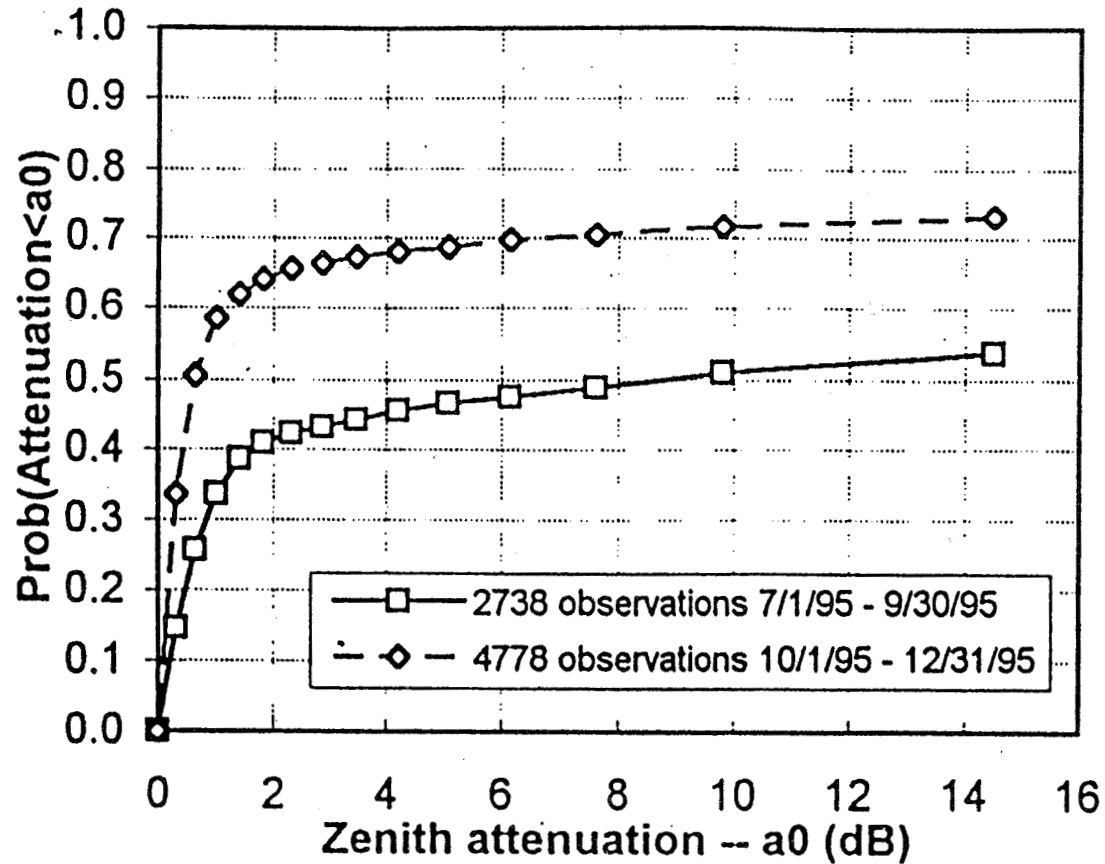
Observation of star #5933 through 860 nm filter from TMF



Visibility Statistics



Site: Mt. Lemmon; Filter 860 nm
Period: 3rd and 4th quarter of 1995

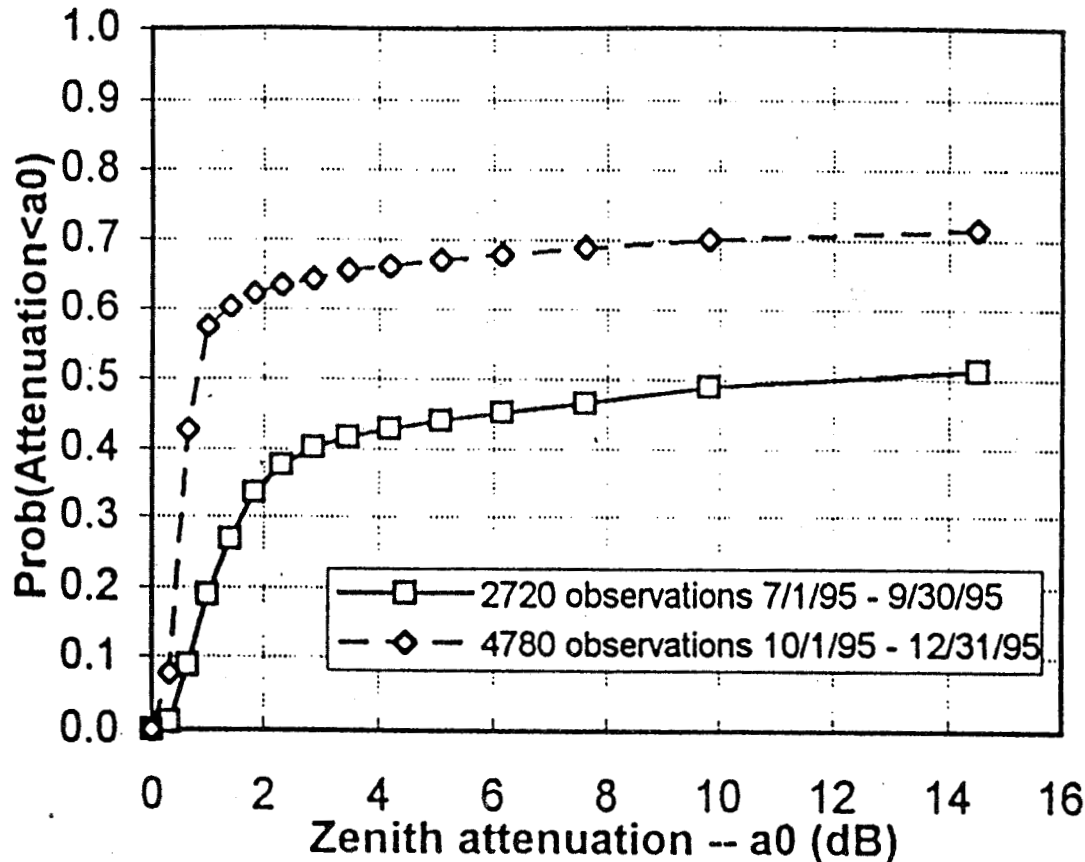




Visibility Statistics



Site: Mt. Lemmon; Filter 532 nm
Period: 3rd and 4th quarter of 1995



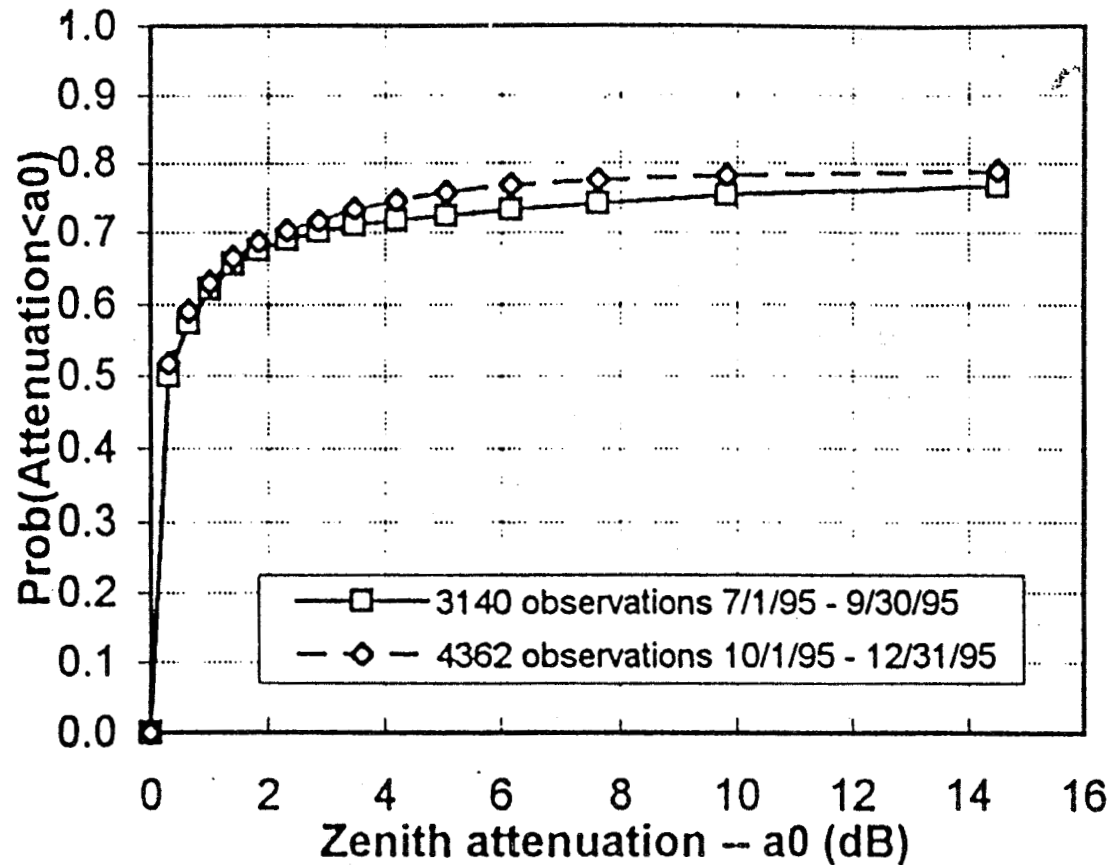


Visibility Statistics



Site: TMF; Filter 860 nm

Period: 3rd and 4th quarter of 1995



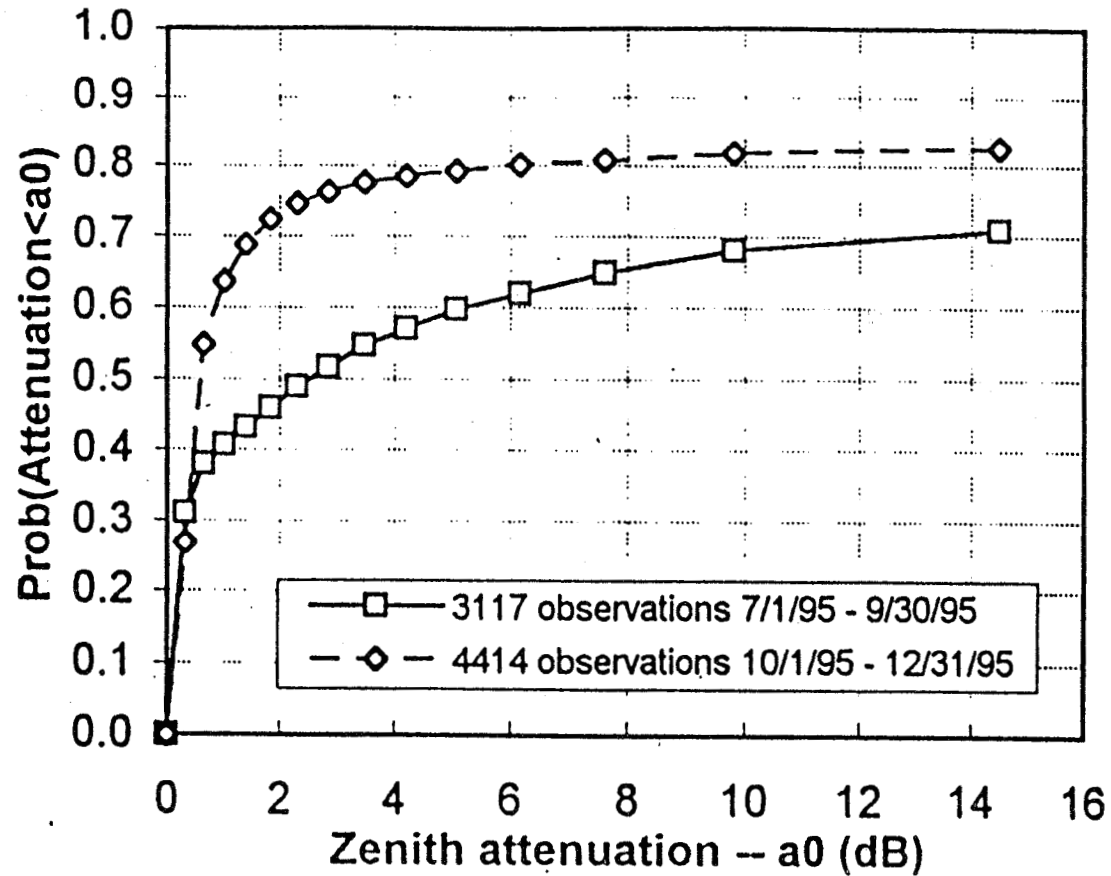


Visibility Statistics



Site: TMF; Filter 532 nm

Period: 3rd and 4th quarter of 1995





Work in Progress



- **Maintain AVM data using MS Access**
- **Use queries to extract necessary data**
- **Analyze extracted data using Interactive Data Language (IDL)**
- **Obtain joint statistics from the three sites (diversified-site availability)**

Planned Activities



- **Capability to collect data in the IR**
 - ◆ especially at the important laser wavelengths of 1.06 μm and 1.55 μm

- **Compare and correlate AVM data to other atmospheric databases**

- **Statistical modeling and prediction**

Conclusions



- **Fully autonomous AVM systems collect atmospheric visibility data from three sites**
- **Database of visibility data is being created to easily extract atmospheric transmission statistics information**

Atmospheric Turbulence Statistics From GOLD Experiments

343



**Muthu Jeganathan,
Keith Wilson & Jim Lesh**



Jet Propulsion Laboratory



- **What is GOLD?**
- **Experimental details**
- **Uplink**
 - ◆ Scintillation
 - ◆ Multi-beam effects
 - ◆ Comparison to experimental data
- **Downlink**
- **Summary**

What is GOLD?



➔ **GOLD: Ground-Orbiter Lasercomm Demonstration**

- ★ Optical communication experiments between Table Mountain Observatory (TMF) and Japanese Engineering Test Satellite (ETS-VI)
- ★ International co-operative effort between NASA, NASDA, CRL and JPL
- ★ Phase I transmissions from October 95 to January 96
Phase II transmissions from March 96 to May 96

GOLD: History

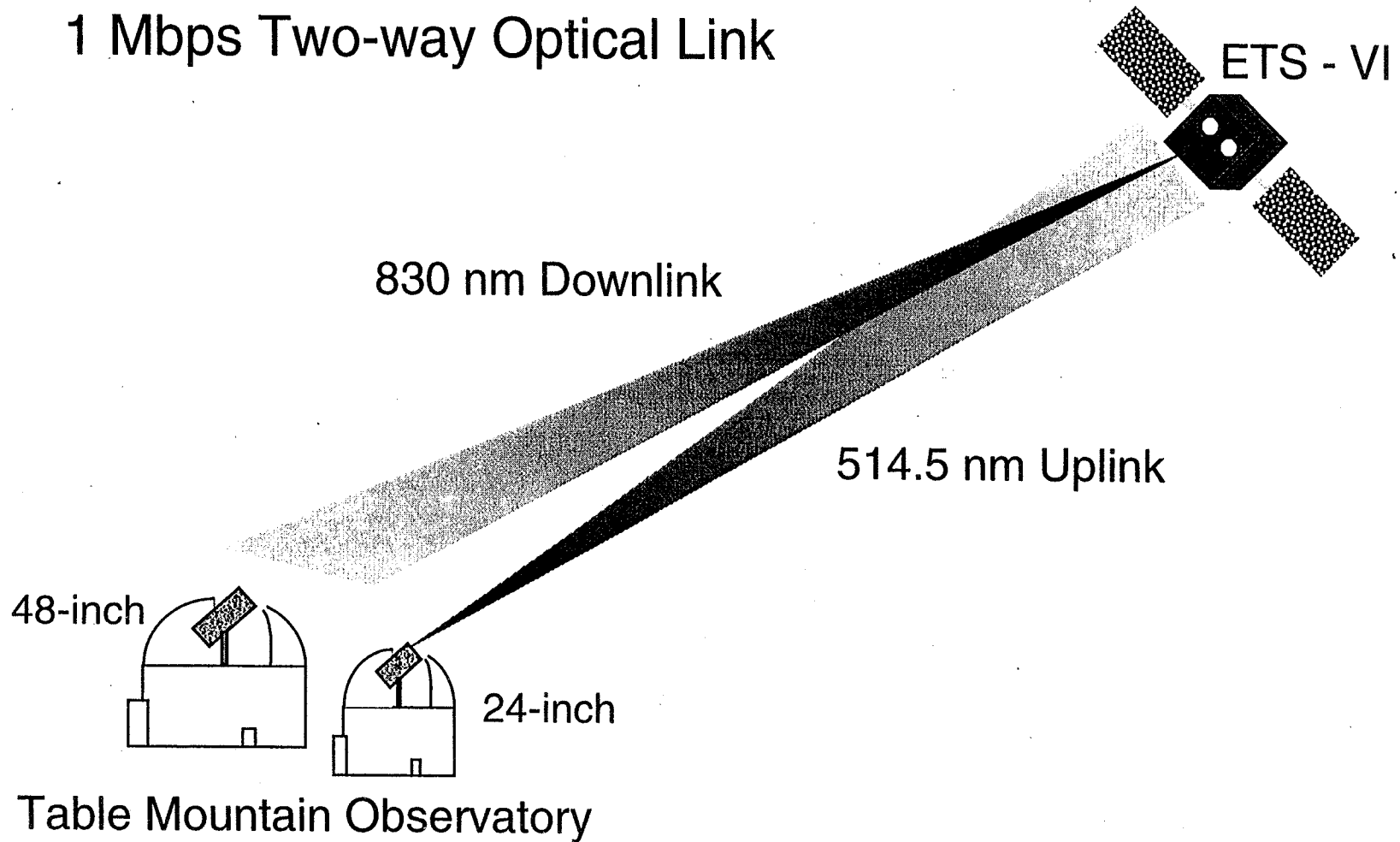


- **ETS-VI launched in August 1994**
- **Passes over TMF every three days**
- **Experiment duration 3 - 5 hours**
- **Accomplishments**
 - ◆ Two-way space-to-ground laser communication from geostationary ranges
 - ◆ Multiple beam uplink
 - ◆ Daytime acquisition/tracking/comm.

Demonstration Overview



1 Mbps Two-way Optical Link



347

JPL

Link Budget: Uplink



Link Distance	37850.0 km	
Elevation Angle	46.2 degrees	
Laser Power	13.2 W	41.21 dBm
Tx Optics Efficiency	0.75	-1.25 dB
Beam Divergence	30.00 micro-rad	
Pointing jitter	0.00 micro-rad	
Pointing offset	4.00 micro-rad	
Pointing loss factor	0.99	-0.04 dB
Propagation loss	9.87E-07 1/m ²	-60.05 dB
Atm transmission	0.80	-1.34 dB
Receiver Aperture	7.5 cm	
	4.42E-03 m ²	-23.55 dB
Rx Optics Efficiency	0.15	-8.24 dB
Received Power	4.7 nW	-53.27 dBm
Required power	631.0 pW	-62.00 dBm
Link Margin		8.73 dB

Does not include fluctuations due to scintillation or beam motion



Uplink: Scintillation



- ➔ **Constructive and destructive interference between waves traveling through different atmospheric cells**
- ➔ **Due to turbulence and dynamics of the atmosphere, interference pattern shifts and changes with time**
- ➔ **Point-detector or small area receiver sees fluctuation in signal strength**

Scintillation: Theory



➔ Scintillation variance described by log-normal distribution

$$S \propto |\exp(\chi + i\phi)|^2$$

amplitude and phase of wave

$$f_S(s) = \frac{1}{\sqrt{2\pi} \sigma_l^2} \frac{1}{s} \exp\left[-\frac{1}{2\sigma_l^2} \cdot (\ln s - l_m)^2\right]$$

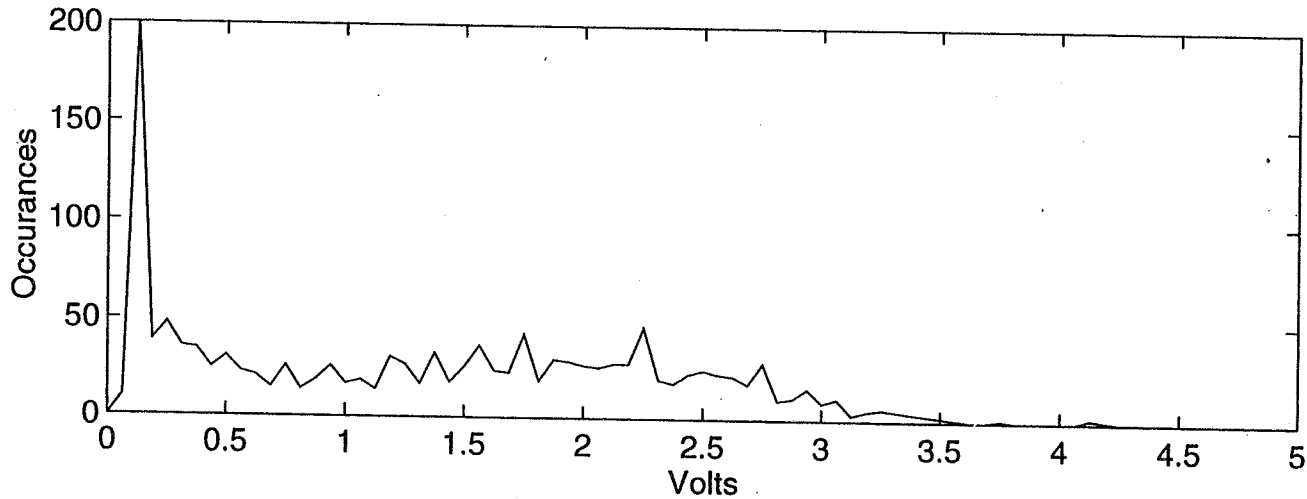
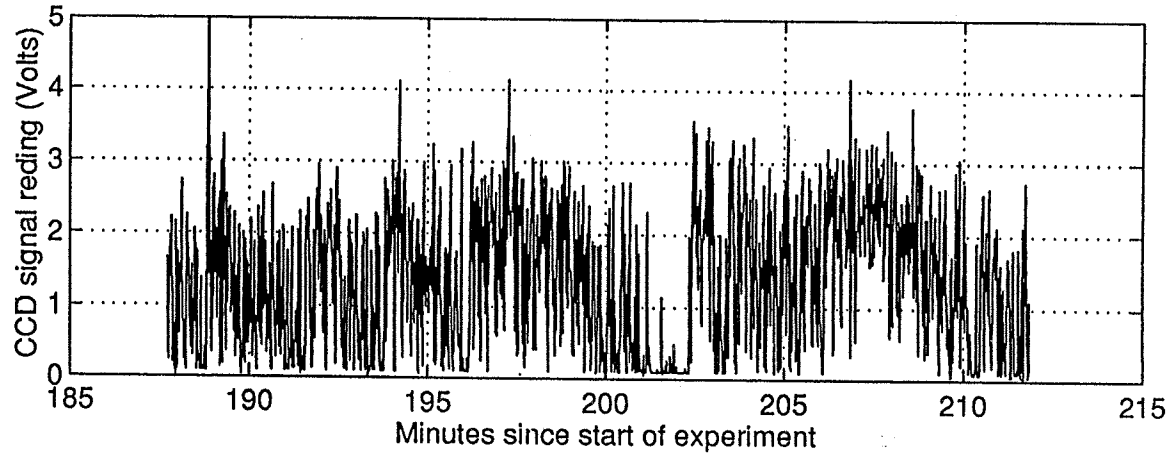
σ_l : Scintillation variance
(variance of 2χ)



One Beam Uplink Data



From November 17, 1995 Experiment



351

Multi-beam effects



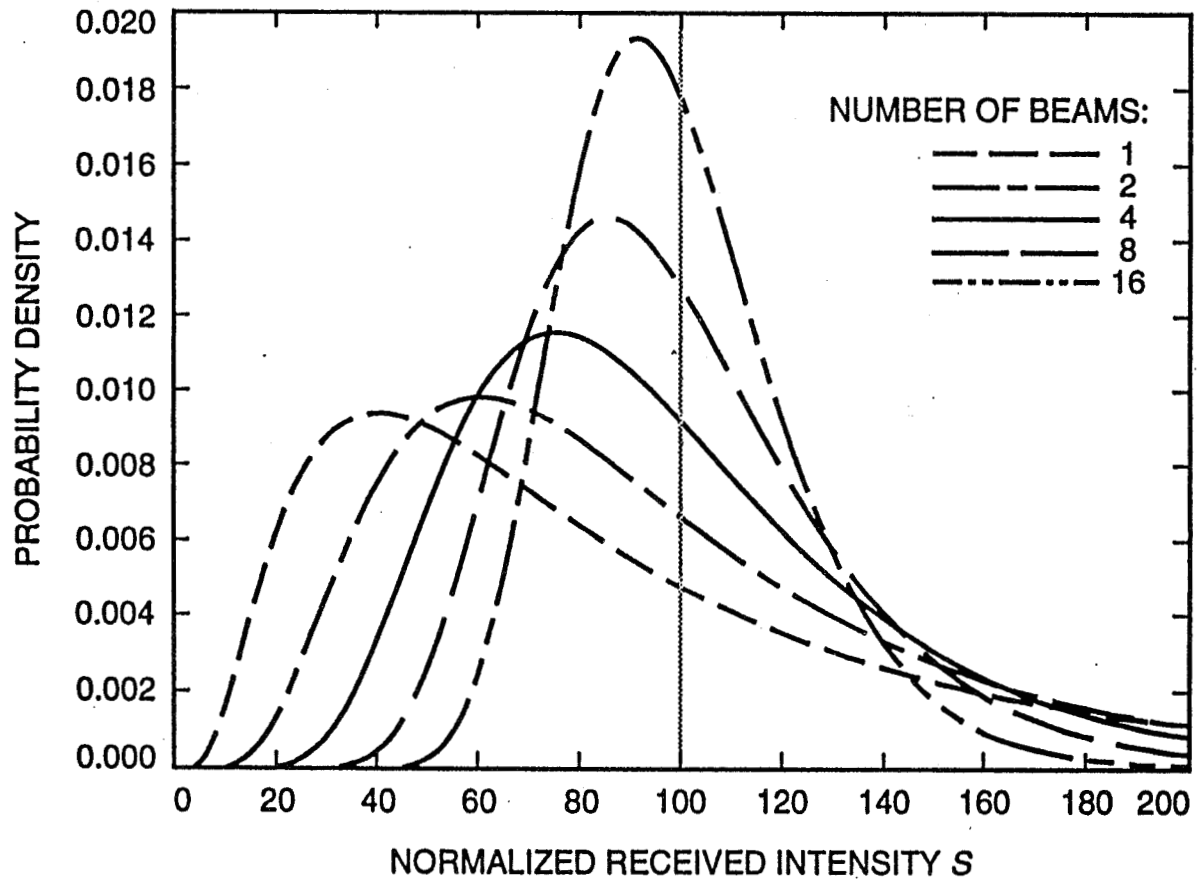
- **Multiple beams can be used to reduce scintillation-induced fades/surges**
 - ◆ beams must have independent phase (incoherent between each other)
 - ◆ beams must be separated by distances larger than the atmospheric coherence length (a measure of turbulence). Typically 1 to 10 cm.
- **PDF is the convolution of log-normal distributions**



Multi-beam Uplink PDF



353



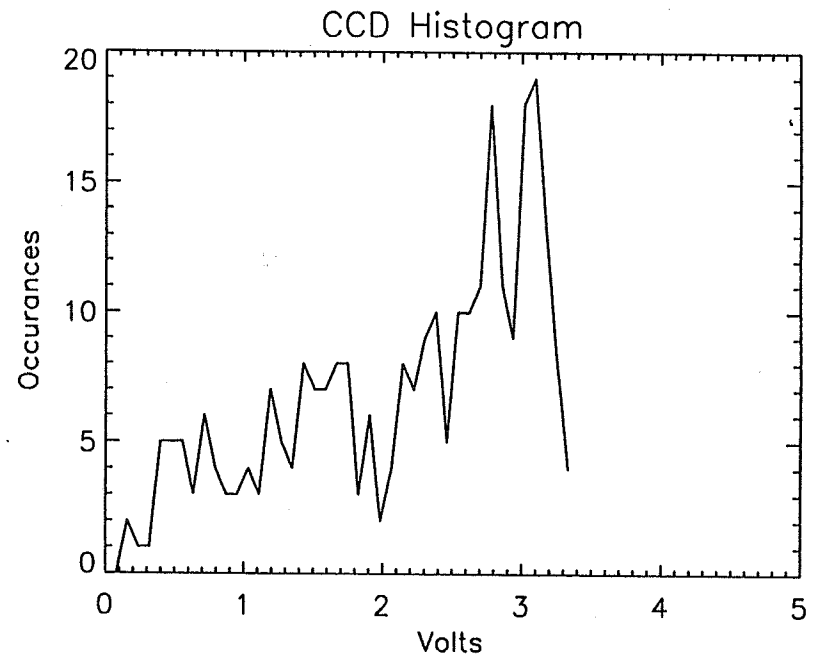
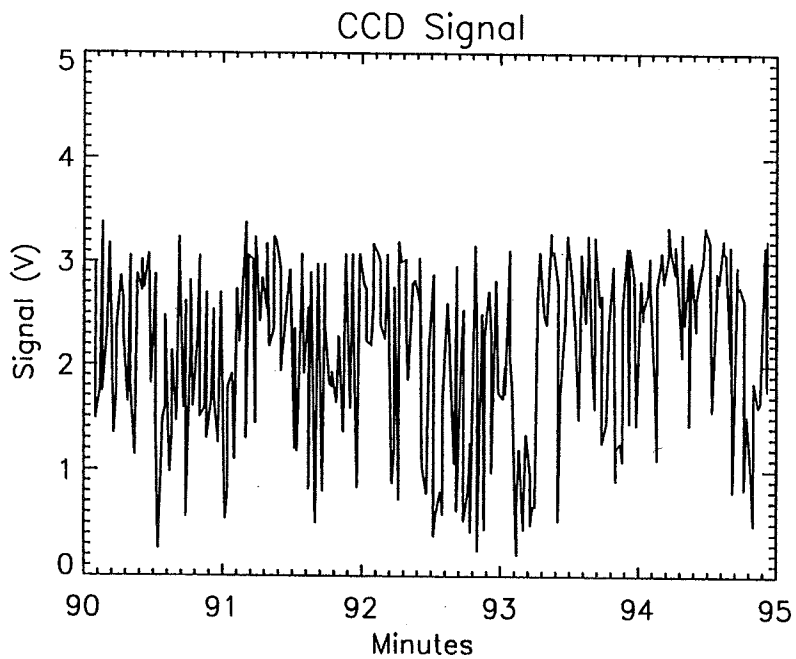


Two Beams



From May 26, 1996 Experiment

354



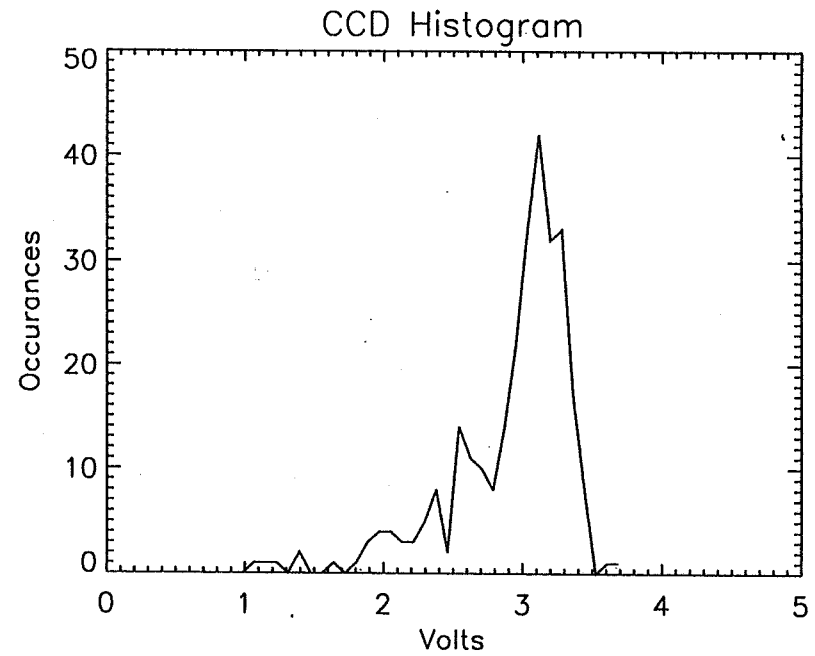
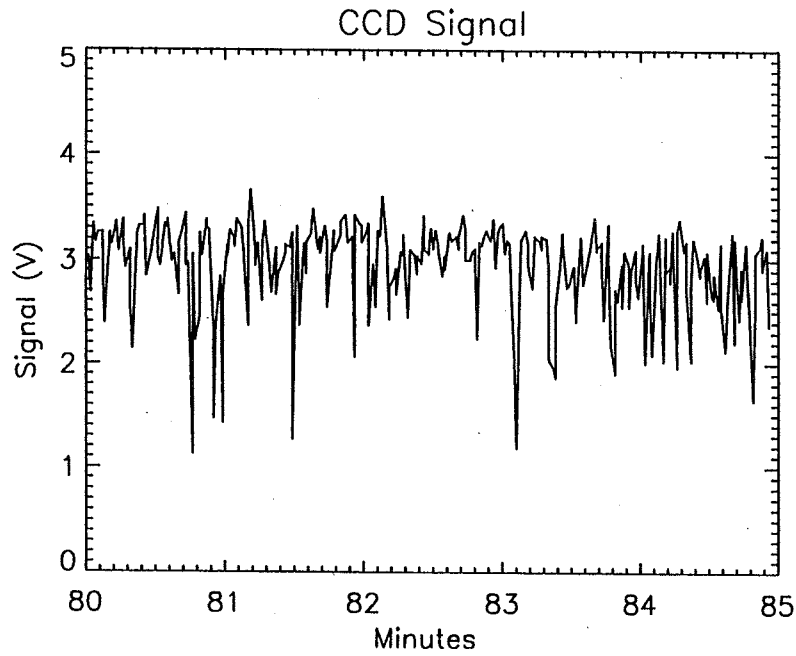


Four Beams



From May 26, 1996 Experiment

355

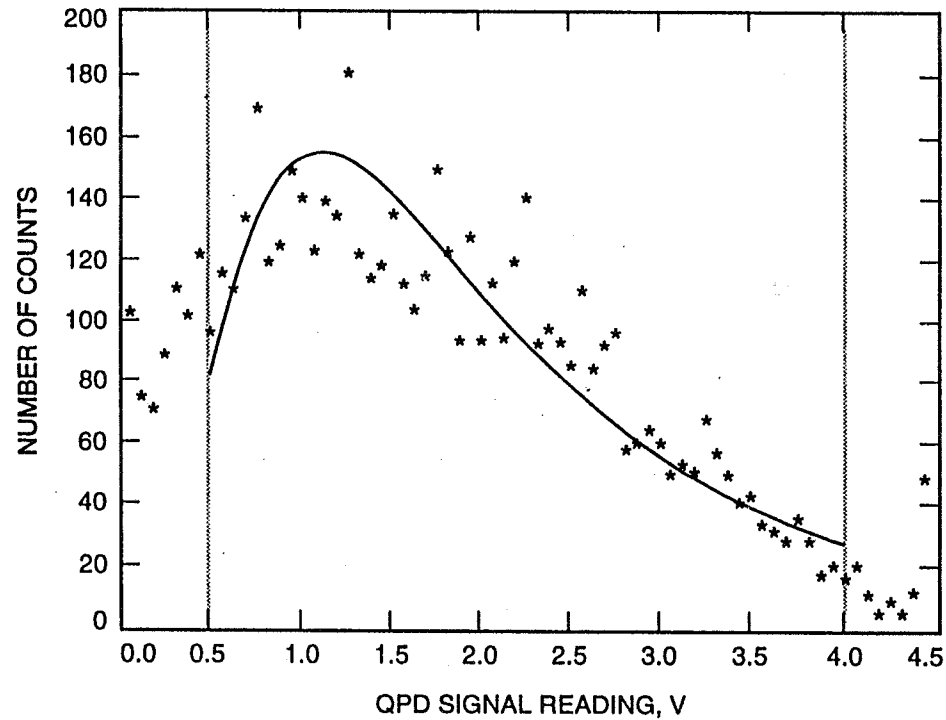




Fit to Experimental Data



Two-beam data from November 17, 1995 Experiment

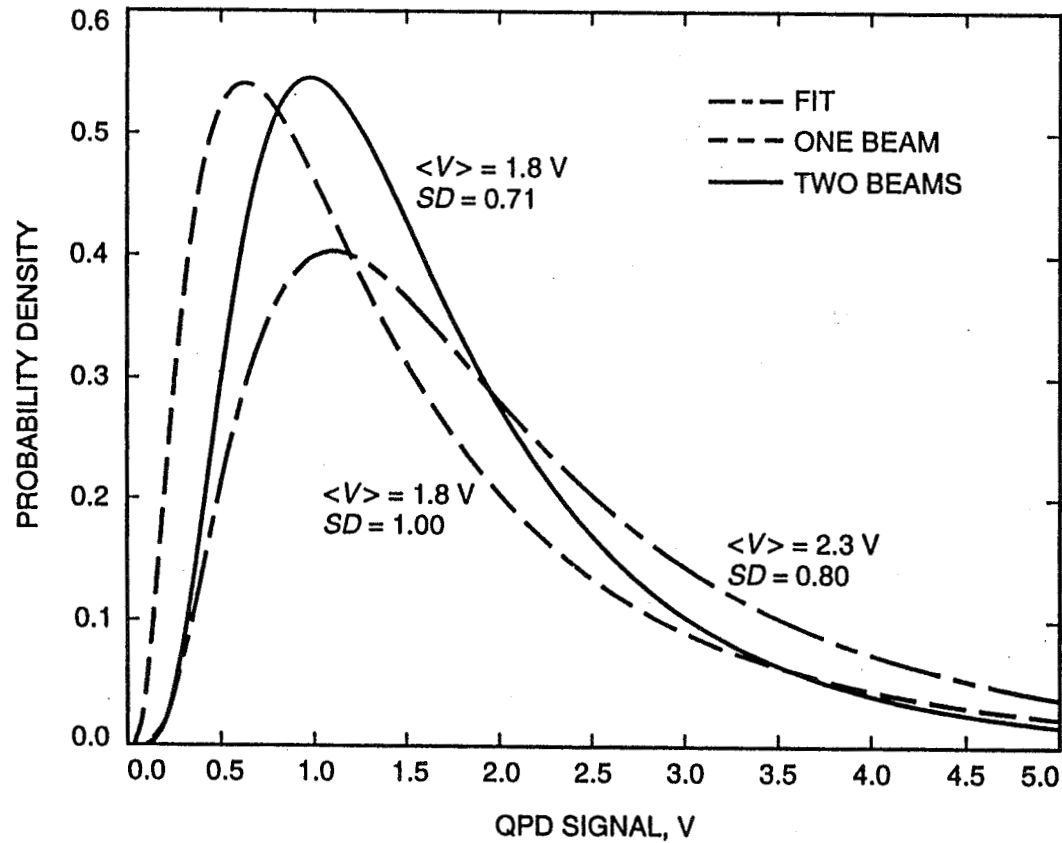




Theory and Experiment



From November 17, 1995 Experiment





Downlink



- **Scintillation significantly reduced by large (greater than 1m) aperture**
 - ◆ Intensity averaged over constructive plus destructive interference

- **Beam wander is the dominant effect**



Link Budget: Downlink



Link Distance	37850 km	
Elevation Angle	46.2 degrees	
Laser Power	28 mW	14.47 dBm
Tx Optical Efficiency	0.3	-5.23 dB
Beam Divergence	30 micro-rad	
Pointing jitter	6 micro-rad	
Pointing offset	6 micro-rad	
Pointing loss	0.98	-0.09 dB
Propagation loss	9.87E-07 1/m ²	-60.05 dB
Atm transmission	0.9	-0.46 dB
Receiver Aperture	120 cm	
Area (w 20% obsc.)	1.09 m ²	0.36 dB
Rx Optical Efficiency	0.75	-1.73 dB
RECEIVED POWER	5.33 nW	-52.73 dBm
THRESHOLD POWER	700 pW	-61.55 dBm
Link Margin		8.82 dB

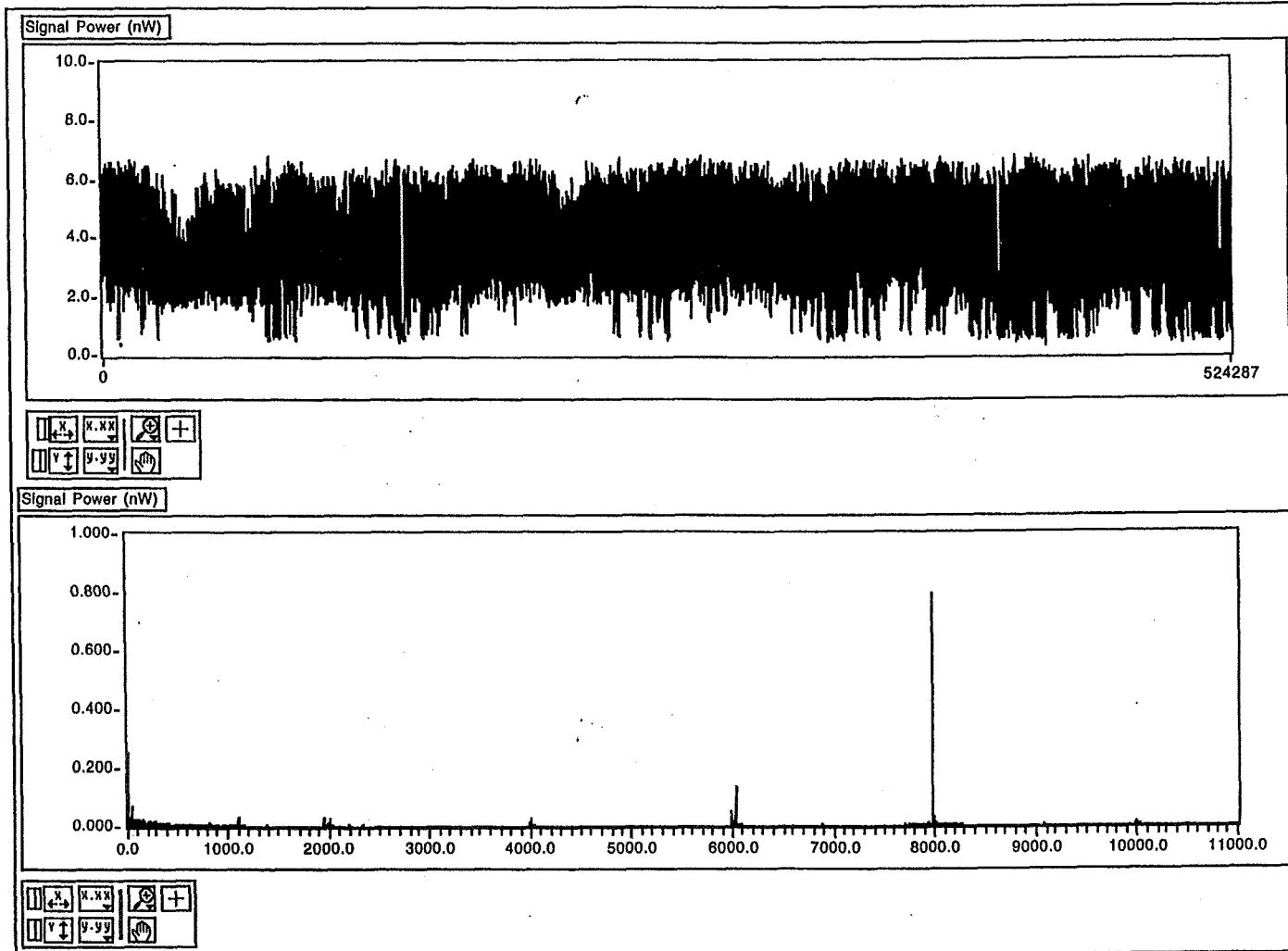


Downlink: Data



22kHz-sampled downlink signal

360





Conclusions



- **Experimental data clearly shows significant reduction in scintillation with multiple beams**
- **Collected data includes combination of atmospheric effects as well as spacecraft vibrations and pointing errors**
- **Further analyses required to deconvolve these effects**

Page intentionally left blank

Earth-Space Propagation Data Bases

Ernest K. Smith

Department of Electrical and Computer Engineering
University of Colorado, Boulder Colorado 80309-0425

Tel. (303) 492-7123; Fax. (303) 492-2758;

e-mail. smithek@colorado.edu

Abstract

This paper, designed for the newcomer rather than the expert, will take a rather broad view of what is meant by "propagation data bases" in that it will take the term to mean both the actual measurements and models of earth-space paths. The text will largely be drawn from CCIR Reports of Study Group 5, now annexed to Recommendations of ITU-R Study Group 3, plus some experience with a course taught at the University of Colorado.

Introduction

As the first JPL Manager for the NASA Propagation Program my interest was aroused by the announcement of its 20th NAPEX meeting (NAPEX derives from NASA Propagation EXperiminters). This paper came about when I called up Dr. Nasser Golshan, the new manager of the NASA Propagation Program at JPL, and offered to present a paper at NAPEX XX on the history of NAPEX. Nasser countered with the suggestion that I do a paper on earth-space propagation data bases, particularly aimed at the newcomer. With some trepidation I agreed to do this.

A little bit of history. I first got involved in the NASA Propagation Program in 1980 when JPL was offered the operational management of the program, and I became its first JPL manager. In 1981 Professor Warren L. Flock of the EE Department at the University of Colorado came to spend a sabbatical year with me at JPL and the idea was conceived of a handbook to parallel Dr. Louis J. Ippolito's famous text Propagation Effects Handbook for Satellite Systems Design - A summary of Propagation Impairments on 10 to 100 GHz Satellite Links with Techniques for System Design, 4th edition 1989, NASA Reference Publication 1082-04. I suggested to Warren that he prepare a companion handbook, so, in order to be complementary, his text was titled "Propagation Effects on Satellite Systems at Frequencies below 10 GHz - A Handbook for Satellite System Design" NASA Reference Publication 1108, first issued in December 1983.

2nd Edition 1987 (as NASA RP-1108-02). When he returned to the University of Colorado, Warren developed a course, ECEN 5264 "Propagation Effect on Satellite Communications," using his NASA RP 1108 as the text. I inherited this course from Warren shortly after I joined the University of Colorado in 1987 after retiring from JPL. I enlisted the help of Dr. David C. Hogg and the two of us have offered the course every one or two years since then.

Initially in the course we used Warren's NASA Reference Publication 1108 (02) and Radiowave Propagation by Lucien Boithias (McGraw Hill 1987) as texts, supplemented by CCIR material. In 1989 when two volumes published by Peter Perigrinus for the IEE: Satellite -to- Ground Radiowave Propagation by Dr. Jeremy Allnut and Ionospheric Radio by Dr. Kenneth Davies, we substituted those volumes for Boithias.

I first become involved in the CCIR, the International Radio Consultative Committee of the International Telecommunications Union (ITU), in the late fifties (I became vice chairman of Study Group 6 in 1959 but since 1976 have been principally involve with Study Group 5) so I am comfortable including CCIR material in my work.

A discussion of pertinent international organizations is given in the first part of this paper with emphasis on the CCIR/ITU-R. This is followed by a discussion of some of the problems encountered in worldwide models used in the preparation of propagation link budgets, plus a bit on a site-specific-model. The intent is to provide the novice engineer with the information to get started in the field.

National and International organizations.

I have tried to be active in three national or international organizations in my professional career: the IEEE, the URSI, and the CCIR (now renamed the ITU-R). I have been involved in radiowave propagation since 1944.

The **Institute of Electrical and Electronic Engineers (IEEE)**, is the world's largest professional organization, now organized in 35 specialized Societies, one of which is the Antennas and Propagation Society, abbreviated AP/S. This Society puts out two publication: the IEEE Transactions on Antennas and Propagation and the IEEE Antennas and Propagation Magazine. The Transaction of AP/S is a highly-rated professional journal for research papers, while the AP/S

Magazine is more informal. I am the propagation editor for the Magazine. The IEEE Home Page is found on the World Wide Web at URL:<http://www.ieee.org>, or the organization can be accessed by telephone at 1-800-678-IEEE.

The **International Union of Radio Science (URSI)** was created in 1919, has just under 40 member countries, and is one of the earliest members of the International Council of Scientific Unions (ICSU). In the United States, the affiliating organization is the National Academy of Sciences. URSI is headquartered in Brussels. It holds a General Assembly every three years, most recently in Kyoto in 1993, to be followed by the XXVth General Assembly in Lille, France August 28 to Sept. 5, 1996.

URSI's work is organized in 10 Commissions. Commission F "Wave Propagation and Remote Sensing" (chaired by Prof. R.K. Moore of Kansas State University) has traditionally dealt with radio propagation through non-ionized media, and Commission G "Ionospheric Radio and Propagation" (chaired by Prof. K.C. Yeh of the University of Illinois) has traditionally dealt with propagation through ionized media. In America the United States National Committee of URSI, supported by the National Research Council holds a meeting of all Commissions once a year - in recent years in January in Boulder hosted by the University of Colorado and a summer meeting joint with the IEEE Antennas and Propagation Society in which not all Commissions participate. Through arrangement with the American Geophysical Union, URSI is supported by the periodical Radio Science. The participants in URSI are largely academics and research scientists.

The **International Radio Consultative Committee (CCIR)** was organized in 1927. In 1932 it became the technical radio advisory body of the newly consolidated International Telecommunications Union (ITU). Following the formation of the United Nations (UN) in 1945 the ITU became a Specialized Agency of the UN. The work of the CCIR has been carried out up to 1994 through twelve Study Groups, two of which, Study Group V (Propagation in Non-Ionized Media) and Study Group VI (Propagation in Ionized Media) deal with applied propagation problems.

Membership in the ITU (and CCIR) is by administrations (e.g., the U.S., Canada, the U.K.) established by treaty. Hence, U.S. participation in the work of the CCIR is through the U.S. Department of State.

In April 1993, following a reorganization of the ITU, the name CCIR disappeared to be replaced by the initials ITU-R (R for Radiocommunications). Simultaneously, the two propagation Study Groups were consolidated into Study Group III. The international Chairman of Study Group III is Leslie Barclay of the U.K. The chairman of U.S. Study Group III is Eldon Haakinson (eldon@its.bldrdoc.gov) at the Institute for Telecommunication Sciences in Boulder. The CCIR held Plenary Assemblies every four years and published their most recent texts as Recommendations and Reports. The Reports, last published in 1990 were well referenced. Now ITU-R only publishes Recommendations (no references), and a great deal of the value has been lost. CCIR and ITU-R volumes can be obtained directly from the ITU in Geneva, or from the National Technical Information Service.

CCIR SG5 & 6/ITU-R SG3

The chairman of the new Study Group 3 is Leslie W. Barclay of the U.K. The most recent version of these texts has the N and I in the title removed, but the only version that I have (1994 PN Series) still has these letters in them so I have retained the N and I. The principal texts of the former CCIR Study Groups 5 and 6, now the new ITU-R Commission 3, as they relate to Earth-Space Propagation are:

Recommendation ITU-R PN.618-3 Propagation Data and Prediction Methods Required for the Design of Earth-Space Telecommunication Systems

This text is derived from the former Study Group 5 text Report 564-4 (1990) of the same title. It is the ITU-R model for Earth-space propagation even though it does not contain any ionospheric data.

Recommendation ITU-R PI.531 Ionospheric Effects upon Earth-Space Propagation

This text, derived from the former CCIR Report 263-6 (1990), is the definitive text on ionospheric effects on earth-space systems. The ionospheric tables included in each of the former Study Group 5 texts below relating to specific services are all derived from the former Tables VII and VIII of Report 263-6.

Recommendation ITU-R PN.679-1 Propagation Data required for the Design of Broadcast-Satellite Systems

This text is an attenuated version of CCIR Report 565-4 (1990).

Recommendation ITU-R PN.680-1 *Propagation Data Required for the Design of Earth-Space Maritime Mobile Telecommunication Systems*

This Text is drawn from CCIR Report 884-2 (1990).

Recommendation ITU-R PN.681-1 *Propagation Data Required for the Design of Earth-Space Land-Mobile Telecommunication Systems*

This text has its roots in CCIR Report 1009-1 (1990) but has been completely rewritten.

Recommendation ITU-R PN.682-1 *Propagation Data Required for the Design of Earth-Space Aeronautical-Mobile Telecommunication Systems*

This text is derived from CCIR Report 1148 (1990).

Unfortunately, the removal of references from the published ITU-R texts makes it almost impossible to track the origin of the material in these texts unless one is privy to the unpublished Study Group documents. However a recent memo from Eldon Haakinson indicates that these working documents of Study Group 3 may be available on the Internet.

ITU Web Site: <http://www.itu.ch>
look for: ITU Radiocommunication Sector
click on: Study Group 3

Data banks are treated in the next text.

Recommendation ITU-R PN.311-7 *Acquisition, Presentation and Analysis of Data in Studies of Tropospheric Propagation*

traces its origins back to 1953. The most recent version that I have had access to came out in 1994. As mentioned above, the new designation in 1996 has deleted the N so that the above would now be listed as Rec. ITU-R P 311-7.

The Introduction to the Recommendation contains the following wording:

"One of the essential requirements for the provision of reliable methods for prediction of radio propagation effects is the establishment of suitable computer data banks. Such data banks must:

- contain all data available that are of adequate standard,

- be widely accepted as the source material on which to conduct testing,

- be readily available.

It is a principle of the data banks that they shall contain only such data as may be used for:

- testing prediction methods recommended by Radiocommunication Study Group 3 (and may of course be used to test other methods): and
- for the creating and updating of radiometeorological maps relevant to the prediction of radio propagation effects."

Data banks are treated in section 5 in the following categories:

Part I Terrestrial line-of-sight path data
Part II Earth-space path data
Part III Terrestrial trans-horizon path and rain-scatter data
Part IV Radiometeorological data
Part V Terrestrial broadcasting data
Part VI Data for mobile satellite services

The actual work of running the data bank has been undertaken by Bertram Arbesser-Rastburg at ESSA-ESTEC at Noordwijk in The Netherlands (bertram@estec.esa.nl). Copies of the data base may be obtained on 3.5 inch DOS disks for 100 Swiss Francs from:

Study Group Department "B", Radiowave Propagation
Attn: Dr. Kevin Hughes
Place Des Nations
CH-1211 Geneva 20
Switzerland

Bertram, through the good offices of Eldon Haakinson, provided me with a copy of the data base. It contains a vast array of data but is probably more useful to the specialist than the newcomer.

Other data in regional and specialized data banks which may or may not have submitted their measurements in response to Rec ITU-R PN.311-7 exist around the world. For Example:

Wolf Vogel: ACTS satellite data
Robert K. Crane: Rain and scintillation data
ESA ESTEC: Data from ESA COST Programs:
Aldo Paraboni: ITALSAT Data

Earth-Space Propagation Modeling

Compact introductory information may be found in recent handbooks (e.g., Smith 1995a,b). Thorough descriptions of the factors entering propagation modeling is found in the NASA Propagation Handbooks

(Ippolito 1989, Flock 1987). Several good texts on Earth-space propagation are Allnutt (1989), Ippolito (1986), and Pratt and Bostian (1986). Fine texts on satellite communications are (Roddy 1989), Miya (1975), Morgan and Gordon 1989, and Rees (1990), to name a few.

The JPL Computer Model. Computer models prepared at JPL have been described by Anil Kantak, Krisjani Suwitra and Choung Le (1993,1994,1995). A presentation and demonstration is scheduled after the break at this meeting. While incorporating many different options the one used for past demonstrations has been the CCIR method. It has the advantage of simplicity and international acceptability.

The method illustrated makes use of world maps of rain rate exceeded 0.01% of the time as illustrated in figure 1 as its basic input in determining rain attenuation. A constant distribution is then assumed of attenuation due to rain to other percents of the time (formula in figure 2) as is shown by the solid curve in figure 2. How good this is can be surmised from figure 3 where the ratios of attenuation values derived for the rain distributions (Table 1) in the various CCIR geographical zones (the alternate zonal approach) are plotted. It can be seen that the fit is not bad for 0.001% to 0.1% of the time, but the formula gives a poor fit above 0.1% of the time (Smith and Flock, 1995). In its favor is the fact that the attenuations are low for rain rates exceeded more than 0.1% of the time.

The alternate approach of geographical zones, such as shown in Figure 4, each with its own rain distribution, has the unfortunate feature that a factor of 4 difference in rain rate can occur at zonal boundaries as illustrated in figure 5. Crane (1993) has suggested that most rain attenuation models provide a prediction accuracy of about 30% which is compounded by a year-to-year natural variability of 20%.

The PARC (Propagation Analysis for Rain and Clear Air) Model . This model (Dissanayake, Allnutt and Haidara 1996) offers a somewhat different approach. propagation factors considered are

- gaseous attenuation
- cloud attenuation
- melting layer attenuation
- rain attenuation
- tropospheric scintillations
- low angle fading

PARC itself is a software package that contains all the above models and associated worldwide data bases necessary to do the calculations. Refractive and ionospheric effects are ignored. Special attention is given as to how to combine the different types of attenuation. A relationship between rain rate and specific attenuation in the melting layer is derived. Rain attenuation is site specific and use is made of the Rice/Holmberg (1973) rain model which requires average annual accumulation of rainfall and fraction of this rain arising from thunderstorm activity as input parameters. A comparison of prediction and measurement is made for paths with elevation angles of 5 degrees on up for 16 locations from around the world. A prediction accuracy of 20% is suggested for Earth-space paths from 4-35 GHz, not including the year-to-year variability.

References

Allnutt, J.E. (1989) Satellite-to-Ground Radiowave Propagation, IEE Electromagnetic Series 29, Peter Perigrinus Ltd., London, on behalf of the Institution of Electrical Engineers

Boithias, L. (1987) Radiowave Propagation, McGraw Hill

CCIR (1990) Reports of the International Radio Consultative Committee

CCIR, XVIIth Plenary Assembly, Dusseldorf May 21-June 6, 1990, Annex to Volume V, Published by the ITU, Geneva

Report 564-4 Propagation data and prediction methods required for Earth-space telecommunication systems, pp 447-505

Report 565-4 Propagation data for broadcasting from satellites, pp 506- 514

Report 884-2 Propagation data for maritime mobile-satellite systems for frequencies above 100 MHz, pp 515-535

Report 1009-1 Propagation data for land mobile-satellite systems for frequencies above 100 Mhz, pp 536-549

Report 1144 Data banks to support evaluation of prediction methods, pp 1-25

Report 1148 Propagation data for aeronautical mobile-satellite systems for frequencies above 100 MHz, pp 550-564

CCIR (1990) Reports of the International Radio Consultative Committee, CCIR, XVIIth Plenary Assembly, Dusseldorf May

- 21- June 6, 1990, Annex to Volume VI, Published by the ITU,
Geneva
Report 263-6 Ionospheric Effects on Earth-space propagation
- Crane R.K. (1982) A two-component rain model for the prediction of attenuation statistics, *Radio Science*, vol 17, 1371-1387
- Crane, R.K. (1993) Estimating risk of earth-satellite propagation, *Proc. IEEE*, vol. 81, 856-864
- Davies, K. (1989) Ionospheric Radio, IEE Electromagnetic Series 31, Peter Perigrinus Ltd., London, on behalf of the Institution of Electrical Engineers
- Dissanayake, A., J.E. Allnutt, and F. Haidara (1996) A prediction model that combines rain attenuation and other impairments along satellite paths, submitted to *IEEE Trans. Ant. and Propag.*
- Flock, W.L. (1987) Propagation Effects on Satellite Systems at Frequencies Below 10 GHz, 2nd Edition, *NASA Reference Publication 1108 (02)*
- Goldhirsh, J. and W.J. Vogel (1992) Propagation Effects for Land Mobile Satellite Systems: Overview of Experimental and Modeling Results, *NASA Reference Publication 1274*
- Ippolito, L.J. (1986) Radiowave Propagation in Satellite Communications. Van Nostrand Reinhold
- Ippolito, L.J. (1989) Propagation Effects Handbook for Satellite System Design - A Summary of Propagation Impairments on 10-100 GHz Satellite Links with Techniques for System Design, 4th Edition, *NASA Reference Publication 1082 (04)*
- Kantak, A.V., K. Suwitra, and C. Le; A data base for propagation models
 (1993) pp 129-141, Proc. NAPEX XVII, JPL Publication 93-21
 (1994) pp 81-102, Proc. NAPEX XVIII, JPL Publication 94-19
 (1995) pp 195-209, Proc. NAPEX XIX, JPL Publication 95-15
- Miya, K. Ed. (1975) Satellite Communications, Lattice Co., Tokyo

- Morgan, W.L. and G.D. Gordon (1989) Communications Satellite Handbook, John Wiley and Sons
- Pratt, T. and C.W. Bostian (1986) Satellite Communications, John Wiley and Sons
- Rees, D.W.E. (1990) Satellite Communications, The First Century of Service, Wiley Interscience, John Wiley and Sons
- Roddy, D. (1989) Satellite Communications, Prentice Hall
- Smith, E.K. and W.L. Flock (1995) Tropospheric Effects on Earth-Space Propagation at VHF, National Radio Science Meeting, Boulder. paper #1, Session F/G/J, Jan3, 1995.
- Smith, E.K. (1995a) Handbook of Microwave Technology, Vol. 2, Applications, T. Koryu Ishii, Ed., Chapter 8: Propagation at microwave frequencies, pp 207-248. Academic Press
- Smith, E.K. (1995b) Worldwide Wireless Communications, F. S. Barnes Et al. Eds., Propagation effects on satellite systems, pp 347-374. International Engineering Consortium, Chicago

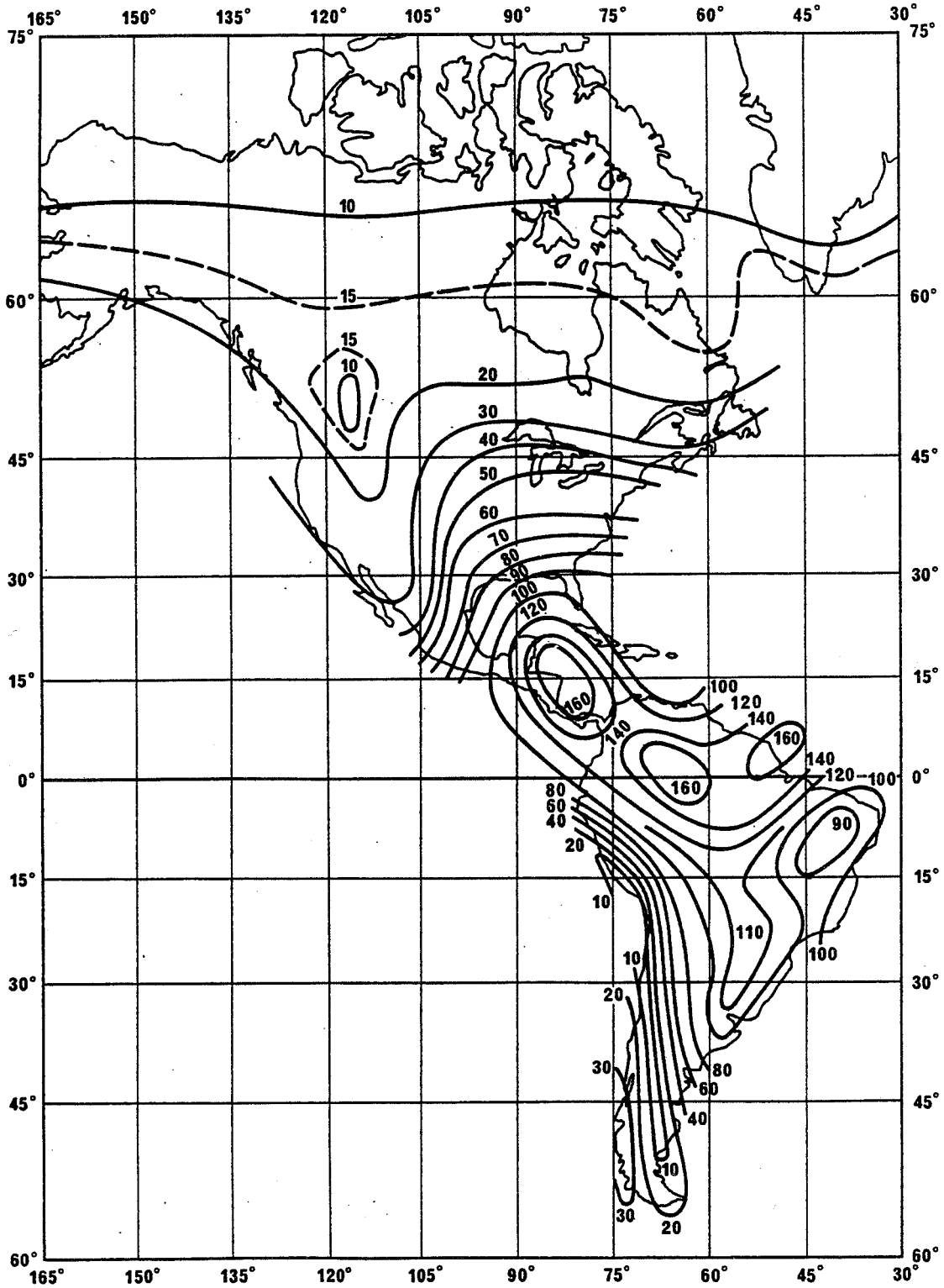
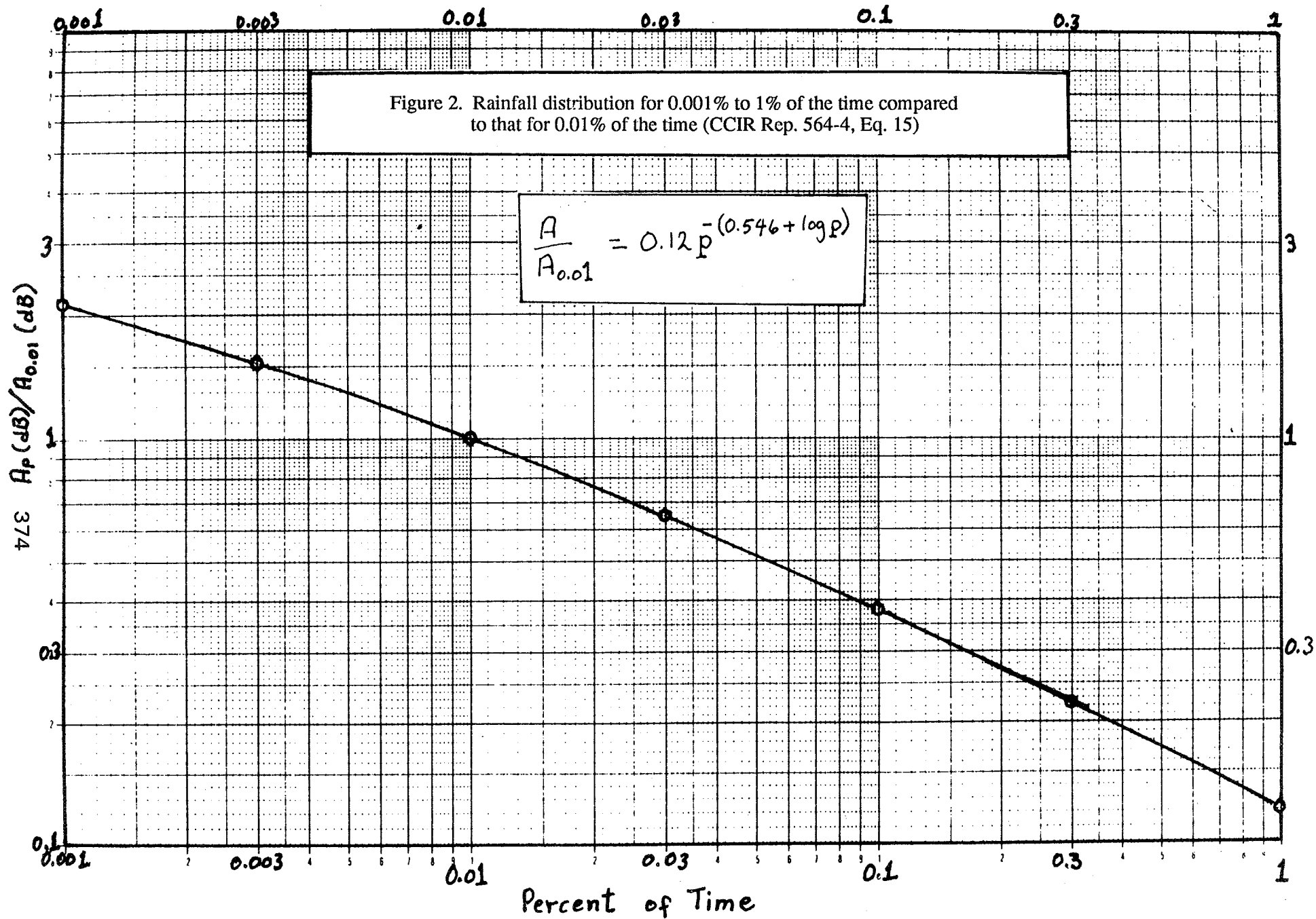


Figure 1. Rainfall contours for 0.01% of the time

Figure 2. Rainfall distribution for 0.001% to 1% of the time compared to that for 0.01% of the time (CCIR Rep. 564-4, Eq. 15)



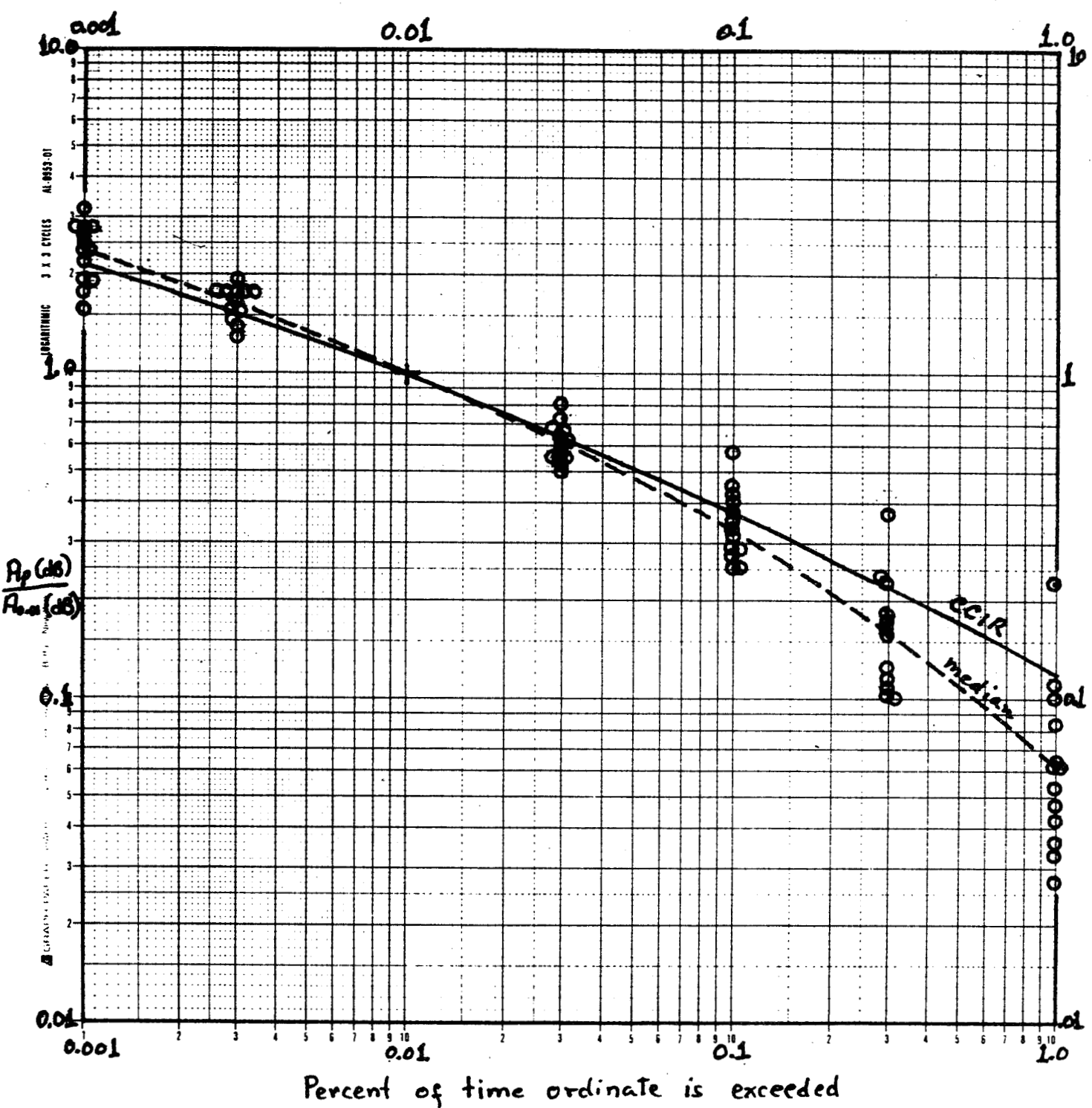


Figure 3. Comparison of the CCIR rainfall intensity distribution of Fig. 2 with the distributions given for rainfall zones in Table 1, Rep. 563-4

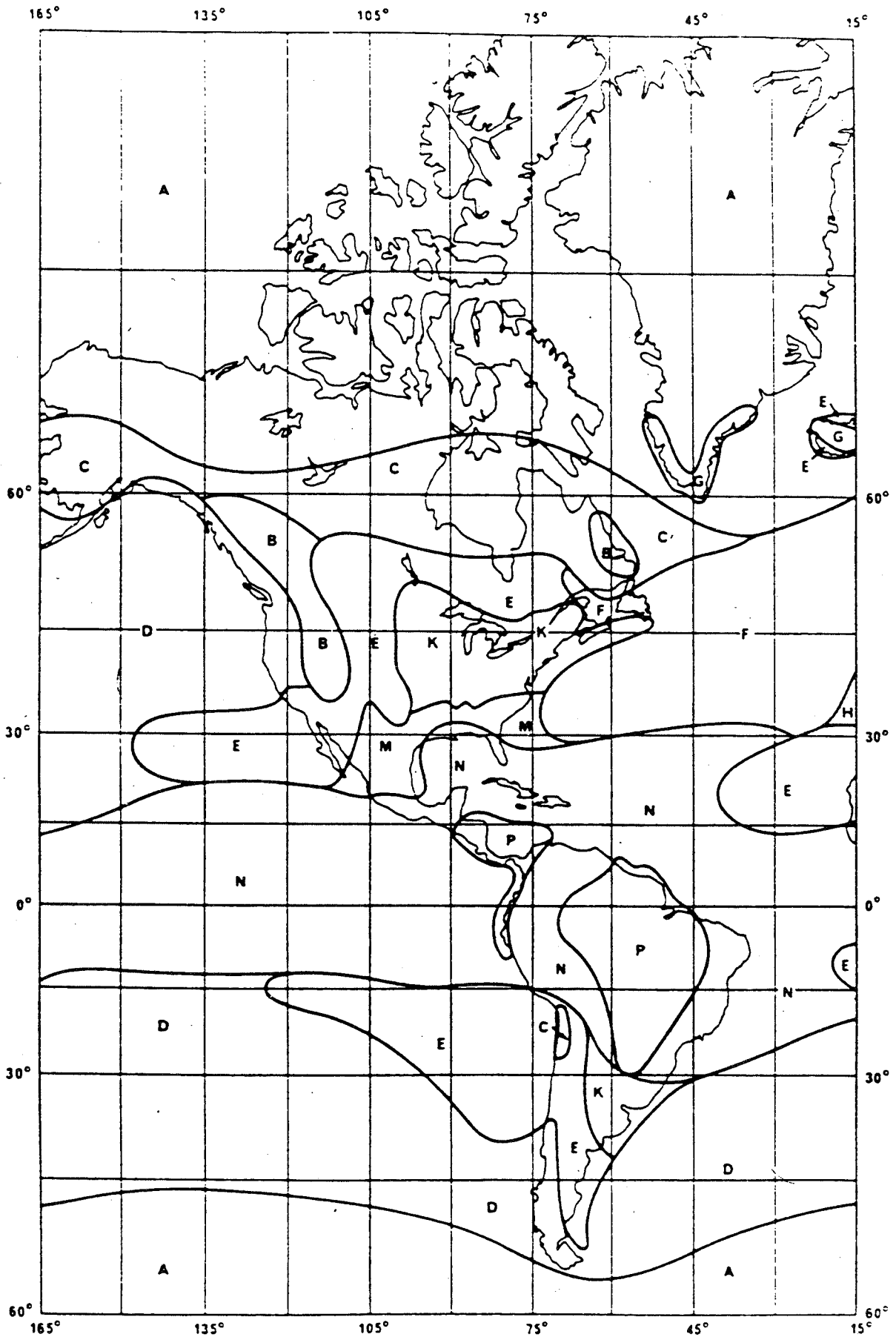


Figure 4. Rain zone map for the Americas
(CCIR Rep. 563-4, Fig 15)

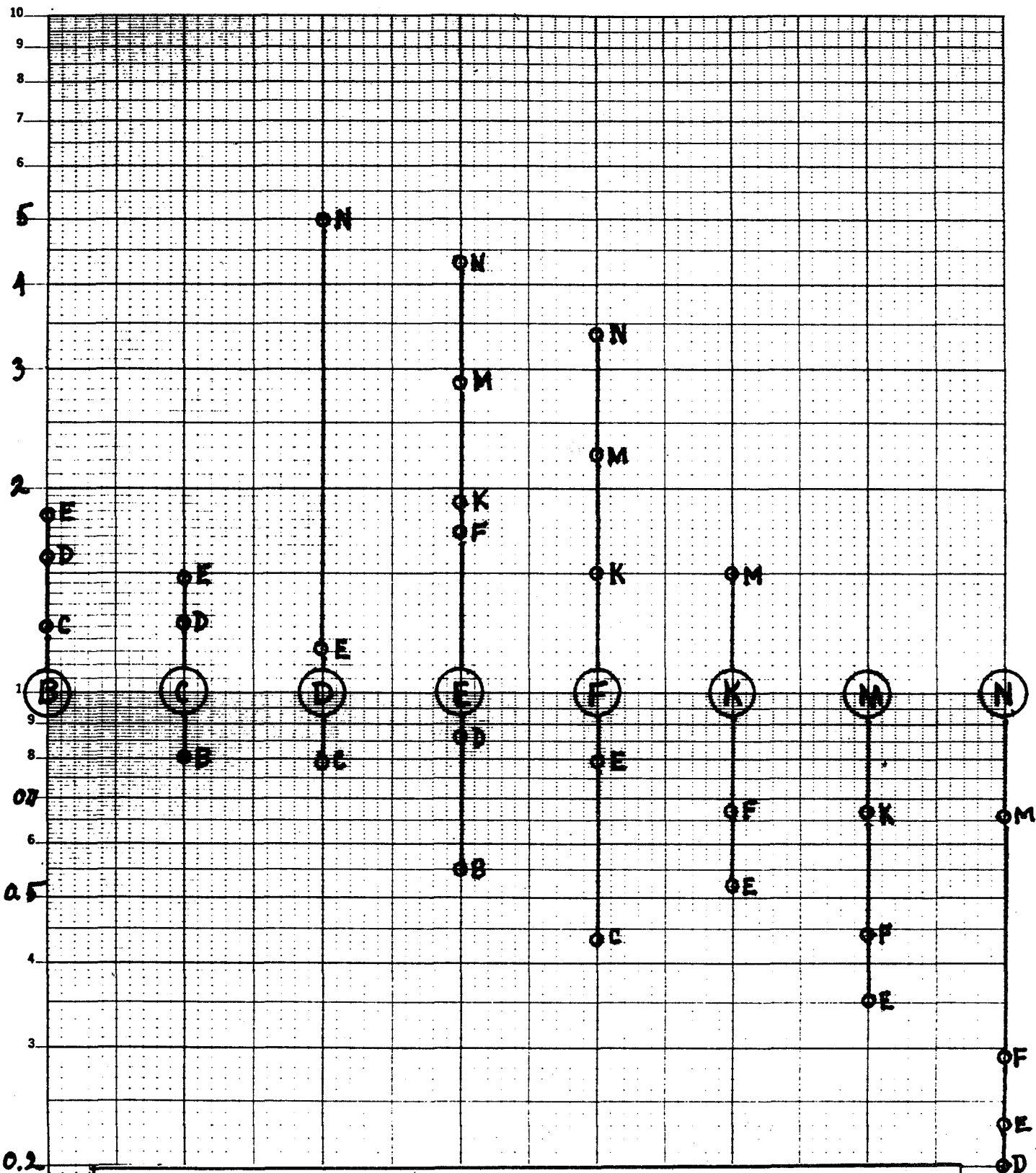


Figure 5. Boundary discontinuities in rain rate at 0.01% of the time for the CCIR zone map for North America (Rep. 563-4, Fig. 15). The large circles with letters inside represent the zone under consideration. The small circles are located at the appropriate ratios of rain rate at the interfaces with those zones.

Table 1. Rain climatic zones, rainfall intensity exceeded (mm/h)
(Reference to Fig. 5)

Percentage of time (%)	A	B	C	D	E	F	G	H	J	K	L	M	N	P
1.0	< 0.5	1	2	3	1	2	3	2	8	2	2	4	5	12
0.3	1	2	3	5	3	4	7	4	13	6	7	11	15	34
0.1	2	3	5	8	6	8	12	10	20	12	15	22	35	65
0.03	5	6	9	13	12	15	20	18	28	23	33	40	65	105
0.01	8	12	15	19	22	28	30	32	35	42	60	63	95	145
0.003	14	21	26	29	41	54	45	55	45	70	105	95	140	200
0.001	22	32	42	42	70	78	65	83	55	100	150	120	180	250



Proposed Revisions To The NASA Propagation Handbooks

Louis J. Ippolito
ACS A Division of Stanford Telecom

NAPEX XX
20th NASA Propagation
Experimenters Meeting

June 5, 1996
Fairbanks, Alaska

Objectives

- Begin the Process of Updating the NASA Propagation Handbooks to Include the Latest Models, Data, and Analysis Tools**
- Include Results of Prior and On-going NASA Studies and the ACTS Propagation Measurements Campaign**
- Update the Systems Analysis Approach to the Evaluation of Atmospheric Degradations on New Applications**
 - Ka-Band Systems**
 - Direct Broadcast Systems**
 - Mobile Satellite Systems**
 - Low Margin VSAT Systems**
 - Frequency Re-Use Systems**

Milestones

Begin Handbook Revisions Study **April 29 1996**

Preliminary Outline: **May 20, 1996**

Peer Review - NAPEX XX Presentation **June 5, 1996**

Handbook Revisions Development Plan **July 15, 1996**

Prior Editions Above 10 GHz Handbooks

- First Edition ORI Technical Report TR 1679
R. Kaul, R. Wallace, G. Kinal
March 1980
- Second Edition NASA Reference Publication 1082
L. Ippolito, R. Kaul, R. Wallace
December 1981
- Third Edition NASA Reference Publication 1082(03)
L. Ippolito, R. Kaul, R. Wallace
June 1983
- Fourth Edition NASA Reference Publication 1082(04)
L. Ippolito
February 1989

Prior Editions Below 10 GHz Handbooks

- First Edition NASA Reference Publication 1108
W. Flock
December 1983
- Second Edition NASA Reference Publication 1108(02)
W. Flock
December 1987



Contents of Current Handbooks

Above 10 GHz Handbook

Below 10 GHz Handbook

Propagation Effects Handbook for Satellite Systems Design

*A Summary of Propagation
Impairments on 10 to 100 GHz
Satellite Links With Techniques
for System Design*

Louis J. Ippolito
[1082(04), February 1989]

- I. INTRODUCTION
- II. CHARACTERISTICS OF RAIN AND RAIN SYSTEMS
- III. AN OVERVIEW OR SEVERAL RAIN AND RAIN
ATTENUATION MODELS
- IV. DEPOLARIZATION IN EARTH-SPACE PATHS
- V. PROPAGATION DATA BASES
- VI. PREDICTION TECHNIQUES
- VII. APPLICATION OF PROPAGATION PREDICTIONS
TO EARTH/SPACE TELECOMMUNICATIONS
SYSTEMS DESIGN

Propagation Effects on Satellite Systems at Frequencies Below 10 GHz

A Handbook for Satellite Systems Design

Warren L. Flock
[1108(02), December 1987]

1. INTRODUCTION
2. IONOSPHERIC EFFECTS
3. TROPOSPHERIC CLEAR-AIR EFFECTS
4. ABSORPTION, SCATTER, AND CROSS POLARIZATION
CAUSED BY PRECIPITATION
5. EFFECTS OF SMALL PARTICLES AND BIOLOGICAL
MATTER
6. PROPAGATION EFFECTS ON MOBILE-SATELLITE
SYSTEMS
7. RADIO NOISE
8. PROPAGATION EFFECTS ON INTERFERENCE
9. ESTIMATION OF PROPAGATION IMPAIRMENTS
10. SPACE-COMMUNICATIONS SYSTEMS DESIGN

Major Developments Since Last Publication of The NASA Handbooks

- New Propagation Measurement Campaigns
- New Propagation Models and Prediction Procedures Developed
- New Satellite Applications - Evolutionary and Revolutionary
- Reorganization of the International Telecommunications Union (ITU)
- Increased Emphasis on Spectrum Sharing and Interference Mitigation

New Propagation Measurement Campaigns

- **Olympus (ESA) - 1989**
 - Propagation Beacons at 12.5, 19.77, 29.65 GHz
 - Measurements in Europe and United States
- **Italsat F1 (Italy) - 1990**
 - Propagation Beacons at 18.7, 40, 50 GHz
 - Measurements in Europe
- **ACTS (NASA) - Launched Sept. 12, 1993**
 - Propagation Beacons at 20.185 and 27.5 GHz
 - Measurements in CONUS, Alaska, Canada
- **Land Mobile 1.5 GHz Measurements - 1987-88**
 - MARECS-B2 , Central Maryland
 - ETS-V and INMARSAT, S.E. Australia

New Propagation Models and Prediction Procedures

- ❑ Land Mobile Satellite Link Fading (*Vogel, Goldhirsh*)
- ❑ Tropospheric Scintillation (*Karasawa, Yamada, Allnutt*)
 - Based on Monthly Temperature and Humidity
 - Provides Both R.M.S. Amplitude Variance and Monthly Fade Level Statistics
- ❑ Extensive New ITU-R Recommendations
 - Rain Attenuation, Site Diversity, Tropospheric Scintillation, Gaseous Attenuation, Frequency Scaling, Worst Month, Ionospheric Effects
- ❑ Enhancements to Global Rain Model (*Crane, 1996*)

New Satellite Applications

- ❑ **Low Margin VSAT Systems (Ku and Ka bands)**
 - 1-3 dB margins, Global Deployment
- ❑ **Direct Broadcast Satellites in the Ku-band**
 - Hughes DSS; Systems in Europe, Japan
- ❑ **Rapid Interest in Development of the Ka-Band**
 - Filings to FCC; 14 GSO, 3 NGSO
 - Applications to ITU; GSO: 21 countries, 380+ Sats.
NGSO: 8 countries, 1200+ Sats.
 - GSO/FSS (Spaceway, VoiceSpan, Astrolink,)
 - NGSO/FSS/MSS (Teledesic)
 - NGSO/MSS Feeder Links (Iridium, Odyssey)

New Satellite Applications (continued)

- **“Big Leo” Mobile Satellite/Personal Communications**
 - **NGSO (LEO, MEO, HEO), 10 to 66 Sat. Constellations (Globalstar, Iridium, Odyssey, ICO, . . .)**
 - **Service Links**
 - **Uplinks: 1610 - 1626.5 MHz**
 - **Downlinks: 2483.5 - 2500 MHz**
 - **CDMA, TDMA/FDMA**
- **“Little Leo” Paging, Messaging Services**
 - **NGSO (LEO) 20 to 24 Sat. Constellations (Orbcom, Starnet, . . .)**
 - **Service Links: 137-138, 148-149.9, 400-401 MHz**

ITU Reorganization

- **Organizational Changes Effective March 1993**
 - CCIR → ITU Radiocommunications Sector (ITU-R)
 - CCITT → ITU Telecommun. Standards Sector (ITU-T)
 - New Telecommunications Development Sector (ITU-D)
- **WARC's, Held Every Eight -Ten years, replaced with World Radiocommunications Conference (WRC) - every two years WRC-93, WRC-95, WRC-97 . . .**
- **Former Study Groups 5 (Propagation in Non-Ionized Media) and 6 (Ionospheric Propagation) replaced with -
Study Group 3 Radiowave Propagation**
- **New/Revised Propagation Models and Prediction Procedures Published in form of ITU-R Recommendations**

ITU-R Recommendations on Earth-Space Propagation

- ❑ **“Propagation data and prediction methods required for the design of Earth-space telecommunications systems”**
[Recommendation ITU-R P.618-4]
- ❑ **“Propagation data required for the design of broadcasting-satellite systems”** *[P.679-1]*
- ❑ **“Propagation data required for the design of Earth-space maritime mobile telecommunications systems”** *[P.680-1]*
- ❑ **“Propagation data required for the design of Earth-space land mobile telecommunications systems”** *[P.681-2]*
- ❑ **“Propagation data required for the design of Earth-space aeronautical mobile telecommunications systems”** *[P.682-1]*
- ❑ **“Ionospheric Effects Influencing Radio Systems Involving Spacecraft”** *[P.531-3]*

New / Revised ITU-R Models and Prediction Procedures

- Rain Attenuation Modeling Procedure [P.618-4]
 - Precipitation Distributions and Global Maps [P.837-1]
 - Specific Attenuation Coefficients [P.838]
 - Rain Height Model [P.839]
- Atmospheric Gaseous Attenuation Model [P.676.2]
 - Reference Standard Atmosphere [P.835-1]
 - Surface Water Vapor Density [P.836]
- Attenuation due to Clouds and Fog [P.840-1]
- Site Diversity [P.618-4]
- Tropospheric Scintillation [P.618-4]
- Worst Month Statistics [P.581-2]
 - Conversion of Annual Statistics to Worst Month [P.841]
- Probability Distributions for Prop. Modeling [P.1057]

Increased Emphasis on Spectrum Sharing and Interference Mitigation

- ❑ **Explosion in Global Satellite Systems**
 - **Ku-band and Ka-band FSS International, Regional, Domestic Systems**
 - **Over 50 Notices to ITU for Global/Regional NGSO Mobile Satellite Systems**
- ❑ **28 GHz Band**
 - **Satellite Links (FSS Up, MSS Feeder) vs LMDS**
 - **FCC Segmentation of 27.5-30 GHz band**
- ❑ **1610-2500 MHz NGSO/ MSS Service Links vs FS**
- ❑ **Space Research Applications vs Space Services**
- ❑ **FCC Spectrum Auctioning**
 - **5 GHz in 5 to 60 GHz band in next 2 years**

Basic Recommendations for Revised NASA Propagation Handbook

- Combine Scope of the Previous Two Handbooks into a Single Document**
- Eliminate Duplication**
- Provide a More Cohesive Structure for the Reader**
 - Offer Several Levels of “Entrance” into Handbook
- Include Tailored Propagation Analysis Procedures For Specific Types of Satellite Applications -**
 - Ka-band Systems, Ku-band Systems
 - Mobile Satellite Systems
 - Low Margin Systems
 - Direct Broadcast Systems
 -
- Provide Electronic Version of Handbook**

Candidate Titles for NASA Handbook

*Propagation Effects Handbook
for Satellite Systems Design*

*Propagation Effects Handbook
for Communications Satellite
Systems Design*

*Propagation Effects Handbook for
Satellite Communications Systems*

Basic Structure of Handbook

Three Sections

SECTION I BACKGROUND

Provide Overview of Propagation Effects, including Theory and Basic Concepts, Propagation Measurements, Available Data Bases.

SECTION II PREDICTION

Provide Descriptions of Prediction Models and Techniques, Organized By Effect. Provide Step-by-Step Procedures For Each, Where Appropriate. Include Sample Calculations.

SECTION III APPLICATIONS

Provide "RoadMaps" {i.e. flow charts} of Application of Prediction Models in SECTION II to Specific Satellite Systems and Applications. Include Evaluation and Impact on Systems Design and Performance. Include Sample Calculations.

Three Section Approach

**SECTION I
BACKGROUND**

**SECTION II
PREDICTION**

**SECTION III
APPLICATIONS**

397



**Researcher,
General Interest
*Enters Here***



**Link Analyst
*Enters Here***

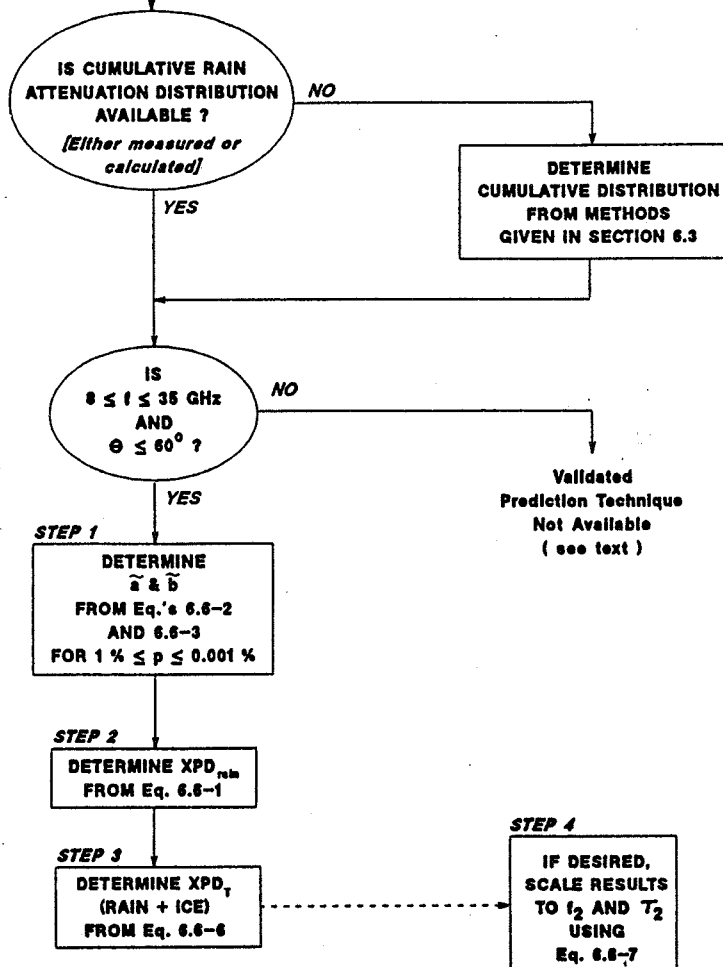


**Systems Designer
*Enters Here***



Sample of "Flow Chart" Depolarization Statistics Prediction

Given: Location
Frequency, f
Elevation Angle, θ
Tilt Angle, τ



Chapters

SECTION I BACKGROUND

- I-1. Overview of Propagation Effects on Satellite Communications**
- I-2. Ionospheric Effects**
- I-3. Tropospheric Effects**
- I-4. Radio Noise**
- I-5. Propagation Data Bases**
 - **Meteorological Parameters**
 - **Slant -Path Measurements**
 - **ITU-R**
 - **Electronic Sources**

Chapters

SECTION II PREDICTION

II-1. Prediction Methods for Satellite Links Operating Below About 3 Ghz

- **Ionspheric Scintillation**
- **Multipath Fading**
- **Group Delay, Phase Advance, Bandwidth Coherence**
- **Polarization, Faraday Rotation**
- **Ducting**
- **Refraction and Turbulence**

Sample Calculations

SECTION II PREDICTION (continued)

II-2. Prediction Methods for Satellite Links Operating Above About 3 Ghz

- **Atmospheric Gaseous Attenuation**
- **Cloud Attenuation**
- **Fog Attenuation**
- **Rain Attenuation**
- **Rain Depolarization**
- **Ice Depolarization**
- **Scintillation**
- **Angle of Arrival**
- **Fade rate, Fade Duration**
- **Dispersive Effects**
- **Combined Effects Statistics**

Sample Calculations

Chapters

SECTION II PREDICTION (continued)

II-3. Link Restoration Models

- Site Diversity
- Orbit Diversity
- Link Power Control
- Adaptive FEC

Sample Calculations

Chapters

SECTION III APPLICATIONS

Flow Charts for Prediction Model Application to Specific Applications

III-1. Application of Prediction Models to Systems Design and Performance

- General Links Analysis Procedures

III-2. Mobile Satellite Systems

- Land Mobile
- Maritime
- Aeronautical

III-3. Ka-band Systems

- Low Margin Fixed Service
- Non-GSO Satellite Links
- Mobile
- Wideband Systems

Chapters
SECTION III APPLICATIONS (continued)

III-4. Direct Broadcast Systems

III-5. Low Margin VSAT Systems

III-6. Frequency Reuse Systems

III-7. Inter- and Intra- System Interference

III-8. ITU Regulatory Considerations

- **PFD Limits**
- **ITU Coordination Procedures**

Sample Calculations

Detailed Preliminary Handbook Outline

- Available for Review by NASA Propagation Community and Interested Industry Representatives

- Suggestions, Comments, Additions, Deletions Welcomed
 - Responses By June 21, 1996
 - Include References for New Information

Additional Considerations

Which Applications / Systems Should Be Emphasized in SECTION III

– Industry Input Important

Relation of Revised NASA Handbook to Current NASA Land Mobile Publication-

“Propagation Effects for Land Mobile Satellite Systems: Overview of Experimental and Modeling Results,” J. Goldhirsh & W. J. Vogel, *NASA Ref. Pub. 1274*, Feb. 1992

– Integrate Results into Revised Handbook

– Reference Document in SECTION III, Chap. 2

Additional Considerations (continued)

Options for Electronic Version of NASA Handbook

- Platform: Workstation, PC, Mac, Other
- Complete S/W Package or Run Under Application (EXCEL, MATLAB, etc.)
- Self-financed(Charge Fee) or Distributed by NASA/JPL

Other Relevant Documents

- OPEX Reference Books, Five Volumes, WPP-083, November 1994.
- ITU-R Working Party 3M, “Radiowave Propagation Information For Earth-Space Path Communications,” draft April 29, 1996.

Summary

- The Process for Revision of the NASA Propagation Handbooks has Begun**
- New and Updated Information Relating to Propagation Measurements, Propagation Models, Evolving Satellite Applications, and International Developments Relevant to the Handbook Have Been Identified**
- A Three Section Structure, which Allows Reader Entrance At Different Levels, Has Been Devised**
- A Detailed Preliminary Handbook Outline Is Available for Community and Industry Review**

Preliminary Outline
**Propagation Effects Handbook
for Satellite Systems Design**

Introduction to the Handbook

SECTION I BACKGROUND

- I-1. Overview of Propagation Effects on Satellite Communications
 - Ionospheric
 - Tropospheric
 - Frequency Dependence

- I-2. Ionospheric Effects
 - Multipath Fading and Scintillation
 - Depolarization
 - Group Delay

- I-3. Tropospheric Effects
 - Atmospheric Gases
 - Clouds, Fog
 - Rain Attenuation and Depolarization
 - Ice Depolarization
 - Scintillation
 - Angle of Arrival
 - Dispersion

- I-4. Radio Noise
 - Uplink Noise Sources
 - Downlink Noise Sources

- I-5. Propagation Data Bases
 - Meteorological Parameters
 - Rain Statistics
 - Water Vapor Density
 - Clouds
 - Slant Path Measurements
 - UHF/VHF Mobile
 - 1-3 GHz Mobile
 - C-Band, Ku-Band, Ka-band Fixed
 - ITU-R
 - Electronic Sources

SECTION II PREDICTION

- II-1. Prediction Methods for Satellite Links Operating Below About 3 Ghz
 - Ionospheric Scintillation
 - Multipath Fading
 - Group Delay, Phase Advance, Bandwidth Coherence
 - Polarization, Faraday Rotation
 - Ducting
 - Refraction and Turbulence
 - Sample Calculations*
- II-2. Prediction Methods for Satellite Links Operating Above About 3 Ghz
 - Attenuation from Atmospheric Gases
 - Cloud Attenuation
 - Fog Attenuation
 - Rain Attenuation
 - Rain Depolarization
 - Ice Depolarization
 - Scintillation
 - Angle of Arrival
 - Fade Rate, Fade Duration
 - Dispersive Effects
 - Combined Effects Statistics
 - Sample Calculations*
- II-3. Link Restoration Models

Site Diversity
Orbit Diversity
Link Power Control
Adaptive FEC
Sample Calculations

SECTION III APPLICATIONS

- III-1. Application of Prediction Models to Systems Design and Performance
 - General Link Analysis Procedures
- III-2. Propagation Effects on Mobile Satellite Systems
 - Land Mobile
 - Maritime Mobile
 - Aeronautical Mobile
- III-3. Propagation Effects on Ka-band Systems
 - Low Margin Fixed Service
 - Non-GSO Satellite Links
 - Mobile Systems
 - Broadband Links
- III-4. Propagation Effects on Direct Broadcast Systems
- III-5. Propagation Effects on Low Margin VSAT Systems
- III-6. Inter- and Intra- System Interference
- III-7. ITU Regulatory Considerations
 - PFD Limits
 - ITU Coordination Procedures

Sample Calculations

Louis J. Ippolito
Stanford Telecom
May 30, 1996

Page intentionally left blank

A Database For Propagation Models And Conversion To C++ Programming Language

Anil V. Kantak, Krisjani Angkasa and James Rucker

**Jet Propulsion Laboratory
California Institute of Technology
Pasadena, California 91109.**

1.0 Introduction

The telecommunications system design engineer generally needs the quantification of effects of the propagation medium (definition of the propagation channel) to design an optimal communications system. To obtain the definition of the channel, the systems engineer generally has a few choices. A search of the relevant publications such as the IEEE Transactions, CCIR's, NASA propagation handbook, etc., may be conducted to find the desired channel values. This method may need excessive amounts of time and effort on the systems engineer's part and there is a possibility that the search may not even yield the needed results.

To help the researcher and the systems engineers, it was recommended by the conference participants of NASA Propagation Experimenters (NAPEX) XV (London, Ontario, Canada, June 28 and 29, 1991) that a software should be produced that would contain propagation models and the necessary prediction methods of most propagation phenomena. Moreover, the software should be flexible enough for the user to make slight changes to the models without expending a substantial effort in programming. In the past few years, a software was produced to fit these requirements as best as could be done. The software was distributed to all NAPEX participants for evaluation and use, the participant reactions, suggestions etc., were gathered and were used to improve the subsequent releases of the software.

The existing database program is in the Microsoft Excel application software and works fine within the guidelines of that environment, however, recently there have

been some questions about the robustness and survivability of the Excel software in the ever changing (hopefully improving) world of software packages.

2.0 The Propagation Database

The Propagation Model Database described here creates a user friendly environment that makes using the database easy for experienced users and novices alike. The database allows sufficient freedom for users to custom fit the propagation phenomena model of interest to their requirements. The database is designed to pass data through the desired models easily and generate relevant results quickly. The database already contains many of propagation phenomena models accepted by the propagation community and every year new models are added to it. Only minimal computer operations knowledge is necessary to run the database.

The major sources of models included in the database are the NASA Propagation Effects Handbook or the CCIR publications, sometimes they are taken from other publications such as the IEEE Journal etc. Every model included in the software contains a reference to the document from which the model was obtained, and if desired, a brief description of the model itself can be brought up on the screen or even printed. Also, when applicable, the related model names to the active model are also indicated. The parameters of every model in the database are shown explicitly, and the units of the parameters are defined completely so that the user does not have to invest time investigating them. Wherever possible, to make the use of the model obvious to the user, default values of the parameters are given. The default values are generally values that are used most frequently with the model, the user is free to change them to more appropriate ones for their own case. One possible use of the default values is to compare the already known results using the default values with the newly obtained values in an experiment.

Sometimes a propagation phenomenon model may have many formulas, numbers generated by one formula are used by the next, and so on until the final result is generated. In such cases, to include them as single step models in the database would make their use and understanding quite difficult, if not

impossible. To avoid this inconvenience, such models are broken down into several logical steps as appropriate, and parameters as well as outputs of each step are described in detail one step at a time. The software makes use of the extensive charting capabilities offered by the Microsoft Excel software to produce charts for the model under use and the users can use these charting capabilities to change any attribute of the produced chart. Where feasible, the actual charting process is made transparent to the user and involves the user only when a choice must be made between the possible inputs or outputs.

The database also allows the user to make changes, within some guidelines, to the model being run. The main restriction is that the user may make changes in mathematical functions and operations used in the model using only already existing input parameters of the model; no new definitions of parameters will be permitted. In general, this restriction is a reasonable restriction and the user can test slight variations of the existing model generated by utilizing different mathematical function and operations than the original model.

Every model in the database has the same operating procedure and instructions, thus the user needs to learn the procedure for only one model in order to use the entire database effectively. All the necessary precautions to ensure the correct use of the database are incorporated in the program. When incorrect inputs are made or when an action conflicts with the general directives of the model at hand, the user is alerted with a warning, and where possible, suggestions are made to correct the input.

User friendly procedures are used to call the available mathematical functions of Excel software, such as curve fitting, statistical analysis, etc. This allows the user to apply these functions to the data whenever needed.

3.0 Software for the Propagation Database

In the early stages of the software development, a study was conducted to evaluate the advantages and disadvantages of currently available compiler-based program versus spreadsheet program for hosting the propagation database

software. The results of this study indicated that between the spreadsheet / database software and the compiler based software available then, because of its very nature of dealing with data in columns without extra effort, the spreadsheet software can easily create a product such as the Propagation Models Database.

Of the many commercially available spreadsheet programs at that time, Microsoft Excel was selected to host the Propagation Models Database. Excel provides an extensive list of the database and mathematical functions necessary to implement the propagation models. Excel also has excellent charting capabilities that include many versions of two-and three-dimensional charts, which can be easily used or automated using the macro language. Excel also offers the dialog box utility, which can be effectively used for input and output functions of the Propagation Models Database. Another notable advantage of Excel is that it can call any executable programs written in C, which is a compiler-based program. This arrangement is ideal because it combines the advantages of a spreadsheet environment with the speed of the compiler-based software for number-crunching purposes.

The reverse of the above statement is also true, i.e., if the Propagation database were to be developed in the C programming language, it could use the Excel functions such as charting etc. to make the C programming easy. At this particular point in time, the C language has developed and evolved such that it has an extensive array of functions and interfaces that can be used to produce the Propagation Database easily. The only thing missing in the C compiler is the 'visual' effect the Excel software can produce for the inputs and outputs of the program. This need is served by the C++ programming language. C++ can be considered as a superset of the C compiler language and has the capability to invoke the windows and table structures which are absolutely needed for the Propagation Database.

The C++ based Propagation Database program will not run faster than the currently Excel based program. The speed increase could be as much as 20 to 50 times depending upon the operation (model) being run. In any case, there will be a general increase of speed for all operations. Another advantage of using C++ as the underlying programming language for the Propagation Database is that once the program is completed, the user does not need the C++ compiler to

run the program. This results in less cost for the user to run the program (does not need to buy the Excel software) as well as the integrity of the program can be preserved because only the compiled code of the program will be distributed to the users.

The C++ may be interfaced with the windows as well as the Excel, and when the later interface is invoked, it can pass the data to Excel program easily and also can use the functions of Excel software to plot and row / column management. This allows the C++ to use Excel's excellent charting routines and this reduces the requirements on the programmer to write the charting routines. The only downside of this arrangement is that the user must also have the Excel software along with the Database Models program. One advantage of the C++ language worth mentioning is that one has complete control over the windows and table creation and hence can create any desirable window forms.

The software Excel 4.0 was a complete program serving almost every programming need of the user, nevertheless, recently Microsoft changed its underlying language from the Excel macro language to Microsoft Visual Basic thereby producing Excel 5.0. This was done to enhance Excel's usability as well as to increase the functionality necessary to make the input / output easy and intuitive. Even though, the step was almost necessary to compete favorably with other similar products in the market place, a converter from the older Excel 4.0 macro language to the newer Excel Visual Basic program was not provided. Even though the Visual Basic Excel (Excel 5.0) could run the older Excel 4.0 programs, any change in the macros is not supported in Excel 5.0 and the windows structures etc. are entirely different in the two languages. This meant that the programmers who created the older programs using Excel 4.0 were faced with the conversion from Excel 4.0 to Excel 5.0 if they desired to use the functionality of the newer Excel. This prompted the authors to search for a more lasting programming language, which may change in incremental steps (like all programming languages do) but not in quantum steps so that a new programming effort will be needed for the same program. Visual C++ compiler seems to fit this need.

The C++ being an Object Oriented Language, various objects may be created independently of other objects. This trait will be useful in putting the software (a

bunch of independent objects) on a network, where the remote user may be able to download either the entire software or only the desired objects and provide the input / output interface necessary for it to run. This is in addition to the distribution of the software via floppy disks through NAPEX participation. The authors feel that this method of creating the Propagation Models Database will have much greater use in the propagation community.

The current effort is converting the older Excel 4.0 based Propagation Models Database program to the visual C++ compiler based software.

4.0 Software and Hardware Requirements

It is anticipated that when the C++ based Propagation Models Database is released, to run it, the user may require Microsoft Windows 95 or Windows NT. Windows 95 is almost becoming a standard and Windows NT is the future of Microsoft Windows, so basing the program on any one of these systems should not cause any problem for the user. Even though the 80486 microprocessor could run the program, it is strongly suggested that a Pentium microprocessor based computer be used. At least 8 Mbytes (preferably 16 Mbytes) of RAM are required to run the software. The clock speed should be at least 50 MHz.

The C++ development is currently done using the IBM compatible PC's and not the Macintosh computers. Later on, once the software is ready for PC's the development will focus on the conversion of the software for the Macintosh computers.

It is recommended that a color monitor be used so that the charting can be done more effectively. Also, needed is a hard disk with at least 5 megabytes of storage space available for the software.

5.0 The Propagation Database

The Propagation Database is divided into six categories: the Ionospheric models, the Tropospheric models, the Land Mobile Systems models, the Effects of Small Particles models, the Rain models, and the Radio Noise models. These six categories are further divided into subcategories to include all the models to be housed in the software.

Ionospheric Models:

Tropospheric Models:

Index of Refraction Profile Model, Gaseous Attenuation Model, Refraction and Fading Model, and Scintillation Model

Mobile Satellite System Models:

The mobile satellite models are subdivided into 'Land Mobile System Models' and 'Maritime Mobile System Models'.

Land Mobile Satellite System Models:

Attenuation Frequency Scaling Model, Cumulative Distribution of Fade Duration Model, Cumulative Distribution of Non Fade Duration Model, Diffusely Scattering Model, Diversity Improvement (Tree Shadowing) Model, Empirical Regression Models, Empirical Roadside Shadowing Model, Faraday Rotation Model, Fresnel Zones, Frequency Reuse Using Orthogonal Polarization Model, Raleigh Model, and Reflection Coefficient Model.

Maritime Mobile Satellite System Models:

Fading Due to Sea Reflection Model, and Interference Due to Reflection Model.

Effect of Small Particles Models:

Cloud Model

Rain Models:

CCIR Model, COMSAT Model, Global Model, Depolarization Model, and Site Diversity Model.

Radio Noise Models:

Noise Model

The access to any model is carried out using Excel's dialog box user interface. Each dialog box is divided into six distinct areas to help the user to provide the inputs easily.

The six areas of the dialog box are described below. The first area is used to provide general information about the model selected by the user. This step describes any particular conditions required by the model, the parameter ranges as well as the number of steps the model has, and so on. The second area is used to display formulas describing the model selected. The formula can be modified by the users to a certain extent using legal expressions in Excel. Once the formula is created, the software will use this formula for the current run only. Loading the software again will bring back the original formula. The third area is the parameter definition area, where all the parameters of the model are defined appropriately. The fourth area is called the input area. This area is used to acquire input parameter(s) for the model. The fifth area is used to display intermediate or final result(s) of the particular model. The sixth area has a few buttons to help the user and to produce the output(s) of the model (or step). For some models, this area also has buttons to allow creation of a table of output values of the model as a function of the range of the selected input parameter. The following figures show the run of the CCIR rain attenuation model included in the database software.

6.0 Future of the Propagation Models Database

From the inception of the idea of Propagation Database till present, Microsoft Excel has been the underlying software. The reason for adopting Excel was that it truly offered unique capabilities of charting and scientific functionality. However, Excel has some drawbacks such as the slow executions of the program, the large memory requirement, and the need to own the Excel software by the users. Another disadvantage Excel entails is that whenever a newer version of Excel is released, such as Excel 5.0, it may not be fully compatible with the older versions such as Excel 4.0. This makes it difficult, if not impossible, for programmers to develop a long-term program. Having taken all these disadvantages into consideration, it was decided that future versions of the database shall be written in the visual C++ language, because this language offers some attractive qualities such as faster execution, efficient use of computer memory, and complete independence from the compiler software once the program is compiled. It also makes the program easier to be put on a network for remote user convenience.

7.0 Conclusion

A database of various propagation phenomena models that can be used by telecommunications systems engineers to obtain parameter values for systems design is presented. This is an easy-to-use tool and will soon be available for a PC using Microsoft C++ software under Windows environment. Macintosh version will be created soon afterwards.

Page intentionally left blank

*NASA Propagation
Studies Website*

(<http://propagation.jpl.nasa.gov>)

*Krisjani S. Angkasa
Jet Propulsion Laboratory*

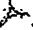


NASA Propagation Studies



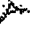
OBJECTIVES: To enable the development of new commercial satellite communication systems and services by providing timely data and models about propagation of satellite radio signals through the intervening environment and to support NASA missions.

APPROACH: In partnership with industry and academia, the program leverages unique NASA assets (currently Advanced Communications Technology Satellite) to obtain propagation data. The findings of the study are disseminated through refereed journals, NASA reference publications, workshops, electronic media, and direct interface with industry.

Viewing Instructions

Some of the files located on this server require Adobe's Acrobat Reader to be installed with your Web browser. These files are marked with the Acrobat Reader logo .

Click here to download Acrobat Reader

- ACTS Propagation Campaign
- Ka-Band Studies
 - Three-Site Space Diversity Experiment at 20 GHz Using ACTS, Julius Goldhirsh, Bert H. Musiani, The John Hopkins University, Applied Physics Laboratory, and Asoka Dissanayake, K.T. Lin, COMSAT Laboratories  (26k)
 - Attenuation Scaling by Frequency in the Ku/Ka-Bands Using the Olympus Satellite, Jeff D. Laster, Warren L. Stutzman, Satellite Communications Group, Bradley Department of Electrical Engineering, Virginia Polytechnic Institute & State University  (22k)
 - An Extended Empirical Roadside Shadowing Model for Estimating Fade Distributions from UHF to K-Band for Mobile Satellite Communications, Julius Goldhirsh, Applied Physics Laboratory, The Johns Hopkins University, and Wolfhard J. Vogel, Electrical Engineering Research Laboratory, The University of Texas at Austin  (116k)

- Mobile Satellite Communications

- Handbook

- NASA Reference Publication 1274
Propagation Effects for land Mobile Satellite Systems: Overview of Experimental and Modeling results, J. Goldhirsh and W. Vogel.

- Experiments

- GPS: A Tool for Mobile Satellite Fade Measurements
Wolfhard J Vogel and Geoffery W. Torrence
University of Texas, Electrical Engineering Research Laboratory
10100 Burnet Road, Austin, Texas 78758-4492 (4.4Mb)
- Fisheye Movies
University of Texas, Electrical Engineering Research Laboratory
10100 Burnet Road, Austin, Texas 78758-4492

- Available Publications

- Handbooks

- NASA Reference Publication 1274
Propagation Effects for land Mobile Satellite Systems: Overview of Experimental and Modeling results, J. Goldhirsh and W. Vogel.
- NASA Reference Publication 1108(02)
Propagation Effects on Satellite Systems at Frequencies Below 10 Ghz, A Handbook for Satellite Systems Design, W. Flock
- NASA Reference Publication 1082(04) -Pending
Propagation Effects handbook for Satellite Systems Design, A Summary of Propagation Impairments to 10 to 100 Ghz Satellite Links With Techniques for System Design, L. Ippolito

- Proceedings, NAPEX Meetings & Workshops

- Proceedings of NAPEX XIX and APSW VII
Fort Collins, Colorado, June 14-15, 1995
- Proceedings of NAPEX XVIII and ACTS miniworkshop
Vancouver, British Columbia, June 16-17, 1994
- Proceedings of NAPEX XVII and ACTS miniworkshop
Pasadena, California, June 14-15, 1993
- Proceedings of NAPEX XVI and ACTS miniworkshop
Houston, Texas, May 29-30, 1992
- Proceedings of NAPEX XV and ACTS miniworkshop
London, Ontario, Canada, June 28-29, 1991
- Presentations of the Eighth ACTS Propagation Studies Workshop
(APSW VIII) Norman, Oklahoma, November 15-16, 1995

- Presentations of the Sixth ACTS Propagation Studies Workshop (APSW VI) Clearwater Beach, Florida, November 28-30, 1994
- Presentations of the Fifth ACTS Propagation Studies Workshop (APSW V) Las Cruces, New Mexico, November 29-December 1, 1993
- Presentations of the Fourth ACTS Propagation Studies Workshop (APSW IV) Santa Monica, California, December 1-2, 1992
- Presentations of the Third ACTS Propagation Studies Workshop (APSW III) Santa Monica, California, January 21-22, 1992
- Presentations of the First ACTS Propagation Studies Workshop (APSW I) Santa Monica, California, November 28-29, 1989

● Related Papers of Propagation Models & Data

- Online Models
- Models not online
- Models from other locations

● Conferences and Workshops

○ NAPEX Meetings/ACTS Workshops

- NASA Propagation Experimenters (NAPEX) XIX and ACTS Propagation Studies Workshop (APSW VII), Fort Collins, Colorado, June 14-15, 1995
- NASA Propagation Experimenters (NAPEX) XVIII and ACTS miniworkshop, Vancouver, British Columbia, June 16-17, 1994
- NASA Propagation Experimenters (NAPEX) XVII and ACTS miniworkshop, Pasadena, California, June 14-15, 1993
- NASA Propagation Experimenters (NAPEX) XVI and ACTS miniworkshop, Houston, Texas, May 29-30, 1992
- NASA Propagation Experimenters (NAPEX) XV and ACTS miniworkshop, London, Ontario, Canada, June 28-29, 1991

- Eighth ACTS Propagation Studies Workshop (APSW VIII) Norman, Oklahoma, November 15-16
- Sixth ACTS Propagation Studies Workshop (APSW VI) Clearwater Beach, Florida, November 28-30, 1994
- Fifth ACTS Propagation Studies Workshop (APSW V) Las Cruces, New Mexico, November 29-December 1, 1993
- Fourth ACTS Propagation Studies Workshop (APSW IV) Santa Monica, California, December 1-2, 1992
- Third ACTS Propagation Studies Workshop (APSW III) Santa Monica, California, January 21-22, 1992
- First ACTS Propagation Studies Workshop (APSW I) Santa Monica, California, November 28-29, 1989

- NAPEX/ACTS Registration

Comments:

Please enter your e-mail address

If your Web browser does not support forms then please e-mail comments to suwitra@java.jpl.nasa.gov

To order reports and propagation models, please contact:

Mardy Wilkins
Jet Propulsion Laboratory
California Institute of Technology
MS 161-260
4800 Oak Grove Drive
Pasadena, CA 91109-8099, USA
Phone: (818)354-7421
Fax: (818)393-4643
e-mail: Mardith.Wilkins@jpl.nasa.gov

ACKNOWLEDGEMENT: The NASA Propagation Studies are conducted by the Jet Propulsion Laboratory, California Institute of Technology, under a contract with the National Aeronautics and Space Administration, in partnership with industry, academia, and NASA LeRC.

The above pages are designed to be of interest to scientists and engineers only.

Related Homepage:

- CRC
- IEEE Antenna & Propagation
- NOAA

Page intentionally left blank

ACTS MINIWORKSHOP

A MINIWORKSHOP

ON

ADVANCED COMMUNICATIONS TECHNOLOGY
SATELLITE (ACTS) PROPAGATION STUDIES

F. Davarian (Hughes Space and Communications Co.),

R.K. Crane, D.V. Rogers (U. Oklahoma)

Page intentionally left blank

ACTS OPENING REMARKS

History

In the early 80s when NASA began its effort to examine the feasibility of Ka-band satellite communications via an experimental program called ACTS, or Advanced Communications Technology, there were no Ka-band applications in sight. At the time, many experts were skeptical of the use of this band for satellite communications. Today, partly because of NASA's foresight, there is such a great deal of interest in this band that some people predict above 50% of all FCC applications for space communications will be for the Ka-band. Therefore, much credit is due to NASA that I gladly acknowledge.

Now let us turn our focus on propagation experiments. As most of you are aware, the NASA Propagation Program has made many contributions to the development of Earth-space communications systems in the last two decades. This program is continuously on the lookout for platforms of opportunity to conduct propagation experiments. Recognizing its potential for propagation studies, the NASA Propagation Program began planning to use ACTS in 1987. I recall the first meeting we had on this subject with David Rogers, John Kiebler and a few others at the COMSAT Laboratory in Maryland in 1987. In 1989, NASA formally announced its decision to support propagation measurements by sponsoring the first ACTS propagation studies workshop attended by representatives from industry, academia and other users of propagation data. The goals of the ACTS propagation campaign were defined in this workshop and a plan was drafted by the participants. In subsequent workshop meetings, this plan was refined and the requirements of the propagation terminal and the data collection and processing software were written. In parallel with the planning activities, NASA released an announcement of opportunity for ACTS propagation experiments in North America in December of 1991. This announcement resulted in the selection of seven experimenters who would use the NASA provided terminal for field measurements. A few months before the experimenter selection began, NASA funded Virginia Polytechnic Institute to build seven identical terminals. As mentioned earlier, the requirements for these terminals were developed at ACTS propagation studies workshops. These terminals were delivered about the same time that ACTS was launched in September 1993. After terminal installation and testing, the data collection phase started December 1, 1993.

Expected Results and Outputs of the Propagation Campaign:

- Ka-band propagation data
- Prediction models of rain and atmospheric attenuation and scintillation
- Fade and nonfade duration distributions
- Frequency scaling models
- Diversity models

- Multiple site analysis
- Mitigation schemes for propagation anomalies
- Wet antenna effect model
- Rain climate region map revision
- Contribution to regulatory organizations

ACTS Propagation Campaign Milestones:

<u>Year</u>	<u>Event</u>
-------------	--------------

1987	First meeting at COMSAT
------	-------------------------

1989	First workshop, Santa Monica, CA
------	----------------------------------

1991	Announcement of Opportunity and Virginia Polytechnic Institute begins to develop the ACTS Propagation Terminal
------	--

1993	Terminal delivery and ACTS launch
------	-----------------------------------

1996	Data delivery, first two years
------	--------------------------------

—F. Davarian

Acknowledgments

I have attended many ACTS workshops before; this is the first time I have had an active role in organizing one. I am looking forward to working with the propagation community. I would like to thank my colleague and friend F. Davarian who has successfully nurtured the NASA Propagation Program and helped with solid advice. Many thanks are due to C. Mayer of the University of Alaska at Fairbanks who hosted this workshop. Last but not least, my sincere thanks to B. Bauer of LeRC for his collegial collaboration and support.

—N. Golshan

1

ACTS PROJECT & PROPAGATION PROGRAM UPDATE

433

Robert Bauer
NASA Lewis Research Center
ACTS Propagation Studies Workshop
June 6, 1996



Lewis Research Center

ACTS PROJECT OFFICE



SPACECRAFT STATUS

- Spacecraft operations continue to be nominal
- Sixth eclipse season completed. Battery reconditioning to be re-evaluated before fall eclipse.



ACTS PROJECT OFFICE



INCLINED ORBIT

- Hydrazine depletion estimate updated to July 1998 (as of 5/20/96)
- Delete last N/S maneuver saves enough fuel for more than 3 yrs. of E/W maneuvers
- Operations will require diurnal stepping of momentum wheel pivot to maintain spot beam locations



ACTS PROJECT OFFICE



INCLINED ORBIT, cont.

- Net result is that ACTS operations could be sustained for 2.3 years beyond July '98
 - Limited by range of S/C pivot
 - Current roll & yaw pointing accuracy expected to be only slightly degraded



ACTS PROJECT OFFICE



INCLINED ORBIT, cont.

***WHAT'S REQ'D TO MAINTAIN PROP.
MEASUREMENTS IN I/O PHASE?***

- **Sufficient margin?**
- **Tracking hardware?**
- **Preprocessing software mod's?**
- **S/C ephemeris data distribution?**
- ***COST to implement?***



ACTS PROJECT OFFICE



EXPERIMENTS PROGRAM

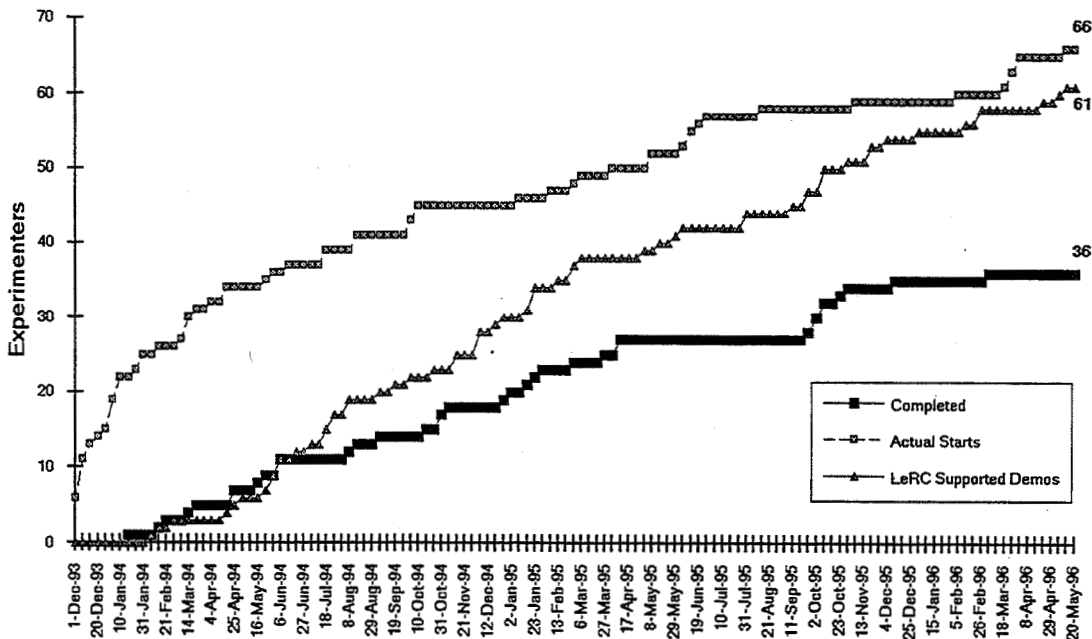
- Number of approved experiments: 81
 - Experiments started: 66
 - Experiments completed: 36
- Current regular users:
 - Mayo Clinic
 - JPL
 - Natl Library Medicine
 - GSFC
 - Georgetown Univ.
 - LeRC
 - Army



ACTS PROJECT OFFICE



ACTS Experiment Starts/Completes



ACTS PROJECT OFFICE

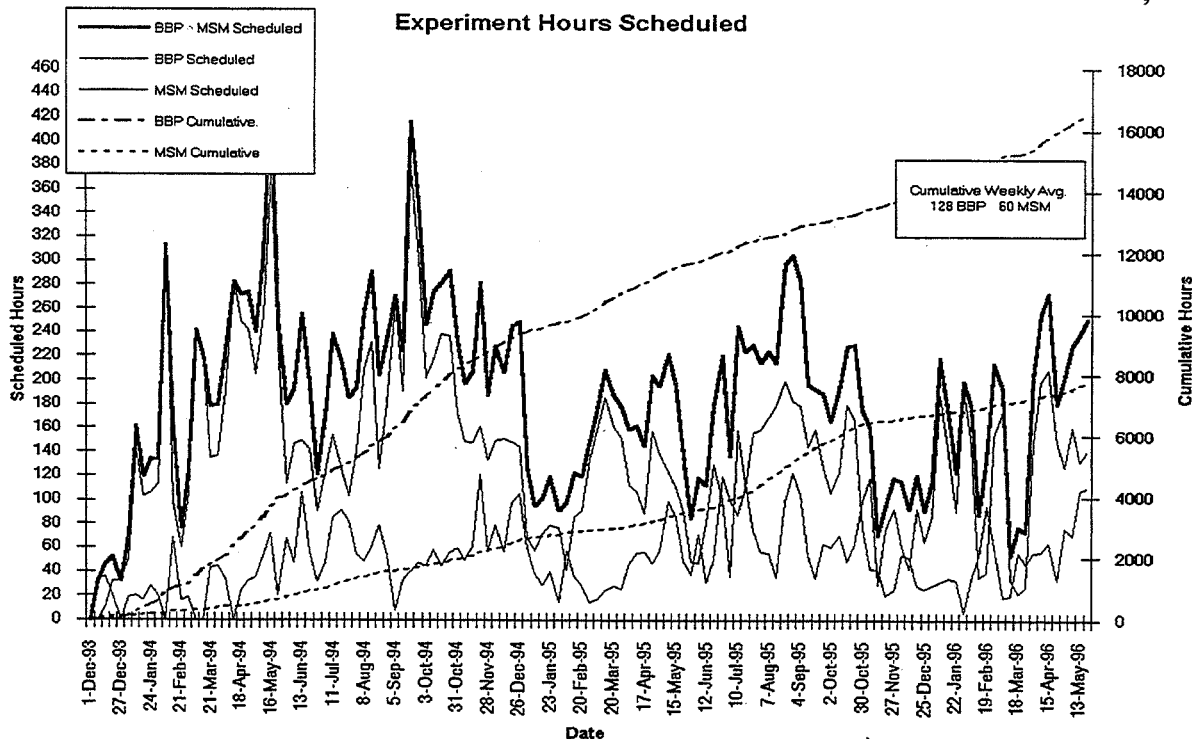


EXPERIMENTS PROGRAM

- Recent demos supported:
 - AIAA ICSS Conf., Feb.'96, Washington DC, USAT
 - Global Legal Info. Network, May '96, Wash. DC, T1VSAT
 - Congressman Sensenbrenner, (R-WI; House Science Committee) at LeRC in April '96, USAT



Lewis Research Center

ACTS PROJECT OFFICE


Lewis Research Center

ACTS PROJECT OFFICE


EARTH STATION STATUS

- Fleet of T1VSAT's remains operational
- All 5 High Data Rate terminals operated together on 5/06/96 (a first!)
- 2 USAT's removed from So.Cal.Edison. Being used in demos & experiments
- ACTS Mobile terminal to support Olympic Torch Relay, shipboard & aero applications



Lewis Research Center

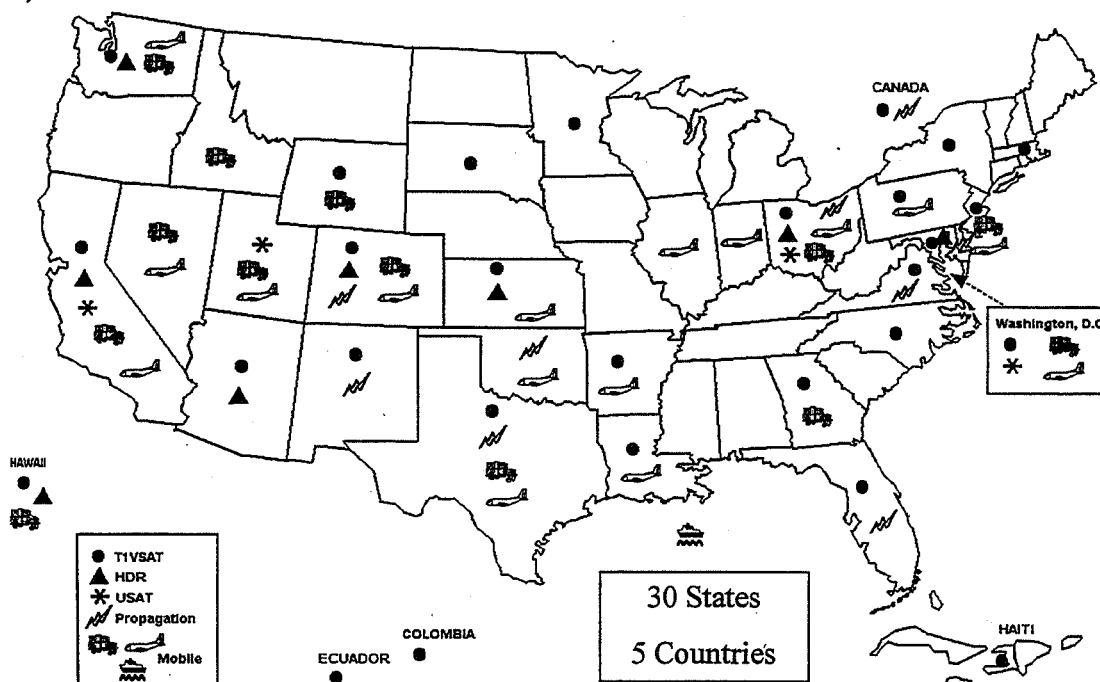
ACTS PROJECT OFFICE



ALASKA

As of: May 24, 1998

Previous/Current Earth Station Locations



Lewis Research Center

ACTS PROJECT OFFICE



Reorganizations

- Zero Base Review (ZBR) has resulted in:
 - NASA HQ downsizing announced
 - Impact unclear, but Level 2 Space Comm. Program Office to move to LeRC
 - Lewis is restructuring
 - Increase Supervisory:Non-Supervisory to 1:14
 - Space Comm Division & ACTS looking at transition to post-ACTS



Lewis Research Center

ACTS PROJECT OFFICE

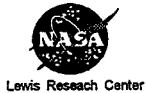


PROPAGATION PROGRAM STATUS

- New Leader at JPL...

Welcome Dr. Nasser Golshan!!

- Program continuation under consideration
 - Satellite Industry Task Force (SITF) input to NASA by late June-early July 1996
 - NASA to notify expts. ASAP of continuation or termination



ACTS PROJECT OFFICE



Prop. Program Status, cont.

- If continued:
 - Contract options exercised by NASA (already negotiated)
 - Provides 1 year of funding (through FY 97)
 - Complete 3rd year of data + 10 mos. of 4th year.
- Continuation must fit into ACTS Project budget/plans.

Reality = If propagation is funded, something else may not be.



ACTS PROJECT OFFICE



Prop. Program Status, cont

- Other considerations:
 - Value added of 1 (or more) year of data
 - Terminal maintenance/age
 - Inclined orbit operations
 - Other studies (e.g., mobile, de-pol, wideband dispersion, tropical data, ...)

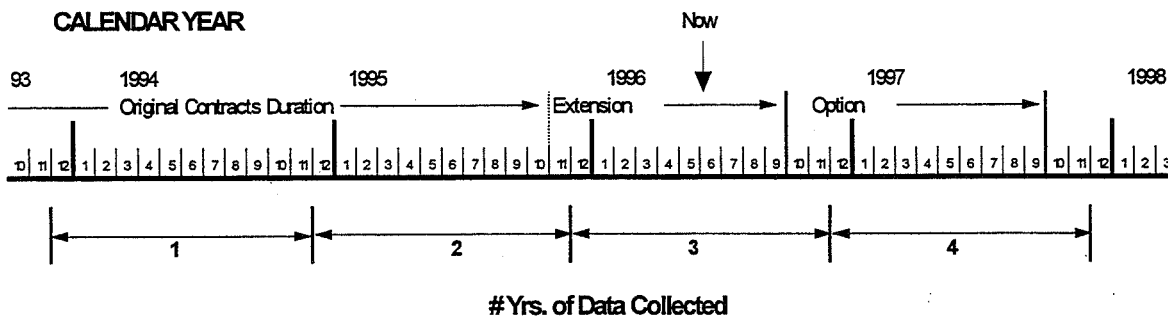


Lewis Research Center

ACTS PROJECT OFFICE



Program Timeline

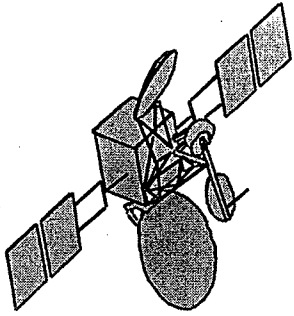


Lewis Research Center

ACTS PROJECT OFFICE



Page intentionally left blank



ACTS Rain Fade Compensation

443

Thom A. Coney

NASA Lewis Research Center
Cleveland, Ohio

Phone: 216.433.2652, Fax: 216.433.6371, E-mail: toney@lerc.nasa.gov

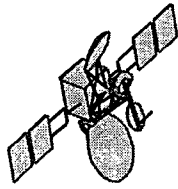


VSAT Architecture

Outdoor Unit

- ◆ 2.4/1.2 meter offset fed parabolic dish
- ◆ 12 watt transmitter
 - Solid state frequency doubler
 - 50 W Ku band TWTA driver

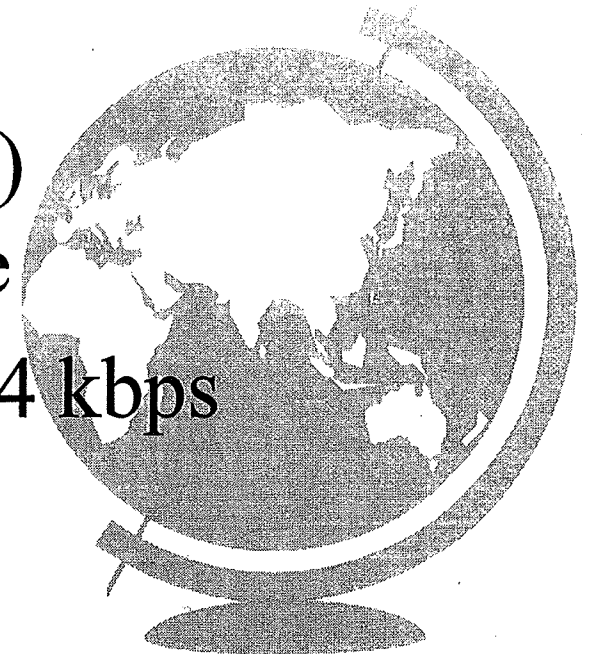


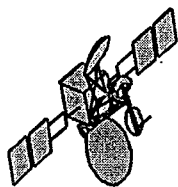


VSAT Architecture

Indoor Unit

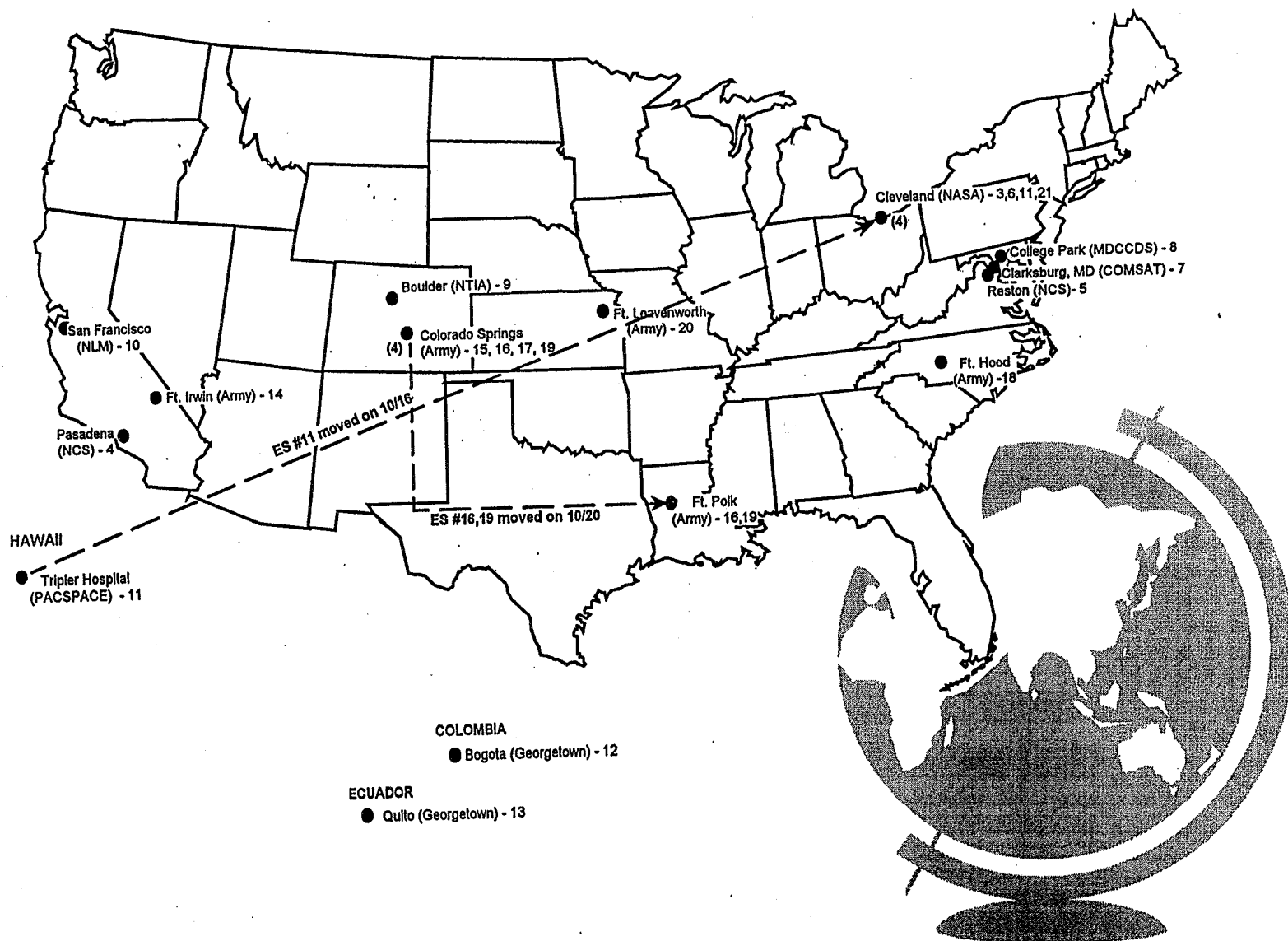
- ◆ Control Processor
- ◆ TDMA Hardware
- ◆ SMSK Modem
- ◆ Public Switched Network (PSN)
Compatible Terrestrial Interface
- ◆ 1.792 Mbps Throughput (28 - 64 kbps
circuits)

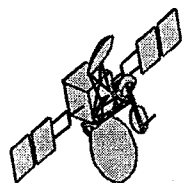




VSAT Locations

446



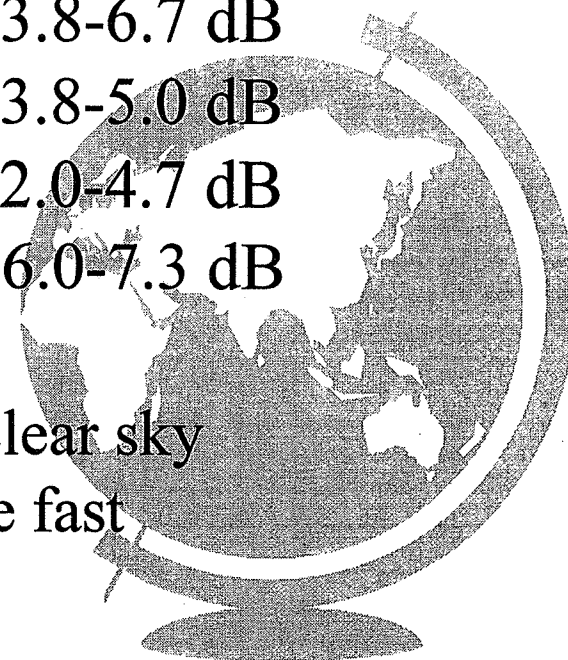


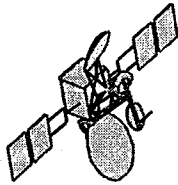
Link Margins

VSAT ID	Beam	Antenna Size	Uplink Margin	Downlink Margin
3	West	2.4m	≥ 11 dB	4.7-7.7 dB
13	West	2.4m	≤ 1.0 dB	4.0 dB
9	West	1.2m	≈ 5.3 dB	3.8-6.7 dB
5	East	1.2m	≈ 3.0 dB	3.8-5.0 dB
7	East	2.4m	≈ 3.3 dB	2.0-4.7 dB
8	East	2.4m	≥ 11 dB	6.0-7.3 dB

447

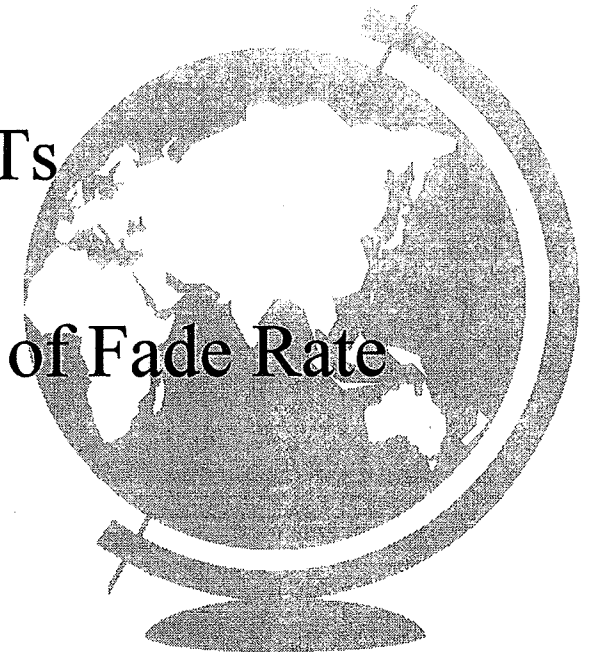
Uplink and downlink BER performance in clear sky conditions is typically $3.3E-10$ excluding the fast varying thermal period.

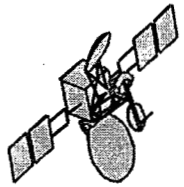




Rain Fade Algorithm Characterization

- ◆ Validate VSAT Downlink Signal Measurement
- ◆ Measure Rain Fade Availability for VSATs
- ◆ Measure BER Availability for VSATs
- ◆ Measure Performance as a Function of Fade Rate

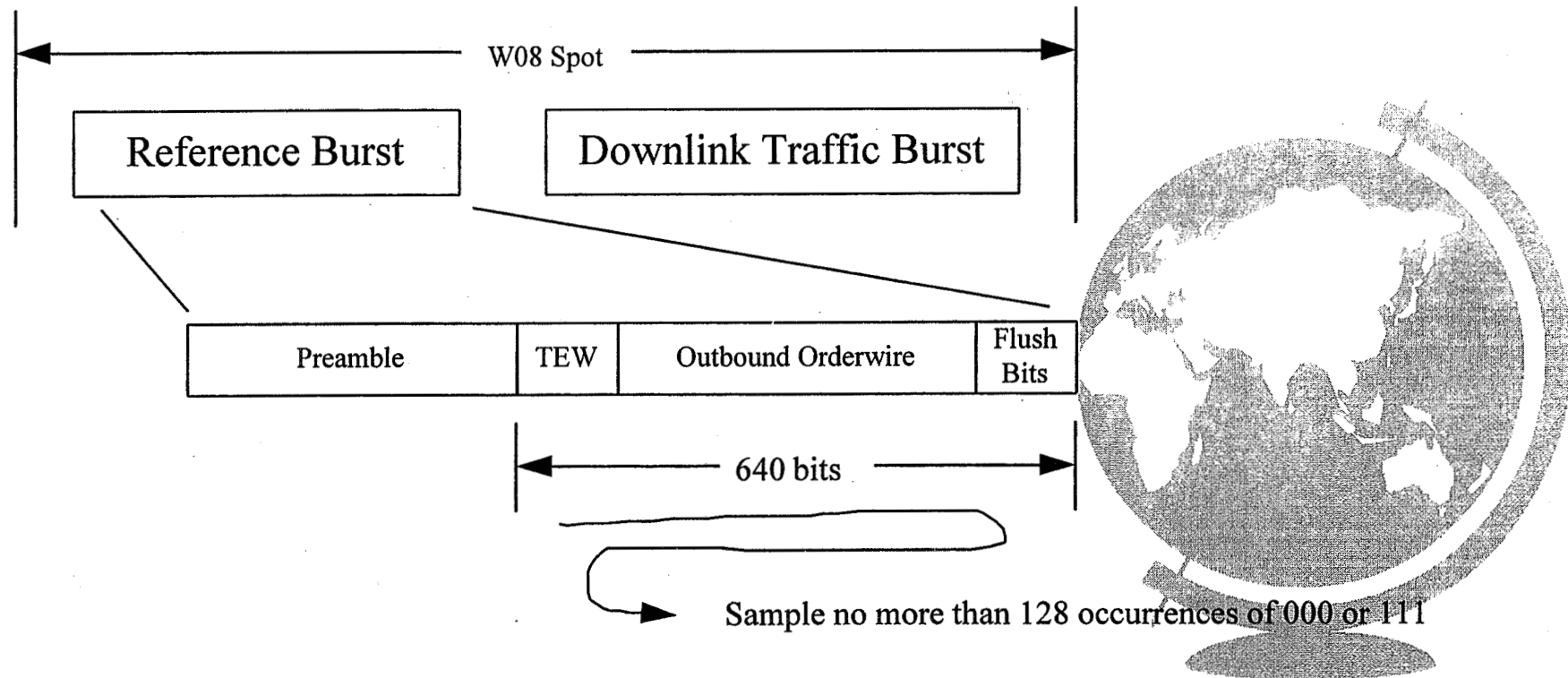


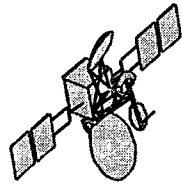


Downlink Signal Level Estimation

- ◆ Sample the VSAT demodulator output voltage of the center bit of 1's and 0's triplets

449



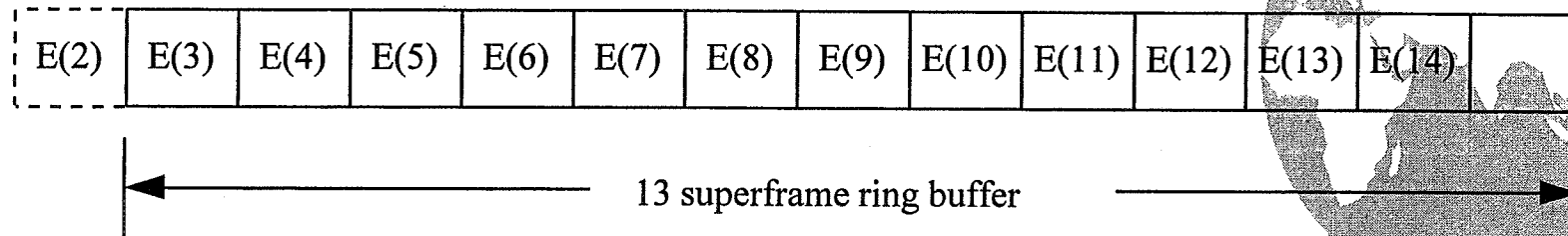


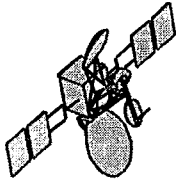
Downlink Signal Level Estimation

- Accumulate 128 samples, v_i , from each of the 75 frames in a superframe; i.e. $i = 9600$
- Estimate E_s/N_0 from the 9600 samples using the mean to variance method and store in a ring buffer

450

$E_s/N_0(j) = \text{function}(v_{i,j})$ where $j = \text{superframes}$; let $E(j) = (E_s/N_0)_j$

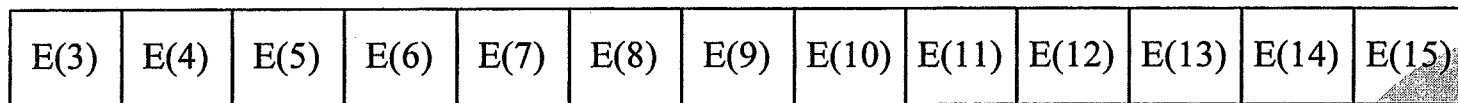




Downlink Signal Level Estimation

- Calculate the 1 second (13 superframe) running average of $E(j)$ thru $E(j+12)$ and report to the Master Control Station every 2 to 13 superframes.

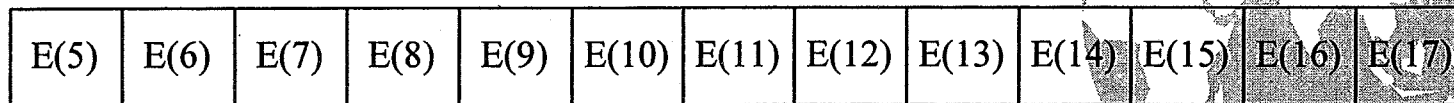
451



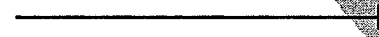
Average $E(3)$ thru $E(15) = \text{Estimated } E_s/N_0$



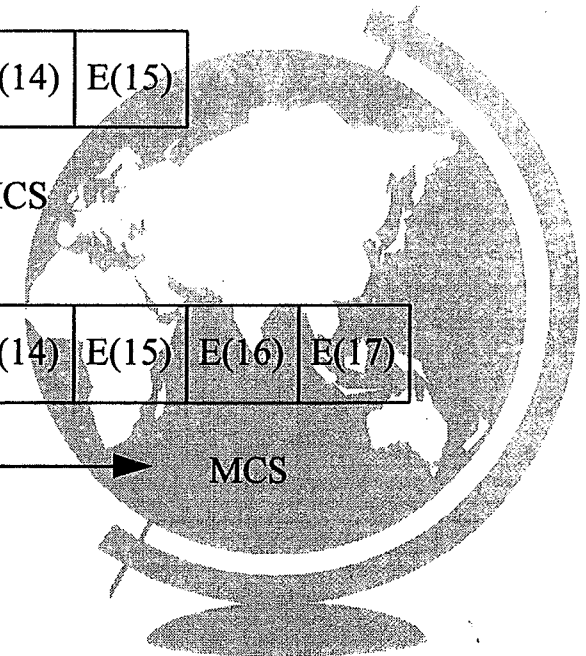
MCS

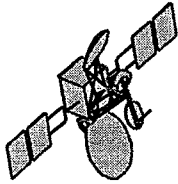


Average $E(5)$ thru $E(17) = \text{Estimated } E_s/N_0$



MCS



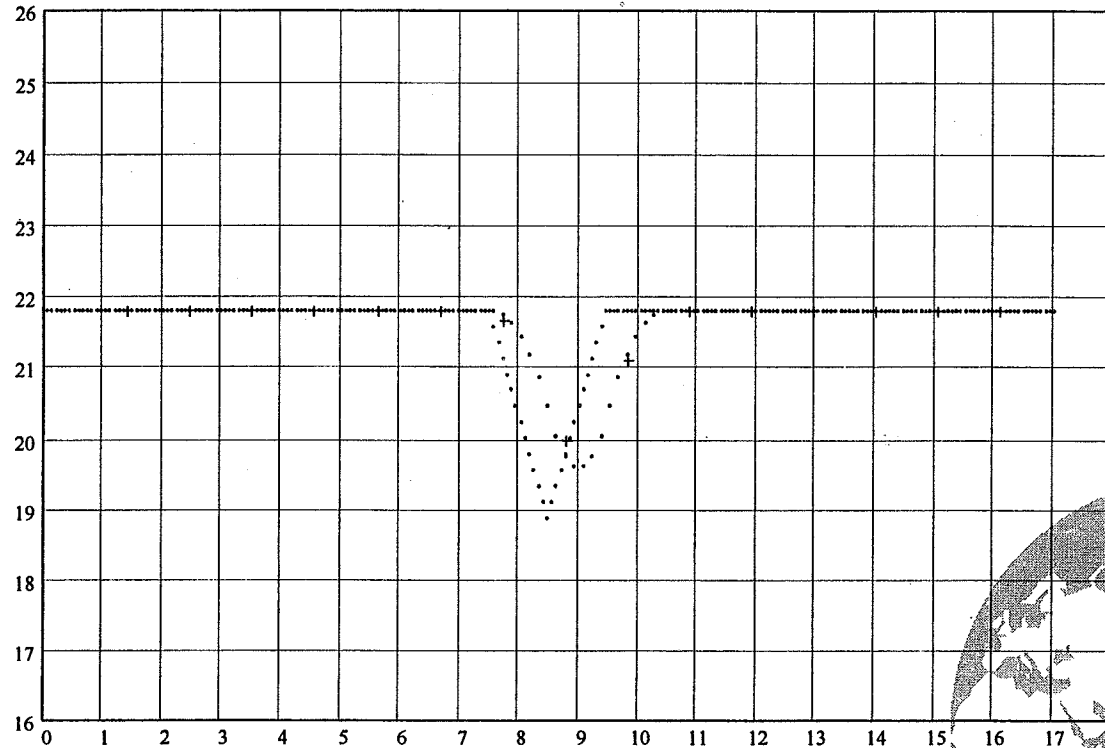


Measurement Impact of 1 Sec. Running Average

Fade Duration - 1 sec., Fade Rate - 3 dB/sec

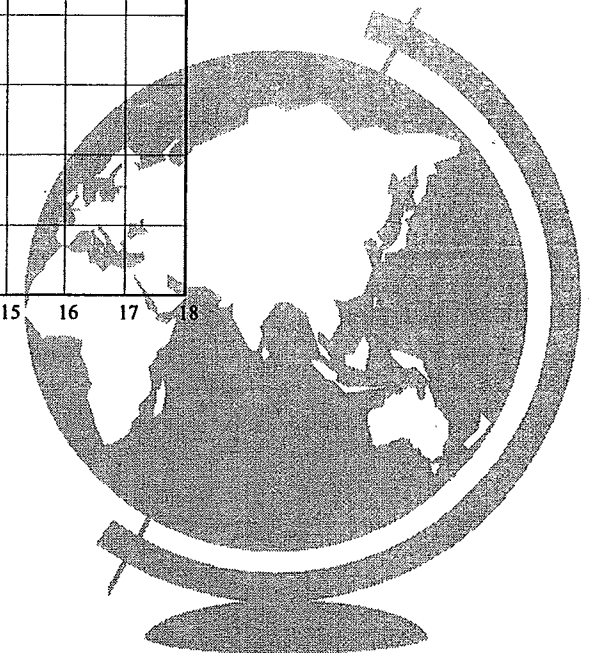
452

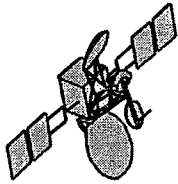
E_b/N_0 , dB



Time, sec

+ 1 sec. average of 150 ms data



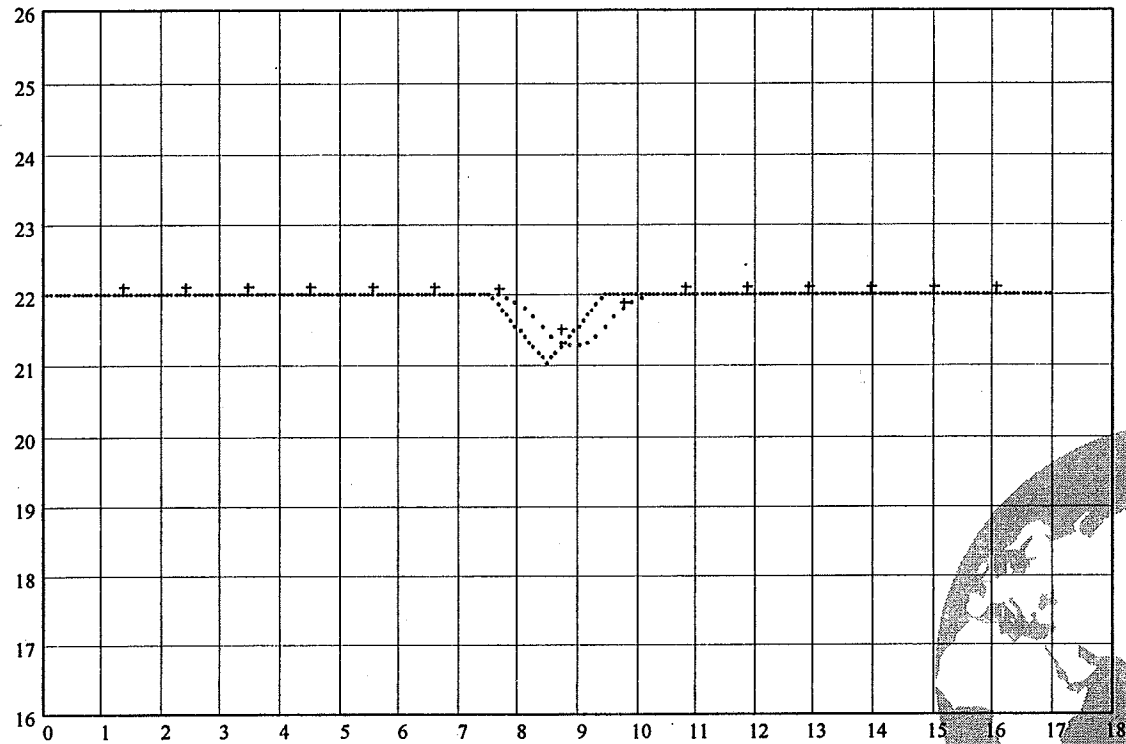


Measurement Impact of 1 Sec. Running Average

Fade Duration -1 sec., Fade Rate - 1 dB/sec

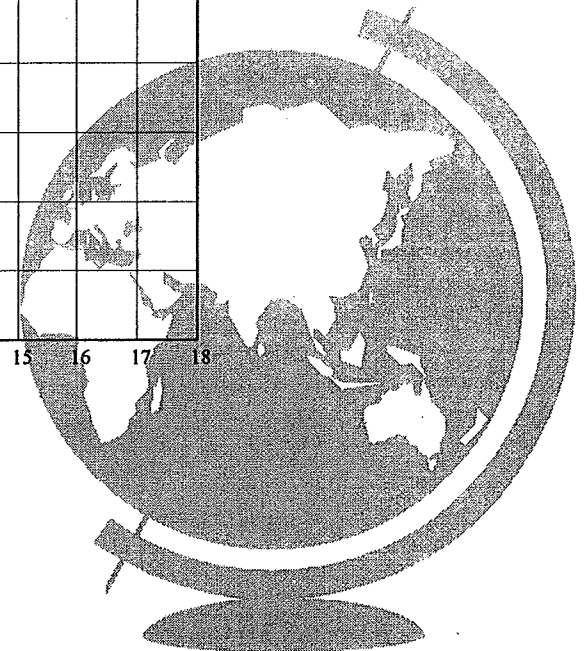
453

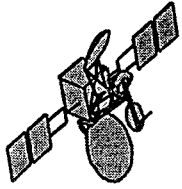
E_b/N_0 , dB



Time, sec

+ 1 sec. average of 150 ms data

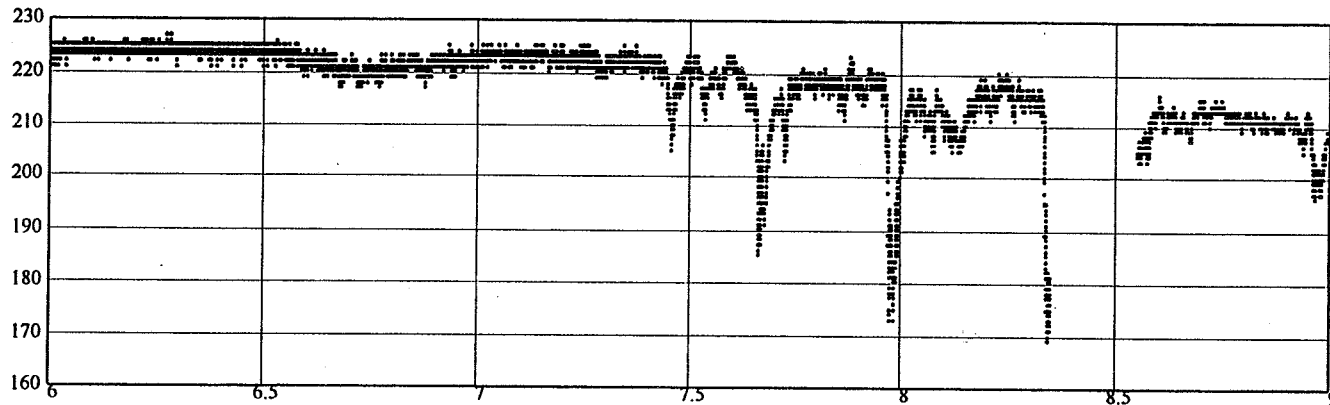




150 ms Fade Data for VSAT #7, 1/20/95

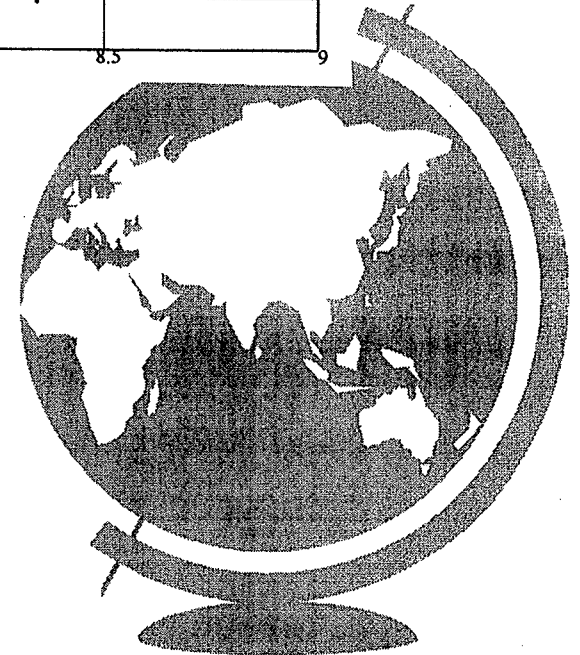
454

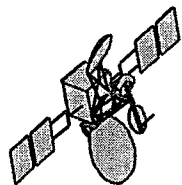
Signal Level,
(1 - 254)*



Time, hours GMT

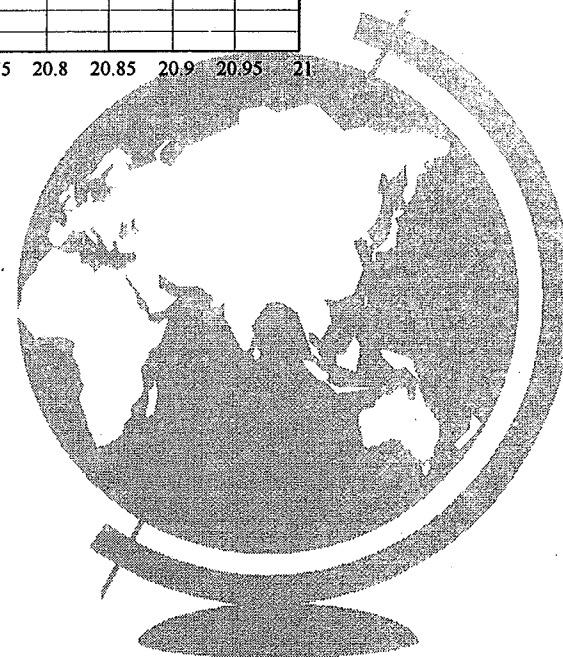
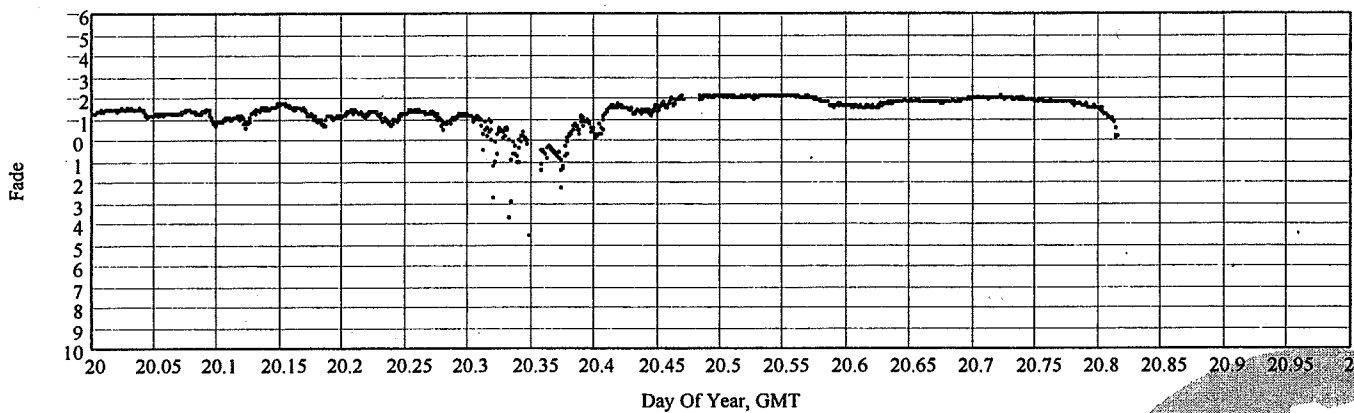
* .15 dB per unit

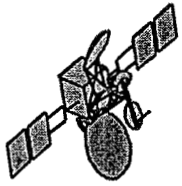




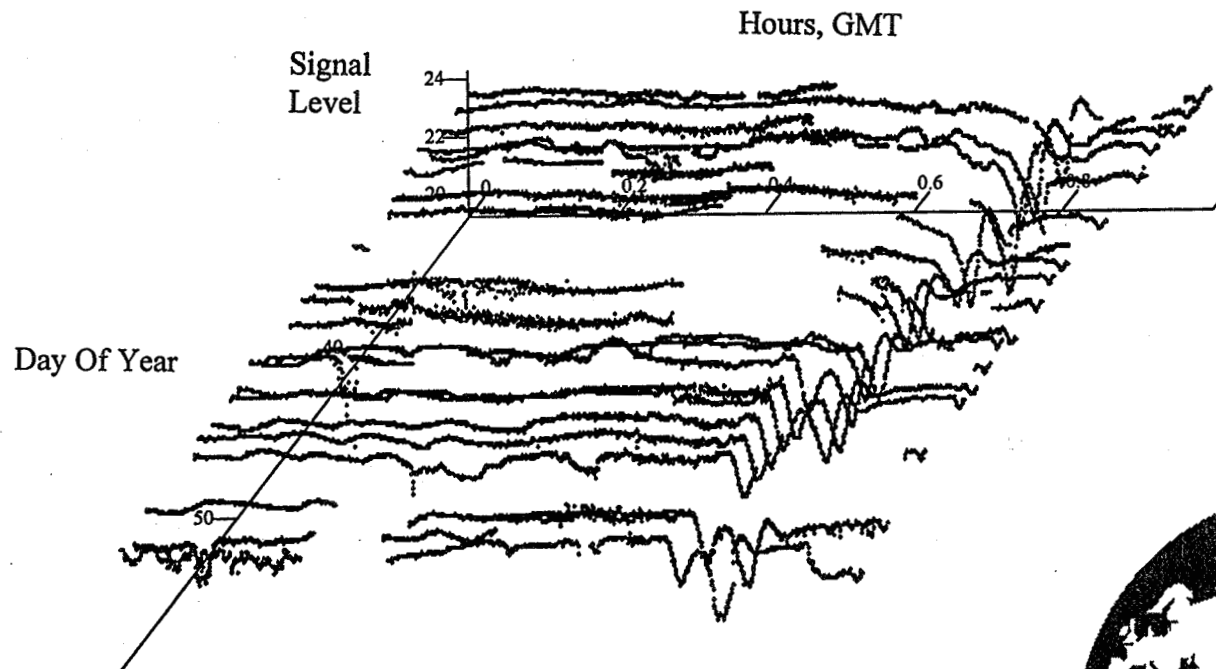
1 min. Fade Data for VSAT #7, 1/20/95

455



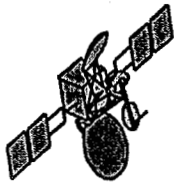


1 min Fade Data for VSAT #7, Feb., 1995

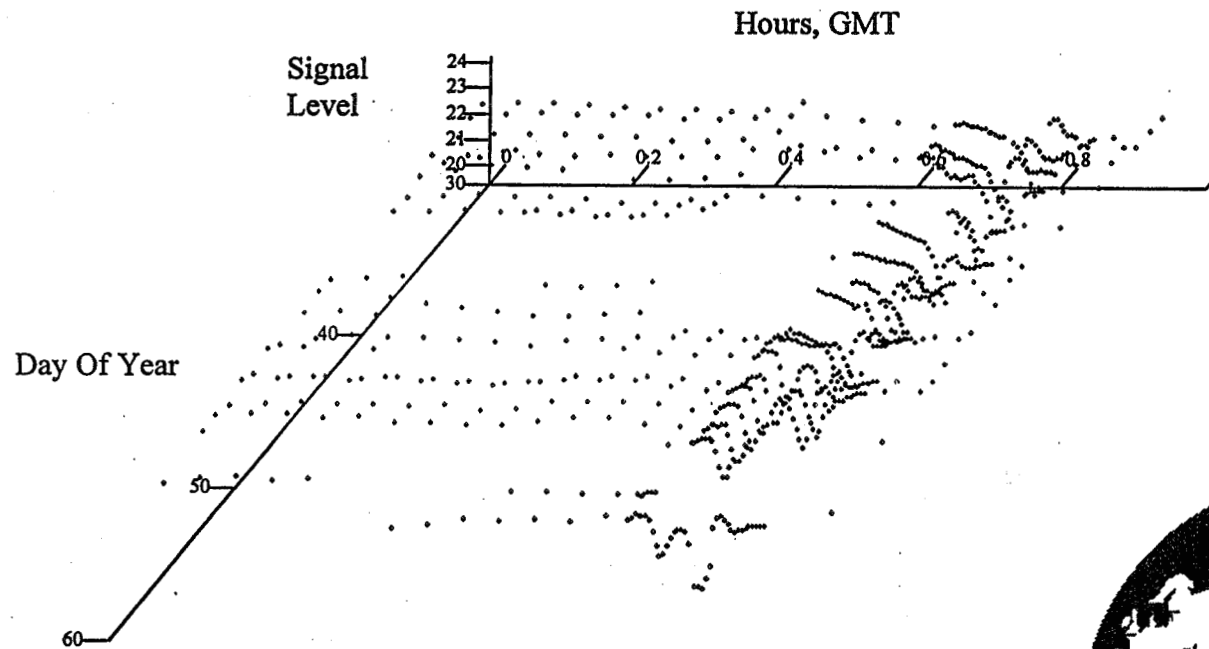


(The variations in signal level in the 1700 - 2300 GMT period is the result of beam mispointing which is in turn caused by thermal effects on the spacecraft antenna.)



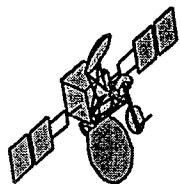


Filtered Fade Data for VSAT #7, Feb., 1995

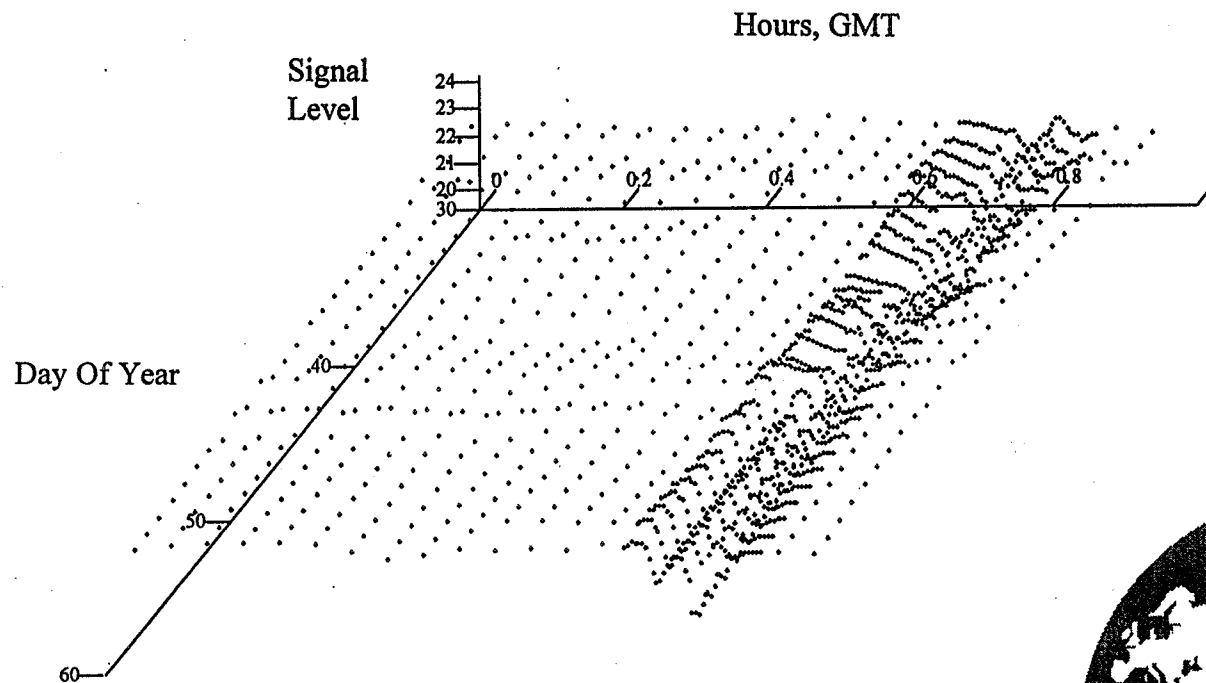


The data is filtered by standard deviation selecting only "clear sky data."



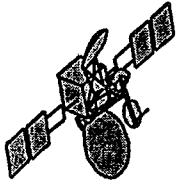


Interpolated Fade Data for VSAT #7, Feb., 1995



The filtered data is linearly interpolated across days so as to estimate the month's clear sky signal levels.

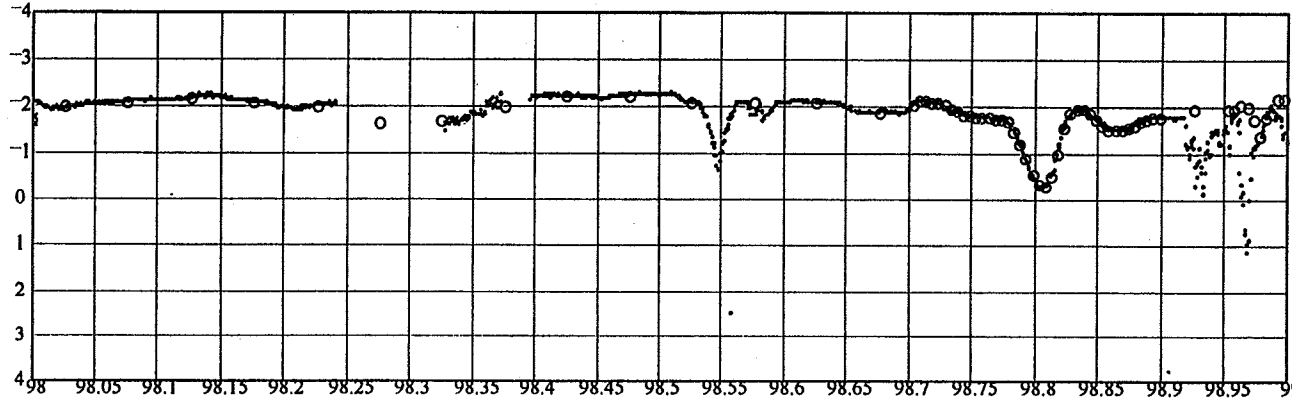




Fade Data and Clear Sky Baseline Fit

459

Downlink
Signal, dB

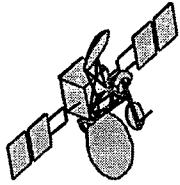


Day Of Year, hours GMT

- o clear sky baseline
- fade data

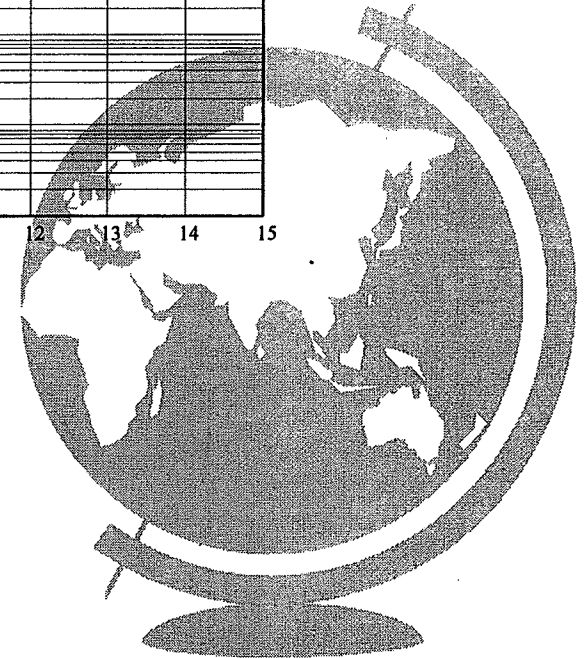
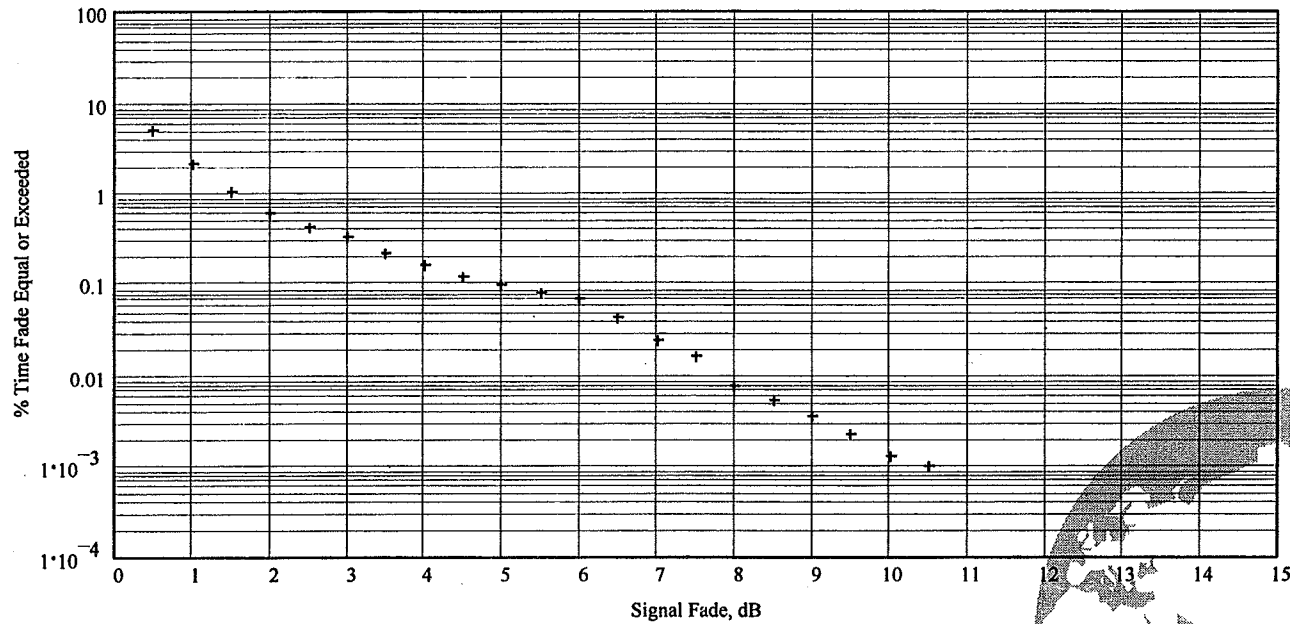
The signal level data is then subtracted from the estimated clear sky levels to yield the signal fade.

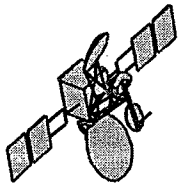




Fade Availability for VSAT #7 1995

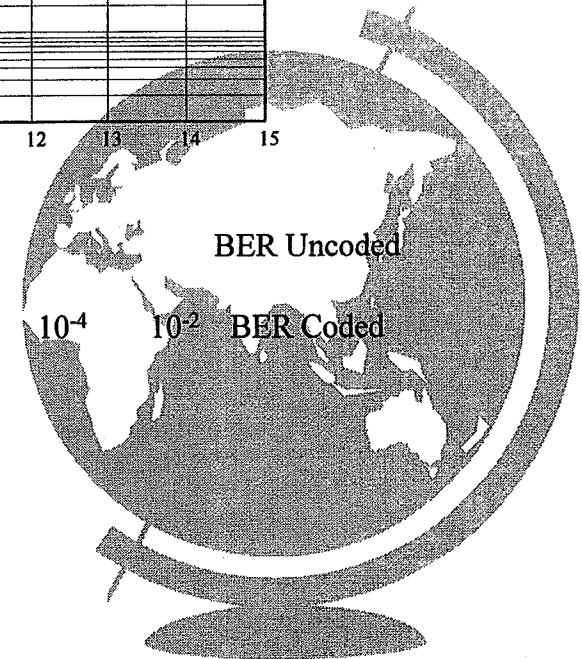
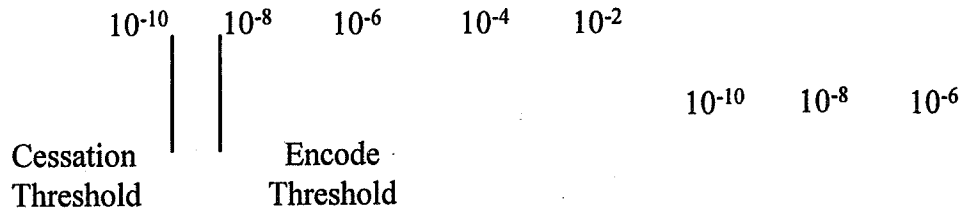
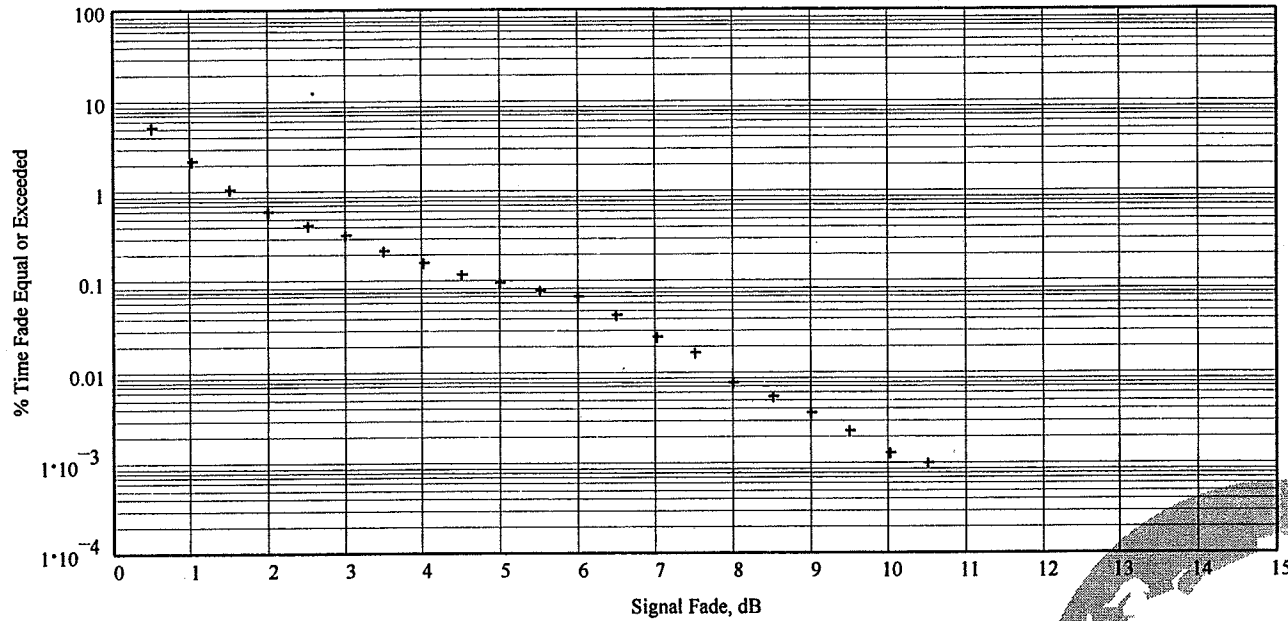
460

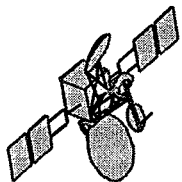




Downlink BER Availability for VSAT #7, 1995

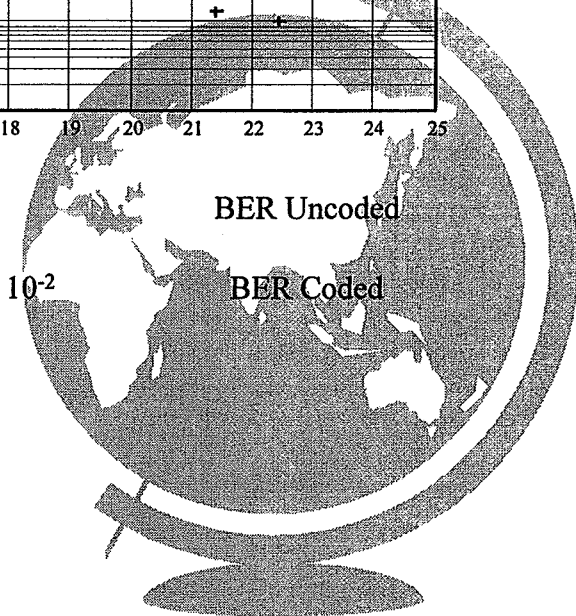
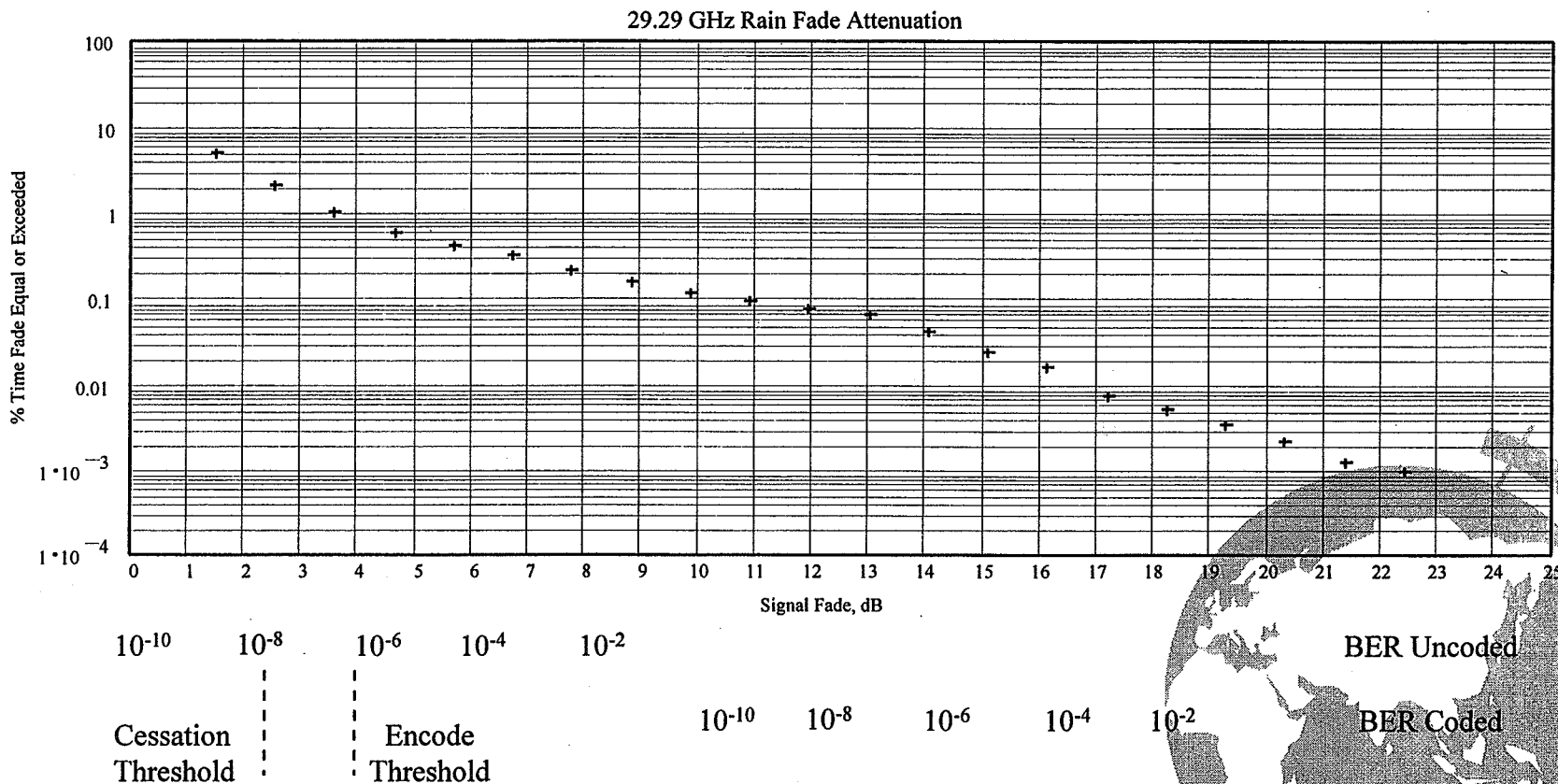
461

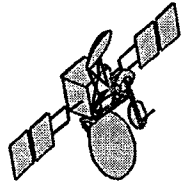




Estimated Uplink BER Availability for VSAT #7, 1995

462





Performance Status

Adaptive Rain Fade Compensation

- ◆ The rain fade protocol is functional detecting fades, providing an additional 10 dB of margin and seamless transitions to and from coded operation
- ◆ The stabilization of the link margins and the optimization of rain fade decision thresholds has resulted in improved BER performance
- ◆ Characterization of the Fade Compensation Algorithm is Ongoing



Page intentionally left blank

“A SENSITIVITY ANALYSIS OF COMBINED EFFECTS MODELING”

Glenn Feldhake

ACS A Division of
STANFORD TELECOM

APSW IX / NAPEX XX
4-6 Jun 96, Fairbanks, AK

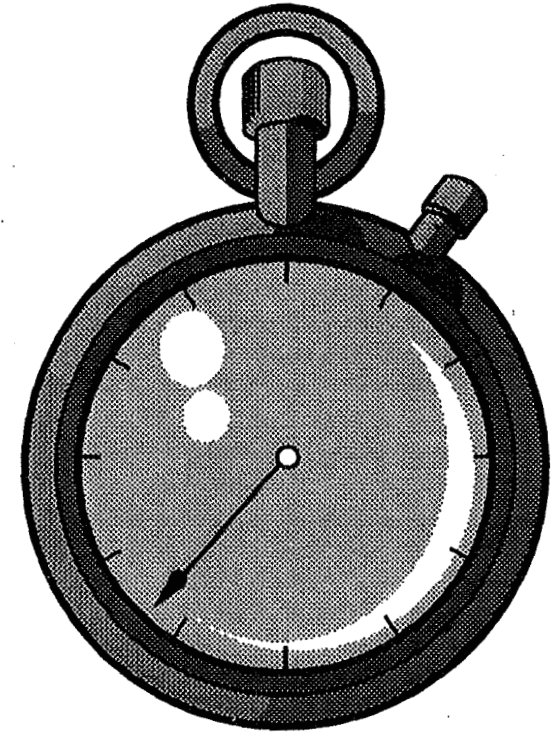
What Does Combined Effects Modeling Do?

- Models Distributions of Weather Characteristics as Random Variables
- Converts Distributions of Weather to Distributions of Attenuation (dB)
- Assumes Dependence/Independence Between Events
- Creates Upper and Lower Bounds of Joint Probability



466

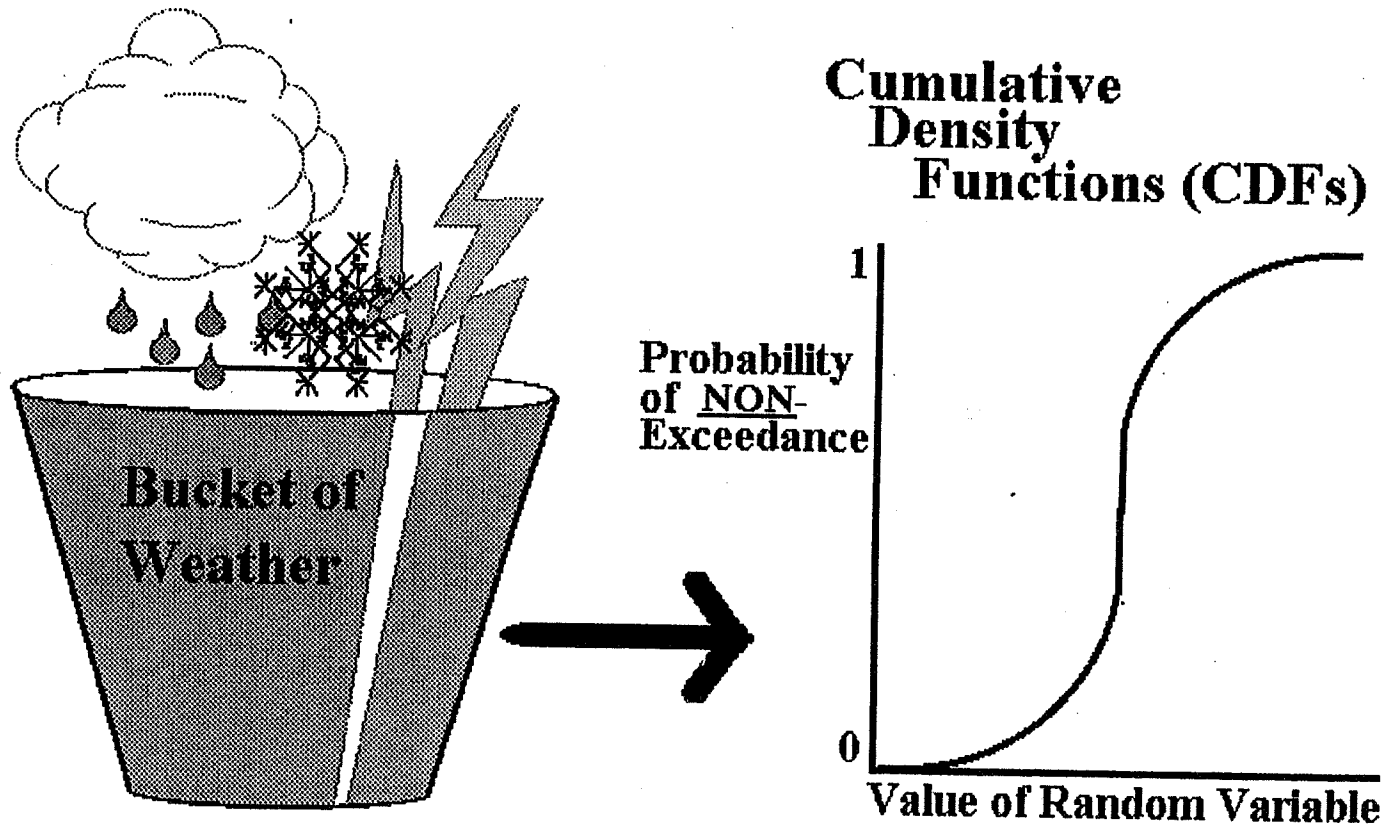
The Five Minute Combined Effects Tutorial...



467

WHERE DO WE START?

- ❑ Step 1) Start with a Pool of Weather Data
- ❑ Step 2) Create CDFs of Weather Statistics



468

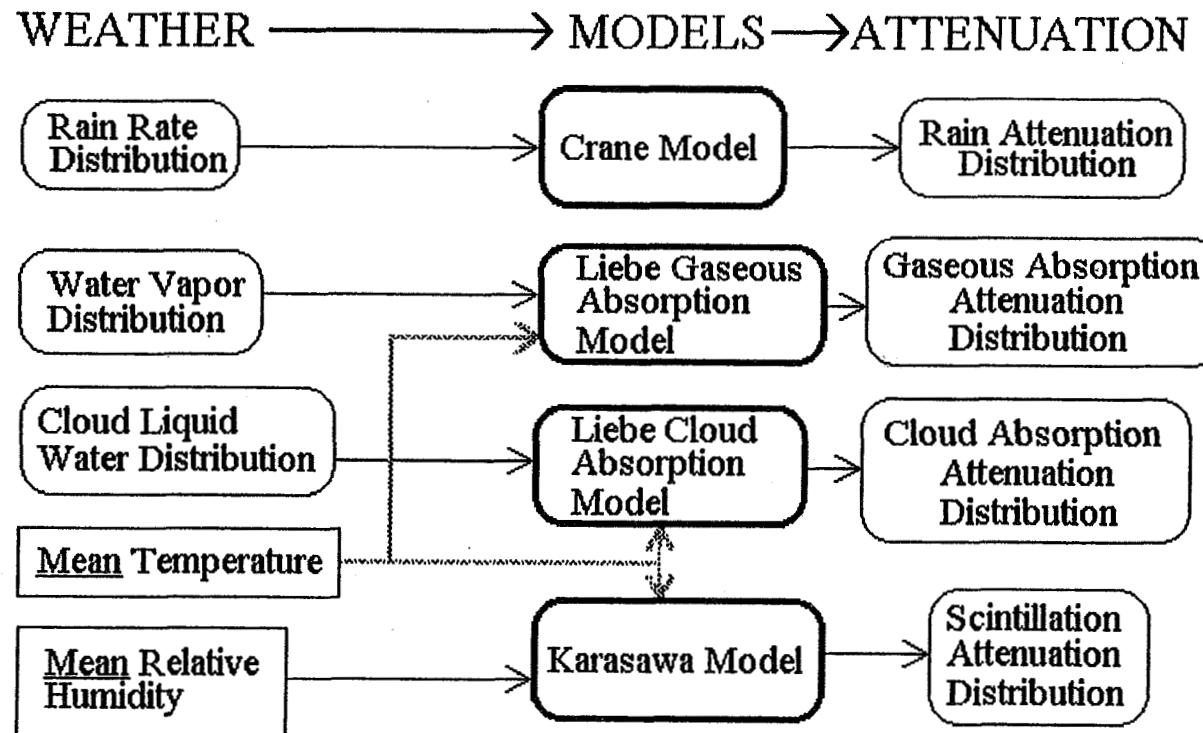
Distributions of Weather Statistics

	JAN	FEB	...	DEC
RAIN RATE STATISTICS			...	
WATER VAPOR STATISTICS			...	
CLOUD LIQUID WATER STATISTICS			...	
SCINTILLATION STATISTICS			...	

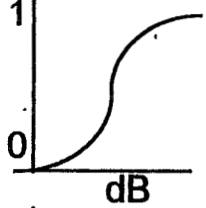
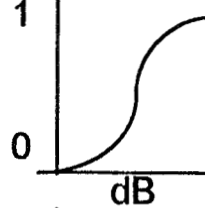
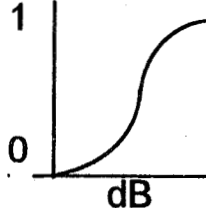
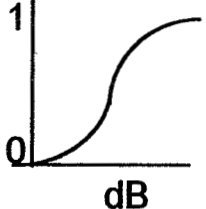
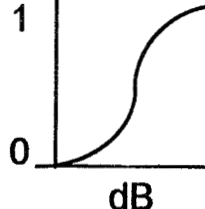
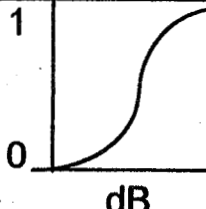
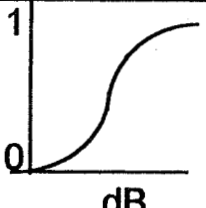
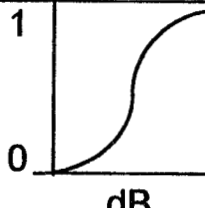
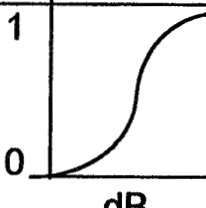
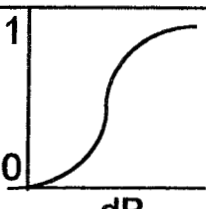
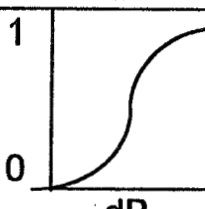
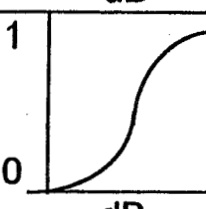
469

MAPPING WEATHER TO ATTENUATION

- Step 3) Use Distributions of Weather with Models to Create Distributions of Attenuation



Distributions of Attenuation Statistics

	JAN	FEB	...	DEC
RAIN ATTENUATIONS			...	
WATER VAPOR ATTENUATIONS			...	
CLOUD ATTENUATIONS			...	
SCINTILLATION ATTENUATION			...	

First, Combine by Effect

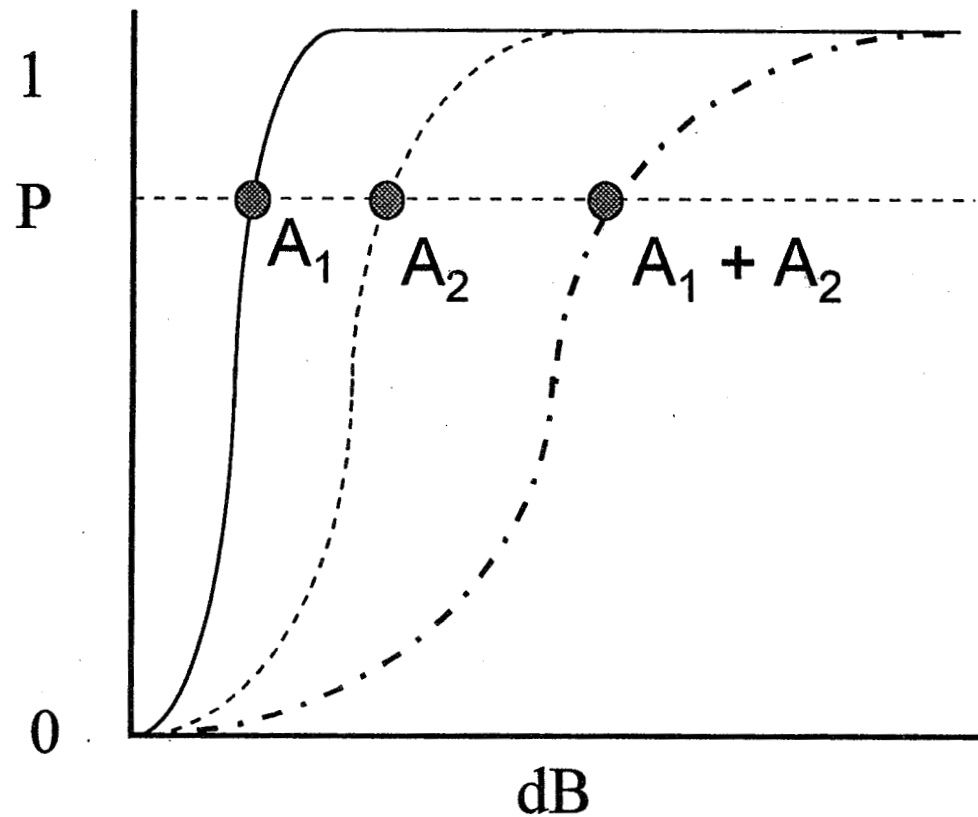
471

STEP 4a) COMBINING CDFs DUE TO VARIOUS EFFECTS

- Equiprobable Summation:
 - Effects Are Perfectly Dependent ($r = 1$)
 - At a Fixed Probability, Attenuations are Added Directly
 - Presents a Worst Case Approximation
- Convolution
 - Effects are Perfectly *Independent* ($r = 0$)
 - The CDF of One Effect Convolved with the PDF of Another Effect Produces the CDF of the Resultant
 - Presents the Most Realistic, Best Case Approximation

Development of a Dependent Curve Through Equiprobable Summation

- For a Fixed Probability, Sum the Corresponding Attenuations Due to Each Effect



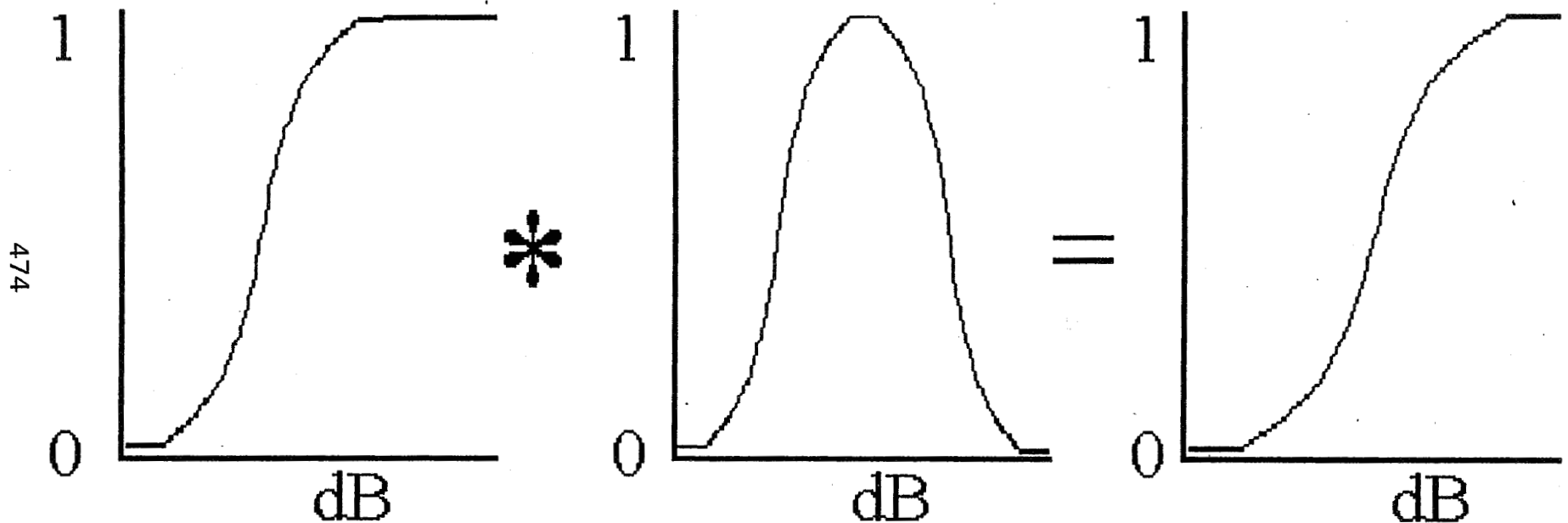
473

Development of an Independent Curve

CDF of Atten.
due to Effect #1

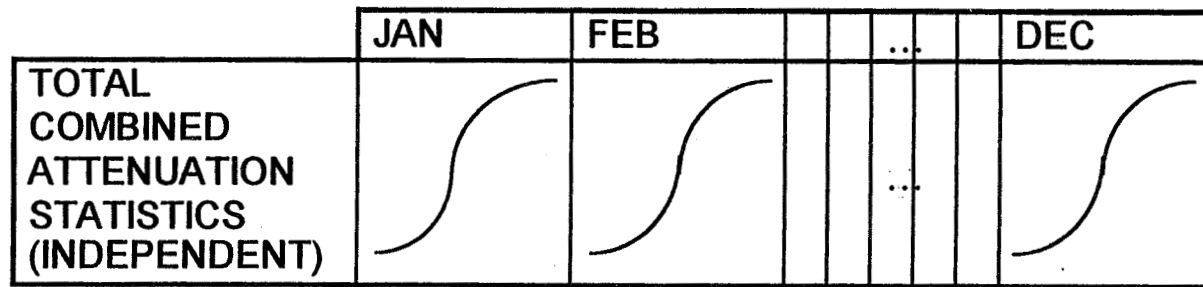
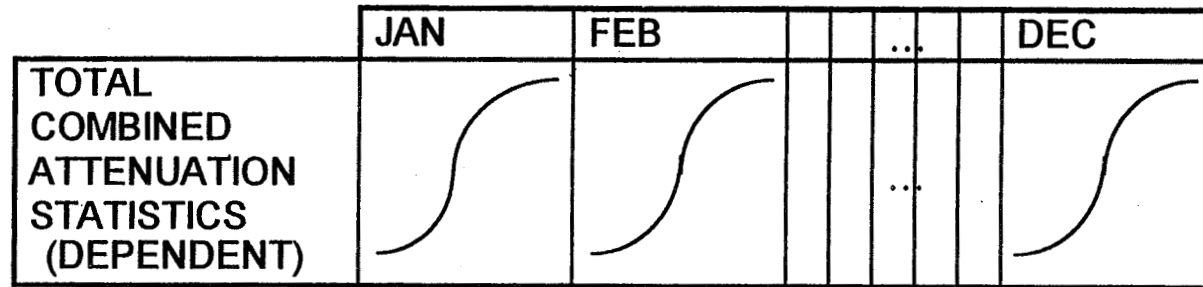
PDF of Atten.
due to Effect #2

Independent
Resultant CDF



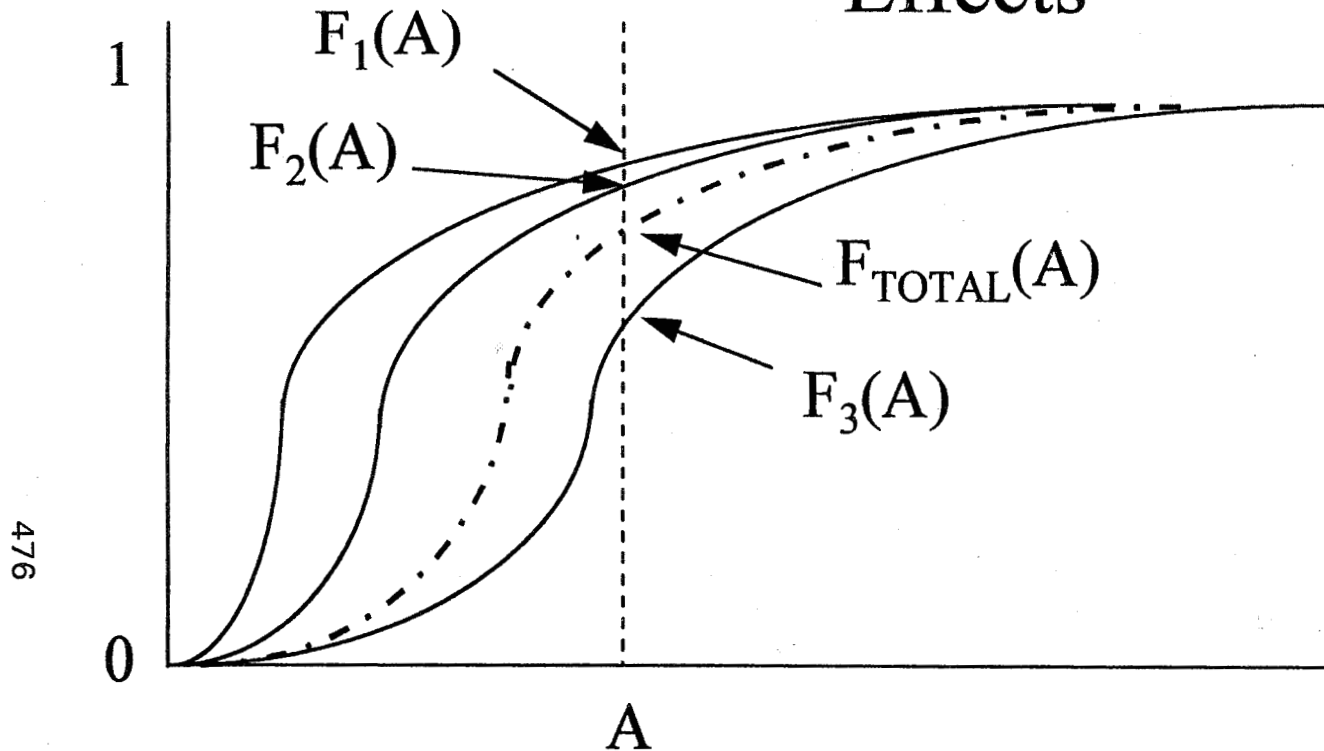
- Where * Represents Convolution
- All Points on the CDF are Required

STEP 4b) COMBINING CDFs FOR DIFFERENT TIMES



Next, Combine by Time Using Bayes Theorem

Applying Bayes Theorem to Combined Effects



Assume Each CDF Represents 1 Month

- Month1: 30 Days
- Month2: 31 Days
- Month3: 30 Days

$$F_{TOTAL}(A) = \frac{F_1(A) * n_1 + F_2(A) * n_2 + \dots + F_N(A) * n_N}{\sum n_1 + n_2 + \dots + n_N}$$

$$= [F_1(A) * 30 + F_2(A) * 31 + F_3(A) * 30] / 91$$



REAL
CALCULATIONS

477

Theoretical System:

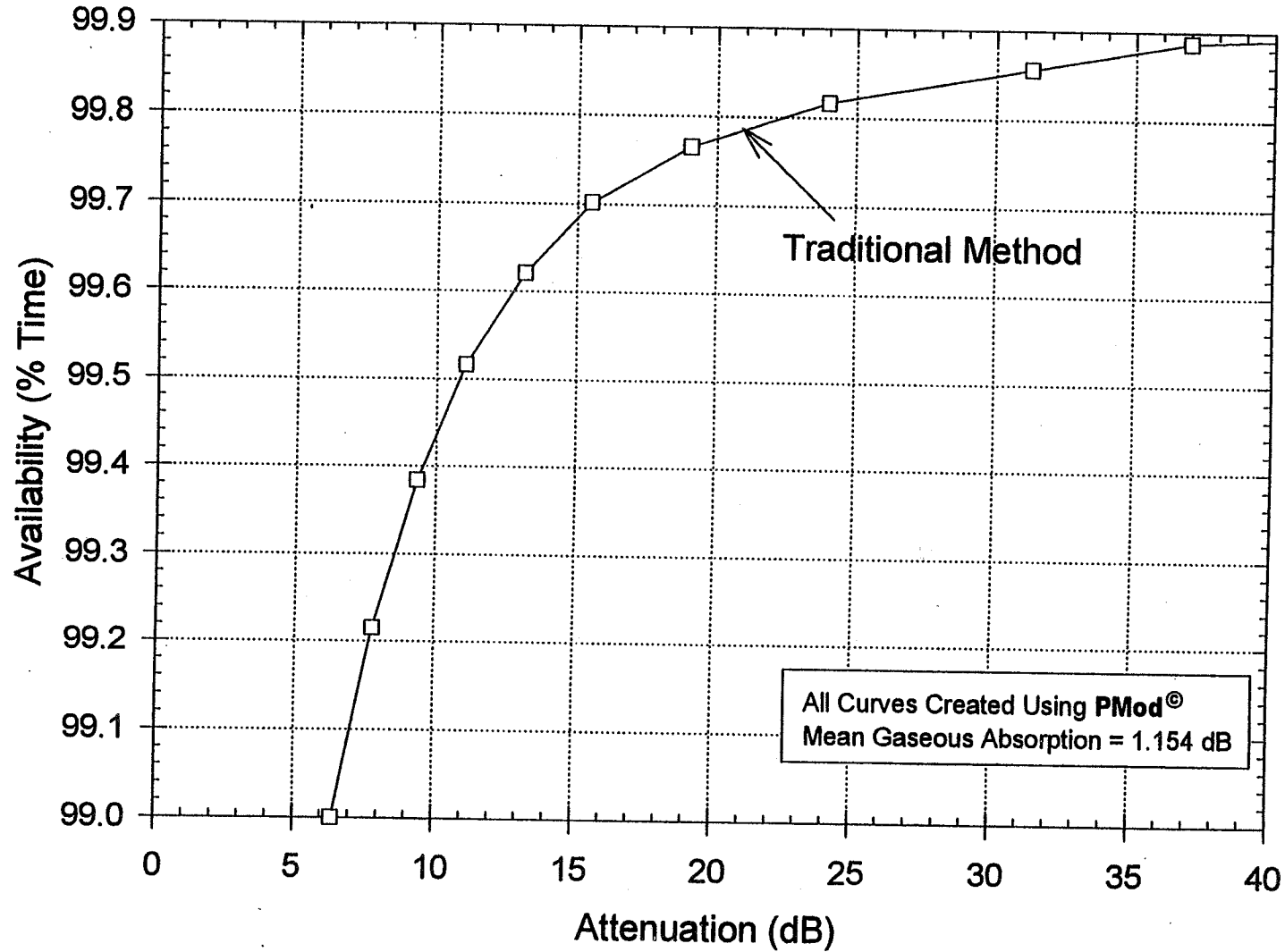
$f=27.505$ GHz

Location: Washington, D.C.

Lat: 38.4° North Lon: 77.0° West

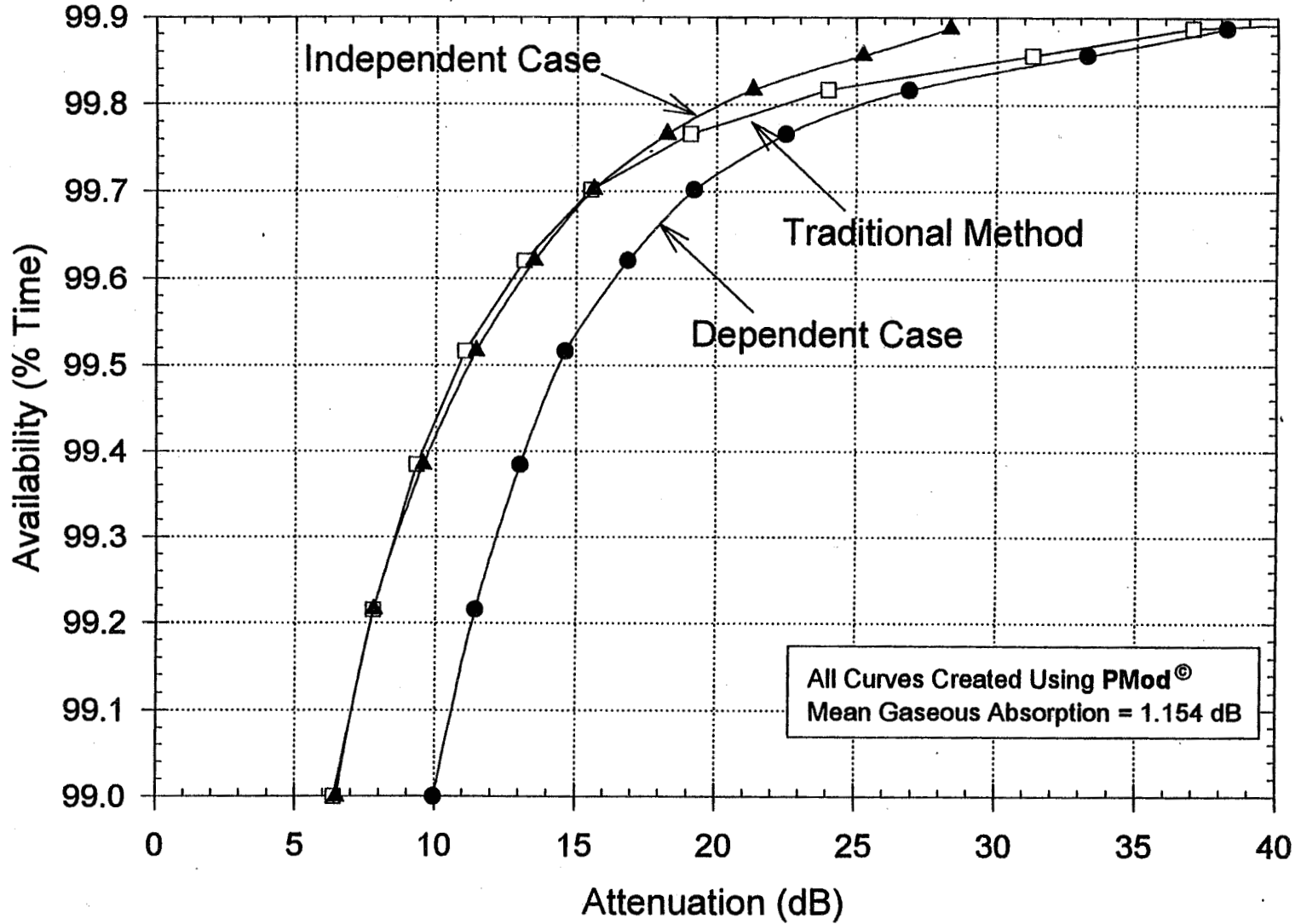
Elevation Angle = 20°

Traditional Approach to Attenuation Approximation (Rain CDF + Mean Gaseous Absorption)



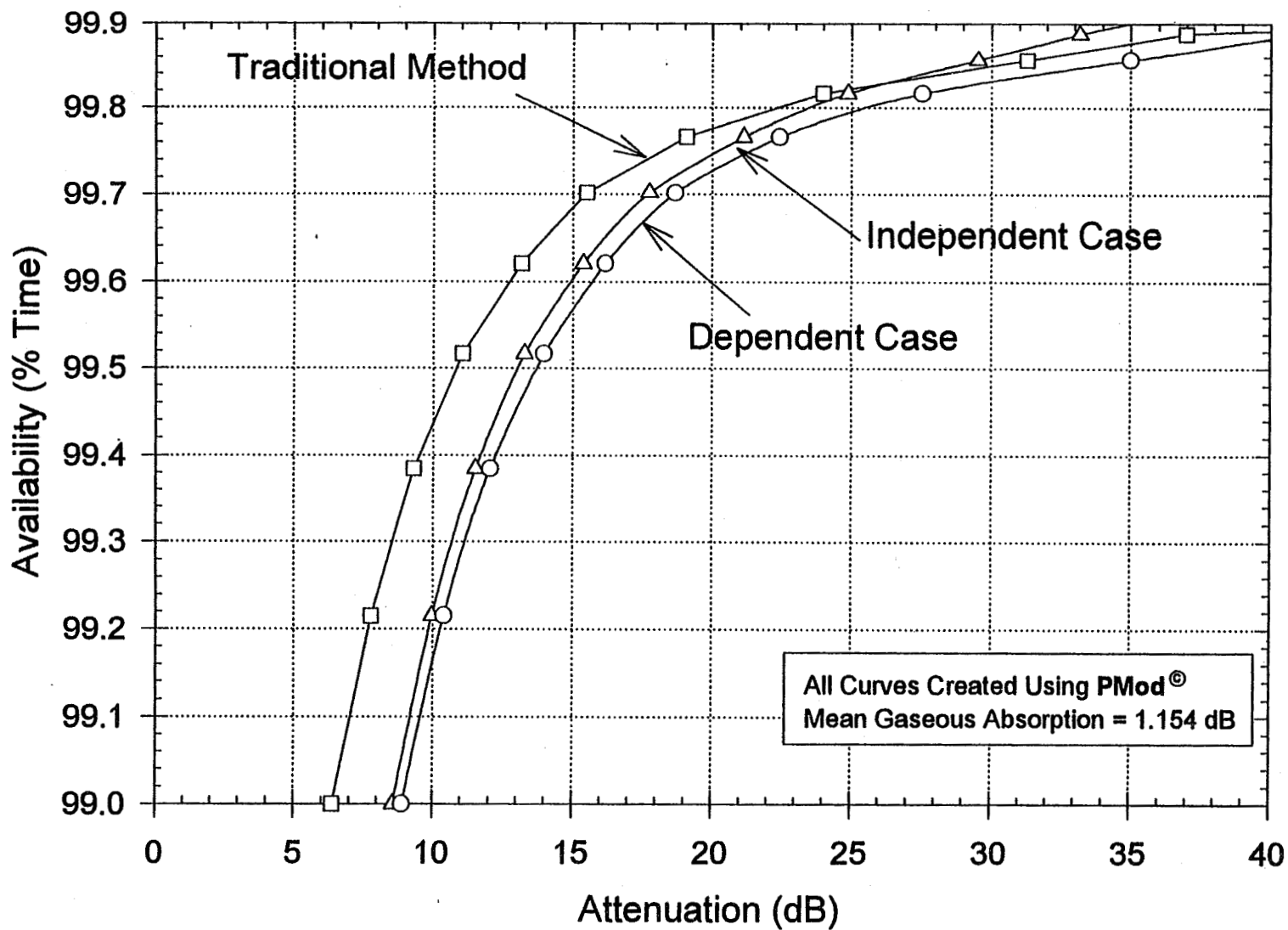
478

Traditional Approach v Annual Combined Effects



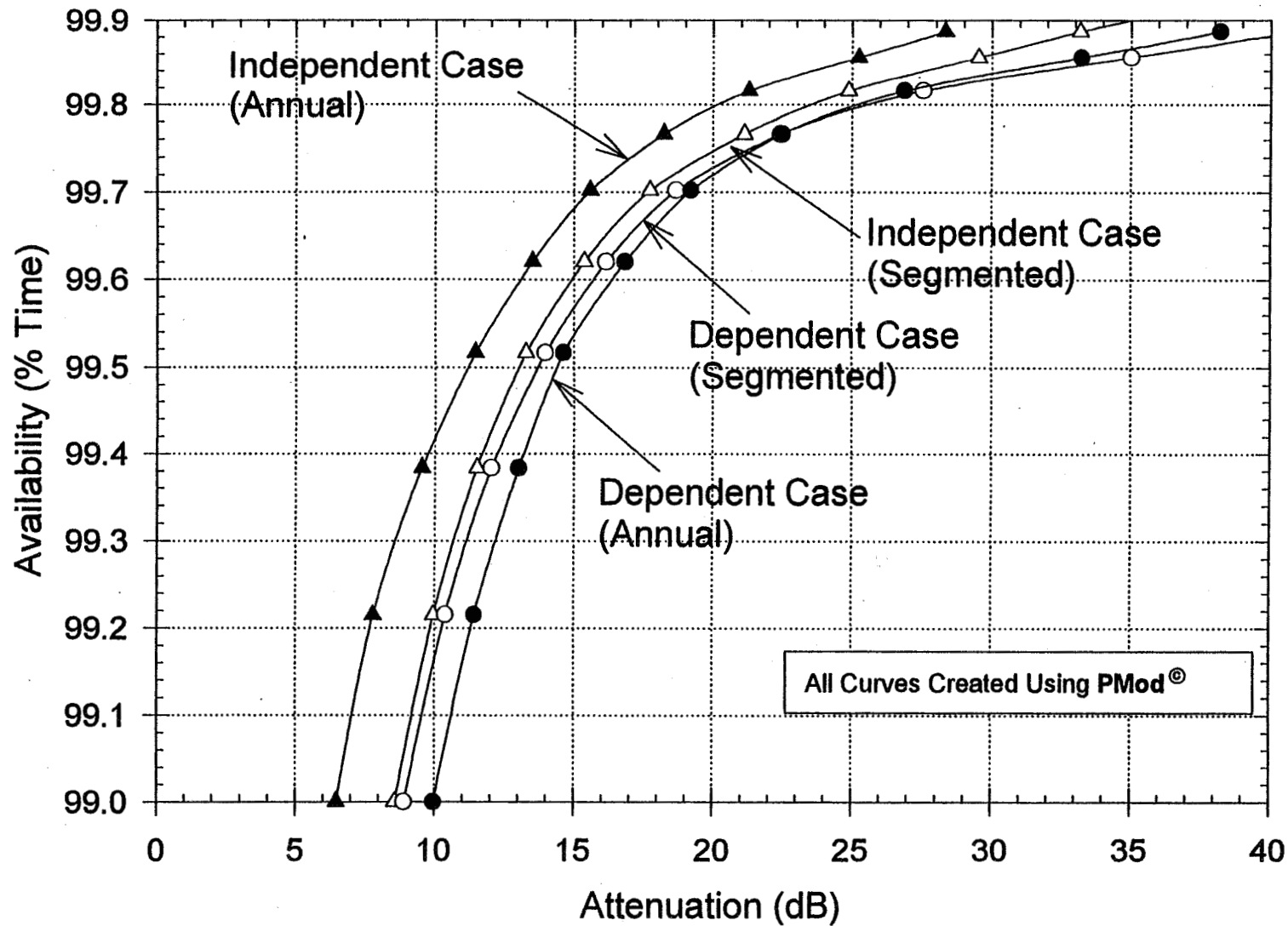
479

Traditional Approach v Segmented Combined Effects



480

Annual v Segmented Combined Effects



481

Page intentionally left blank

Acts Propagation Terminals

Engineering Support and Systems Upgrades

David Westenhaver

Westenhaver Wizard Works, Inc.

June 6, 1996

Software Status / Deficiencies and Known Problems

DRX software status:

Current version 17 of 4/25/96.

Fixed data dropouts during High Data Rate Collection.

Fixed FFT coding error.

DACS software status:

Current version 10 of 4/01/96.

Improved automatic restart of DRX.

TSR software status:

Current version 10 of 4/01/96.

Will Automatically collect High Data Rate data.

Will Accept GPS Time via RS-232.

Data missing from RV0; Defragment Disk.

ActsView software status:

Current version 3 of 9/26/94.

Need to be able to read CD directly.

Need to add display of tipping bucket gauge.

Actspp PreProcessing software status:

Current version 6.9 of 5/22/96.

System Hardware Status / Deficiencies and Known Problems

27 Beacon one-second dropouts.

Cause is the master local oscillator is microphonic.

The DRX fans create low-frequency shaking.

Solution is to replace fans and loosen 7 of the 8 mounting bolts.

Bad LNBS.

20-GHz LNB at OU has low gain and high noise figure.

Awaiting repaired unit to install, but not losing data now.

May have unstable 20-GHz LNB at CSU.

Radiometer 0.25 -0.5 Volt Jumps

This effect is seen at several sites.

Cause is being investigated.

WWW clock:

Problems: Start up & signal loss; Date jumps.

Solution: Code changes in DACS TSR should prevent data loss.

The GPS solution at UAF has been installed.

Westenhaver Wizard Works, Inc.

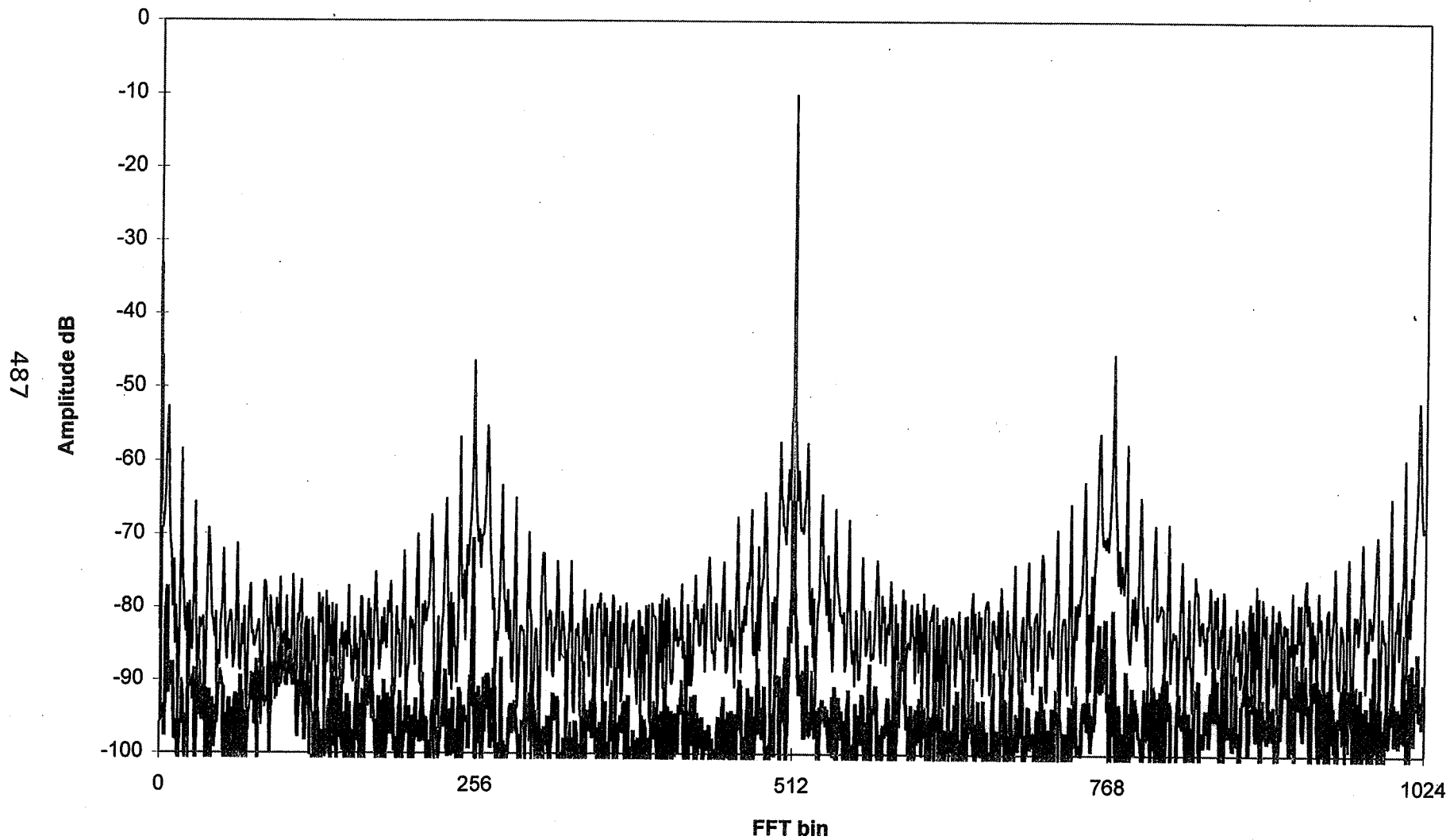
**Summary plots of Digital Receiver
Investigation and Correction Efforts**

**Summary plots of the Sites System
Calibration to Date**

All Sites Data Accumulation Summary

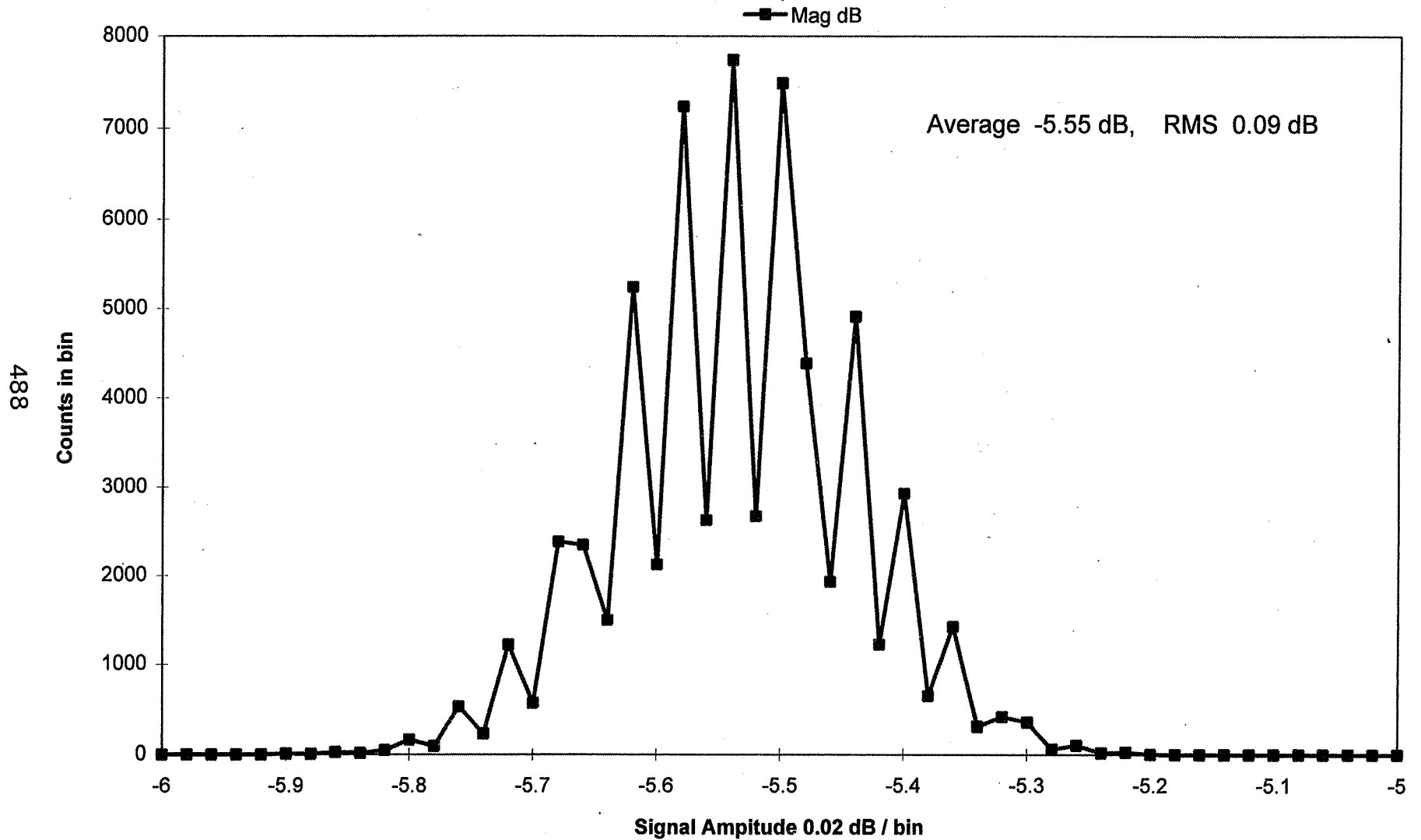
1 K FFT Spectrum Side Lobes

— Signal -10dB - - - - - Signal -40dB

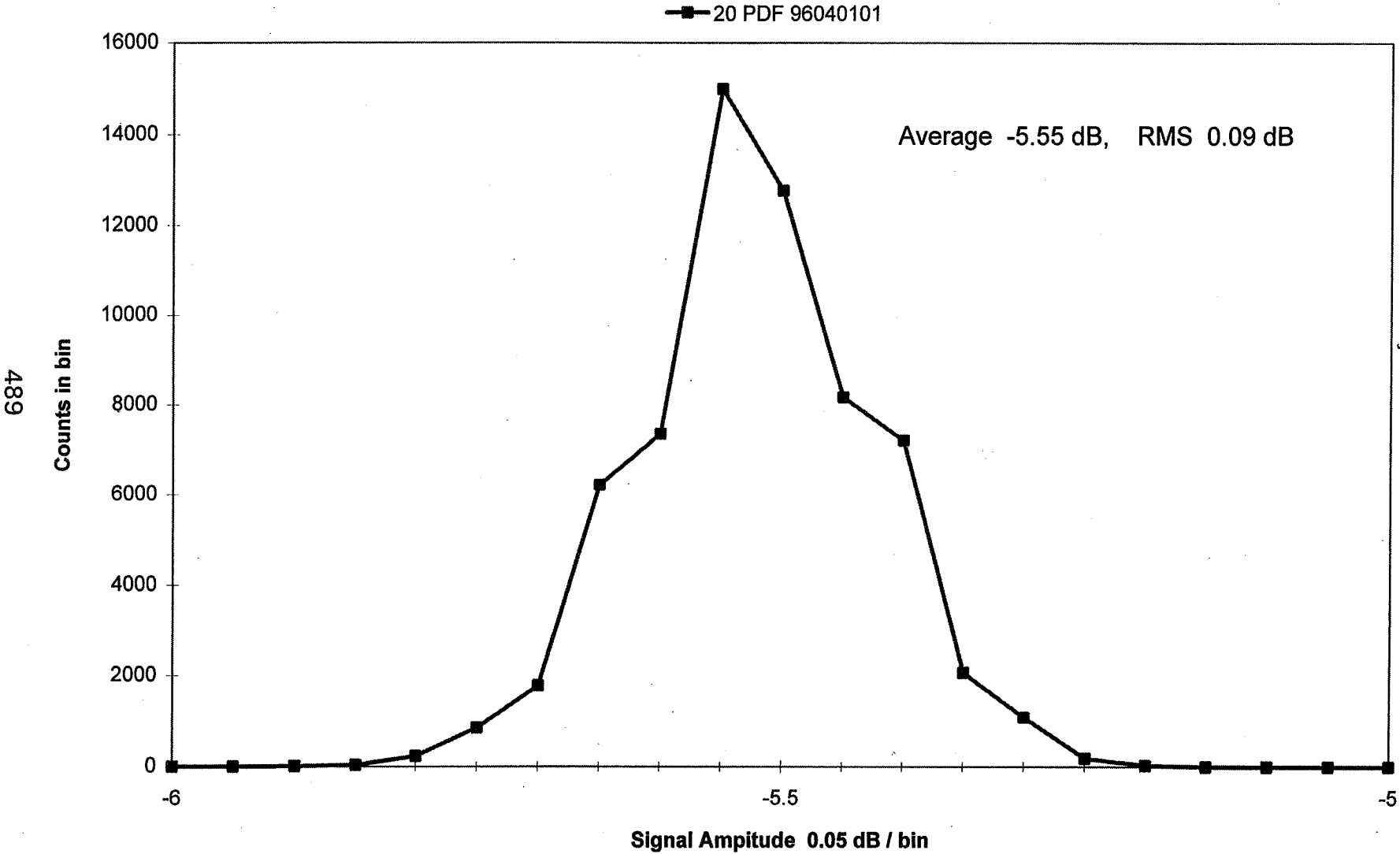


487

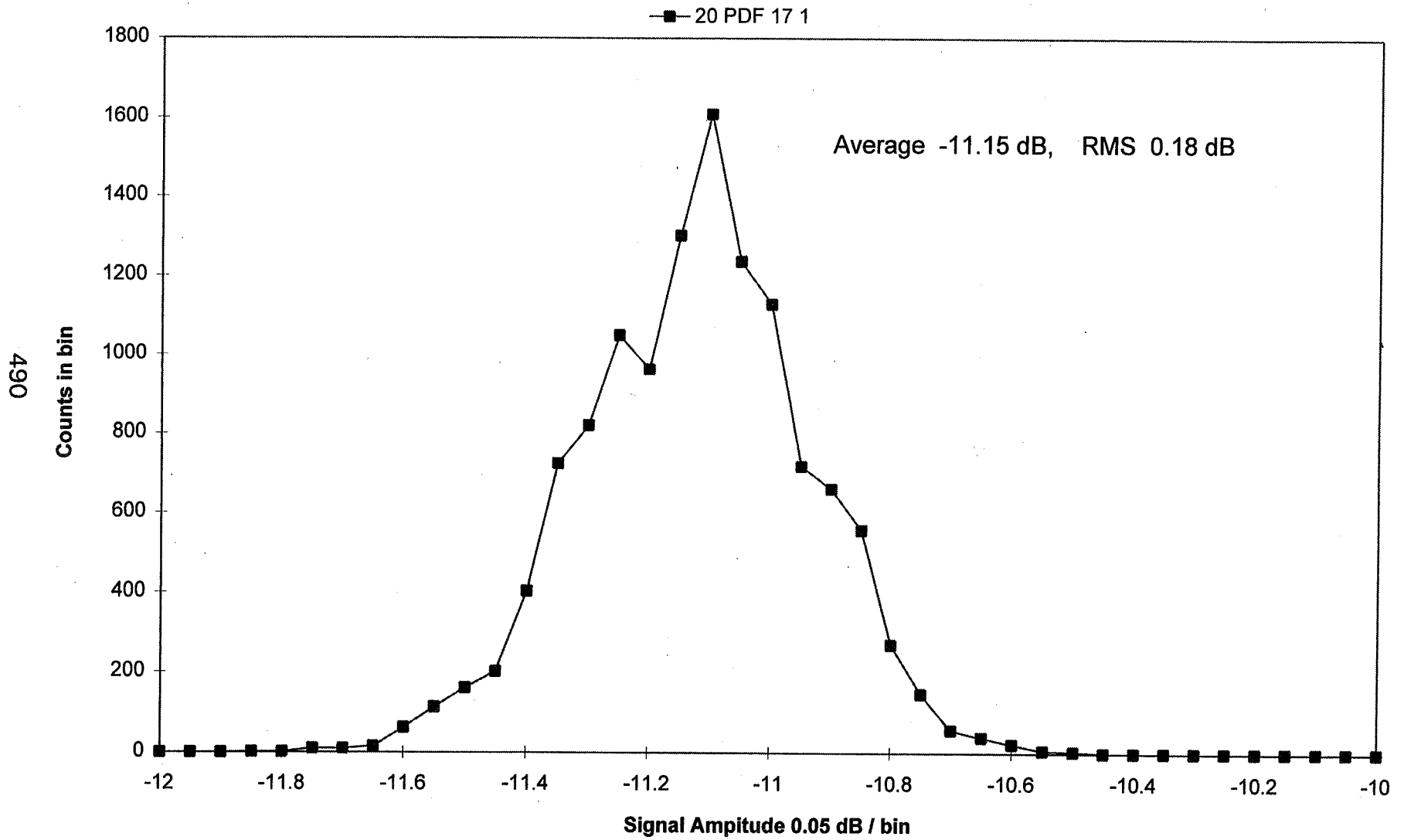
High Data Rate Amplitude Histogram at 0.02 dB / bin



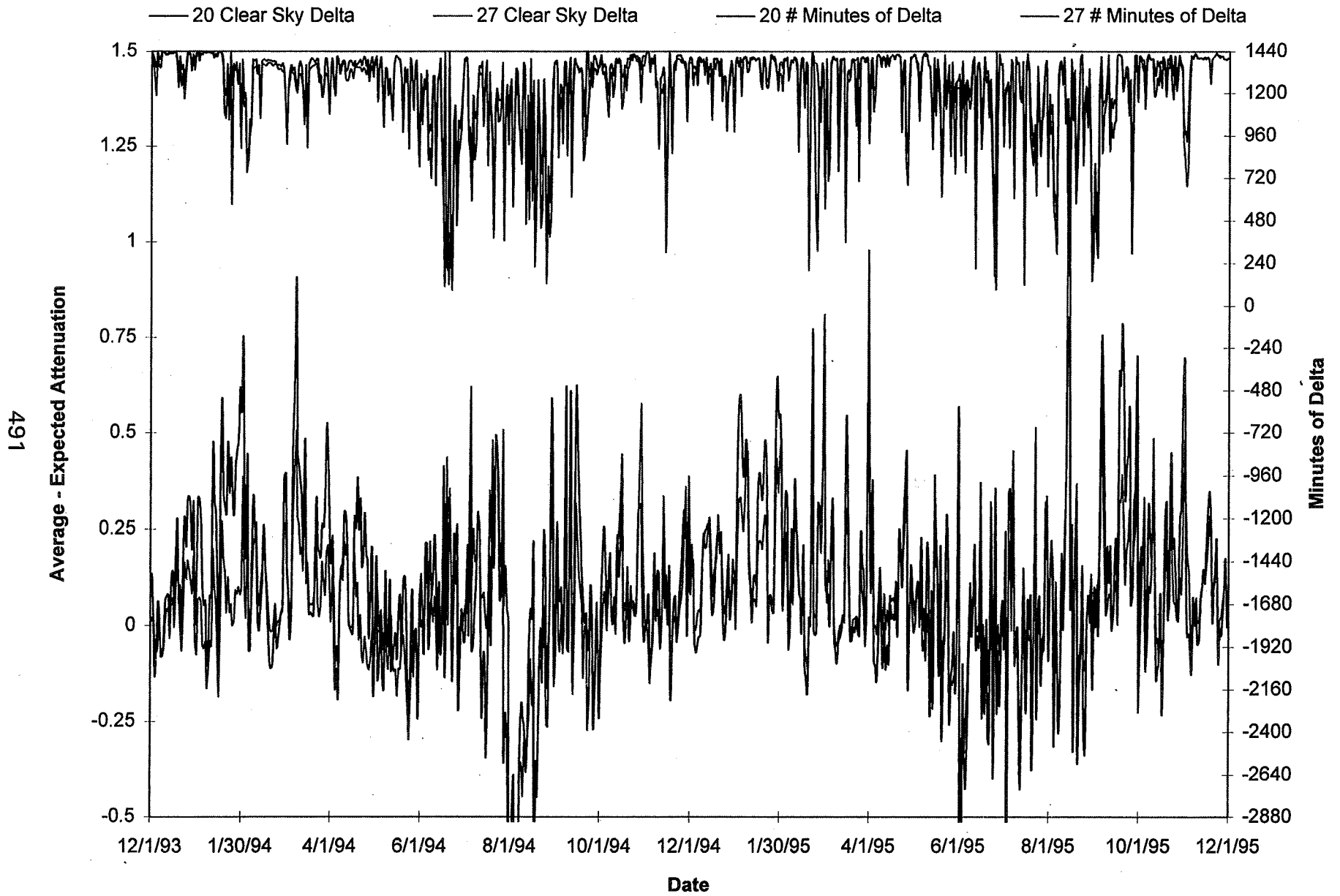
High Data Rate Amplitude Histogram at 0.05 dB / bin



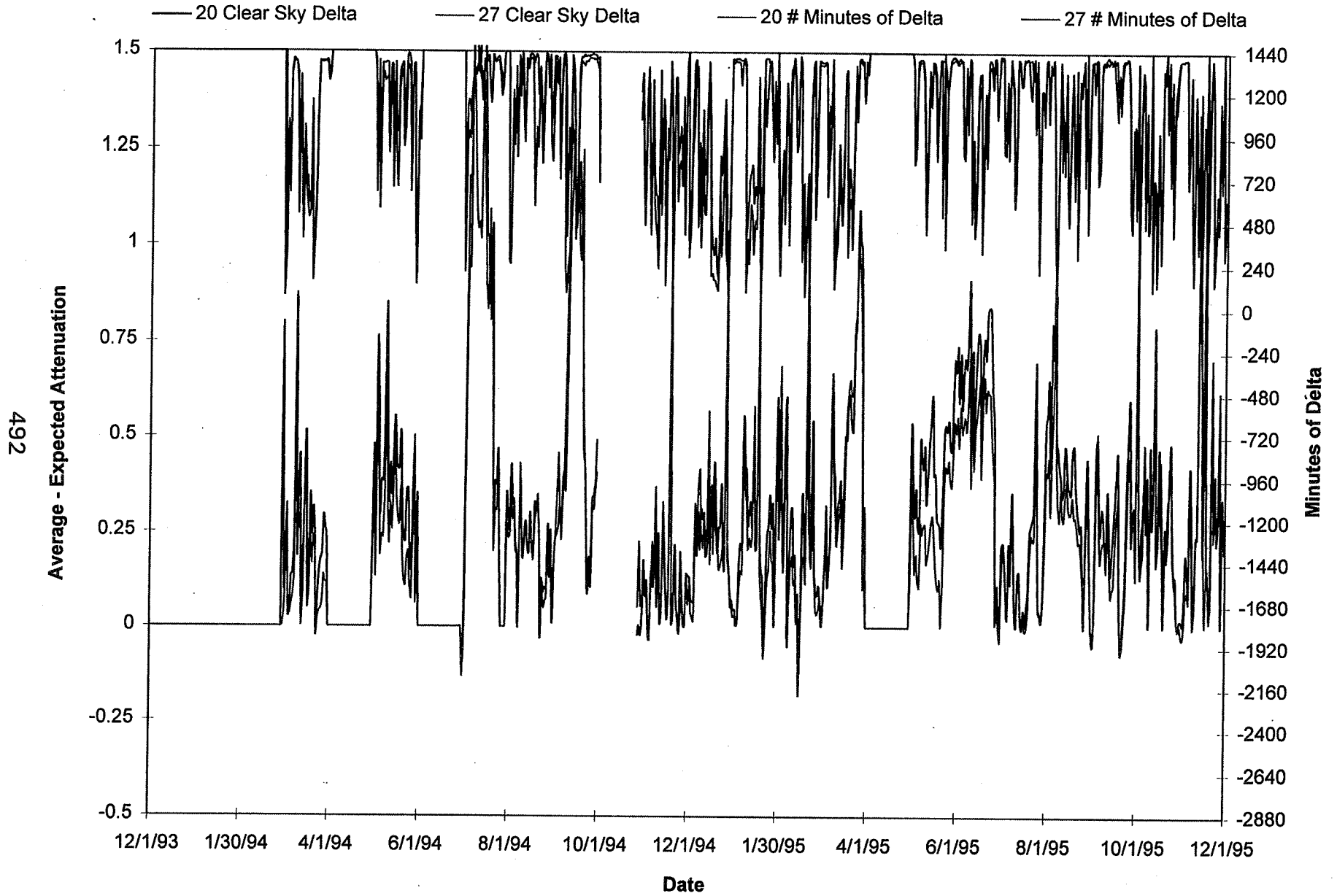
High Data Rate Amplitude Histogram at 0.05 dB / bin



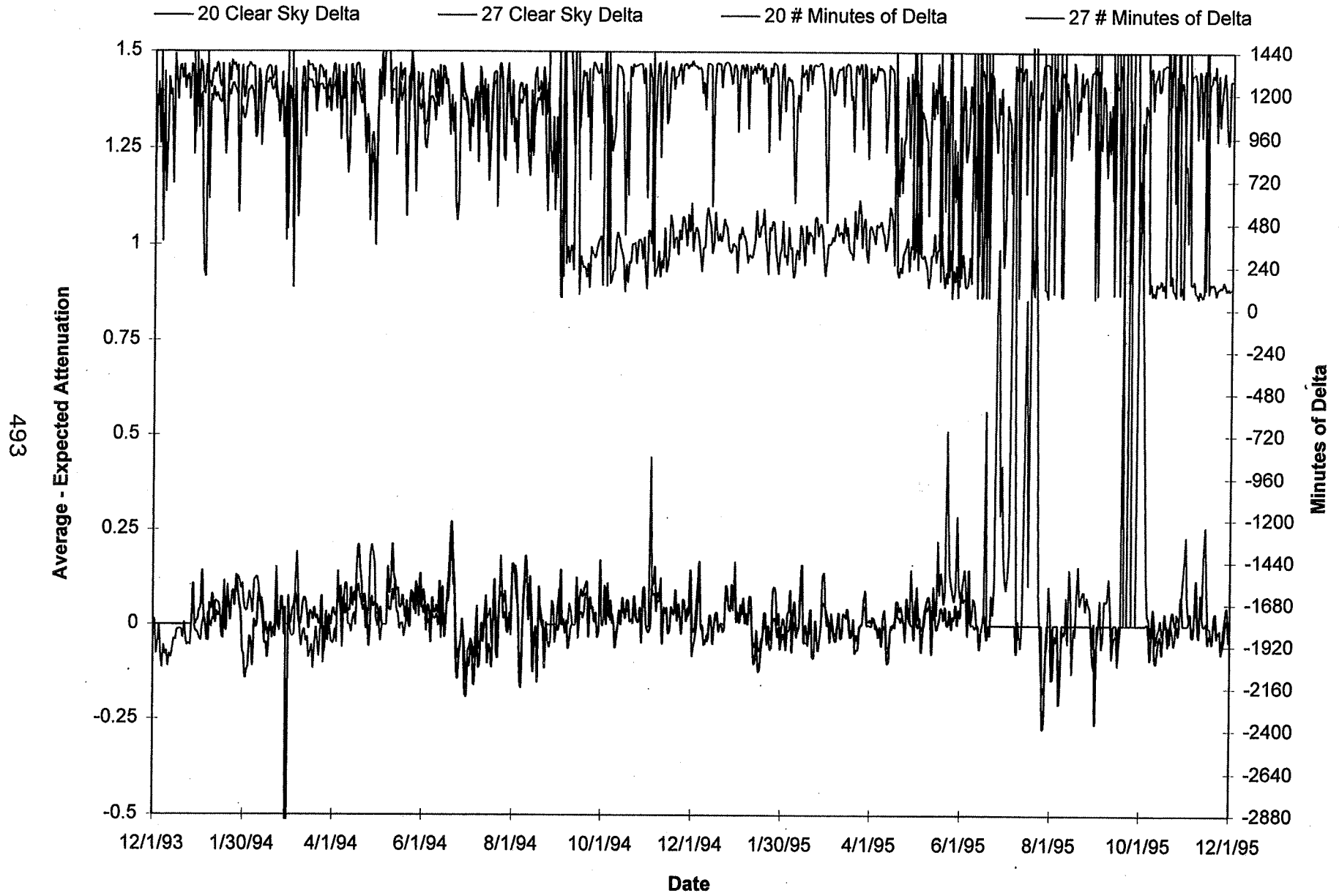
AK System Calibration



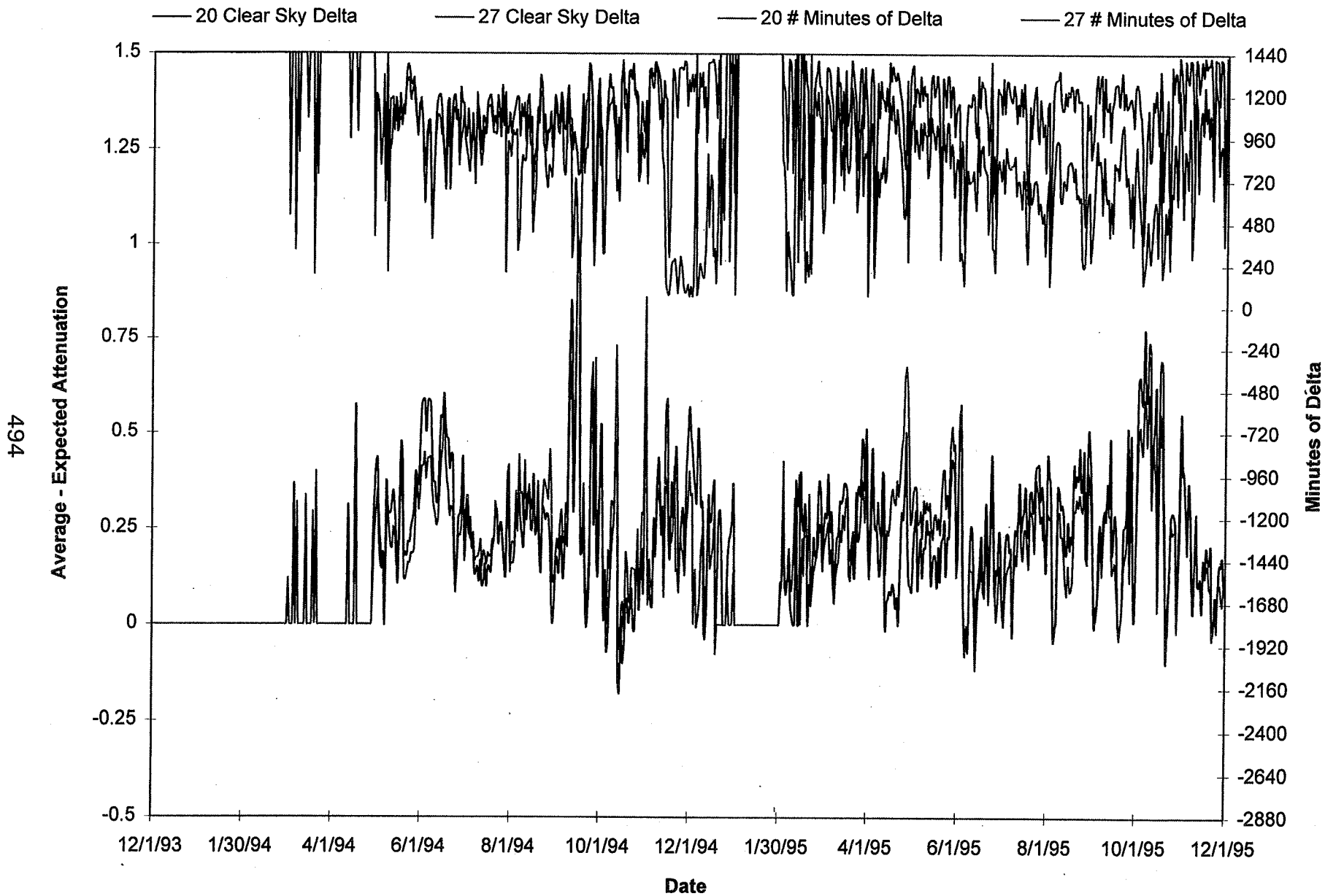
BC System Calibration



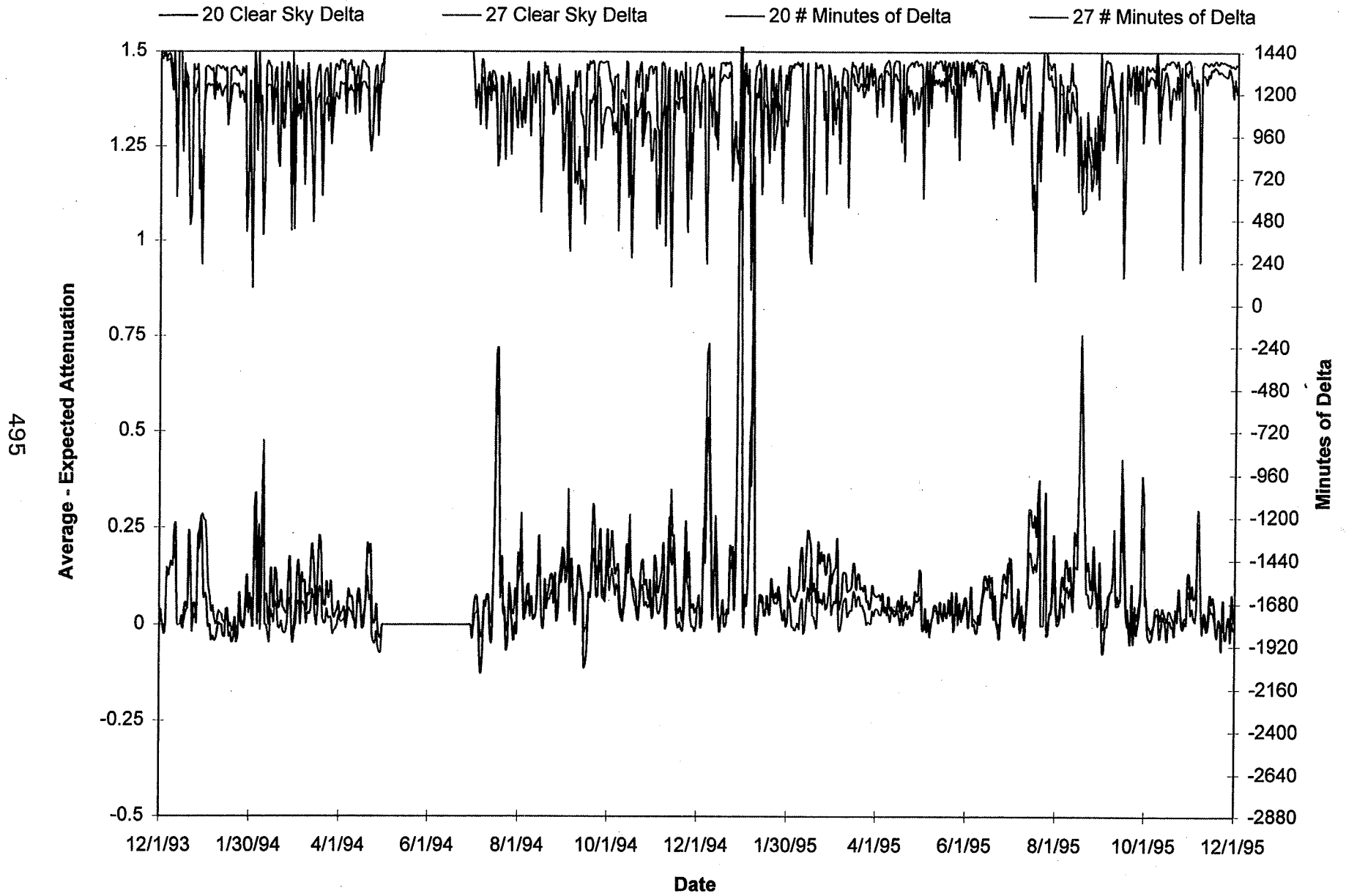
CO System Calibration



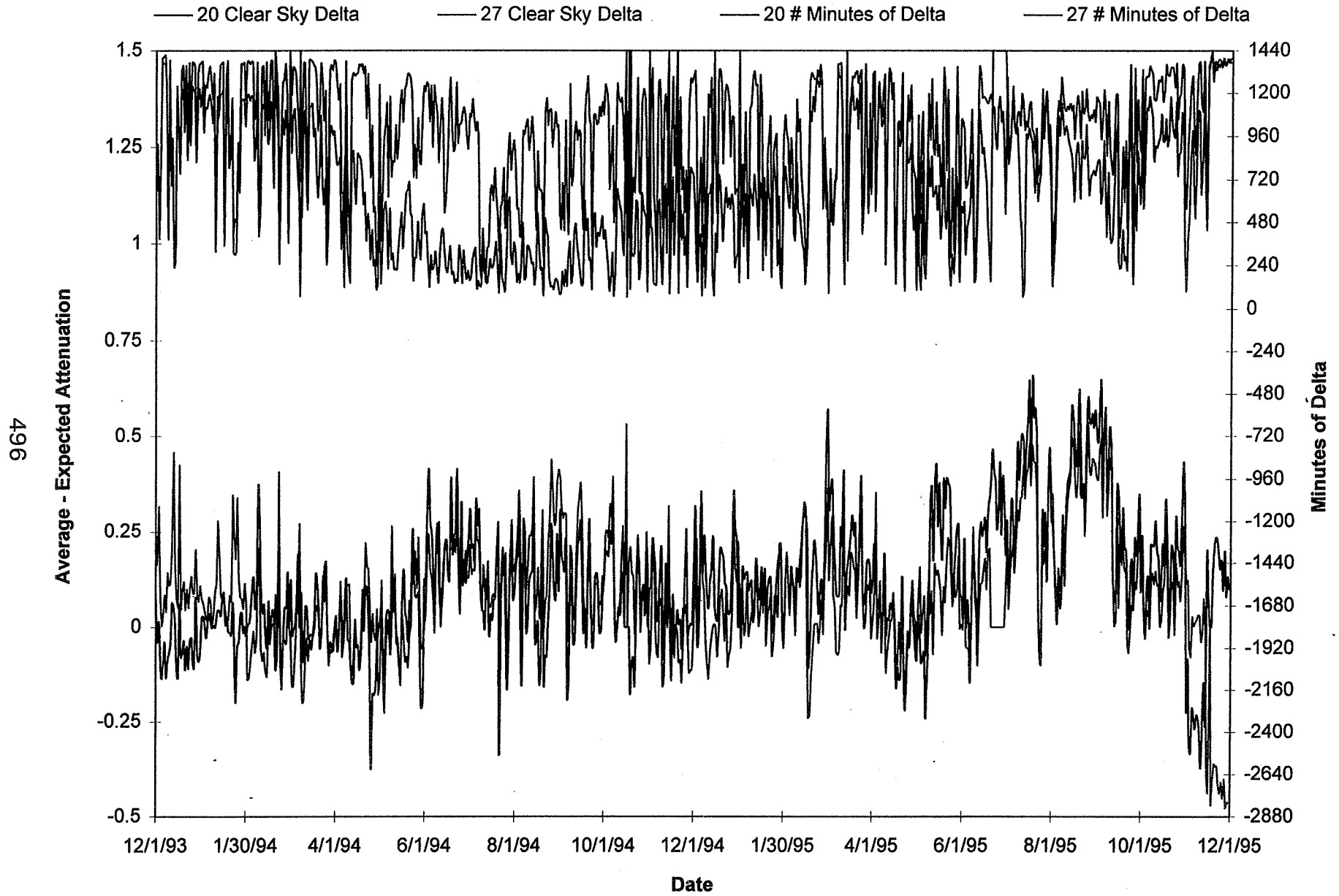
FL System Calibration



NM System Calibration



OK System Calibration



Total Data Accumulation Summary

Site	Total Days	Total Days Collected		Lost Time During Collection		Total Good Days Collected		Total Lost or Missing Days	
AK	730.0	725.2	99.34%	1.9	0.26%	723.3	99.08%	6.7	0.92%
BC	730.0	726.1	99.46%	1.9	0.26%	724.2	99.21%	5.8	0.79%
CO	730.0	717.6	98.30%	6.4	0.88%	711.2	97.42%	18.8	2.58%
FL	730.0	718.6	98.44%	6.9	0.95%	711.7	97.49%	18.3	2.51%
MD	351.0	329.1	93.76%	2.4	0.68%	326.7	93.08%	24.3	6.92%
NM	730.0	721.3	98.81%	4.8	0.66%	716.5	98.15%	13.5	1.85%
OK	730.0	729.1	99.87%	3.4	0.46%	725.7	99.41%	4.3	0.59%

497

Page intentionally left blank

ACTS Data Center Status

Geoffrey W. Torrence

Electrical Engineering Research Laboratory
The University of Texas at Austin

Presented at APWS IX
Fairbanks, AK
June 6, 1996

1

Raw Data Received

RV0 Files as of 05-23-1996

Year	Month	AK	BC	CO	FL	MD	NM	OK
93	Sep	03	10	29
93	Oct	31	26	30	31
93	Nov	..	27	..	28	..	15	29
93	Dec	31	31	30	29	..	29	31
94	Jan	31	31	31	31	..	31	31
94	Feb	28	28	28	28	..	25	28
94	Mar	31	31	31	29	17	31	31
94	Apr	30	30	30	30	30	30	30
94	May	31	31	25	30	31	31	31
94	Jun	30	30	30	30	30	30	30
94	Jul	31	31	31	31	31	31	31
94	Aug	31	31	31	31	31	31	31
94	Sep	30	30	29	30	30	30	30
94	Oct	31	31	29	31	31	31	31
94	Nov	27	30	30	30	30	30	30
94	Dec	31	31	31	28	22	31	31

95	Jan	31	31	31	31	19	31	31
95	Feb	28	28	28	28	28	28	28
95	Mar	31	31	31	31	31	31	31
95	Apr	30	30	30	30	28	30	30
95	May	31	31	31	31	31	31	31
95	Jun	30	30	30	30	30	30	30
95	Jul	31	31	31	31	31	31	31
95	Aug	31	31	31	31	31	31	31
95	Sep	30	30	30	30	30	30	30
95	Oct	31	31	31	31	31	31	31
95	Nov	30	30	30	30	30	30	30
95	Dec	31	31	31	31	31	31	31
96	Jan	..	31	..	31	31	..	31
96	Feb	..	29	..	29	29	..	29
96	Mar	..	31	..	31
96	Apr	..	30	..	30
96	May

Total Daily RV0 Files: 5795
Total Compressed MegaBytes: 3945

2

PV2 Data Received

FV2 Files as of 05-23-1996

Year	Month	AK	BC	CO	FL	MD	NM	OK
93	Sep
93	Oct
93	Nov	..	27	29
..
94	Jan	31	31	31	31	..	31	31
94	Feb	28	28	28	28	..	25	28
94	Mar	31	31	31	29	17	31	31
94	Apr	30	30	30	30	30	30	30
94	May	31	31	25	30	31	31	31
94	Jun	30	30	30	30	30	30	30
94	Jul	31	31	31	31	31	31	31
94	Aug	31	31	31	31	30	31	31
94	Sep	30	30	29	30	30	30	30
94	Oct	31	31	29	31	31	31	31
94	Nov	27	30	30	30	30	30	30
94	Dec	31	31	31	28	22	31	31

95	Jan	31	31	31	31	19	31	31
95	Feb	28	28	28	28	28	28	28
95	Mar	31	31	31	31	31	31	31
95	Apr	30	30	30	30	28	30	30
95	May	31	31	31	31	31	31	31
95	Jun	30	30	30	30	30	30	30
95	Jul	31	31	31	31	31	31	31
95	Aug	31	31	31	31	31	31	31
95	Sep	30	30	30	30	30	30	30
95	Oct	31	31	31	31	31	31	31
95	Nov	30	30	30	30	30	30	30
95	Dec	..	31	31
96	Jan	..	31	31
96	Feb	..	29	29
96	Mar
96	Apr
96	May

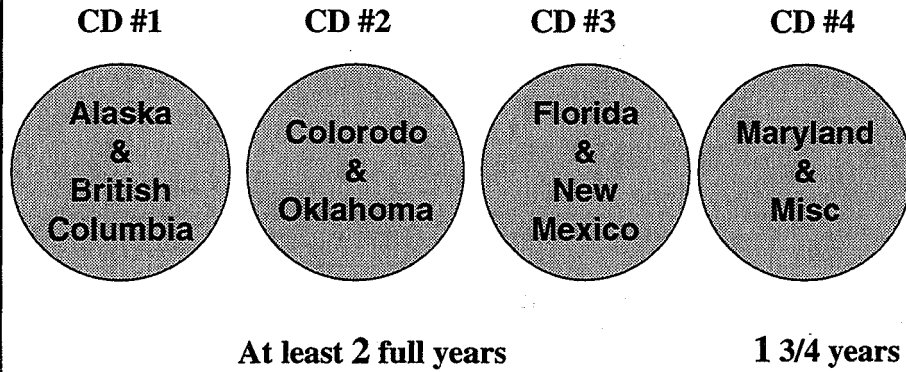
Total Daily FV2 Files: 5193
 Total Compressed MegaBytes: 1991

Miscellaneous Files as of 05-23-1996

Year	Month	AK	BC	CO	FL	MD	NM	OK
93	NovLDSRELD..E
93	DecLDSRE	.LDSRE	.LDSRELDS.E	.LD..E
94	JanLDSRE	.LDSRE	.LDSRELDS.E	.LD..E
94	FebLDSRE	.LDSRE	.LDSRELDS.E	.LD..E
94	MarLDSRE	.LDSRE	.LDSRE	.LDSRE	.LDS.E	.LD..E
94	AprLDSRE	.LDSRE	.LDSRE	.LDSRE	.LDS.E	.LD..E
94	MayLDSRE	.LDSRE	.LDSRE	.LDSRE	.LDS.E	.LD..E
94	JunLDSRE	.LDSRE	.LDSRE	.LDSRE	.LDS.E	.LD..E
94	JulLDSRE	.LDSRE	.LDSRE	.LDSRE	.LDS.E	.LD..E
94	AugLDSRE	.LDSRE	.LDSRE	.LDSRE	.LDS.E	.LD..E
94	SepLDSRE	.LDSRE	.LDSRE	.LDSRE	.LDS.E	.LD..E
94	OctLDSRE	.LDSRE	.LDSRE	.LDSRE	.LDS.E	.LD..E
94	NovLDSRE	.LDSRE	.LDSRE	.LDSRE	.LDS.E	.LD..E
95	JanLDSRE	.LDSRE	.LDSRE	.LDSRE	.LDS.E	.LD..E
95	FebLDSRE	.LDSRE	.LDSRE	.LDSRE	.LDS.E	.LD..E
95	MarLDSRE	.LDSRE	.LDSRE	.LDSRE	.LDS.E	.LD..E
94	DecLDSRE	.LDSRE	.LDSRE	.LDSRE	.LDS.E	.LD..E
95	AprLDSRE	.LDSRE	.LDSRE	.LDSRE	.LDS.E	.LD..E
95	MayLDSRE	.LDSRE	.LDSRE	.LDSRE	.LDS.E	.LD..E
95	JunLDSRE	.LD.RE	CLDSRE	.LDSRE	.LDS.E	.LD..E
95	JulLDSRE	.LD.RE	CLDSRE	.LDSRE	.LDS.E	.LD..E
95	AugLDSRE	.LD..E	CLDSRE	.LDSRE	.LDS.E	.LD..E
95	SepLDSRE	.LD..E	.LDSRE	.LDSRE	.LDS.E	.LD..E
95	OctLDSRE	.LD.RE	.LDSRE	.LDSRE	.LDS.E	.LD..E
95	NovLDSRE	.LD..E	.LDSRE	.LDSRE	.LDS.E	.LD..E
95	DecLDSRELD..E
96	JanLDSRELD..E
96	FebLDSRELD..E

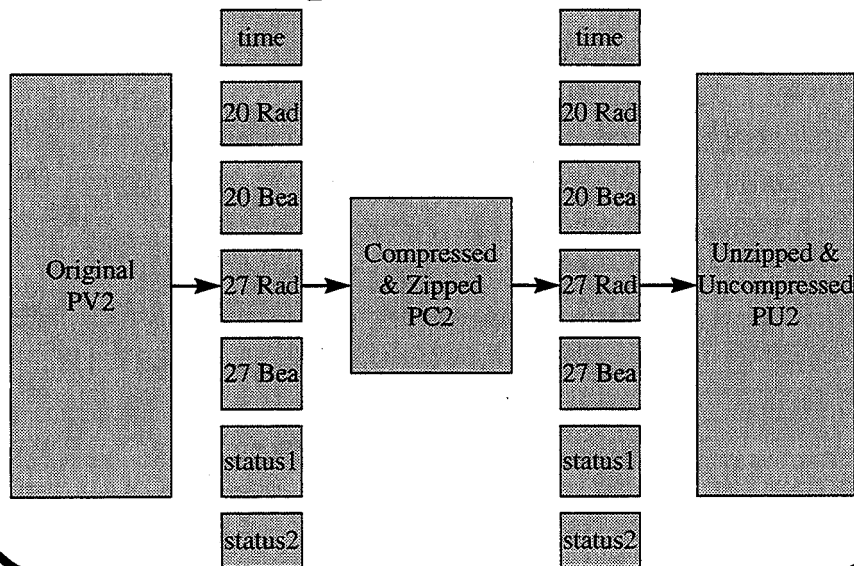
Key: C=CAL, L=LOG, D=DFC, S=SRF, R=RTN, E=EDF

PP CD-ROM Organization



5

PP File Compression



6

CD-ROM Directory

CD-ROM Volume

Year-Month

Station

PC2 files for month

EDF file for month

misc. files for month

Station....

Year-Month....

7

CD-ROM #4 Misc. Files

- All EDF Files for all sites (in \EDFFiles)
 - compressed & uncompressed
 - Excel spreadsheet with all edf files etc. (not the 9505BC update) & result graphs & models
- Sample Directory Structure (in \ACTSP)
 - for running pp program in c:\ACTSP
- Program for uncompressing data (decomp.exe)
- Programs for viewing data (in \ACTSP)
- Information on data file structure (in \ACTSP)
- last minute revised PC2 and EDFiles
 - BC 9312, 9505

8

Plans for CD-ROM distribution

- ◆ Made 20 sets
 - 2 ACTS Propagation Data Center
 - 1 WWW Inc.
 - 1 LeRC
 - 1 JPL
 - 7 Doers
 - 3 Double Doers (BC, FL, NM)
- ◆ 5 left to distribute
- ◆ More can be made if required

9

CD-ROM Requests

EMSAT: Advanced Technology for Emergency Medical Services
A Non-Profit, Public Benefit Corporation
P.O. Box 41136, Los Angeles, CA 90041
(213) 258-4440



February 21, 1996

Wolfhard Vogel, PhD
ACTS Data Center
Electrical Engineering Research Laboratory
University of Texas at Austin
10100 Burnet Road
Austin, TX 78758-4497

Dear Dr. Vogel:

I am the Principle Investigator for an ACTS mobile telemedicine experiment. EMSAT work with the JPL AMT during early 1994. I understand from Dr. Faramaz Davarian, NASA Propagation Program, that CD-ROM disks are available from the ACTS Data Center. I would like to obtain a copy of the available ACTS data. A Macintosh formatted CD-ROMs would be preferred, but IBM compatible disks would be acceptable. Please forward the data to the above address. Your assistance is appreciated.

Sincerely,

Bruce P. Jackson
President, EMSAT

10

Page intentionally left blank

NASA PROPAGATION PROGRAM STATUS AND
PROPAGATION NEEDS OF SATCOM INDUSTRY

NASSER GOLSHAN

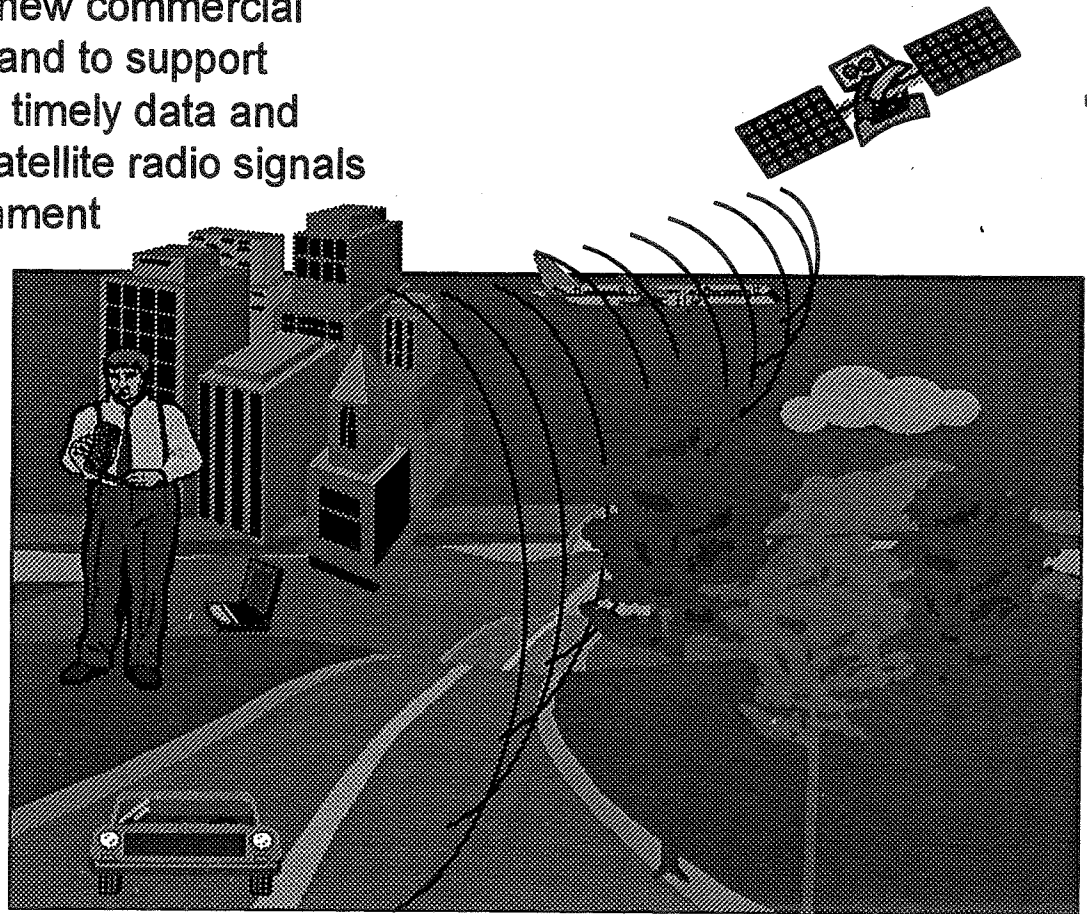
Propagation Studies
Jet Propulsion Laboratory
California Institute of Technology

**NASA PROPAGATION PROGRAM
PRESENTATION OUTLINE**

- **OBJECTIVE**
- **APPROACH**
- **THE NASA PROPAGATION PROGRAM: A PARTNERSHIP BETWEEN NASA, INDUSTRY, AND ACADEMIA**
- **SUMMARY OF INDUSTRY FEEDBACK AT NAPEX XX**
- **PLANS TO MEET THE SHORT-TERM PROPAGATION NEEDS OF THE SATCOM INDUSTRY**
- **UNDERSTANDING THE LONG-TERM PROPAGATION NEEDS OF THE SATCOM INDUSTRY**
- **FY 97 PLANS**
- **ACKNOWLEDGMENTS**

NASA PROPAGATION PROGRAM OBJECTIVES

- To enable the development of new commercial satellite systems and services and to support NASA's programs by providing timely data and models about propagation of satellite radio signals through the intervening environment
 - New services
 - Higher frequencies
 - Higher data rates
 - Different environments
 - Mobile
 - Indoors
 - Fixed
 - Different orbits
 - Geostationary
 - Low Earth Orbit

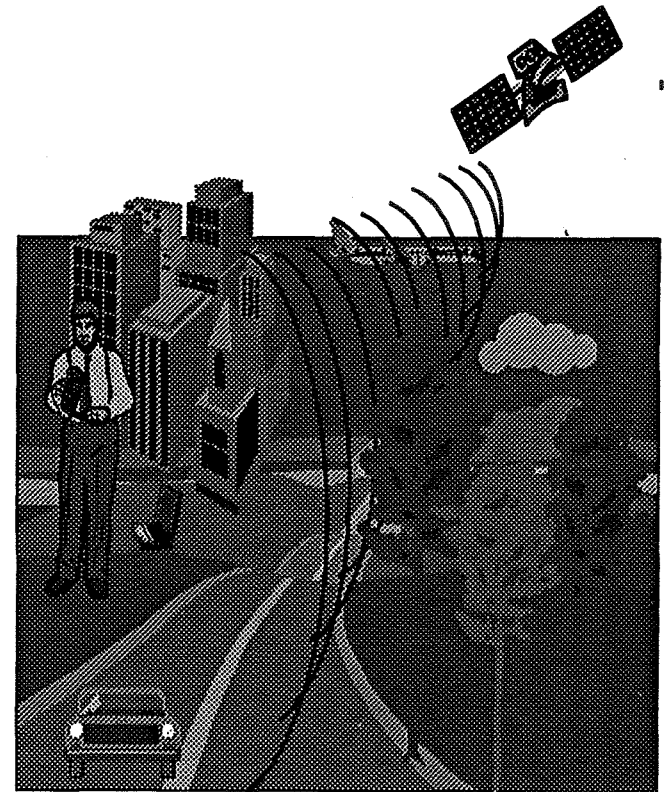


NASA PROPAGATION PROGRAM

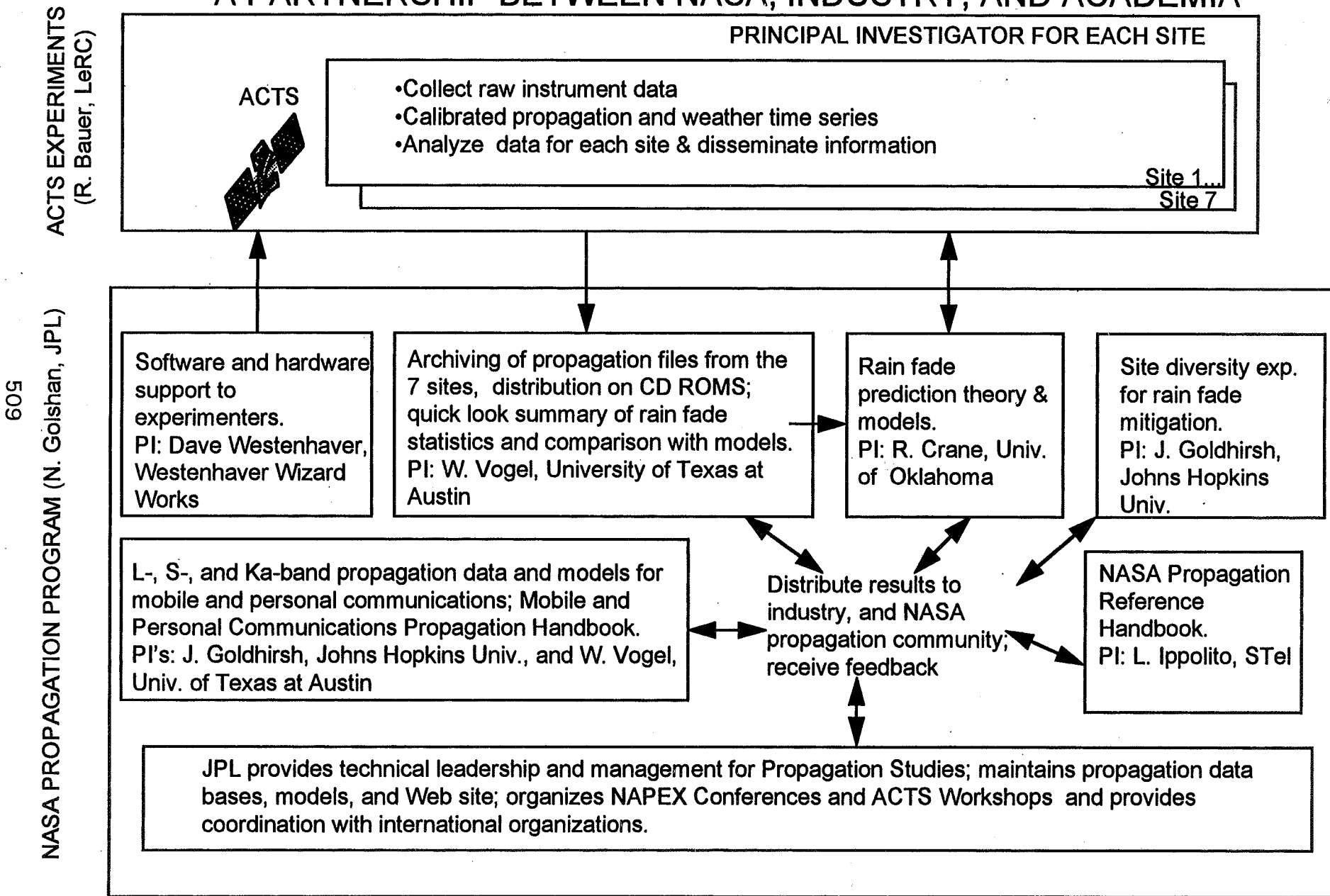
APPROACH

- Leverage unique NASA assets (currently ACTS) and other resources to obtain propagation data
- Strong partnership between NASA, industry, and universities
- Dissemination of data and models through refereed journals, NASA reference handbooks, workshops, electronic media, and direct interface with industry

508



NASA PROPAGATION PROGRAM A PARTNERSHIP BETWEEN NASA, INDUSTRY, AND ACADEMIA



**NASA PROPAGATION PROGRAM
SUMMARY OF INDUSTRY FEEDBACK AT NAPEX XX**

- **The NAPEX XX Conference provided an opportunity to present the status of the NASA Propagation Program to the U.S. Satcom Industry and get feedback.**
 - **U.S. Satcom Industry considers NASA Propagation Studies a national asset and critical to the industry.**
 - **U.S. Satcom Industry needs timely, easy-to-use propagation effects handbooks and internationally accepted, reliable prediction models for system design and coordination purposes across the globe.**
 - **Urgent need to revise the NASA propagation handbooks and publish electronically to allow timely, low-cost incremental updates.**
 - **Urgent need to have internationally accepted global model for prediction of rain & atmospheric propagation effects on satcom links.**
 - **Long-term plans needed to meet the future propagation needs of Satcom Industry.**

NASA PROPAGATION PROGRAM

Plans to Meet the Short-term Propagation Needs of the Satcom Industry

- Will accelerate efforts to validate and improve models for prediction of weather related impairments of Ka-Band satellite links to meet the urgent needs of the U.S. Satcom Industry.
 - 13 station-years of ACTS Ka-Band propagation data collected so far at 7 sites is an invaluable data base to validate and improve models for prediction of weather related impairments of Ka-Band satellite links.
 - This data represents the most extensive and reliable Ka-Band propagation data base existing today, thanks to extensive efforts to maintain the quality and continuity of ACTS Propagation Experiments.
 - Data is becoming available just in time for preliminary design of future Ka-Band satcom systems.
 - Summary comparison of ACTS Ka-Band data with prediction models indicates a need to revise the prediction models.
 - Extension of ACTS Propagation Experiments to November 1998 would provide 35 station-years of high quality data which would greatly facilitate international acceptance of ACTS propagation models by international and regulatory bodies.

NASA PROPAGATION PROGRAM

Plans to Meet the Short-term Propagation Needs of the Satcom Industry (Cont'd)

- Will accelerate revision of NASA reference propagation handbooks to meet the urgent need of the Satcom Industry.
 - NASA Reference Publications 1182 (1982) and 1082 (1989) are being overhauled into an updated, one-volume “Propagation Effects Handbook for Satellite Systems Design”
 - NASA Reference Publication 1274 (1992) is being revised into an easy-to-use “Propagation Effects for Vehicular and Personal Communications Satellite Systems” handbook.
- The Propagation Web Site at JPL is being expanded along a fast track approach intended to streamline distribution of NASA propagation documents, data, and models electronically.
 - Low cost, quick implementation by leveraging an existing system already working at JPL.

NASA PROPAGATION PROGRAM

Understanding the Long-term Propagation Needs of the Satcom Industry

- **NAPEX XX provided a dialogue between the U.S. Satcom Industry and the NASA Propagation Program to understand the long-term propagation needs of the U.S. Satcom Industry for implementation of communications systems at Ka-band and higher frequencies, as well as for second-generation mobile satellite systems.**
 - **There is a strong need for easy-to-use global models to predict first & second order temporal and spatial propagation statistics about attenuation, coherence bandwidth & depolarization due to weather (precipitation & atmosphere) for line of sight satellite systems at Ka-Band and higher frequencies up to and including optical systems.**
 - **Second-generation mobile and personal satellite systems can greatly benefit from global models to predict first & second order temporal and spatial statistics about attenuation, coherence bandwidth and depolarization over the 1.0-30 GHz range due to blockage, reflection and scattering by objects near the mobile or personal terminal.**

NASA PROPAGATION PROGRAM

ACKNOWLEDGMENTS

- The research described in this overview was carried out by the Jet Propulsion Laboratory, California Institute of Technology, under a contract with the National Aeronautics and Space Administration.
- Many individuals from NASA, academia, and industry have contributed to the success of the NASA Propagation Program and the NAPEX XX Conference; their contributions are reported separately as papers and overviews in this publication.

REPORT OF APSW IX PLENARY MEETING

D.V. Rogers and R.K. Crane

On 6 June 1996, the ACTS Working Groups held their customary joint Plenary meeting in Fairbanks to address issues related to experiments being conducted with NASA's ACTS Propagation Terminals (APTs). Results of that meeting are reported here.

I. Issues Related to Interaction with Industry

In recognition of the active participation by industry representatives in this workshop and the increasing interest in commercial Ka-band applications, several issues related to the reliability of the ACTS results, and how propagation information in general might best be disseminated to the engineering community, were discussed during the first part of the Plenary meeting. That discussion is summarized here.

A. *Extension of Measurement Period*

Concern was expressed regarding the potential benefits that might accrue from extending the ACTS measurement period; *i.e.*, is extension worth the cost? R. Crane provided data that indicated the uncertainty in estimating monthly statistics of 5-dB attenuation at the 0.1 significance level decreases to (± 3.0 , ± 2.5 , ± 2.1 , ± 1.9) dB for (2, 3, 4, 5) years of data, respectively. It was noted that additional years of data permit analyses of interannual variability, important in estimating risk factors in satellite systems design. It was further pointed out that continuing the measurements is likely to consume a small fraction of the cost of initially making the ACTS resource available.

B. *Data Dissemination/Need for Specific Results*

The data for the first two years of ACTS measurements are now available on CDs from the Data Center. J. Goldhirsh noted there was interest in seasonal models for propagation impairments, and indicated the benefits to the system designer. C. Mitchell concurred, and asked if such a model might be available by April 1997. Strong appreciation for reliable propagation prediction models was expressed. There was some discussion of the features and merits of some prediction models for rain attenuation (*e.g.*, Crane Global model, ITU-R method) and acknowledgment that the prediction accuracy for specific applications (*e.g.*, tropical predictions) is poorly known as yet.

Y. Lee expressed an interest to have propagation results presented in terms of quantities (such as bit error rate) that are directly applicable to systems design. However, it was noted that the conversion of measured data into such quantities are usually systems specific and consequently might best be made by the system designer himself.

C. Provision of General Propagation Information

Issues related to possible revision of the NASA handbooks (now currently available in three volumes for general topics related to propagation at frequencies above 10 GHz, below 10 GHz, and for land mobile-satellite services) were discussed. There appeared to be general support to update the handbooks. Additional opinions were expressed regarding the format of updated volumes, with the two generally recognized options being a single volume or separate volumes focused on fixed- and mobile-satellite applications. The final configuration is of course the purview of NASA. H. Berger recommended that the handbooks be made available on the world wide web. N. Golshan of JPL noted NASA's intention to do so, and stated that the current handbooks will in fact soon be available.

II. ACTS Experimenter Issues and Concerns

A. High Data-Rate Sampling for Scintillation

The capability to sample and analyze ACTS beacon data at 20 Hz is now available, and the system can be configured to automatically initiate a 6-minute sampling interval at 11 minutes after every hour. R. Crane recommended use of this feature at every ACTS site to collect statistically valid data for each propagation path. Some experimenters expressed concern that the large amount of additional data might cause problems of data handling for individual sites, and impact data archiving at the ACTS Data Center. A large amount of data is transferred to disk in this mode, and must be dumped to tape fairly quickly to ensure adequate disk storage.

C. Mayer cautioned that the present ACTS data-collection system is not optimum to support this mode (limited disk space, PCs are slow) and should be configured so that high data-rate sampling cannot crash the disk if improperly set up. He also noted that there should be a justification for using this feature, and

for how much 20-Hz data are required for valid statistics. Furthermore, the current file designators are not unique for each site.

ACTIONS:

ACTS experimenters are strongly encouraged to adopt the high data-rate sampling feature for at least the next three (summer) months, but its use is optional. D. Westenhaver will ensure that file names for each site are unique. W. Vogel offered to transfer the scintillation data for each site onto a CD for detailed analysis by R. Crane, who volunteered to critically review the data and compile a reference data set for each site.

B. Site Support/Maintenance

A great deal of concern was raised regarding the availability of critical site spares. Several experimenters had the view that the current data-collection computers and disk drives are becoming marginal for the ACTS requirements (*e.g.*, such as the 20-Hz data sampling mode mentioned above). The LNAs used in the beacon receive chains have been troublesome, and replacement of defective units can take several months. Loss of an LNA could therefore disable beacon measurements for a large fraction of a year. Strong endorsement for maintaining a supply of critical hardware spares, especially for long-lead items (LNAs, noise diodes, etc.), was expressed as essential to protecting the integrity of statistical results.

C. Mayer observed that the independent development of the APTs means that individual site experimenters lack intimate knowledge of terminal design and operation, and this knowledge must be supplied via site support. J. Feil stated that site services (as provided by D. Westenhaver) are vital to successful operation of the experiments.

S. Horan questioned the integrity of the 386-based computers, especially if the experiments are extended. Other experimenters expressed similar views regarding the current disk drives and the issue of data-collection reliability in general.

ACTIONS:

Subject to funding and necessary authorizations, D. Westenhaver is requested to upgrade the site hard drives, and to configure these units with necessary software, etc., for direct on-site exchange. Subject to the same constraints, urgent attention is recommended to acquiring a set of critical spares that can support site hardware failures. Subsequent consideration is requested

regarding upgrading the ACTS 386-based computers with high-quality 486-based machines.

C. *General Operations*

In his presentation, R. Bauer informed the group that NASA currently estimates that there is sufficient fuel on-board the satellite to maintain normal operations through July 1998, and perhaps an additional three years in inclined-orbit operation (by ceasing to perform N-S stationkeeping). In inclined-orbit operation the inclination of the satellite increases by about 0.8° per year, indicating that after July 1998, another 4-6 months of operation would be feasible for the APTs, with the satellite remaining in the 3-dB beamwidth of the antennas (*i.e.*, pointing would not be essential). In this case, a full five-year measurement APT period (through November 1998) is achievable.

Several sites reported recent difficulties with the beacon receivers at one or both frequencies. D. Westenhaver is aware of these problems and is collaborating with the experimenters to resolve the problems. In general, the day-to-day operations of the APTs are basically routine, and focus on data analysis and model development continues to increase.

As a follow-up to results already presented by M. Kharadly on antenna wetting experiments performed at UBC, both H. Helmken and R. Crane noted the importance of this effect for developing propagation models. There was discussion of the possibility of shielding the antenna feeds somehow, but since 2.5 years of data have already been collected, such protection would change the nature of the collected data and preclude further possibilities to investigate the effect on signal-loss statistics. M. Kharadly stated that the best efforts must be made to characterize the effect as a loss mechanism.

There appeared to be a consensus that the ACTS propagation data sets constitute the best data to date for development and validation of attenuation prediction models.

ACTIONS:

ACTS sites are encouraged to review their data records and try to identify wet antenna events. Each site is also encouraged to perform an antenna-wetting experiment if possible.